Synthesis and Application of Supramolecular Catalysts in the Oxidation of Unactivated C(sp^3)-H Bonds

Inauguraldissertation

Zur Erlangung der Würde eines Doktors der Philosophie

vorgelegt der

Philosophisch-Naturwissenschaftlichen Fakultät

der Universität Basel

Von

Melina Knezevic

2023

Genehmigt von der Philosophisch-Naturwissenschaftlichen Fakultät

Auf Antrag von

Prof. Dr. Konrad Tiefenbacher, Prof. Dr. Thomas R. Ward und Prof. Dr. Miquel Costas

Basel, den 21.02.2023

Prof. Dr. Marcel Mayor

(Dekan)

Die vorliegende Arbeit wurde von März 2019 bis Februar 2023 an der Universität Basel unter der Betreuung von Prof. Dr. Konrad Tiefenbacher angefertigt.

Teile dieser Arbeit wurden veröffentlich:

(1) **Knezevic, M.**;† Heilmann, M.; Piccini, G. M.; Tiefenbacher, K. Overriding Intrinsic Reactivity in Aliphatic C–H Oxidation: Preferential C3/C4 Oxidation of Aliphatic Ammonium Substrates, *Angew. Chem. Int. Ed.* **2020**, *59*, 12387–12391.

(2) Heilmann, M.;† **Knezevic, M.**; Piccini, G. M.; Tiefenbacher, K. Understanding the Binding Properties of Phosphorylated Glycoluril-Derived Molecular Tweezers and Selective Nanomolar Binding of Natural Polyamines in Aqueous Solution, *Org. Biomol. Chem.* **2021**, *19*, 3628-3633.

(3) **Knezevic, M.**;† Tiefenbacher, K. Tweezer-Based C-H Oxidation Catalysts Overriding the Intrinsic Reactivity of Aliphatic Ammonium Substrates, *Chem. Eur. J.* **2022**, doi.org/10.1002/chem.202203480.

† Erstautor

Acknowledgments

First of all, I wish to express my deepest gratitude to Prof. Dr. Konrad Tiefenbacher for giving me the opportunity to work in his group and in the exciting field of supramolecular chemistry. I am very thankful for the particularly interesting project, and all the support, assistance, and motivation he shared with me throughout my master`s thesis and this study.

Also, I would like to thank Prof. Dr. Thomas R. Ward for his advice and input in our yearly discussions as my second supervisor.

Furthermore, I would like to express my gratitude to all my colleagues from the Tiefenbacher group for the amazing working atmosphere. Special thanks go to all my direct lab mates, and especially to Dr. Jesper Köster and Dr. Michael Heilmann, who received me so warmly in their lab and even tolerated my special taste in music. Furthermore, I am very thankful to Dr. Michael Heilmann for his technical supervision during my master`s project and for all the knowledge he shared with me during my ongoing studies. Special thanks also go to Dr. Suren Nemat, Dr. Jonathan Pfeuffer-Rooschütz, and Dr. Daria Sokolova who were my colleagues almost throughout the whole time and became good friends. My deepest gratitude also goes to Dr. Jonathan Pfeuffer-Rooschütz and Iris Martyn for proofreading this manuscript as well as to Dr. Leonidas-Dimitrios Syntrivanis for all the helpful discussions and advice. Furthermore, I would like to acknowledge Yiheng Lu, who was an outstanding student to supervise and became a great colleague.

Also, I am extremely grateful to Prof. Dr. Giovanni-Maria Piccini for our collaboration, and his valuable contribution to the first publication presented in this thesis by adding important computational studies. Special thanks also go to Dr. Joan Serrano-Plana, for sharing his great knowledge about C-H oxidation catalysts with me.

I want to thank the entire staff of the chemistry department for their support whenever needed. Special thanks go to Dr. Michael Pfeffer for HR-MS analysis, Dr. Jonas Zurflüh for support concerning any analytical issues, and Isa Worni for all the administrative work she has done. Furthermore, I greatly acknowledge and thank the technical staff (Markus Hauri and Susanne Foley) as well as the workshop team (Markus Ast, Pascal Andrek, Andreas Sohler, and Isny Meha) and IT Service Center (Dr. Bernhard Jung and Christoph Heidenreich).

Last but not least, I want to thank my family, friends, and most of all my wonderful partner, Christian, for their unconditional love and support.

Deutsche Zusammenfassung

Im Laufe der letzten Jahrzehnte sind beeindruckende Fortschritte bei der selektiven Funktionalisierung von nicht aktivierten, aliphatischen C(sp^3)-H Bindungen gemacht worden. In Anbetracht des inerten Charakters und der Allgegenwärtigkeit dieser Bindungen, gilt ihre selektive Umsetzung als eine der schwierigsten. Zur gleichen Zeit jedoch hat die selektive Umwandlung von C-H Bindungen, insbesondere im Falle von Late-Stage-Funktionalisierungen, großes Potenzial und ist aus wirtschaftlicher Sichtweise sehr attraktiv. Um eine gute Aktivität und Selektivität bei C-H Oxidationen zu erreichen, haben Synthesechemiker verschiedene Ansätze entwickelt, einschließlich gerichteter, ungerichteter und supramolekularer Strategien. Für uns war besonders der supramolekulare Ansatz von Interesse, bei dem die Bindung zwischen Katalysator und Substrat über mehrere schwache Kräfte erfolgt.

Im ersten Teil dieser Arbeit wurden supramolekulare Katalysatoren hergestellt, die aus einer Glycoluril-basierten, molekularen Pinzette und den gut etablierten M(pdp)- oder M(mcp)-Katalysatoren bestehen. Insgesamt wurden fünf verschiedene Versionen in jeweils zehn Schritten synthetisiert. In allen Fällen wurde eine bevorzugte Oxidation von Decylammonium an den intrinsisch deaktivierten Positionen in der Nähe des Ammoniumsalzes beobachtet (C3/C4). Je nach verwendetem Katalysator wurden allerdings leicht unterschiedliche Ergebnisse beobachtet. Die besten Ergebnisse hinsichtlich der Selektivität für die deaktivierten Positionen C3/C4 wurden mit **Fe(pdp)Twe** erzielt. Außer Decylammonium wurden auch eine Reihe anderer linearer aliphatischer Ammoniumsalze, zwei Ammoniumsubstrate mit einem Terpensubstitutionsmuster und zwei Cyclohexanderivate in der Oxidation mit **Fe(pdp)Twe** studiert. Schließlich untersuchten wir auch noch das Oxidationsverhalten unseres Katalysators in verschiedenen Lösungsmitteln (MeCN, TFE, HFIP).

Im zweiten Teil wurde der Nicht-Häm **Mn(mcp)**-Katalysator mit zwei verschiedenen Cyclophaneinheiten funktionalisiert, was zu **Mn(mcp)CY3** und **Mn(mcp)CY5** führte. Die Katalysatoren wurden beide in einer sieben-stufigen Synthese hergestellt. Wir vermuteten, dass aufgrund eines solvophoben Effekts selektive Oxidationen von aliphatischen Substraten ohne jegliche funktionelle Griffe in TFE und HFIP möglich sein könnten. Leider beobachteten wir bei allen untersuchten Substraten mit unseren supramolekularen Katalysatoren das gleiche Oxidationsmuster wie mit dem unfunktionalisierten **Mn(mcp)**. Es sollte jedoch erwähnt werden, dass die Arbeit an diesem Konzept weitergeht und dass erste, vielversprechende Ergebnisse von einem anderen Gruppenmitglied mit anderen Makrocyclen beobachtet wurden.

English Abstract

Over recent decades, impressive progress was achieved in the selective functionalization of unactivated aliphatic C(sp^3)-H bonds. Considering the inert character and ubiquity of these bonds, they are considered among the most challenging ones to selectively convert. However, at the same time, the selective reaction of C-H bonds, especially in the form of late-stage functionalizations, has great potential and is very attractive from an economic point of view. Synthetic chemists have established different approaches to achieve good activity and selectivity in C-H oxidations, including directed, undirected, and supramolecular strategies. To us, the supramolecular approach, in which binding between the catalyst and the substrate is achieved *via* multiple weak forces, was of great interest in particular.

In the first part of this thesis, supramolecular catalysts consisting of a glycoluril-based molecular tweezer and well-established M(pdp) or M(mcp) catalysts were prepared. In total, five different versions were synthesized in ten steps each. In all cases, preferential oxidation of decylammonium at the intrinsically deactivated positions close to the ammonium salt was observed (C3/C4). However, slightly different results were obtained depending on the catalyst used. The best results regarding the selectivity for the deactivated positions C3/C4 were achieved with **Fe(pdp)Twe**. Other than decylammonium, a handful of other linear aliphatic ammonium salts, two ammonium substrates possessing a terpene substitution pattern, and two cyclohexane derivatives were investigated in the oxidation with **Fe(pdp)Twe**. Finally, we also studied the oxidation behavior of our catalyst in different solvents (MeCN, TFE, HFIP).

In the second part, the non-heme Mn(mcp) catalyst was functionalized with two distinct cyclophane moieties, leading to **Mn(mcp)CY3** and **Mn(mcp)CY5**. The catalysts were both made in a seven-step synthesis. We hypothesized that selective oxidations of aliphatic substrates lacking any functional handle might be possible in TFE and HFIP, due to a solvophobic effect. Unfortunately, we observed the same oxidation pattern with our supramolecular catalysts as with the unfunctionalized **Mn(mcp)** for all investigated substrates. However, it should be noted that the work on this concept is ongoing and that promising first results have been observed by another group member with different macrocycles.

Table of Contents

1 Introduction

The elegance and efficiency of biochemical machinery have always been a great source of inspiration for synthetic chemists.[1] Especially when it comes to the synthesis of complex oxygenated hydrocarbon frameworks, performance in nature remains unmatched by artificial approaches. For instance, the biochemical synthesis of complex terpenes can usually be divided into two phases.[2] In the "cyclase phase", enzymes stitch together C-C bonds and construct the hydrocarbon framework from only a few small precursors. Subsequently, in an "oxidation phase", a second class of enzymes introduces C-O bonds into the structure, which are often crucial for biological activity.[3] Despite the beauty and near-to-perfect redox economy of this approach, synthetic chemists have only recently started to mimic it in total synthesis strategies.[4-6] This is due to the relatively inert character of C-H bonds and the similar reactivity between different C(sp^3)-H bonds of the same degree of substitution (e.g. secondary).[7] An even greater challenge is the oxidation of deactivated positions in the presence of more activated positions. To achieve site-selectivity in C-H bond functionalizations, chemists have developed different approaches which can be divided into three groups (Scheme 1).[8-10] Firstly, in a directed strategy, C-H bonds are oxidized in intramolecular reactions, either by applying directing groups or *via* the incorporation of the reactant into the substrate (Scheme 1A).[8-9] However, this approach usually is limited to proximal positions (β, γ, and δ) to the directing groups and their preinstallation is necessary.

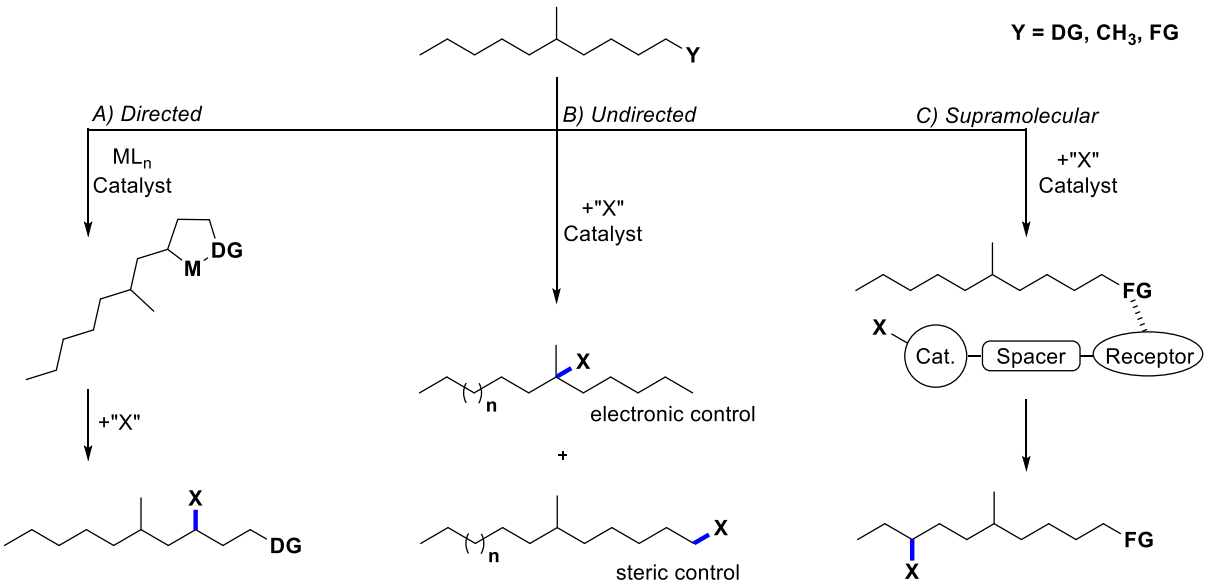

Scheme 1: Different approaches towards selective C(sp^3)-H oxidations. A) Directed approach: selectivity for β, γ, or δ positions. B) Undirected approach: selectivity for the most reactive and/or accessible position. C) Supramolecular approach: selectivity for the positions closest to the active center.

In a second strategy, undirected C-H oxidation catalysts are used, which rely on the small electronic, steric, and stereoelectronic differences of C-H bonds (Scheme 1B).[8-9] Therefore, the most reactive, accessible positions will be oxidized. However, deactivated positions usually remain inaccessible. Finally, a supramolecular approach can be used (Scheme 1C).[10] The field of supramolecular chemistry is based on the concept of molecular recognition of two or more molecules *via* weak, non-covalent forces, such as dipole-dipole interactions, hydrogen bonding, dispersion forces, and different kinds of π-interactions. Applications of these intermolecular bonding forces include host-guest systems, molecular machines, and processes like self-assembly.[11] Supramolecular chemistry is defined as the chemistry of the intermolecular bond and has been described as "chemistry beyond the molecule" by *Lehn*, one of its pioneering leaders.[12] Together with *Pederson*[13] and *Cram*,[14] he was awarded the Nobel Prize in Chemistry for the "syntheses of molecules that mimic important biological processes", showing the close relationship between supramolecular chemistry and molecular biology. Using a supramolecular approach in C-H oxidations allows for the oxidation of positions closest to the active center, even if those are distant from the recognition site or intrinsically deactivated.

1.1 Reactivity of C(sp^3)-H Bonds

The inert character and ubiquity of C-H bonds render them the most challenging bonds to functionalize. A good first indication of the strength of C-H bonds in alkanes are their high pK_a values (~ 50)[15] and bond dissociation energies (BDE ≈ 96 – 101 kcal/mol).[7] Benzylic and allylic positions, by comparison, are noticeably more reactive (BDE ≈ 83 – 90 kcal/mol) and can be targeted more easily.[7] In recent years, catalysts have been developed that are capable of distinguishing between the different aliphatic C(sp^3)-H bond types. As a result, they can selectively oxidize primary C-H sites in the presence of secondary and tertiary sites (e.g. metal-catalyzed C-H activation reactions) or, *vice versa*, oxidize tertiary sites in the presence of secondary and primary sites (e.g. radical promoted functionalizations).[8-10] However, if multiple C-H bonds of the same degree of substitution are present, selectivity usually is more difficult, with selective methylene oxidation being among the most challenging examples.[16]

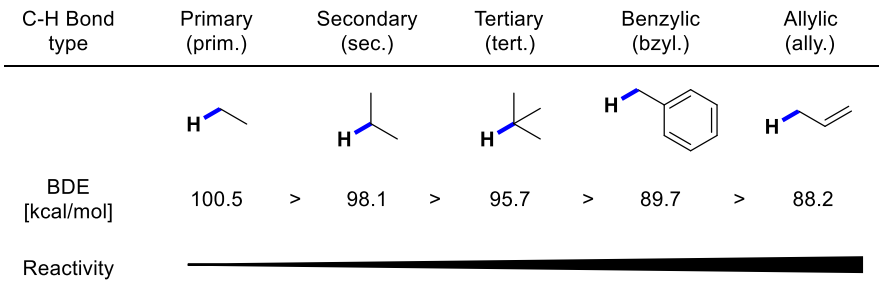

Figure 1: Bond dissociation energies of different aliphatic bond types.

In the following section, an overview will be given of the different techniques used to achieve selectivity in C-H oxidations/functionalizations (C-H → C-X; X=O, N, C, halogen), with a slight focus on C-H oxygenations (C-O bond formation).

1.2 Directed C(sp^3)-H Oxidation

1.2.1 Non-Metal Directed C(sp^3)-H Oxidation

Possibly the oldest strategy in directed C(sp^3)-H oxidations is based on radical-mediated selective hydrogen atom transfer (HAT) (Scheme 2).[17-18] Early results in these C(sp^3)-H functionalizations were obtained almost 140 years ago by *Hofmann*, by taking advantage of the photolytic homolysis of cationic *N*-haloamines.[19] In these reactions (known today as Hofmann-Löffler-Freytag (HLF) reactions), an N-centered radical **3** undergoes a 1,5-regioselective HAT *via* a chair-like transition state.[20-21] The new δ C-centered radical **4** is subsequently trapped, generating the corresponding halide **5**. Base-induced intramolecular cyclization gives access to the corresponding pyrrolidine **6**. This formal C-H amination is, therefore, a C-H halogenation which leads only to a net amination.[22] *Löffler* and *Freytag* extended the substrate scope and successfully applied it to the synthesis of nicotine (**7**) (Scheme 2B).[23-24] Later, Corey employed the strategy for aminated steroid substrates, furnishing dihydroconessine (**8**) (Scheme 2C).[25] Original drawbacks, such as the need to use strong acids and high temperatures to generate the N-radical, were later overcome due to further modification by *Suárez* and coworkers by employing molecular iodine and a hypervalent iodine oxidant (PhI(OAc)$_2$).[26]

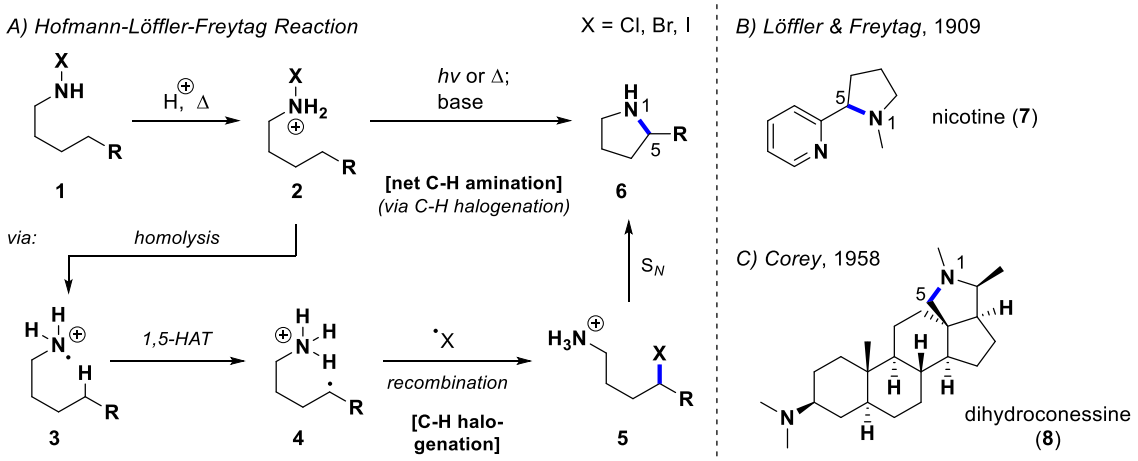

Scheme 2: Directed C(sp^3)-H functionalizations *via* N-centered radicals.

Although most work in this field has been carried out on N-centered radicals, C-centered and O-centered radicals have also been studied.[18] Due to their higher electronegativity, the open shell in O-centered radicals is less stable and therefore promotes the HAT step.[18] However, the formation of the O-radical is consequently more challenging compared to nitrogen. The earliest example of an alcohol-derived alkoxy radical was reported by *Barton* in 1960 *via* nitrite ester photolysis (Barton reaction, Scheme 3A).[27] Preparation of the nitrite can be achieved by the reaction of an alcohol **9** with nitrosyl chloride in dry pyridine. Homolysis of the nitrite ester

10 upon irradiation gives the highly reactive O-radical, which usually undergoes selective 1,5-HAT. By means of recombination of the formed δ C-radical with ˙NO and subsequent tautomerization, a δ-aminated oxime product **11** is obtained. *Barton* and coworkers successfully applied this new method in the synthesis of aldosterone acetate (**13**), involving hydrolysis of the observed oxime **12** (Scheme 3B).[28] Only a few years later, *Kalvoda* and coworkers reported the direct generation of the alkoxy radical from an alcohol *via in situ* formation of the O-X bond with $Pb(OAc)_2$ and I_2 (Scheme 3C/D).[29] In this way, it was possible to observe tetrahydrofuran **16**. Significant improvements in the reaction were achieved again by *Suárez* and coworkers, employing hypervalent $PhI(OAc)_2$ and iodine instead of Pb reagents (Scheme 3E).[30-31] The versatility of these conditions was further demonstrated by employing a range of steroid and carbohydrate substrates. Once again, it should be noted that this method is only a net C-H oxygenation. It proceeds *via* a C-H halogenation step followed by intramolecular nucleophilic substitution, in a manner analogous to the HLF reaction.

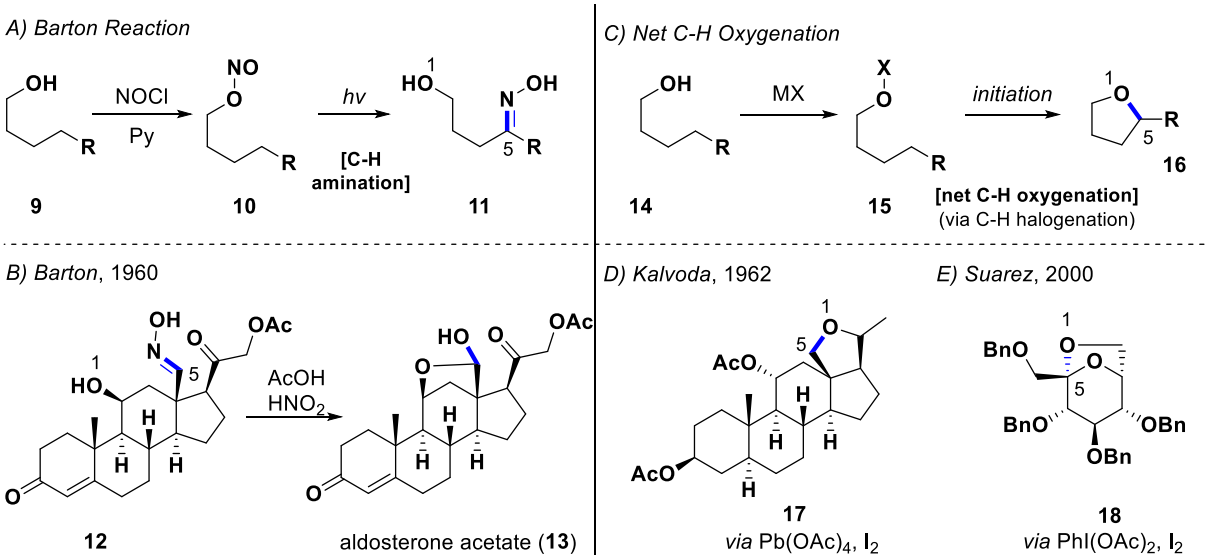

Scheme 3: Directed C(sp^3)-H functionalizations *via* O-centered radicals.

As previously mentioned, radical-mediated C-H oxidations usually react in a 1,5-HAT *via* a chair-like transition state. Both the 1,4- or 1,6- alternatives are typically higher in energy, due to enthalpic[32] and entropic[33] reasons, respectively. Only a few exceptions to this rule are known, for instance, if the δ C lacks an H-bond, or if other close C-H bonds are significantly more reactive (benzylic > tert. > sec. > prim. C-H bond).[34] Some examples for 1,n-HAT reactions other than n = 5 are depicted in Figure 2. *Baran* and coworkers for instance reported the 1,6-HAT in trifluoroethyl carbamate substrates to give, for example, ε-brominated carbamate **19** *via* a modified HLF reaction (Figure 2A).[35] After subsequent cyclization and hydrolysis, 1,3-diol **20** could be obtained in 69% yield. Good 1,6-selectivity could only be

obtained with the use of these special trifluoroethyl carbamates and for substrates in which the δ C-H bond was less reactive than the ε C-H bond (e.g., secondary vs. tertiary; tertiary vs. benzylic). Another example of selective 1,n-HAT with n ≠ 5 was provided by *Griesbeck* (Figure 2B).[36] In this case, product **21** was obtained *via* a Norrish type II reaction starting from the corresponding carbonyl compound. Photochemical activation of the carbonyl promotes intramolecular 1,7-HAT and the formation of a 1,6-biradical, which subsequently cyclizes to **21** (90% yield). Another example of O-centered radical promoted HAT was given by *Suárez* in 2002, reporting the selective 1,8-HAT of methyl β-D-maltoside (Figure 2C).[37] This occurs *via* activation of the primary alcohol with DIB and I_2, leading to disaccharide **22** in 62% yield. Finally, two very early examples of remote intramolecular C-H functionalizations using HAT should be mentioned. In both examples, *Breslow* and coworkers employed rigid steroid scaffolds in remote HAT functionalizations. In 1973, they reported that irradiation of benzophenone-4-acidic ester of 3-α-cholestanol results in a selective 1,14-HAT reaction (Figure 2D).[38] The generated diradical **24** undergoes internal disproportionation giving alkene **23** in 55% yield. Furthermore, in 1977, they achieved selective remote chlorination *via* irradiation of 3-α-cholestanol iodobenzoate and $ArICl_2$ giving **25** in 81% yield (Figure 2E).[39] By switching the linker length, they also achieved other 1,n-HAT reactions (e.g. 1,14 and 1,19).

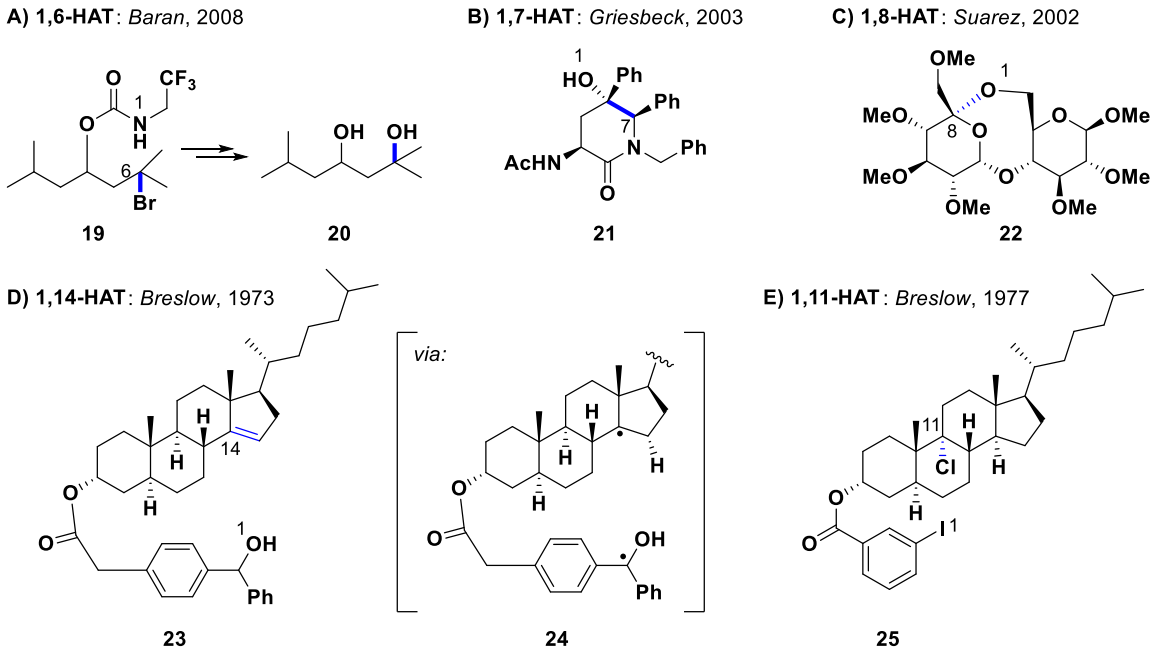

Figure 2: Examples of directed C(sp^3)-H functionalizations *via* radical mediated 1,n-HAT with n ≠ 5.

Besides these very impressive examples, the general application of radical-mediated C-H functionalizations for positions other than δ C-H bonds remains limited. Similarly, the

functionalization of deactivated positions in the presence of more reactive ones is usually only possible in the case of 1,5-HAT reactions.[18]

Besides radicals, nitrenes and carbenes can be used in C(sp^3)-H oxidations.[22] Both nitrenes and carbenes are highly reactive and can therefore insert into a C-H bond, giving access to **28** and **31**, respectively (Scheme 4A/B). Early contributions were carried out by *Cory* and coworkers in 1977, by applying the C-H insertion strategy to the total synthesis of the tetracyclic sesquiterpene ishwarane (**32**) (Scheme 4C).[40] In this case, the crucial carbene was formed by treatment of the corresponding alkene with CBr_4 to generate the dibromocyclopropane intermediate, which undergoes elimination upon addition of MeLi. In 1964, *Masamune* reported the total synthesis of garryine (**34**), by applying a nitrene insertion reaction to form lactame **33** from an unstable acyl azide starting material by irradiation with light (Scheme 4D).[41]

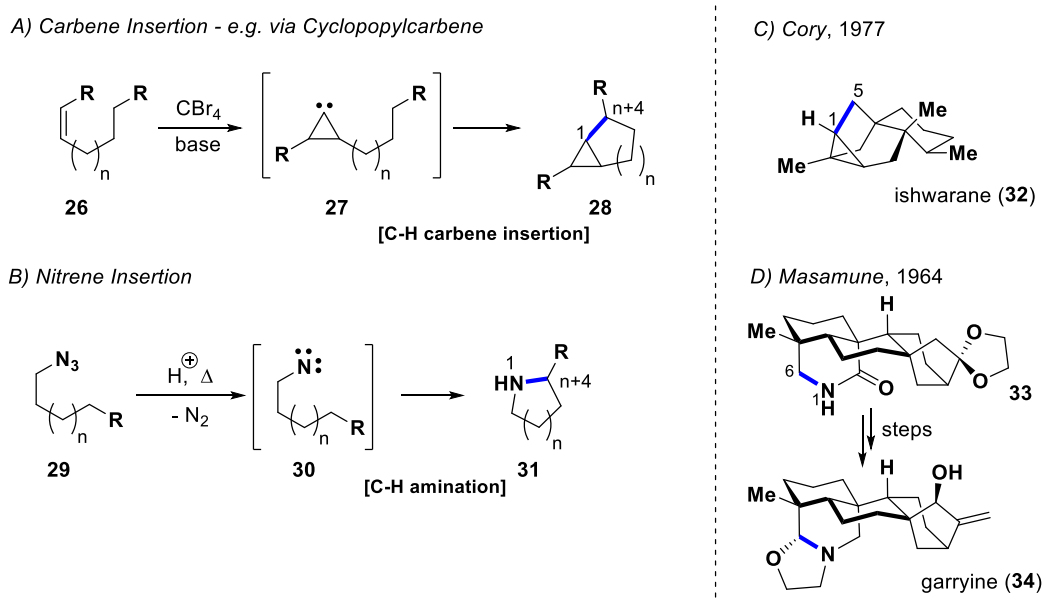

Scheme 4: Directed C(sp^3)-H functionalizations *via* nitrene/carbene insertion.

Since those early contributions, further examples involving metal-free directed nitrene or carbene insertion reactions have been reported.[22] In the case of carbene insertion, most work has been performed using alkylidene carbenes, which can be synthesized by several different methods, e.g. *via* a retro-1,2-shift from alkynes, base-induced α-elimination of terminal 1-haloalkenes, or elimination of nitrogen from diazoalkenes.[42] However, analogous to the radical-promoted C-H functionalization, carbenes and nitrenes usually insert in a regiocontrolled fashion to form five-membered carbo- or heterocycles. For the functionalization of other positions, this approach is of limited usage.[22]

1.2.2 Metal-Catalyzed Directed C(sp^3)-H Oxidation

Transition metal-catalyzed C-H functionalizations (both directed and undirected) can be subdivided into two groups, depending on the mechanistic pathway they follow (Scheme 5).[43] Common terms used for the two distinct pathways are 'organometallic' and 'coordination' chemistry after *Crabtree*[43] or 'inner-sphere' and 'outer-sphere' mechanism after *Sanford.*[44]

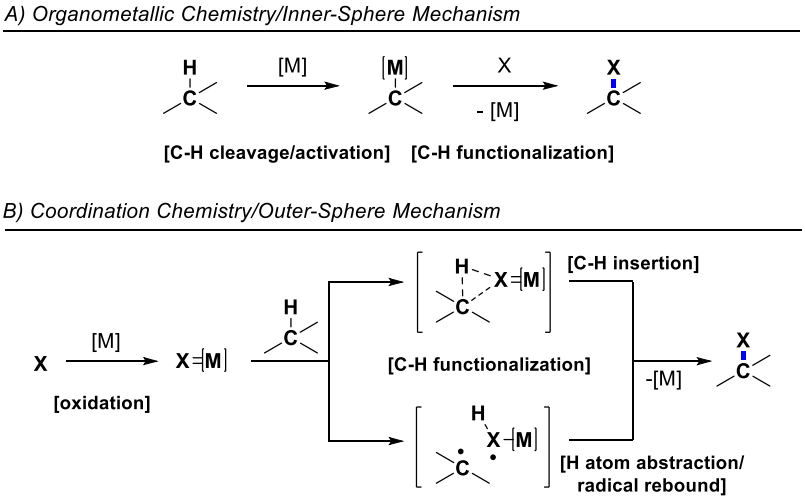

Scheme 5: Different mechanisms for metal-catalyzed C(sp^3)-H functionalizations.

In the organometallic/inner-sphere approach, the C-H functionalization begins by cleavage of a C-H bond to give a new C-M bond (C-H activation),[45] followed by functionalization (Scheme 5A).[43-44] The functionalization step can proceed either *via* a reductive process (e.g. reductive elimination), or by reaction with an electrophilic reagent (*via* direct electrophilic cleavage, one-electron oxidation, or two-electron oxidation).[46] 2nd and 3rd-row transition metals are typically used for this transformation, with Pd playing a dominant role.[46-48] Due to the lack of a radical or electrophilic intermediate, an inverted selectivity trend compared to the previously discussed approaches is observed (prim. > sec. > tert.), favoring the formation of the least sterically hindered C-M bond. In ligand-directed C(sp^3)-H oxidations (Scheme 6A), the key cyclometalation intermediate **36** is formed, with a high preference observed for the formation of a 5-membered metallocycle.[46-47] The reactivity preferences can be demonstrated by the highly selective formation of **38** (>95% selectivity) in 75% yield, in the presence of other proximal primary and secondary positions (Scheme 6B).[49] In fact, the directed functionalization of secondary and tertiary bonds *via* C-H activation proved to be challenging even in the absence of proximal primary bonds, and can often only be achieved for positions adjacent to activating groups (e.g. oxygen).[46]

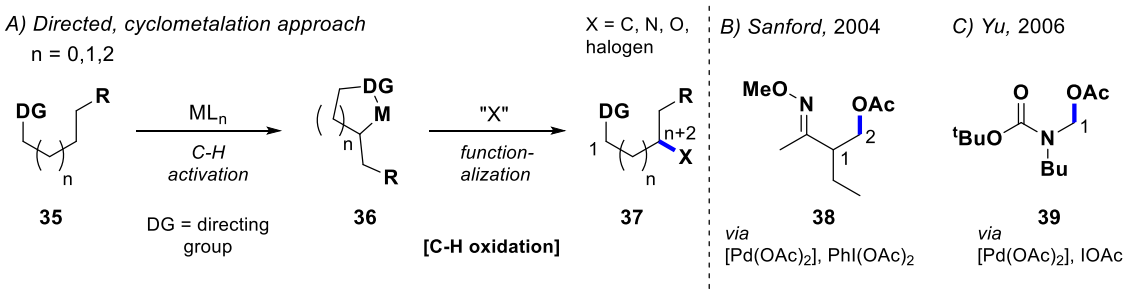

Scheme 6: Directed C(sp^3)-H functionalizations *via* cyclometalation.

Besides hypervalent iodine(III) reagents (PhI(OAc)$_2$),[49-50] iodine(I) oxidants (IOAc)[51] or inorganic peroxide oxidants (Oxone, $K_2S_2O_8$)[52-53] can also be utilized to achieve C-O bond formation.[46] For instance, *Yu* and coworkers reported the synthesis of **39** in 83% yield by the use of IOAc (Scheme 6C).[51] The proposed mechanism proceeds *via* a C-H halogenation (i.e. a C-I bond-forming reductive elimination) followed by a nucleophilic substitution with acetate to give **39**. However, the direct C-OAc bond formation could not be excluded with certainty. Besides C-O bond formation, many other C-X bonds can also be obtained *via* this approach with the use of different reagents.[46-47]

In the coordination/other-sphere mechanism, a high oxidation state metal complex with an activated ligand (X=[M]) is initially formed, which subsequently interacts with a C-H bond (Scheme 5B).[43-44] This second step can proceed either by direct insertion or by an H atom abstraction/radical rebound mechanism. In both pathways, preferential selectivity for weaker C-H bonds is observed (tert. > sec. > prim.). A frequently used directed outer-sphere approach involves the intramolecular insertion of metal carbenoids or nitrenoids into C-H bonds (Scheme 7A).[22, 54-55] Common starting materials for the directed C-H insertion of carbenoids are diazo compounds such as **40**.[54] Upon transition metal-catalyzed nitrogen extrusion, the metal carbenoid **41** is formed, which subsequently inserts into a nearby C-H bond affording the cyclic product **42** (mostly cyclopentanes and -hexanes). The most frequently used starting materials for C-H amination are carbamates and sulfamate esters of the general structure **43**.[55] Pioneering work was done by *Breslow*, reporting the rhodium(II) catalyzed intramolecular C(sp^3)-H amination of 2,5-diisopropylbenzenesulfonamide with PhI(OAc)$_2$.[56]

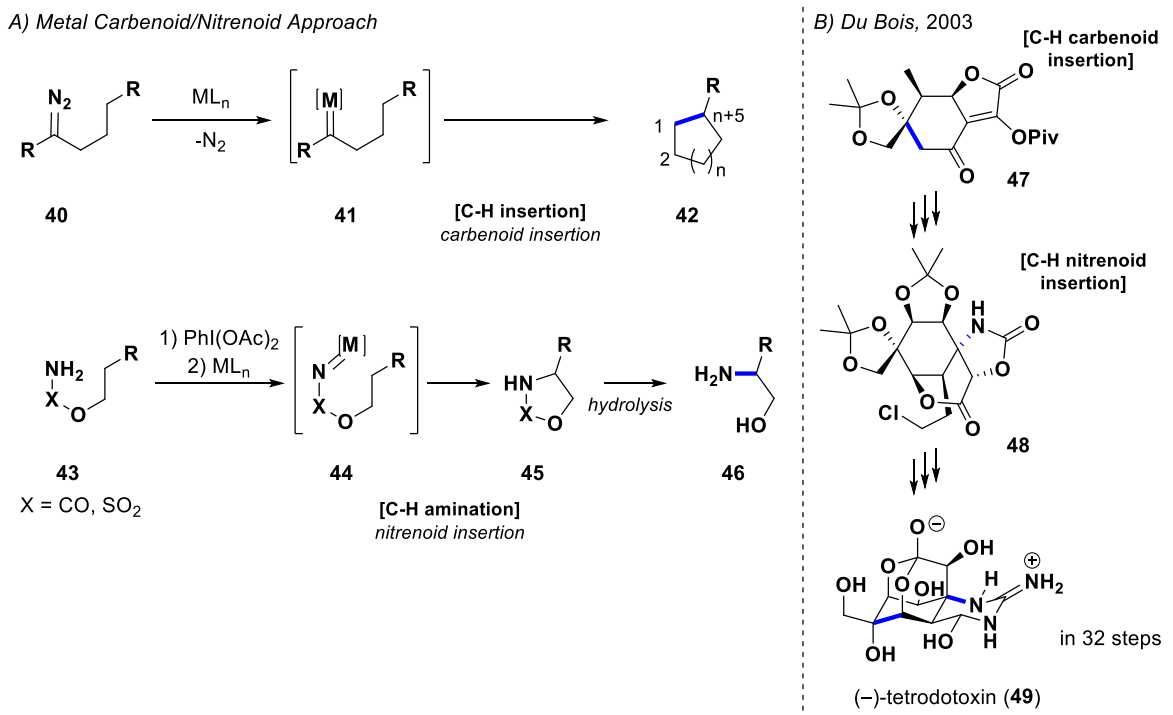

Scheme 7: Directed C(sp^3)-H functionalizations *via* metal carbenoid/nitrenoid insertion.

Later, *Du Bois* and coworkers showed that carbamates and sulfamate esters also react with PhI(OAc)$_2$ in the presence of a Rh(II) catalyst to give the corresponding oxazolidinones and oxathiazinones **45**, respectively.[57-58] A particularly remarkable application of this method is the total synthesis of (-)-tetrodotoxin (**49**) by *Du Bois*.[59] He and his group achieved **49** in half as many steps as in the previous synthesis reported by *Isobe* (32 and 67 steps, respectively).[60] In their synthetic strategy, they employed both a C-H carbenoid insertion and a C-H nitrenoid insertion step (Scheme 7B).

In summary, directed C(sp^3)-H bond functionalizations have proved to be a very powerful tool for synthetic chemists. Very high selectivities can often be observed, however, the general usage is limited, due to the need for a directing group or the incorporation of the reactant into the substrate. And despite the reports of some beautiful examples of remote functionalizations, directed C(sp^3)-H bond functionalizations are typically limited to proximal positions.

1.3 Undirected C(sp^3)-H Oxidation

For a long time, undirected aliphatic C-H oxidations were considered too unselective to be of general utility. Only in recent years have chemists started to achieve more and more selective undirected C-H oxidations, by employing catalysts that distinguish between the small electronic, steric, and stereoelectronic differences of those bonds in a molecule (Figure 3).[16, 61-62] Since most C-H oxidation catalysts/reagents are electrophilic, the most electron-rich C-H bond is usually preferentially oxidized. Electronic effects due to bonding are evident in the commonly observed reactivity trend of C-H bond types (tert. > sec. > prim.). Furthermore, electron-withdrawing groups (EWGs) have a distinct impact on the reactivity of their proximal positions, by decreasing the electron density and deactivating them towards oxidation (Figure 3A). Similarly, steric factors such as a bulky group can have a great impact on the oxidation rate, especially if the catalyst itself is sterically demanding (Figure 3B). Finally, stereoelectronic activation or deactivation influences the reactivity of C-H bonds (Figure 3C). This can, for example, be observed in the preferential oxidation of C-H bonds vicinal to some heteroatoms or cyclopropanes due to hyperconjugation. In this case, the non-bonding electrons of the heteroatom or the C-C σ bonding orbital of the cyclopropane overlap with the neighboring C-H σ antibonding orbital, increasing the electron density and its reactivity.[61]

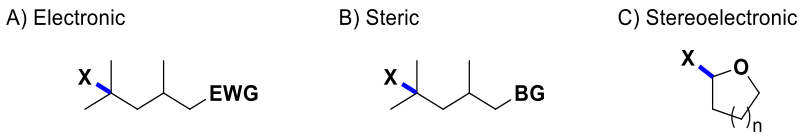

Figure 3: C-H oxidation selectivity on basis of electronic, steric, and stereoelectronic differences.

One frequently used class of non-metal oxidants is dioxiranes (Scheme 8).[16, 61, 63] Common representatives are dimethyldioxirane (DDO) and trifluoromethylmethyldioxirane (TFDO). These highly strained cyclic peroxides are very reactive and need to be handled carefully due to their instability towards various conditions (e.g. TFDO decomposes under visible light, at temperatures above -20 °C, or in the presence of trace metals).[16] Despite their delicate handling, dioxiranes oxidize unactivated C-H bonds under very mild conditions and have been widely applied. The precise mechanism has been the subject of longstanding debate, with evidence for both a concerted "oxenoid" insertion mechanism[64-68] as well as for a free radical mechanism.[69-70] However, the more recent publications by *Bach*[71] and *Houk*[72-73] support an H atom abstraction/oxygen rebound mechanism mostly based on computational results (Scheme 8A).

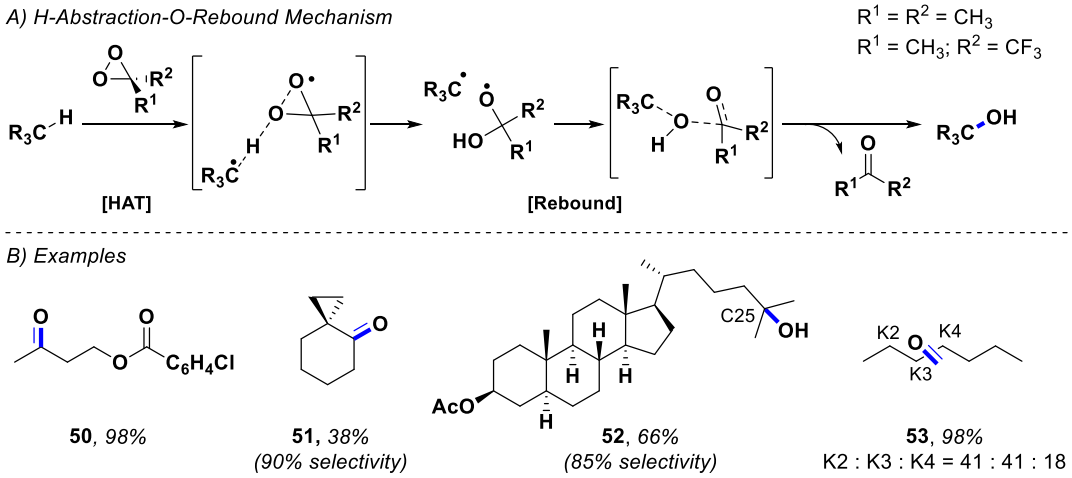

Scheme 8: Undirected C(sp^3)-H oxygenation with dioxirane.

And indeed, impressive selectivities can be observed in the oxidation with dioxiranes (Scheme 8B).[16, 61] For instance, *Asensio* and coworkers applied TFDO to the oxidation of some aliphatic esters.[74] Due to the strong deactivation of the proximal positions, **50** was formed exclusively. However, it should be noted that the deactivating effect and selectivity are rapidly lost with longer aliphatic chains. Extensive work has also been carried out by *Curci* and coworkers, who studied the oxidation of some cyclopropyl-bearing substrates and the effect of hyperconjugation.[75-77] One example is the oxidation of spiro[2.5]octane to **51** with 90% selectivity.[75] In another report from this group, good selectivity for the unhindered C25 positions of 3β-acetoxy-5α-cholestane was observed to produce **52**.[76] However, in the oxidation of simple *n*-alkanes such as heptane, almost statistical product distribution of the possible ketone products **53** is observed.[77] This is due to the lack of any strong electronic, steric, or stereoelectronic differences, other than the less reactive primary C-H bonds.

Organometallic/inner-sphere chemistry can also be applied to undirected C-H oxidations.[16, 43, 62] Perhaps the earliest report of transition-metal catalyzed undirected C(sp^3)-H oxidations dates back to 1972 by *Shilov*, who reported the C-H oxygenation and halogenation of alkanes in water *via* high-valent Pt catalysis (Scheme 9A).[78-79] Back then, it was a remarkable result that a preference for the oxidation of primary C-H bonds was observed. However, only modest rates and conversions were obtained. Further improvements in the reactions were achieved by *Periana* utilizing a bipyrimidine Pt catalysts, enabling impressive yields based on the starting material at relatively low catalyst loading (5 mol%) and good turnover numbers (Scheme 9B).[80] Almost two decades later, *Sanford* and coworkers reported good selectivities in the oxidation of the terminal CH_3 groups in tertiary ammonium substrates such as **54**, increasing the selectivity by further deactivating the proximal methylene bonds (Scheme 9C).[81]

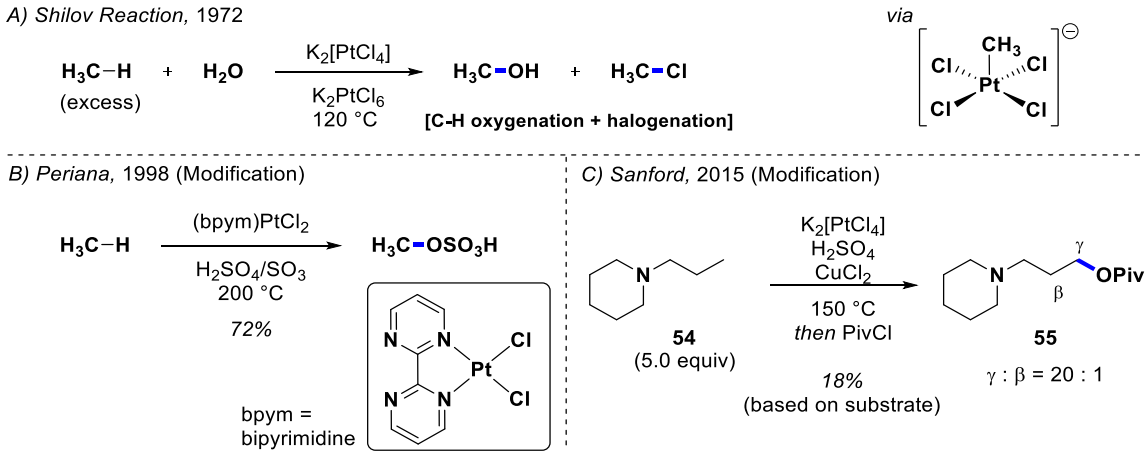

Scheme 9: Undirected C(sp^3)-H oxidation with organometallic/inner-sphere catalysts.

Extensive research has also been conducted on metalloporphyrin catalysts, inspired by the exceptional efficiency of cytochrome P450.[82-87] The first generation of catalysts was developed by *Groves* and coworkers, who reported the **Fe(TPP)Cl** (iron(III)tetraphenylporphyrin chloride) catalyst, which is capable of the hydroxylation of simple alkanes with PhIO acting as an oxidant (Scheme 10A).[88-89] For example, cyclohexane (**56**) was oxidized to cyclohexanol (**57**) in 8% yield. It should be noted that the phenyl groups in *meso*- positions are crucial features to obtain reactivity. Planar metalloporphyrins lacking substituents at these positions quickly decompose due to oxidative degradation.[90] In a second generation of catalysts, the porphyrin ligands were further derivatized to yield the more electron-deficient catalysts (e.g. **Fe(TMP)Cl**,[91] **Fe(TDCPP)Cl**,[92] **Fe(TPFPP)Cl**),[93] resulting in higher activities (up to 45% yield with **Fe(TDCPP)Cl**) (Scheme 10B). However, in all these cases an excess of starting material was needed, and the yields were usually reported with respect to the oxidant. Later, a third generation of even more electron-deficient catalysts was synthesized (e.g. **F_8TPFPP**, Scheme 10C).[94-97] Regarding the mechanism, *Groves* proposed an oxygen rebound mechanism *via* an active Fe^{V}=O species for the P450 hydroxylation.[98] The mechanism has been extensively studied ever since, both for P450 and artificial analogs.[84-86, 99-101] The current assumption is that the electronic structure of the reactive intermediate is best described as an oxo-iron(IV) porphyrin radical [Fe^{IV}(O)($Porph^{+\bullet}$)] performing a HAT followed by a hydroxyl rebound (Scheme 10D).[101] Furthermore, it was shown that the reactivity of artificial metalloporphyrin catalysts can be highly dependent on the nature of the axial ligand.[102-103] Among other things, the axial ligand can influence the O-O bond cleavage process, giving access to either [Fe^{IV}(O)($Porph^{+\bullet}$)] *via* heterolysis or [Fe^{IV}(O)(Porph)] *via* homolysis. Ligands mediating the former were much more reactive both in epoxidations as well as hydroxylations.[102]

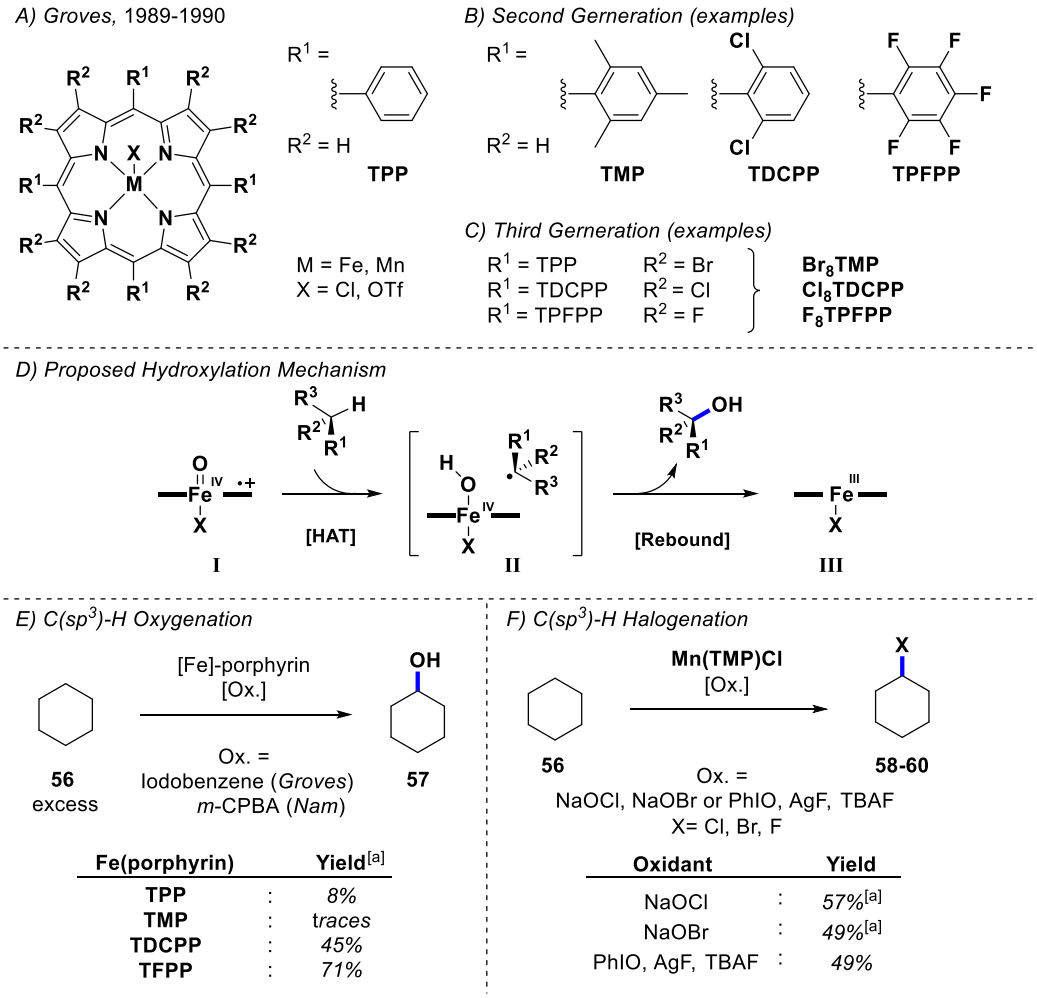

Scheme 10: Undirected C(sp^3)-H functionalization with Fe and Mn porphyrins. [a] Yield is based on oxidant.

Groves and coworkers also applied Mn porphyrin catalysts to the halogenation of aliphatic C-H bonds (Scheme 10F).[104] The formation of chlorocyclohexane (**58**) and bromocyclohexane (**59**) from cyclohexane were achieved by the use of NaOCl and NaOBr as oxidants, in 57% and 49% yield, respectively.[105] However, an excess of starting material was again used (3:1, substrate:oxidant). Impressively, even the fluorination of cyclohexane with **Mn(TMP)Cl** and a mixture of PhIO, AgF, and TBAF resulted in fluorocyclohexane (**60**) in 49% yield based on substrate.[106] These conditions were also applied in some late-stage functionalization of more complex hydrocarbon motifs with usable selectivities and yields. Furthermore, metalloporphyrins have also been utilized in C-H amination and alkylation reactions.[87]

Since the oxidations with metalloporphyrins proceed *via* an electrophilic species, the typical reactivity trend is observed (tert. > sec. > prim.). An impressive example of shape-selective reactivity was reported by *Suslick* in 1986 (Scheme 11).[107] Oxidation with the sterically demanding **Mn(TTPPP)OAc** catalyst resulted in the preferential oxidation of primary C-H bonds in the presence of more reactive methylene groups. Thus, in the oxidation of 2,2-

dimethylbutane (**61**) the selectivity for primary alcohol **64** increased from less than 1% to a remarkable 69% due to the poor steric accessibility of the other positions. For less sterically demanding *n*-alkanes, for instance, *n*-heptane (**65**), the selectivity for primary alcohol **67** still increased from 2% to 26%.

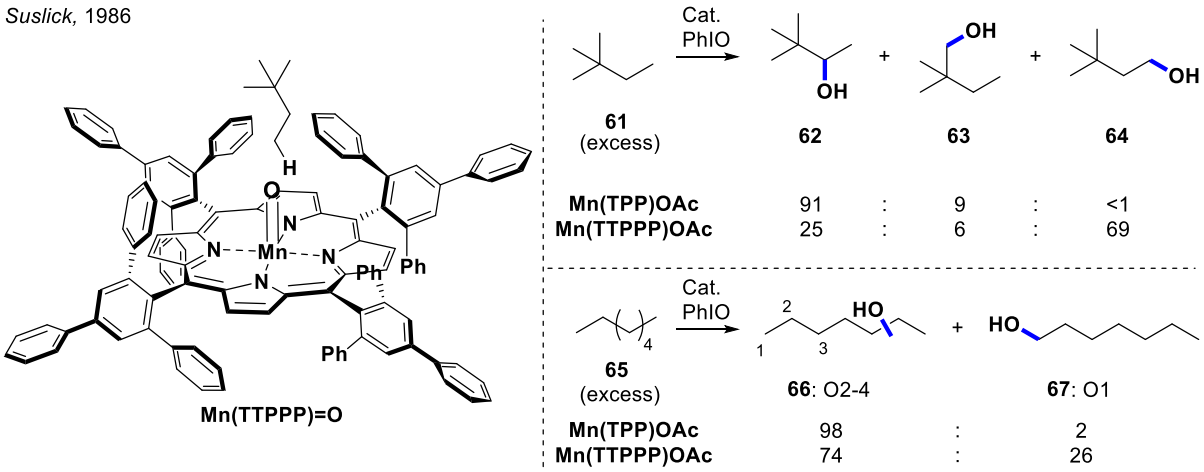

Scheme 11: Shape-selective undirected C(sp^3)-H oxygenation with **Mn(TTPPP)=O**.

Finally, enantioselective C(sp^3)-H oxidations of benzylic positions have also been reported by utilizing metalloporphyrin as well as -salen catalysts (Scheme 12).[108-110] Again, pioneering work was conducted by *Groves* and coworkers, reporting **68** as capable of enabling the asymmetric oxygenation of benzylic positions. For instance, ethylbenzene (**71**) was oxidized to (*R*)-**72** in 40% yield (based on oxidant) and 40% *ee*.[108]

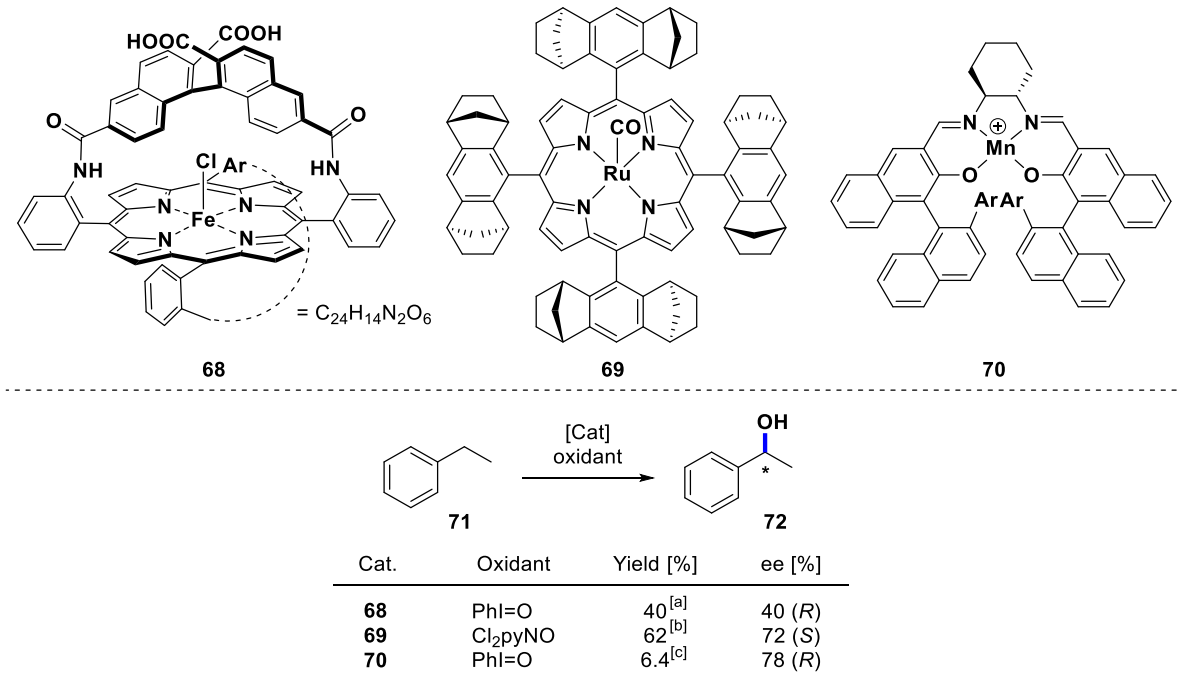

Cat.	Oxidant	Yield [%]	ee [%]
68	PhI=O	40[a]	40 (*R*)
69	Cl_2pyNO	62[b]	72 (*S*)
70	PhI=O	6.4[c]	78 (*R*)

Scheme 12: Undirected enantioselective C(sp^3)-H oxygenation with Fe and Mn porphyrins/salen. [a] Yield is based on oxidant. [b] Yield is based on the converted starting material. [c] Yield is based on staring material.

With the more recent chiral catalysts **69**[109] and **70**,[110] even higher enantioselectivities could be achieved (for ethylbenzene, 72% and 78% *ee*, respectively).

A wider scope of reagents and catalysts for aliphatic C-H bond functionalizations, apart from oxygenations, has been explored in recent years (Figure 4).[62] For example, *Alexanian* and coworkers reported the application of *N*-bromoamide **73** in the selective radical-mediated C-H bromination of stoichiometric amounts of starting material under visible light irradiation (Figure 4A).[111] Reasonably good yields (e.g. 70% of bromocyclohexane (**59**)) were achieved, with no formation of dibromo products (due to deactivation by the newly installed bromide). Furthermore, **73** selectively brominates secondary C(sp^3)-H bonds in the presence of tertiary ones, due to the bulky *tert*-butyl residue. Two years later, the same group reported the chloro-derivative **74**. A notable example of its application is in the selective oxidation of (+)-sclareolide to **75** in 82% yield.[112] Furthermore, a few undirected versions of nitrenoid and carbenoid insertions using rhodium catalysts were established. *Du Bois* and coworkers reported the selective intermolecular C-H amination of tertiary bonds with a dirhodium catalyst, **DfsNH2**, an oxidant, and an acid additive (Figure 4B).[113] Thereby, they selectively aminated the less sterically hindered tertiary position of a menthol derivative to give **76** in 68% isolated yield. In contrast, *Hartwig* and coworkers reported a method for C(sp^3)-H amination utilizing a radical-promoted azidation reaction, which showed a preference for the most electron-rich C-H bonds (benzylic, tertiary) (Figure 4C).[114] Steric factors seemed to play a minor role, as the alternative selectivity in the amination of menthol acetate to **78** was observed in 35% yield (*Note*: for other substrates yields up to 75% were achieved). Undirected carbenoid insertion reaction into C(sp^3)-H bonds has also experienced great interest and progress in the last decades (Figure 4D).[54, 115]

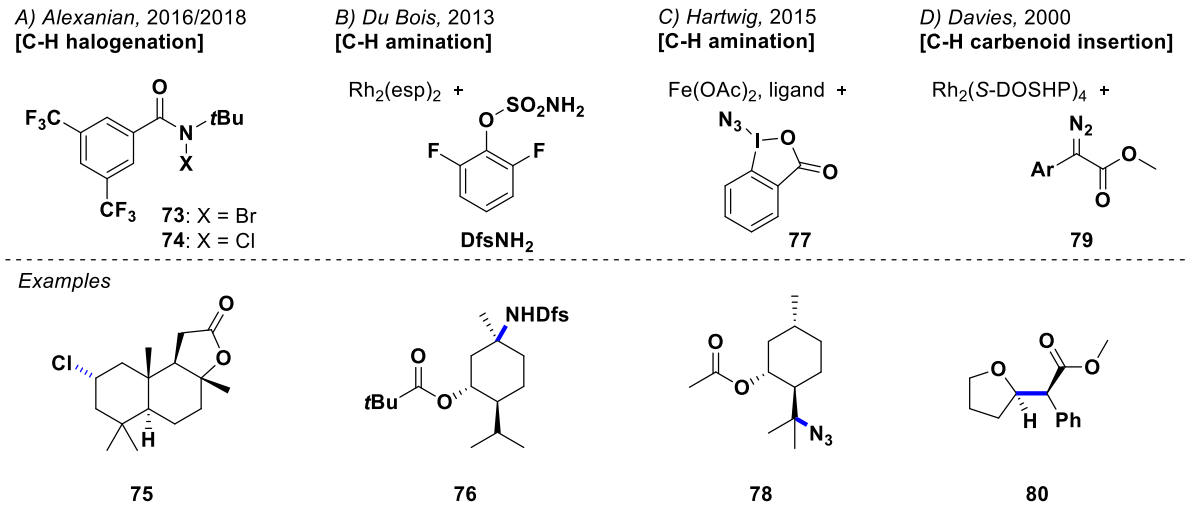

Figure 4: Examples of undirected C(sp^3)-H oxidations other than C-H oxygenations.

In particular, the functionalization of activated positions, such as allylic or benzylic positions and those adjacent to heteroatoms were explored, and asymmetric C-H functionalization methods were established. An example of the latter is the functionalization of tetrahydrofuran, by applying a chiral dirhodium catalyst together with **79** at -50 °C to afford **80** in 67% combined yield of the two diastereomers (d.r. = 2.8) in 97% *ee* for the major diastereomer.[116]

Finally, non-heme Fe and Mn catalysts shall be discussed in more depth. Again, nature acted as a major role model with very active oxidase enzymes (e.g. α-ketoglutarate dependent hydroxylases,[117] methane monooxygenase),[118-120] suggesting the potential of artificial non-heme catalysts.[121] Mononuclear non-heme Fe oxygenases are a very versatile class of enzymes, in which the active center often consists of an Fe^{II} surrounded by two histidines, a carboxylate, and three labile ligands (e.g. water).[121-123] One of the earliest artificial non-heme Fe complexes capable of mimicking the reactivity of such enzymes was **Fe(tpa)** (**tpa** = tris(2-pyridylmethyl)amine).[124-126] This catalyst only approximately represents the active binding site of non-heme oxygenases, with one aliphatic amine and three pyridine donors. Impressively, this catalyst and its relatives are nevertheless capable of performing most reactions mediated by non-heme Fe oxygenases, including C(sp^3)-H oxidations.[127-129] Since this discovery, a range of different tetraazadentate ligands have been synthesized with different amine/pyridine (or similar N-heterocycles) ratios from N_4 to Py_4.[124, 130-133] Here, the focus will be set on the N_2Py_2 versions, which emerged as the most effective derivatives (Figure 5).[16, 134] In particular, the well-explored, chiral *N*,*N*'-bis(2-pyridylmethyl)-2,2'-bipyrrolidine (**pdp**)[135-136] and *N*1,*N*2-dimethyl-*N*1,*N*2-bis(pyridin-2-ylmethyl)cyclohexane-1,2-diamine (**mcp**)[137-138] -based catalysts are presented. Besides several other backbones,[139-141] different modifications of the pyridine were explored, which enable the tuning of the electronic and steric properties of the final catalysts.[134] For instance, electron-donating groups have been attached at R^4 to manipulate the electronic properties of the pyridine (e.g. NMe_2[142], OMe[143]) without having a large steric impact on the reaction outcome. In epoxidation reactions, this strongly influences the reactivity, but displays only a minor impact on C(sp^3)-H oxidations.[134] Another important modification is the introduction of bulky groups at R^3 (e.g., TIPS,[144] $C_5H_3(CF_3)_2$),[145] which gives access to preferential oxidation of secondary over tertiary C-H bonds. Furthermore, it should be noted that the two labile sites (**X**) in the *cis* positions of the catalyst are crucial for reactivity in general.[133-134] They act as the binding site for the oxidant (often environmentally friendly H_2O_2 can be used) and an additive (water or carboxylic acid, with the latter usually being more effective). Regarding the topology of the N_2Py_2 ligand, two different types of *cis*-labile coordination complexes can be formed.[146] In the first case, the two pyridine groups are

trans to each other (*cis*-α, depicted in Figure 5), and in the second case, they are *cis* to each other (*cis*-β, not shown). The former is by far more active and therefore the topology referred to in all the following work.

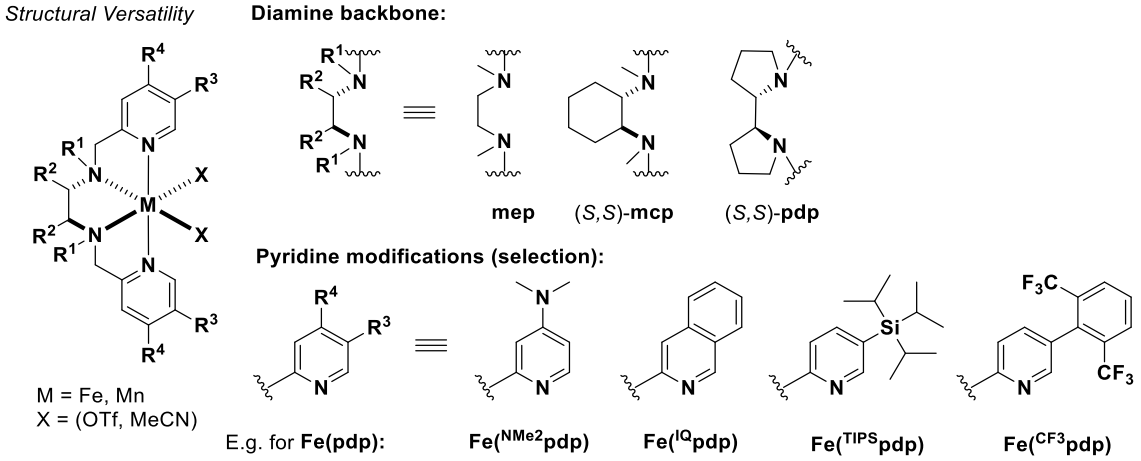

Figure 5: Undirected C(sp^3)-H oxygenation with non-heme Fe and Mn catalysts.

The proposed mechanistic cycle for the carboxylic acid-assisted pathway is depicted schematically in Scheme 13B.[127, 147-149] The cycle begins with the oxidation of the M^{II} precatalyst to form the M^{III} complex **I**. By coordination of H_2O_2, intermediate **II** is formed, which subsequently undergoes heterolytic O-O bond cleavage to form a high-valent M^{V}=O carboxylate species **III**. This highly reactive M^{V}=O species then reacts in a HAT step to form a short-lived carbon-centered radical and **IV**. The carbon-centered radical is quickly trapped *via* hydroxyl rebound under retention of the configuration.

Although **Fe(tpa)** was reported as early as the 1990s,[124-125] the synthetic potential of these non-heme Fe and Mn complexes in C(sp^3)-H oxidation was particularly highlighted in 2007 by *White* and *Chen*.[135] For the first time, preparatively useful conversions and yields with this catalyst class could be observed in C(sp^3)-H oxidations. This was enabled by using the more rigid and stronger σ-donating amine backbone **pdp** instead of **mep** and by utilizing AcOH as an additive. Furthermore, the electrophilic nature of the catalysts and their sensitivity to the electronic and steric differences of C(sp^3)-H bonds were highlighted.[135] For example, this was illustrated in the oxidation of 2,6-dimethylheptyl acetate to **81** in 49% yield and with very good selectivities for the more electron-rich tertiary C-H bond distal from the EWG (Scheme 13C). Another example is the previously discussed oxidation of menthol acetate to **82**. Although two tertiary C(sp^3)-H bonds equidistant from the EWG are present, good selectivity for product **82** was observed, presumably due to better accessibility. **Fe(pdp)** was also applied to the oxidation of spiro[2.5]octane to **51**.[136] Analogous to TFDO, preferential oxidation of the methylene

groups adjacent to the cyclopropane was observed due to hyperconjugation, however, the effect was less pronounced (84% selectivity with **Fe(pdp)**[136] vs 90% with TFDO).[75] This may be due to the steric and electronic sensitivity of **Fe(pdp),** whereas the reactivity of less steric TFDO is mostly dependent on the electronic properties.[16]

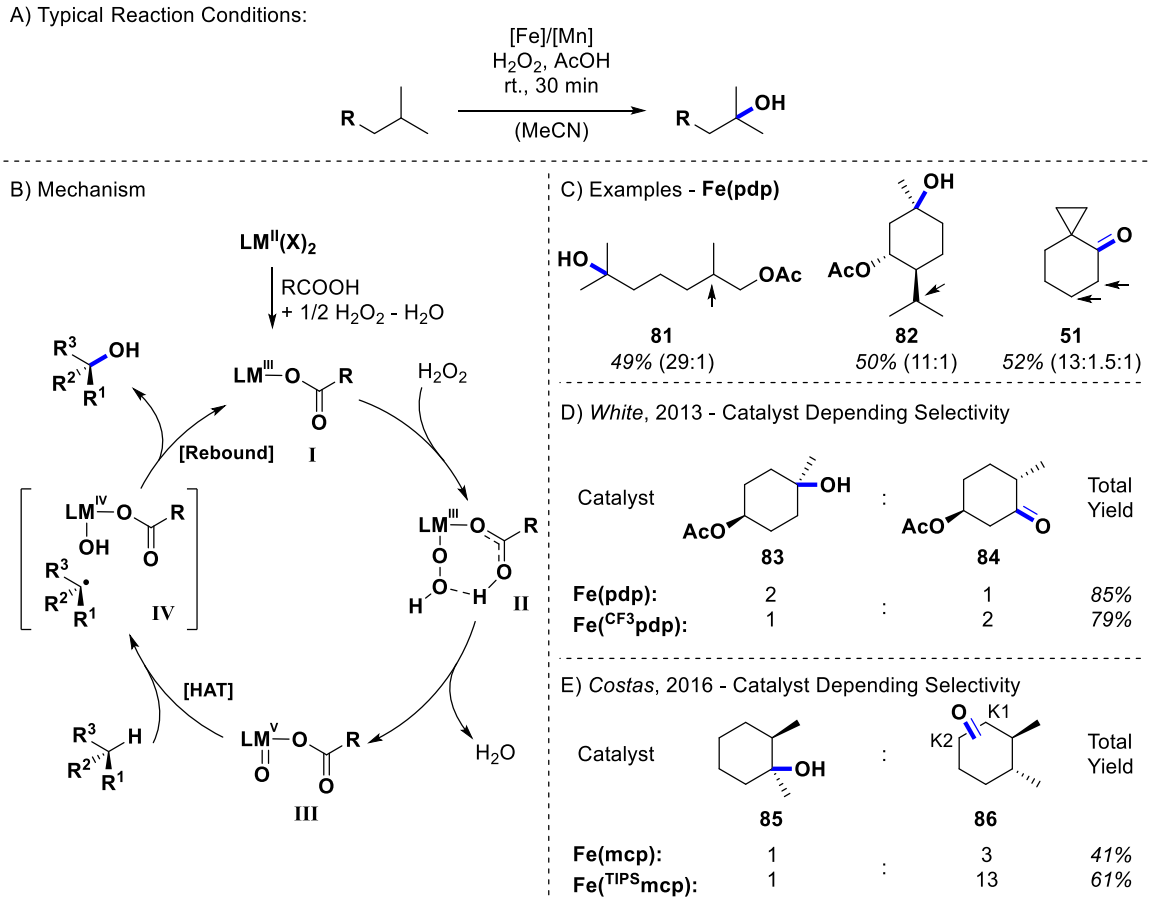

Scheme 13: Mechanism and examples of undirected C(sp^3)-H oxygenations with non-heme Fe and Mn catalysts.

As previously mentioned, the N_2Py_2-type catalysts can be easily modified to be more sterically demanding by introducing bulky substituents on the pyridines. Two examples are depicted in Scheme 13D and E. With **Fe(pdp)**, the preferential oxidation of *trans*-4-methylcyclohexyl acetate to the tertiary alcohol **83** is observed.[145] However, with the sterically demanding **Fe(CF3pdp)**, the selectivity is inverted to give **84** as the major product (in 2:1 vs 1:2 ratio, respectively). A similar trend was observed in the oxidation of *trans*-1,2-dimethylcyclohexane.[144] With both catalysts, **Fe(mcp)** and **Fe(TIPSmcp)**, alcohol **85** is the minor product compared to the possible ketone products K1 and K2. However, the ratio of **85**:**86** is significantly increased from 1:3 for **Fe(mcp)** to 1:13 for **Fe(TIPSmcp)** due to the bulky TIPS groups.

Furthermore, it has been shown that the selectivity in C(sp^3)-H oxidations following HAT mechanisms can be influenced by applying polyfluorinated H-bond donor solvents like trifluoroethanol (TFE) and hexafluoroisopropanol (HFIP).[150-153] As discussed before, methylene oxidation reactions with an electrophilic catalyst like **Fe(pdp)** in MeCN usually result in overoxidized ketone products. This can be explained by the activation of the α C-H bonds of the intermediate alcohols towards HAT due to stereoelectronic effects (Scheme 14A). In contrast, solvents like TFE and HFIP, which act as H-bond donors, deactivate the α C-H bonds of the intermediate alcohols (=H-bond acceptors) towards HAT by decreasing the electron density of the α C-H bond. This effect is also observed in the case of other electron-donating groups such as amines,[154] amides,[155] and ethers.[156] Two examples of this changed selectivity are depicted in Scheme 14B.[153]

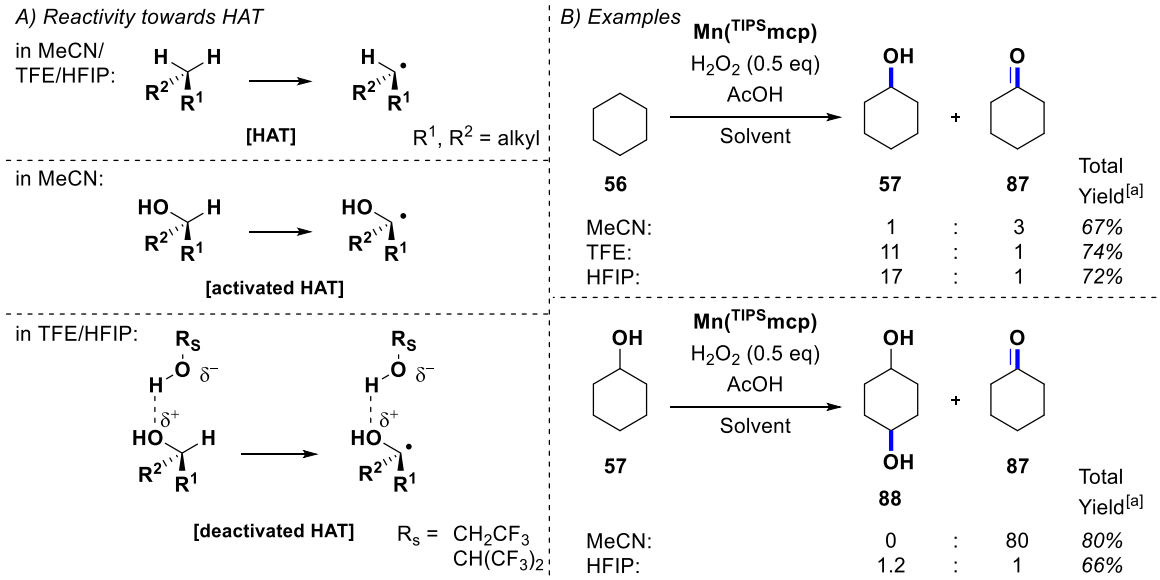

Scheme 14: Solvent-dependent reactivity and selectivity of HATs. [a] Total yield refers to the combined yield of both products based on oxidant.

The oxidation of cyclohexane with **Mn(TIPSmcp)**, H_2O_2, and AcOH in MeCN affords cyclohexanone (**87**) as the major product (74% selectivity, 50% yield based on H_2O_2).[153] In contrast, the same reaction in TFE or HFIP affords cyclohexanol (**86**) as the major product in 68% yield, with 96% and 94% selectivity, respectively. Starting from cyclohexanol as substrate, the corresponding ketone **87** was exclusively observed in 80% yield in MeCN. However, in HFIP, the corresponding ketone and 1,4-cyclohexanol (**88**, 1:1, *cis*:*trans*-mixture) were obtained in a 1:1.2 ratio.

Finally, some cases of undirected, enantioselective oxidations using these non-heme catalysts shall also be discussed. Analogously to the heme and salen catalysts discussed before, most examples reported so far are oxidations of activated benzylic positions (Scheme 15). *Bryliakov*

and coworkers, for instance, published the enantioselective oxidation of ethylbenzene (**71**) with **Mn(**$^{CH3,\ OCH2CH3}$**pdp)** and various acid additives (Scheme 15A).[157-158] With 2-ethylhexanoic acid (2-eha) as an additive and ***R,R*-Mn** catalyst, alcohol (*R*)-**72** was observed in 15% and 34% *ee* (with respect to H_2O_2). The reactions were performed in MeCN, therefore H_2O_2 had to be used as the limiting factor in order to decrease the amount of overoxidized ketone **89** (24% yield). With (tert-butoxycarbonyl)-*L*-proline (Boc-*L*-Pro) as the acid, the enantiomeric excess of (*R*)-**72** could be further increased to 76% *ee* in 10% yield (and 12% ketone **89**). In the same year, *Company*, *Bietti*, *Costas*, and coworkers reported comparable reactions, however, with TFE as solvent (Scheme 15B).[153] By virtue of this, a lower excess of starting material was needed and the alcohol:ketone ratio improved considerably. However, H_2O_2 was still used as the limiting factor. More precisely, oxidation of propylbenzene (**90**) afforded alcohol **91** in 25% yield and 66% *ee* with **Mn(**^{dMM}**pdp)** and **2-eha** as the acid. Only 2% of ketone product **92** was formed. With **Mn(**^{NMe2}**pdp)**, alcohol **91** was obtained in higher yields (44%) albeit with slightly worse enantioselectivity (60% *ee*).

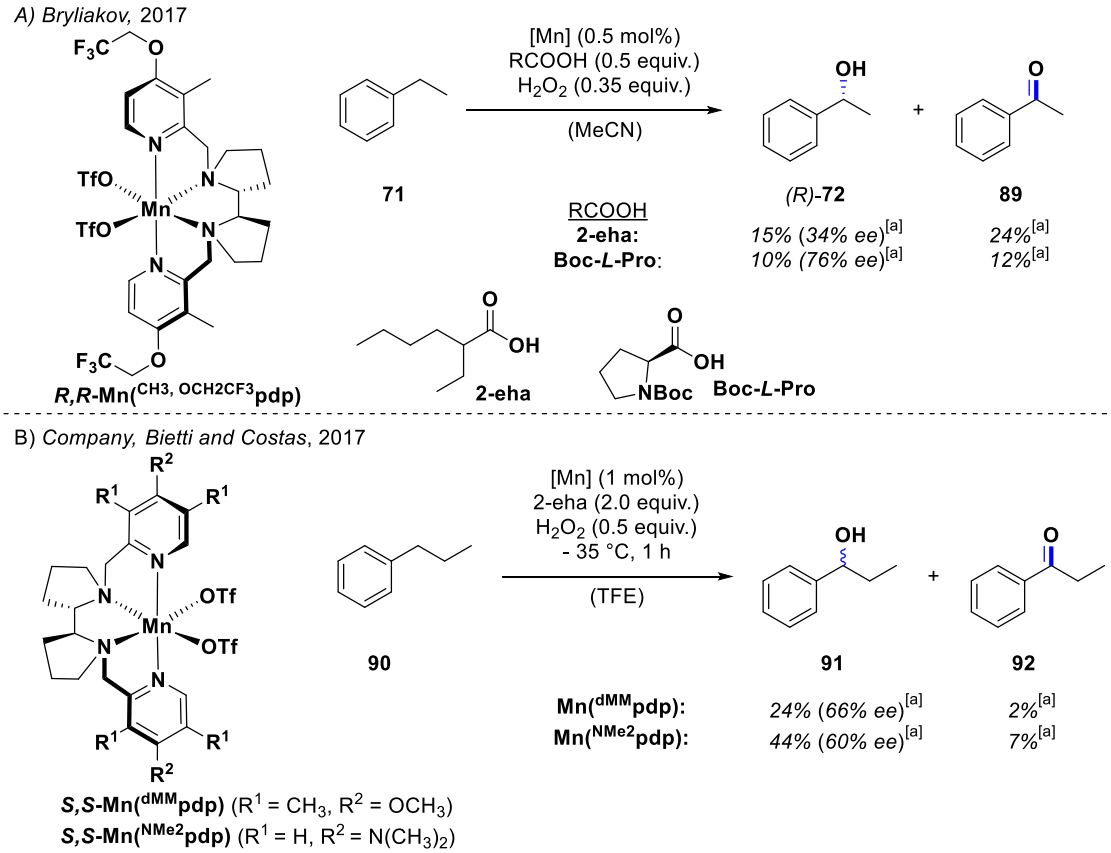

Scheme 15: Undirected enantioselective C(sp^3)-H oxygenation of benzylic positions with non-heme Mn catalysts. [a] Yield is based on hydrogen peroxide.

In the same year, *Bietti*, *Costas*, and coworkers also reported the first example of undirected, enantioselective oxidation of unactivated methylene positions using an artificial non-heme

catalyst (Scheme 16).[159] By exploring the oxidation of several monosubstituted cyclohexanes, they found that particularly good results were obtained with cyclohexane substrates possessing bulky amide groups. For example, amide **93** gave ketone **94** in 90% yield and 76% *ee* with acetic acid as the additive. Only 1% of the K4 oxidation product was formed. Screening of different acids showed that with cyclopropanecarboxylic acid the enantioselectivity could be further improved to a remarkable 94% *ee* in 84% yield. The observed excellent regioselectivity can be explained by several previously established reactivity observations. First, the primary and axial tertiary C-H bonds are not very reactive towards HAT. The former can be attributed to the high BDE,[7] and the latter to sterics and an increase in torsional strain in the HAT transition state (due to planarization effects of the C-centered radical, which forces the *t*-Bu residue into disadvantageous eclipsed interactions).[160] The observed C3/C4 selectivity depends mostly on the electronic effect of the substituent (electron donating groups (EDGs) favor C3, EWGs C4 oxidation),[161] however, other factors may play a role as well.[159] For instance, the oxidation of cyclohexanes with EWGs such as cyclohexyl methyl ketone (**95**) increased the amount of K4 oxidation product significantly (19% yield). However, the K3 oxidation product **96** remained the major product (47% yield). Furthermore, the enantioselectivity for K3 decreased to 8% *ee*. The excellent results for **94** indicate strong interactions between the substrate and the Mn catalyst. Consequently, both the bulkiness of the amide group as well as the Lewis basic character can be said to play a crucial role.[159]

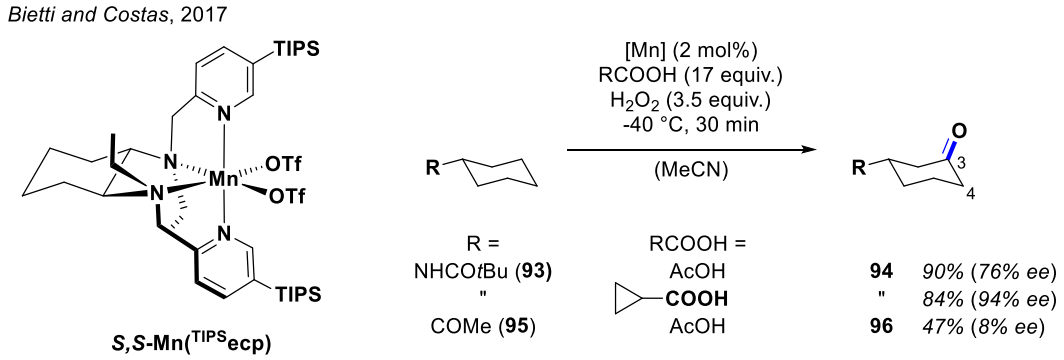

Scheme 16: Undirected enantioselective C(sp^3)-H oxygenation of unactivated positions with a non-heme Mn catalyst.

In summary, impressive progress has been achieved in the field of undirected C(sp^3)-H oxidations throughout the years. This even enables differentiation between C-H bonds of the same degree of substitution, if they possess large enough electronic, steric, or stereoelectronic differences. However, the reaction of intrinsically deactivated positions in the presence of more reactive ones (if both are accessible) remains beyond reach with this strategy.

1.4 Supramolecular C(sp^3)-H Oxidation

In contrast to the two previous strategies, supramolecular chemistry could enable the selective functionalization of any C-H bond that is accessible to the active site - even if it is intrinsically deactivated and/or remote from functional groups in the substrate.[11-12] To accomplish this, substrate recognition is necessary, which is usually achieved by multiple non-covalent interactions.[162-163] Furthermore, the size and shape of the cavity/binding site of the host should be approximately complementary to the guest. For catalysis, weak interactions such as hydrogen bonding,[164-165] different kinds of π–interactions[166-168] as well as dispersion forces.[169] between catalyst and substrate can be advantageous over stronger bonding interactions (such as ligand-to-metal bonding[170-171] or dynamic covalent chemistry),[172-173] since they have more often been reported to entail better turnover numbers.[174] More generally, the binding rate of the substrate and catalyst should exceed or at least match the oxidation rate to prevent product inhibition and low turnover. Naturally, substrate binding should also be stronger than product binding. Regarding the host structure/receptor, several different supramolecular structures have been established and reported over the last decades. This includes, for example, a variety of different macrocycles, like cyclodextrins (CDs),[175-178] crown ethers (CRs),[13] cucurbit[*n*]urils (CB[*n*]),[179] cyclophanes,[180-181] and cryptophanes.[182] Besides macrocycles, also self-assembled supramolecular capsules[183-185] and noncyclic molecular clips and tweezers[186-187] have been reported.

In the following, examples of recognition-driven, aliphatic C(sp^3)-H oxidation are presented. There are also many supramolecular catalysts for selective aromatic (e.g. borylations)[188-191] and olefinic (e.g. hydroformylation,[192-193] epoxidation,[194-196] oxidative cleavage)[197] functionalizations,[198] however, they are not discussed in more detail in this manuscript. In the last part, a very brief introduction to the supramolecular structures of interest for this thesis is given.

1.4.1 Binding *via* Lipophilic Interactions and the Hydrophobic Effect

Regarding the concept of undertaking a supramolecular approach towards selective C-H functionalization, one can differentiate between two strategies.[174] In a usually simpler strategy, the supramolecular host molecule and the active catalysts are not linked. An example of such a system was reported by *Wong* and coworkers, who conducted oxidation of aliphatic esters with in-situ formed dioxirane in the presence of β-cyclodextrins (**β-CD**s) (Scheme 17).[199] Without **β-CD**, the oxidation of **97** with TFDO resulted in a 1:7 mixture of the two tertiary oxidation products **98** and **99**. (As before, the terminal tertiary C-H bond is favored due to the electron-

withdrawing effect of the ester group.) When **β-CD** was added, the reaction selectivity was enhanced to a 1:20 ratio in water, however, it stayed the same in a water/MeCN solvent mixture. This can be explained by the binding properties of the substrate in **CD**. The well-studied cyclodextrins are water-soluble due to their hydrophilic surface, additionally, they possess a hydrophobic cavity that can bind apolar guests.[175] The main reason for substrate binding is therefore the hydrophobic effect,[200-201] which usually diminishes quickly in solvent mixtures containing organic solvents. In addition, **α**- and **γ-CD**s were tested in the oxidation of **97**. Both resulted in no selectivity enhancement, showing the size sensitivity of host-guest binding.

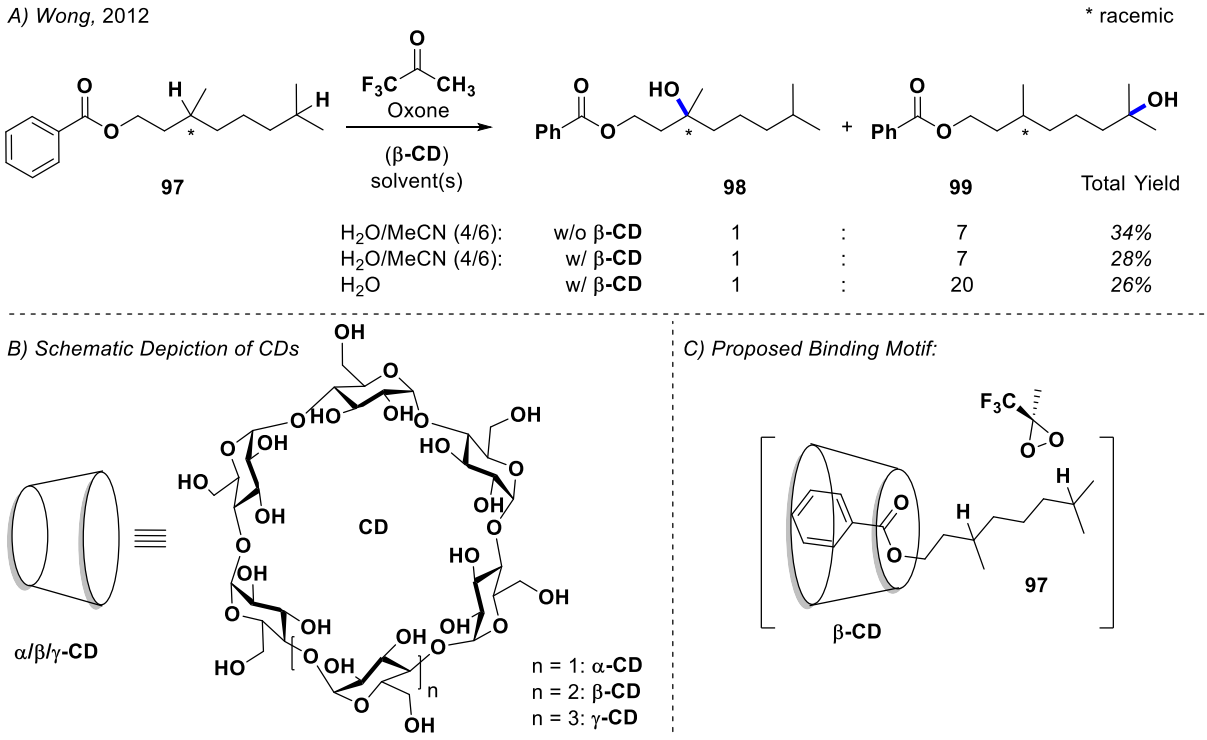

Scheme 17: Supramolecular C(sp^3)-H oxygenation *via* host:guest adducts and discrete TFDO.

Other than **97,** other ester groups were also studied, however, the effect was less distinct. Lower selectivity enhancement was observed with simple alkyl groups (Me, *t*Bu) due to weaker binding, and with larger aromatic systems (*p*-(*t*Bu)Ph) due to the less efficient steric shielding of the proximal tertiary C-H bond after binding. Furthermore, it was necessary to use stoichiometric amounts of **β-CD** to exclude background reactions with unbound starting material and TFDO.

To us, the second strategy, in which the supramolecular moiety and the active center are linked, is of greater interest. Although such systems are consequently more challenging to synthesize, they also resemble enzymes to a greater extent.[174] One example of shape-selective C-H oxidation using a functionalized Mn porphyrin catalyst was reported by *Groves* and coworkers

in 1988 (Scheme 18, *note:* stereoconfiguration of cholesterol was corrected)[16, 202] By attaching four steroid units to the catalyst they formed **Mn(ChP)Cl**. The catalyst was then positioned in a synthetic bilayer to achieve a highly ordered receptor, with the alcohol groups of the four steroids pointing towards the polar groups of the bilayer (presumably also preventing intramolecular oxidation of the catalyst). That way, a membrane-spanning Mn porphyrin catalyst was obtained possesing a hydrophobic pocket capable of binding apolar substrates in water. This catalyst was applied in the hydroxylation of simple alkanes as well as to the oxidation of cholesterol (**100**). Impressively, the C25 oxidation product **101** was formed exclusively without any attack of the more reactive double bond. This presice selectivity can be explained by the very specific conformation of the bound substrate, due to the bilayer. However, the catalyst suffers from product inhibition and achieves less than one turnover (TON = 0.8), due to the strong binding of the product.

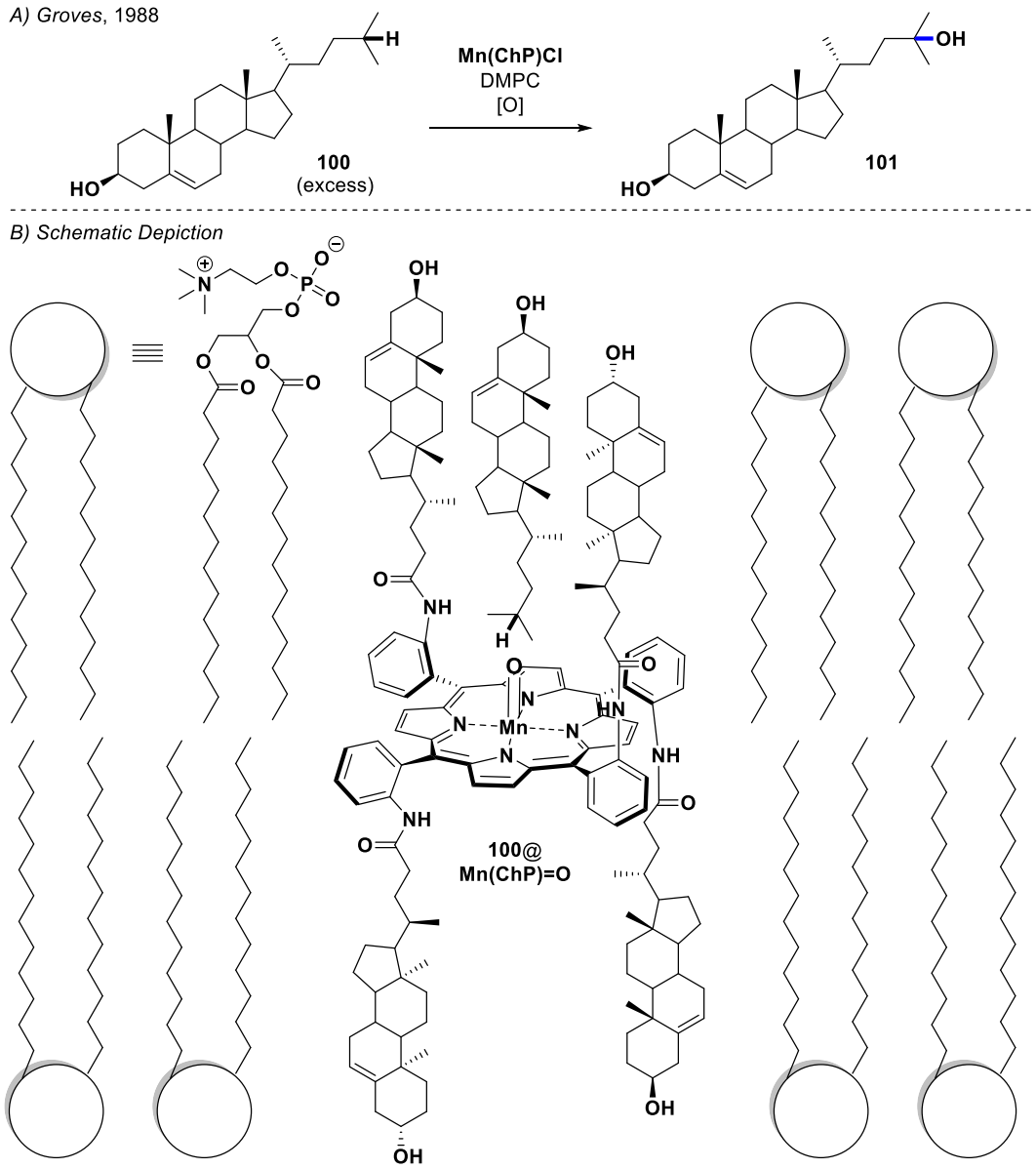

Scheme 18: Supramolecular C(sp^3)-H oxygenation *via* lipophilic Interactions.

Nevertheless, it is an inspiring early example of how lipophilic interaction can be used to achieve good molecular recognition and precise orientation in a hydrophobic pocket, enabling site-selectivity in unactivated C(sp^3)-H bond oxidation.

Extensive work in the field has also been carried out by *Breslow* and coworkers.[178, 203] They studied the use of cyclodextrins as supramolecular receptors and applied them to selective C(sp^3)-H oxidation reactions by merging an Mn porphyrin catalyst with different numbers of β-cyclodextrins (for three illustrative examples, see Scheme 19A). Firstly, they studied the oxidation of a dihydrostilbene derivative possessing two *tert*-butylphenyl residues (Scheme 19B/C).[204-205] In water, these groups bind to two opposite cyclodextrins of e.g **Mn(^{CD4}Porph)Cl** due to the hydrophobic effect. This gives access to oxidation product **102** with very high catalytic activity (up to 650 turnovers). Iodosobenzene was used as an oxidant,

since neither the more environmentally friendly H_2O_2 nor NaOCl were sufficient for the reaction. When a substrate analog lacking the two *tert*-butylphenyl groups was used, no formation of the analogous product was observed. Furthermore, only catalysts with at least two *trans*-**CDs** moieties gave good selectivities. Catalysts with only one **CD**, or two **CDs** *cis* to each other were not sufficient to achieve precise binding and orientation of the substrate. *Breslow* and coworkers also applied the catalysts to the oxidation of an androstanediol derivative.[204-205] Again, *tert*-butylphenyl moieties were installed for binding, and additionally, two sulfonate residues were introduced to achieve water-solubility. Impressively, oxidation with **Mn(CD4Porph)Cl** resulted in the selective hydroxylation of carbon C6 to give compound **103** in 40% conversion and yield. However, the catalyst activity was much lower than before, with only up to 4 turnovers. This was attributed to the sensitivity of the **Mn(CD4Porph)Cl** towards oxidation, and could be improved by using more electron-deficient aromatic groups on the porphyrins, such as the polyfluorinated catalyst **Mn(F-CD4Porph)Cl**.[206] With this catalyst, the turnover number could be increased distinctly to 96 TONs, achieving a remarkable 95% yield with 1 mol% catalyst.

If unfunctionalized androstanediol was used instead, no oxidation was observed at all (presumably due to the insolubility of the steroid in water). Compound **103** was subsequently functionalized with another binding/solubility group installed at the newly formed alcohol at C6.[207] Models indicated, that for binding of all three *tert*-butylphenyl groups to the CDs of **Mn(F - CD4Porph)Cl**, the substrate had to face the Mn porphyrin in a 180° rotated manner. That way, a new position was exposed to the active center. And indeed, the selective oxidation of the C9 position could be achieved to give **104** in 72% yield with 1 mol% catalyst. Unfortunately, the substrate scope remains limited and additional steps are necessary for the introduction and removal of the ester groups. Nevertheless, *Breslow's* catalysts and their selectivities remain exceptional examples of how supramolecular control can be applied to achieve selective C-H bond oxidation with single hydroxylation products.

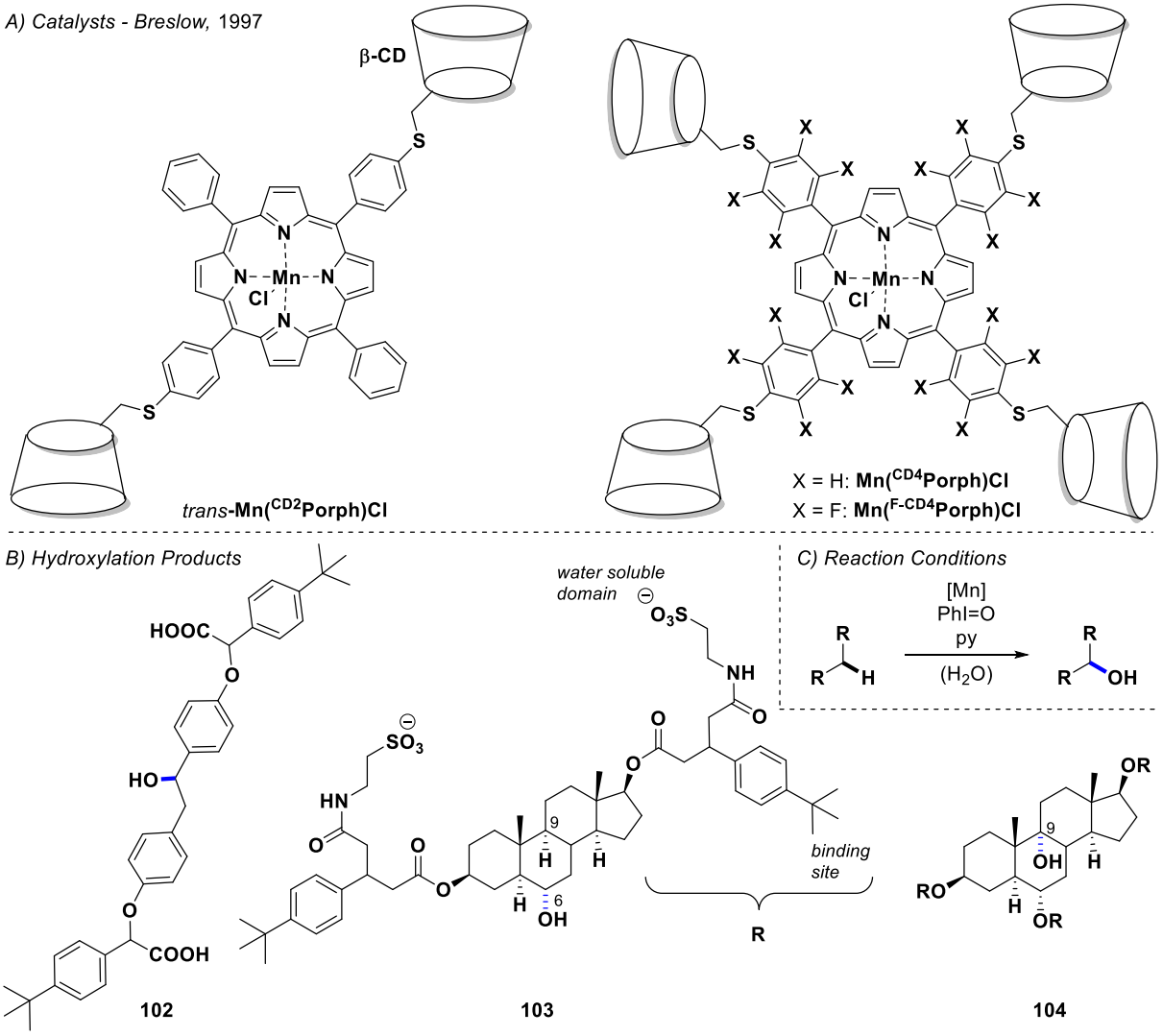

Scheme 19: Supramolecular C(sp^3)-H oxygenation *via* the hydrophobic effect.

1.4.2 Binding due to Metal Coordination

Breslow and coworkers have also investigated ligand-to-metal coordination catalysts for C-H oxidations. As early as 1989, they reported salen- and porphyrin-based Mn catalysts decorated with metal coordinating groups (e.g. bipyridine).[208] In this way, substrates possessing coordination ligands were preferentially epoxidized in the presence of substrates lacking such ligands. Cu^{2+} was used as the metal for coordination between the substrate and catalyst, enabling the fast exchange of the ligands and preventing product inhibition. Then, two years later, they reported the **Mn(($^{(bipy)4}$Porph)Cl** catalyst and its application to C(sp^3)-H oxygenation (Scheme 20A).[209] For instance, two different androsterone bipyridine derivates were investigated (Scheme 20B/C). When the bipyridine was attached to the C17-alcohol, oxidation products **105** at C15 (17%, ketone:alcohol = 1.0:1.4) were mainly observed alongside minor amounts of C16 alcohol (3%). In contrast, when substrates lacking the bipyridine motif were

used, C5 and C6 oxidation products were predominantly obtained. Despite the relatively good selectivity for C15 oxidation, the catalyst suffered from low activity (TON = 0.4). This was ascribed to several factors, including: pyridine oxidation; the possibility of trans configuration around the Cu^{2+} such that steroid and catalysts point in opposite directions; and the possible formation of substrate-substrate and porphyrin-porphyrin coordination species. In the second substrate, the binding site was attached at C3 leading to C6α alcohol **106** as the only product, however with only 3% conversion. Under more forcing conditions, (60 equiv. PhIO) the conversion could be increased to 41% (TON = 2) resulting in **106** as a C6α alcohol/ketone (1.0:1.7) mixture.

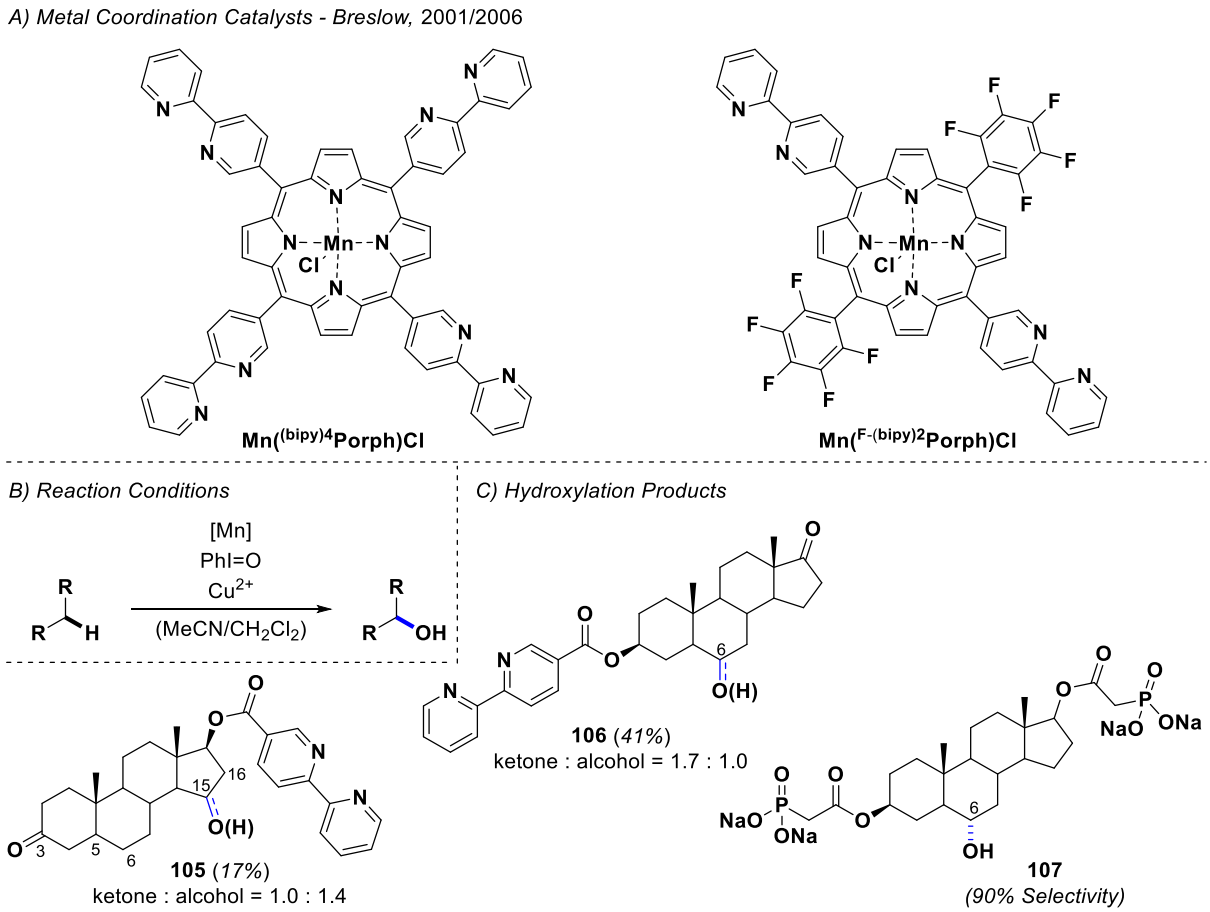

Scheme 20: Supramolecular C(sp^3)-H oxygenation *via* ligand-to-metal coordination.

In 2006, they issued a follow-up report, utilizing phosphonates as coordination groups on the substrates instead of bipyridine to avoid undesired pyridine oxidation.[210] With **Mn((bipy)4Porph)Cl**, the C6 oxidation product was observed in a mixture including 5 side products and with only 10 turnovers. By using the perfluorinated version **Mn(F-(bipy)2Porph)Cl** instead, alcohol **107** was observed in 90% selectivity with an improved 32 turnovers.

1.4.3 Binding due to Hydrogen Bonding

In recent years, several catalysts have been reported that enable selective C(sp^3)-H oxidation *via* hydrogen bonding between substrate and catalyst.[174, 198, 211-212] One of the first examples was developed by *Crabtree* and *Brudvig*, who reported a di-μ-oxo dimanganese catalyst (**Mn_2(Terpy-COOH)**) featuring two ligands based on terpyridine and a Kemp's triacid motif.[211, 213-214] This motif possesses a U-shape and terminates with a -COOH group oriented towards the active catalytic Mn center, and enables molecular recognition of carboxylic acid-containing substrates (Scheme 21A). For instance, 1 mol% of **Mn_2(Terpy-COOH)** catalyzed the oxidation of ibuprofen (**108**) with TBAO to give **109** with 98% selectivity and 50% conversion (Scheme 21B).[213] Only very little formation of **110** was observed. In contrast, if **Mn_2(Terpy)** (a catalyst lacking the COOH recognition groups) was used, both **109** and **110** were formed (with 75% selectivity for **109**). The reaction could be further improved regarding yield and catalyst turnover (71%, 710 TONs) by switching to CD_3CN as the solvent and using only 0.1 mol% **Mn_2(Terpy-COOH)**. That way, only a slightly lower selectivity (97%) for **109** was observed. In addition to ibuprofen, the oxidation of a mixture of *cis*/*trans*-2-(4-methylcyclohexyl) acetic acid (**111**) was also investigated. Both catalysts (**Mn_2(Terpy)** and **Mn_2(Terpy-COOH)**) gave lower conversions in the oxidation of *cis*/*trans*-**111** in contrast to ibuprofen, probably due to the lower reactivity of the C-H bonds (tert./sec. vs benzylic). However, very impressive regioselectivity was observed in the oxidation with **Mn_2(Terpy-COOH),** which oxidizes almost exclusively *trans*- and *cis*-**111** to *trans*-**112** (>99% selectivity). This was explained by a 180° rotation of the *cis*-**111** derived C-centered radical intermediate to reduce steric hindrance prior to hydroxyl rebound. With (**Mn_2(Terpy)** a mixture of *trans*-**112**, *cis*-**112,** and other products was formed (1:1:1.3).

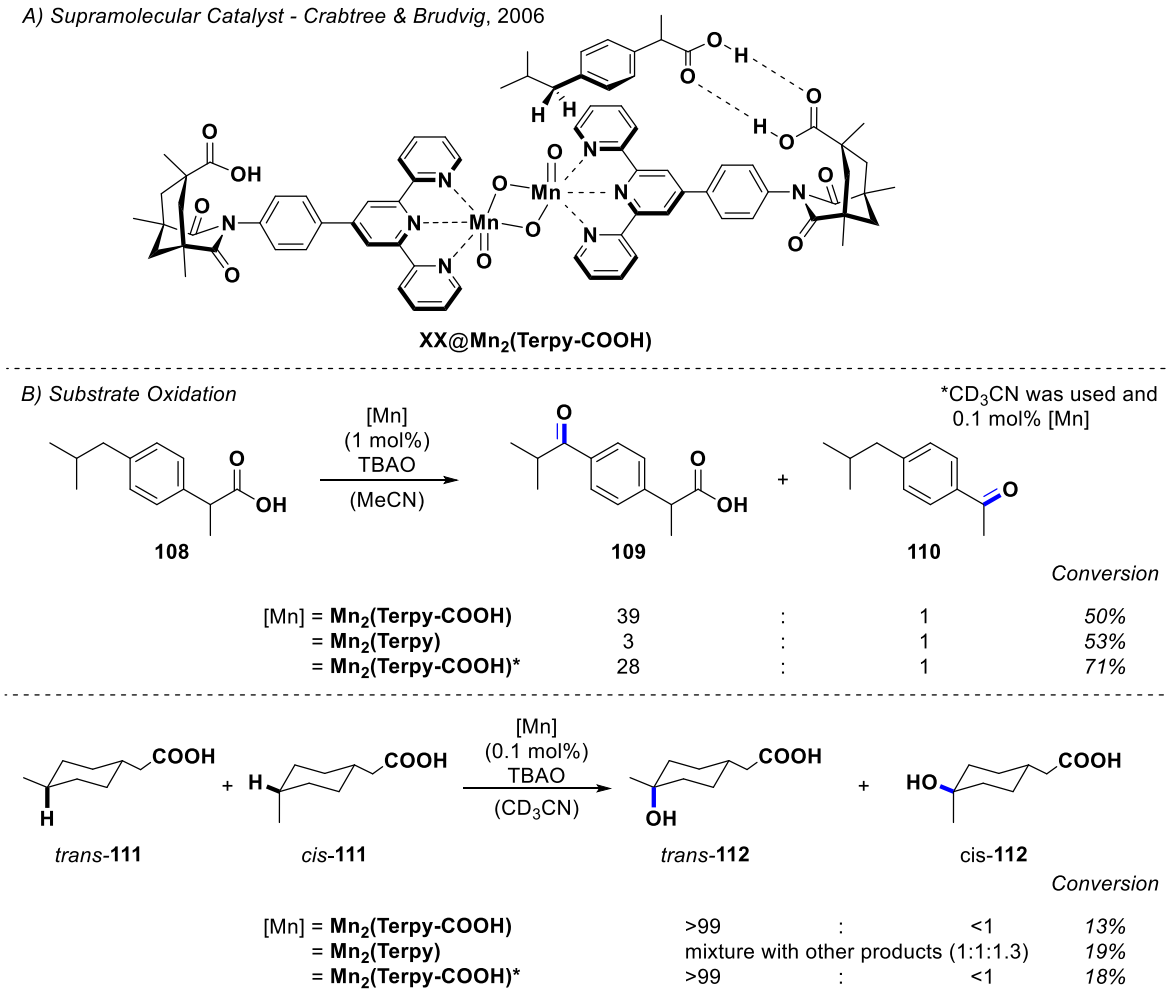

Scheme 21: Supramolecular C(sp^3)-H oxygenation *via* hydrogen bonding by *Crabtree, Brudvig,* and coworkers.

Impressive examples of enantioselective C(sp^3)-H oxidation reactions were reported by *Bach* and coworkers by using a similar approach.[212, 215-217] They synthesized different catalysts possessing a U-turning chiral lactam moiety capable of recognizing primary amides *via* hydrogen bonding (**(Lactam)M(Porph)**, **(Lactam)Ag(phen$_2$)** Scheme 22A). In their initial publication, they applied the Ru porphyrin version to the enantioselective, benzylic oxygenation of spirocyclic oxindoles (with nine examples, up to 94% *ee*).[215] In the case of model substrate **113**, oxidation with **(Lactam)Ru(Porph)** and 2,6-dichloropyridine-*N*-oxide gave product **115** in 90% *ee* in 20% yield (Scheme 22B). The low yield was attributed to unconverted alcohol intermediates. Through subsequent oxidation of the crude material under Swern or PCC oxidation conditions, the yield could be increased to 70% leading to only slightly worse enantiomeric ratios (80% *ee*). The challenging aspect of this second oxidation was the possibility of competing retro-aldol reaction, eliminating any enantioselectivity.

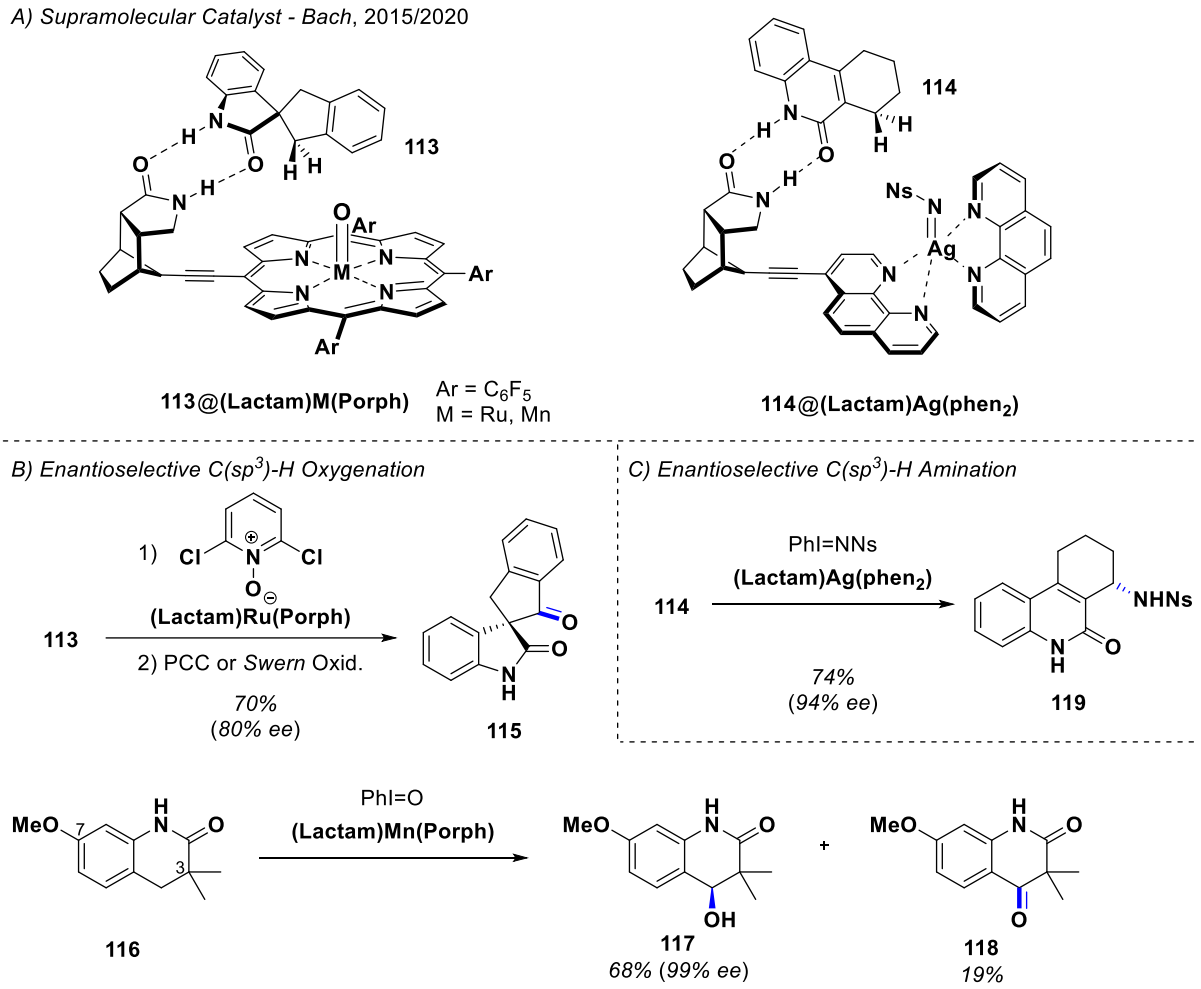

Scheme 22: Supramolecular C(sp^3)-H oxygenation *via* hydrogen bonding by *Bach* and coworkers.

A few years later, the same group utilized the Mn version of the catalysts in the enantioselective oxidation of **116**, with PhIO as the oxidant, to give **117** in 68% yield and 99% *ee*.[216] Up to 12 examples were reported with different groups at C7 (halogen, triflate, alky) as well as at C3 (cyclopropyl, -pentyl, -hexyl) in 19-68% yield and 97-99% *ee*. In 2020, they reported the same principle in the enantioselective C(sp^3)-H amination using **(Lactam)Ag(phen2)** (Scheme 22C).[217] The reaction of **114** with the Ag catalysts and PhI=NNs as nitrene precursor resulted in product **119** in 74% yield and 94% *ee.* Likewise, up to 14 different quinolones and pyridines have been oxidized with 29-88% yield and 83-97% *ee.*

In 2017, *Olivo*, *Di Stefano*, *Costas*, and coworkers reported a supramolecular catalyst for the site-selective C(sp^3)-H oxidation of linear aliphatic ammonium salts (Scheme 23A/B).[174, 218]

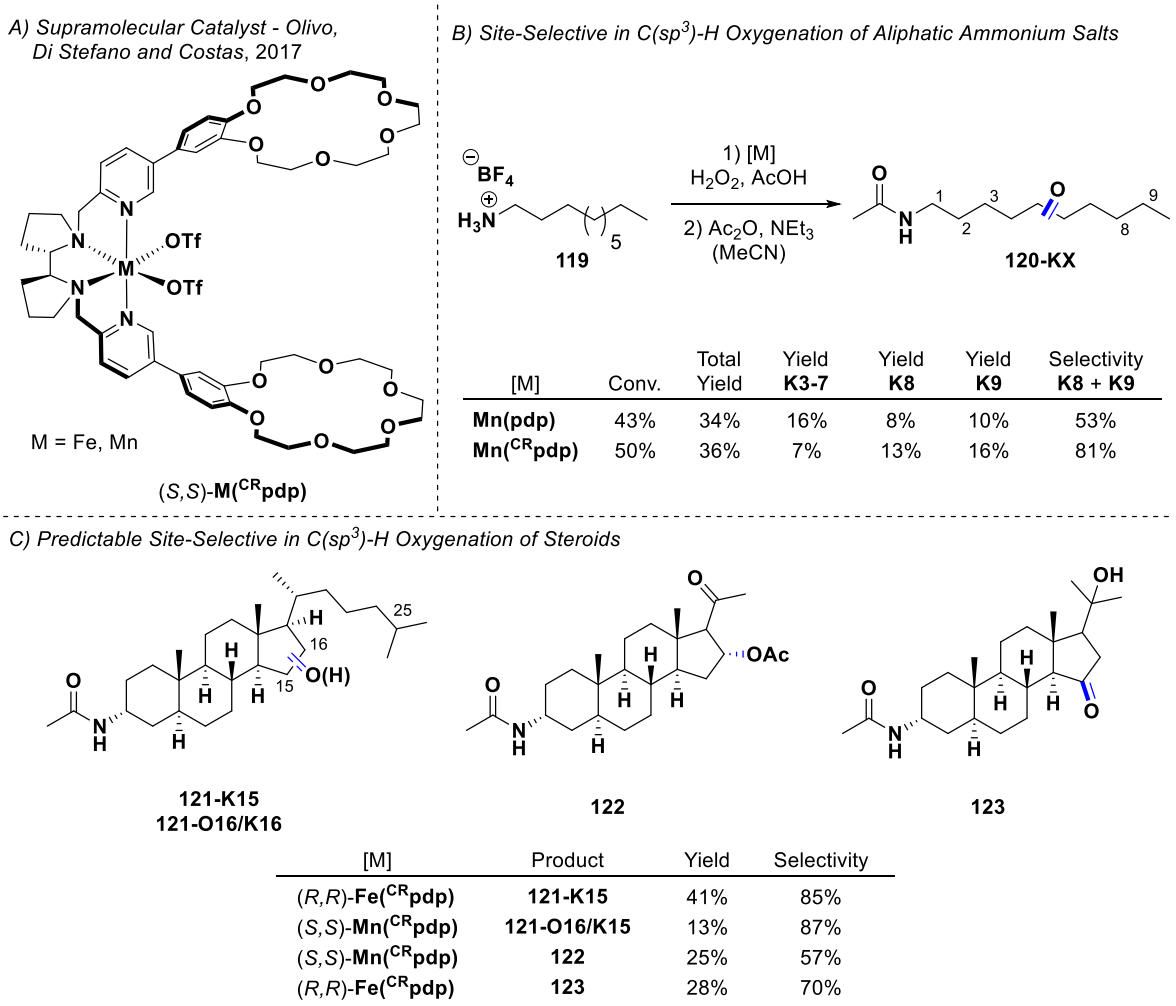

[M]	Conv.	Total Yield	Yield **K3-7**	Yield **K8**	Yield **K9**	Selectivity **K8 + K9**
Mn(pdp)	43%	34%	16%	8%	10%	53%
Mn(CRpdp)	50%	36%	7%	13%	16%	81%

[M]	Product	Yield	Selectivity
(*R*,*R*)-**Fe(CRpdp)**	**121-K15**	41%	85%
(*S*,*S*)-**Mn(CRpdp)**	**121-O16/K15**	13%	87%
(*S*,*S*)-**Mn(CRpdp)**	**122**	25%	57%
(*R*,*R*)-**Fe(CRpdp)**	**123**	28%	70%

Scheme 23: Supramolecular C(sp^3)-H oxygenation *via* hydrogen bonding by *Olivo, Di Stefano, Costas*, and coworkers.

The system consists of the well-known **M(pdp)** catalysts linked with two 18-benzocrown-6-ether (**CR**) motifs for substrate recognition *via* hydrogen bonding. Oxidation with unfunctionalized catalysts (e.g. **Fe(pdp)**) resulted predominantly in the formation of the ketone products distant from the ammonium group (K6 and higher), with minor amounts of K3-5. In contrast, in the presence of the supramolecular **Fe(CRpdp)** and **Mn(CRpdp)** catalysts, site-selectivity for the remote C8 and C9 positions was observed. In particular, for decylammonium **119** the selectivity for K8/K9 increased from 53% to a remarkable 81% from **Mn(pdp)** to **Mn(CRpdp)**, respectively. Besides decylammonium, both longer and shorter aliphatic chains were oxidized, showing a preference for C8/C9 oxidation.[218] Upon oxidation of the dimethylated derivative of decylammonium (C10-NMe_2H^+), the total yield of the reaction dropped to 3% with no evidence for increased C8/C9 selectivity (50%). The low yield was attributed to the oxidation of the unprotected crown ethers of the catalyst (due to the lack of a cationic binding partner).

In 2020, the same groups reported the application of the **M(CRpdp)** catalysts to the selective oxidation of some steroid substrates.[219] Furthermore, the group showed remarkable predictive power of which positions would be the favored ones and observed different products depending on the catalyst's chirality. For example, in the oxidation of 3α-ammonium-5α-cholestane, good selectivity for the formation of ketone **121-K15** was observed using (*R*,*R*)-**Fe(CRpdp)** as the catalyst (41% yield, 85% selectivity). Oxidation with (*S*,*S*)-**Mn(CRpdp)** on the other side resulted mainly in the formation of the **121-O16/K16** (25% yield, 87% selectivity). These positions are 8 and 9 carbons away from the ammonium binding side, respectively. This is in accord with the results from the decylammonium oxidation. In contrast, the unfunctionalized catalysts gave the C25 alcohol as the major product (up to 60% selectivity). Similar tunability of the oxidation positions depending on the chirality was observed with two other amino steroids. With (*S*,*S*)-**Mn(CRpdp),** acetylated alcohol **122** was mostly formed, whereas with (*R*,*R*)-**Fe(CRpdp),** ketone **123** was the major product. (57% and 70% selectivity, respectively). In both cases, oxidation with unfunctionalized catalysts resulted in a mixture of products (8-10 products) in low yields (11-22% total yield).

In summary, some impressive examples of selective C(sp^3)-H oxidations using supramolecular catalysts have been reported. It has been shown that less reactive positions can be targeted in the presence of more reactive ones. Moreover, the functionalization of remote positions even in challenging linear substrates can be achieved with good selectivities. However, the examples have also shown that the choice of a suitable supramolecular host can be very challenging. In particular, low turnovers due to product inhibition and catalyst decomposition under oxidation conditions have to be taken into account. Nevertheless, to us, the approach of supramolecular chemistry enables selectivities that would not otherwise be accessible either with directed or undirected C(sp^3)-H oxidations. Therefore, we aimed to synthesize new supramolecular catalysts capable of performing selective C(sp^3)-H oxidations.

1.4.4 Supramolecular Structures of Interest for this Work

Regarding the recognition site, we were especially interested in the use of molecular tweezers and cyclophanes. The term “molecular tweezer” was introduced by *Chen* and *Whitlock* and describes receptors possessing two flat, typically aromatic and identical panels, which are connected by a more or less rigid linker (e.g. **124**).[186] Furthermore, they defined that at least two out of three requirements had to be fulfilled to achieve binding of aromatic molecules in water: i) prevention of self-association of the panels, ii) a distance of approx. 7 Å between the panels (either plane to plane or centroid to centroid), and iii) a more or less rigid *syn* conformation of the two panels. Ever since the first molecular tweezer **124** was described by

Chen and *Whitlock*, many different versions have been reported (including di- to tetramethylene-bridged compounds,[220] porphyrin-based tweezers,[221] *Kagan`s* ethers[222] and glycoluril based structurs).[223] Depending on the properties of the spacer, tweezers can be more or less rigid. The use of a more rigid and preorganized tweezer can be advantageous regarding the thermodynamic stability of the host-guest complex (if they are well-fitting). However, at the same time, the substrate scope is usually limited, since badly fitting substrates will result in low binding or no binding at all.[221]

The term "cyclophane" on the other side goes back to the synthesis of [2.2]paracyclophane (**125**) by *Cram* and *Steinberg* in 1951 (although this was not the first report of such cyclic structures).[224-225] Ever since, cyclophanes have been described as cyclic molecular receptors with at least one aromatic ring connected between two non-adjacent positions by at least one aliphatic bridge. Consequently, the number of different cyclophanes reported to date is huge.[225-226] Intensive work on cyclophanes, for instance, was carried out by *Diederich* and coworkers.[181, 201] They investigated cyclophanes (with additional polar groups for water solubility) and their guest-uptake properties of aromatic and neutral compounds in water. They also studied the influence of different solvents on the binding of a neutral aromatic guest in a cyclophane host.[227] Interestingly, they observed a linear free energy relationship between the solvent polarity parameter $E_T(30)$ and complex formation. For water, the most polar solvent investigated ($E_T(30) = 63.0\ kcal\ mol^{-1}$), a free energy of $\Delta G° = -9.4\ kcal\ mol^{-1}$ was observed for complexation. In contrast in carbon disulfide, the least polar solvent studied ($E_T(30) = 32.6\ kcal\ mol^{-1}$), the free energy of the formation of the complex decreased to $\Delta G° = -1.3\ kcal\ mol^{-1}$. TFE was among the solvents tested and showed the second highest free energy $\Delta G° = -7.8\ kcal\ mol^{-1}$ for complex formation after water possessing the second highest polarity parameter ($E_T(30) = 63.0\ kcal\ mol^{-1}$).

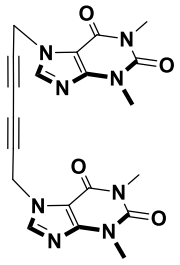

124

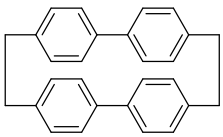

[2.2]paracyclophane (**125**)

Figure 6: First molecular tweezer **124** and name-giving cyclophane **125**.

Both, molecular tweezers and cyclophanes gained our interest for their application in selective C(sp^3)-H oxidation *via* substrate recognition. In the case of the first, we aimed for a tweezer

enabling binding *via* hydrogen bonding. In the case of the second, we envisioned that binding of neutral apolar guest might be possible due to a solvophobic effect in TFE and HFIP based on the studies reported by *Diederich*. Although HFIP was not included in this study, we expected molecular recognition might be feasible, since its solvent polarity parameter is even higher than the one of water ($E_T(30) = 65.3\ kcal\ mol^{-1}$).[228]

2 Objective of this Thesis

The tetraazadentate non-heme Fe and Mn catalysts, especially the **M(pdp)**[135, 229] and **M(mcp)**[137, 146, 230] versions, have been proven to be very active C(sp^3)-H oxidation catalysts.[16, 134] Furthermore, they can be easily derivatized *via* their pyridine rings. To us, the application of these catalysts in a supramolecular approach was especially interesting. We envisioned that the addition of a recognition motif would enable new selectivities in C-H oxidations (Scheme 24). In order to achieve this, we wanted to explore a glycoluril-based molecular tweezer, which has been previously shown to be able to bind ammonium salts *via* hydrogen bonding and ion-dipole interactions and was first reported by *Isaacs*.[231-232] The first steps towards such a molecular tweezer catalyst were already achieved in the master`s thesis project prior to this work.[233] Therefore, the synthesis began from tweezer **125**. We hypothesized that the final catalysts could be synthesized in only a few more steps *via* reductive amination of **125** and **127** followed by alkylation with **126** and metal complexation. The supramolecular catalysts should then be explored in the methylene oxidation of aliphatic ammonium salts. From SPARTAN models, we expected preferential oxidation of the positions C6-C8. Furthermore, we hoped to observe better selectivities compared to the approach with CRs by *Olivo*, *Di Stefano*, *Costas*, and coworkers[218] due to the higher rigidity of the molecular tweezer.

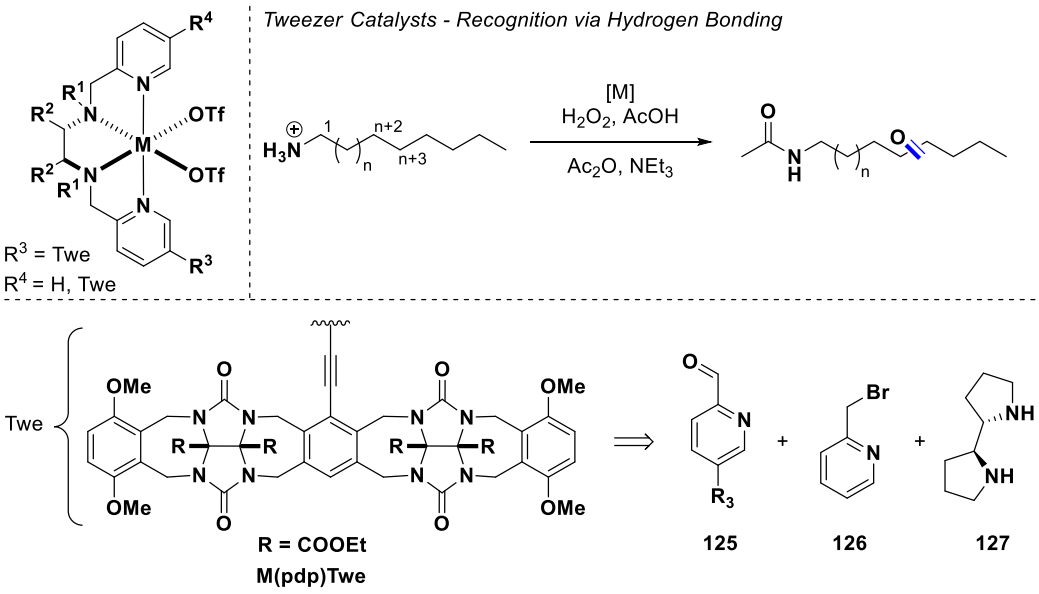

Scheme 24: Strategy towards a supramolecular C(sp^3)-H oxygenation catalysts based on a molecular tweezer.

In the second phase of this work, we wanted to explore macrocyclic catalysts derived from cyclophanes[181, 234] (**Mn(mcp)CY3Br** and **Mn(mcp)CY5Br** (Scheme 25)). We envisioned that the binding of apolar guests lacking any functional handles might be possible in HFIP and TFE due to a solvophobic effect. This assumption was based on host-guest studies by *Diederich* and

coworkers, which showed a distinct solvophobic effect of aromatic substrates depending on the polarity of the solvent.[227, 235] The synthetic strategy included monobromination of bisphenol A (**128**) followed by monoalkyation with **130/131** and subsequent macrocyclization with two equivalents of the substrate. Thereafter, macrocycle **CY3Br** /**CY5Br** should be attached to the catalyst pyridines *via* twofold Suzuki cross-coupling. In theory, the second unreacted bromide of the macrocycle could be later used to forge an additional macrocyclic connection between the two distinct CY3 or CY5 cycles in the catalyst, increasing the rigidity of the system. As substrates, simple *n*-alkanes should be applied for the smaller CY3 version. CY5 should then also enable the investigation of larger substrates.

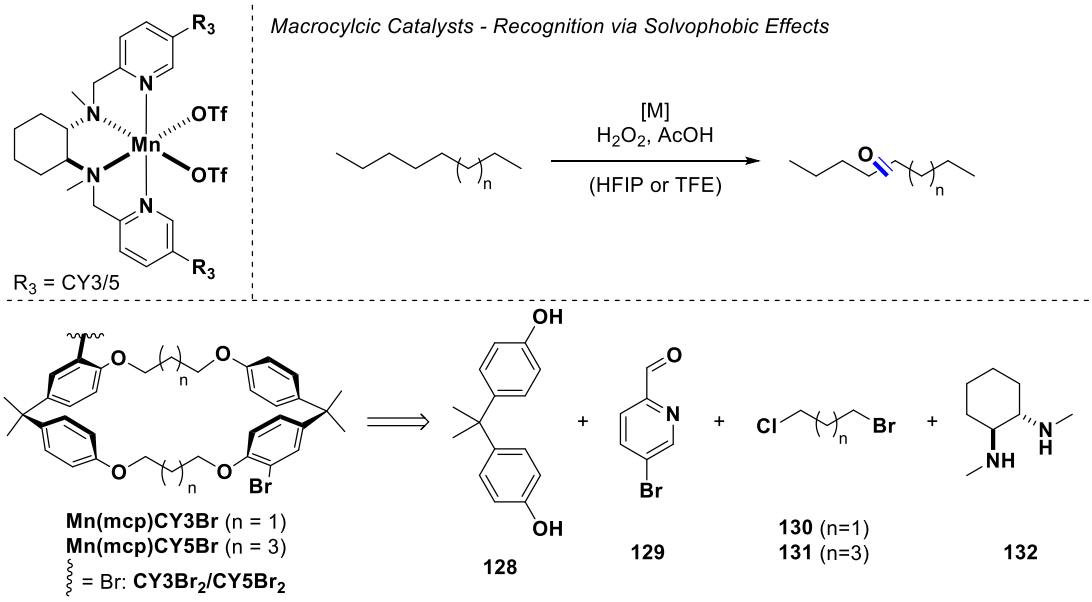

Scheme 25: Strategy towards a supramolecular C(sp^3)-H oxygenation catalysts based on macrocycles.

3 Results and Discussion

In the following, a short summary of the publications that were produced in the course of this dissertation is given (chapter 3.1, excluding the co-authored publication). Furthermore, the results of preliminary and unpublished work regarding macrocyclic C-H oxidation catalysts are discussed (chapter 3.2).

3.1 Tweezer-Based C-H Oxidation Catalyst: Publication Summary

3.1.1 Overriding Intrinsic Reactivity in Aliphatic C–H Oxidation: Preferential C3/C4 Oxidation of Aliphatic Ammonium Substrates[236]

Following the aim to synthesize **Fe(pdp)Twe**, we started with commercially available iododurene (**133**, Scheme 26). Introduction of TBS-acetylene *via* Sonogashira cross-coupling followed by benzylic bromination with NBS gave access to **134**. In a literature-known procedure, 1,2,4,5-tetrakis(bromomethyl)benzene compounds can be reacted with two equivalents of **135** resulting in tweezer **136**.[231] Deprotection followed by a second Sonogashira cross-coupling resulted in compound **125**. Subsequently, the aldehyde was reduced to the alcohol, which was then converted with PBr_3 to the benzylic bromide. Reaction with **193** resulted in the formation of free ligand **(pdp)Twe**. Note, that we switch the substrates for the reductive amination and alkylation of **127** compared to our initial plan, due to better product separation and yields. In the last step, complexation with $Fe(OTf)_2(MeCN)_2$ gave the desired catalyst **Fe(pdp)Twe**. Originally we planned a more concerted approach, however, it was not possible to achieve direct cross-coupling between **137** and a free **(pdp)Br** ligand.[233]

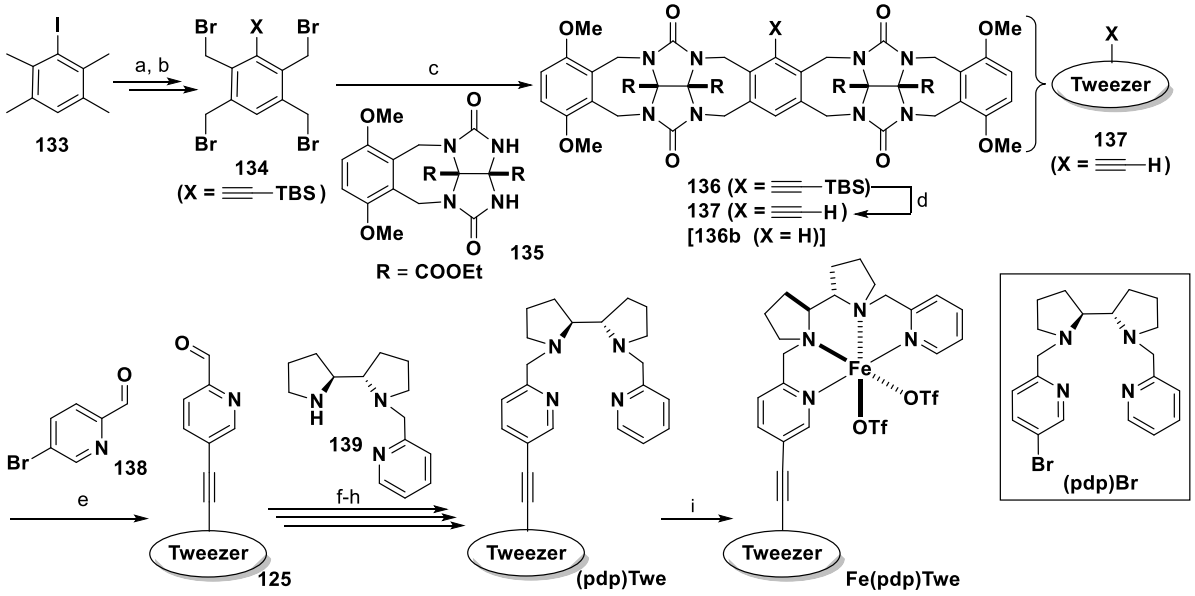

Scheme 26: Synthesis of the Fe(pdp)-functionalized tweezer **Fe(pdp)Twe**. a) TBS-acetylene, $PdCl_2(PPh_3)_2$, CuI, Et_2NH, 50 °C, 16 h, 97%. b) NBS, AIBN, CCl_4, 95 °C, 72 h, 58%. c) 7, KO*t*Bu, **135**, DMSO, rt, 16 h, 44%. d) TBAF, THF, 0 °C, 2 h,

80%. e) **137**, **138**, $PdCl_2(PPh_3)_2$, CuI, PPh_3, THF, µw, 120 °C, 90 min, 76%. f) $NaCNBH_3$, TFA, MeOH, CH_2Cl_2, rt, 4 h, 96%. g) PBr_3, CH_2Cl_2, 0 °C → rt, 16 h, 75%. h) **139**, K_2CO_3, TBAB, MeCN, 90 °C, 16 h, 97%. i) $Fe(OTf)_2(MeCN)_2$, MeCN, rt, 2.5 h, 58%. AIBN: azobis-*iso*-butyronitrile, TBS: (*tert*-butyldimethylsilyl), TBAB: tetra-*n*-butylammonium bromide, TBAF: tetra-*n*-butylammonium fluoride, TFA: trifluoroacetic acid, NBS: *N*-bromosuccinimide

Next, we wanted to investigate the behavior of the catalyst with some substrates. We chose decylammonium tetrafluoroborate (**119**) as the model substrate and performed NMR titration experiments to determine the binding constant. Surprisingly, relatively weak binding was observed for decylammonium and **Fe(pdp)Twe** (K_a = 29.5 ± 1.9 M^{-1}, K_d = 34.0 mM ± 2.2 mM), in contrast to unfunctionalized tweezer **136b** (K_a = 210 ± 7.6 M^{-1}, K_d = 4.77 mM ± 0.17 mM). Further dilution experiments showed that **Fe(pdp)Twe** possesses a distinct dimerization constant (K_{dim} = 160 ± 2.2 M^{-1}), whereas **136b** showed no aggregation. For the oxidation of decylammonium with **Fe(pdp)Br**, the expected reactivity trend for the formation of ketone products K4 to K9 was observed (Table 1, entry 1). The positions proximal to the ammonium salt were clearly deactivated and only minor amounts of K3 and K4 were formed. With **Fe(pdp)Twe** product mixtures were unfortunately also observed, however, with a remarkable selectivity change (Table 1, entry 2). The deactivated positions K3 and K4 proximal to the ammonium salt were now preferentially oxidized. In addition to decylammonium, shorter and longer linear ammonium salts were also investigated (entries 9-20). For all the substrates tested, the same selectivity trend was observed, with increased formation of intrinsically deactivated products K3/K4 (three examples depicted in Figure 7a). Subsequently, some control experiments were performed. First, **Fe(pdp)Br** and tweezer **136b** were added as separate moieties. And indeed, with this combination, a similar reactivity as with **Fe(pdp)Br** alone was observed (Table 1, entry 3 vs. 4), showing the need for a linked supramolecular catalyst.

Table 1: C(sp^3)-H oxygenation of different linear aliphatic ammonium salts with **Fe(pdp)Br** or **Fe(pdp)Twe**.[a]

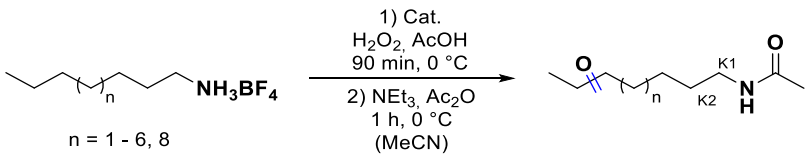

Entry	Substrate	Catalyst	Conv. [%]	Total yield[b] [%]	Selectivity[c] K3/K4 [%]	Selectivity[c] K3-K5 [%]
1 vs. 2[d]	C10-NH_3^+	**Fe(pdp)Br** vs. **Fe(pdp)Twe**	75 vs. 47	34 vs. 25	5.3 vs. 28	17 vs. 43
3 vs. 4	C10-NH_3^+	**Fe(pdp)Br** vs. **Fe(pdp)Br/136b**	75 vs. 52	34 vs. 19	5.3 vs. 7.8	17 vs. 18
5 vs. 6	C10-$NMeH_2^+$	**Fe(pdp)Br** vs. **Fe(pdp)Twe**	57 vs. 43	27 vs. 18	7.1 vs. 16	20 vs. 32
7[e] vs. 8[e]	C10-NMe_2H^+	"	60 vs. 41	32 vs. 14	5.2 vs. 6.2	17 vs. 17
9 vs. 10	C7-NH_3^+	"	34 vs. 34	3.8 vs. 6.4	46 vs. 80	70 vs. 92
11 vs. 12	C8-NH_3^+	"	37 vs. 22	17 vs. 8.2	19 vs. 51	36 vs. 64
13 vs. 14	C9-NH_3^+	"	49 vs. 39	30 vs. 16	10 vs. 40	24 vs. 53
15 vs. 16	C11-NH_3^+	"	57 vs. 36	42 vs. 24	3.9 vs. 24	12 vs. 37
17 vs. 18	C12-NH_3^+	"	63 vs. 39	28 vs. 10	3.8 vs. 23	9.9 vs. 37
19 vs. 20	C14-NH_3^+	"	77 vs. 68	33 vs. 18	2.1 vs. 21	8.8 vs. 34

[a] General reaction conditions: substrate (18.5 µmol, 1.0 equiv.), catalyst (925 nmol, 5 mol%), AcOH (148 µmol, 8.0 equiv.), H_2O_2 (278 µmol, 15 equiv., addition *via* a syringe pump over 90 min), MeCN, 0 °C. After 15 min, internal standard (biphenyl, 9.25 µmol, 0.5 equiv.), NEt_3 (100 µL), Ac_2O (150 µL), 0 °C. After 1 h, washing with H_2O, 2 M H_2SO_4, $NaHCO_3$, H_2O, dried (Na_2SO_4) and analyzed by GC. [b] Total yield refers to mixture of all isomers. [c] Selectivity refers to yield of selected ketones/total yield. [d] 5 mol% of Tweezer **136b** was added additionally. [e] Different work-up, see SI.

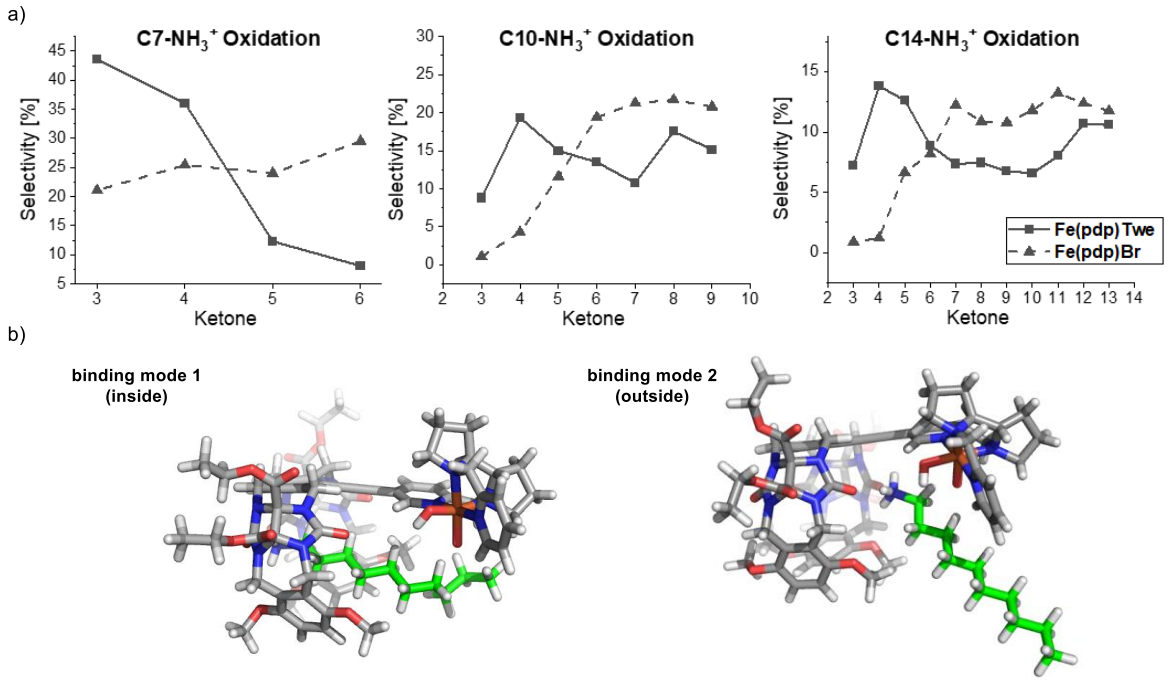

Figure 7: a) Graphic depiction of the selectivities in the C-H oxidation of selected substrates. b) Binding models of decylammonium and **Fe(pdp)Twe**.

Next, the binding of the substrate should be decreased by weakening the H-bonding ability through the addition of methyl groups to the ammonium salt (Table 1, entries 5-7). With C10-$NMeH_2^+$, lower amounts of K3/K4 were already observed compared to C10-NH_3^+ (16% and 28% selectivity, respectively). In the case of C10-NMe_2H^+, the selectivity for K3/K4 was

almost completely lost (6.2% in contrast to 5.2% for **Fe(pdp)Twe** and **Fe(pdp)Br**, respectively). To explain the observed preference for the proximal positions, we performed molecular modeling. In theory, we envisioned two different binding modes (Figure 7b): one inside the tweezer (binding mode 1); and one outside of the tweezer (binding mode 2). Only in the case of the latter would one expect preferential oxidation of C3 and C4. And indeed, according to the calculations, the binding mode 2 (with an additional acetonitrile solvent in the cavity of the tweezer, not shown in Figure 7b) is approximately 5 kJ/mol lower in energy.

In conclusion, we synthesized new supramolecular catalysts capable of the preferential C-H oxidation of intrinsically deactivated positions close to the ammonium (C3/C4) in aliphatic ammonium salts. For more general usability the selectivities need to be further improved, however, these results still highlight the possibility of a supramolecular approach in C-H oxidations.

3.1.2 Tweezer-Based C-H Oxidation Catalysts Overriding the Intrinsic Reactivity in Aliphatic Ammonium Substrates[237]

After our initial results with **Fe(pdp)Twe**, we wanted to explore such tweezer catalysts further, and investigate their ability to oxidize intrinsically deactivated positions. Firstly, we aimed for an increased catalyst scope. Therefore, we synthesized the twofold tweezer-functionalized catalyst **Fe(pdp)Twe$_2$**, as well as the **Fe(mcp)Twe** and the two Mn versions (**Mn(pdp)Twe** and **Mn(mcp)Twe**) (Figure 8). For comparison, the unfunctionalized counterparts were prepared as well.[135, 137, 146, 229-230]

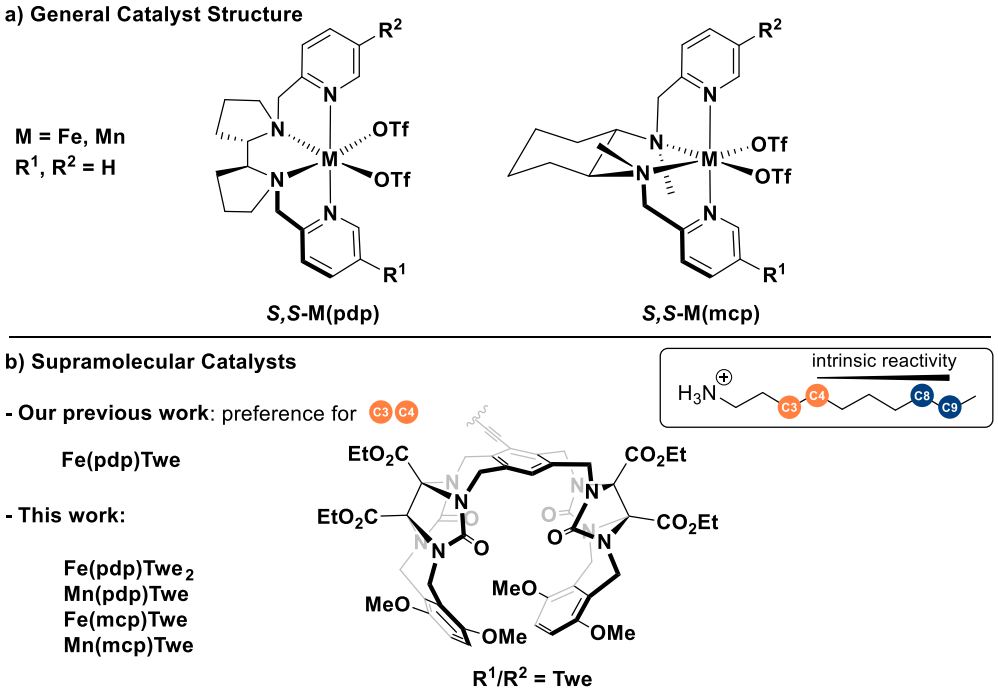

Figure 8: Depiction of the functionalized and tweezer-based catalysts.

In the case of the twofold functionalized **Fe(pdp)Twe$_2$**, we hoped to achieve better selectivities for K3 and K4 in contrast to the monofunctionalized **Fe(pdp)Twe**. Unfortunately, the opposite was true, with slightly lower conversion and yields in the oxidation of decylammonium as well as worse selectivities for the proximal positions (Table 2). Therefore, we performed a NMR titration experiment to determine the binding constant between decylammonium and **Fe(pdp)Twe$_2$**. Initially, we expected it to be higher, due to the additional tweezer binding side. However, to our surprise, an even lower binding constant was observed compared to **Fe(pdp)Twe** (K_a = 19.7 ± 1.2 M^{-1} vs. K_a = 29.5 ± 1.9 M^{-1}, respectively).

Table 2: Oxidation of decylammonium **119** with **Fe(pdp)Twe** and **Fe(pdp)Twe$_2$**.[a]

Catalyst	Conv. [%]	Total Yield[b] [%]	K3/K4 Selectivity[c] [%]	K3-K5 Selectivity[c] [%]
Fe(pdp)Twe	47	25	28	43
Fe(pdp)Twe$_2$	34	24	19	34

[a] General reaction conditions: substrate (9.25 µmol, 1.0 equiv.), Fe (463 nmol, 5 mol%), AcOH (74.0 µmol, 8.0 equiv.), H_2O_2 (139 µmol, 15 equiv., addition *via* a syringe pump over 90 min), MeCN, 0 °C. After 15 min, internal standard (biphenyl, 4.63 µmol, 0.5 equiv.), NEt_3 (50 µL), Ac_2O (75 µL), 0 °C. After 1 h, washing with H_2O, 2 M H_2SO_4, $NaHCO_3$, dried (Na_2SO_4) and analyzed by GC. [b] Total yield refers to the mixture of all isomers. [c] Selectivity refers to the yield of selected ketones/total yield.

Next, we investigated the behavior of the different supramolecular tweezer catalysts (Table 3). As previously observed,[218-219] the two new Mn catalysts (**Mn(mcp)Twe** and **Mn(pdp)Twe**) both behaved as relatively active catalysts, enabling the use of 1 mol% catalyst loading compared to 3 mol% for the Fe versions. Furthermore, a significant increase in C3/C4 oxidation was observed compared to their unfunctionalized counterparts **Mn(mcp)** and **Mn(pdp)** (entries 1-4). However, this increase was less distinct than with **Fe(pdp)Twe**. In addition to C3/C4, the C5 positions were also oxidized to a greater extent. In the case of **Fe(mcp)Twe**, however, only low activity in the oxidation of decylammonium was observed despite repeated attempts to synthesize it under various conditions (entry 6).[146, 159, 238]

Table 3: Oxidation of decylammonium **119** with several catalysts and in different solvents.[a]

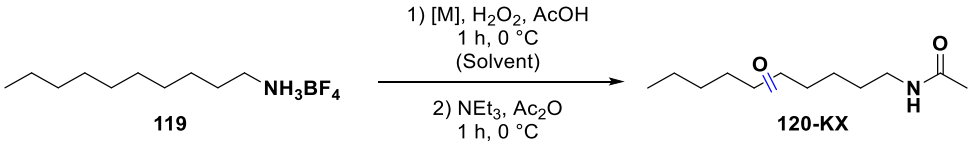

Entry	Catalyst	[Cat] [mol%]	Solvent	Conv. [%]	Total Yield[c] [%]	K3/K4 Selectivity[d] [%]	K3-K5 Selectivity[d] [%]
1 vs 2	**Mn(mcp)** vs **Mn(mcp)Twe**	1	MeCN	69 vs 58	55 vs 40	5.8 vs 14	15 vs 29
3 vs 4	**Mn(pdp)** vs **Mn(pdp)Twe**	1	MeCN	58 vs 45	32 vs 26	7.2 vs 13	16 vs 28
5 vs 6	**Fe(mcp)** vs **Fe(mcp)Twe**	3	MeCN	18 vs 6.8	15 vs 2.0	3.6 vs 9.0	7.9 vs 15
7 vs 8	**Fe(pdp)** vs **Fe(pdp)Twe**	3	MeCN	35 vs 17	31 vs 14	6.4 vs 27	13 vs 36
9[b] vs 10[b]	**Fe(pdp)** vs **Fe(pdp)Twe**	3	TFE	63 vs 38	34 vs 20	1.6 vs 5.6	9.5 vs 20
11[b] vs 12[b]	**Fe(pdp)** vs **Fe(pdp)Twe**	3	HFIP	94 vs 45	73 vs 30	0.7 vs 15	3.3 vs 34

[a] General reaction conditions: substrate (18.5 µmol, 1.0 equiv.), Fe (555 nmol, 3 mol%) or Mn catalyst (185 nmol, 1 mol%), AcOH (148 µmol, 8.0 equiv. or 407 µmol, 22 equiv., respectively), H_2O_2 (46.3 µmol, 2.5 equiv., addition via a syringe pump over 16 min), solvent, 0 °C. After 45 min, internal standard (biphenyl, 9.25 µmol, 0.5 equiv.), NEt_3 (100 µL), Ac_2O (150 µL), 0 °C. After 1 h, washing with H2O, 2 m H_2SO_4, $NaHCO_3$, dried (Na_2SO_4) and analyzed by GC. [b] Additional IBX oxidation of alcohol products, see SI p. S20. [c] Total yield refers to the mixture of all isomers. [d] Selectivity refers to the yield of selected ketones/total yield.

Next, we wanted to investigate the effect of H-bond donor solvents like TFE and HFIP. Both solvents are known to activate H_2O_2[239-240] and to deactivate the α-CH bond of intermediate alcohol products.[150-151] Already in our first publication,[236] we performed a short screening of these solvents, however, since we were not aware of this strong deactivation effect, we misinterpreted the observed alcohol products as ketones (O3-O9 possess similar retention times on the GC as K8 and K9). Therefore, we concluded that no selectivity for C3 was observed in these solvents for proximal positions. Once we realized this mistake, we repeated the experiments and added a subsequent oxidation step with IBX to convert the alcohol products to ketones. And indeed, also in TFE and HFIP, selectivity for the proximal positions C3 and C4 was observed. The best results were still obtained in MeCN, however, the relative 21-fold increase in K3/K4 selectivity in HFIP from **Fe(pdp)** to **Fe(pdp)Twe** was extraordinary (Table 3, entries 11-12.). Furthermore, as expected, higher conversions and yields were observed in TFE and HFIP compared to MeCN.

Finally, we investigated the oxidation of some new substrates (Table 4). In particular, we were interested in the oxidation of two substrates with a terpene substitution pattern, **140** and **141**, as well as the two cyclohexyl substrates **142** and **143**. In all four cases, a distinct increase in C3 or C4 selectivity was observed with **Fe(pdp)Twe**, compared to unfunctionalized **Fe(pdp)**. For both catalysts (unfunctionalized and supramolecular), the oxidation of **140** results in the formation of the tertiary alcohols at C3 and C7. The amount of C3 alcohol, however, increased from **Fe(pdp)** to **Fe(pdp)Twe** from 11% to 41%, respectively. In the case of the substrate that is one carbon longer, **141**, oxidation of the less deactivated C4 position increased from 25% to 57% selectivity, respectively, making the proximal alcohol product the major one. In the case of substrates **142** and **143** a similar trend was observed, however, with generally lower amounts of C3 and C4, presumably due to the deactivation by the ammonium salt plus sterical hindrance and torsional effects in the HAT transition state.[160] In the case of **142**, the main products were K5 and K6, with a selectivity increase in proximal O3 from 4.9% to 16% from **Fe(pdp)** to **Fe(pdp)Twe**. In the case of substrate **143** which is longer by one carbon, the selectivity for O4 formation increased from 9% to 27%, respectively.

Table 4: Oxidation of new substrates with **Fe(pdp)** and **Fe(pdp)Twe**.[a]

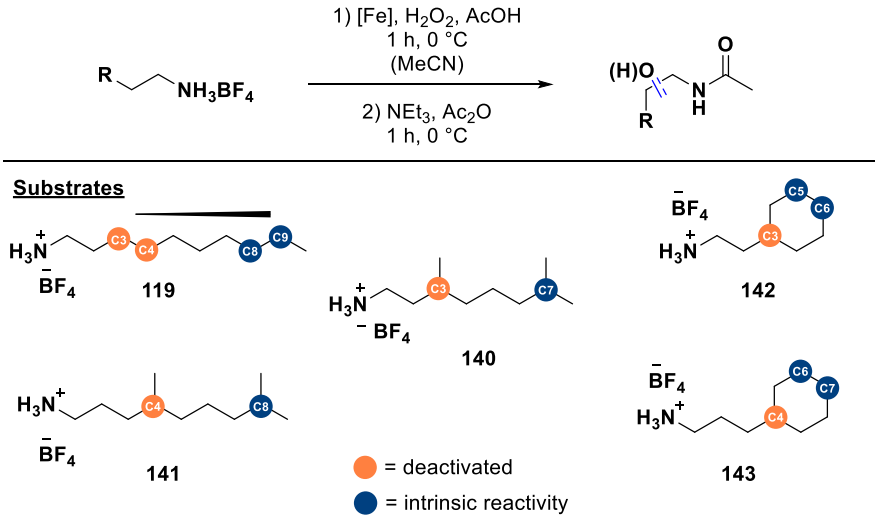

Substrate[a]	Fe(pdp)		Fe(pdp)Twe	
	Total Yield[b] [%]	● Selectivity[c] [%]	Total Yield[b] [%]	● Selectivity[c] [%]
	31	6.4	14	27
	34	11	16	41
	24	25	15	57
	28	4.9	11	16
	36	9.0	14	27

[a] General reaction conditions: substrate (18.5 µmol, 1.0 equiv.), Fe (3 mol%), AcOH (8.0 equiv.), H_2O_2 (2.5 equiv., addition *via* a syringe pump over 16 min), MeCN, 0 °C. After 45 min, internal standard (biphenyl, 0.5 equiv.), NEt_3, Ac_2O, 0 °C. After 1 h, work up, see SI p. S19-S20. [b] Additional IBX oxidation of alcohol products, see SI p. S20. [c] Total yield refers to the mixture of all isomers. [d] Selectivity refers to the yield of selected ketones/total yield.

In summary, we synthesized four new versions of our tweezer-based C-H oxidation catalyst and investigated their efficiency in the oxidation of decylammonium. The best-performing catalyst, **Fe(pdp)Twe** was applied in the hydroxylation of decyl ammonium in TFE and HFIP and in the oxidation of four new substrates in MeCN. In all cases, preferential oxidation of C3 and/or C4 was observed.

3.2 Macrocyclic C-H Oxidation Catalyst: Preliminary Work

3.2.1 Synthesis of Intrinsic and new Macrocyclic Catalysts

In aiming for a macrocyclic C-H oxidation catalyst, the synthesis of **Mn(mcp)CY3** was attempted. First, commercially available bisphenol A (BPA, **128**) was brominated with NBS (Scheme 27), according to a previously reported method (Lit: 80% yield).[241] To achieve reasonable yields of the mono-brominated product **144**, an excess of starting material is necessary. Since bisphenol A (**128**) is reasonably cheap and can be easily recovered after the reaction, this was accepted without trying to improve the reaction conditions further. In our case, slightly lower yields were obtained compared to the literature, which might be due to imperfect separation on the MPLC, resulting in minor amounts of mixed fractions of starting material and **144**.

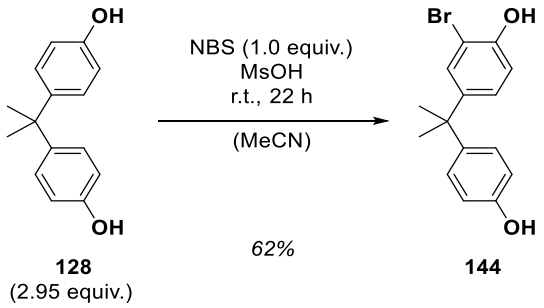

Scheme 27: Monobromination of bisphenol A to obtain **144**.

Next, we aspired to synthesize macrocycle **CY3Br2** in two steps (Scheme 28). In the first step, bisphenol **144** should be mono-alkylated. We assumed that the bromide ortho- to one of the two phenols might result in some reactivity difference in the alkylation. And indeed, it was possible to achieve **145** in up to 73% yield by using one equivalent of 1-bromo-3-chloropropane (**130**) and potassium carbonate as a base. The higher reactivity of the phenol ortho- to the bromide might be due to an inductive effect of Br, making the O-H bond more acidic compared to its non-brominated counterpart. The subsequent macrocyclization to **CY3Br2** at low concentration was achieved in reasonably good yield (40%) by using caesium carbonate and potassium iodide.

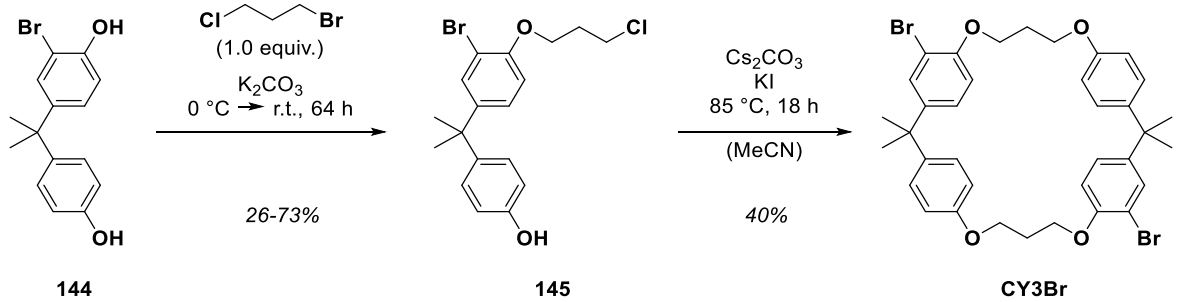

Scheme 28: Synthesis of macrocycle **CY3Br2** *via* monoalkylation of **144** followed by cyclization of two parts of **145**.

Unfortunately, upon scaling up the two reactions, we observed a distinct decrease in the yield of our desired monoalkylated product **144**, with the worst result being 26% yield. Instead, higher amounts of unreacted starting material and the dialkylated product **146** were observed. Therefore, we decided to change the synthetic strategy and aim for the synthesis of macrocycle **CY3Br** possessing only one bromide (Scheme 29). For the non-macrocyclic catalyst, the second bromide would not be necessary, and by removing it, the subsequent cross-coupling reaction would also not suffer from selectivity issues. The alkylation was performed exactly as before, except using 2.1 equivalents of 1-bromo-3-chloropropane, resulting in **146** in 76% yield. For the macrocyclization, compound **146** was reacted with 1.0 equivalent of BPA (**128**) giving macrocycle **CY3Br** in 48% yield.

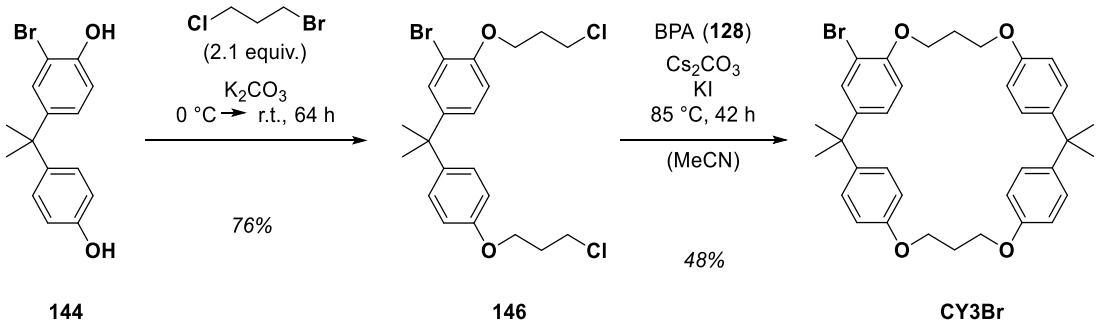

Scheme 29: Synthesis of **CY3Br** *via* double alkylation of **144** followed by cyclization of **146** and BPA.

Thereafter, macrocycle **CY3Br** should be converted with **147** in a Suzuki cross-coupling reaction (Scheme 30). To achieve this, **147** was synthesized from 5-bromopyridine-2-carbaldehyde (**129**) and bis(pinacolato)diboron (B_2pin_2) in a Miyaura borylation, and was then directly submitted to the Suzuki cross-coupling without further purification. Among the conditions tested, the best results were observed with K_3PO_4 as the base and in a DMF/H_2O (9/1) mixture. The cross-coupling also showed lower conversion and yields upon up-scaling. Under small-scale conditions (200 µmol), yields of up to 68% were achieved, however, at a 1.00 mmol scale, the best yield observed was 49%. Higher yields in the Suzuki cross-coupling could be probably achieved by switching the boron and halogen functionalities in the reactants (most reactive partners in Suzuki reactions are usually unhindered, electron-deficient halides/triflates with electron-rich organoboranes).[242] However, this would result in an additional step in the longest synthetic route.

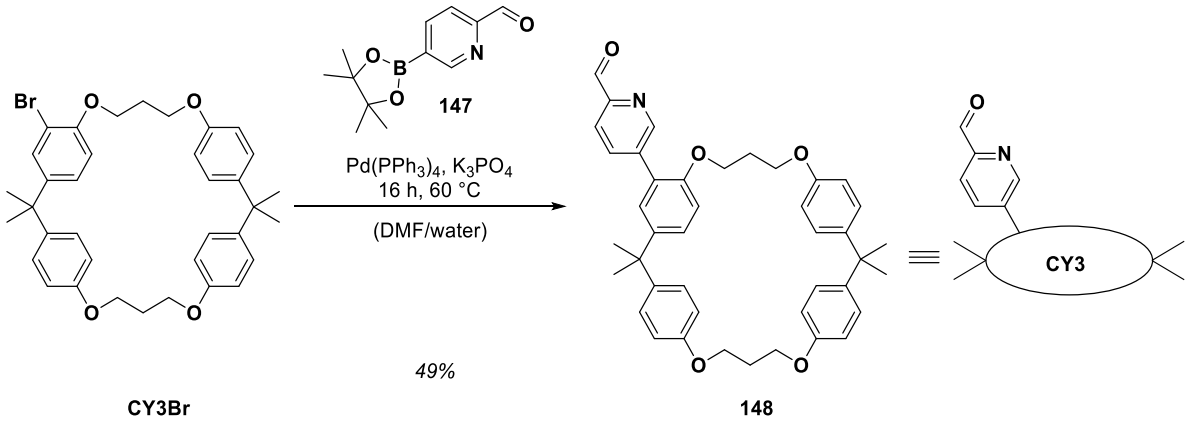

Scheme 30: Suzuki cross-coupling of **CY3Br** and **147** to obtain aldehyde **148**.

The final steps were all performed according to the previous tweezer project, except that in the reduction, $NaBH_4$ and a CH_2Cl_2/MeOH mixture were used (Scheme 31). The former is due to lower toxicity compared to $NaCNBH_3$ and the latter is due to the low solubility of **148** in pure MeOH. After bromination with PBr_3, alkylation of (1*S*,2*S*)-*N*,*N*'-dimethyl-1,2-cyclohexane-diamine (**132**), and complexation with $Mn(OTf)_2$, the final complex **Mn(mcp)CY3** was achieved in 27% yield over those four steps.

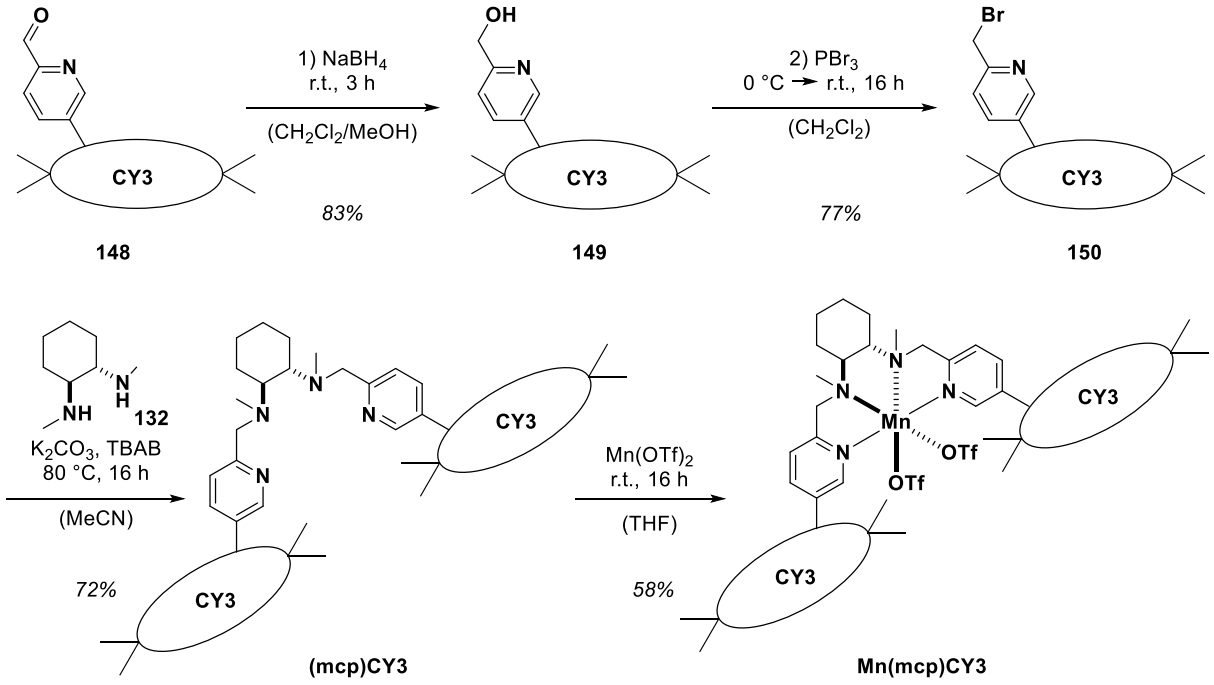

Scheme 31: Final steps towards the formation of **Mn(mcp)CY3** according to the previous strategy in the tweezer project.

In addition to the CY3 macrocycle, an enlarged derivative, CY5, should also be synthesized, opening the investigation of larger hydrocarbon skeletons such as steroids. To achieve this, the whole synthesis was repeated accordingly, using 1-bromo-5-chloropentane (**131**) as the linkage

between the two bisphenol moieties (Scheme 32). All the reactions were conducted successfully in similar yields. For comparison, the unfunctionalized catalyst **Mn(mcp)**[137, 230] was used.

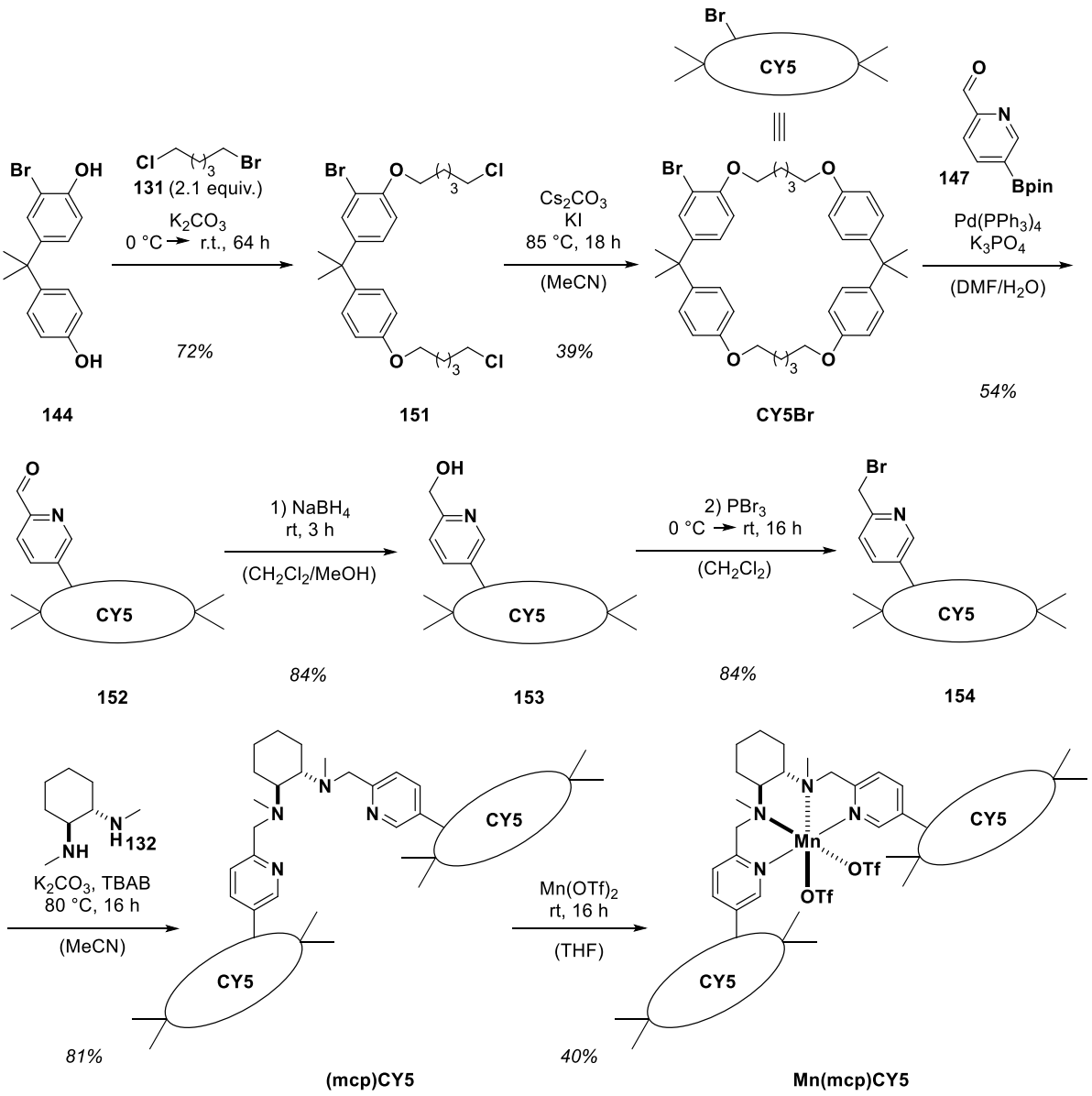

Scheme 32: Analog synthesis of **Mn(mcp)CY5** according to the previous strategy for **Mn(mcp)CY3** using 1-bromo-5-chloropentane (**131**) as linker instead of 1-bromo-3-chloropropane (**130**).

3.2.2 Substrates and their C-H Oxidation

We were especially interested in two kinds of substrates. First, we wanted to investigate *n*-alkanes. Although those substrates appear very simple, the selective oxidation of a single methylene group remains an unsolved challenge. This is due to the lack of any functional handle or group which would either enable binding or have an impact on the electronic, steric, and stereo-electronic properties of CH_2 groups in its proximity. However, we hypothesized that an enhancement of the medial methylene C-H oxidation might be observed if the substrate takes a linear conformation within the two macrocycles of **Mn(mcp)CY3**. For that reason, we decided

to start with *n*-tetradecane (**155**), a relatively long substrate that could fill both macrocycles according to our SPARTAN model (Figure 9).

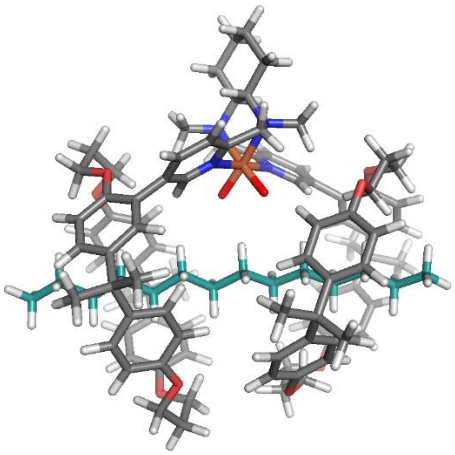

Figure 9: SPARTAN model of the binding of *n*-tetradecane **(155)** in **Mn(mcp)CY3**.

The oxidation reactions were performed according to the general oxidation conditions for *n*-alkanes, using 4.0 equivalents of acetic acid and 4.0 equivalents of H_2O_2 in MeCN and 1.0 equiv. of H_2O_2 in TFE and HFIP, respectively. Lower amounts of the peroxide were used in the latter solvent to minimize the formation of overoxidized diol products. The conversion and yield were calculated *via* GC utilizing biphenyl (BP) as an internal standard. As predicted, the supramolecular catalyst resulted in an active C-H oxidation catalyst (see Table 5). Although lower conversions and yields were observed compared to the unfunctionalized catalyst, the general catalytic activity was the first important result to us. The lower conversion could be due to the slow decomposition of **Mn(mcp)CY3** under the oxidation conditions, which was also observed with our tweezer catalyst. However, it should be noted that the conversions and yields were also lower for the unfunctionalized catalysts. With **Mn(mcp)**, we observed total yields of up to 55% in MeCN for the oxidation of decylammonium, but only 23% in the case of *n*-tetradecane (**155**). An explanation for this marked decrease could be the different solubility of the substrates. Decylammonium is soluble in all free solvents, *n*-tetradecane in none, presumably making the substrate less accessible to the catalyst. Hence, higher yields might be also possible for **Mn(mcp)CY3** in the oxidation of other substrates.

Table 5: Oxidation of *n*-tetradecane **(155)** with **Mn(mcp)** and **Mn(mcp)CY3** in several solvents.[a]

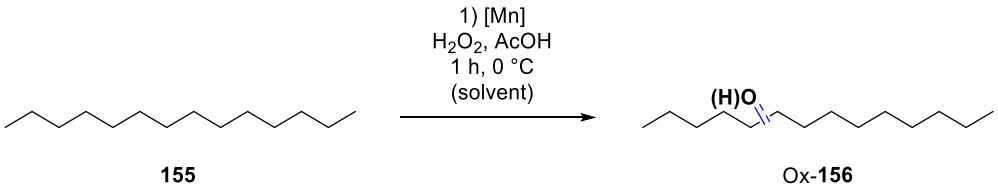

Entry	Cat.	Solvent	Conversion	Total Yield[b]
1	**Mn(mcp)**	MeCN	39%	23%
2	**Mn(mcp)CY3**	"	26%	13%
3	**Mn(mcp)**	TFE	76%	20%
4	**Mn(mcp)CY3**	"	42%	11%
5	**Mn(mcp)**	HFIP	59%	29%
6	**Mn(mcp)CY3**	"	31%	14%

[a] Reactions were performed according to the *General small-scale oxidation procedure with Mn catalysts in MeCN* or *in TFE/HFIP*, respectively (see Chapter 5.3). Conversion and total yield were observed *via* GC analysis of the crude mixtures and are based on an internal standard. [b] Total yield refers to the mixture of all products.

To analyze whether some differences in the oxidation selectivity were observed, the GC spectra of the crude mixtures of the different reactions were compared (see Figure 10). To start with, a clear difference between the oxidation in MeCN and HFIP was visible. However, this was expected, since MeCN should mainly result in the ketone products, whereas reactions in HFIP should terminate at the alcohols. Looking at the oxidation of **Mn(mcp)** and **Mn(mcp)CY3** in HFIP, three main peaks were observed on the GC, although in total 6 different alcohol constitution isomers of the oxidation of methylene C-H bonds are possible. Unfortunately, it was not possible to achieve better separation even under improved GC conditions. Regarding the isolated signals, unfortunately, almost no relative intensity change was observed with **Mn(mcp)** or **Mn(mcp)CY3** in HFIP. In MeCN, it seems like there could be some selectivity change, however, the most likely explanation for the observation is a different alcohol-to-ketone ratio for the two catalysts. It should be noted, that the assignment of ketone and alcohol products was not proven and represents only an assumption based on the observed signals and the expected reactivity of the HAT step in the different solvents used.[150-153] However, it was surprising to us to obtain such high amounts of alcohol products in MeCN. Presumably, this is also due to the low solubility of the substrates and low conversion of our catalysts. The results for the oxidation in TFE were intermediate between those in MeCN and HFIP. The yields were somewhat lower than in MeCN, and alcohol products were mainly observed, however, small amounts of ketones were also formed. In conclusion, we were not able to observe any distinct selectivity change with our supramolecular catalyst for the oxidation of C14. Nevertheless, we learned that our catalyst was generally active and gained first information about its oxidation behavior in the different solvents.

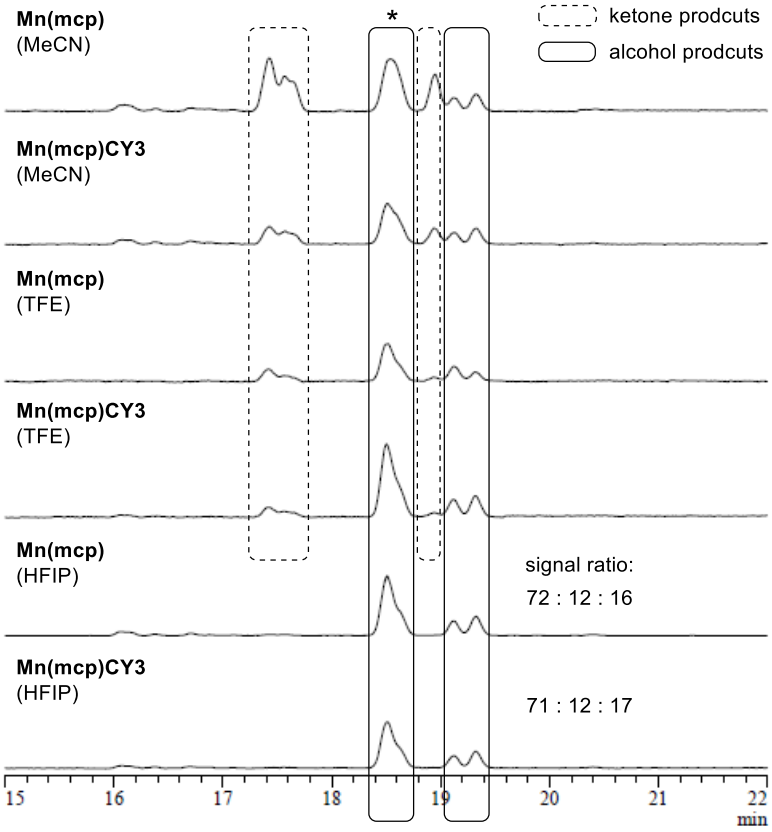

Figure 10: GC-spectra of the oxidation of **155** with **Mn(mcp)** and **Mn(mcp)CY3** in several solvents.

Next, we decided to look at shorter substrates, the oxidation products of which would still be separable on the GC. Furthermore, we focused on oxidations in HFIP and MeCN. The former, because they gave the best yields and resulted exclusively in alcohol products, and the latter, to have an additional comparison to our results in HFIP. The results of the oxidation of *n*-octane are shown in Table 6. Again, in MeCN, mixtures of ketone and alcohol products were observed and only very low yields were obtained for the oxidation with **Mn(mcp)CY3** (see Figure 11). In HFIP, a 19% total yield was observed, with **Mn(mcp)CY3** leading only to the alcohol products. The product assignment displayed was made according to a literature reference.[243-244] For better comparison with the results in HFIP, we decided to further oxidize the observed alcohol products of the oxidation with **Mn(mcp)** using IBX. In this way, it was possible to compare the ratios of the three ketone products with the ratios of the alcohol products in HFIP. Unfortunately, the change in selectivity for the oxidation using **Mn(mcp)CY3** was not significant enough to be interesting.

Table 6: Oxidation of *n*-octane with **Mn(mcp)** and **Mn(mcp)CY3** in MeCN and HFIP.[a]

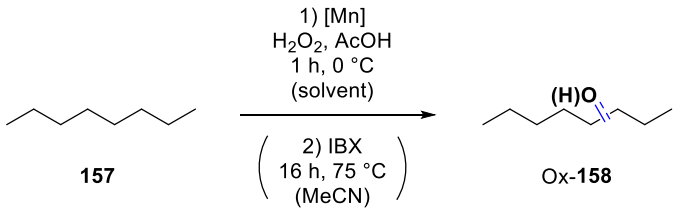

Entry	Cat.	Solvent	Conversion	Total Yield[b]
1[c]	**Mn(mcp)**	MeCN	71%	20%
2[c]	**Mn(mcp)CY3**	"	55%	5.8%
3	**Mn(mcp)**	HFIP	88%	45%
4	**Mn(mcp)CY3**	"	61%	19%

[a] Reactions were performed according to the *General small-scale oxidation procedure with Mn catalysts in MeCN* or *in TFE/HFIP*, respectively (see Chapter 5.3). Conversion and total yield were observed *via* GC analysis of the crude mixtures and are based on an internal standard. [b] Total yield refers to the mixture of all products. [c] Additional oxidation in a *Second step for small-scale oxidation reactions* (see Chapter 5.3).

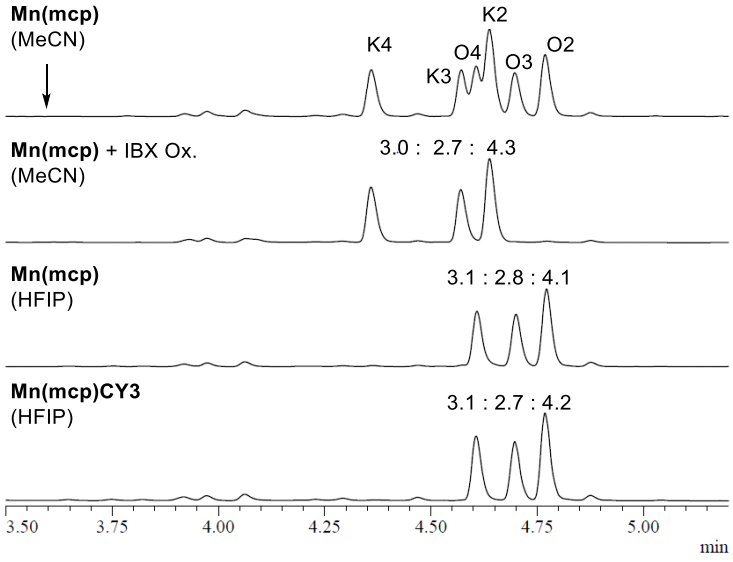

Figure 11: GC-spectra of the oxidation of **157** with **Mn(mcp)** and **Mn(mcp)CY3** in MeCN and HFIP.

Next, the oxidation of substrates with a bulkier group at one end was investigated. We envisioned that this could help due to decreased flexibility of the substrate within the macrocycles. In particular, we studied the oxidations of 1-bromododecane (**159**) and tridecan-2-one (**161**). The results of the oxidation of 1-bromododecane (**159**) are depicted in Table 7 and Figure 12. It should be noted that for **159**, higher yields were generally observed, (except for **Mn(mcp)CY3** in MeCN) with a 39% total yield for our supramolecular catalyst in HFIP.

Table 7: Oxidation of 1-bromododecane (**159**) with **Mn(mcp)** and **Mn(mcp)CY3** in MeCN and HFIP.[a]

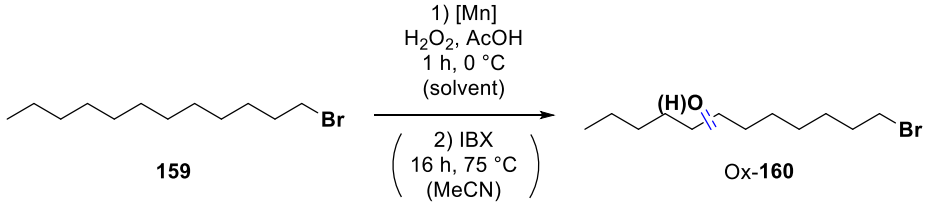

Entry	Cat.	Solvent	Conversion	Total Yield[b]
1	**Mn(mcp)**	MeCN	54%	32%
2	**Mn(mcp)CY3**	"	12%	4.8%
3[c]	**Mn(mcp)**	HFIP	78%	72%
4[c]	**Mn(mcp)CY3**	"	45%	39%

[a] Reactions were performed according to the *General small-scale oxidation procedure with Mn catalysts in MeCN* or *in TFE/HFIP*, respectively (see Chapter 5.3). Conversion and total yield were observed *via* GC analysis of the crude mixtures and are based on an internal standard. [b] Total yield refers to the mixture of all products. [c] Additional oxidation in a *Second step for small-scale oxidation reactions* (see Chapter 5.3).

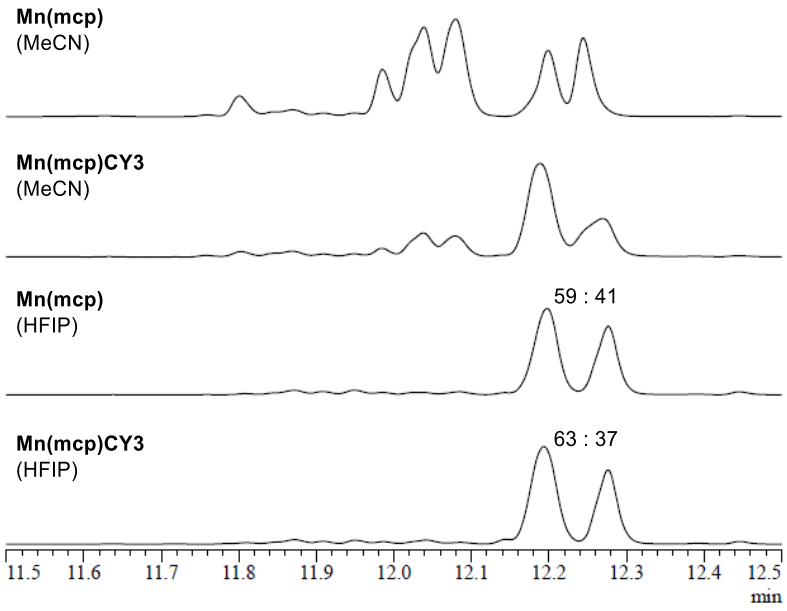

Figure 12: GC-spectra of the oxidation of **159** with **Mn(mcp)** and **Mn(mcp)CY3** in MeCN and HFIP.

Two interesting patterns were observed in the GC spectra. Firstly, the ketone products are more separable than the alcohol products, and secondly, a small selectivity change was observed in the case of the oxidation in HFIP. Although this change was not large, we decided to investigate it in further detail. To be able to gain more information about the pattern, we oxidized the alcohol products from the reactions in HFIP in a subsequent step with IBX to observe the corresponding ketones (see Figure 13). The results could hint towards a slight enhancement of the proximal C-H oxidation products, but again, the effect was very small. The assumption of

which peak corresponds to which product was based on two factors. Firstly, we would expect a clear reactivity difference between the oxidation of the proximal and distal methylene groups in 1-bromododecane (**159**), due to the negative inductive effect of the bromide. And secondly, we assumed that the pattern observed on the GC would be comparable with those observed for the oxidation of decylammonium. One way to investigate this further would be via GC-MS, looking for the fragmentation patterns (e.g. McLafferty fragmentations) as was done for decylammonium. Alternatively, the products could be isolated, however, this is extremely challenging due to their high similarity. At this stage, we were more interested in the reproducibility of the selectivity pattern. Again, different ratios and therefore presumably different selectivities in HFIP were observed, however, the second time the observed selectivity difference decreased with a 59:41 ratio for **Mn(mcp)** and a 61:39 ratio for **Mn(mcp)CY3**, respectively. All in all, the selectivity change was too small and we did not further investigate this substrate.

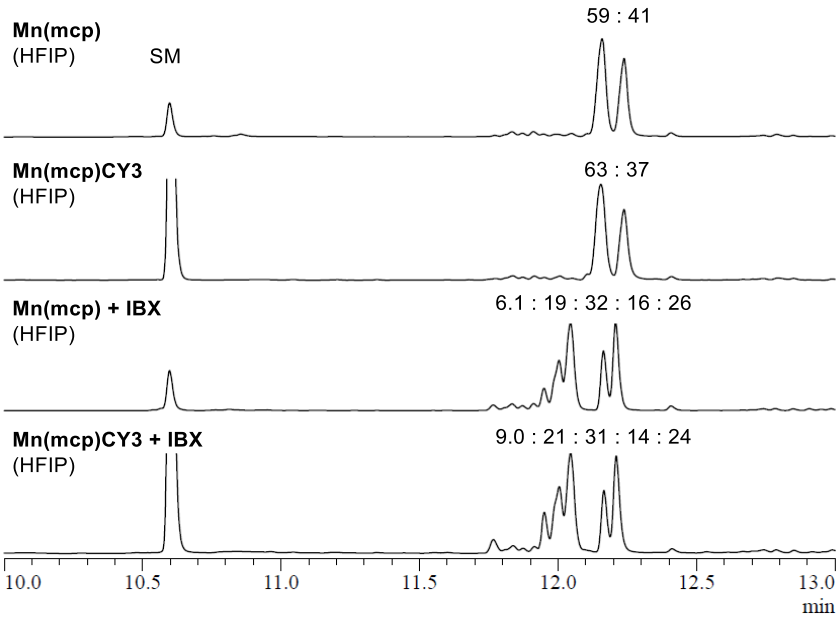

Figure 13: GC-spectra of the oxidation of **159** before and after additional IBX oxidation.

Next, the oxidation of tridecan-2-one (**161**) was conducted (Table 8, Figure 14). Note that in the case of the oxidation with **Mn(mcp)CY3** in HFIP no reliable conversions and yields were observed, due to an error during the addition of our internal standard. However, from the signal intensities, it can be stated that reasonable yields were observed. Furthermore, it was still possible to investigate the oxidation pattern, and again, in the case of the oxidation reactions in HFIP a slight selectivity change was observed. As before, we oxidized the alcohol products with IBX and looked at the pattern of the corresponding ketones. A good separation was observed on the GC, showing a distinct reactivity difference between the methylene groups.

But unfortunately, it was observed again that there was no conclusive selectivity change for the oxidation with our supramolecular catalysts compared to the unfunctionalized catalysts.

Table 8: Oxidation of tridecan-2-one (**161**) with **Mn(mcp)** and **Mn(mcp)CY3** in MeCN and HFIP.[a]

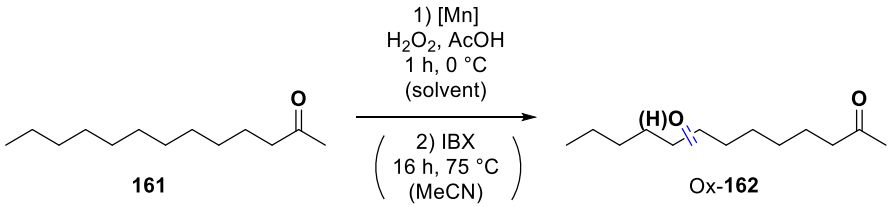

Entry	Cat.	Solvent	Conversion	Total Yield[b]
1	**Mn(mcp)**	MeCN	51%	35%
2	**Mn(mcp)CY3**	"	6.7%	0.6%
3[c]	**Mn(mcp)**	HFIP	92%	91%
4[c]	**Mn(mcp)CY3**	"	n.d.	n.d.

[a] Reactions were performed according to the *General small-scale oxidation procedure with Mn catalysts in MeCN* or *in TFE/HFIP*, respectively (see Chapter 5.3). Conversion and total yield were observed *via* GC analysis of the crude mixtures and are based on an internal standard. [b] Total yield refers to the mixture of all products.

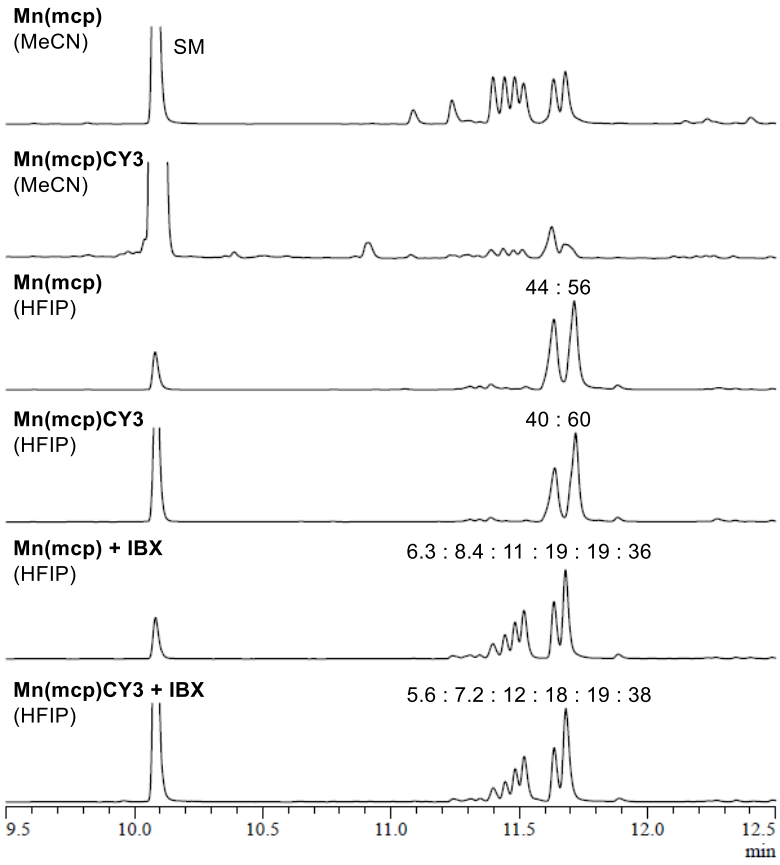

Figure 14: GC-spectra of the oxidation of **161** with **Mn(mcp)** and **Mn(mcp)CY3** in MeCN and HFIP..

Finally, some non-linear substrates should be investigated. In particular, we were interested in the oxidation of menthol acetate **163** and menthol hexanoate **165**. The former was also oxidized

by the group of *White* with **Fe(pdp)** in MeCN, leading to products **82** and **164** in an 11:1 ratio due to steric differences (the C-H bond in the isopropyl group is oriented towards the neighboring acetate, making it less accessible to the catalyst).[135] In our case, the oxidation with **Mn(mcp)** resulted in two signals on the GC in a 9:1 ratio (Table 9, Figure 15). The oxidation with **Mn(mcp)CY3** resulted in the same two signals in a 10:1 ratio. Although the products were not isolated, it was assumed that they are the same as observed by *White* and coworkers. The two tertiary C-H bonds should be the most reactive ones independent of the different solvents used. As no significant change was observed, we did not investigate the substrate or its products further.

Table 9: Oxidation of *rac*-**163** with **Mn(mcp)** and **Mn(mcp)CY3** in HFIP.[a]

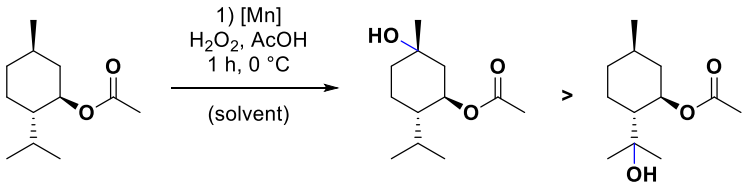

Entry	Cat.	Solvent	Conversion	Total Yield[b]
1	**Mn(mcp)**	HFIP	94%	63%
2	**Mn(mcp)CY3**	"	32%	23%

[a] Reactions were performed according to the *General small-scale oxidation procedure with Mn catalysts in TFE/HFIP* (see p. Chapter 5.3). Conversion and total yield were observed *via* GC analysis of the crude mixtures and are based on an internal standard. [b] Total yield refers to the mixture of all products.

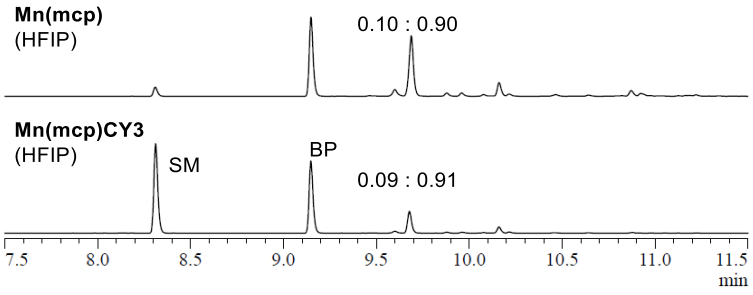

Figure 15: GC-spectra of the oxidation of **163** with **Mn(mcp)** and **Mn(mcp)CY3** in HFIP.

In the case of the oxidation of menthol hexanoate, three main peaks were observed (Table 10, Figure 16). Note that, again, no reasonable conversion and yield was observed for the oxidation with **Mn(mcp)CY3**. Since once again no promising differences in the ratio of the peaks were observed on the GC for the different catalysts, the oxidation reaction with **Mn(mcp)CY3** was not repeated. Regarding the signal at approx. 14.0 min, we assumed that this could be some overoxized diol product(s), however, we did not further investigate it. It could also just be an impurity.

Table 10: Oxidation of *rac*-**165** with **Mn(mcp)** and **Mn(mcp)CY3** in HFIP.[a]

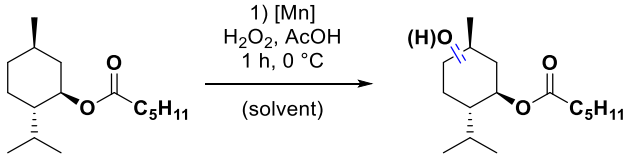

rac-**165** *rac*-**166**

Entry	Cat.	Solvent	Conversion	Total Yield[b]
1	**Mn(mcp)**	HFIP	88%	42%
2	**Mn(mcp)CY3**	"	n.d.	n.d.

[a] Reactions were performed according to the *General small-scale oxidation procedure with Mn catalysts in TFE/HFIP* (see Chapter 5.3). Conversion and total yield were observed *via* GC analysis of the crude mixtures and are based on an internal standard. [b] Total yield refers to the mixture of all products.

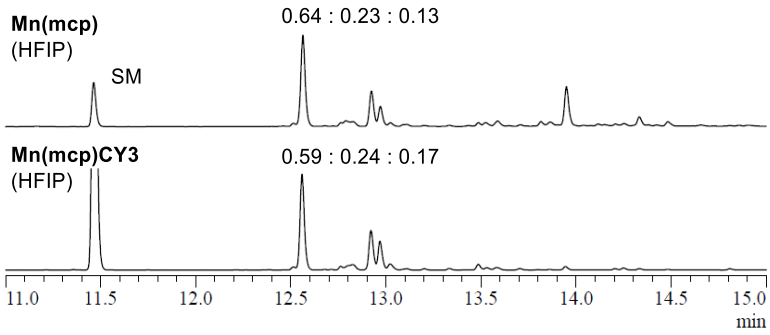

Figure 16: GC-spectra of the oxidation of **165** with **Mn(mcp)** and **Mn(mcp)CY3** in HFIP.

Next, we focused on oxidation reactions with macrocyclic catalyst **Mn(mcp)CY5** enabling the investigation of larger substrates. The first substrate studied was bicyclohexane **167**. We performed the oxidation both in MeCN and HFIP, but the former gave very diminished conversion and yields (Table 11). However, the oxidation in HFIP showed conversion of the starting material and formation of products, both with the unfunctionalized as well as with the macrocyclic catalyst (Figure 17). Therefore, the synthesis of the second macrocycle also resulted in an active catalyst. On the GC spectra, six different product signal were detected, with four of them being the major products. From an electronic point of view, it would make sense that these are the oxidation products of the four tertiary C-H bonds. However, the peaks were not assigned to the corresponding products, and the possibility cannot be excluded that the observed peaks in fact consist of several overlapping products. The selectivity difference was not very distinct. The strongest reactivity change was observed for the least intense product peak in the **Mn(mcp)** oxidation. The selectivity for this first product peak increased from 3% to 8% with **Mn(mcp)** and **Mn(mcp)CY5**, respectively. But again, the differences were too small and we did not carry out further investigation.

Table 11: Oxidation of **167** with **Mn(mcp)** and **Mn(mcp)CY5** in MeCN and HFIP.[a]

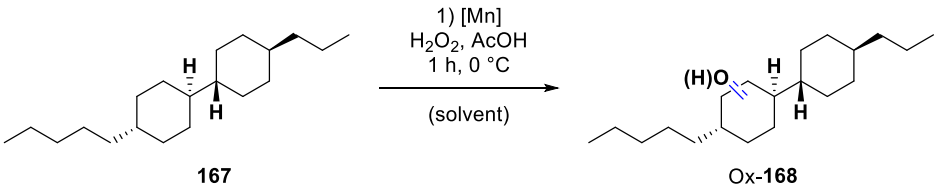

167 Ox-**168**

Entry	Cat.	Solvent	Conversion	Total Yield[b]
1	**Mn(mcp)**	MeCN	22%	4.2%
2	**Mn(mcp)CY5**	"	10%	0.9%
3	**Mn(mcp)**	HFIP	34%	34%
4	**Mn(mcp)CY5**	"	25%	18%

[a] Reactions were performed according to the *General small-scale oxidation procedure with Mn catalysts in MeCN* or *in TFE/HFIP*, respectively (see Chapter 5.3). Conversion and total yield were observed *via* GC analysis of the crude mixtures and are based on an internal standard. [b] Total yield refers to the mixture of all products.

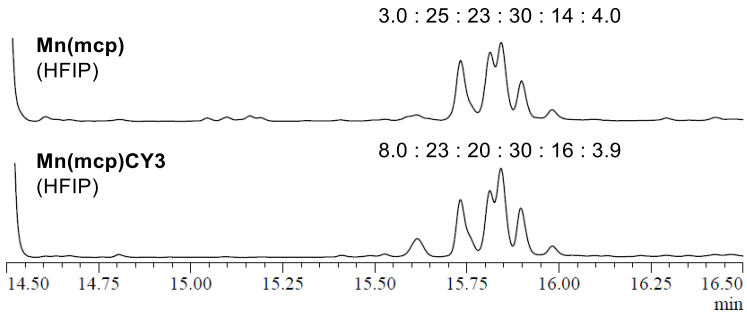

Figure 17: GC-spectra of the oxidation of **167** with **Mn(mcp)** and **Mn(mcp)CY5** in HFIP.

Finally, two steroid substrates (**169** and **171**) were oxidized. For their analysis, it was not possible to use GC due to their high molecular weights. Instead, the crude mixtures of the oxidation reactions were analyzed *via* NMR. Below the ^{13}C NMR spectra are depicted, showing that only in the case of the oxidation with unfunctionalized **Mn(mcp)** in HFIP were reasonable conversions and yields obtained (Scheme 33, Scheme 34).

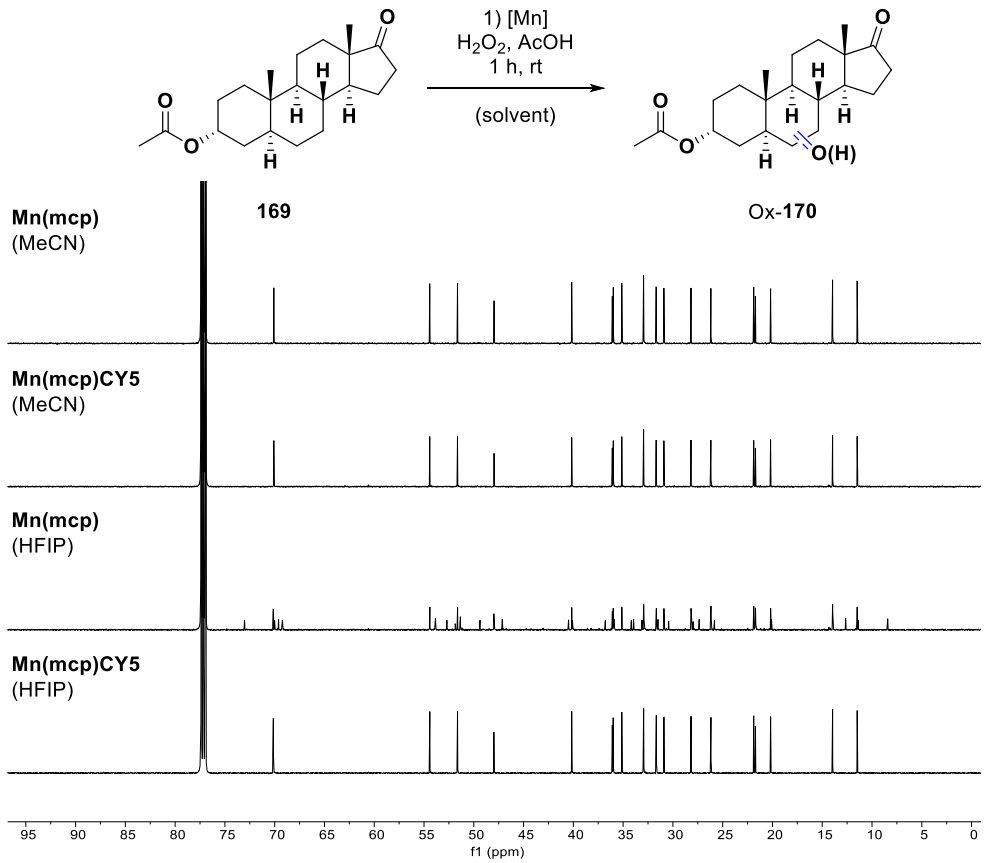

Scheme 33: Oxidation of **169** with **Mn(mcp)** and **Mn(mcp)CY5** in MeCN and HFIP. Reactions were performed according the *General small-scale oxidation procedure with Mn catalysts in MeCN* or *in TFE/HFIP*, respectively (see Chapter 5.3). Instead of GC analysis NMR was used.

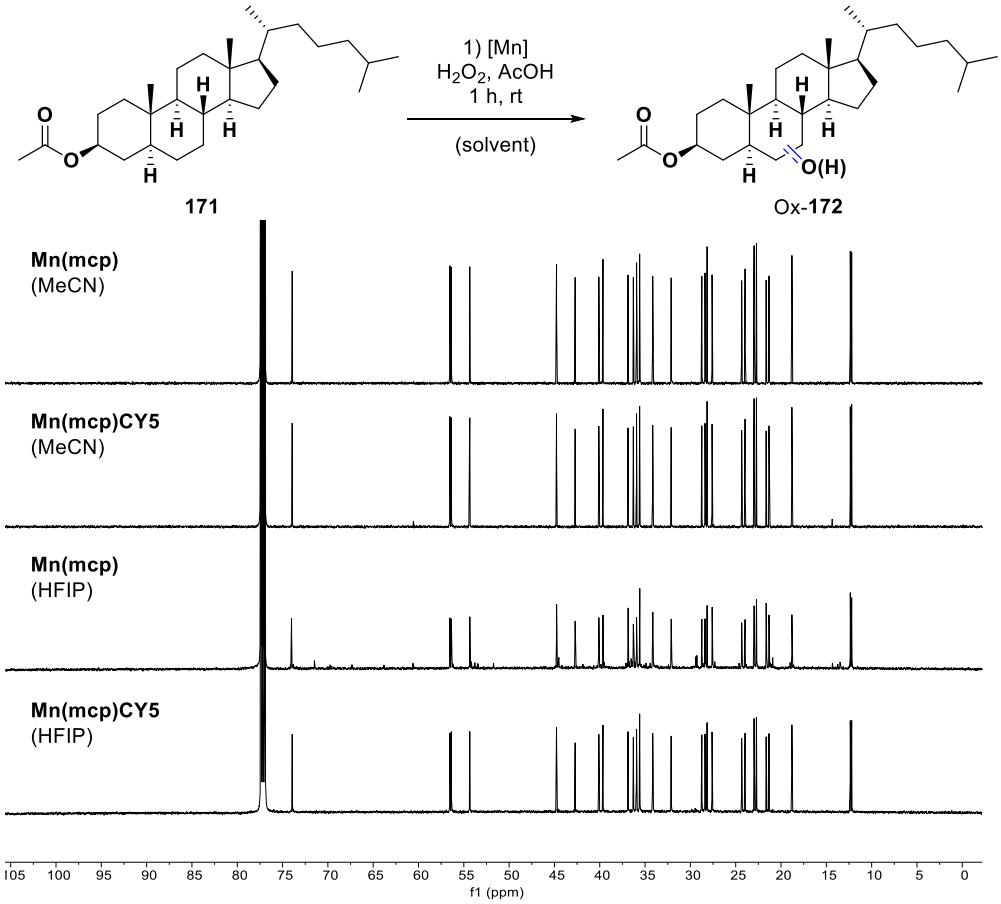

Scheme 34: Oxidation of **171** with **Mn(mcp)** and **Mn(mcp)CY5** in MeCN and HFIP. Reactions were performed according the *General small-scale oxidation procedure with Mn catalysts in MeCN* or *in TFE/HFIP*, respectively (see Chapter 5.3). Instead of GC analysis NMR was used.

4 Summary and Outlook

In recent years, the M(pdp) and M(mcp) catalysts have been shown to be very active C(sp^3)-H oxidation catalysts. Furthermore, they can be easily derivatized *via* their pyridine rings. Over the course of this dissertation, several supramolecular catalysts were obtained based on these M(pdp) and M(mcp) scaffolds. In the first part, a handful of tweezer catalysts based on glycoluril were synthesized in 10 steps each (Figure 18). First, we applied **Fe(pdp)Twe** to the oxidation of linear aliphatic ammonium salts. Similarly to the unfunctionalized catalysts, we observed product mixtures, however, with an impressive change in selectivity. The oxidation of the intrinsically *de*activated C3 and C4 positions increased distinctly. Of all catalyst versions synthesized, **Fe(pdp)Twe** gave the best selectivities for the oxidation of C3/C4. In contrast, the Mn versions, **Mn(mcp)Twe** and **Mn(pdp)Twe**, showed lower selectivities for C3. However, oxidation of the C5 positions increased and higher conversions and total yields were observed using lower amounts of catalyst. In addition to linear substrates, two ammonium substrates with terpene substitution patterns as well as two cyclohexane derivatives were investigated. In all cases, preferential oxidation of C3 or C4 was observed.

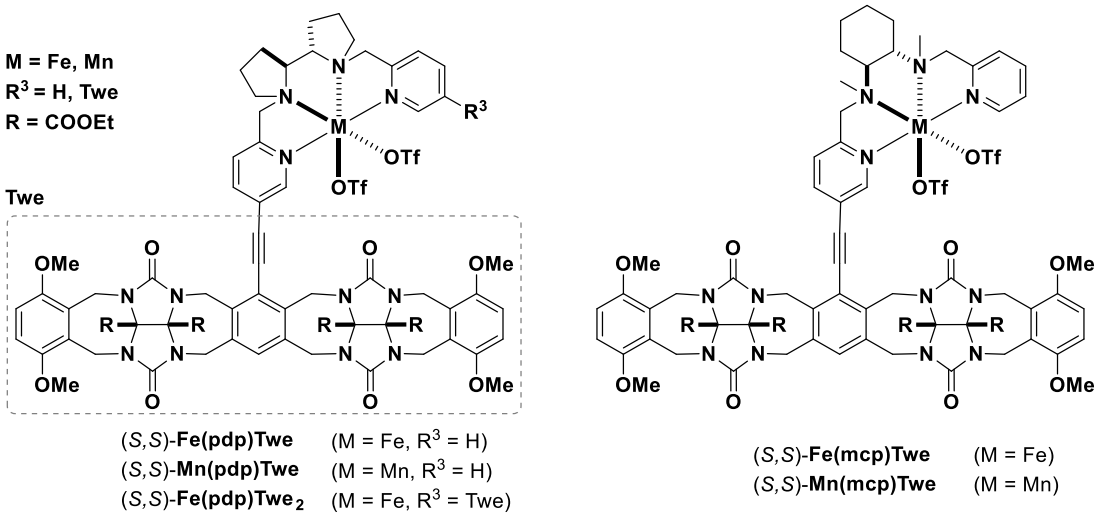

Figure 18: Overview of the tweezer-based C-H oxidation catalysts achieved during this dissertation.

In the second part, we aimed for the synthesis of supramolecular catalysts based on macrocyclic recognition sites (Figure 19). And indeed, both the **Mn(mcp)CY3** and **Mn(mcp)CY5** could be obtained in 7 steps each. We envisioned that binding might be possible in TFE and HFIP due to a solvophobic effect. Therefore, we investigated several apolar substrates lacking distinct functional handles. Unfortunately, in none of the cases was a change in selectivity observed compared to the unfunctionalized catalysts. This might be due to several reasons, including too much flexibility of the catalysts as well as of the substrates. Furthermore, the binding might be

too weak. However, due to the special solvents of interest (TFE and HFIP) and the low amount of available catalysts, we did not measure any binding constants.

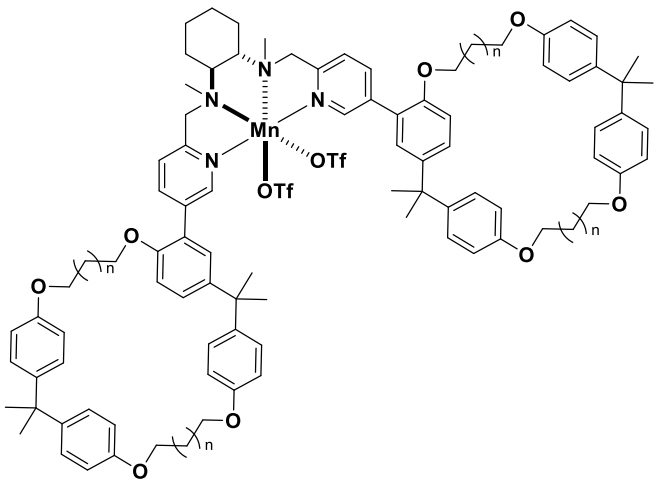

Figure 19: Overview of the macrocyclic C-H oxidation catalysts achieved during this dissertation.

However, the work done with **Mn(mcp)CY3** and **Mn(mcp)CY5** proved to be helpful in a closely related project of our group. In the course of this dissertation, Yiheng Lu started his master`s thesis aiming for the synthesis of supramolecular catalysts analogous to **Mn(mcp)CY3/CY5** but featuring different macrocycles. And indeed, the first promising results were observed, for example, in the oxidation of *n*-octane. These results present a first proof of concept of our initial assumption that selective C(sp^3)-H oxidation could be achieved *via* binding in TFE and HFIP through a solvophobic effect. The work is now continued by Yiheng Lu in a Ph.D. program in the Tiefenbacher group.

5 Experimental Section

This chapter contains only the experimental work concerning the unpublished macrocyclic project (Chapter 3.2). The supporting information on the published tweezer projects is depicted in the appendix (Chapter 10).

5.1 General Information

Experimental: Reactions were carried out under an atmosphere of argon in dried glassware unless otherwise indicated. Analytical thin-layer chromatography (TLC) was performed on Merck silica gel 60 F254 glass-backed plates, which were analyzed under UV light or after exposure to standard staining solution (basic $KMnO_4$).[245] Medium Pressure Liquid Chromatography (MPLC) was carried out with RediSep® Silica Gel Disposable Flash Columns SiO_2 columns (particle size 40-63 μm) and Al_2O_3 basic columns (particle size 40-63 μm) on a CombiFlash NextGen 300+ version 5.0.55 by Teledyne ISCO with a fraction collector version 00.92.00, detector version 11, and a pump version: 1.47. For all the runs the column type and size, flow rate [ml/min], solvent mixture, column volumes (CV) and run time [min] is given. All NMR experiments were performed on a Bruker Avance Neo and a Bruker Avance III HD NMR spectrometer operating at 500 MHz and 600 MHz proton frequency, respectively. The instruments were equipped with a direct observe 5-mm BBFO smart probe (500 MHz) or a five-channel cryogenic 5 mm QCI probe (600 MHz). All probes were equipped with actively shielded z-gradients (10 A). The experiments were performed at 300 K. Chemical shifts of ^{1}H NMR and ^{13}C NMR are given in ppm. The following solvent residual signals of the deuterated solvents were used as reference: $CDCl_3$: 7.26 ppm ($\delta^{1}H$), 77.16 ppm ($\delta^{13}C$).[246] Coupling constants (*J*) are reported in Hertz (Hz). Standard abbreviations indicating multiplicity were used as follows: br (broad), s (singlet), d (doublet), t (triplet), dd (doublet of doublets), etc., m (multiplet). Infrared spectra were measured on a Brucker Alpha IR spectrometer (ATR, attenuated total reflection). Abbreviations indicating intensity were used as follows: vs (very strong), s (strong), m (medium), w (weak), vw (very weak). Melting points were recorded on a Büchi Melting Point M-565 apparatus using open capillary tubes. GC analyses were carried out on a Shimadzu GC-2010 Plus instrument equipped with a FID (flame ionization detector) and an Rtx-5 capillary column (length = 30 m). Hydrogen was used as the carrier gas and the constant-flow mode was used (flow rate = 40 mL/min) with a split ratio of 1:20. The following temperature program was used: 60 °C for 3 min, 15 °C/min to 250 °C, and 250 °C for 5 min. The response factors of the analyzed compounds were calculated as previously reported.[236, 247] GC-MS analyses were performed on an AGLIENT 5977B GC/MSD instrument equipped with a

single quadrupole GC/MS and a HP-5MS UI capillary column (length = 30 m). Helium was used as the carrier gas and a constant-flow mode (flow rate = 1 mL/min) with a split ration of 1:100. The following temperature-program was used: 50 °C for 2.25 min, +10 °C/min to 300 °C, and 300 °C for 3 min. High-resolution mass spectra were obtained on a Thermo Scientific LTQ-FT Ultra via electrospray ionization (ESI) or a Finnigan MAT 8200 (EI) (ESI source parameters for positive polarity mode were: spray voltage, 4.0 kV; capillary temperature, 275 °C; capillary voltage, 48 V; and tube lens, –120 V).

Sources of chemicals: Anhydrous acetonitrile (MeCN), dichloromethane (CH_2Cl_2), diethyl ether (Et_2O), dimethylformamide (DMF), 1,4-dioxane, methanol (MeOH), and tetrahydrofuran (THF) were purchased from Acros Organics. Deuterated chloroform (stabilized over silver foil) ($CDCl_3$, 99.8%) was purchased from Cambridge Isotope Laboratories. Acetic acid, acetic anhydride, aluminum oxide (activated, basic, Brockmann I), biphenyl, 1-bromo-3-chloropropane, 1-bromododecane, decylamine, dichlorobis-(triphenylphosphine)palladium ($PdCl_2(PPh_3)_2$), *rac*-menthol, methanesulfonic acid (MsOH), *n*-octane, phosphorus tribromide, potassium acetate, sodium borohydride ($NaBH_4$), hydrogen peroxide water solution (50% w/w), tetra-*n*-butylammonium bromide (TBAB), *n*-tetradecane, tetrafluoroboric acid diethyl ether complex, tetrakis(triphenylphosphine)palladium ($Pd(PPh_3)_4$), tridecan-2-one, triethylamine, and trifluoroethanol (TFE) were purchased from Sigma-Aldrich. Androsterone, bisphenol A, *N*-bromosuccinimide (NBS), potassium carbonate, and potassium phosphate, tribasic were purchased from Acros Organics. 5α-Cholestan-3β-ol and potassium iodide were purchased from Alfa Aesar. Bis(pinacolato)diboron (B_2pin_2), 1-bromo-5-chloropentane, 5-bromopyridine-2-carbaldehyde, cesium carbonate, (1*S*,2*S*)-*N*,*N*'-dimethyl-1,2-cyclohexane-diamine, 1,1,1,3,3,3-hexafluoro-2-isopropanol (HFIP), and (*trans*,*trans*)-4-pentyl-4'-propyl-1,1'-bi(cyclohexane) were purchased from FluoroChem. Manganese bis(trifluoromethanesulphonate) was purchased from Apollo. Iron (II) bis (trifluoromethanesulfonate) bis (acetonitrile) was prepared according to a literature procedure.[248] Silica gel (0.040-0.063 mm, 230-400 mesh ASTM) and Celite 545 (0.02-0.1 mm) were purchased from Merck KGaA.

5.2 Synthetic porcedure

5.2.1 Ligand Synthesis

2-Bromo-4-(2-(4-hydroxyphenyl)propan-2-yl)phenol (144)

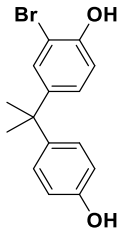

$C_{15}H_{15}BrO_2$
MW: 307.19 g/mol

According to a previously reported method,[241] a one-neck 500 mL round-round bottom flask was charged with bisphenol A (**128**, 30.3 g, 133 mmol, 2.95 equiv.) and dissolved in anhydrous MeCN (115 mL). NBS (8.01 g, 45.0 mmol, 1.0 equiv.) and $MeSO_3H$ (2.83 mL, 4.20 g, 43.6 mmol, 0.97 equiv.) were added and the mixture was stirred at room temperature for 22 h. After this time, water (150 mL) was added and the mixture was extracted with EtOAc (3 x 150 mL). The combined organic layers were washed with brine (100 mL), dried (Na_2SO_4), filtered, and concentrated under reduced pressure. The crude material was purified by MPLC (RediSep® Column: Silica 3 x 80 g; 80 ml/min; CH_2Cl_2/CH_2Cl_2:MeOH (9:1) 100:0 to 0:100, 20.7 CV, 29.4 min) to obtain **144** (8.61 g, 28.0 mmol, 62%) as a colorless oil.

TLC *R*f = 0.18 (CyHex/EtOAc = 4/1) [UV, KMnO4].

^{1}H NMR ($CDCl_3$, 600 MHz, 300 K) δ [ppm] = 7.31 (d, *J* = 2.3 Hz, 1H), 7.10 – 7.06 (m, 2H), 7.04 (dd, *J* = 8.5, 2.3 Hz, 1H), 6.90 (d, *J* = 8.6 Hz, 1H), 6.76 – 6.71 (m, 2H), 5.35 (s, 1H), 4.57 (s, 1H), 1.61 (s, 6H).

The spectroscopic data matches the data reported in the literature.[241]

4-(2-(3-Bromo-4-(3-chloropropoxy)phenyl)propan-2-yl)phenol (145)

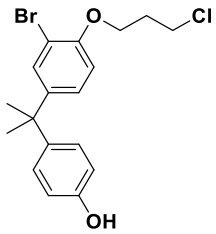

$C_{18}H_{20}BrClO_2$
MW: 383.71 g/mol

A one-neck 25 mL round-bottom flask was charged with 2-bromo-4-(2-(4-hydroxyphenyl)propan-2-yl)phenol (**144**) (922 mg, 3.00 mmol, 1.0 equiv.) and 1-bromo-3-chloropropane (**130**) (296 µL, 472 mg, 3.00 mmol, 1.0 equiv.). The starting materials were dissolved in anhydrous DMF (3 mL) followed by the addition of K_2CO_3 (456 mg, 3.30 mmol,

1.1 equiv.) at 0 °C. The mixture was allowed to reach room temperature and was stirred at this temperature for 16 h. Next, water (40 mL) and EtOAc (20 mL) were added, the two layers were separated, and the aqueous layer was extracted with EtOAc (3 x 20 mL). The combined organic layers were washed with brine (20 mL), dried (Na_2SO_4), filtered and the solvent removed under reduced pressure. The crude material was purified by MPLC (RediSep® Column: Silica 40 g; 60 ml/min; CyHex/EtOAc 100:0 to 80:20 to 0:100, 14.2 CV, 13 min) to obtain **145** (856 mg, 2.23 mmol, 74%) as a colorless oil.

TLC *R*f = 0.29 (CyHex/EtOAc = 4/1) [UV, KMnO4].

IR (ATR): ṽ (cm-1) = 3356 (brw), 3032 (vw), 2966 (m), 2872 (w), 1703 (w), 1610 (w), 1597 (w), 1565 (m), 1509 (m), 1499 (m), 1488 (w), 1467 (w), 1442 (w), 1387 (w), 1362 (w), 1289 (m), 1249 (s), 1177 (m), 1104 (w), 1087 (w) 1049 (m), 1015 (w), 950 (w), 882 (w), 830 (m) 812 (m), 764 (w), 731 (w), 719 (w), 689 (w), 657 (w), 610 (w), 577 (m), 556 (w), 436 (w).

^{1}H NMR ($CDCl_3$, 500 MHz, 300 K) δ [ppm] = 7.41 (d, *J* = 2.3 Hz, 1H), 7.08 (dd, *J* = 8.7, 2.4 Hz, 3H), 6.80 (d, *J* = 8.6 Hz, 1H), 6.77 – 6.68 (m, 2H), 4.69 (d, *J* = 1.7 Hz, 1H), 4.14 (t, *J* = 5.7 Hz, 2H), 3.81 (t, *J* = 6.3 Hz, 2H), 2.55 – 2.10 (m, 2H), 1.62 (s, 6H).

^{13}C NMR ($CDCl_3$, 126 MHz, 300 K) δ [ppm] = 153.5 (s), 153.0 (s), 145.3 (s), 142.7 (s), 131.7 (s), 128.0 (s), 127.0 (s), 115.0 (s), 112.9 (s), 112.0 (s), 65.6 (s), 41.9 (s), 41.7 (s), 32.4 (s), 31.1 (s).

HRMS (ESI): $C_{18}H_{20}BrClO_2$ calculated: $[(M - H)^-]$: 381.0262

found: $[(M - H)^-]$: 381.0268.

2-Bromo-1-(3-chloropropoxy)-4-(2-(4-(3-chloropropoxy)phenyl)propan-2-yl)benzene (146)

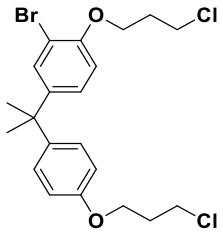

$C_{21}H_{25}BrCl_2O_2$
MW: 460.23 g/mol

A one-neck 25 mL round-bottom flask was charged with 2-bromo-4-(2-(4-hydroxyphenyl)propan-2-yl)phenol (**144**) (2.70 g, 8.80 mmol, 1.0 equiv.) and 1-bromo-3-chloropropane (**130**) (1.82 mL, 2.91 g, 18.5 mmol, 2.1 equiv.). The starting materials were dissolved in anhydrous DMF (8.8 mL) followed by the addition of K_2CO_3 (2.68 g, 19.4 mmol,

2.2 equiv.) at 0 °C. The mixture was allowed to reach room temperature and was stirred at this temperature for 16 h. Next, water (40 mL) and EtOAc (20 mL) were added, the two layers were separated, and the aqueous layer was extracted with EtOAc (3 x 20 mL). The combined organic layers were washed with brine (20 mL), dried (Na_2SO_4), filtered and the solvent removed under reduced pressure. The crude material was purified by MPLC (RediSep® Column: Silica 40 g; 60 ml/min; CyHex/EtOAc 100:0 to 89:11, 7.7 CV, 7.1 min) to obtain **146** (2.98 g, 6.48 mmol, 74%) as a colorless oil.

TLC *R*f = 0.57 (CyHex/EtOAc = 4/1) [UV, KMnO4].

IR (ATR): ṽ (cm-1) = 3036 (vw), 2965 (w), 2873 (w), 1736 (w), 1607 (w), 1581 (w), 1509 (s), 1490 (s), 1468 (m), 1444 (m), 1421 (w), 1387 (m), 1362 (w), 1290 (m), 1245 (vs), 1182 (s), 1142 (w), 1110 (w), 1089 (w), 1048 (s), 948 (m), 883 (w), 829 (s), 811 (m), 751 (w), 732 (w), 720 (m), 694 (m), 652 (m), 589 (m), 562 (m), 513 (m), 464 (m), 437 (w).

^{1}H NMR ($CDCl_3$, 600 MHz, 300 K) δ [ppm] = 7.41 (d, *J* = 2.4 Hz, 1H), 7.14 – 7.10 (m, 2H), 7.07 (dd, *J* = 8.6, 2.4 Hz, 1H), 6.81 (*virt.* dd, *J* = 8.8, 7.0 Hz, 3H), 4.14 (t, *J* = 5.7 Hz, 2H), 4.09 (t, *J* = 5.8 Hz, 2H), 3.81 (t, *J* = 6.3 Hz, 2H), 3.74 (t, *J* = 6.3 Hz, 2H), 2.27 (p, *J* = 6.2 Hz, 2H) 2.22 (p, *J* = 6.2 Hz, 2H), 1.62 (s, 6H).

^{13}C NMR ($CDCl_3$, 151 MHz, 300 K) δ [ppm] = 156.8 (s), 152.9 (s), 145.2 (s), 142.7 (s), 131.7 (s), 127.8 (s), 127.0 (s), 114.1 (s), 112.9 (s), 111.9 (s), 65.5 (s), 64.3 (s), 41.9 (s), 41.7 (s), 41.7 (s), 32.5 (s), 32.3 (s), 31.1 (s).

HRMS (ESI): $C_{21}H_{25}BrCl_2O_2$

calculated: $[(M + Ag)^+]$: 564.9460

found: $[(M + Ag)^+]$: 564.9450.

Macrocycle CY3Br$_2$

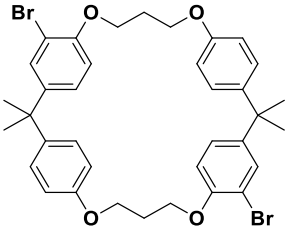

$C_{36}H_{38}Br_2O_4$
MW: 694.50 g/mol

A one-neck 2 L round-bottom flask was charged with compound **145** (384 mg, 1.00 mmol, 2.0 equiv.). The starting material was dissolved in anhydrous MeCN (200 mL), followed by the addition of Cs_2CO_3 (489 mg, 1.50 mmol, 3.0 equiv.) and KI (16.6 mg, 100 µmol, 0.2 equiv.).

The reaction mixture was then stirred at reflux for 2 d. After this time, the solvent was removed under reduced pressure, and water (100 mL) and EtOAc (60 mL) were added. The two layers were separated, and the aqueous layer was extracted with EtOAc (3 x 60 mL). The combined organic layers were washed with brine (100 mL), dried (Na_2SO_4), filtered and the solvent removed under reduced pressure. The crude material was purified by MPLC (RediSep® Column: Silica 12 g; 30 ml/min; CyHex/EtOAc 100:0 to 85:15 to 0:100, 23.5 CV, 13.9 min) to obtain **CY3Br2** (138 mg, 199 μmol, 40%) as a white solid.

TLC *R*f = 0.50 (CyHex/EtOAc = 4/1) [UV, KMnO4].

M.P.: 202 - 204°C.

IR (ATR): ṽ (cm-1) = 3031 (w), 2966 (w), 2930 (w), 2873 (w), 1738 (w), 1601 (w), 1566 (w), 1507 (m), 1489 (m), 1460 (m), 1420 (w), 1393 (w), 11361 (w), 1291 (m), 1249 (s), 1222 (m), 1213 (m), 1177 (m), 1113 (w), 1082 (w), 1056 (m), 1039 (m), 1012 (w), 985 (m), 967 (m), 923 (w), 902 (w), 887 (w), 853 (m), 828 (m), 812 (w), 777 (w), 760 (w), 731 (w), 717 (w), 685 (w), 654 (w), 613 (w), 601 (w), 590 (w), 524 (w), 498 (w), 438 (w).

^{1}H NMR ($CDCl_3$, 500 MHz, 300 K) δ [ppm] = 7.35 (d, *J* = 2.4 Hz, 2H), 7.10 – 7.02 (m, 4H), 6.92 (dd, *J* = 8.6, 2.4 Hz, 2H), 6.80 – 6.73 (m, 4H), 6.70 (d, *J* = 8.6 Hz, 2H), 4.21 (t, *J* = 5.5 Hz, 4H), 4.18 (t, *J* = 5.6 Hz, 4H), 2.21 (p, *J* = 5.5 Hz, 4H), 1.62 (s, 12H).

^{13}C NMR ($CDCl_3$, 151 MHz, 300 K) δ [ppm] = 157.2 (s), 153.4 (s), 145.3 (s), 142.3 (s), 131.2 (s), 127.5 (s), 126.8 (s), 114.8 (s), 114.3 (s), 112.4 (s), 76.9 (s), 65.9 (s), 64.2 (s), 41.5 (s), 30.4 (s), 29.8 (s).

HRMS (ESI): $C_{36}H_{38}Br_2O_4$ calculated: $[(M + Na)^+]$: 715.1029

found: $[(M + Na)^+]$: 715.1026.

Macrocycle CY3Br

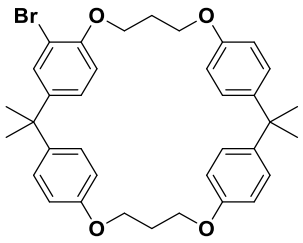

$C_{36}H_{39}BrO_4$
MW: 615.61 g/mol

A one-neck 2 L round-bottom flask was charged with compound **146** (1.38 g, 3.00 mmol, 1.0 equiv.) and bisphenol A (**128**) (685 mg, 3.00 mmol, 1.0 equiv.). The starting materials were dissolved in anhydrous MeCN (600 mL), followed by the addition of Cs_2CO_3 (2.93 g,

9.00 mmol, 3.0 equiv.) and KI (99.6 mg, 600 µmol, 0.2 equiv.). The reaction mixture was then stirred at reflux for 2 d. After this time, the solvent was removed under reduced pressure, and water (150 mL) and EtOAc (150 mL) were added. The two layers were separated, and the aqueous layer was extracted with EtOAc (3 x 100 mL). The combined organic layers were washed with brine (100 mL), dried (Na_2SO_4), filtered and the solvent removed under reduced pressure. The crude material was purified by MPLC (RediSep® Column: Silica 40 g; 60 ml/min; CyHex/EtOAc 100:0 to 90:10, 17.8 CV, 16.3 min) to obtain **CY3Br** (795 mg, 1.29 mmol, 43%) as a white solid.

TLC *R*f = 0.51 (CyHex/EtOAc = 4/1) [UV, KMnO4].

M.P.: 164 – 166 °C.

IR (ATR): ṽ (cm-1) = 3059 (vw), 3034 (vw), 2938 (w), 2931 (w), 2874 (w), 1606 (w), 1581 (w), 1507 (s), 1489 (m), 1467 (m), 1420 (w), 1398 (w), 1380 (m), 1461 (w), 1297 (m), 1245 (s), 1228 (vs), 1183 (s), 1111 (m), 1087 (m), 1065 (s), 1046 (m), 1010 (m), 988 (m), 968 (m), 885 (w), 826 (vs), 808 (s), 769 (w), 735 (m), 692 (m) 666 (m), 653 (w), 617 (m), 601 (m), 577 (s), 553 (m), 537 (m), 439 (w).

^{1}H NMR ($CDCl_3$, 600 MHz, 300 K) δ [ppm] = 7.38 (d, *J* = 2.4 Hz, 1H), 7.07 (*virt.* dd, *J* = 12.2, 8.8 Hz, 6H), 6.92 (dd, *J* = 8.6, 2.4 Hz, 1H), 6.79 – 6.66 (m, 7H), 4.18 (q, *J* = 5.5 Hz, 4H), 4.13 (q, *J* = 5.6 Hz, 4H), 2.20 (p, *J* = 5.5 Hz, 2H), 2.16 (p, *J* = 5.5 Hz, 2H), 1.64 (s, 6H), 1.62 (s, 6H).

^{13}C NMR ($CDCl_3$, 151 MHz, 300 K) δ [ppm] = 157.2 (s), 157.0 (s), 157.0 (s), 153.4 (s), 145.2 (s), 143.4 (s), 143.3 (s), 142.4 (s), 131.2 (s), 127.5 (s), 127.5 (s), 127.5 (s), 126.9 (s), 114.8 (s), 114.7 (s), 114.7 (s), 114.1 (s), 112.3 (s), 65.9 (s), 64.6 (s), 64.5 (s), 64.4 (s), 41.5 (s), 41.4 (s), 30.4 (s), 30.4 (s), 29.9 (s), 29.8 (s).

HRMS (ESI): $C_{36}H_{39}BrO_4$ calculated: $[(M + Ag)^+]$: 721.1077.

found: $[(M + Ag)^+]$: 721.1077.

Macrocycle 148

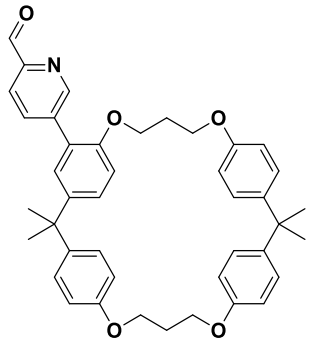

$C_{42}H_{43}NO_5$
MW: 641.81 g/mol

Step A): 5-Bromopyridine-2-carbaldehyde (**129**, 558 mg, 3.00 mmol, 1.0 eq.), B_2pin_2 (838 mg, 3.30 mmol, 1.1 eq.), $PdCl_2(PPh_3)_2$ (105 mg, 150 µmol, 0.05 eq.) and KOAc (972 mg, 9.90 mmol, 3.3 eq.) were dissolved in degassed, anhydrous 1,4-dioxane (10 mL). The reaction mixture was stirred at 80 °C overnight. After cooling down to room temperature, the mixture was filtered over Celite and washed with CH_2Cl_2 (50 mL). The filtrate was concentrated under reduced pressure to give a dark oil. The purity of the crude product **147** (53%) was determined *via* NMR using vinyltrimethylsilane as an external standard. The material was then submitted to the next reaction without further purification (*Note:* Purification from the byproduct *via* column chromatography was not successful.)

Step B): A one-neck 25 mL round-bottom flask was charged with macrocycle **CY3Br** (246 mg, 400 µmol, 1.0 equiv.), compound **147** (53%, 246 mg, 560 µmol, 1.4 equiv.), $Pd(PPh_3)_4$ (37 mg, 32.0 µmol, 8 mol%) and K_3PO_4 (340 mg, 1.60 mmol, 4.0 equiv.). The compounds were dissolved in a mixture of degassed DMF/water (9/1) (8 mL) and stirred at 60 °C for 24 h. Next, the reaction mixture was filtered over Celite and washed with CH_2Cl_2 (20 mL). The solvents were removed under reduced pressure and the crude material was purified by MPLC (RediSep® Column: Silica 12 g; 30 ml/min; CyHex/EtOAc 100:0 to 80:20, 26.4 CV, 15.6 min) to obtain **148** (109 mg, 170 µmol, 43%) as an off-white solid.

TLC *R*f = 0.37 (CyHex/EtOAc = 4/1) [UV, KMnO4].

M.P.: 94 – 95 °C.

IR (ATR): ṽ (cm-1) = 3035 (vw), 2963 (w), 2933 (w), 2872 (w), 1708 (m), 1606 (m), 1581 (w), 1507 (vs), 1468 (m), 1383 (w), 1362 (w), 1293 (m), 1246 (s), 1228 (s), 1180 (s), 1113 (w), 1084 (w), 1051 (m), 1013 (m), 987 (m), 900 (vw), 828 (vs), 766 (w), 736 (m), 721 (m), 694 (w), 636 (w), 622 (w), 578 (m), 555 (m), 519 (w), 456 (w), 417 (w).

^{1}H NMR ($CDCl_3$, 600 MHz, 300 K) δ [ppm] = 10.12 (d, *J* = 0.8 Hz, 1H), 8.80 (dd, *J* = 2.1, 0.9 Hz, 1H), 7.84 (dd, *J* = 8.1, 0.9 Hz, 1H), 7.67 (ddd, *J* = 8.0, 2.1, 0.8 Hz, 1H), 7.15 (dd, *J* = 8.7, 2.5 Hz, 1H), 7.14 – 7.06 (m, 5H), 7.04 – 6.97 (m, 2H), 6.86 (d, *J* = 8.7 Hz, 1H), 6.82 – 6.75 (m, 2H), 6.75 – 6.70 (m, 2H), 6.57 – 6.50 (m, 2H), 4.15 (td, *J* = 5.5, 2.6 Hz, 4H), 4.12 (t, *J* = 5.6 Hz, 2H), 3.93 (t, *J* = 5.5 Hz, 2H), 2.17 (p, *J* = 5.5 Hz, 2H), 2.10 (p, *J* = 5.5 Hz, 2H), 1.68 (s, 6H), 1.64 (s, 6H).

^{13}C NMR ($CDCl_3$, 151 MHz, 300 K) δ [ppm] = 193.5 (s), 157.3 (s), 157.1 (s), 156.8 (s), 154.2 (s), 150.9 (s), 150.8 (s), 144.3 (s), 143.4 (s), 143.2 (s), 142.5 (s), 139.3 (s), 137.6 (s), 129.0 (s), 128.5 (s), 127.6 (s), 127.5 (s), 127.4 (s), 125.9 (s), 121.3 (s), 114.8 (s), 114.6 (s), 114.2 (s), 113.3 (s), 65.2 (s), 64.7 (s), 64.4 (s), 64.0 (s), 41.6 (s), 41.3 (s), 30.4 (s), 30.3 (s), 29.9 (s), 29.4 (s).

HRMS (ESI): $C_{42}H_{43}NO_5$ calculated: $[(M + H)^+]$: 642.3214

found: $[(M + H)^+]$: 642.3215.

Macrocycle 149

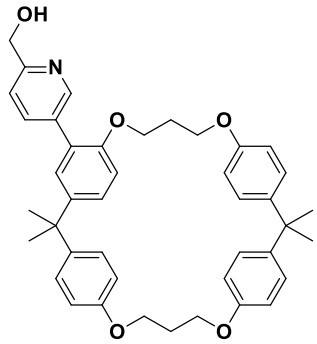

$C_{42}H_{45}NO_5$
MW: 643.82 g/mol

Compound **148** (257 mg, 400 µmol, 1.0 equiv.) was dissolved in a mixture of anhydrous MeOH and CH_2Cl_2 (1:1, 20 mL). Then, $NaBH_4$ (15.1 mg, 37.8 µmol, 1.0 equiv.) was added at 0 °C and the mixture was stirred for 3 h at room temperature. The reaction mixture was diluted with CH_2Cl_2 (20 mL), neutralized by the addition of water (10 mL), and then extracted with CH_2Cl_2 (3 × 15 mL). The combined organic layers were washed with brine (15 mL), dried (Na_2SO_4), filtered, and concentrated under reduced pressure and the crude material was purified by MPLC (RediSep® Column: Silica 12 g; 30 ml/min; CyHex/EtOAc 100:0 to 0:100, 12.3 CV, 7.3 min) to obtain **149** (240 mg, 373 µmol, 83%) as an off-white solid.

TLC *R*f = 0.25 (CyHex/EtOAc = 1/1) [UV, KMnO4].

M.P.: 73 – 74 °C.

IR (ATR): ṽ (cm-1) = 3033 (vw), 2964 (w), 2933 (w), 2873 (w), 1734 (w), 1606 (w) 1580 (w), 1506 (s), 1485 (m), 1468 (m), 1382 (w), 1362 (w), 1297 (m), 1245 (s), 1227 (s), 1180 (s), 1111 (w), 1049 (s), 1013 (m), 987 (m), 967 (m), 896 (w), 828 (vs), 769 (w), 734 (w), 652 (w), 633 (w), 574 (m), 553 (m), 484 (w), 465 (w), 407 (w).

^{1}H NMR ($CDCl_3$, 500 MHz, 300 K) δ [ppm] = 8.95 – 8.11 (m, 1H), 7.59 (dd, *J* = 8.0, 2.2 Hz, 1H), 7.19 – 6.99 (m, 9H), 6.82 (d, *J*= 9.3 Hz, 1H), 6.77 (d, *J* = 8.8 Hz, 2H), 6.72 (d, *J* = 8.8 Hz, 2H), 6.61 – 6.53 (m, 2H), 4.79 (d, *J* = 4.2 Hz, 2H), 4.28 – 4.06 (m, 7H), 3.96 (t, *J* = 5.5 Hz, 2H), 3.72 (t, *J* = 5.1 Hz, 1H), 2.16 (p, *J* = 5.5 Hz, 2H), 2.09 (p, *J* = 5.5 Hz, 2H), 1.67 (s, 6H), 1.64 (s, 6H).

^{13}C NMR ($CDCl_3$, 126 MHz, 300 K) δ [ppm] = 157.3 (s), 157.1 (s), 157.0 (s), 156.8 (s), 154.1 (s), 149.0 (s), 144.1 (s), 143.5 (s), 143.2 (s), 142.8 (s), 137.7 (s), 133.6 (s), 128.9 (s), 127.6 (s), 127.6 (s), 127.5 (s), 127.4 (s), 126.8 (s), 119.6 (s), 114.8 (s), 114.7 (s), 114.4 (s), 113.2 (s), 65.2 (s), 64.9 (s), 64.5 (s), 64.2 (s), 64.2 (s), 41.6 (s), 41.4 (s), 30.5 (s), 30.4 (s), 29.9 (s), 29.6 (s).

HRMS (ESI): $C_{42}H_{45}NO_5$ calculated: $[(M + Na)^+]$: 666.3190

found: $[(M + Na)^+]$: 666.3189.

Macrocycle 150

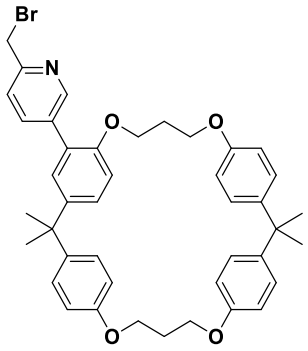

$C_{42}H_{44}BrNO_4$
MW: 706.72 g/mol

Compound **149** (235 mg, 365 µmol, 1.0 equiv.) was dissolved in anhydrous CH_2Cl_2 (4.6 mL) and cooled to 0 °C. After dropwise addition of PBr_3 (34.3 µL, 98.8 mg, 365 µmol, 1.0 equiv.) and stirring for 1 h at 0 °C, the mixture was allowed to reach room temperature and was stirred for 16 h. Next, CH_2Cl_2 (20 mL) and saturated aqueous $NaHCO_3$ solution (20 mL) were added, and the two layers were separated. The aqueous layer was extracted with CH_2Cl_2 (3 x 15 mL) and the combined organic layers were washed with brine (15 mL), dried (Na_2SO_4), filtered, and concentrated under reduced pressure. The crude material was purified by MPLC (RediSep® Column: Silica 4 g; 13 ml/min; CyHex/EtOAc 100:0 to 45:55, 15.9 CV, 7.5 min) to obtain **150** (198 mg, 280 µmol, 77%) as a pinkish solid.

TLC *R*f = 0.37 (CyHex/EtOAc = 4/1) [UV, KMnO4].

M.P.: 171 – 172 °C.

IR (ATR): ṽ (cm-1) = 3034 (vw), 2962 (w), 2929 (w), 2872 (w), 1606 (w), 1579 (w), 1506 (s), 1468 (m), 1383 (w), 1362 (w), 1297 (w), 1245 (s), 1227 (s), 1179 (s), 1108 (w), 1083 (w), 1050 (m), 1012 (m), 986 (m), 827 (vs), 731 (m), 633 (w), 608 (w), 568 (m), 553 (m), 481 (w), 454 (w), 407 (w).

^{1}H NMR ($CDCl_3$, 600 MHz, 300 K) δ [ppm] = 8.62 (d, *J* = 2.3 Hz, 1H), 7.56 (dd, *J* = 8.0, 2.2 Hz, 1H), 7.33 (d, *J* = 8.0 Hz, 1H), 7.11 (d, *J* = 8.7 Hz, 2H), 7.10 – 7.06 (m, 4H), 7.04 (d, *J* = 8.7 Hz, 2H), 6.82 (d, *J* = 8.5 Hz, 1H), 6.77 (d, *J* = 8.7 Hz, 2H), 6.73 (d, *J* = 8.7 Hz, 2H), 6.57 (d, *J* = 8.7 Hz, 2H), 4.61 (s, 2H), 4.14 (*virt.* dq, *J* = 11.2, 5.6 Hz, 6H), 3.96 (t, *J* = 5.5 Hz, 2H), 2.16 (p, *J* = 5.5 Hz, 2H), 2.10 (p, *J* = 5.5 Hz, 2H), 1.67 (s, 6H), 1.64 (s, 6H).

^{13}C NMR ($CDCl_3$, 151 MHz, 300 K) δ [ppm] = 157.2 (s), 157.1 (s), 156.9 (s), 154.1 (s), 149.4 (s), 144.2 (s), 143.4 (s), 143.2 (s), 142.6 (s), 138.5 (s), 134.6 (s), 128.8 (s), 128.0 (s), 127.6 (s), 127.4 (s), 125.9 (s), 123.1 (s), 114.8 (s), 114.6 (s), 114.3 (s), 113.2 (s), 77.4 (s), 77.2 (s), 76.9 (s), 65.2 (s), 64.8 (s), 64.4 (s), 64.0 (s), 41.6 (s), 41.3 (s), 33.2 (s), 30.4 (s), 30.3 (s), 29.9 (s), 29.5 (s).

HRMS (ESI): $C_{42}H_{44}BrNO_4$ calculated: $[(M + H)^+]$: 706.2526

found: $[(M + H)^+]$: 706.2537.

Ligand (mcp)CY3

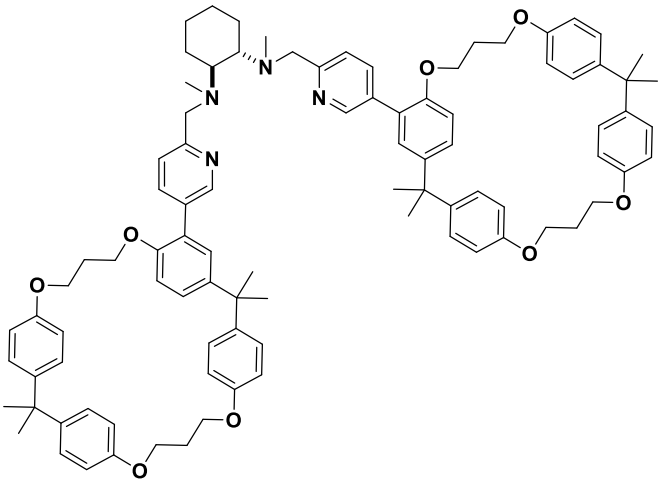

$C_{92}H_{104}N_4O_8$
MW: 1393.86 g/mol

Benzyl bromide **150** (50.9 mg, 72.0 µmol, 2.05 equiv.) and (2*S*,2'*S*)-N^1,N^2-dimethylcyclohexane-1,2-diamine (**132**, 4.99 mg, 35.1 µmol, 1.0 equiv.) were dissolved in anhydrous MeCN (1.8 mL). Then, K_2CO_3 (19.4 mg, 140 µmol, 4.0 equiv.) and TBAB

(0.57 mg, 1.76 μmol, 0.05 equiv.) were added and the reaction mixture was stirred at reflux for 16 h. Thereafter, the mixture was cooled down to room temperature, filtered and the residue was washed with CH_2Cl_2 (10 mL). The filtrate was concentrated under reduced pressure, 1 m NaOH (10 mL) was added and the mixture was extracted with CH_2Cl_2 (3 ×10 mL). The combined organic layers were washed with brine (10 mL), dried (Na_2SO_4), filtered, and concentrated by rotatory evaporation. The crude compound was purified *via* flash column chromatography (10 g SiO_2, CH_2Cl_2/MeOH/NH_4OH = 93/5/2) to obtain the desired product **(mcp)CY3** (35.0 mg, 25.1 μmol, 72%) as a yellow solid.

TLC R_f = 0.22 (CH_2Cl_2/MeOH/NH_4OH = 93/5/2) [UV, $KMnO_4$].

M.P.: 114 – 116 °C.

IR (ATR): $\tilde{\nu}$ (cm^{-1}) = 3034 (vw), 2962 (w), 2928 (w), 2876 (w), 1607 (w), 1579 (w), 1507 (s), 1468 (m), 1382 (w), 1362 (w), 1297 (w), 1246 (s), 1227 (s), 1180 (s), 1113 (w), 1083 (w), 1051 (m), 1014 (w), 987 (m), 882 (w), 828 (vs), 766 (w), 734 (w), 640 (w), 554 (m), 521 (w), 471 (w), 414 (w).

^{1}H NMR ($CDCl_3$, 500 MHz, 300 K) δ [ppm] = 8.57 (dd, *J* = 2.0, 1.0 Hz, 2H), 7.68 – 7.53 (m, 4H), 7.18 (d, *J* = 2.5 Hz, 2H), 7.12 – 7.09 (m, 4H), 7.07 – 7.01 (m, 8H), 6.97 (dd, *J* = 8.7, 2.5 Hz, 2H), 6.78 (d, *J* = 8.7 Hz, 2H), 6.78 – 6.72 (m, 4H), 6.73 – 6.69 (m, 4H), 6.62 – 6.58 (m, 4H), 4.17 – 4.07 (m, 12H), 4.06 – 3.89 (m, 8H), 2.78 – 2.64 (m, 2H), 2.38 (s, 6H), 2.15 (p, *J* = 5.4 Hz, 4H), 2.10 – 1.97 (m, 6H), 1.82 – 1.76 (m, 2H), 1.66 (s, 12H), 1.62 (s, 12H), 1.41 – 1.31 (m, 2H), 1.22 – 1.14 (m, 2H).

^{13}C NMR ($CDCl_3$, 126 MHz, 300 K) δ [ppm] = 159.4 (s), 157.1 (s), 157.1 (s), 156.9 (s), 154.1 (s), 149.3 (s), 144.0 (s), 143.3 (s), 143.2 (s), 142.8 (s), 137.4 (s), 132.7 (s), 128.5 (s), 127.8 (s), 127.6 (s), 127.4 (s), 127.1 (s), 122.0 (s), 114.8 (s), 114.6 (s), 114.5 (s), 113.4 (s), 65.3 (s), 64.7 (s), 64.3 (s), 64.2 (s), 61.1 (s), 41.5 (s), 41.4 (s), 36.9 (s), 30.5 (s), 30.3 (s), 29.9 (s), 29.7 (s), 26.9 (s), 26.0 (s).

HRMS (ESI): $C_{92}H_{104}N_4O_8$ calculated: $[(M + Na)^+]$: 1414.7746

found: $[(M + Na)^+]$: 1415.7750.

2-Bromo-1-(3-chloropropoxy)-4-(2-(4-(3-chloropropoxy)phenyl)propan-2-yl)benzene (151)

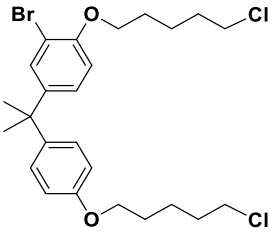

$C_{25}H_{33}BrCl_2O_2$
MW: 516.34 g/mol

A one-neck 50 mL round-bottom flask was charged with 2-bromo-4-(2-(4-hydroxyphenyl)propan-2-yl)phenol (**144**) (3.99 g, 13.0 mmol, 1.0 equiv.) and 1-bromo-5-chloropentane (**131**) (5.06 g, 27.3 mmol, 2.1 equiv.). The starting materials were dissolved in anhydrous DMF (13 mL) followed by the addition of K_2CO_3 (2.43 g, 28.6 mmol, 2.2 equiv.) at 0 °C. The mixture was allowed to reach room temperature and was stirred at this temperature for 16 h. Next, water (150 mL) and EtOAc (50 mL) were added, the two layers were separated, and the aqueous layer was extracted with EtOAc (3 x 50 mL). The combined organic layers were washed with brine (50 mL), dried (Na_2SO_4), filtered and the solvent removed under reduced pressure. The crude material was purified by MPLC (RediSep® Column: Silica 40 g; 60 ml/min; CyHex/EtOAc 100:0 to 90:10, 8.9 CV, 8.1 min) to obtain **151** (4.82 g, 9.33 mmol, 72%) as a colorless oil which solidified to a white solid upon storage.

TLC *R*f = 0.59 (CyHex/EtOAc = 4/1) [UV, KMnO4].

IR (ATR): $\tilde{\nu}$ (cm^{-1}) = 3036 (vw), 2941 (m), 2868 (m), 1737 (w), 1607 (m), 1580 (w), 1509 (s), 1490 (s), 1470 (m), 1389 (m), 1362 (w), 1287 (s), 1246 (vs), 1182 (s), 1110 (w), 1046 (s), 1013 (m), 919 (w), 882 (w). 829 (s), 810 (s), 732 (m), 719 (m), 692 (w), 650 (m), 614 (w), 591 (w), 563 (w), 437 (w).

^{1}H NMR ($CDCl_3$, 600 MHz, 300 K) δ [ppm] = 7.40 (d, *J* = 2.3 Hz, 1H), 7.18 – 7.09 (m, 2H), 7.06 (dd, *J* = 8.6, 2.4 Hz, 1H), 6.84 – 6.77 (m, 2H), 6.76 (d, *J* = 8.6 Hz, 1H), 4.00 (t, *J* = 6.2 Hz, 2H), 3.95 (t, *J* = 6.3 Hz, 2H), 3.57 (*virt.* dt, *J* = 7.6, 6.7 Hz, 4H), 1.93 – 1.76 (m, 8H), 1.70 – 1.63 (m, 4H), 1.62 (s, 6H).

^{13}C NMR ($CDCl_3$, 151 MHz, 300 K) δ [ppm] = 157.1 (s), 153.2 (s), 144.9 (s), 142.4 (s), 131.7 (s), 127.8 (s), 126.9 (s), 114.0 (s), 112.7 (s), 111.8 (s), 68.9 (s), 67.6 (s), 45.1 (s), 45.1 (s), 41.8 (s), 32.5 (s), 32.4 (s), 31.1 (s), 28.8 (s), 28.5 (s), 23.7 (s), 23.7 (s).

HRMS (ESI): $C_{25}H_{33}BrCl_2O_2$

calculated: $[(M + Ag)^+]$: 621.0086

found: [(M + Ag)$^+$]: 621.0088.

Macrocycle CY5Br

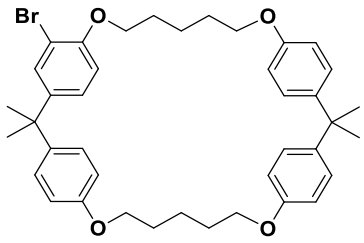

$C_{40}H_{47}BrO_4$
MW: 671.72 g/mol

A one-neck round-bottom flask was charged with compound **151** (2.06 g, 3.99 mmol, 1.0 equiv.) and bisphenol A (**128**) (911 mg, 3.99 mmol, 1.0 equiv.). The starting materials were dissolved in anhydrous MeCN (800 mL), followed by the addition of Cs_2CO_3 (3.90 g, 12.0 mmol, 3.0 equiv.) and KI (132 mg, 798 µmol, 0.2 equiv.). The reaction mixture was then stirred at reflux for 2 d. After this time, the solvent was removed under reduced pressure, and water (200 mL) and EtOAc (100 mL) were added. The two layers were separated, and the aqueous layer was extracted with EtOAc (3 x 50 mL). The combined organic layers were washed with brine (100 mL), dried (Na_2SO_4), filtered and the solvent removed under reduced pressure. The crude material was purified by MPLC (RediSep® Column: Silica 40 g; 60 ml/min; CyHex/EtOAc 100:0 to 92:8, 18.4 CV, 16.8 min) to obtain **CY5Br** (1.05 g, 1.56 mmol, 39%) as a white solid.

TLC *R*f = 0.57 (CyHex/EtOAc = 4/1) [UV, KMnO4].

M.P.: 181 – 182 °C.

IR (ATR): ṽ (cm-1) = 3056 (vw), 2941 (m), 2920 (m), 2871 (m), 1608 (m), 1581 (w), 1508 (s), 1490 (m), 1471 (m), 1413 (w), 1388 (m), 1359 (w), 1298 (m), 1247 (vs), 1181 (s), 1133 (w), 1108 (w), 1087 (w), 1062 (m), 1046 (m), 1032 (m), 1010 (m), 988 (m), 924 (w), 888 (w), 829 (s), 812 (s), 736 (m), 691 (m), 664 (w), 636 (w), 616 (w), 579 (m), 553 (m), 486 (w), 451 (w), 427 (w), 416 (w).

^{1}H NMR ($CDCl_3$, 600 MHz, 300 K) δ [ppm] = 7.32 (d, *J* = 2.3 Hz, 1H), 7.10 – 7.02 (m, 7H), 6.77 – 6.68 (m, 7H), 4.02 (t, *J* = 6.1 Hz, 2H), 3.96 (ddd, *J* = 8.2, 4.6, 1.9 Hz, 6H), 1.90 – 1.75 (m, 8H), 1.71 – 1.59 (m, 16H).

^{13}C NMR ($CDCl_3$, 151 MHz, 300 K) δ [ppm] = 157.1 (s), 156.9 (s), 156.9 (s), 153.3 (s), 144.9 (s), 143.2 (s), 142.4 (s), 131.9 (s), 127.7 (s), 127.7 (s), 127.6 (s), 126.4 (s), 114.1 (s), 114.0 (s), 114.0 (s), 112.6 (s), 112.0 (s), 69.2 (s), 67.9 (s), 67.9 (s), 67.8 (s), 41.6 (s), 41.5 (s), 30.7 (s), 30.7 (s), 29.0 (s), 28.9 (s), 28.9 (s), 28.8 (s), 23.1 (s), 22.9 (s).

HRMS (ESI): $C_{40}H_{47}BrO_4$ calculated: $[(M + Ag)^+]$: 777.1703

found: $[(M + Ag)^+]$: 777.1691.

Macrocycle 152

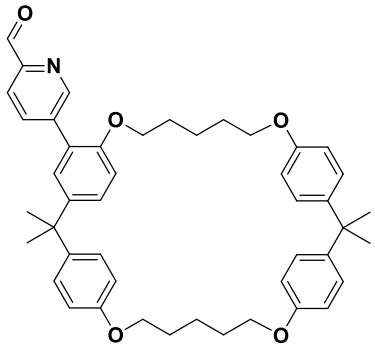

$C_{46}H_{51}NO_5$
MW: 697.92 g/mol

Step 1): 5-Bromopyridine-2-carbaldehyde (**129**, 558 mg, 3.00 mmol, 1.0 eq.), B_2pin_2 (838 mg, 3.30 mmol, 1.1 eq.), $PdCl_2(PPh_3)_2$ (105 mg, 150 µmol, 0.05 eq.) and KOAc (972 mg, 9.90 mmol, 3.3 eq.) were dissolved in degassed, anhydrous 1,4-dioxane (10 mL). The reaction mixture was stirred at 80 °C overnight. After cooling down to room temperature, the mixture was filtered over Celite and washed with CH_2Cl_2 (50 mL). The filtrate was concentrated under reduced pressure to give a dark oil. The purity of the crude product **147** (58%) was determined *via* NMR using vinyltrimethylsilane as an external standard. The material was then submitted to the next reaction without further purification (*Note:* Purification from the byproduct *via* column chromatography was not successful.)

Step 2): A one-neck round-bottom flask was charged with macrocycle **CY5Br** (672 mg, 1.00 mmol, 1.0 equiv.), **147** (58%, 563 mg, 1.40 mmol, 1.4 equiv.), $Pd(PPh_3)_4$ (92.4 mg, 80.0 µmol, 8 mol%) and K_3PO_4 (849 mg, 4.00 mmol, 4.0 equiv.). The solids were dissolved in a mixture of degassed DMF/water (9/1) (20 mL) and stirred at 65 °C for 24 h. Next, the reaction mixture was filtered over Celite and washed with CH_2Cl_2 (50 mL). The solvents were removed under reduced pressure and the crude material was purified by MPLC (RediSep® Column: Silica 12 g; 30 ml/min; CyHex/EtOAc 100:0 to 75:25 to 0:100, 24.6 CV, 14.5 min) to obtain **152** (374 mg, 536 µmol, 54%) as an off-white solid.

TLC *R*f = 0.41 (CyHex/EtOAc = 4/1) [UV, KMnO4].

M.P.: 84 – 85 °C.

IR (ATR): ṽ (cm-1) = 3049 (vw), 2936 (w), 2866 (w), 1708 (m), 1607 (w), 1580 (w), 1506 (s), 1469 (m), 1413 (w), 1383 (w), 1361 (w), 1293 (w), 1241 (s), 1179 (s), 1107 (w), 1043 (m),

1012 (m), 943 (w), 910 (w), 826 (vs), 725 (m), 663 (w), 636 (w), 572 (m), 555 (s), 513 (w), 467 (w), 454 (w), 415 (m).

^{1}H NMR ($CDCl_3$, 600 MHz, 300 K) δ [ppm] = 10.10 (d, *J* = 0.8 Hz, 1H), 8.90 – 8.84 (m, 1H), 8.01 – 7.97 (m, 1H), 7.92 (dd, *J* = 8.0, 0.8 Hz, 1H), 7.23 (dd, *J* = 8.6, 2.5 Hz, 1H), 7.17 (d, *J* = 2.5 Hz, 1H), 7.12 (d, *J* = 8.8 Hz, 2H), 7.08 (*virt.* dd, *J* = 8.9, 3.1 Hz, 4H), 6.86 (d, *J* = 8.7 Hz, 1H), 6.76 (d, *J* = 8.8 Hz, 2H), 6.73 (d, *J* = 8.8 Hz, 2H), 6.70 (d, *J* = 8.8 Hz, 2H), 4.00 (t, *J* = 6.2 Hz, 2H), 3.96 (td, *J* = 6.1, 1.3 Hz, 4H), 3.91 (t, *J* = 6.1 Hz, 2H), 1.83 – 1.72 (m, 8H), 1.70 (s, 6H), 1.66 – 1.60 (m, 8H), 1.58 – 1.49 (m, 2H).

^{13}C NMR ($CDCl_3$, 151 MHz, 300 K) δ [ppm] = 193.4 (s), 157.1 (s), 156.9 (s), 156.8 (s), 154.1 (s), 150.9 (s), 150.8 (s), 143.9 (s), 143.3 (s), 143.1 (s), 142.6 (s), 139.3 (s), 137.9 (s), 129.4 (s), 128.4 (s), 127.7 (s), 127.6 (s), 127.6 (s), 125.3 (s), 121.2 (s), 114.1 (s), 113.9 (s), 113.8 (s), 111.7 (s), 68.3 (s), 67.9 (s), 67.8 (s), 67.7 (s), 41.7 (s), 41.5 (s), 30.7 (s), 30.7 (s), 29.0 (s), 28.9 (s), 28.7 (s), 28.7 (s), 23.1 (s), 23.1 (s).

HRMS (ESI): $C_{46}H_{51}NO_5$ calculated: [(M + Na)+]: 720.3659

found: [(M + Na)+]: 720.3666.

Macrocycle 153

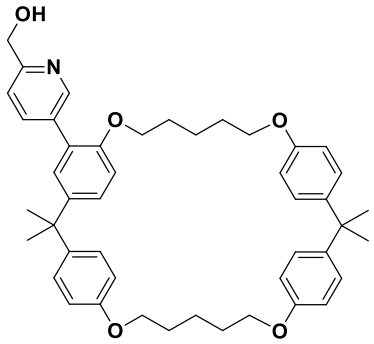

$C_{46}H_{53}NO_5$
MW: 699.93 g/mol

Compound **152** (133 mg, 190 µmol, 1.0 equiv.) was dissolved in a mixture of anhydrous MeOH and CH_2Cl_2 (1:1) (10 mL). Then, $NaBH_4$ (7.19 mg, 190 µmol, 1.0 equiv.) was added at 0 °C and the mixture was stirred for 3 h at room temperature. The reaction mixture was diluted with CH_2Cl_2 (10 mL), neutralized by the addition of water (10 mL), and was then extracted with CH_2Cl_2 (3 × 5 mL). The combined organic layers were washed with brine (10 mL), dried (Na_2SO_4), filtered, and concentrated under reduced pressure and the crude material was purified by MPLC (RediSep® Column: Silica 4 g; 13 ml/min; CyHex/EtOAc 100:0 to 37:63, 18.2 CV, 8.6 min) to obtain **153** (112 mg, 160 µmol, 84%) as an off-white wax-like substance.

TLC *R*f = 0.35 (CyHex/EtOAc = 1/1) [UV, KMnO4].

IR (ATR): ṽ (cm-1) = 3035 (vw), 2938 (m), 2869 (m), 1607 (m), 1580 (w), 1507 (s), 1486 (w), 1470 (m), 1384 (w), 1362 (w), 1299 (m), 1243 (s), 1180 (s), 1139 (w), 1109 (w), 1053 (m), 1012 (m), 945 (w), 907 (s), 827 (s), 727 (vs), 648 (m), 575 (m), 555 (m), 455 (w), 411 (w).

^{1}H NMR ($CDCl_3$, 600 MHz, 300 K) δ [ppm] = 8.64 (d, *J* = 2.1 Hz, 1H), 7.83 (dd, *J* = 8.0, 2.2 Hz, 1H), 7.17 (*virt.* dd, *J* = 8.5, 2.7 Hz, 2H), 7.12 (*virt.* dd, *J* = 8.6, 2.2 Hz, 3H), 7.08 (d, *J* = 8.7 Hz, 4H), 6.83 (d, *J* = 8.6 Hz, 1H), 6.80 – 6.63 (m, 6H), 4.77 (d, *J* = 2.5 Hz, 2H), 4.02 – 3.93 (m, 6H), 3.91 (t, *J* = 6.1 Hz, 2H), 3.81 (br s, 1H), 1.86 – 1.71 (m, 8H), 1.69 (s, 6H), 1.67 – 1.60 (m, 8H), 1.59 – 1.52 (m, 2H).

^{13}C NMR ($CDCl_3$, 151 MHz, 300 K) δ [ppm] = 157.0 (s), 157.0 (s), 156.9 (s), 156.9 (s), 154.0 (s), 149.0 (s), 143.6 (s), 143.3 (s), 143.1 (s), 142.8 (s), 137.9 (s), 133.5 (s), 129.4 (s), 127.7 (s), 127.6 (s), 127.6 (s), 127.4 (s), 126.3 (s), 119.6 (s), 114.1 (s), 114.0 (s), 113.9 (s), 111.6 (s), 68.2 (s), 67.9 (s), 67.8 (s), 64.2 (s), 41.6 (s), 41.6 (s), 30.7 (s), 29.0 (s), 29.0 (s), 28.8 (s), 28.7 (s), 23.1 (s), 23.0 (s).

HRMS (ESI): $C_{46}H_{53}NO_5$ calculated: $[(M + Na)^+]$: 722.3816

found: $[(M + Na)^+]$: 722.3818.

Macrocycle 154

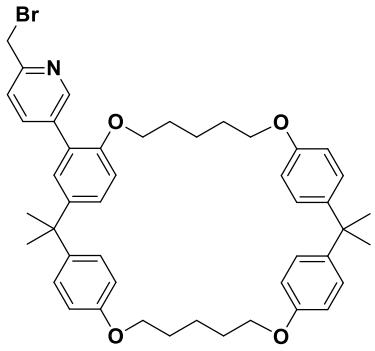

$C_{46}H_{52}BrNO_4$
MW: 762.83 g/mol

Compound **153** (385 mg, 550 µmol, 1.0 equiv.) was dissolved in anhydrous CH_2Cl_2 (7 mL) and cooled to 0 °C. After dropwise addition of PBr_3 (51.7 µL, 149 mg, 550 µmol, 1.0 equiv.) and stirring for 1 h at 0 °C, the mixture was allowed to reach room temperature and was stirred for 16 h. Next, CH_2Cl_2 (30 mL) and saturated aqueous $NaHCO_3$ solution (20 mL) were added, and the two layers were separated. The aqueous layer was extracted with CH_2Cl_2 (3 x 10 mL) and the combined organic layers were washed with brine (20 mL), dried (Na_2SO_4), filtered, and concentrated under reduced pressure. The crude material was purified by MPLC (RediSep® Column: Silica 12 g; 30 ml/min; CyHex/EtOAc 100:0 to 60:40, 11.6 CV, 6.8 min) to obtain **154** (353 mg, 463 µmol, 84%) as a pinkish solid.

TLC *R*f = 0.46 (CyHex/EtOAc = 4/1) [UV, KMnO4].

M.P.: 135 – 137 °C.

IR (ATR): ṽ (cm-1) = 3032 (vw), 2924 (m), 2868 (m), 1710 (w), 1607 (m), 1579 (w), 1505 (s), 1469 (m), 1383 (w), 1362 (w), 1299 (m), 1272 (w), 1241 (vs), 1179 (s), 1158 (w), 1114 (w), 1075 (w), 1054 (w), 1014 (m), 1002 (m), 942 (w), 900 (w), 828 (vs), 813 (s), 731 (m), 717 (w), 650 (w), 622 (w), 603 (w), 579 (m), 548 (s), 503 (w), 476 (w), 465 (w), 449 (w), 430 (w), 409 (w).

^{1}H NMR ($CDCl_3$, 600 MHz, 300 K) δ [ppm] = 8.65 (d, *J* = 2.2 Hz, 1H), 7.86 (dt, *J* = 8.0, 2.0 Hz, 1H), 7.36 (d, *J* = 8.1 Hz, 1H), 7.19 (dd, *J* = 8.6, 2.5 Hz, 1H), 7.13 – 7.10 (m, 3H), 7.08 (d, *J* = 8.7 Hz, 4H) 6.83 (d, *J* = 8.6 Hz, 1H), 6.76 (d, *J* = 8.8 Hz, 2H), 6.73 (d, *J* = 8.8 Hz, 2H), 6.71 (d, *J* = 8.8 Hz, 2H), 4.58 (s, 2H), 4.05 – 3.94 (m, 6H), 3.90 (t, *J* = 6.1 Hz, 2H), 1.88 – 1.72 (m, 8H), 1.68 (s, 6H), 1.66 – 1.61 (m, 8H), 1.56 – 1.50 (m, 2H).

^{13}C NMR ($CDCl_3$, 151 MHz, 300 K) δ [ppm] = 157.0 (s), 157.0 (s), 156.9 (s), 154.3 (s), 154.0 (s), 149.8 (s), 143.7 (s), 143.3 (s), 143.1 (s), 142.7 (s), 138.5 (s), 134.4 (s), 129.4 (s), 127.7 (s), 127.6 (s), 127.6 (s), 125.7 (s), 122.8 (s), 114.1 (s), 114.0 (s), 113.9 (s), 111.7 (s), 68.3 (s), 67.9 (s), 67.8 (s), 67.8 (s), 41.6 (s), 41.6 (s), 30.7 (s), 30.7 (s), 29.0 (s), 29.0 (s), 28.7 (s), 23.2 (s), 23.1 (s).

HRMS (ESI): $C_{46}H_{52}BrNO_4$ calculated: $[(M + Na)^+]$: 784.2972

found: $[(M + Na)^+]$: 784.2965.

Ligand (mcp)CY5

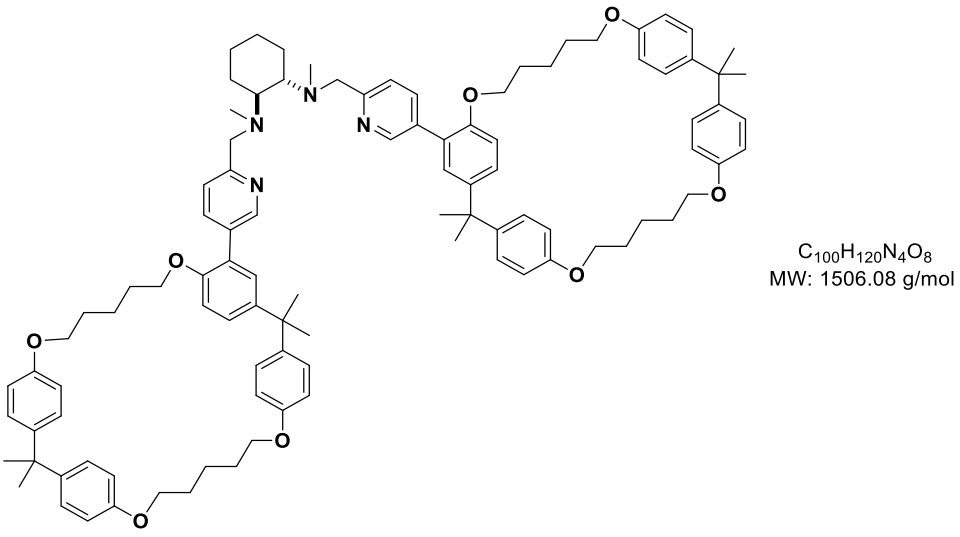

Benzylic bromide **154** (156 mg, 205 µmol, 2.05 equiv.) and (2*S*,2'*S*)-N^1,N^2-dimethylcyclohexane-1,2-diamine (**132**, 14.2 mg, 100 µmol, 1.0 equiv.) were dissolved in anhydrous MeCN (5.0 mL). Then, K_2CO_3 (55.2 mg, 400 µmol, 4.0 equiv.) and TBAB (1.61 mg, 5.00 µmol, 0.05 equiv.) were added and the reaction mixture was stirred at reflux for 16 h. Thereafter, the mixture was cooled down to room temperature, filtered and the residue was washed with CH_2Cl_2 (40 mL). The filtrate was concentrated under reduced pressure, 1 m NaOH (20 mL) was added and the mixture was extracted with CH_2Cl_2 (3 × 20 mL). The combined organic layers were washed with brine (10 mL), dried (Na_2SO_4), filtered, and concentrated by rotatory evaporation. The crude compound was purified *via* MPLC (RediSep® Column: Alumina, Basic 8 g, 13 mL/min; CH_2Cl_2/CH_2Cl_2:MeOH (9:1) 100:0 to 0:100, 27.1 CV, 12.8 min) to obtain the desired product **(mcp)CY5** (122 mg, 81.0 µmol, 81%) as a yellow solid.

TLC R_f = 0.25 (CH_2Cl_2/MeOH/NH_4OH = 93/5/2) [UV, $KMnO_4$].

M.P.: 118 – 119 °C.

IR (ATR): $\tilde{\nu}$ (cm^{-1}) = 3037 (vw), 2958 (m), 2928 (m), 2868 (m), 1709 (w), 1607 (m), 1580 (w), 1506 (s), 1470 (m), 1383 (w), 1362 (w), 1299 (m), 1242 (vs), 1179 (s), 1159 (m), 1114 (w), 1075 (w), 1048 (m), 1013 (s), 943 (w), 900 (w), 868 (w), 827 (vs), 761 (w), 730 (m), 682 (w), 650 (w), 638 (w), 578 (m), 552 (s), 516 (w), 503 (w), 495 (w), 476 (w), 461 (w), 444 (w), 435 (w), 415 (w).

^{1}H NMR ($CDCl_3$, 500 MHz, 300 K) δ [ppm] = 8.60 (d, *J* = 2.2 Hz, 2H), 7.80 (dd, *J* = 8.1, 2.3 Hz, 2H), 7.61 (d, *J* = 8.1 Hz, 2H), 7.21 (d, *J* = 2.5 Hz, 2H), 7.11 (d, *J* = 8.8 Hz, 4H), 7.08 – 7.01 (m, 10H), 6.79 (d, *J* = 8.7 Hz, 2H), 6.74 (d, *J* = 8.8 Hz, 4H), 6.72 (d, *J* = 8.8 Hz, 4H), 6.69 (d, *J* = 8.8 Hz, 4H), 3.99 – 3.83 (m, 20H), 2.72 – 2.65 (m, 2H), 2.33 (s, 6H), 2.01 – 1.93 (m, 2H), 1.82 – 1.76 (m, 8H), 1.75 – 1.68 (m, 10H), 1.66 (s, 12H), 1.64 – 1.59 (m, 16H), 1.53 – 1.47 (m, 4H), 1.38 – 1.26 (m, 2H), 1.20 – 1.11 (m, 2H).

^{13}C NMR ($CDCl_3$, 126 MHz, 300 K) δ [ppm] = 159.4 (s), 157.0 (s), 157.0 (s), 156.8 (s), 154.0 (s), 149.3 (s), 143.6 (s), 143.3 (s), 143.1 (s), 142.8 (s), 137.6 (s), 132.6 (s), 129.0 (s), 127.7 (s), 127.7 (s), 127.6 (s), 126.7 (s), 121.9 (s), 114.0 (s), 114.0 (s), 113.9 (s), 111.9 (s), 68.4 (s), 67.9 (s), 67.9 (s), 67.7 (s), 64.5 (s), 61.0 (s), 41.6 (s), 41.6 (s), 36.9 (s), 30.7 (s), 29.0 (s), 29.0 (s), 28.7 (s), 26.7 (s), 26.0 (s), 23.2 (s), 22.8 (s).

HRMS (ESI): $C_{100}H_{120}N_4O_8$ calculated: $[(M + Na)^+]$: 1527.8998

found: $[(M + Na)^+]$: 1527.8997.

5.2.2 Complex Synthesis

All reactions were performed in a glove box and anhydrous and degassed (*via* freeze-pump-thaw) solvents were used.

Synthesis **(*S*,*S*)-Mn(mcp)** was carried out as previously described.[229-230]

_S,S_-Mn(mcp)CY3

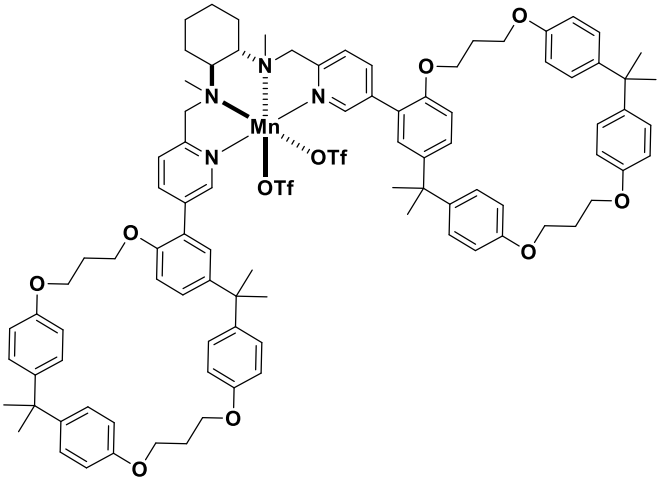

$C_{94}H_{104}F_6MnN_4O_{14}S_2$
MW: 1746.93 g/mol

Ligand **(mcp)CY3** (41.1 mg, 30.0 µmol, 1.0 equiv.) and $Mn(OTf)_2$ (10.6 mg, 30.0 µmol, 1.0 equiv.) were dissolved in MeCN (0.2 mL) and stirred at room temperature for 2.5 h. Subsequently, diethyl ether (4 mL) was added which resulted in the precipitation of a yellow solid out of the solution. The supernatant was removed and the solid was washed two times with diethyl ether (2x2 mL) and dried under reduced pressure for 30 min resulting in the desired complex ***S*,*S*-Mn(mcp)CY3** (30.0 mg, 17.4 µmol, 58%) as an off-white solid.

M.P.: 186 – 188 °C.

IR (ATR): $\tilde{\nu}$ (cm^{-1}) = 3035 (vw), 2962 (m), 2931 (m), 2868 (w), 1711 (w), 1608 (w), 1581 (w), 1508 (vs), 1473 (m), 1384 (w), 1363 (w), 1305 (w), 1246 (vs), 1181 (s), 1108 (w), 1084 (w), 1051 (w), 1031 (m), 990 (w), 949 (w), 869 (w), 830 (s), 743 (w), 665 (w), 638 (s), 610 (w), 570 (w), 560 (w), 514 (w), 493 (w), 486 (w), 452 (w), 439 (w), 421 (w).

HRMS (ESI): $C_{94}H_{104}F_6MnN_4O_{14}S_2$

calculated: $[(M - 2OTf + HCOO)^+]$: 1492.7206

found: $[(M - 2OTf + HCOO)^+]$: 1492.7229.

***S,S*-Mn(mcp)CY5**

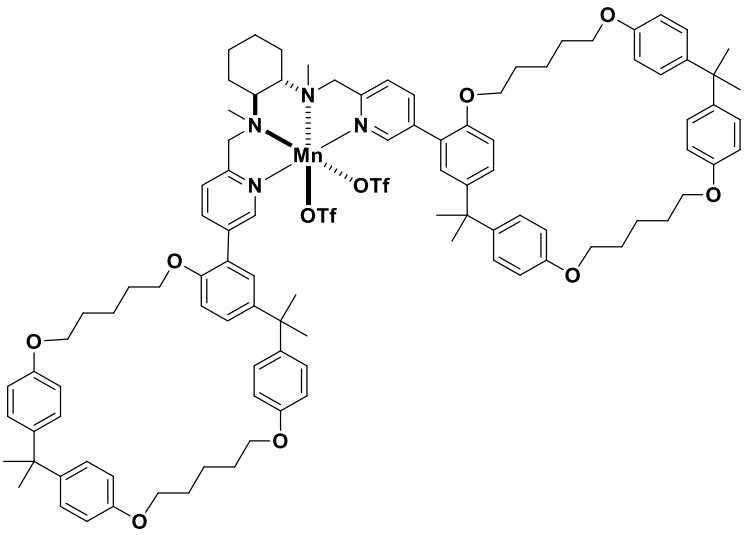

$C_{102}H_{120}F_6MnN_4O_{14}S_2$
MW: 1859.14 g/mol

Ligand **(mcp)CY5** (56.5 mg, 37.5 µmol, 1.0 equiv.) and $Mn(OTf)_2$ (13.2 mg, 37.2 µmol, 1.0 equiv.) were dissolved in THF (0.2 mL) and stirred at room temperature overnight. Subsequently, diethyl ether (4 mL) was added which resulted in the precipitation of a yellow solid out of the solution. The supernatant was removed and the solid was washed two times with diethyl ether (2x2 mL) and dried under reduced pressure for 30 min resulting in the desired complex **Mn(mcp)CY5** (27.6 mg, 14.8 µmol, 40%) as an off-white solid.

M.P.: 184 – 185 °C.

IR (ATR): $\tilde{\nu}$ (cm^{-1}) = 2935 (w), 2871 (w), 1607 (w), 1579 (w), 1507 (m), 1471 (w), 1383 (w), 1362 (w), 1300 (w), 1240 (s), 1179 (s), 1106 (w), 1028 (s), 945 (w), 899 (w), 868 (w), 828 (s), 760 (w), 731 (w), 695 (w), 662 (w), 636 (vs), 578 (m), 514 (m), 496 (w), 481 (w), 459 (w), 449 (w), 437 (w), 417 (w), 405 (w).

HRMS (ESI): $C_{74}H_{80}F_6MnN_{12}O_{22}S_2$ calculated: $[(M - 2OTf)^{2+}]$: 712.2578

found: $[(M - 2OTf)^{2+}]$: 712.2586.

5.2.3 Substrate Synthesis

***rac*-(1*R*,2*S*,5*R*)-2-Isopropyl-5-methylcyclohexyl acetate (163)**

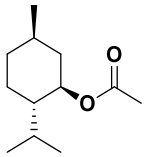

$C_{12}H_{22}O_2$
MW: 198.31 g/mol

rac-Menthol (500 mg, 3.20 mmol, 1.0 equiv.) was suspended in acetic anhydride (1.66 mL, 1.80 g, 17.6 mmol, 5.5 equiv.). $MeSO_3H$ (4.15 µL, 6.15 mg, 64.0 µmol, 0.02 equiv.) was added and the mixture was stirred at 30 °C overnight. The next day, the reaction was poured into an ice-cold saturated $NaHCO_3$ solution (40 mL). The mixture was extracted with EtOAc (3 x 60 mL). The combined organic layers were washed with brine (40 mL), dried (Na_2SO_4), filtered, and carefully concentrated under reduced pressure to give *rac*-**163** (472 mg, 2.38 mmol, 74%) as a colorless liquid.

^{1}H NMR ($CDCl_3$, 500 MHz, 300 K) δ [ppm] = 4.67 (td, *J* = 10.9, 4.4 Hz, 1H), 2.03 (s, 3H), 1.99 (dddd, *J* = 12.1, 4.4, 3.5, 2.0 Hz, 1H), 1.86 (pd, *J* = 7.0, 2.7 Hz, 1H), 1.74 – 1.63 (m, 2H), 1.48 (dddt, *J* = 15.3, 8.9, 6.7, 3.4 Hz, 1H), 1.36 (ddt, *J* = 12.6, 10.8, 3.2 Hz, 1H), 1.11 – 1.00 (m, 1H), 0.96 (td, *J* = 12.2, 11.0 Hz, 1H), 0.91 – 0.84 (m, 7H), 0.76 (d, *J* = 7.0 Hz, 3H).

The spectroscopic data matches the data reported in the literature.[249]

***rac*-(1*R*,2*S*,5*R*)-2-Isopropyl-5-methylcyclohexyl hexanoate (165)**

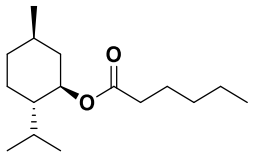

$C_{16}H_{30}O_2$
MW: 254.41 g/mol

rac-Menthol (200 mg, 1.28 mmol, 1.0 equiv.) was suspended in hexonic anhydride (296 µL, 274 mg, 1.28 mmol, 1.0 equiv.). $MeSO_3H$ (1.66 µL, 2.46 mg, 25.6 µmol, 0.02 equiv.) was added and the mixture was stirred at 30 °C overnight. The next day, the reaction was poured into an ice-cold saturated $NaHCO_3$ solution (20 mL). The mixture was extracted with EtOAc (3 x 30 mL). The combined organic layers were washed with brine (20 mL), dried (Na_2SO_4), filtered, and carefully concentrated under reduced pressure to give *rac*-**165** (301 mg, 1.18 mmol, 92%) as a white solid.

^{1}H NMR ($CDCl_3$, 500 MHz, 300 K) δ [ppm] = 4.67 (td, *J* = 10.9, 4.4 Hz, 1H), 2.27 (td, *J* = 7.4, 0.9 Hz, 2H), 1.98 (dddd, *J* = 12.0, 4.4, 3.5, 2.0 Hz, 1H), 1.87 (pd, *J* = 7.0, 2.8 Hz, 1H),

1.71 – 1.57 (m, 4H), 1.49 (dddt, *J* = 15.4, 8.9, 6.7, 3.4 Hz, 1H), 1.41 – 1.23 (m, 5H), 1.05 (qd, *J* = 13.4, 12.8, 3.7 Hz, 1H), 0.99 – 0.92 (m, 1H), 0.92 – 0.86 (m, 10H), 0.76 (d, *J* = 7.0 Hz, 3H).

The spectroscopic data matches the data reported in the literature.[250]

(3*R*,8*R*,9*S*,10*S*,13*S*,14*S*)-10,13-Dimethyl-17-oxohexadecahydro-1*H*-cyclopenta[*a*]phenanthren-3-yl acetate (169)

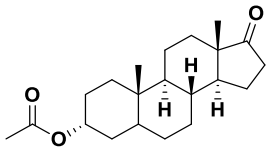

$C_{21}H_{32}O_3$
MW: 332.48 g/mol

Androsterone (145 mg, 500 µmol, 1.0 equiv.) was dissolved in anhydrous CH_2Cl_2 (0.5 mL). Acetic anhydride (260 µL, 281 mg, 2.75 mmol, 5.5 equiv.) and $MeSO_3H$ (1.0 µL, 1.48 mg, 15.4 µmol, 0.03 equiv.) were added and the mixture was stirred at 30 °C overnight. The next day, the reaction was poured into an ice-cold saturated $NaHCO_3$ solution (10 mL). The mixture was extracted with EtOAc (3 x 15 mL). The combined organic layers were washed with brine (10 mL), dried (Na_2SO_4), filtered, and carefully concentrated under reduced pressure to give **169** (157 mg, 472 µmol, 94%) as a white solid.

^{1}H NMR ($CDCl_3$, 500 MHz, 300 K) δ [ppm] = 5.02 (t, *J* = 2.8 Hz, 1H), 2.44 (ddd, *J* = 19.2, 8.9, 1.1 Hz, 1H), 2.05 (s, 4H), 2.00 – 1.89 (m, 1H), 1.86 – 1.78 (m, 2H), 1.74 (dd, *J* = 14.0, 3.2 Hz, 1H), 1.70 – 1.54 (m, 3H), 1.53 – 1.45 (m, 5H), 1.35 – 1.16 (m, 6H), 1.02 (qd, *J* = 12.6, 4.8 Hz, 1H), 0.87 (s, 3H), 0.82 (d, *J* = 0.6 Hz, 4H).

The spectroscopic data matches the data reported in the literature.[251-252]

(3*S*,5*S*,8*R*,9*S*,10*S*,13*R*,14*S*,17*R*)-10,13-Dimethyl-17-((*R*)-6-methylheptan-2-yl)hexadecahydro-1*H*-cyclopenta[*a*]phenanthren-3-yl acetate (171)

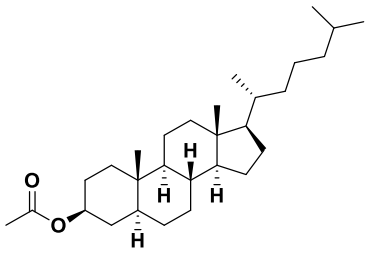

$C_{29}H_{50}O_2$
MW: 430.72 g/mol

5*α*-Cholestan-3*β*-ol (194 mg, 500 µmol, 1.0 equiv.) was dissolved in anhydrous CH_2Cl_2 (0.5 mL). Acetic anhydride (260 µL, 281 mg, 2.75 mmol, 5.5 equiv.) and $MeSO_3H$ (1.0 µL, 1.48 mg, 15.4 µmol, 0.03 equiv.) were added and the mixture was stirred at 30 °C overnight. The next day, the reaction was poured into an ice-cold saturated $NaHCO_3$ solution (10 mL).

The mixture was extracted with EtOAc (3 x 15 mL). The combined organic layers were washed with brine (10 mL), dried (Na_2SO_4), filtered, and carefully concentrated under reduced pressure to give **171** (175 mg, 406 µmol, 81%) as a white solid.

^{1}H NMR ($CDCl_3$, 500 MHz, 300 K) δ [ppm] = 4.68 (tt, *J* = 11.4, 4.9 Hz, 1H), 2.02 (s, 3H), 1.96 (dt, *J* = 12.7, 3.4 Hz, 1H), 1.85 – 1.76 (m, 2H), 1.72 (dt, *J* = 13.3, 3.7 Hz, 1H), 1.65 (dq, *J* = 12.9, 3.5 Hz, 1H), 1.61 – 0.93 (m, 25H), 0.90 (d, *J* = 6.6 Hz, 3H), 0.86 (dd, *J* = 6.6, 2.3 Hz, 6H), 0.82 (d, *J* = 0.6 Hz, 3H), 0.64 (s, 4H).

The spectroscopic data matches the data reported in the literature.[253]

5.3 Oxidation Conditions

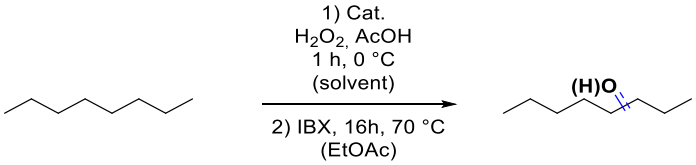

General small-scale oxidation procedure with Mn catalysts in MeCN

Mn catalyst (185 nmol, 1 mol%) and substrate (18.5 µmol, 1.0 equiv.) were dissolved in 200 µL MeCN in a 1 mL screw vial. After the addition of AcOH (2.12 µL, 37.0 µmol, 2.0 equiv.), the mixture was cooled to 0 °C. Next, a solution of commercially available aq. H_2O_2 (50% w/w, Sigma Aldrich, 51.4 µL, 46.2 µmol, 2.5 equiv.) diluted in MeCN (~ 0.9 M) was slowly added over 15 min by a syringe pump. After the addition, the mixture was left to stir for another 45 min. After the time indicated, biphenyl (internal standard, 9.25 µmol, 0.5 equiv.) was added and the reaction mixture was diluted with CH_2Cl_2, filtered over basic AlOx, and washed with CH_2Cl_2. The product mixture was analyzed *via* GC, GC-MS and/or NMR.

General small-scale oxidation procedure with Mn catalysts in TFE/HFIP

Mn catalyst (185 nmol, 1 mol%) and substrate (18.5 µmol, 1.0 equiv.) were dissolved in 200 µL solvent in a 1 mL screw vial. After the addition of AcOH (2.12 µL, 37.0 µmol, 2.0 equiv.), the mixture was cooled to 0 °C. Next, a solution of commercially available aq. H_2O_2 (50% w/w, Sigma Aldrich, 20.6 µL, 18.5 µmol, 1.0 equiv.) diluted in solvent (~ 0.9 M) was slowly added over 6 min by a syringe pump. After the addition, the mixture was left to stir for another 45 min. After the time indicated, biphenyl (internal standard, 9.25 µmol, 0.5 equiv.) was added and the reaction mixture was diluted with CH_2Cl_2, filtered over basic AlOx, and washed with CH_2Cl_2. The product mixture was analyzed *via* GC, GC-MS and/or NMR.

Second step for small-scale oxidation reactions

The oxidation of the alcohol products obtained in MeCN/TFE/HFIP as solvents turned out to be advantageous due to better separation. Therefore, after removal of the solvents under reduced pressure, the crude material was dissolved in anhydrous EtOAc (0.5 mL) and IBX (10.4 mg, 37 µmol, 2.00 equiv.) was added. The mixture was stirred at 70 °C overnight, cooled down to r.t., filtered over Celite, and analyzed *via* GC, GC-MS and/or NMR.

5.4 ^{1}H and ^{13}C NMR Spectra

145: ^{1}H NMR (600 MHz, 300 K, $CDCl_3$)

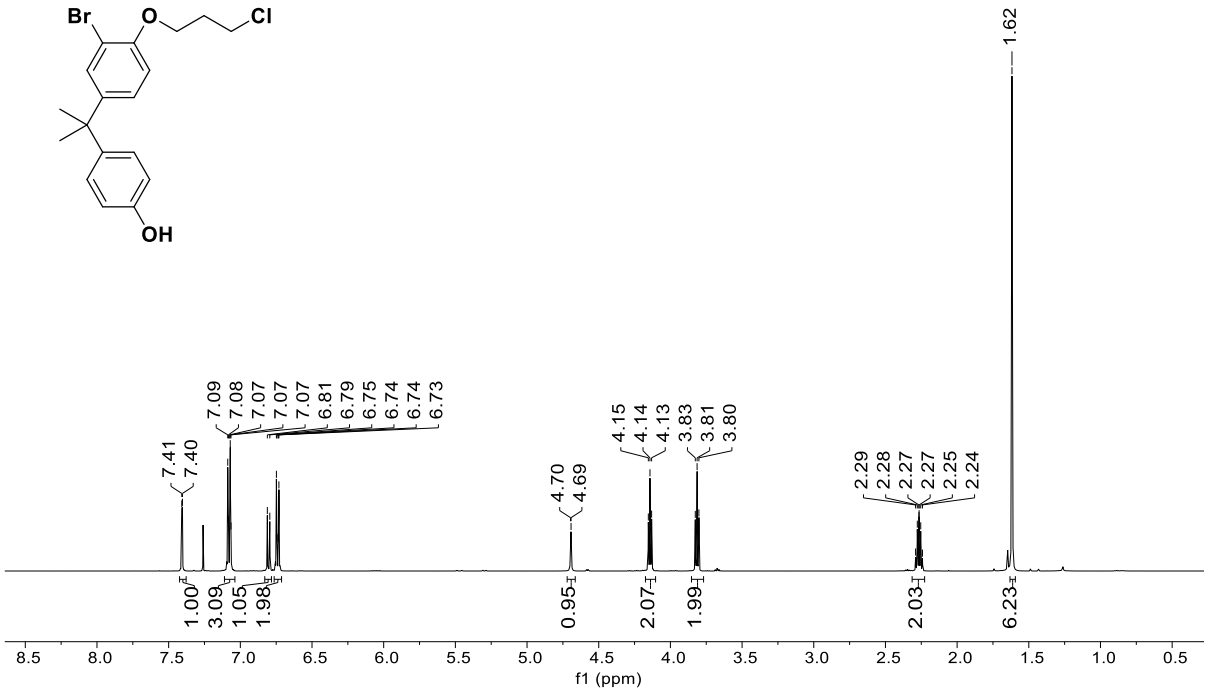

145: ^{13}C NMR (126 MHz, 300 K, $CDCl_3$)

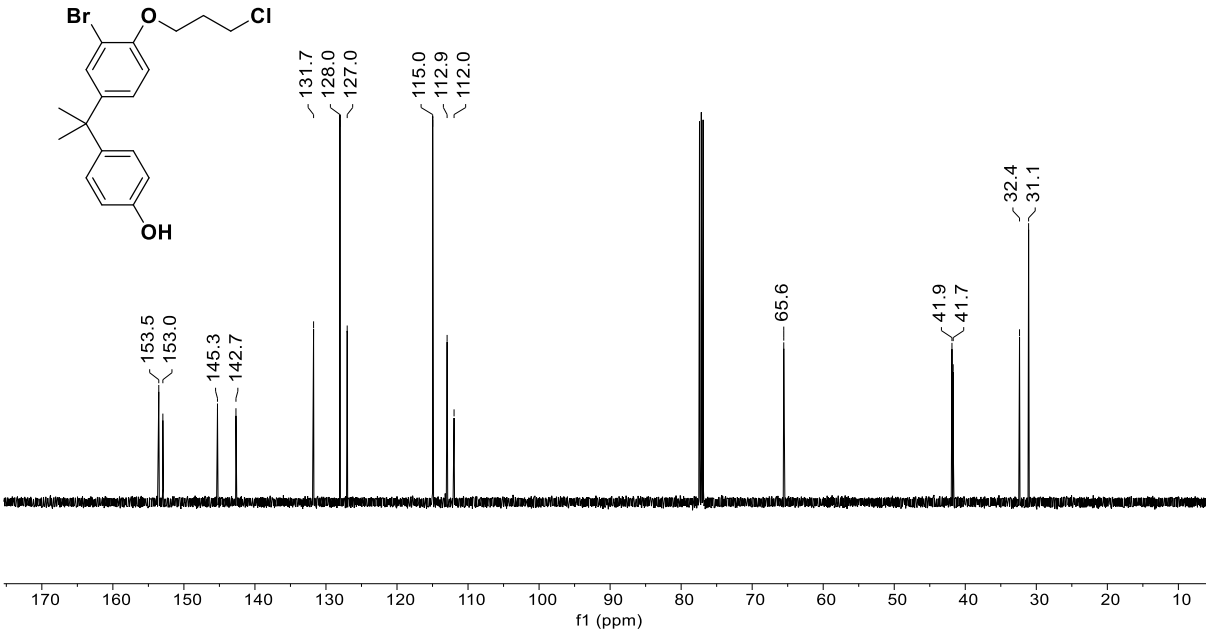

146: ^{1}H NMR (600 MHz, 300 K, $CDCl_3$)

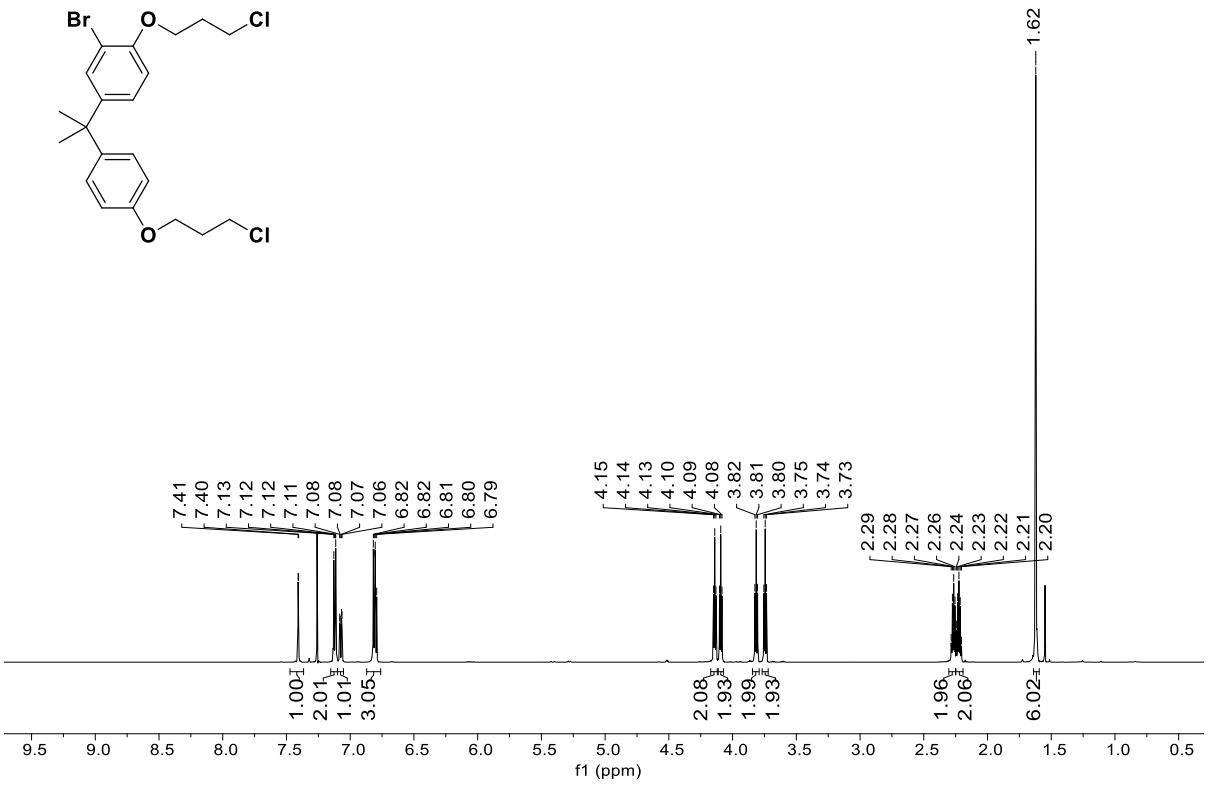

146: ^{13}C NMR (126 MHz, 300 K, $CDCl_3$)

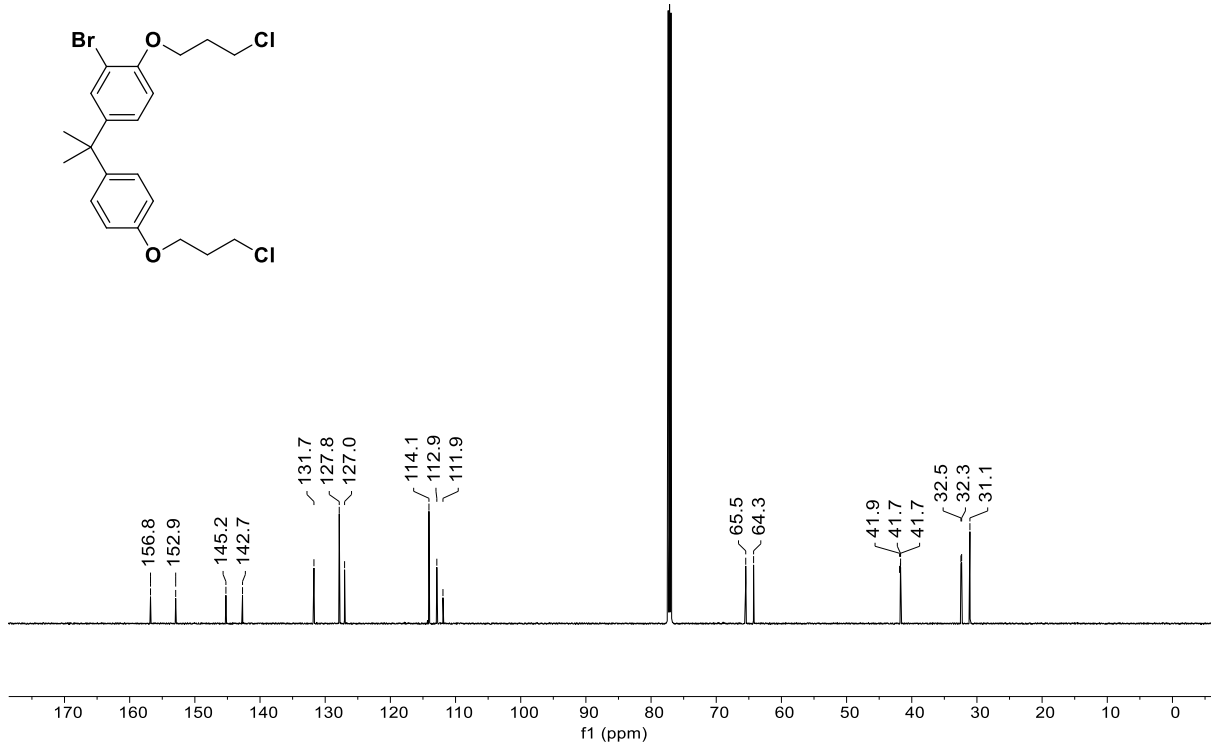

CY3Br$_2$: ^{1}H NMR (600 MHz, 300 K, $CDCl_3$)

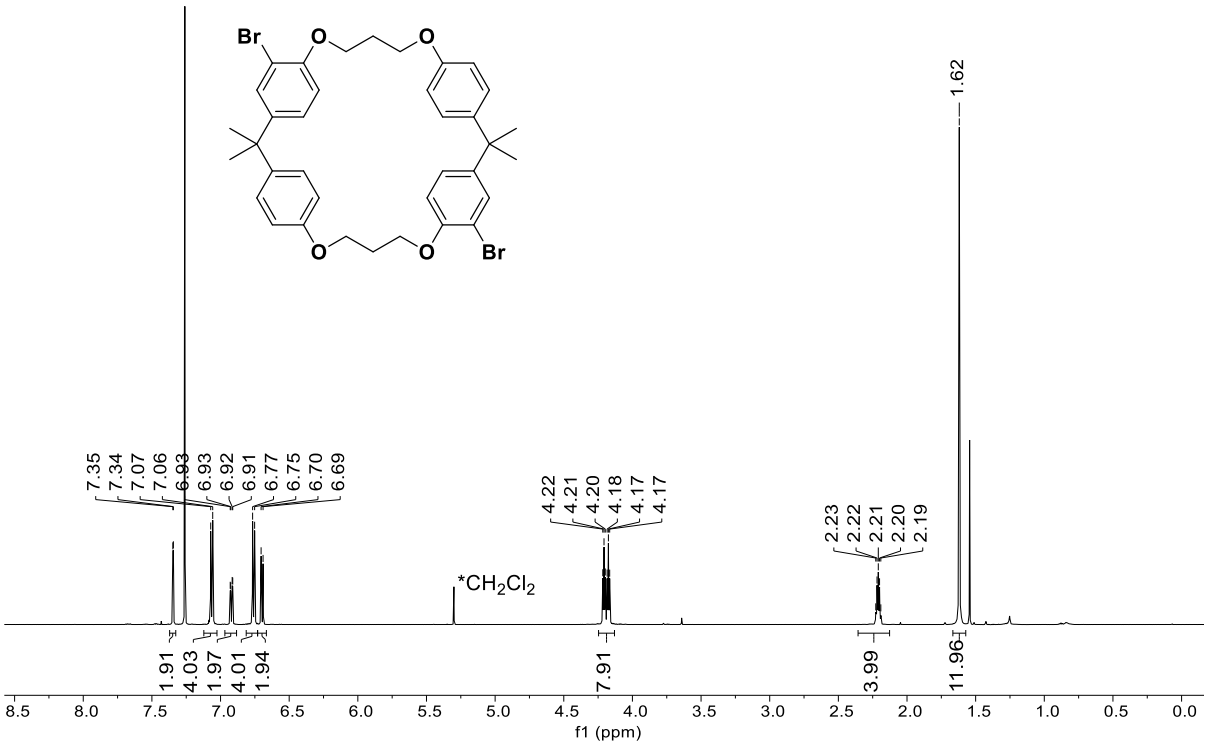

CY3Br$_2$: ^{13}C NMR (126 MHz, 300 K, $CDCl_3$)

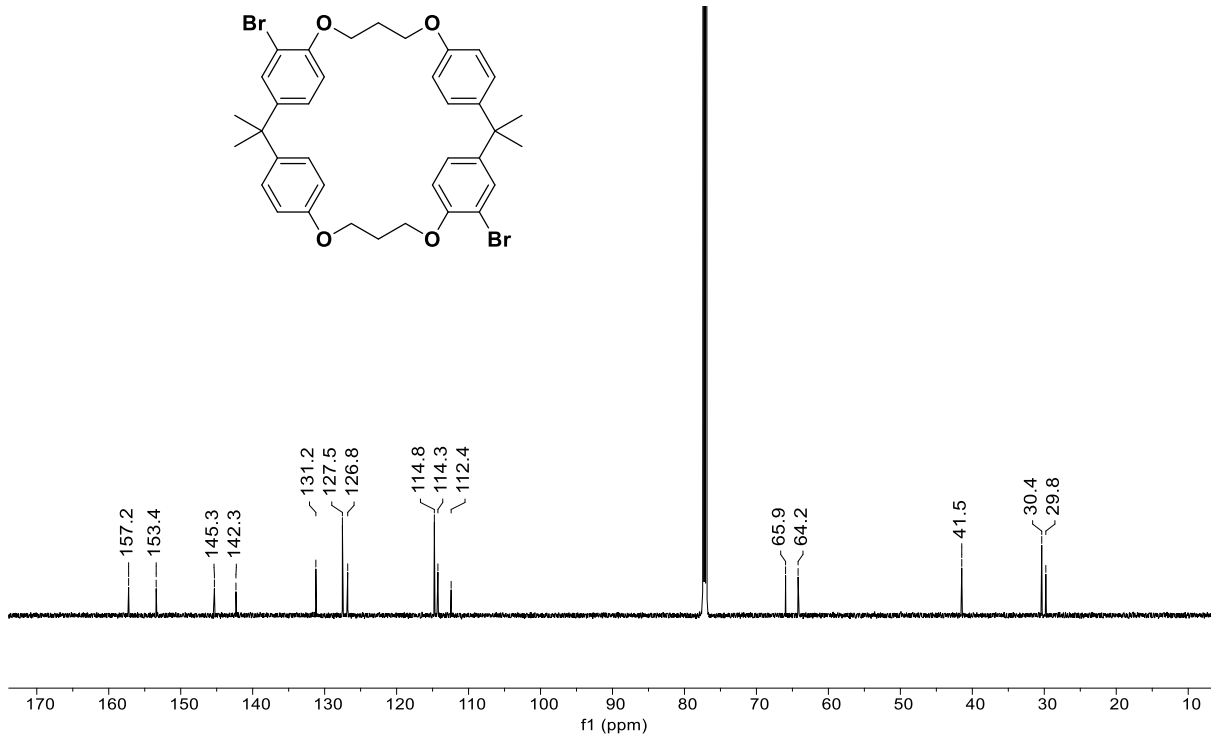

CY3Br: ^{1}H NMR (600 MHz, 300 K, $CDCl_3$)

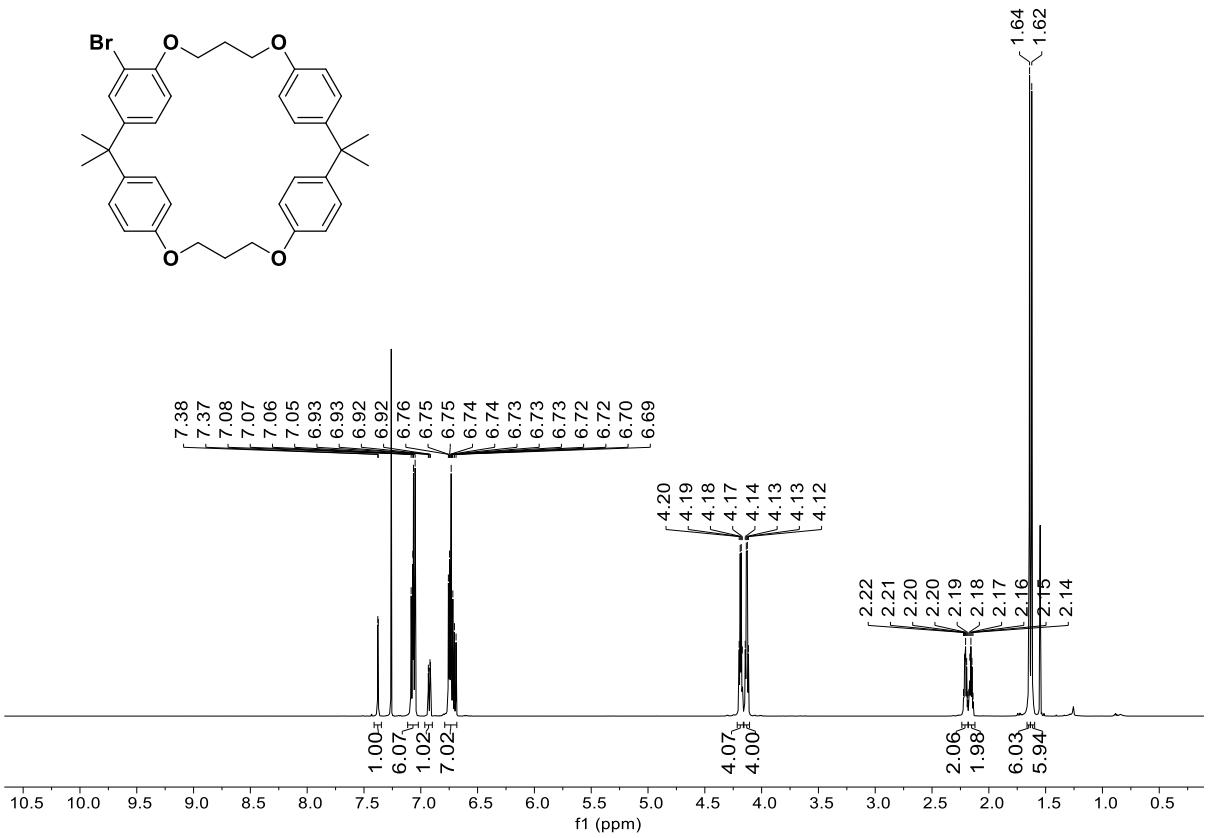

CY3Br: ^{13}C NMR (126 MHz, 300 K, $CDCl_3$)

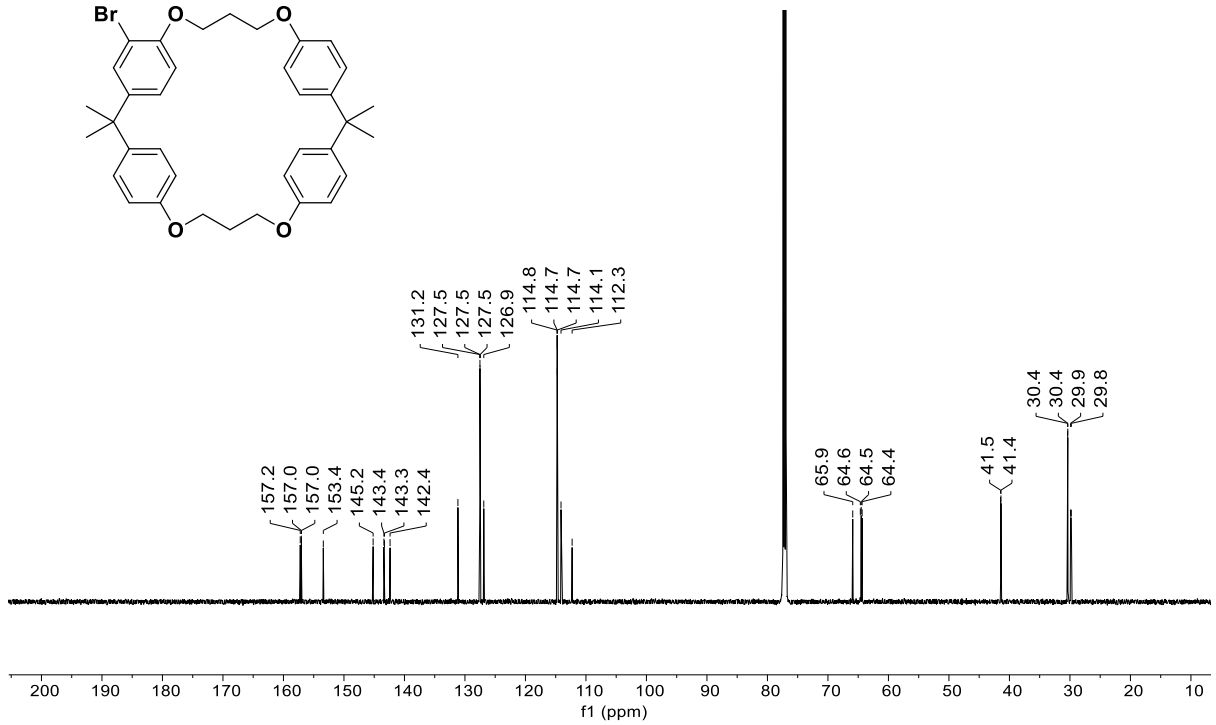

148: ^{1}H NMR (600 MHz, 300 K, $CDCl_3$)

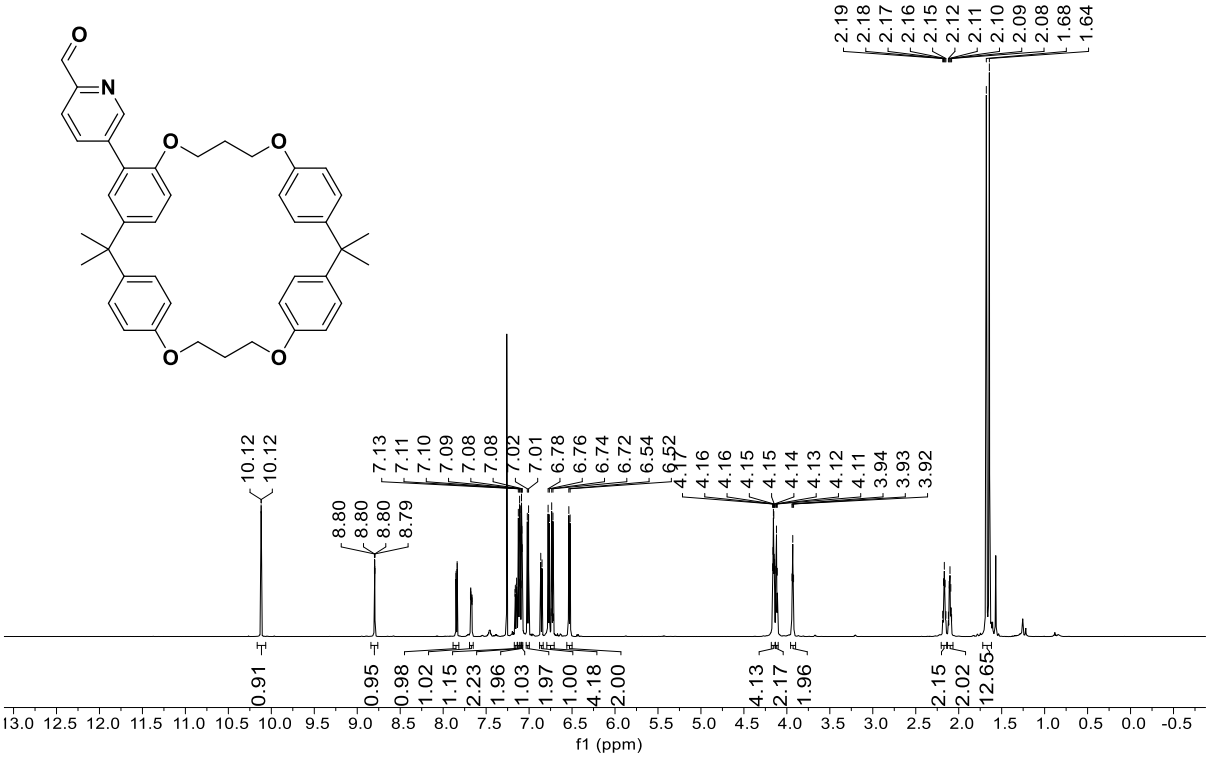

148: ^{13}C NMR (126 MHz, 300 K, $CDCl_3$)

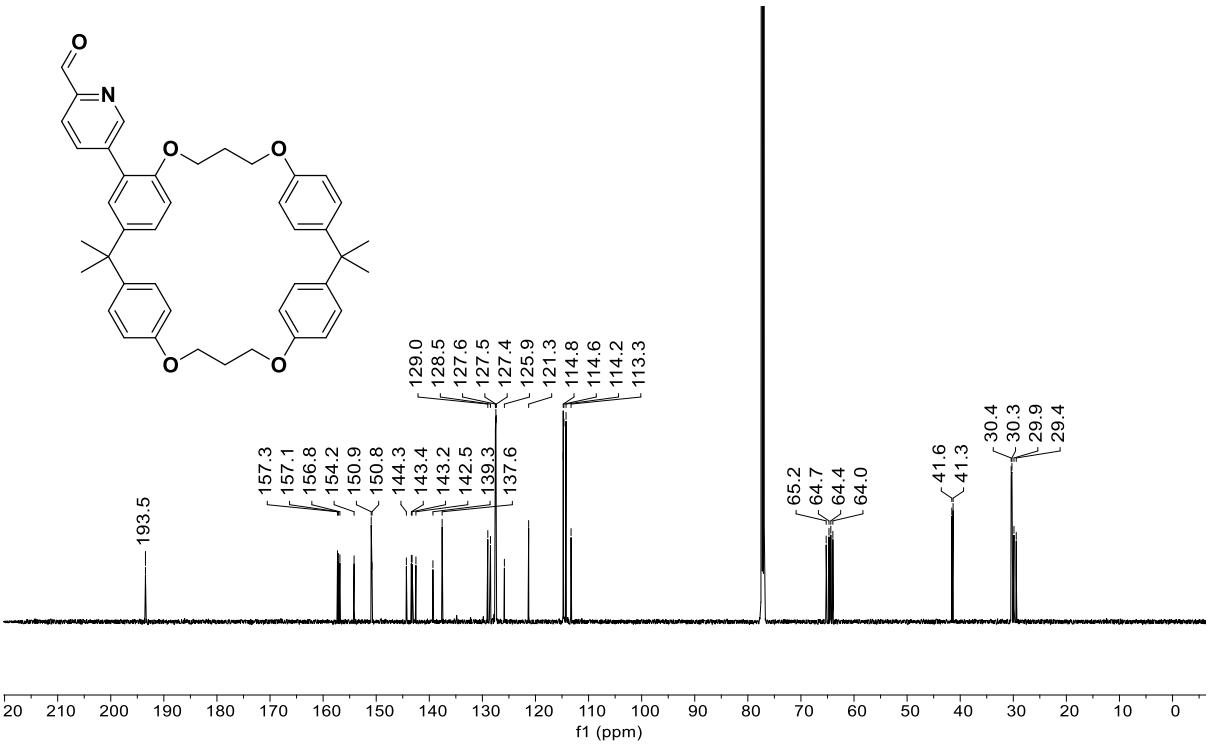

149: ^{1}H NMR (500 MHz, 300 K, $CDCl_3$)

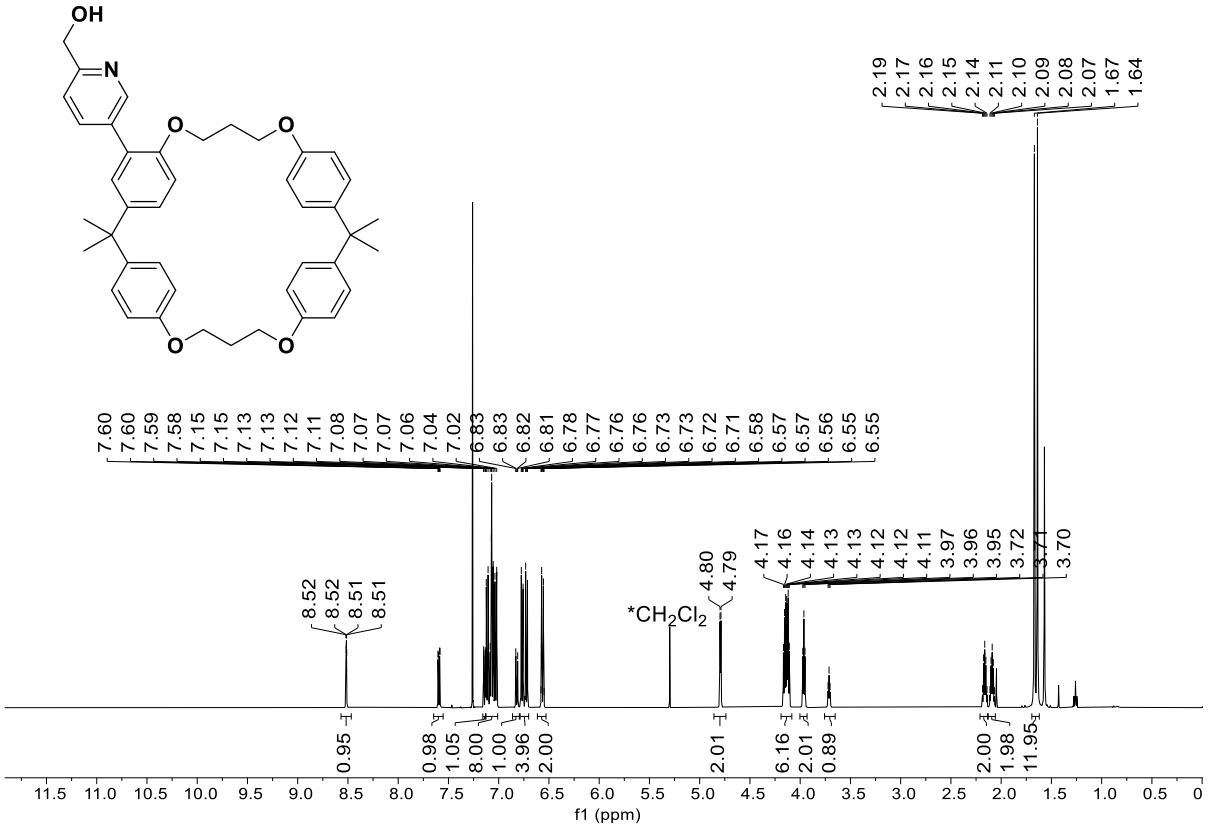

149: ^{13}C NMR (126 MHz, 300 K, $CDCl_3$)

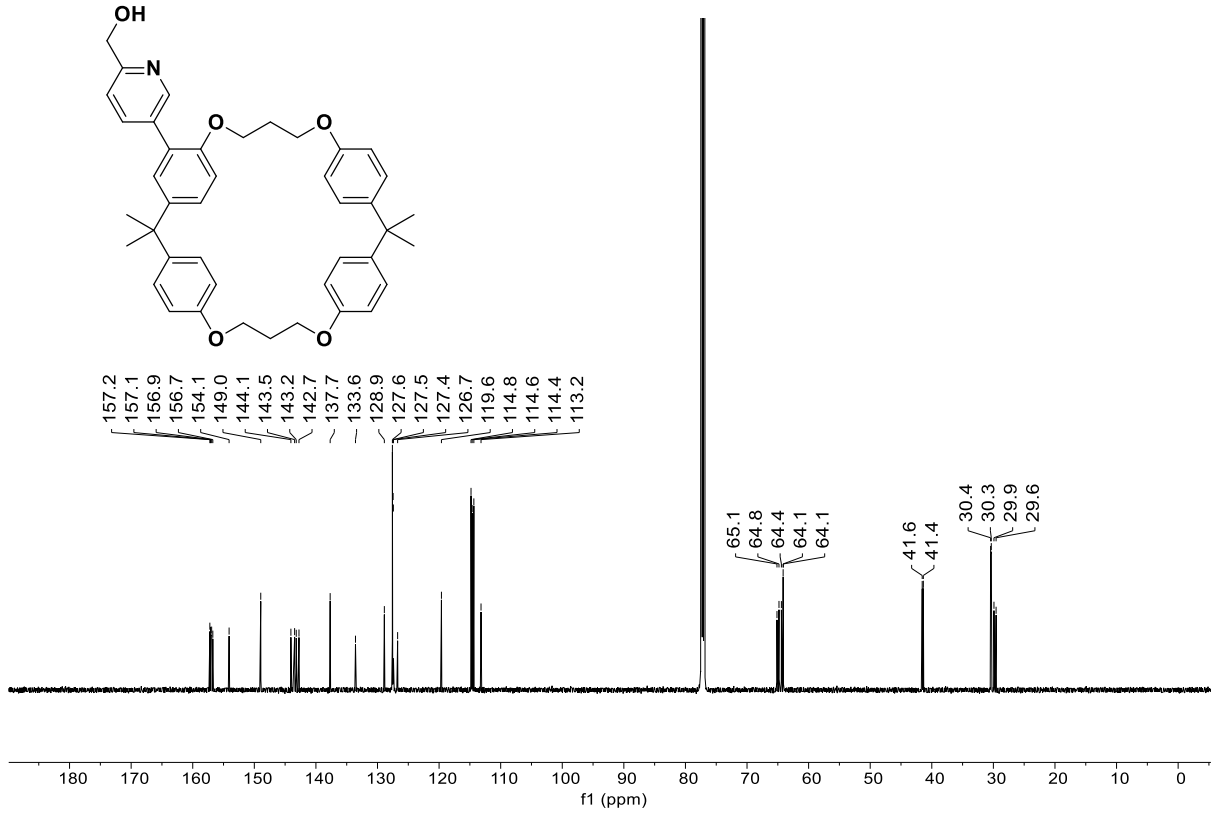

150: ^{1}H NMR (600 MHz, 300 K, $CDCl_3$)

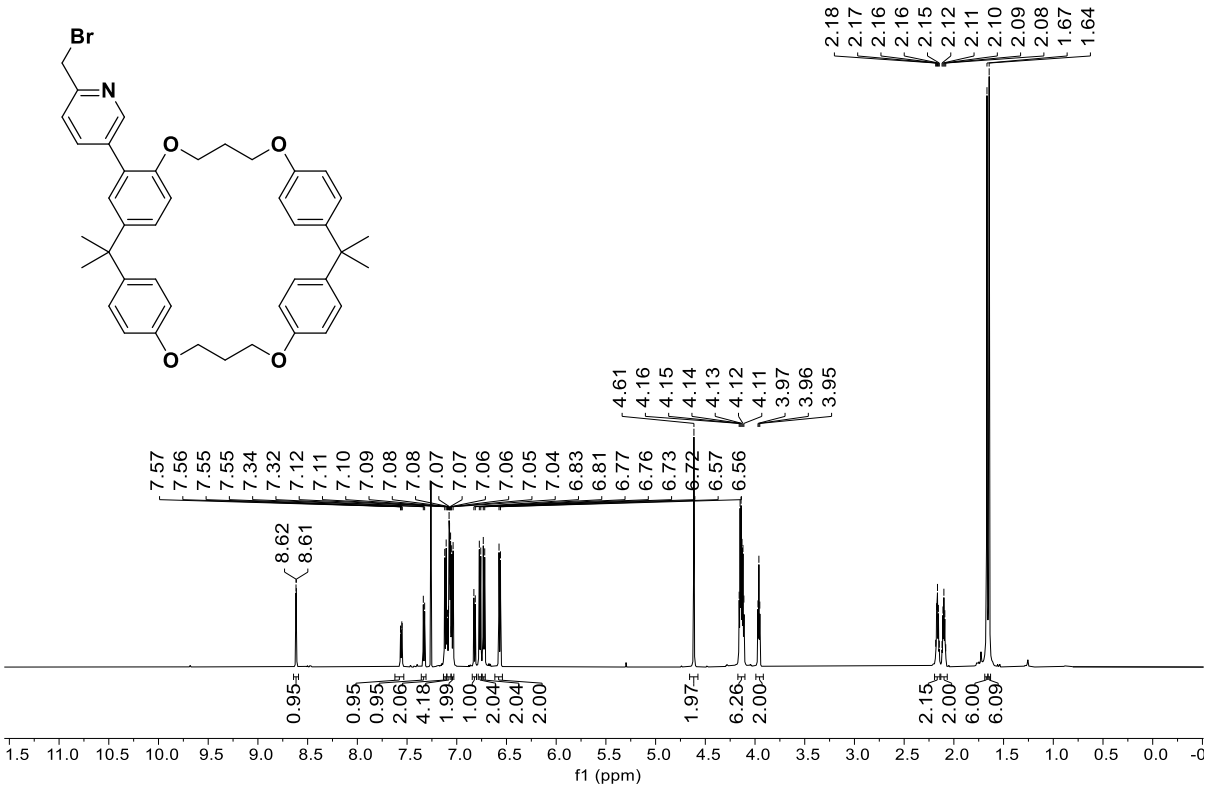

150: ^{13}C NMR (126 MHz, 300 K, $CDCl_3$)

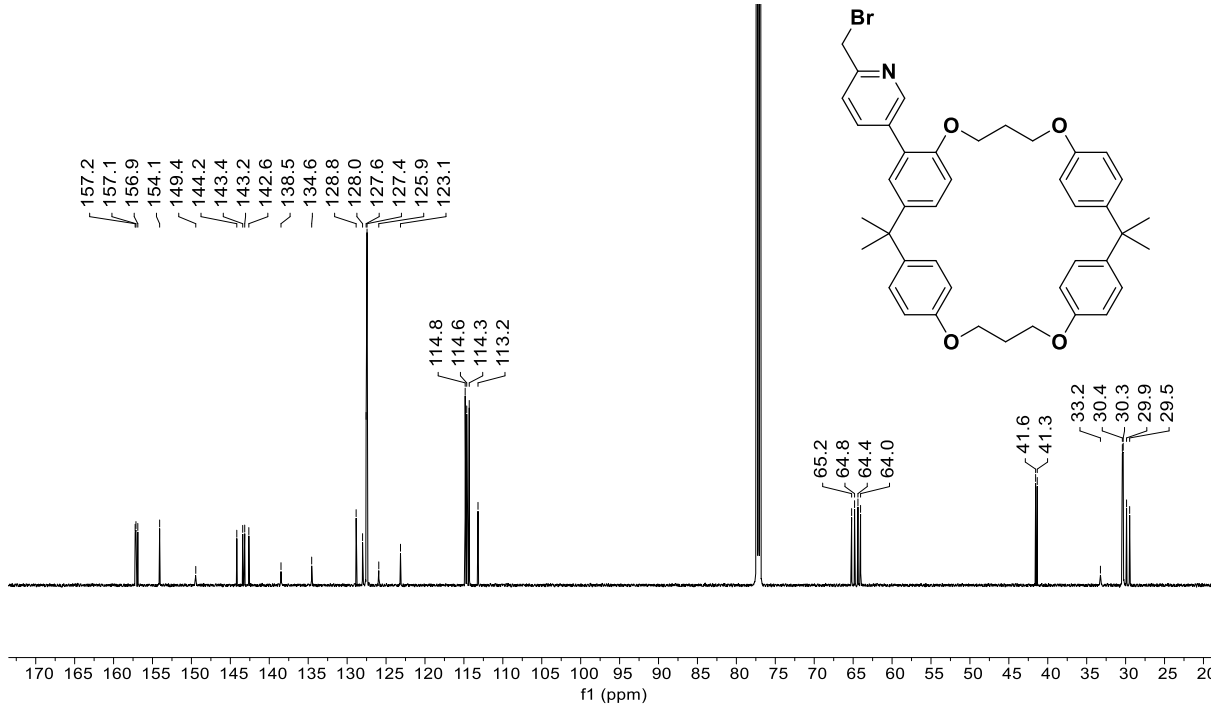

(mcp)CY3: ^{1}H NMR (500 MHz, 300 K, $CDCl_3$)

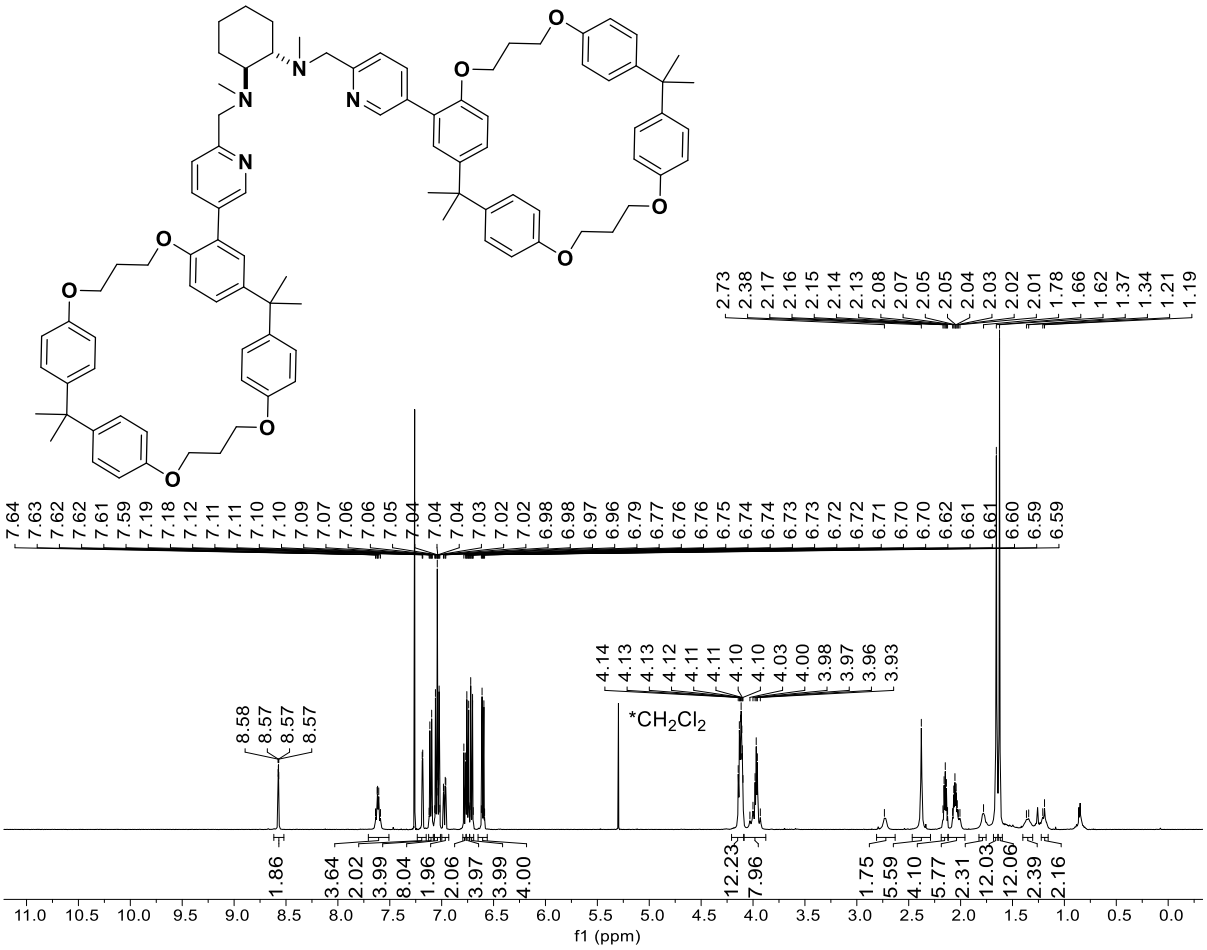

(mcp)CY3: ^{13}C NMR (126 MHz, 300 K, $CDCl_3$)

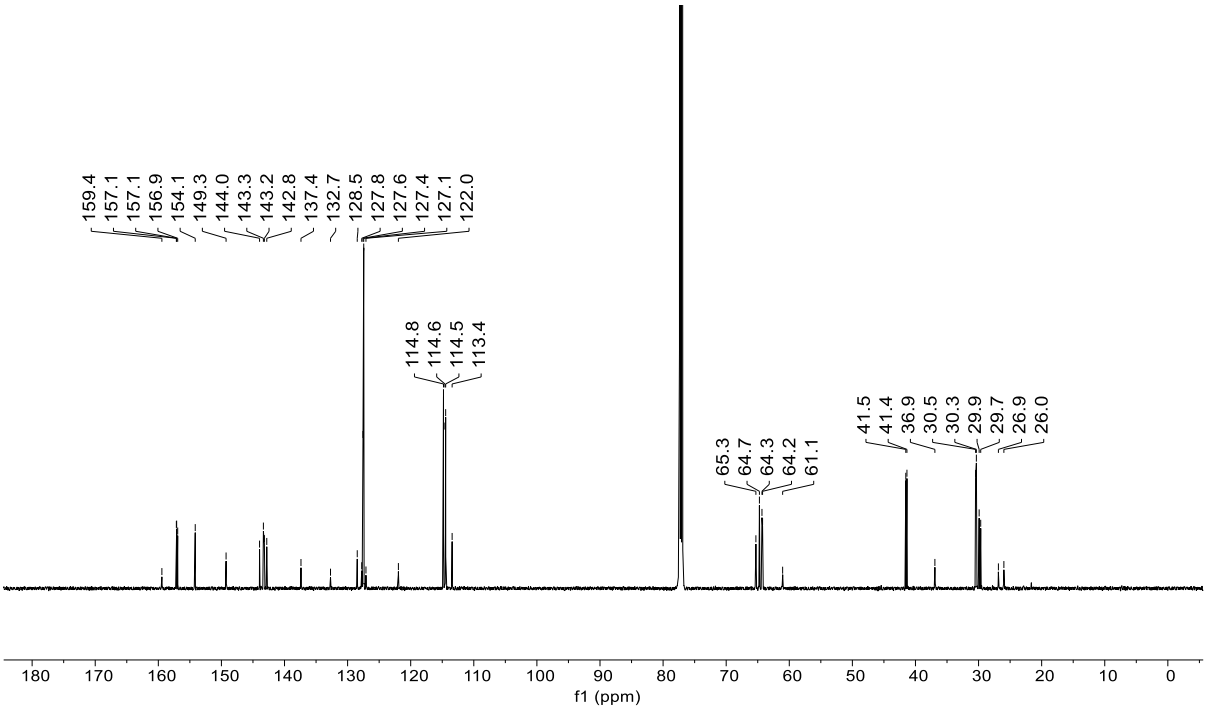

151: ^{1}H NMR (600 MHz, 300 K, $CDCl_3$)

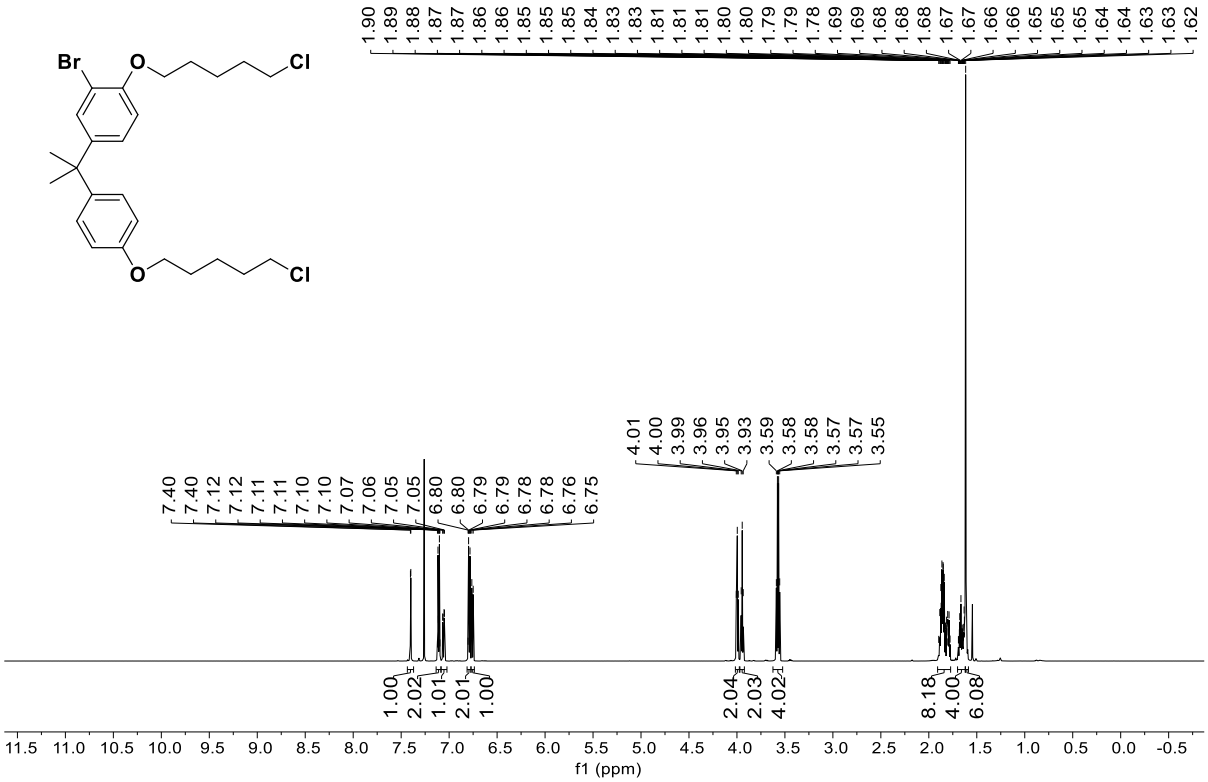

151: ^{13}C NMR (126 MHz, 300 K, $CDCl_3$)

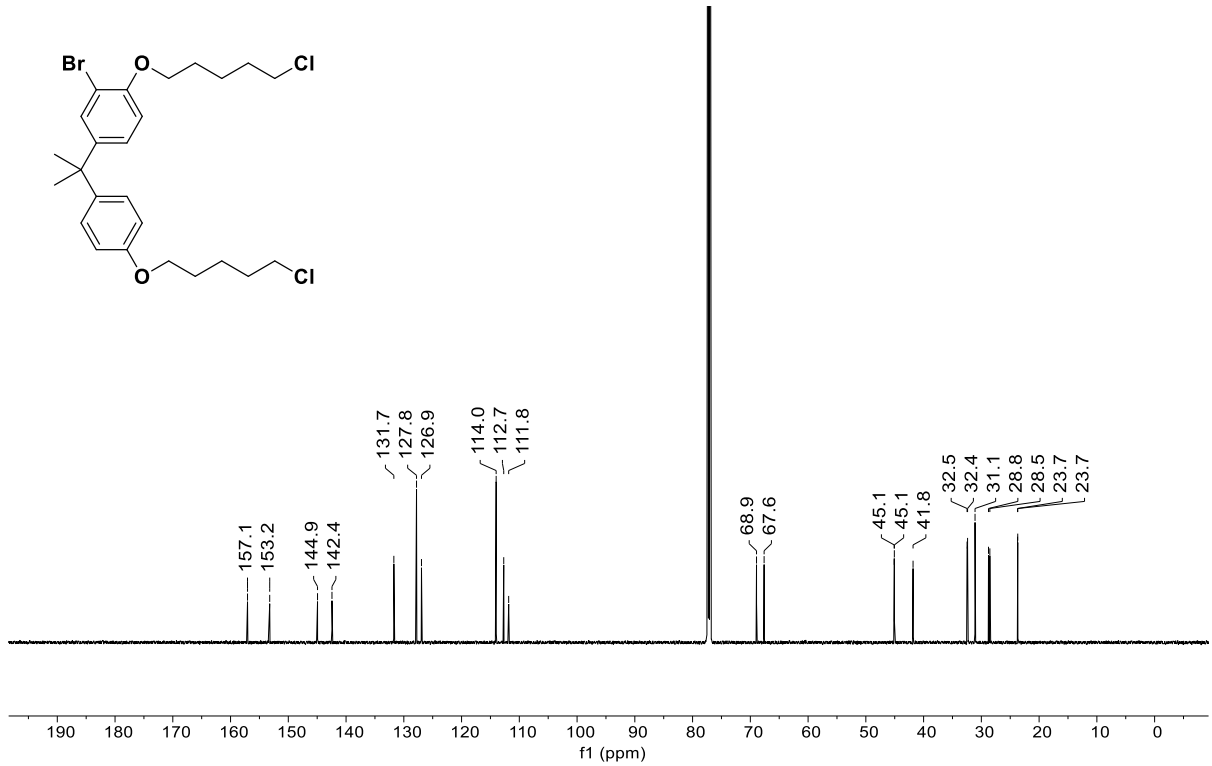

CY5Br: ^{1}H NMR (600 MHz, 300 K, $CDCl_3$)

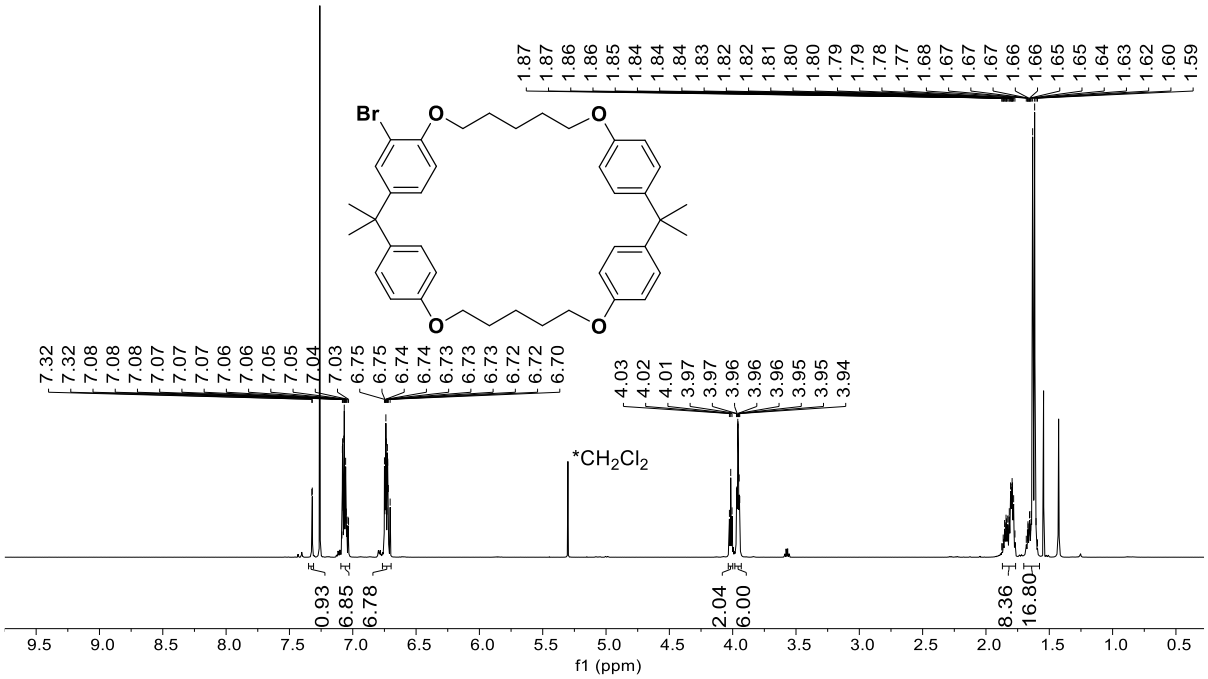

CY5Br: ^{13}C NMR (126 MHz, 300 K, $CDCl_3$)

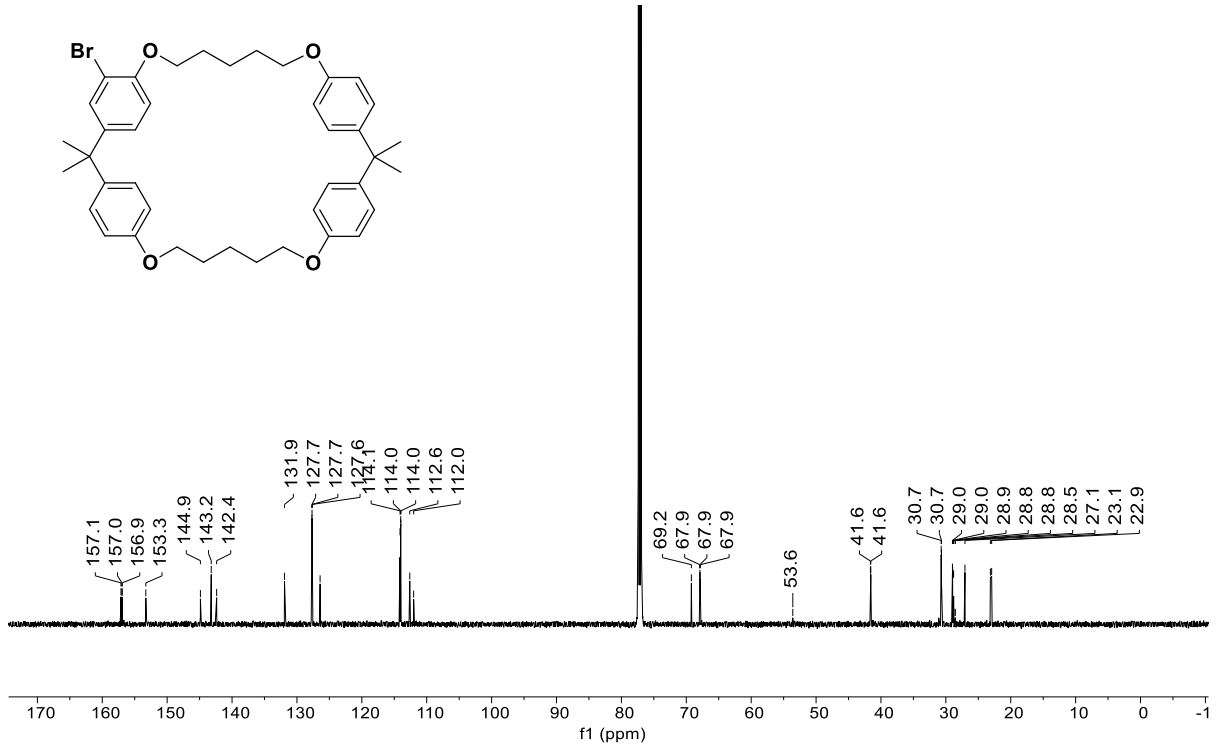

152: ^{1}H NMR (600 MHz, 300 K, $CDCl_3$)

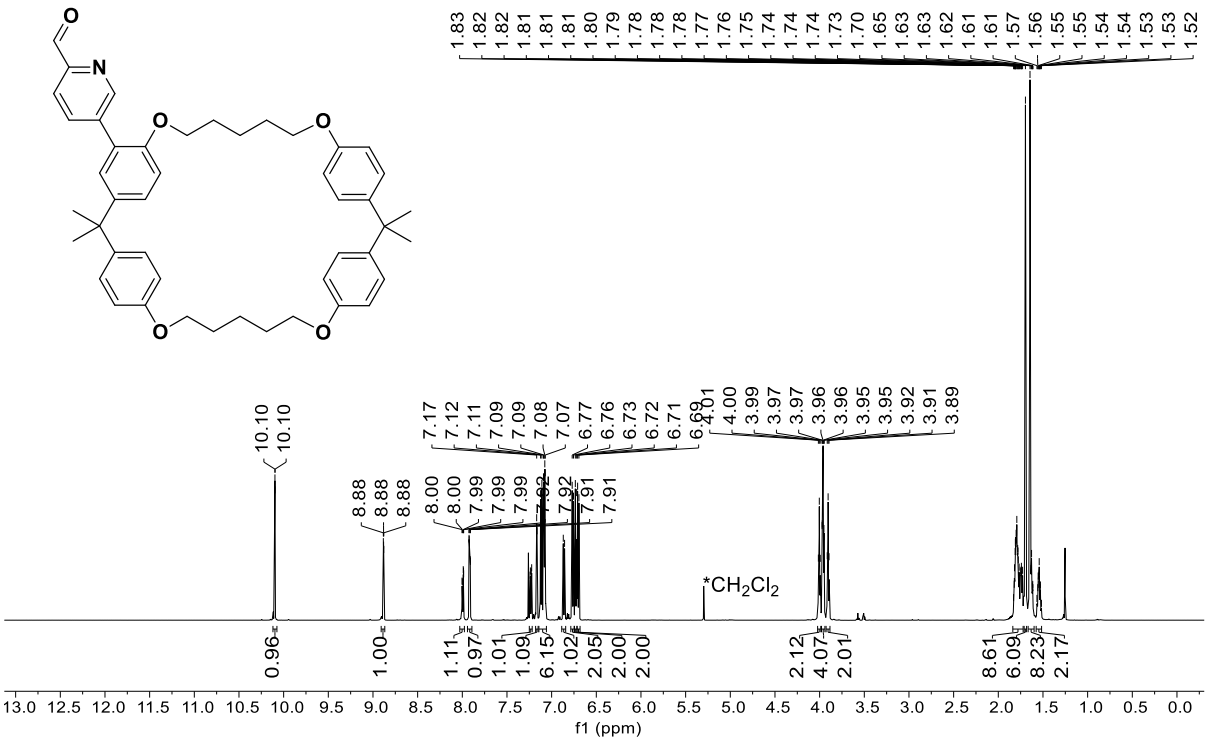

152: ^{13}C NMR (126 MHz, 300 K, $CDCl_3$)

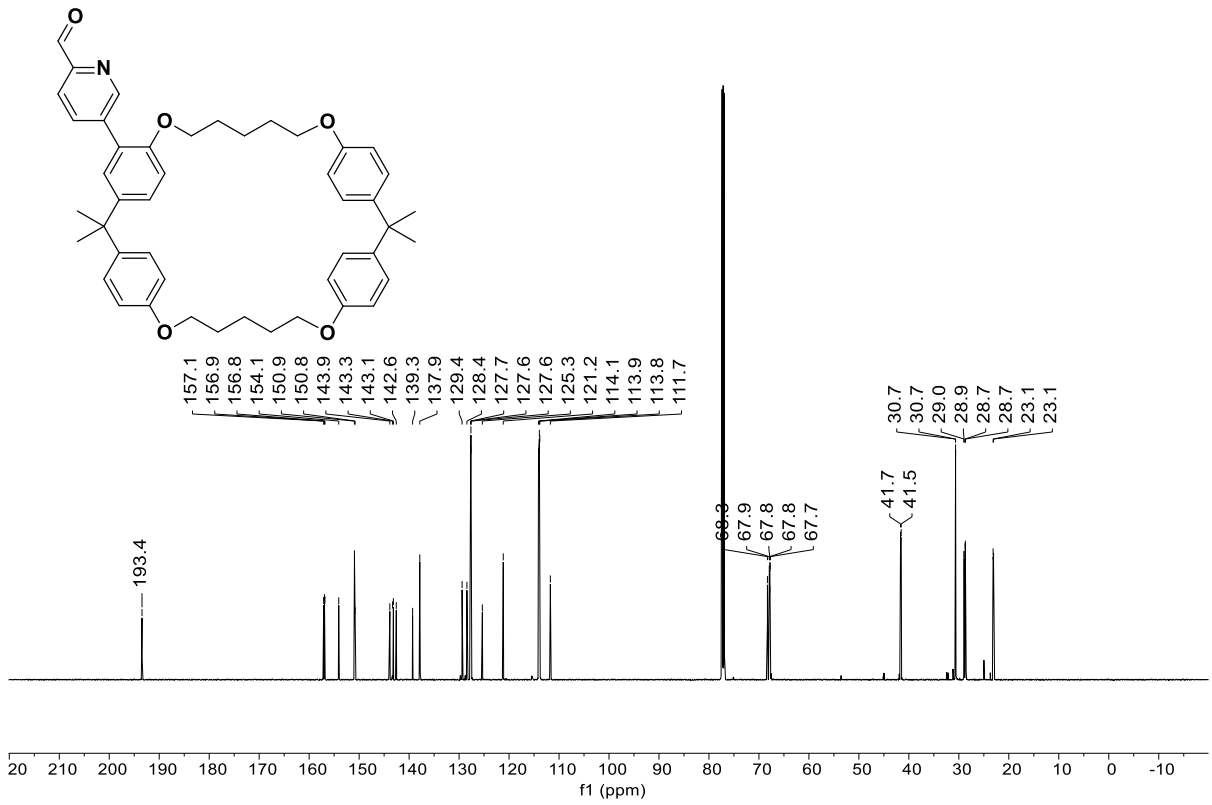

153: ^{1}H NMR (600 MHz, 300 K, $CDCl_3$)

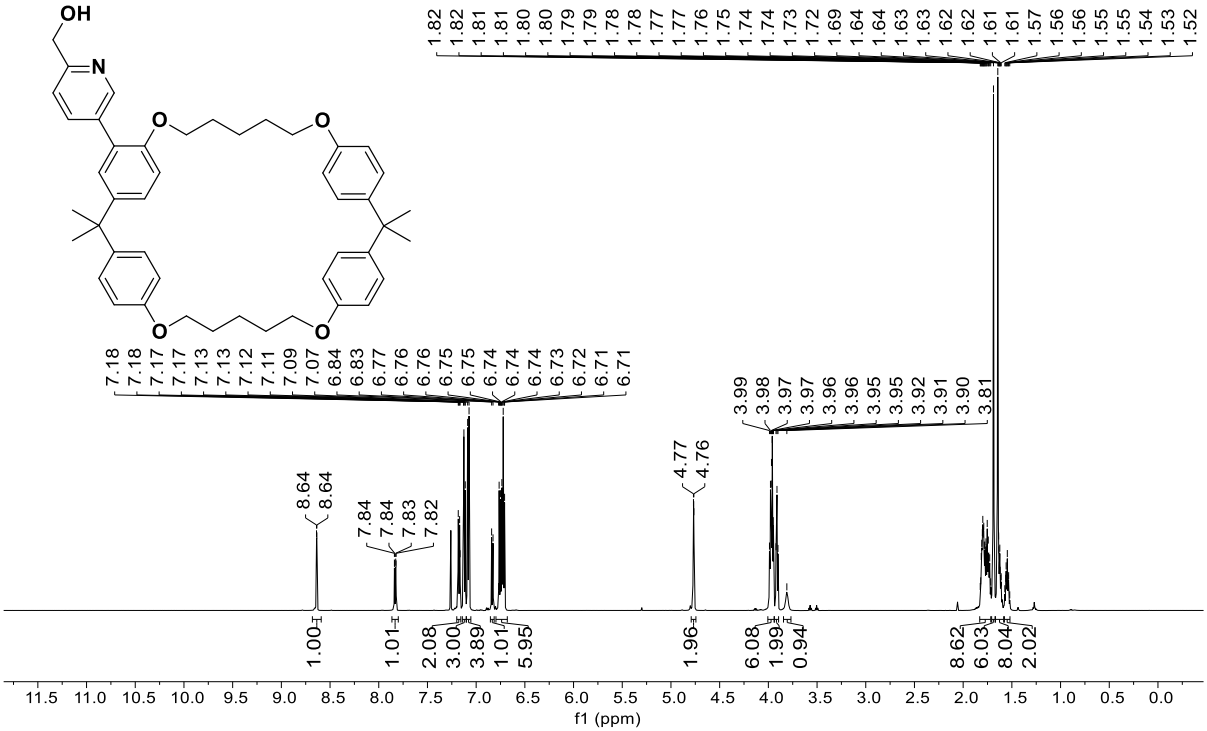

153: ^{13}C NMR (126 MHz, 300 K, $CDCl_3$)

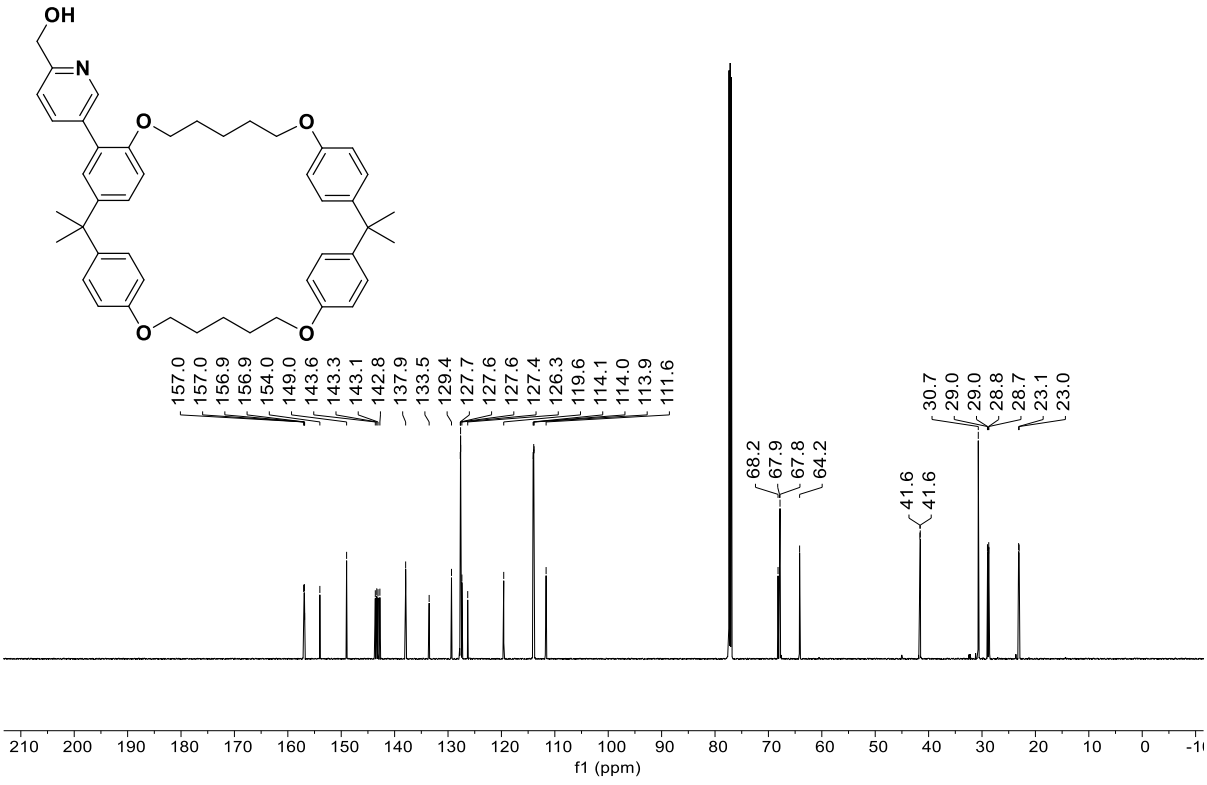

154: ^{1}H NMR (600 MHz, 300 K, $CDCl_3$)

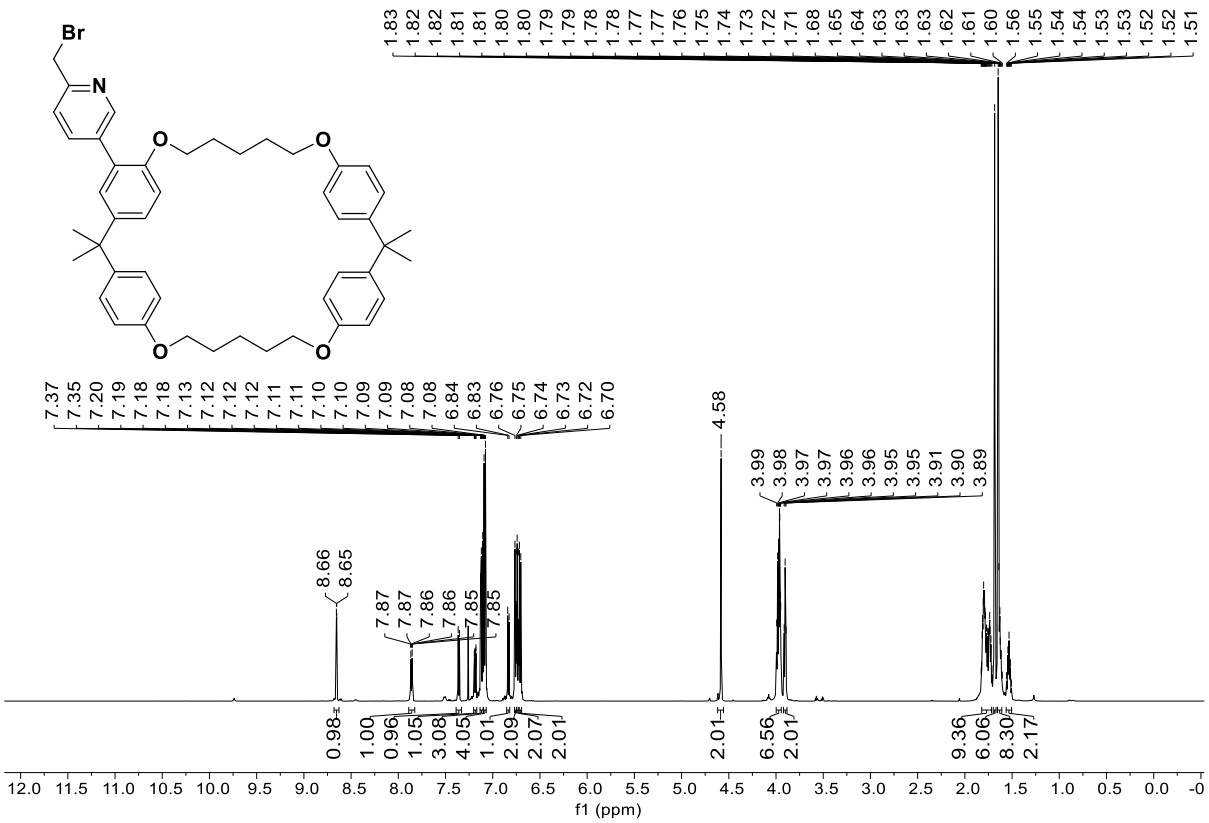

154: ^{13}C NMR (126 MHz, 300 K, $CDCl_3$)

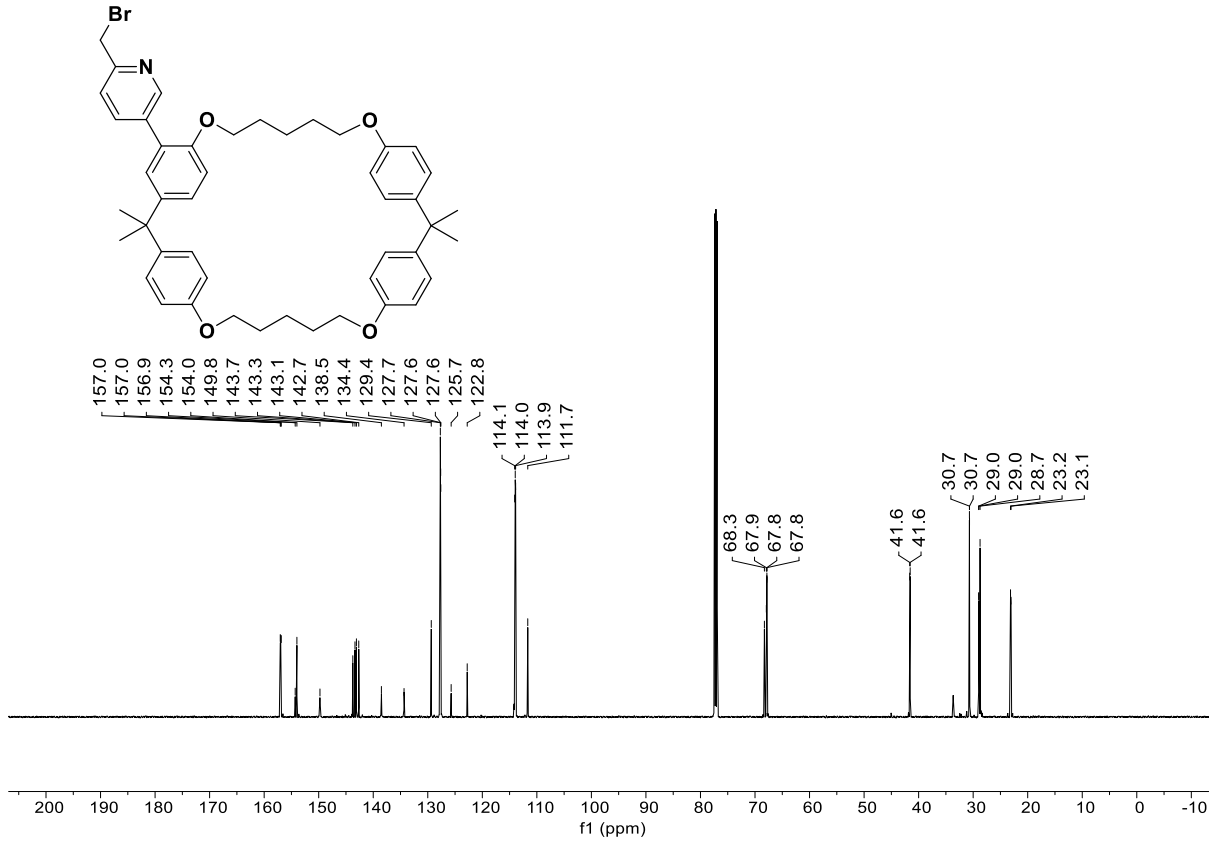

(mcp)CY5: ^{1}H NMR (600 MHz, 300 K, $CDCl_3$)

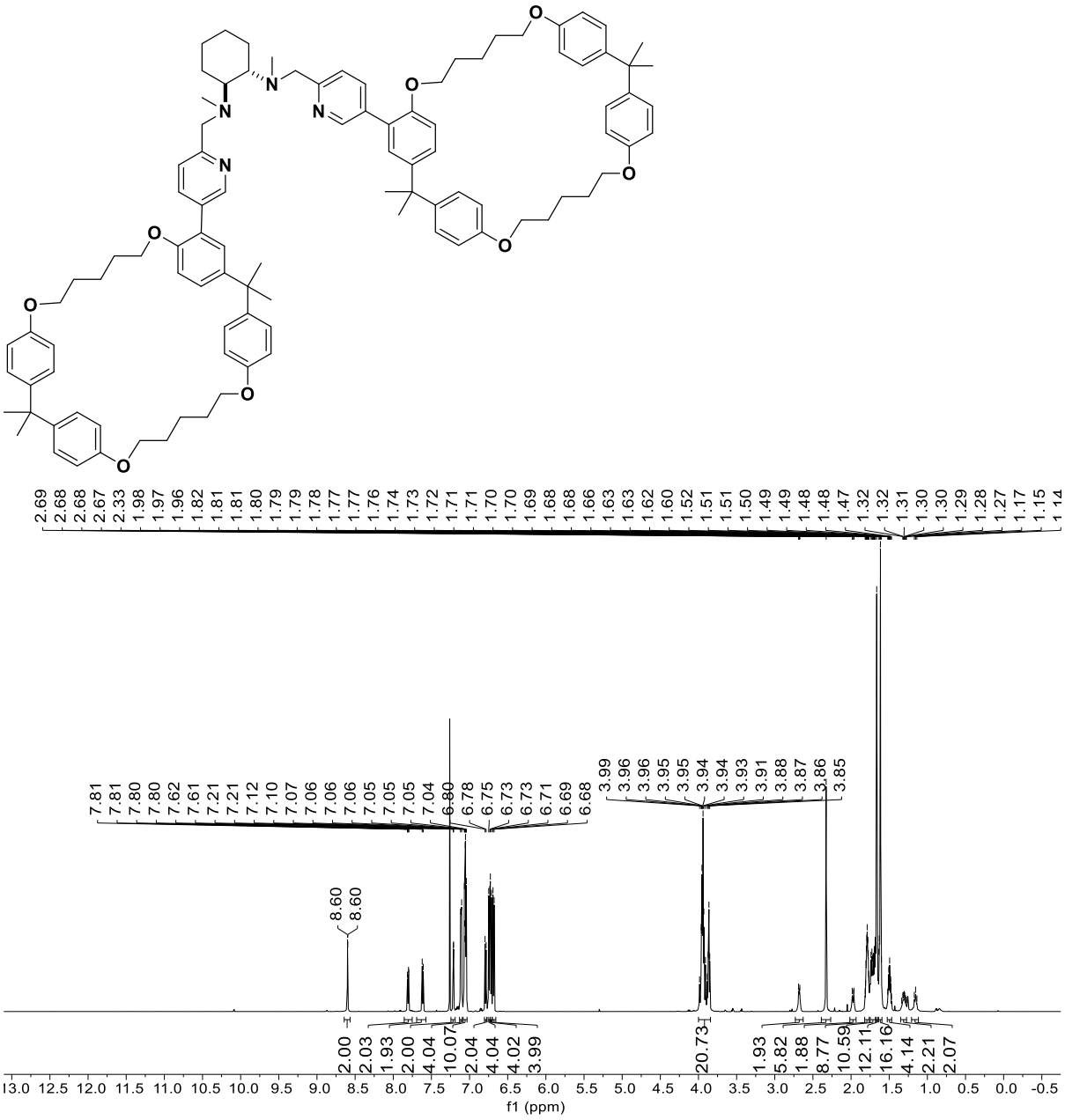

(mcp)CY5: ^{13}C NMR (126 MHz, 300 K, $CDCl_3$)

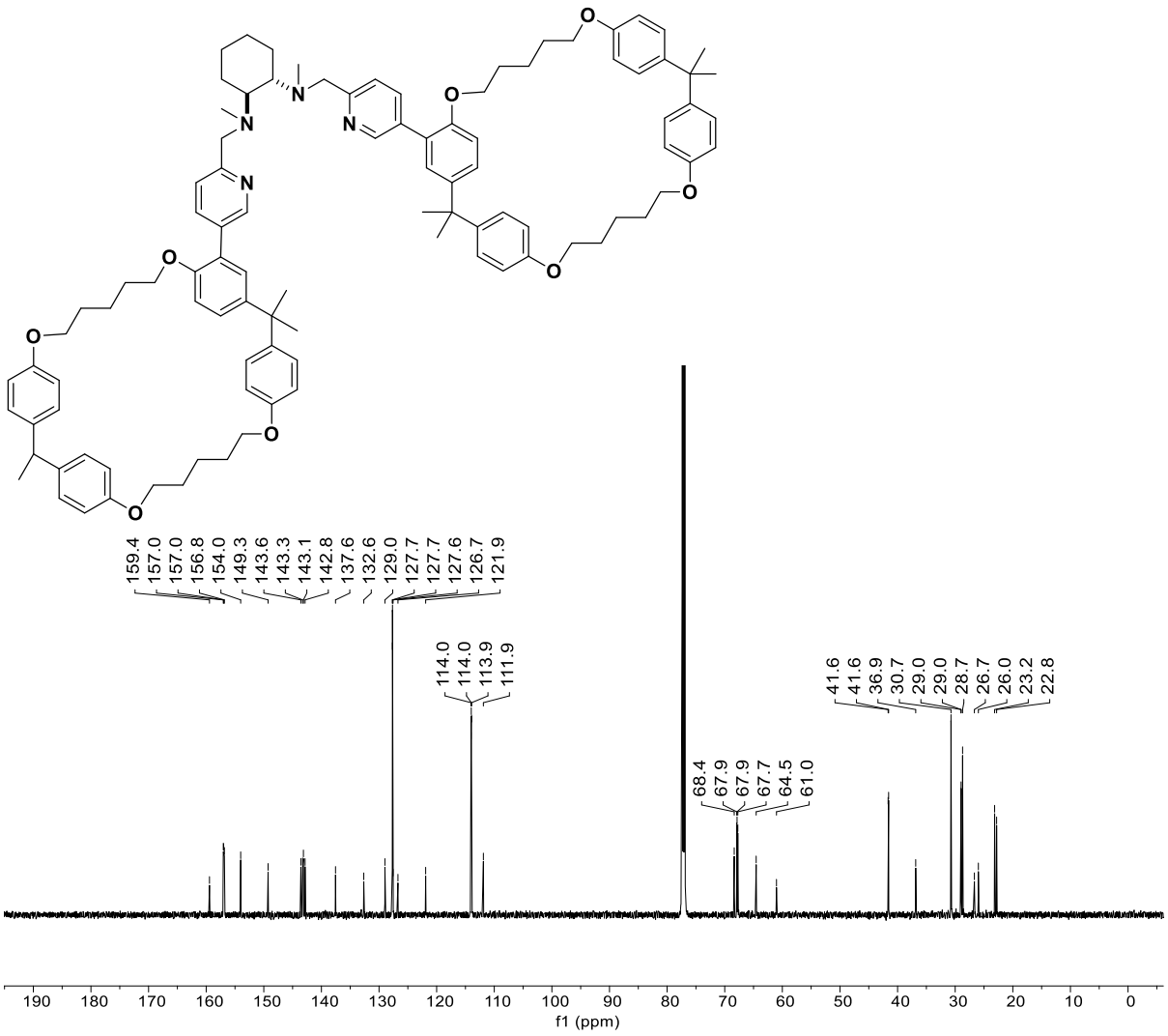

6 Index of Abbreviations

Å	Ångström, 10^{-10} m
Ac	acetyl
Ar	aryl
ATR	attenuated total reflection
BDE	bond dissociation energie
B_2pin_2	bis(pinacolato)diboron
Bpin	pinacolatoboron
BPA	bisphenol A
BP	biphenyl
Bu	butyl
CD	cyclodextrin
ChP	α,β,α,β-*meso*-tetrakis[*o*-(3β-hydroxy-5-cholenamido)phenyl]porphyrin
CR	crown ether
Cy	cyclohexyl
CY3	cyclophane 3
CY5	cyclophane 5
dMM	3,5-dimethyl-4-methoxy
DDO	dimethyldioxirane
DMF	dimethylformamide
DMPC	dimyristoylphosphocholine
EDG	electron donating group
equiv.	equivalents
ESI	electrospray ionization
et al.	et alii (and others)

Et	ethyl
EWG	electron withdrawing group
FID	flame ionization detector
GC	gas chromatography
GC-MS	gas chromatography-mass spectrometry
HAT	hydrogen atom transfer
Hex	hexane
HFIP	1,1,1,3,3,3-hexafluoro-2-isopropanol
HLF	Hofmann-Löffler-Freytag
HRMS	high resolution mass spectrometry
IBX	2-iodoxybenzoic acid
IR	infrared
mcp	*N*1,*N*2-dimethyl-*N*1,*N*2-bis(pyridin-2-ylmethyl)cyclohexane-1,2-diamine
Me	methyl
mep	*N*,*N*'-dimethyl-*N,N'*-bis(2-pyridylmethyl)ethylene-1,2-diamine
Ms	methansulfonyl
M.p.	melting point
MPLC	medium pressure liquid chromatography
NBS	*N*-bromosuccinimide
NMR	nuclear magnetic resonance
pdp	1,1'-bis(pyridin-2-ylmethyl)-2,2'-bipyrrolidine
Ph	phenyl
phen	1,10-phenanthroline
Porph	porphyrine

ppm	parts per million
prim.	primary
Py	pyridine
rt	room temperature
resp.	respectively
sec.	secondary
TBAB	tetrabutylammonium bromide
TBAF	tetrabutylammonium fluoride
TDCPP	5,10,15,20-tetrakis(2,6-dichlorophenyl)porphyrin
Terpy	2,2';6',2''-terpyridine
tert.	tertiary
Tf	trifluoromethansulfonyl
TFDO	trifluoromethylmethyldioxirane
TFE	trifluoroethanol
THF	tetrahydrofuran
TIPS	triisopropylsilyl
TLC	thin layer chromatography
TMP	5,10,15,20-tetramesitylporphyrin
TON	turnover number
tpa	tris(2-pyridylmethyl)amine
TPFPP	5,10,15,20-tetrakis(pentafluorophenyl)porphyrin
TPP	5,10,15,20-tetraphenylporphyrin
Twe	tweezer
TTPPP	5,10,15,20-tetrakis(2',4,,6'-tri-methoxyphenyl)porphyrin

7 References

[1] J.-M. Lehn, J. Benyus, *Bioinspiration and biomimicry in chemistry: reverse-engineering nature*, John Wiley & Sons, **2012**.

[2] E. M. Davis, R. Croteau, Cyclization enzymes in the biosynthesis of monoterpenes, sesquiterpenes, and diterpenes, *Biosynthesis* **2000**, 53-95.

[3] J. Gershenzon, N. Dudareva, The function of terpene natural products in the natural world, *Nat. Chem. Biol.* **2007**, *3*, 408-414.

[4] N. C. Wilde, M. Isomura, A. Mendoza, P. S. Baran, Two-phase synthesis of (−)-taxuyunnanine D, *J. Am. Chem. Soc.* **2014**, *136*, 4909-4912.

[5] Y. Kanda, H. Nakamura, S. Umemiya, R. K. Puthukanoori, V. R. Murthy Appala, G. K. Gaddamanugu, B. R. Paraselli, P. S. Baran, Two-phase synthesis of taxol, *J. Am. Chem. Soc.* **2020**, *142*, 10526-10533.

[6] L. A. Wein, K. Wurst, T. Magauer, Total Synthesis and Late-Stage C− H Oxidations of ent-Trachylobane Natural Products, *Angew. Chem. Int. Ed.* **2022**, *61*, e202113829.

[7] X.-S. Xue, P. Ji, B. Zhou, J.-P. Cheng, The essential role of bond energetics in C–H activation/functionalization, *Chem. Rev.* **2017**, *117*, 8622-8648.

[8] J.-Q. Yu, Z. Shi, *C-H activation*, Springer, **2010**.

[9] J. J. Li, *C-H bond activation in organic synthesis*, CRC press, **2015**.

[10] D. Maiti, S. Guin, *Remote C-H Bond Functionalizations: Methods and Strategies in Organic Synthesis*, John Wiley & Sons, **2021**.

[11] J. W. Steed, J. L. Atwood, *Supramolecular chemistry*, John Wiley & Sons, **2022**.

[12] J. M. Lehn, Supramolecular chemistry—scope and perspectives molecules, supermolecules, and molecular devices (Nobel Lecture), *Angew. Chem. Int. Ed.* **1988**, *27*, 89-112.

[13] C. J. Pedersen, The discovery of crown ethers (Noble Lecture), *Angew. Chem. Int. Ed.* **1988**, *27*, 1021-1027.

[14] D. J. Cram, The design of molecular hosts, guests, and their complexes (Nobel lecture), *Angew. Chem. Int. Ed.* **1988**, *27*, 1009-1020.

[15] F. G. Bordwell, Equilibrium acidities in dimethyl sulfoxide solution, *Acc. Chem. Res.* **1988**, *21*, 456-463.

[16] M. C. White, J. Zhao, Aliphatic C–H oxidations for late-stage functionalization, *J. Am. Chem. Soc.* **2018**, *140*, 13988-14009.

[17] H. Yi, G. Zhang, H. Wang, Z. Huang, J. Wang, A. K. Singh, A. Lei, Recent advances in radical C–H activation/radical cross-coupling, *Chem. Rev.* **2017**, *117*, 9016-9085.

[18] L. M. Stateman, K. M. Nakafuku, D. A. Nagib, Remote C–H functionalization via selective hydrogen atom transfer, *Synthesis* **2018**, *50*, 1569-1586.

[19] A. Hofmann, Ueber die Einwirkung des Broms in alkalischer Lösung auf die Amine, *Ber. Dtsch. Chem. Ges.* **1883**, *16*, 558-560.

[20] E. Corey, W. R. Hertler, A Study of the Formation of Haloamines and Cyclic Amines by the Free Radical Chain Decomposition of N-Haloammonium Ions (Hofmann-Löffler Reaction), *J. Am. Chem. Soc.* **1960**, *82*, 1657-1668.

[21] M. E. Wolff, Cyclization of N-Halogenated Amines (The Hofmann-Löffler Reaction), *Chem. Rev.* **1963**, *63*, 55-64.

[22] J. Yamaguchi, A. D. Yamaguchi, K. Itami, C– H Bond Functionalization: Emerging Synthetic Tools for Natural Products and Pharmaceuticals, *Angew. Chem. Int. Ed.* **2012**, *51*, 8960-9009.

[23] K. Löffler, C. Freytag, Über eine neue Bildungsweise von N-alkylierten Pyrrolidinen, *Ber. Dtsch. Chem. Ges.* **1909**, *42*, 3427-3431.

[24] K. Löffler, S. Kober, Über die Bildung des i-Nicotins aus N-Methyl-p-pyridyl-butylamin (Dihydrometanicotin), *Ber. Dtsch. Chem. Ges.* **1909**, *42*, 3431-3438.

[25] E. Corey, W. Hertler, The synthesis of dihydroconessine. A method for functionalizing steroids at C18, *J. Am. Chem. Soc.* **1958**, *80*, 2903-2904.
[26] P. De Armas, R. Carrau, J. I. Concepción, C. G. Francisco, R. Hernández, E. Suárez, Synthesis of 1, 4-epimine compounds. Iodosobenzene diacetate, an efficient reagent for neutral nitrogen radical generation, *Tetrahedron Lett.* **1985**, *26*, 2493-2496.
[27] D. Barton, J. Beaton, L. Geller, M. Pechet, A new photochemical reaction, *J. Am. Chem. Soc.* **1960**, *82*, 2640-2641.
[28] D. Barton, J. Beaton, A synthesis of aldosterone acetate, *J. Am. Chem. Soc.* **1960**, *82*, 2641-2641.
[29] C. Meystre, K. Heusler, J. Kalvoda, P. Wieland, G. Anner, A. Wettstein, Reaktionen von Steroid-Hypojoditen II. Über die Herstellung 18-oxygenierter Pregnanverbindungen. Über Steroide, 187. Mitteilung, *Helv. Chim. Acta* **1962**, *45*, 1317-1343.
[30] J. I. Concepción, C. G. Francisco, R. Hernández, J. A. Salazar, E. Suárez, Intramolecular hydrogen abstraction. Iodosobenzene diacetate, an efficient and convenient reagent for alkoxy radical generation, *Tetrahedron Lett.* **1984**, *25*, 1953-1956.
[31] C. G. Francisco, A. J. Herrera, E. Suárez, Intramolecular hydrogen abstraction reaction in carbohydrate chemistry. Synthesis of chiral 2, 7-dioxabicyclo [2.2. 1] heptane and 6, 8-dioxabicyclo [3.2. 1] octane ring systems, *Tetrahedron Lett.* **2000**, *41*, 7869-7873.
[32] X. Huang, J. Dannenberg, Molecular orbital estimation of the activation enthalpies for intramolecular hydrogen transfer as functions of size of the cyclic transition state and carbon-hydrogen-carbon angle, *J. Org. Chem.* **1991**, *56*, 5421-5424.
[33] H. G. Roth, N. A. Romero, D. A. Nicewicz, Experimental and calculated electrochemical potentials of common organic molecules for applications to single-electron redox chemistry, *Synlett* **2016**, *27*, 714-723.
[34] M. Nechab, S. Mondal, M. P. Bertrand, 1, n-Hydrogen-Atom Transfer (HAT) Reactions in Which n≠ 5: An Updated Inventory, *Chem. Eur. J.* **2014**, *20*, 16034-16059.
[35] K. Chen, J. M. Richter, P. S. Baran, 1, 3-diol synthesis via controlled, radical-mediated C− H functionalization, *J. Am. Chem. Soc.* **2008**, *130*, 7247-7249.
[36] A. G. Griesbeck, Spin-selectivity in photochemistry: a tool for organic synthesis, *Synlett* **2003**, *2003*, 0451-0472.
[37] C. G. Francisco, A. J. Herrera, A. R. Kennedy, D. Melián, E. Suárez, Intramolecular 1, 8-Hydrogen Abstraction Between Glucopyranose Units in a Disaccharide Model Promoted by Alkoxy Radicals, *Angew. Chem. Int. Ed.* **2002**, *41*, 856-858.
[38] R. Breslow, S. Baldwin, T. Flechtner, P. Kalicky, S. Liu, W. Washburn, Remote oxidation of steroids by photolysis of attached benzophenone groups, *J. Am. Chem. Soc.* **1973**, *95*, 3251-3262.
[39] R. Breslow, R. J. Corcoran, B. B. Snider, R. J. Doll, P. L. Khanna, R. Kaleya, Selective halogenation of steroids using attached aryl iodide templates, *J. Am. Chem. Soc.* **1977**, *99*, 905-915.
[40] R. M. Cory, F. R. McLaren, Carbon atom insertion: an efficient synthesis of ishwarane 1, *J. Chem. Soc., Chem. Commun.* **1977**, 587-588.
[41] S. Masamune, Total Syntheses of Diterpenes and Diterpene Alkaloids. IV. 1 Garryine, *J. Am. Chem. Soc.* **1964**, *86*, 290-291.
[42] W. Kirmse, Alkenylidenes in organic synthesis, *Angew. Chem. Int. Ed.* **1997**, *36*, 1164-1170.
[43] R. H. Crabtree, Alkane C–H activation and functionalization with homogeneous transition metal catalysts: A century of progress—A new millennium in prospect, *J. Chem. Soc., Dalton Trans.* **2001**, 2437-2450.
[44] A. R. Dick, M. S. Sanford, Transition metal catalyzed oxidative functionalization of carbon–hydrogen bonds, *Tetrahedron* **2006**, *11*, 2439-2463.

[45] A. E. Shilov, G. B. Shul'pin, Activation of C− H bonds by metal complexes, *Chem. Rev.* **1997**, *97*, 2879-2932.
[46] T. W. Lyons, M. S. Sanford, Palladium-catalyzed ligand-directed C− H functionalization reactions, *Chem. Rev.* **2010**, *110*, 1147-1169.
[47] K. M. Engle, T.-S. Mei, M. Wasa, J.-Q. Yu, Weak coordination as a powerful means for developing broadly useful C–H functionalization reactions, *Acc. Chem. Res.* **2012**, *45*, 788-802.
[48] J. He, M. Wasa, K. S. Chan, Q. Shao, J.-Q. Yu, Palladium-catalyzed transformations of alkyl C–H bonds, *Chem. Rev.* **2017**, *117*, 8754-8786.
[49] L. V. Desai, K. L. Hull, M. S. Sanford, Palladium-catalyzed oxygenation of unactivated sp3 C− H bonds, *J. Am. Chem. Soc.* **2004**, *126*, 9542-9543.
[50] A. R. Dick, K. L. Hull, M. S. Sanford, A highly selective catalytic method for the oxidative functionalization of C− H bonds, *J. Am. Chem. Soc.* **2004**, *126*, 2300-2301.
[51] D.-H. Wang, X.-S. Hao, D.-F. Wu, J.-Q. Yu, Palladium-Catalyzed Oxidation of Boc-Protected N-Methylamines with IOAc as the Oxidant: A Boc-Directed sp3 C− H Bond Activation, *Org. Lett.* **2006**, *8*, 3387-3390.
[52] L. V. Desai, H. A. Malik, M. S. Sanford, Oxone as an inexpensive, safe, and environmentally benign oxidant for C− H bond oxygenation, *Org. Lett.* **2006**, *8*, 1141-1144.
[53] B. S. Reddy, L. R. Reddy, E. Corey, Novel acetoxylation and C− C coupling reactions at unactivated positions in α-amino acid derivatives, *Org. Lett.* **2006**, *8*, 3391-3394.
[54] H. M. Davies, J. R. Manning, Catalytic C–H functionalization by metal carbenoid and nitrenoid insertion, *Nature* **2008**, *451*, 417-424.
[55] J. L. Roizen, M. E. Harvey, J. Du Bois, Metal-catalyzed nitrogen-atom transfer methods for the oxidation of aliphatic C–H bonds, *Acc. Chem. Res.* **2012**, *45*, 911-922.
[56] R. Breslow, S. H. Gellman, Intramolecular nitrene carbon-hydrogen insertions mediated by transition-metal complexes as nitrogen analogs of cytochrome P-450 reactions, *J. Am. Chem. Soc.* **1983**, *105*, 6728-6729.
[57] C. G. Espino, J. Du Bois, A Rh-Catalyzed C− H Insertion Reaction for the Oxidative Conversion of Carbamates to Oxazolidinones, *Angew. Chem. Int. Ed.* **2001**, *40*, 598-600.
[58] C. G. Espino, P. M. Wehn, J. Chow, J. Du Bois, Synthesis of 1, 3-difunctionalized amine derivatives through selective C− H bond oxidation, *J. Am. Chem. Soc.* **2001**, *123*, 6935-6936.
[59] A. Hinman, J. Du Bois, A stereoselective synthesis of (−)-tetrodotoxin, *J. Am. Chem. Soc.* **2003**, *125*, 11510-11511.
[60] N. Ohyabu, T. Nishikawa, M. Isobe, First asymmetric total synthesis of tetrodotoxin, *J. Am. Chem. Soc.* **2003**, *125*, 8798-8805.
[61] T. Newhouse, P. S. Baran, If C-H Bonds Could Talk: Selective C-H Bond Oxidation, *Angew. Chem. Int. Ed.* **2011**, *50*, 3362-3374.
[62] J. F. Hartwig, M. A. Larsen, Undirected, homogeneous C–H bond functionalization: challenges and opportunities, *ACS Cent. Sci.* **2016**, *2*, 281-292.
[63] L. D'Accolti, C. Annese, C. Fusco, Continued Progress towards Efficient Functionalization of Natural and Non-natural Targets under Mild Conditions: Oxygenation by C− H Bond Activation with Dioxirane, *Chem. Eur. J.* **2019**, *25*, 12003-12017.
[64] R. W. Murray, R. Jeyaraman, L. Mohan, Chemistry of dioxiranes. 4. Oxygen atom insertion into carbon-hydrogen bonds by dimethyldioxirane, *J. Am. Chem. Soc.* **1986**, *108*, 2470-2472.
[65] R. W. Murray, M. Singh, R. Jeyaraman, Dioxiranes. 20. Preparation and properties of some new dioxiranes, *J. Am. Chem. Soc.* **1992**, *114*, 1346-1351.

[66] R. Curci, A. Dinoi, M. F. Rubino, Dioxirane oxidations: Taming the reactivity-selectivity principle, *Pure Appl. Chem.* **1995**, *67*, 811-822.
[67] W. Adam, G. Asensio, R. Curci, M. E. Gonzalez-Nunez, R. Mello, Oxygen atom insertion into the benzylic carbon-hydrogen bond of (R)-(-)-2-phenylbutane by methyl (trifluoromethyl) dioxirane: an efficient and mild regio-and stereoselective synthesis of (S)-(-)-2-phenyl-2-butanol, *J. Org. Chem.* **1992**, *57*, 953-955.
[68] M. N. Glukhovtsev, C. Canepa, R. D. Bach, The nature of the transition structure for the oxidation of alkanes with dioxiranes, *J. Am. Chem. Soc.* **1998**, *120*, 10528-10533.
[69] F. Minisci, L. Zhao, F. Fontana, A. Bravo, Free-radicals in the oxidation and halogenation of alkanes by dimethyldioxirane: an oxygen rebound mechanism, *Tetrahedron Lett.* **1995**, *36*, 1697-1700.
[70] A. Bravo, H.-R. Bjorsvik, F. Fontana, F. Minisci, A. Serri, Radical versus "oxenoid" oxygen insertion mechanism in the oxidation of alkanes and alcohols by aromatic peracids. New synthetic developments, *J. Org. Chem.* **1996**, *61*, 9409-9416.
[71] R. D. Bach, The DMDO hydroxylation of hydrocarbons via the oxygen rebound mechanism, *J. Phys. Chem. A* **2016**, *120*, 840-850.
[72] L. Zou, R. S. Paton, A. Eschenmoser, T. R. Newhouse, P. S. Baran, K. Houk, Enhanced reactivity in dioxirane C–H oxidations via strain release: A computational and experimental study, *J. Org. Chem.* **2013**, *78*, 4037-4048.
[73] Z. Yang, P. Yu, K. Houk, Molecular dynamics of dimethyldioxirane C–H oxidation, *J. Am. Chem. Soc.* **2016**, *138*, 4237-4242.
[74] G. Asensio, G. Castellano, R. Mello, M. González Núñez, Oxyfunctionalization of aliphatic esters by methyl (trifluoromethyl) dioxirane, *J. Org. Chem.* **1996**, *61*, 5564-5566.
[75] L. D'Accolti, A. Dinoi, C. Fusco, A. Russo, R. Curci, Oxyfunctionalization of Non-Natural Targets by Dioxiranes. 5. Selective Oxidation of Hydrocarbons Bearing Cyclopropyl Moieties1, *J. Org. Chem.* **2003**, *68*, 7806-7810.
[76] P. Bovicelli, P. Lupattelli, E. Mincione, T. Prencipe, R. Curci, Oxidation of natural targets by dioxiranes. 2. Direct hydroxylation at the side chain C-25 of cholestane derivatives and of vitamin D3 Windaus-Grundmann ketone, *J. Org. Chem.* **1992**, *57*, 5052-5054.
[77] R. Mello, M. Fiorentino, C. Fusco, R. Curci, Oxidations by methyl (trifluoromethyl) dioxirane. 2. Oxyfunctionalization of saturated hydrocarbons, *J. Am. Chem. Soc.* **1989**, *111*, 6749-6757.
[78] N. F. Gol'Dshleger, V. V. Es'Kova, A. E. Shilov, A. A. Shteinman, Reactions of alkanes in solutions of platinum chloride complexes, *Zh. Fiz. Khim.* **1972**, *46*, 1353-1354.
[79] V. V. Es'Kova, A. E. Shilov, A. A. Shteinman, *Kinet. Katal.* **1972**, *13*, 534.
[80] R. A. Periana, D. J. Taube, S. Gamble, H. Taube, T. Satoh, H. Fujii, Platinum catalysts for the high-yield oxidation of methane to a methanol derivative, *Science* **1998**, *280*, 560-564.
[81] M. Lee, M. S. Sanford, Platinum-catalyzed, terminal-selective C (sp3)–H oxidation of aliphatic amines, *J. Am. Chem. Soc.* **2015**, *137*, 12796-12799.
[82] B. Meunier, Metalloporphyrins as versatile catalysts for oxidation reactions and oxidative DNA cleavage, *Chem. Rev.* **1992**, *92*, 1411-1456.
[83] D. Mansuy, Activation of alkanes: The biomimetic approach, *Coord. Chem. Rev.* **1993**, *125*, 129-141.
[84] P. R. O. De Montellano, *Cytochrome P450: structure, mechanism, and biochemistry*, Springer, **2005**.
[85] W. Nam, High-valent iron (IV)–oxo complexes of heme and non-heme ligands in oxygenation reactions, *Acc. Chem. Res.* **2007**, *40*, 522-531.

[86] M. Costas, Selective C–H oxidation catalyzed by metalloporphyrins, *Coord. Chem. Rev.* **2011**, *255*, 2912-2932.
[87] H. Lu, X. P. Zhang, Catalytic C–H functionalization by metalloporphyrins: recent developments and future directions, *Chem. Soc. Rev.* **2011**, *40*, 1899-1909.
[88] J. T. Groves, T. E. Nemo, R. S. Myers, Hydroxylation and epoxidation catalyzed by iron-porphine complexes. Oxygen transfer from iodosylbenzene, *J. Am. Chem. Soc.* **1979**, *101*, 1032-1033.
[89] J. T. Groves, W. J. Kruper Jr, R. C. Haushalter, Hydrocarbon oxidations with oxometalloporphinates. Isolation and reactions of a (porphinato) manganese (V) complex, *J. Am. Chem. Soc.* **1980**, *102*, 6375-6377.
[90] C. Chang, M.-S. Kuo, Reaction of iron (III) porphyrins and iodosoxylene. The active oxene complex of cytochrome P-450, *J. Am. Chem. Soc.* **1979**, *101*, 3413-3415.
[91] J. T. Groves, T. E. Nemo, Aliphatic hydroxylation catalyzed by iron porphyrin complexes, *J. Am. Chem. Soc.* **1983**, *105*, 6243-6248.
[92] P. S. Traylor, D. Dolphin, T. G. Traylor, Sterically protected hemins with electronegative substituents: efficient catalysts for hydroxylation and epoxidation, *J. Chem. Soc., Chem. Commun.* **1984**, 279-280.
[93] C. K. Chang, F. Ebina, NIH shift in haemin–iodosylbenzene-mediated hydroxylations, *J. Chem. Soc., Chem. Commun.* **1981**, 778-779.
[94] T. G. Traylor, S. Tsuchiya, Perhalogenated tetraphenylhemins: stable catalysts of high turnover catalytic hydroxylations, *Inorg. Chem.* **1987**, *26*, 1338-1339.
[95] P. Hoffmann, G. Labat, A. Robert, B. Meunier, Highly Selective Bromination of Tetramesitylporphyrin: An Easy Access to Robust Metalloporphyrins, M-Br8TMP and M-Br8TMPS. Examples of application in catalytic oxygenation and oxidation reactions, *Tetrahedron Lett.* **1990**, *31*, 1991-1994.
[96] T. Wijesekera, A. Matsumoto, D. Dolphin, D. Lexa, Perchlorinated and Highly Chlorinated meso-Tetraphenylporphyrins, *Angew. Chem. Int. Ed.* **1990**, *29*, 1028-1030.
[97] S. Tsuchiya, M. Seno, Novel synthetic method of phenol from benzene catalysed by perfluorinated hemin, *Chem. Lett.* **1989**, *18*, 263-266.
[98] J. T. Groves, G. A. McClusky, R. E. White, M. J. Coon, Aliphatic hydroxylation by highly purified liver microsomal cytochrome P-450. Evidence for a carbon radical intermediate, *Biochem. Biophys. Res. Commun.* **1978**, *81*, 154-160.
[99] I. Schlichting, J. Berendzen, K. Chu, A. M. Stock, S. A. Maves, D. E. Benson, R. M. Sweet, D. Ringe, G. A. Petsko, S. G. Sligar, The catalytic pathway of cytochrome P450cam at atomic resolution, *Science* **2000**, *287*, 1615-1622.
[100] J. Rittle, M. T. Green, Cytochrome P450 compound I: capture, characterization, and CH bond activation kinetics, *Science* **2010**, *330*, 933-937.
[101] P. R. Ortiz de Montellano, Hydrocarbon hydroxylation by cytochrome P450 enzymes, *Chem. Rev.* **2010**, *110*, 932-948.
[102] W. Nam, M. H. Lim, S. Y. Oh, J. H. Lee, H. J. Lee, S. K. Woo, C. Kim, W. Shin, Remarkable Anionic Axial Ligand Effects of Iron (III) Porphyrin Complexes on the Catalytic Oxygenations of Hydrocarbons by H2O2 and the Formation of Oxoiron (IV) Porphyrin Intermediates by m-Chloroperoxybenzoic Acid, *Angew. Chem. Int. Ed.* **2000**, *39*, 3646-3649.
[103] Y. Kang, H. Chen, Y. J. Jeong, W. Lai, E. H. Bae, S. Shaik, W. Nam, Enhanced Reactivities of Iron (IV)-Oxo Porphyrin π-Cation Radicals in Oxygenation Reactions by Electron-Donating Axial Ligands, *Chem. Eur. J.* **2009**, *15*, 10039-10046.
[104] W. Liu, J. T. Groves, Manganese catalyzed C–H halogenation, *Acc. Chem. Res.* **2015**, *48*, 1727-1735.
[105] W. Liu, J. T. Groves, Manganese porphyrins catalyze selective C− H bond halogenations, *J. Am. Chem. Soc.* **2010**, *132*, 12847-12849.

[106] W. Liu, X. Huang, M.-J. Cheng, R. J. Nielsen, W. A. Goddard III, J. T. Groves, Oxidative aliphatic CH fluorination with fluoride ion catalyzed by a manganese porphyrin, *Science* **2012**, *337*, 1322-1325.
[107] B. R. Cook, T. J. Reinert, K. S. Suslick, Shape-selective alkane hydroxylation by metalloporphyrin catalysts, *J. Am. Chem. Soc.* **1986**, *108*, 7281-7286.
[108] J. T. Groves, P. Viski, Asymmetric hydroxylation, epoxidation, and sulfoxidation catalyzed by vaulted binaphthyl metalloporphyrins, *J. Org. Chem.* **1990**, *55*, 3628-3634.
[109] R. Zhang, W.-Y. Yu, T.-S. Lai, C.-M. Che, Enantioselective hydroxylation of benzylic C–H bonds by D4-symmetric chiral oxoruthenium porphyrins, *Chem. Commun.* **1999**, 1791-1792.
[110] T. Hamada, R. Irie, J. Mihara, K. Hamachi, T. Katsuki, Highly enantioselective benzylic hydroxylation with concave type of (salen) manganese (III) complex, *Tetrahedron* **1998**, *54*, 10017-10028.
[111] V. A. Schmidt, R. K. Quinn, A. T. Brusoe, E. J. Alexanian, Site-selective aliphatic C–H bromination using N-bromoamides and visible light, *J. Am. Chem. Soc.* **2014**, *136*, 14389-14392.
[112] R. K. Quinn, Z. A. Könst, S. E. Michalak, Y. Schmidt, A. R. Szklarski, A. R. Flores, S. Nam, D. A. Horne, C. D. Vanderwal, E. J. Alexanian, Site-selective aliphatic C–H chlorination using N-chloroamides enables a synthesis of chlorolissoclimide, *J. Am. Chem. Soc.* **2016**, *138*, 696-702.
[113] J. L. Roizen, D. N. Zalatan, J. Du Bois, Selective Intermolecular Amination of C□ H Bonds at Tertiary Carbon Centers, *Angew. Chem. Int. Ed.* **2013**, *52*, 11343-11346.
[114] A. Sharma, J. F. Hartwig, Metal-catalysed azidation of tertiary C–H bonds suitable for late-stage functionalization, *Nature* **2015**, *517*, 600-604.
[115] H. M. Davies, R. E. Beckwith, Catalytic enantioselective C− H activation by means of metal− carbenoid-induced C− H insertion, *Chem. Rev.* **2003**, *103*, 2861-2904.
[116] H. M. Davies, T. Hansen, M. R. Churchill, Catalytic asymmetric C− H activation of alkanes and tetrahydrofuran, *J. Am. Chem. Soc.* **2000**, *122*, 3063-3070.
[117] R. P. Hausinger, Fe (II)/α-ketoglutarate-dependent hydroxylases and related enzymes, *Crit. Rev. Biochem. Mol. Biol.* **2004**, *39*, 21-68.
[118] M. Merkx, D. A. Kopp, M. H. Sazinsky, J. L. Blazyk, J. Müller, S. J. Lippard, Dioxygen activation and methane hydroxylation by soluble methane monooxygenase: a tale of two irons and three proteins, *Angew. Chem. Int. Ed.* **2001**, *40*, 2782-2807.
[119] B. J. Wallar, J. D. Lipscomb, Dioxygen activation by enzymes containing binuclear non-heme iron clusters, *Chem. Rev.* **1996**, *96*, 2625-2658.
[120] C. E. Tinberg, S. J. Lippard, Dioxygen activation in soluble methane monooxygenase, *Acc. Chem. Res.* **2011**, *44*, 280-288.
[121] E. I. Solomon, T. C. Brunold, M. I. Davis, J. N. Kemsley, S.-K. Lee, N. Lehnert, F. Neese, A. J. Skulan, Y.-S. Yang, J. Zhou, Geometric and electronic structure/function correlations in non-heme iron enzymes, *Chem. Rev.* **2000**, *100*, 235-350.
[122] P. C. Bruijnincx, G. van Koten, R. J. K. Gebbink, Mononuclear non-heme iron enzymes with the 2-His-1-carboxylate facial triad: recent developments in enzymology and modeling studies, *Chem. Soc. Rev.* **2008**, *37*, 2716-2744.
[123] E. L. Hegg, L. Q. Jr, The 2-His-1-carboxylate facial triad—an emerging structural motif in mononuclear non-heme iron (II) enzymes, *Eur. J. Biochem.* **1997**, *250*, 625-629.
[124] R. A. Leising, J. Kim, M. A. Perez, L. Que Jr, Alkane functionalization at (. mu.-oxo) diiron (III) centers, *J. Am. Chem. Soc.* **1993**, *115*, 9524-9530.
[125] R. A. Leising, R. E. Norman, L. Que Jr, Alkane functionalization by nonporphyrin iron complexes: mechanistic insights, *Inorg. Chem.* **1990**, *29*, 2553-2555.
[126] M. Costas, K. Chen, L. Que Jr, Biomimetic nonheme iron catalysts for alkane hydroxylation, *Coord. Chem. Rev.* **2000**, *200*, 517-544.

[127] W. N. Oloo, L. Que Jr, Bioinspired Nonheme Iron Catalysts for C–H and C–C Bond Oxidation: Insights into the Nature of the Metal-Based Oxidants, *Acc. Chem. Res.* **2015**, *48*, 2612-2621.
[128] N. V. Tkachenko, R. V. Ottenbacher, O. Y. Lyakin, A. M. Zima, D. G. Samsonenko, E. P. Talsi, K. P. Bryliakov, Highly Efficient Aromatic C− H Oxidation with H2O2 in the Presence of Iron Complexes of the PDP Family, *ChemCatChem* **2018**, *10*, 4052-4057.
[129] M. A. Bigi, S. A. Reed, M. C. White, Diverting non-haem iron catalysed aliphatic C–H hydroxylations towards desaturations, *Nat. Chem.* **2011**, *3*, 216.
[130] L. Chen, X.-J. Su, J. W. Jurss, Selective Alkane C–H Bond Oxidation Catalyzed by a Non-Heme Iron Complex Featuring a Robust Tetradentate Ligand, *Organometallics* **2018**, *37*, 4535-4539.
[131] T. Okuno, S. Ito, S. Ohba, Y. Nishida, μ-Oxo bridged diiron (III) complexes and hydrogen peroxide: Oxygenation and catalase-like activities, *J. Chem. Soc., Dalton Trans.* **1997**, 3547-3551.
[132] A. Company, L. Gómez, X. Fontrodona, X. Ribas, M. Costas, A Novel Platform for Modeling Oxidative Catalysis in Non-Heme Iron Oxygenases with Unprecedented Efficiency, *Chem. Eur. J.* **2008**, *14*, 5727-5731.
[133] Y. Feng, J. England, L. Que Jr, Iron-catalyzed olefin epoxidation and cis-dihydroxylation by tetraalkylcyclam complexes: the importance of cis-labile sites, *ACS Catal.* **2011**, *1*, 1035-1042.
[134] L. Vicens, G. Olivo, M. Costas, Rational design of bioinspired catalysts for selective oxidations, *ACS Catal.* **2020**, *10*, 8611-8631.
[135] M. S. Chen, M. C. White, A predictably selective aliphatic C–H oxidation reaction for complex molecule synthesis, *Science* **2007**, *318*, 783-787.
[136] M. S. Chen, M. C. White, Combined effects on selectivity in Fe-catalyzed methylene oxidation, *Science* **2010**, *327*, 566-571.
[137] A. Murphy, G. Dubois, T. Stack, Efficient epoxidation of electron-deficient olefins with a cationic manganese complex, *J. Am. Chem. Soc.* **2003**, *125*, 5250-5251.
[138] M. Canta, D. Font, L. Gómez, X. Ribas, M. Costas, The iron (II) complex [Fe (CF3SO3) 2 (mcp)] as a convenient, readily available catalyst for the selective oxidation of methylenic sites in alkanes, *Adv. Synth. Catal.* **2014**, *356*, 818-830.
[139] B. Wang, S. Wang, C. Xia, W. Sun, Highly Enantioselective Epoxidation of Multisubstituted Enones Catalyzed by Non-Heme Iron Catalysts, *Chem. Eur. J.* **2012**, *18*, 7332-7335.
[140] E. A. Mikhalyova, O. V. Makhlynets, T. D. Palluccio, A. S. Filatov, E. V. Rybak-Akimova, A new efficient iron catalyst for olefin epoxidation with hydrogen peroxide, *Chem. Commun.* **2012**, *48*, 687-689.
[141] C. Clarasó, L. Vicens, A. Polo, M. Costas, Enantioselective Epoxidation of β, β-Disubstituted Enamides with a Manganese Catalyst and Aqueous Hydrogen Peroxide, *Org. Lett.* **2019**, *21*, 2430-2435.
[142] O. Cusso, I. Garcia-Bosch, X. Ribas, J. Lloret-Fillol, M. Costas, Asymmetric epoxidation with H2O2 by manipulating the electronic properties of non-heme iron catalysts, *J. Am. Chem. Soc.* **2013**, *135*, 14871-14878.
[143] G. Olivo, O. Lanzalunga, L. Mandolini, S. Di Stefano, Substituent effects on the catalytic activity of bipyrrolidine-based iron complexes, *J. Org. Chem.* **2013**, *78*, 11508-11512.
[144] D. Font, M. Canta, M. Milan, O. Cussó, X. Ribas, R. J. Klein Gebbink, M. Costas, Readily accessible bulky iron catalysts exhibiting site selectivity in the oxidation of steroidal substrates, *Angew. Chem. Int. Ed.* **2016**, *55*, 5776-5779.
[145] P. E. Gormisky, M. C. White, Catalyst-controlled aliphatic C–H oxidations with a predictive model for site-selectivity, *J. Am. Chem. Soc.* **2013**, *135*, 14052-14055.

[146] M. Costas, J. Que, Lawrence, Ligand topology tuning of iron-catalyzed hydrocarbon oxidations, *Angew. Chem. Int. Ed.* **2002**, *41*, 2179-2181.
[147] K. Chen, L. Que, Stereospecific alkane hydroxylation by non-heme iron catalysts: mechanistic evidence for an FeV O active species, *J. Am. Chem. Soc.* **2001**, *123*, 6327-6337.
[148] R. Mas-Ballesté, L. Que, Iron-catalyzed olefin epoxidation in the presence of acetic acid: insights into the nature of the metal-based oxidant, *J. Am. Chem. Soc.* **2007**, *129*, 15964-15972.
[149] L. Que, W. B. Tolman, Biologically inspired oxidation catalysis, *Nature* **2008**, *455*, 333-340.
[150] M. Salamone, M. Bietti, Tuning reactivity and selectivity in hydrogen atom transfer from aliphatic C–H bonds to alkoxyl radicals: role of structural and medium effects, *Acc. Chem. Res.* **2015**, *48*, 2895-2903.
[151] M. Salamone, L. Mangiacapra, M. Bietti, Kinetic solvent effects on the reactions of the cumyloxyl radical with tertiary amides. Control over the hydrogen atom transfer reactivity and selectivity through solvent polarity and hydrogen bonding, *J. Org. Chem.* **2015**, *80*, 1149-1154.
[152] E. Gaster, S. Kozuch, D. Pappo, Selective Aerobic Oxidation of Methylarenes to Benzaldehydes Catalyzed by N-Hydroxyphthalimide and Cobalt (II) Acetate in Hexafluoropropan-2-ol, *Angew. Chem. Int. Ed.* **2017**, *56*, 5912-5915.
[153] V. Dantignana, M. Milan, O. Cussó, A. Company, M. Bietti, M. Costas, Chemoselective Aliphatic C–H bond oxidation enabled by polarity reversal, *ACS Cent. Sci.* **2017**, *3*, 1350-1358.
[154] M. Salamone, R. Martella, M. Bietti, Hydrogen abstraction from cyclic amines by the cumyloxyl and benzyloxyl radicals. The role of stereoelectronic effects and of substrate/radical hydrogen bonding, *J. Org. Chem.* **2012**, *77*, 8556-8561.
[155] M. Salamone, M. Milan, G. A. DiLabio, M. Bietti, Absolute rate constants for hydrogen atom transfer from tertiary amides to the cumyloxyl radical: evaluating the role of stereoelectronic effects, *J. Org. Chem.* **2014**, *79*, 7179-7184.
[156] V. Malatesta, J. Scaiano, Absolute rate constants for the reactions of tert-butoxyl with ethers: importance of the stereoelectronic effect, *J. Org. Chem.* **1982**, *47*, 1455-1459.
[157] E. P. Talsi, D. G. Samsonenko, K. P. Bryliakov, Asymmetric autoamplification in the oxidative kinetic resolution of secondary benzylic alcohols catalyzed by manganese complexes, *ChemCatChem* **2017**, *9*, 2599-2607.
[158] E. P. Talsi, D. G. Samsonenko, R. V. Ottenbacher, K. P. Bryliakov, Highly Enantioselective C− H Oxidation of Arylalkanes with H2O2 in the Presence of Chiral Mn-Aminopyridine Complexes, *ChemCatChem* **2017**, *9*, 4580-4586.
[159] M. Milan, M. Bietti, M. Costas, Highly enantioselective oxidation of nonactivated aliphatic C–H bonds with hydrogen peroxide catalyzed by manganese complexes, *ACS Cent. Sci.* **2017**, *3*, 196-204.
[160] M. Salamone, V. B. Ortega, M. Bietti, Enhanced Reactivity in Hydrogen Atom Transfer from Tertiary Sites of Cyclohexanes and Decalins via Strain Release: Equatorial C–H Activation vs Axial C–H Deactivation, *J. Org. Chem.* **2015**, *80*, 4710-4715.
[161] M. González-Núñez, G. Castellano, C. Andreu, J. Royo, M. Báguena, R. Mello, G. Asensio, Influence of Remote Substituents on the Equatorial/Axial Selectivity in the Monooxygenation of Methylene C− H Bonds of Substituted Cyclohexanes, *J. Am. Chem. Soc.* **2001**, *123*, 7487-7491.
[162] M. Raynal, P. Ballester, A. Vidal-Ferran, P. W. van Leeuwen, Supramolecular catalysis. Part 1: non-covalent interactions as a tool for building and modifying homogeneous catalysts, *Chem. Soc. Rev.* **2014**, *43*, 1660-1733.

[163] Y. Jiao, X.-Y. Chen, J. F. Stoddart, Weak bonding strategies for achieving regio-and site-selective transformations, *Chem* **2022**, *8*, 414-438.
[164] G. A. Jeffrey, W. Saenger, *Hydrogen bonding in biological structures*, Springer, **2012**.
[165] J. Emsley, Very strong hydrogen bonding, *Chem. Soc. Rev.* **1980**, *9*, 91-124.
[166] C. R. Martinez, B. L. Iverson, Rethinking the term "pi-stacking", *Chem. Sci.* **2012**, *3*, 2191-2201.
[167] D. A. Dougherty, Cation-π interactions in chemistry and biology: a new view of benzene, Phe, Tyr, and Trp, *Science* **1996**, *271*, 163-168.
[168] L. M. Salonen, M. Ellermann, F. Diederich, Aromatic rings in chemical and biological recognition: energetics and structures, *Angew. Chem. Int. Ed.* **2011**, *50*, 4808-4842.
[169] L. Yang, C. Adam, G. S. Nichol, S. L. Cockroft, How much do van der Waals dispersion forces contribute to molecular recognition in solution?, *Nat. Chem.* **2013**, *5*, 1006-1010.
[170] M. Fujita, Metal-directed self-assembly of two-and three-dimensional synthetic receptors, *Chem. Soc. Rev.* **1998**, *27*, 417-425.
[171] C. J. Brown, F. D. Toste, R. G. Bergman, K. N. Raymond, Supramolecular catalysis in metal–ligand cluster hosts, *Chem. Rev.* **2015**, *115*, 3012-3035.
[172] S. J. Rowan, S. J. Cantrill, G. R. Cousins, J. K. Sanders, J. F. Stoddart, Dynamic covalent chemistry, *Angew. Chem. Int. Ed.* **2002**, *41*, 898-952.
[173] Y. Jin, C. Yu, R. J. Denman, W. Zhang, Recent advances in dynamic covalent chemistry, *Chem. Soc. Rev.* **2013**, *42*, 6634-6654.
[174] D. Vidal, G. Olivo, M. Costas, Controlling Selectivity in Aliphatic C− H Oxidation through Supramolecular Recognition, *Chem. Eur. J.* **2018**, *24*, 5042-5054.
[175] J. Szejtli, Introduction and general overview of cyclodextrin chemistry, *Chem. Rev.* **1998**, *98*, 1743-1754.
[176] V. T. D'Souza, M. L. Bender, Miniature organic models of enzymes, *Acc. Chem. Res.* **1987**, *20*, 146-152.
[177] I. Tabushi, Cyclodextrin catalysis as a model for enzyme action, *Acc. Chem. Res.* **1982**, *15*, 66-72.
[178] R. Breslow, S. D. Dong, Biomimetic reactions catalyzed by cyclodextrins and their derivatives, *Chem. Rev.* **1998**, *98*, 1997-2012.
[179] L. Isaacs, Cucurbit [n] urils: from mechanism to structure and function, *Chem. Commun.* **2009**, 619-629.
[180] D. J. Cram, J. M. Cram, Cyclophane chemistry: bent and battered benzene rings, *Acc. Chem. Res.* **1971**, *4*, 204-213.
[181] F. Diederich, Complexation of neutral molecules by cyclophane hosts, *Angew. Chem. Int. Ed.* **1988**, *27*, 362-386.
[182] T. Brotin, J.-P. Dutasta, Cryptophanes and their complexes - present and future, *Chem. Rev.* **2009**, *109*, 88-130.
[183] M. M. Conn, J. Rebek, Self-assembling capsules, *Chem. Rev.* **1997**, *97*, 1647-1668.
[184] S. J. Dalgarno, N. P. Power, J. L. Atwood, Metallo-supramolecular capsules, *Coord. Chem. Rev.* **2008**, *252*, 825-841.
[185] Q. Zhang, K. Tiefenbacher, Terpene cyclization catalysed inside a self-assembled cavity, *Nat. Chem.* **2015**, *7*, 197-202.
[186] C. Chen, H. Whitlock Jr, Molecular tweezers: a simple model of bifunctional intercalation, *J. Am. Chem. Soc.* **1978**, *100*, 4921-4922.
[187] M. Hardouin–Lerouge, P. Hudhomme, M. Sallé, Molecular clips and tweezers hosting neutral guests, *Chem. Soc. Rev.* **2011**, *40*, 30-43.
[188] Y. Kuninobu, H. Ida, M. Nishi, M. Kanai, A meta-selective C–H borylation directed by a secondary interaction between ligand and substrate, *Nat. Chem.* **2015**, *7*, 712.

[189] H. J. Davis, M. T. Mihai, R. J. Phipps, Ion pair-directed regiocontrol in transition-metal catalysis: a meta-selective C–H borylation of aromatic quaternary ammonium salts, *J. Am. Chem. Soc.* **2016**, *138*, 12759-12762.
[190] H. J. Davis, R. J. Phipps, Harnessing non-covalent interactions to exert control over regioselectivity and site-selectivity in catalytic reactions, *Chem. Sci.* **2017**, *8*, 864-877.
[191] M. E. Hoque, R. Bisht, C. Haldar, B. Chattopadhyay, Noncovalent interactions in Ir-catalyzed C–H activation: L-shaped ligand for para-selective borylation of aromatic esters, *J. Am. Chem. Soc.* **2017**, *139*, 7745-7748.
[192] T. Šmejkal, B. Breit, A supramolecular catalyst for regioselective hydroformylation of unsaturated carboxylic acids, *Angew. Chem. Int. Ed.* **2008**, *47*, 311-315.
[193] P. Dydio, W. I. Dzik, M. Lutz, B. de Bruin, J. N. Reek, Remote supramolecular control of catalyst selectivity in the hydroformylation of alkenes, *Angew. Chem. Int. Ed.* **2011**, *50*, 396-400.
[194] P. Thordarson, E. J. Bijsterveld, A. E. Rowan, R. J. Nolte, Epoxidation of polybutadiene by a topologically linked catalyst, *Nature* **2003**, *424*, 915-918.
[195] P. Fackler, C. Berthold, F. Voss, T. Bach, Hydrogen-bond-mediated enantio-and regioselectivity in a Ru-catalyzed epoxidation reaction, *J. Am. Chem. Soc.* **2010**, *132*, 15911-15913.
[196] S. a. Korom, P. Ballester, Attachment of a RuII complex to a self-folding hexaamide deep cavitand, *J. Am. Chem. Soc.* **2017**, *139*, 12109-12112.
[197] R. R. French, P. Holzer, M. G. Leuenberger, W. D. Woggon, A Supramolecular Enzyme Mimic That Catalyzes the 15, 15′ Double Bond Scission of β, β-Carotene, *Angew. Chem. Int. Ed.* **2000**, *39*, 1267-1269.
[198] G. Olivo, G. Capocasa, D. Del Giudice, O. Lanzalunga, S. Di Stefano, New horizons for catalysis disclosed by supramolecular chemistry, *Chem. Soc. Rev.* **2021**, *50*, 7681-7724.
[199] Y.-S. Fung, S.-C. Yan, M.-K. Wong, Selective oxidation of unactivated C–H bonds by supramolecular control, *Org. Biomol. Chem.* **2012**, *10*, 3122-3130.
[200] N. T. Southall, K. A. Dill, A. Haymet, A view of the hydrophobic effect, *J. Phys. Chem. B* **2002**, *106*, 521-533.
[201] E. A. Meyer, R. K. Castellano, F. Diederich, Interactions with aromatic rings in chemical and biological recognition, *Angew. Chem. Int. Ed.* **2003**, *42*, 1210-1250.
[202] J. T. Groves, R. Neumann, Enzymic regioselectivity in the hydroxylation of cholesterol catalyzed by a membrane-spanning metalloporphyrin, *J. Org. Chem.* **1988**, *53*, 3891-3893.
[203] R. Breslow, Biomimetic chemistry and artificial enzymes: catalysis by design, *Acc. Chem. Res.* **1995**, *28*, 146-153.
[204] R. Breslow, Y. Huang, X. Zhang, J. Yang, An artificial cytochrome P450 that hydroxylates unactivated carbons with regio-and stereoselectivity and useful catalytic turnovers, *Proc. Natl. Acad. Sci. U.S.A.* **1997**, *94*, 11156-11158.
[205] R. Breslow, X. Zhang, Y. Huang, Selective catalytic hydroxylation of a steroid by an artificial cytochrome P-450 enzyme, *J. Am. Chem. Soc.* **1997**, *119*, 4535-4536.
[206] R. Breslow, B. Gabriele, J. Yang, Geometrically directed selective steroid hydroxylation with high turnover by a fluorinated artificial cytochrome P-450, *Tetrahedron Lett.* **1998**, *39*, 2887-2890.
[207] J. Yang, R. Breslow, Selective Hydroxylation of a Steroid at C-9 by an Artificial Cytochrome P-450, *Angew. Chem. Int. Ed.* **2000**, *39*, 2692-2695.
[208] R. Breslow, A. B. Brown, R. D. McCullough, P. W. White, Substrate selectivity in epoxidation by metalloporphyrin and metallosalen catalysts carrying binding groups, *J. Am. Chem. Soc.* **1989**, *111*, 4517-4518.

[209] S. Belvedere, R. Breslow, Regioselective oxidation of steroids by a manganese porphyrin carrying metal coordinating groups, *Bioorg. Chem.* **2001**, *29*, 321-331.
[210] Z. Fang, R. Breslow, Metal coordination-directed hydroxylation of steroids with a novel artificial P-450 catalyst, *Org. Lett.* **2006**, *8*, 251-254.
[211] S. Das, G. W. Brudvig, R. H. Crabtree, Molecular recognition in homogeneous transition metal catalysis: a biomimetic strategy for high selectivity, *Chem. Commun.* **2008**, 413-424.
[212] F. Burg, T. Bach, Lactam Hydrogen Bonds as Control Elements in Enantioselective Transition-Metal-Catalyzed and Photochemical Reactions, *J. Org. Chem.* **2019**, *84*, 8815-8836.
[213] S. Das, C. D. Incarvito, R. H. Crabtree, G. W. Brudvig, Molecular recognition in the selective oxygenation of saturated CH bonds by a dimanganese catalyst, *Science* **2006**, *312*, 1941-1943.
[214] S. Das, G. W. Brudvig, R. H. Crabtree, High turnover remote catalytic oxygenation of alkyl groups: How steric exclusion of unbound substrate contributes to high molecular recognition selectivity, *J. Am. Chem. Soc.* **2008**, *130*, 1628-1637.
[215] J. R. Frost, S. M. Huber, S. Breitenlechner, C. Bannwarth, T. Bach, Enantiotopos-Selective C− H Oxygenation Catalyzed by a Supramolecular Ruthenium Complex, *Angew. Chem. Int. Ed.* **2015**, *54*, 691-695.
[216] F. Burg, M. Gicquel, S. Breitenlechner, A. Pöthig, T. Bach, Site-and Enantioselective C− H Oxygenation Catalyzed by a Chiral Manganese Porphyrin Complex with a Remote Binding Site, *Angew. Chem. Int. Ed.* **2018**, *57*, 2953-2957.
[217] R. R. Annapureddy, C. Jandl, T. Bach, A chiral phenanthroline ligand with a hydrogen-bonding site: application to the enantioselective amination of methylene groups, *J. Am. Chem. Soc.* **2020**, *142*, 7374-7378.
[218] G. Olivo, G. Farinelli, A. Barbieri, O. Lanzalunga, S. Di Stefano, M. Costas, Supramolecular Recognition Allows Remote, Site-Selective C− H Oxidation of Methylenic Sites in Linear Amines, *Angew. Chem. Int. Ed.* **2017**, *129*, 16565-16569.
[219] G. Olivo, G. Capocasa, B. Ticconi, O. Lanzalunga, S. Di Stefano, M. Costas, Predictable selectivity in remote C− H oxidation of steroids: analysis of substrate binding mode, *Angew. Chem. Int. Ed.* **2020**, *59*, 12703-12708.
[220] F.-G. Klärner, B. Kahlert, Molecular tweezers and clips as synthetic receptors. Molecular recognition and dynamics in receptor− substrate complexes, *Acc. Chem. Res.* **2003**, *36*, 919-932.
[221] V. Valderrey, G. Aragay, P. Ballester, Porphyrin tweezer receptors: Binding studies, conformational properties and applications, *Coord. Chem. Rev.* **2014**, *258*, 137-156.
[222] M. Harmata, Chiral molecular tweezers, *Acc. Chem. Res.* **2004**, *37*, 862-873.
[223] A. E. Rowan, J. A. Elemans, R. J. Nolte, Molecular and supramolecular objects from glycoluril, *Acc. Chem. Res.* **1999**, *32*, 995-1006.
[224] D. J. Cram, H. Steinberg, Macro rings. I. Preparation and spectra of the paracyclophanes, *J. Am. Chem. Soc.* **1951**, *73*, 5691-5704.
[225] F. N. Diederich, *Cyclophanes*, The Royal Society of Chemistry, **1991**.
[226] P. Keehn, *Cyclophanes*, Elsevier, **2012**.
[227] D. Smithrud, E. Sanford, I. Chao, S. Ferguson, D. Carcanague, J. Evanseck, K. Houk, F. Diederich, Solvent effects in molecular recognition, *Pure Appl. Chem.* **1990**, *62*, 2227-2236.
[228] C. Reichardt, Solvatochromic dyes as solvent polarity indicators, *Chem. Rev.* **1994**, *94*, 2319-2358.
[229] R. V. Ottenbacher, K. P. Bryliakov, E. P. Talsi, Non-Heme Manganese Complexes Catalyzed Asymmetric Epoxidation of Olefins by Peracetic Acid and Hydrogen Peroxide, *Adv. Synth. Catal.* **2011**, *353*, 885-889.

[230] R. V. Ottenbacher, K. P. Bryliakov, E. P. Talsi, Nonheme manganese-catalyzed asymmetric oxidation. A Lewis acid activation versus oxygen rebound mechanism: evidence for the "Third Oxidant", *Inorg. Chem.* **2010**, *49*, 8620-8628.
[231] C. A. Burnett, D. Witt, J. C. Fettinger, L. Isaacs, Acyclic congener of cucurbituril: synthesis and recognition properties, *J. Org. Chem.* **2003**, *68*, 6184-6191.
[232] M. Heilmann, K. Tiefenbacher, A Modular Phosphorylated Glycoluril-Derived Molecular Tweezer for Potent Binding of Aliphatic Diamines, *Chem. Eur. J.* **2019**, *25*, 12900-12904.
[233] M. Knezevic, Synthesis of Novel Functionalized, Alkyl Ammonium Binding Molecular Tweezers, Master`s thesis, Technical University of Munich **2018**.
[234] K. Odashima, A. Itai, Y. Iitaka, K. Koga, Host-guest complex formation between a water-soluble polyparacyclophane and a hydrophobic guest molecule, *J. Am. Chem. Soc.* **1980**, *102*, 2504-2505.
[235] D. B. Smithrud, F. Diederich, Strength of molecular complexation of apolar solutes in water and in organic solvents is predictable by linear free energy relationships: a general model for solvation effects on apolar binding, *J. Am. Chem. Soc.* **1990**, *112*, 339-343.
[236] M. Knezevic, M. Heilmann, G. M. Piccini, K. Tiefenbacher, Overriding intrinsic reactivity in aliphatic C− H oxidation: preferential C3/C4 oxidation of aliphatic ammonium substrates, *Angew. Chem. Int. Ed.* **2020**, *59*, 12387-12391.
[237] M. Knezevic, K. Tiefenbacher, Tweezer-Based C-H Oxidation Catalysts Overriding the Intrinsic Reactivity of Aliphatic Ammonium Substrates, *Chem. Eur. J.* **2022**.
[238] K. Chen, M. Costas, J. Kim, A. K. Tipton, L. Que, Olefin cis-dihydroxylation versus epoxidation by non-heme iron catalysts: two faces of an FeIII− OOH coin, *J. Am. Chem. Soc.* **2002**, *124*, 3026-3035.
[239] K. Neimann, R. Neumann, Electrophilic activation of hydrogen peroxide: selective oxidation reactions in perfluorinated alcohol solvents, *Org. Lett.* **2000**, *2*, 2861-2863.
[240] A. Berkessel, J. A. Adrio, Dramatic acceleration of olefin epoxidation in fluorinated alcohols: activation of hydrogen peroxide by multiple H-bond networks, *J. Am. Chem. Soc.* **2006**, *128*, 13412-13420.
[241] K. Suyama, S. Kaneko, H. Kesamaru, X. Liu, A. Matsushima, Y. Kakuta, T. Okubo, K. Kasatani, T. Nose, Evaluation of the Influence of Halogenation on the Binding of Bisphenol A to the Estrogen-Related Receptor γ, *Chem. Res. Toxicol.* **2020**, *33*, 889-902.
[242] S. R. Chemler, D. Trauner, S. J. Danishefsky, The B-Alkyl Suzuki–Miyaura Cross-Coupling Reaction: Development, Mechanistic Study, and Applications in Natural Product Synthesis, *Angew. Chem. Int. Ed.* **2001**, *40*, 4544-4568.
[243] L. Leckie, S. F. Mapolie, Triazole complexes of ruthenium immobilized on mesoporous silica as recyclable catalysts for octane oxidation, *Catal. Commun.* **2019**, *131*, 105803.
[244] S. G. Mncube, M. D. Bala, Application of 1, 2, 3-triazolylidene nickel complexes for the catalytic oxidation of n-octane, *Mol. Catal.* **2020**, *482*, 100107.
[245] W. C. Still, M. Kahn, A. Mitra, Rapid chromatographic technique for preparative separations with moderate resolution, *J. Org. Chem.* **1978**, *43*, 2923-2925.
[246] H. E. Gottlieb, V. Kotlyar, A. Nudelman, NMR chemical shifts of common laboratory solvents as trace impurities, *J. Org. Chem.* **1997**, *62*, 7512-7515.
[247] J. T. Scanlon, D. E. Willis, Calculation of flame ionization detector relative response factors using the effective carbon number concept, *J. Chromatogr. Sci.* **1985**, *23*, 333-340.
[248] A. Diebold, A. Elbouadili, K. S. Hagen, Crystal Structures and Solution Behavior of Paramagnetic Divalent Transition Metal Complexes (Fe, Co) of the Sterically Encumbered Tridentate Macrocycles 1, 4, 7-R3-1, 4, 7-Triazacyclononane: Coordination Numbers 5 (R= i-Pr) and 6 (R= i-Bu), *Inorg. Chem.* **2000**, *39*, 3915-3923.

[249] J. L. Débieux, A. Cosandey, C. Helgen, C. G. Bochet, Photoacylation of alcohols in neutral medium, *Eur. J. Org. Chem.* **2007**, 2073-2077.
[250] L. Zhao, L. Fang, Y. Xu, S. Liu, Z. He, Y. Zhao, Transdermal delivery of penetrants with differing lipophilicities using O-acylmenthol derivatives as penetration enhancers, *Eur. J. Pharm. Biopharm.* **2008**, *69*, 199-213.
[251] R. B. Porter, W. A. Gallimore, P. B. Reese, Steroid transformations with Exophiala jeanselmei var. lecanii-corni and Ceratocystis paradoxa☆, *Steroids* **1999**, *64*, 770-779.
[252] J. M. Howell, K. Feng, J. R. Clark, L. J. Trzepkowski, M. C. White, Remote oxidation of aliphatic C–H bonds in nitrogen-containing molecules, *J. Am. Chem. Soc.* **2015**, *137*, 14590-14593.
[253] S. Mukherjee, B. Maji, A. Tlahuext-Aca, F. Glorius, Visible-light-promoted activation of unactivated C (sp3)–H bonds and their selective trifluoromethylthiolation, *J. Am. Chem. Soc.* **2016**, *138*, 16200-16203.

8 Bibliographic Data of Complete Publications

This chapter contains the bibliographic data of the publications included in this thesis (except for the co-author publication. Summaries of these publications are given in Chapter 3.1.

Overriding Intrinsic Reactivity in Aliphatic C–H Oxidation: Preferential C3/C4 Oxidation of Aliphatic Ammonium Substrates

Melina Knezevic,[a] Michael Heilmann,[a] GiovanniMaria Piccini,[b] and Konrad Tiefenbacher*[a][c]

[a] Department of Chemistry, University of Basel, Mattenstrasse 24a, 4058 Basel, Switzerland

[b] Department of Chemistry and Applied Biosciences, ETH Zurich, c/o USI Campus, Via Giuseppe Buffi 13, CH-6900 Lugano, Switzerland; Facoltàdi Informatica, Istituto di Scienze Computazionali, Universitàdella SvizzeraItaliana (USI), Via Giuseppe Buffi 13, CH-6900 Lugano, Switzerland

[c] Department of Biosystems Science and Engineering, ETH Zurich, Mattenstrasse 24, 4058 Basel, Switzerland

*Corresponding Author: Konrad.tiefenbacher@unibas.ch

Originally published in: *Angew. Chem. Int. Ed.* **2020**, *59*, 12387–12391.

DOI: 10.1002/anie.202004242

URL: https://onlinelibrary.wiley.com/doi/10.1002/anie.202004242

Tweezer-Based C-H Oxidation Catalysts Overriding the Intrinsic Reactivity in Aliphatic Ammonium Substrates

Melina Knezevic,[a] and Konrad Tiefenbacher*[a][b]

[a] Department of Chemistry, University of Basel, Mattenstrasse 24a, 4058 Basel, Switzerland

[b] Department of Biosystems Science and Engineering, ETH Zurich, Mattenstrasse 24, 4058 Basel, Switzerland

*Corresponding Author: Konrad.tiefenbacher@unibas.ch

Originally published in: *Chem. Eur. J.* **2022**, *accepted*.

DOI: 10.1002/chem.202203480

URL: https://chemistry-europe.onlinelibrary.wiley.com/doi/abs/10.1002/chem.202203480

9 Reprints and Reprint Permission

The manuscript published in Angewandte Chemie International Edition, Figure 26, Table 1, and Figure 7 were reproduced with the permission of John Wiley and Sons.

	Switzerland Attn: Melina Knezevic
Publisher Tax ID	EU826007151
Total	0.00 CHF

GDCh **Communications** Angewandte International Edition Chemie

How to cite: *Angew. Chem. Int. Ed.* **2020**, *59*, 12387–12391
International Edition: doi.org/10.1002/anie.202004242
German Edition: doi.org/10.1002/ange.202004242

C–H Oxidation

Overriding Intrinsic Reactivity in Aliphatic C–H Oxidation: Preferential C3/C4 Oxidation of Aliphatic Ammonium Substrates

*Melina Knezevic, Michael Heilmann, Giovanni Maria Piccini, and Konrad Tiefenbacher**

In memory of Rolf Huisgen

Abstract: *The site-selective C–H oxidation of unactivated positions in aliphatic ammonium chains poses a tremendous synthetic challenge, for which a solution has not yet been found. Here, we report the preferential oxidation of the strongly deactivated C3/C4 positions of aliphatic ammonium substrates by employing a novel supramolecular catalyst. This chimeric catalyst was synthesized by linking the well-explored catalytic moiety Fe(pdp) to an alkyl ammonium binding molecular tweezer. The results highlight the vast potential of overriding the intrinsic reactivity in chemical reactions by guiding catalysis using supramolecular host structures that enable a precise orientation of the substrates.*

Over the last few decades, synthetic methodology has progressed enormously. However, the site-selective oxidation of unactivated C(sp^3)–H bonds still poses a remarkable challenge.[1] Although it is possible to predict and exploit differences in the intrinsic reactivity of the C–H bonds in a given molecule, the oxidation of less-reactive positions generally remains elusive.[2] Arguably, such a method would considerably simplify the synthesis of complex oxygenated organic molecules. Nature—in many cases a role model for chemists—clearly demonstrates the potential of such methodology through the use of complex cytochrome P450 enzymes.[3] The optimized binding pocket of the active site is crucial in orienting a specific C–H bond that is not necessarily the most reactive one towards the oxidant. Mimicking such selective binding modes with synthetic catalysts has been very challenging.[4]

[*] M. Sc. M. Knezevic, M. Sc. M. Heilmann, Prof. Dr. K. Tiefenbacher
Department of Chemistry, University of Basel
Mattenstrasse 24a, 4058 Basel (Switzerland)
E-mail: Konrad.tiefenbacher@unibas.ch
Dr. G. M. Piccini
Department of Chemistry and Applied Biosciences
ETH Zurich
c/o USI Campus, Via Giuseppe Buffi 13
CH-6900 Lugano (Switzerland)
and
Facoltàdi Informatica, Istituto di Scienze Computazionali
Universitàdella SvizzeraItaliana (USI)
Via Giuseppe Buffi 13, CH-6900 Lugano (Switzerland)
Prof. Dr. K. Tiefenbacher
Department of Biosystems Science and Engineering, ETH Zurich
Mattenstrasse 24, 4058 Basel (Switzerland)
Supporting information and the ORCID identification number for one of the authors of this article can be found under: https://doi.org/10.1002/anie.202004242.

One promising approach is the covalent merger of a well-developed oxidation catalyst with a supramolecular binding motif.[4b–d,5] For example, seminal work by Breslow et al. involved cyclodextrin(CD)-modified metalloporphyrin complexes.[4b,6] Several covalently modified substrates (to enable binding to the CD moieties of the catalyst) were selectively oxidized using this strategy. Selective oxidation without the covalent attachment of recognition moieties to the substrate has been less successful, although remarkable examples were reported by the groups of Crabtree and Brudvig[7] as well as of Bach.[8] The oxidation of unactivated positions remains problematic.[4d] Longer alkyl chains comprise one of the most challenging substrate classes for selective oxidation, as the methylene C–H bonds differ little in their reactivity.[9] For example, the oxidation of a decyl ammonium substrate (Figure 1) with the White–Chen[11a,2d,10] catalyst **1** yields mixtures of ketone products with a preference for oxidation at carbon atoms C6 and higher.[11] Remarkably, the Costas group recently reported a novel method for the selective oxidation of alkyl ammonium substrates preferably at positions C8/C9 (Figure 1).[11] The catalyst utilized in their work features

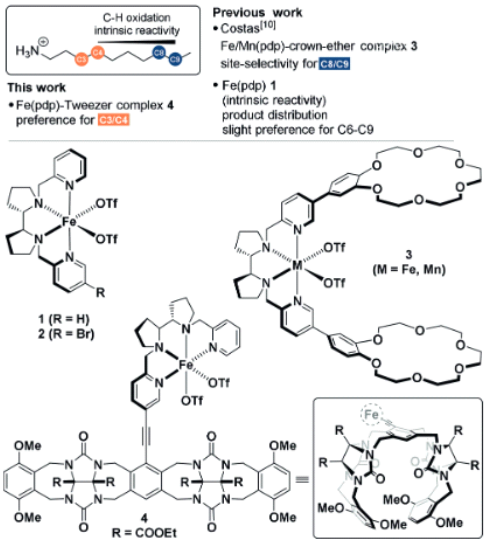

Figure 1. C–H Oxidation catalysts with different selectivities for alkyl ammonium chains.

a catalytic center (Mn- or Fe-*N*,*N*′-bis(2-pyridylmethyl)-2,2′-bipyrrolidine (Mn-/Fe(pdp)) attached to two 18-benzocrown-6 ether (BC) receptors (**3**) that are able to bind primary aliphatic ammonium ions.[11]

Our recent interest in molecular tweezers,[12] combined with their ability to bind alkyl ammonium ions prompted us to investigate their potential for selective C–H oxidation. Molecular tweezers are host molecules with an open cavity defined by two rigid arms.[13] Specifically, we decided to utilize a framework similar to the glycoluril-based tweezer **8b** (Scheme 1) originally developed by Isaacs and co-workers.[14] We speculated that it may bind alkylammonium cations more rigidly than the flexible crown ethers in catalyst **3**, thereby potentially delivering an increased oxidation selectivity. Here we report the synthesis of the chimeric tweezer-oxidation catalyst **4**, and its unprecedented selectivity for the deactivated positions C3/C4.

Although the ability of tweezer **8b** (R = COOH, Scheme 1) to bind alkyl ammonium species in water has been documented,[14] this project depended on binding in acetonitrile, the standard solvent for oxidations with catalyst **1** and its derivatives.[2c,10,11,15] The binding constant of decyl ammonium tetrafluoroborate (C10-NH_3^+) with **8b** (R = COOEt) in acetonitrile was determined by NMR titration experiments (see Supporting Information, p. S95–96) and indicated reasonably strong binding ($K_a = 210 \pm 7.6\,M^{-1}$, $K_d = 4.77\,mM \pm 0.17\,mM$). Under the general oxidation concentrations adapted from those used by Costas (1.0 equiv substrate, 74 mM in MeCN, 5 mol% Fe-Twe **8b**; see below),[11] >93% of tweezer **8b** would be occupied with substrate.

Encouraged by these initial results, we decided to explore a synthetic route towards the tweezer catalyst **4**, which comprises the well-explored catalytic moiety Fe(pdp)[1a,10] linked to the tweezer binding motif by an alkyne residue. Initially, we envisioned a convergent approach based on the coupling of tweezer **9** and ligand **14** (Scheme 1). However, attempts to achieve such a coupling failed, which led us to develop a more linear approach.

Commercially available iododurene (**5**) was coupled with TBS-acetylene under Sonogashira coupling conditions. Subsequent tetrabromination with NBS and AIBN yielded compound **6**, which was linked through alkylation with two equivalents of **7**[14] to produce tweezer **8a**. Cleavage of the TBS group using TABF resulted in tweezer **9**, which subsequently was coupled with 5-bromo-2-pyridinecarboxaldehyde (**10**). Surprisingly, reductive amination with **12** resulted in low yields under a variety of conditions. Therefore, the desired ligand **13** was constructed by alkylation (after reduction of the aldehyde and Appel-like bromination). The final complex **4** was obtained by coordination of **13** with $Fe(OTf)_2(MeCN)_2$.[11] Catalyst **2** (Figure 1) was also synthesized as a reference oxidation catalyst lacking the tweezer binding motif but carrying a substituent at the pyridine 5-position (see the Supporting Information).

Surprisingly, the determination of the binding constant of decyl ammonium tetrafluoroborate with Fe-Twe **4** showed a rather weak binding ($K_a = 29.5 \pm 1.9\,M^{-1}$, $K_d = 34.0\,mM \pm 2.2\,mM$). Subsequent dilution titration experiments, however, revealed that Fe-Twe **4** displays a relatively large dimerization constant ($K_{dim} = 160 \pm 2.2\,M^{-1}$), in contrast to tweezer **8b**, which did not show significant aggregation (see the Supporting Information, p. S94–99).

Initially, decyl ammonium tetrafluoroborate was chosen as a model substrate and investigated in the oxidation reactions with Fe-Br **2** (intrinsic reactivity) and Fe-Twe **4** (Figure 2). As expected,[11] the nondirected oxidation with Fe-Br **2** resulted in mixtures of ketone products (K4–K9; ketones at C4–C9). Oxidation at the more proximal positions (K3/K4) was barely detectable because of deactivation by the nearby ammonium moiety.[16] The main products were K6–K9 in nearly equal amounts. Employing catalyst Fe-Twe **4** also led

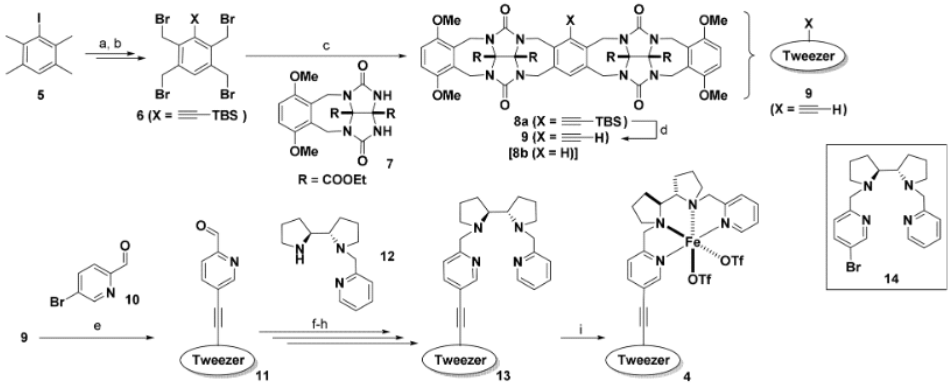

Scheme 1. Synthesis of the Fe(pdp)-functionalized tweezer Fe-Twe **4.** a) TBS-acetylene, $PdCl_2(PPh_3)_2$, CuI, Et_2NH, 50 °C, 16 h, 97%. b) NBS, AIBN, CCl_4, 95 °C, 72 h, 58%. c) **7**, KO*t*Bu, **6**, DMSO, rt, 16 h, 44%. d) TBAF, THF, 0 °C, 2 h, 80%. e) **10**, $PdCl_2(PPh_3)_2$, CuI, PPh_3, THF, microwaves, 120 °C, 90 min, 76%. f) $NaCNBH_3$, TFA, MeOH, CH_2Cl_2, rt, 4 h, 96%. g) PBr_3, CH_2Cl_2, 0 °C→rt, 16 h, 75%. h) **11**, K_2CO_3, TBAB, MeCN, 90 °C, 16 h, 97%. i) $Fe(OTf)_2(MeCN)_2$, MeCN, rt, 2.5 h, 58%. AIBN: azobis(isobutyronitrile), TBS: *tert*-butyldimethylsilyl, TBAB: tetra-*n*-butylammonium bromide, TBAF: tetra-*n*-butylammonium fluoride, TFA: trifluoroacetic acid, NBS: *N*-bromosuccinimide.

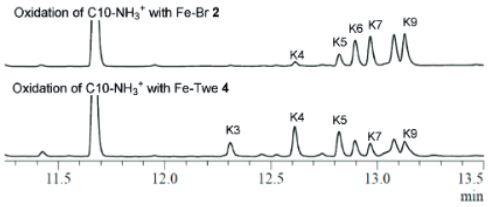

Figure 2. GC Chromatograms of the oxidation of C10-NH_3^+ with Fe-Br **2** (top) and Fe-Twe **4** (bottom).

to mixtures, but resulted in an inversed selectivity. Interestingly, the deactivated positions K3–K5 were those preferred by the supramolecular catalyst **4**, overriding the intrinsic reactivity of the substrate (Table 1, entry 1 vs. entry 2).

Several control experiments were carried out to elucidate the role of the supramolecular recognition motif. First an experiment in which the two parts of Fe-Twe **4** were added as separate entities (tweezer **8b** (5 mol%), and Fe-Br **2** (5 mol%)) was performed (Table 1, entry 4). The selectivity was significantly reduced and similar to the results obtained with Fe-Br **2**, thus demonstrating that the tweezer has to be covalently linked to the oxidation catalyst to achieve high selectivity. In separate experiments, we tried to reduce the binding ability of the substrate through methylation of the amine residue. The oxidation of C10-$NMeH_2^+$ already delivered reduced selectivities (entry 5 vs. entry 6) while the use of dimethylated C10-NMe_2H^+ as the substrate resulted in an almost complete loss of the selectivity. These results strongly indicate that the substrate binds to the tweezer through hydrogen bonds. The yields in these two cases (entries 6 and 8) were only slightly reduced in comparison to entry 2, which suggests that oxidation without specific binding to the tweezer takes place as a background reaction. This is also indicated by the oxidation of cyclohexane by both catalysts (see the Supporting Information, p. S37). In a competition experiment, decyl ammonium and cyclohexane were subjected to oxidation reactions with Fe-Br **2** and Fe-Twe **4** in equal amounts, which resulted in only a slightly increased selectivity for decyl ammonium with Fe-Twe **4**. The background reaction was much less pronounced with **3**,[11] presumably because of the oxidant being blocked from two sides by the crown ether moieties. A third series of control experiments was performed with the aim of inhibiting substrate binding inside Fe-Twe **4**. NH_4PF_6, NaOTf, and methyl viologen dichloride hydrate were explored as inhibitors. The yields of the oxidation products, as well as the selectivity for C3 and C4 decreased. However, these results are difficult to interpret, since the inhibitor also inhibits the oxidation of the regular catalyst Fe-Br **2**, which is devoid of a tweezer moiety. However, the reduced selectivity with these experiments also indicates some background oxidation with regular "solution" selectivity at C6–C9.

Subsequently, we studied the oxidation of several aliphatic ammonium salts with different chain lengths (Table 1 and Figure 3). For all oxidation reactions with Fe-Twe **4**, a pronounced selectivity increase for the C3 and C4 positions was observed compared to the nondirected oxidations. In fact, with most substrates, ketones K3 or K4 were the favored products in the Fe-Twe **4** oxidation reactions. The yields, however, were generally lower for catalyst **4**, which is presumably due to catalyst decomposition during the oxidation reaction (see the Supporting Information, p. S39–42). The only exception is the oxidation of C7-NH_3^+, in which almost all the positions are deactivated.[16] Moreover, substrates with longer alkyl chains mostly resulted in higher yields compared to the short ones, a trend also observed with **3**.[11] In terms of the selectivity, two different binding motifs can, in principle, be envisioned for catalyst **4** (Figure 3b): 1) The binding of the aliphatic chain inside the cavity of the

Table 1: Oxidation of aliphatic ammonium salts by catalysts Fe-Br **2** and Fe-Twe **4**.[a]

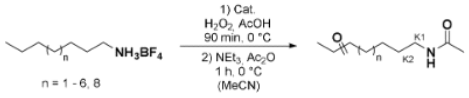

Entry	Substrate	Catalyst	Conv. [%]	Total yield[b] [%]	Yield K3/K4 [%]	Yield K3–K5 [%]	Selectivity[c] K3/K4 [%]	Selectivity[c] K3–K5 [%]
1 vs. 2[d]	C10-NH_3^+	Fe-Br **2** vs. Fe-Twe **4**	75 vs. 47	34 vs. 25	1.8 vs. 7.0	5.9 vs. 11	5.3 vs. 28	17 vs. 43
3 vs. 4	C10-NH_3^+	Fe-Br **2** vs. Fe-Br **2** + **8b**	75 vs. 52	34 vs. 19	1.8 vs. 1.5	5.9 vs. 3.4	5.3 vs. 7.8	17 vs. 18
5 vs. 6	C10-$NMeH_2^+$	Fe-Br **2** vs. Fe-Twe **4**	57 vs. 43	27 vs. 18	1.9 vs. 2.9	5.5 vs. 5.6	7.1 vs. 16	20 vs. 32
7[e] vs. 8[e]	C10-NMe_2H^+	"	60 vs. 41	32 vs. 14	1.7 vs. 0.9	5.3 vs. 2.4	5.2 vs. 6.2	17 vs. 17
9 vs. 10	C7-NH_3^+	"	34 vs. 34	3.8 vs. 6.4	1.8 vs. 5.1	2.7 vs. 5.9	46 vs. 80	70 vs. 92
11 vs. 12	C8-NH_3^+	"	37 vs. 22	17 vs. 8.2	3.2 vs. 4.2	6.1 vs. 5.2	19 vs. 51	36 vs. 64
13 vs. 14	C9-NH_3^+	"	49 vs. 39	30 vs. 16	2.9 vs. 6.6	7.3 vs. 8.7	10 vs. 40	24 vs. 53
15 vs. 16	C11-NH_3^+	"	57 vs. 36	42 vs. 24	1.6 vs. 5.7	5.0 vs. 8.7	3.9 vs. 24	12 vs. 37
17 vs. 18	C12-NH_3^+	"	63 vs. 39	28 vs. 10	1.0 vs. 2.4	2.8 vs. 3.8	3.8 vs. 23	9.9 vs. 37
19 vs. 20	C14-NH_3^+	"	77 vs. 68	33 vs. 18	0.7 vs. 3.8	2.1 vs. 6.1	2.1 vs. 21	8.8 vs. 34

[a] General reaction conditions:[11] substrate (18.5 µmol, 1.0 equiv), catalyst (925 nmol, 5 mol%), AcOH (148 µmol, 8.0 equiv), H_2O_2 (278 µmol, 15 equiv, addition by a syringe pump over 90 min), MeCN, 0°C. After 15 min, internal standard (biphenyl, 9.25 µmol, 0.5 equiv), NEt_3 (100 µL), and Ac_2O (150 µL) added, 0°C. After 1 h, washed with H_2O, 2 M H_2SO_4, $NaHCO_3$, H_2O, dried (Na_2SO_4), and analyzed by GC. [b] Total yield refers to the mixture of all isomers. [c] Selectivity refers to the yield of selected ketones/total yield. [d] 5 mol% of tweezer **8b** was added additionally. [e] Different work-up, see the Supporting Information.

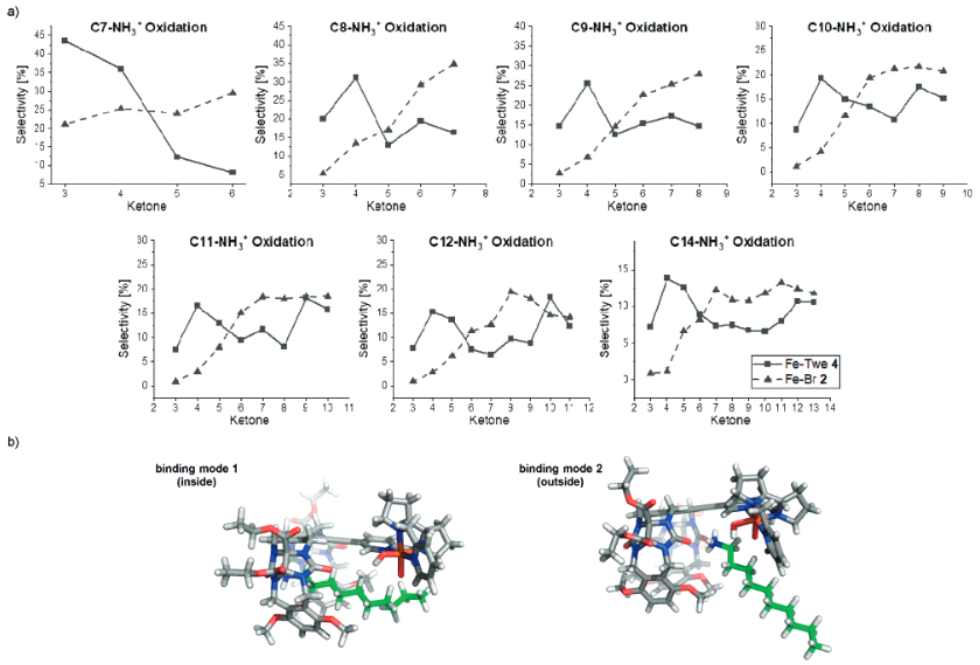

Figure 3. a) Reaction selectivities of the possible ketone products for the oxidation of different aliphatic ammonium ions with Fe-Br **2** and Fe-Twe-**4**. b) Binding modes 1 and 2 of Fe-**4** and decyl ammonium (optimized at the PM3 level).

tweezer. This binding mode is observed in aqueous solution, presumably as a result of the hydrophobic effect.[14] It would expose positions C6–C8 to the oxidant. 2) Without the hydrophobic effect, sole binding to the polar end groups (urea carbonyl group and methoxy oxygen atom) of the tweezer would be feasible, thereby favoring oxidation of positions C3–C5. The oxidation results obtained clearly suggest that the second binding mode is the predominant one. Molecular modeling studies were performed to investigate the suggested binding modes of the ammonium substrate to the tweezer (see the Supporting Information, p. S101–107). According to the calculations, the two binding modes are relatively close in energy, thus indicating that C6–C9 oxidation not only stems from a background reaction but also from binding mode 1. However, binding mode 2 (the cavity is filled with acetonitrile solvent, not shown in Figure 3) is preferred by approximately 5 kJ mol^{-1}, in accordance with the experimental results. Since binding mode 2 depends on the guest acetonitrile molecule, the observed selectivity for K3–K5 should be solvent-dependent. Indeed, the selectivity is greatly reduced with trifluoroethanol and disappears completely when the larger hexafluoro-2-propanol is used as solvent (see the Supporting information, p. S35–36). These results provide further evidence that the observed oxidation of the unactivated positions C3–C5 stem from substrate binding to the tweezer moiety of catalyst **4**.

In summary, we reported the synthesis of a supramolecular oxidation catalyst capable of overriding the intrinsic reactivity in the aliphatic C–H oxidation of alkyl ammonium salts. The main products formed were ketones at carbon atoms C3 and C4, positions that are intrinsically strongly deactivated and, therefore, not formed to a significant degree with other catalysts. Although the selectivities clearly have to be improved to achieve synthetically useful yields, these results augur well for the selective oxidation of unactivated C–H positions of complex carbon frameworks.

Acknowledgements

This work was supported by the Swiss National Science Foundation as part of the NCCR Molecular Systems Engineering program. We thank Fabian Bissegger for VT-NMR experiments, Dr. Michael Pfeffer for HR-MS analysis, and Dr. Joan Serrano Plana for helpful discussions. Calculations were carried out on the ETH Euler cluster.

Conflict of interest

The authors declare no conflict of interest.

Keywords: catalysis · C–H oxidation · molecular recognition · regioselectivity · supramolecular chemistry

[1] a) M. C. White, J. Zhao, *J. Am. Chem. Soc.* **2018**, *140*, 13988–14009; b) W. R. Gutekunst, P. S. Baran, *Chem. Soc. Rev.* **2011**, *40*, 1976–1991.

[2] a) T. Brückl, R. D. Baxter, Y. Ishihara, P. S. Baran, *Acc. Chem. Res.* **2012**, *45*, 826–839; b) J. F. Hartwig, M. A. Larsen, *ACS Cent. Sci.* **2016**, *2*, 281–292; c) T. Newhouse, P. S. Baran, *Angew. Chem. Int. Ed.* **2011**, *50*, 3362–3374; *Angew. Chem.* **2011**, *123*, 3422–3435; d) M. S. Chen, M. C. White, *Science* **2010**, *327*, 566–571; e) P. E. Gormisky, M. C. White, *J. Am. Chem. Soc.* **2013**, *135*, 14052–14055; f) K. Chen, J. M. Richter, P. S. Baran, *J. Am. Chem. Soc.* **2008**, *130*, 7247–7249; g) B. Li, M. Driess, J. F. Hartwig, *J. Am. Chem. Soc.* **2014**, *136*, 6586–6589; h) M. A. Bigi, S. A. Reed, M. C. White, *J. Am. Chem. Soc.* **2012**, *134*, 9721–9726.

[3] a) P. R. Ortiz de Montellano, *Chem. Rev.* **2010**, *110*, 932–948; b) R. Fasan, *ACS Catal.* **2012**, *2*, 647–666.

[4] a) P. Dydio, J. N. Reek, *Chem. Sci.* **2014**, *5*, 2135–2145; b) R. Breslow, S. D. Dong, *Chem. Rev.* **1998**, *98*, 1997–2012; c) S. Das, G. W. Brudvig, R. H. Crabtree, *Chem. Commun.* **2008**, 413–424; d) D. Vidal, G. Olivo, M. Costas, *Chem. Eur. J.* **2018**, *24*, 5042–5054; e) F. Burg, T. Bach, *J. Org. Chem.* **2019**, *84*, 8815–8836; f) N. R. Mote, S. H. Chikkali, *Chem. Asian J.* **2018**, *13*, 3623–3646; g) M. Raynal, P. Ballester, A. Vidal-Ferran, P. W. van Leeuwen, *Chem. Soc. Rev.* **2014**, *43*, 1660–1733; h) S. Carboni, C. Gennari, L. Pignataro, U. Piarulli, *Dalton Trans.* **2011**, *40*, 4355–4373.

[5] Examples of similar approaches concerning C–H borylation: a) Y. Kuninobu, H. Ida, M. Nishi, M. Kanai, *Nat. Chem.* **2015**, *7*, 712; b) H. J. Davis, M. T. Mihai, R. J. Phipps, *J. Am. Chem. Soc.* **2016**, *138*, 12759–12762; c) M. E. Hoque, R. Bisht, C. Haldar, B. Chattopadhyay, *J. Am. Chem. Soc.* **2017**, *139*, 7745–7748; examples of similar approaches concerning olefin functionalization: d) P. Thordarson, E. J. Bijsterveld, A. E. Rowan, R. J. Nolte, *Nature* **2003**, *424*, 915–918; e) T. Šmejkal, B. Breit, *Angew. Chem. Int. Ed.* **2008**, *47*, 311–315; *Angew. Chem.* **2008**, *120*, 317–321; f) P. Dydio, W. I. Dzik, M. Lutz, B. de Bruin, J. N. Reek, *Angew. Chem. Int. Ed.* **2011**, *50*, 396–400; *Angew. Chem.* **2011**, *123*, 416–420; g) S. a. Korom, P. Ballester, *J. Am. Chem. Soc.* **2017**, *139*, 12109–12112; h) P. Fackler, C. Berthold, F. Voss, T. Bach, *J. Am. Chem. Soc.* **2010**, *132*, 15911–15913.

[6] a) R. Breslow, X. Zhang, Y. Huang, *J. Am. Chem. Soc.* **1997**, *119*, 4535–4536; b) R. Breslow, Y. Huang, X. Zhang, J. Yang, *Proc. Natl. Acad. Sci. USA* **1997**, *94*, 11156–11158; c) J. Yang, R. Breslow, *Angew. Chem. Int. Ed.* **2000**, *39*, 2692–2695; *Angew. Chem.* **2000**, *112*, 2804–2806; d) J. Yang, B. Gabriele, S. Belvedere, Y. Huang, R. Breslow, *J. Org. Chem.* **2002**, *67*, 5057–5067.

[7] a) S. Das, C. D. Incarvito, R. H. Crabtree, G. W. Brudvig, *Science* **2006**, *312*, 1941–1943; b) S. Das, G. W. Brudvig, R. H. Crabtree, *J. Am. Chem. Soc.* **2008**, *130*, 1628–1637.

[8] a) J. R. Frost, S. M. Huber, S. Breitenlechner, C. Bannwarth, T. Bach, *Angew. Chem. Int. Ed.* **2015**, *54*, 691–695; *Angew. Chem.* **2015**, *127*, 701–705; b) F. Burg, M. Gicquel, S. Breitenlechner, A. Pöthig, T. Bach, *Angew. Chem. Int. Ed.* **2018**, *57*, 2953–2957; *Angew. Chem.* **2018**, *130*, 3003–3007; c) F. Burg, S. Breitenlechner, C. Jandl, T. Bach, *Chem. Sci.* **2020**, *11*, 2121–2129.

[9] X.-S. Xue, P. Ji, B. Zhou, J.-P. Cheng, *Chem. Rev.* **2017**, *117*, 8622–8648.

[10] M. S. Chen, M. C. White, *Science* **2007**, *318*, 783–787.

[11] G. Olivo, et al., *Angew. Chem. Int. Ed.* **2017**, *56*, 16347–16351; *Angew. Chem.* **2017**, *129*, 16565–16569.

[12] M. Heilmann, K. Tiefenbacher, *Chem. Eur. J.* **2019**, *25*, 12900–12904.

[13] Reviews: a) M. Hardouin-Lerouge, P. Hudhomme, M. Salle, *Chem. Soc. Rev.* **2011**, *40*, 30–43; b) F.-G. Klärner, T. Schrader, *Acc. Chem. Res.* **2013**, *46*, 967–978; c) V. Valderrey, G. Aragay, P. Ballester, *Coord. Chem. Rev.* **2014**, *258*, 137–156; d) A. E. Rowan, J. A. Elemans, R. J. Nolte, *Acc. Chem. Res.* **1999**, *32*, 995–1006; e) F.-G. Klärner, B. Kahlert, *Acc. Chem. Res.* **2003**, *36*, 919–932; f) S. Ganapati, L. Isaacs, *Isr. J. Chem.* **2018**, *58*, 250–263; g) J. Rebek, Jr., *Science* **1987**, *235*, 1478–1484; h) S. C. Zimmerman, in *Top. Curr. Chem.* Springer, Berlin, **1993**, pp. 71–102; i) S. C. Zimmerman, *Beilstein J. Org. Chem.* **2016**, *12*, 125–138; early contributions: j) C. Chen, H. Whitlock, Jr., *J. Am. Chem. Soc.* **1978**, *100*, 4921–4922; k) J. Rebek, Jr., et al., *J. Am. Chem. Soc.* **1985**, *107*, 6736–6738; l) C. S. Wilcox, L. M. Greer, V. Lynch, *J. Am. Chem. Soc.* **1987**, *109*, 1865–1867; m) S. C. Zimmerman, C. M. VanZyl, *J. Am. Chem. Soc.* **1987**, *109*, 7894–7896.

[14] C. A. Burnett, D. Witt, J. C. Fettinger, L. Isaacs, *J. Org. Chem.* **2003**, *68*, 6184–6191.

[15] R. V. Ottenbacher, D. G. Samsonenko, E. P. Talsi, K. P. Bryliakov, *Org. Lett.* **2012**, *14*, 4310–4313.

[16] a) M. Lee, M. S. Sanford, *J. Am. Chem. Soc.* **2015**, *137*, 12796–12799; b) J. M. Howell, K. Feng, J. R. Clark, L. J. Trzepkowski, M. C. White, *J. Am. Chem. Soc.* **2015**, *137*, 14590–14593.

Manuscript received: March 23, 2020
Revised manuscript received: May 20, 2020
Accepted manuscript online: May 26, 2020
Version of record online: June 29, 2020

The manuscript published in Chemistry – A European Journal, Figure 8 and Tables 2 to 4 were reproduced with the permission of John Wiley and Sons. The reprint represents the accepted version since the final version was not available at the time of writing.

Chemistry - A European Journal

10.1002/chem.202203480

WILEY-VCH

RESEARCH ARTICLE

Tweezer-Based C-H Oxidation Catalysts Overriding the Intrinsic Reactivity of Aliphatic Ammonium Substrates

Melina Knezevic,[a] and Konrad Tiefenbacher*[a,b]

[a] MSc. M. Knezevic, Prof. Dr. K. Tiefenbacher
Department of Chemistry
University of Basel
Mattenstrasse 24a, 4058 Basel, Switzerland
E-mail: Konrad.tiefenbacher@unibas.ch

[b] Prof. Dr. K. Tiefenbacher
Department of Biosystems Science and Engineering,
ETH Zurich
Mattenstrasse 24, 4058 Basel, Switzerland

Supporting information for this article is given via a link at the end of the document.

Abstract: The site-selective C-H oxygenation of alkyl chains as well as deactivated positions remains a great challenge for chemists. Here, we report the synthesis and application of four new supramolecular tweezer-based oxidation catalysts. They consist of the well-explored M(pdp/mcp) oxidation moiety and a molecular tweezer capable of binding ammonium salts. All catalysts display preferential oxidation of the strongly deactivated C3/C4 positions, however to different degrees. Furthermore, the best performing catalyst **Fe(pdp)Twe** was explored with an expanded substrate scope. It was demonstrated that the deactivated positions C3/C4 are also preferentially oxidized in these cases.

Introduction

Oxygenated hydrocarbon skeletons are abundant in nature and are crucial in many biological interactions. In nature, enzymes like cytochrome P450 enable the selective C-H oxygenation of unactivated positions in complex hydrocarbon frameworks, even if those are intrinsically the least reactive ones.[1] Due to the enormous scientific work over the last decades, chemists have learned to mimic such C-H oxygenations of unactivated positions with man-made catalysts.[2] The intrinsic reactivity of C-H bonds is now well-understood and even predictable, as shown by the groups of White,[2d, 3] and Baran.[2a] Moreover, the groups of White,[4] and Gebbink and Costas[5] reported catalysts that favor oxidation at less hindered sites over more electron-rich ones. Despite these great advances, the site-selective oxidation of unactivated C-H bonds still represents a great challenge for synthetic chemists. Especially when it comes to longer flexible carbon chains (alkyl groups), as they feature a multitude of C-H bonds with very similar reactivity and steric hindrance, leading to mixtures of products. Even more challenging is the oxidation of *de*activated C-H bonds close to electron-withdrawing substituents. Related to the field of C-H oxygenation, similar challenges exist for other C(sp^3)-H bond functionalizations.[6]

One way of addressing the selectivity issue of flexible carbon chains (alkyl groups) and *de*activated C-H bonds is the development of catalysts capable of binding and orientating substrates via non-covalent supramolecular recognition.[7] One of the first pioneering supramolecular C(sp^3)-H oxidation catalysts was developed by Breslow and coworkers. They reported a manganese porphyrin catalyst with up to four cyclodextrin moieties capable of binding and precisely orientating covalently modified steroid substrates.[8] Further impressive examples were reported by Brudvig and Crabtree[9] as well as by Bach and coworkers.[10] They developed catalysts that bind substrates via hydrogen bonding, however, oxidation was limited in both cases to activated benzylic positions.

A few years ago, Olivio, Di Stefano, Costas, and coworkers reported the site-selective C-H oxidation of unactivated

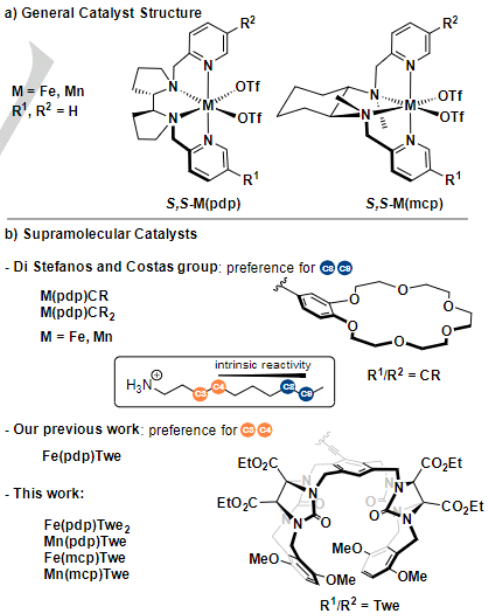

Figure 1. Supramolecular C-H oxidation catalysts for the oxidation of linear aliphatic ammonium salts.

Chemistry - A European Journal

10.1002/chem.202203480

WILEY-VCH

RESEARCH ARTICLE

methylene units in aliphatic ammonium salts by merging the **Fe(pdp)**[3] and **Mn(pdp)**[11] catalysts (Figure 1a) with two crown ether (CR) units (Figure 1b).[12] They achieved high selectivities for the C8/C9 positions of aliphatic ammonium substrates despite the very similar reactivity of all the methylene groups remote from the electron-withdrawing ammonium group (C6 and higher). Subsequently, they also applied the crown ether catalysts in the oxidation of steroid substrates and demonstrated impressive predictability in these cases.[13]

Examples in which intrinsically deactivated positions are oxidized in the presence of more reactive C-H bonds, however, are still limited, despite the significant interest in such functionalizations. For instance, very recently the groups of Luis, Bietti, and Costas reported the site-selective γ-lactonization of very strong primary C-H bonds in carboxylic acid substrates even in the presence of more reactive secondary and tertiary bonds, enabled via a directed intramolecular oxidation strategy.[14] Our group merged the White-Chen catalyst **Fe(pdp)**[3a] with a molecular glycoluril-based tweezer[15] to deliver **Fe(pdp)Twe** (Figure 1b).[16] A molecular tweezer is a host molecule with an open cavity defined by two rigid arms.[17] Similar to crown ethers, this tweezer moiety is capable of binding ammonium salts.[15] The shorter distance between the oxidation site and the binding site resulted in the preferential oxidation of C3/C4, positions that are strongly deactivated due to the nearby positive charge of the ammonium moiety. As catalyst-directed oxygenations of deactivated positions remain underexplored, we decided to further expand our initial investigations by increasing the catalyst and substrate scope. We here report the synthesis of four new supramolecular catalysts and their application to the oxidation of challenging aliphatic ammonium substrates.

Results and Discussion

Catalyst Scope

First, the catalyst scope was expanded. In particular, we were interested in the attachment of two molecular tweezer units to the pdp backbone instead of only one (Figure 2b, for models see SI, p. S66). This was of interest to us, as the original catalyst **Fe(pdp)Twe** (Figure 2a) suffered to some extent from an unspecific background reaction.[16] We hypothesized that it might be caused by the relatively open structure of the catalyst that may enable oxidation even without specific tweezer-substrate binding. The synthesis of the difunctionalized catalyst **Fe(pdp)Twe$_2$** involved the double alkylation of bipyrrolidine (**4**) with the tweezer bromide **3** (see Scheme 1) that was accessed via our route developed earlier.[16] Subsequent complexation with $Fe(OTf)_2(MeCN)_2$ resulted in the desired *S,S*-**Fe(pdp)Twe$_2$** in a similar step count (10 steps) as the original catalyst. To our surprise, the oxidation of decylammonium tetrafluoroborate (**7**) with **Fe(pdp)Twe$_2$** in the presence of H_2O_2 and acetic acid gave inferior results to the monofunctionalized **Fe(pdp)Twe** (Table 1). Interestingly, the catalyst **Fe(pdp)Twe$_2$** also displayed a lower affinity towards substrate **7** than the monosubstitued catalyst **Fe(pdp)Twe** (K_a = 19.7 ± 1.2 M^{-1} vs K_a = 29.5 ± 1.9 M^{-1}, respectively). Thus, we assume that the reduced affinity is responsible for the decreased selectivity. Therefore, the focus of the remaining study was put on novel mono-functionalized catalysts.

Next, the scope of the catalysts was expanded to the mcp-ligand (Figure 1a), as well as to the manganese metal center. The synthesis of the supramolecular catalysts started from tweezer bromide **3** that was reacted with amines **5**[18] and **6**[19] resulting in the two free ligands *S,S*-**(mcp)-Twe** and *S,S*-**(pdp)-Twe**, respectively (Scheme 1). Complexation with either $FeCl_2$/AgOTf or $Mn(OTf)_2$ gave the desired complexes. Furthermore, the established unfunctionalized *S,S*-**Fe(pdp)**[3a] and *S,S*-**Fe(mcp)**[20] complexes as well as the two Mn versions *S,S*-**Mn(pdp)**[11] and *S,S*-**Mn(mcp)**[21] were synthesized and compared with the

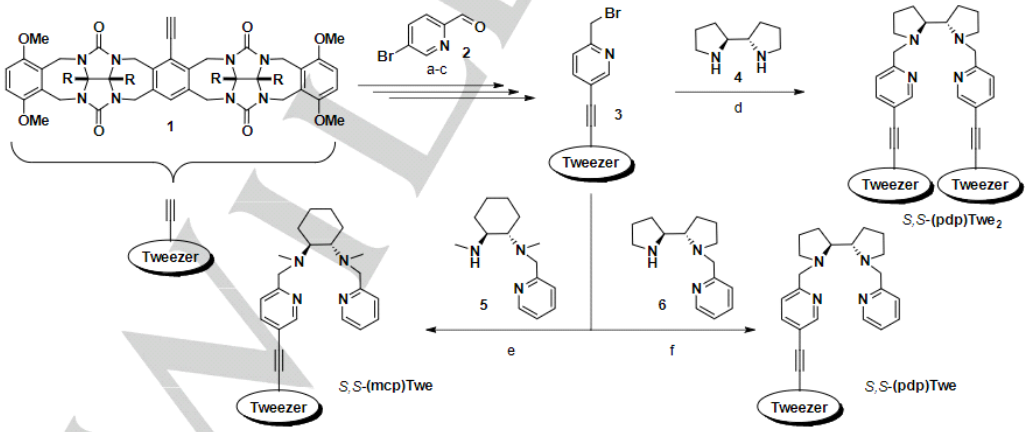

Scheme 1. Synthesis of the three ligands *S,S*-**(pdp)Twe**, *S,S*-**(mcp)Twe** and *S,S*-**(pdp)Twe$_2$**. The Synthesis of tweezers **1** and **3**, compound **6**, and ligand *S,S*-**(pdp)-Twe** was previously reported.[16] a) **2**, $PdCl_2(PPh_3)_2$, CuI, PPh_3, THF, mw, 120 °C, 90 min, 76%. B) $NaCNBH_3$, TFA, MeOH, CH_2Cl_2, rt, 4 h, 96%. C) PBr_3, CH_2Cl_2, 0 °C → rt, 16 h, 75%. D) **3** (2 equiv.), **4** (1 equiv.), K_2CO_3, TBAB, MeCN, 90 °C, 16 h, 88%. E) **3** (1 equiv.), **5**[18] (1 equiv.), K_2CO_3, TBAB, MeCN, 90 °C, 16 h, 94%. F) **3** (1 equiv.), **6**[19] (1 equiv.), K_2CO_3, TBAB, MeCN, 90 °C, 16 h, 97%. TBAB: tetra-*n*-butylammonium bromide, TFA: trifluoroacetic acid.

Chemistry - A European Journal

10.1002/chem.202203480

WILEY-VCH

RESEARCH ARTICLE

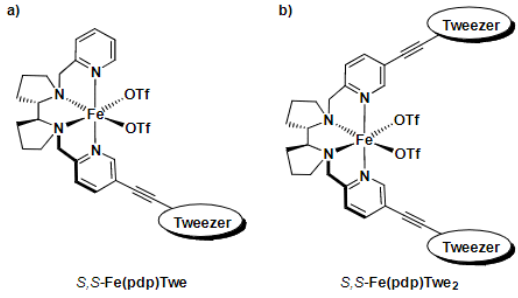

Figure 2. Depiction of *S,S*-**Fe(pdp)Twe** and *S,S*-**Fe(pdp)Twe2**.

Table 1. Oxidation of decylammonium **7** with **Fe(pdp)Twe** and **Fe(pdp)Twe2**.[a]

Catalyst	Conv [%]	Total Yield[b] [%]	K3/K4 Selectivity[c] [%]	K3-K5 Selectivity[c] [%]
Fe(pdp)Twe	47	25	28	43
Fe(pdp)Twe2	34	24	19	34

[a] General reaction conditions: substrate (9.25 µmol, 1.0 equiv.), Fe (463 nmol, 5 mol%), AcOH (74.0 µmol, 8.0 equiv.), H_2O_2 (139 µmol, 15 equiv., addition *via* a syringe pump over 90 min), MeCN, 0 °C. After 15 min, internal standard (biphenyl, 4.63 µmol, 0.5 equiv.), NEt_3 (50 µL), Ac_2O (75 µL), 0 °C. After 1 h, washing with H_2O, 2 M H_2SO_4, $NaHCO_3$, dried (Na_2SO_4) and analyzed by GC. [b] Total yield refers to the mixture of all isomers. [c] Selectivity refers to the yield of selected ketones/total yield.

respective tweezer complexes *S,S*-**Fe(pdp)Twe**, *S,S*-**Fe(mcp)Twe**, *S,S*-**Mn(pdp)Twe**, and *S,S*-**Mn(mcp)Twe** in the oxidation of decylammonium tetrafluoroborate (**7**, Table 2, Figure 3a-b). Whereas the *S,S*-**Mn(pdp)Twe** and *S,S*-**Mn(mcp)Twe** resulted in active catalysts, **Fe(mcp)Twe** gave only low conversions and yields in the oxidation experiments (Table 2, entry 6) despite repeated attempts of synthesizing it under various reported conditions.[20, 22] Interestingly, the Fe(mcp) combination is often excluded in catalytic studies, potentially indicating that it is generally less accessible/active.[13-14]

In agreement with previous results,[12-13] the manganese complexes gave higher yields at lower catalyst loading as compared to the **Fe(pdp)Twe** catalyst (1 vs. 3 mol%). They also displayed a significant increase in C3/C4 selectivity (5.8 vs. 14, and 7.2 vs. 13, respectively) compared to their unfunctionalized counterparts **Mn(mcp)** and **Mn(pdp)** (Table 2, entries 1-4, Figure 3a). However, the selectivity increase was not as marked as for the **Fe(pdp)**-series (Table 2, entries 7-8). A closer inspection of the results revealed that both K3 and K4 selectivity are affected to a similar extent (Figure 3b). Furthermore, for both Mn Twe catalysts, a distinct increase in C5 oxidation is observed compared to their unfunctionalized versions.

This is in stark contrast to the original **Fe(pdp)Twe**, which shows only a slight increase in K5 product compared to its unfunctionalized counterpart. A comparison of the two catalyst backbones reveals that the **Mn(mcp)Twe** not only gives slightly better selectivities for the proximal C3-C5 positions compared to **Mn(pdp)Twe** but also higher yields (Table 2). In conclusion, both **Fe(pdp)Twe** and **Mn(mcp)Twe** possess interesting features. The first displays the best selectivity for the deactivated positions C3/C4 of all the catalysts investigated, whereas the second one gives the best yields and the highest selectivity for the K5 product. Since to us the oxidation of the strongly deactivated positions C3 and C4 was most interesting, we decided to focus on the **Fe(pdp)Twe** catalyst in the subsequent oxidation experiments that aimed at expanding the substrate scope.

Solvent screening

Before expanding the substrate scope, we decided to explore alternative solvents besides acetonitrile. Specifically, we wanted to investigate the polar solvents trifluoroethanol (TFE) and hexafluoroisopropanol (HFIP). Both solvents are known to activate H_2O_2, and therefore facilitate the hydrogen atom transfer (HAT) to form the reactive $[LM^{V}(O)OAc]^{2+}$ species in Fe and Mn catalyzed C-H oxidation reaction.[23] Since these solvents also deactivate the α C-H bond of the alcohols formed,[24] higher amounts of alcohol products are observed (in HFIP almost exclusively). Being not aware of this strong deactivation of the α C-H bond in the past, led to a misinterpretation in our initial publication, and the incorrect conclusion that no selectivity for the proximal positions was observed in TFE and HFIP.[16]

Table 2. Oxidation of decylammonium tetrafluoroborate (**7**) using different catalysts and solvents.[a]

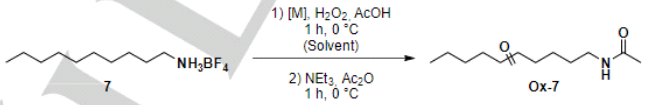

Entry	Catalyst	[Cat] [mol%]	Solvent	Conv. [%]	Total Yield[c] [%]	K3/K4 Selectivity[c] [%]	K3-K5 Selectivity[c] [%]
1 vs 2	**Mn(mcp)** vs **Mn(mcp)Twe**	1	MeCN	69 vs 58	55 vs 40	5.8 vs 14	15 vs 29
3 vs 4	**Mn(pdp)** vs **Mn(pdp)Twe**	1	MeCN	58 vs 45	32 vs 26	7.2 vs 13	16 vs 28
5 vs 6	**Fe(mcp)** vs **Fe(mcp)Twe**	3	MeCN	18 vs 6.8	15 vs 2.0	3.6 vs 9.0	7.9 vs 15
7 vs 8	**Fe(pdp)** vs **Fe(pdp)Twe**	3	MeCN	35 vs 17	31 vs 14	6.4 vs 27	13 vs 36
9[b] vs 10[b]	**Fe(pdp)** vs **Fe(pdp)Twe**	3	TFE	63 vs 38	34 vs 20	1.6 vs 5.6	9.5 vs 20
11[b] vs 12[b]	**Fe(pdp)** vs **Fe(pdp)Twe**	3	HFIP	94 vs 45	73 vs 30	0.7 vs 15	3.3 vs 34

[a] General reaction conditions: substrate (18.5 µmol, 1.0 equiv.), Fe (555 nmol, 3 mol%) or Mn catalyst (185 nmol, 1 mol%), AcOH (148 µmol, 8.0 equiv. or 407 µmol, 22 equiv., respectively), H_2O_2 (46.3 µmol, 2.5 equiv., addition *via* a syringe pump over 16 min), solvent, 0 °C. After 45 min, internal standard (biphenyl,

Chemistry - A European Journal

10.1002/chem.202203480

WILEY-VCH

RESEARCH ARTICLE

9.25 µmol, 0.5 equiv.), NEt_3 (100 µL), Ac_2O (150 µL), 0 °C. After 1 h, washing with H_2O, 2 M H_2SO_4, $NaHCO_3$, dried (Na_2SO_4) and analyzed by GC. [b] Additional IBX oxidation of alcohol products, see SI p. S20. [c] Total yield refers to the mixture of all isomers. [d] Selectivity refers to the yield of selected ketones/total yield.

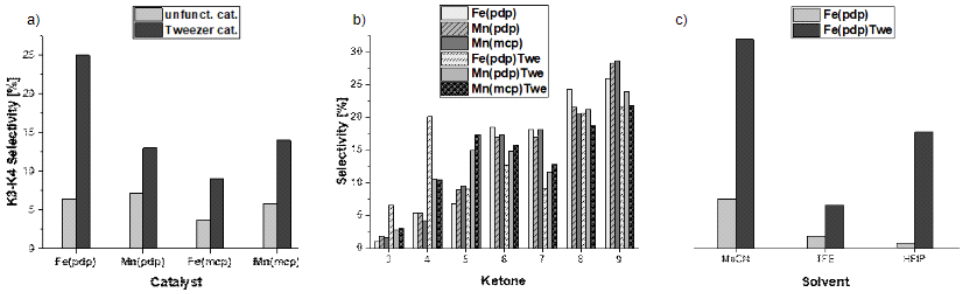

Figure 3. Graphical depictions of the decylammonium tetrafluoroborate (7) oxidation results from Table 2: a) the K3-K4 oxidation selectivity of various catalysts; b) the oxidation selectivity of the observed ketone products; c) the K3-K4 selectivity in different solvents in the oxidation with **Fe(pdp)** and **Fe(pdp)Twe**.

The alcohol products observed in the oxidation of decylammonium possess very similar retention times and additionally overlap with the signals of the ketone products K8 and K9. This led to the misinterpretation of the products in the HFIP and TFE experiment in the initial publication. Because an excess of H_2O_2 was used, it was assumed that the observed product signals correspond to ketones, and concluded that the selectivity of our supramolecular catalyst was lost in TFE and HFIP. Once we realized this, the product mixtures obtained were further oxidized in a subsequent step with IBX to exclusively obtain the ketone products. And indeed, in both solvents, an increased selectivity of the deactivated C3/C4 positions was observed for the supramolecular catalyst compared to the unfunctionalized one (Table 2, Figure 3c). Although the best selectivity was still obtained in MeCN (Table 2, entry 8), the 21-fold C3/C4 selectivity increase in HFIP for the switch from **Fe(pdp)** to **Fe(pdp)Twe** was exceptional (Table 2, entries 11-12). Furthermore, as expected the activation of H_2O_2 by TFE and HFIP increased the conversion and yield in the oxidation of decylammonium distinctly (Table 2, entries 7-12).

Substrate Scope

Finally, the oxidation of new substrates was investigated (Table 3, Figure 4). It was decided to utilize the standard conditions using **Fe(pdp)**/**Fe(pdp)Twe** in MeCN, as they delivered the highest selectivities. In particular, we were interested in the oxidation of 3,7-dimethyloctan-1-ammonium (**8**) and 4,8-dimethylnonan-1-ammonium tetrafluoroborate (**9**), substrates with terpene substitution pattern. The substrates can be readily synthesized from 1-bromo-3,7-dimethyloctane in three steps. First, the bromide was reacted with NaN_3 or NaCN, respectively.[25] Subsequent reduction with $LiAlH_4$ and direct ammonium salt formation of the crude amines with HBF_4•OEt_2 resulted in the desired substrates **8** and **9** (see SI, p. S12-S14). Both substrates possess two tertiary C-H bonds: an intrinsically deactivated one in proximity to the positive charge (C3 and C4, respectively) and a remote one (C7 and C8, respectively). For analysis of the oxidation products, a combination of GC a NMR analysis was used. The conversion and yield were calculated *via* GC using an internal standard. The regioselectivity, however, was determined by 1H NMR analysis of the isolated product mixture by comparison of the methyl groups and the methylene signal α- to the amide (for details, see SI p. S25-S26 and S30-S32).

Regarding substrate **8**, the oxidation with the unfunctionalized **Fe(pdp)** catalyst gave mainly the remote alcohol product **8**-O7 and only minor amounts of the proximal C3 alcohol product **8**-O3 (11% selectivity for C3, Table 3). Notably, no ketone products from the oxidation of less reactive secondary C-H bonds were observed. As expected, the usage of **Fe(pdp)Twe** catalyst promoted the oxidation of the deactivated C3 C-H bond leading to a distinct selectivity increase from 11 to 41%. When switching to the extended substrate **9**, comparable results were observed with a general increase in the formation of the less deactivated tertiary **9**-O4 alcohol compared to **8**-O3. More precisely, the selectivity for C4 was 25% and 57% for **Fe(pdp)** and **Fe(pdp)Twe**, respectively, making it the major product in the oxidation with the supramolecular catalyst. Comparing the two substrates, a similar performance was achieved by **Fe(pdp)Twe** as it increased the selectivity for the deactivated position by about 30 percentage points in each case. Considering the relative selectivity change, more impressive results were obtained with substrate **8**. While for compound **9** a 2.3-fold increase for the oxidation of C4 was observed, the increase for C3 selectivity was 3.7-fold for **8**, despite the stronger deactivation at C3 as compared to C4.

Next, the oxidations of substrates **10** and **11** were investigated. They can be synthesized in one step from the corresponding commercial amines by reaction with HBF_4•OEt_2 (see SI p. S14-S15). Both substrates possess only one tertiary C-H bond (at C3 and C4, respectively), hence we envisioned the intrinsic reactivity for these positions would be higher compared to the substrates **8** and **9**. Interestingly, this was not the case. For **10**, the C3 oxidation selectivity was only 4.9% for the unfunctionalized **Fe(pdp)** catalyst, which could be increased up to 16% with **Fe(pdp)Twe**. The two major products were the ketone products (*rac*-**10**-K5 and **10**-K6) at the remote cyclohexane positions C5/C6 and also minor amounts of *rac*-**10**-K4 ketone were formed (for details, see SI p. S34-S49). Similarly, in the oxidation of **11,** the selectivity for alcohol product **11**-O4 increased from 9.0% to 27% for **Fe(pdp)** and **Fe(pdp)Twe**, respectively. Again, the main products were the ketone products at the remote cyclohexane positions C6/C7 (for details, see SI p.S50-S61). The reason for the low reactivity of the tertiary C3-H and C4-H bonds in **10** and **11** may be due to steric effects. The electronic difference should

Chemistry - A European Journal

10.1002/chem.202203480

WILEY-VCH

RESEARCH ARTICLE

favor the tertiary bonds over the cyclic secondary C-H bonds despite their proximity to the positive charge. This is supported by the observation, that no ketone products were formed in the case of the linear substrates **8** and **9**.[26] Again, considering the relative selectivity change, slightly better results were observed for the C3 oxidation in **10** compared to C4 in **11** with a 3.2-fold increase compared to a 3.0-fold increase, respectively.

Overall, it seems that the substrate-tweezer binding slightly favors C3 over C4, as the C3 selectivity is amplified to a stronger extent than the C4 counterpart. This is most evident for substrates **8** and **9** (Figure 4). Thus, we assume that C3 is closer to the oxidation center in the substrate-tweezer complex.

Table 3. Oxidation of **7** and new substrates (**8**-**11**) with **Fe(pdp)** and **Fe(pdp)Twe**.[a]

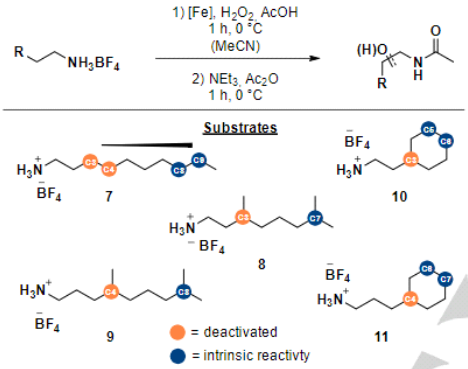

Substrate[a]	Fe(pdp)		Fe(pdp)Twe	
	Total Yield[b] [%]	Selectivity[c] [%]	Total Yield[b] [%]	Selectivity[c] [%]
7	31	6.4	14	27
8	34	11	16	41
9	24	25	15	57
10	28	4.9	11	16
11	36	9.0	14	27

[a] General reaction conditions: substrate (1.0 equiv.), Fe (3 mol%), AcOH (8.0 equiv.), H_2O_2 (2.5 equiv., addition *via* a syringe pump over 16 min), MeCN, 0 °C. After 45 min, internal standard (biphenyl, 9.25 µmol, 0.5 equiv.), NEt_3, Ac_2O, 0 °C. After 1 h, work up, see SI p. S19-S20. [b] Total yield refers to the mixture of all isomers. [c] Selectivity refers to the yield of selected ketones/total yield.

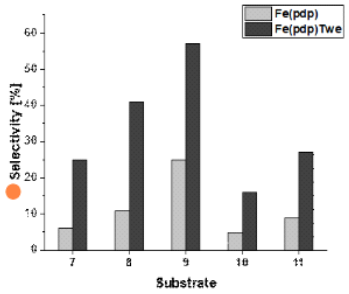

Figure 4. Oxidation selectivity of **Fe(pdp)** and **Fe(pdp)Twe** for C3 and/or C4.

Conclusion

In summary, we synthesized four new supramolecular oxidation catalysts that are based on well-established Fe/Mn oxidation catalysts linked to a molecular glycoluril-based tweezer. The **Fe(pdp)Twe$_2$**, unfortunately, did not improve yield and even showed a slightly lower C3/C4 selectivity, presumingly due to the lower binding affinity to the substrate.

The two Mn tweezer catalysts (**Mn(mcp)Twe** and **Mn(pdp)Twe**) resulted in a distinct increase in conversion and yield. They both showed a significant increase in C3/C4 selectivity compared to the unfunctionalized catalysts, however not as marked as with the **Fe(pdp)Twe** catalyst. Moreover, in both cases, C5 oxidation was substantially amplified.

The oxidation of four additional substrates with the **Fe(pdp)Twe** catalyst was investigated. In the case of substrate **9**, it was possible to observe the deactivated C4 oxidation product as the major product. Moreover, the relative increase in selectivity for the strongly deactivated C3 positions in compound **8** was exceptional. These results highlight the potential of supramolecular catalysts for the oxidation of deactivated C-H bonds that are very difficult to oxidize with alternative means. However, further improvements in the design and efficiency of these systems are required to enable more general applicability. The main points that require improvement are certainly the low affinity of the catalyst to the substrate, as well as the conformational freedom of the binding site linkage.

Experimental Section

General small-scale Fe oxidation reactions: Substrate (18.5 µmol, 1.0 equiv.) and Fe catalyst (555 nmol, 3 mol%) were dissolved in 200 µL solvent in a 1 mL screw vial. After the addition of AcOH (8.5 µL, 148 µmol, 8.0 equiv.), the mixture was cooled to 0 °C. Next, a solution of commercially available aq. H_2O_2 (50% w/w, Sigma Aldrich, 51.4 µL, 46.2 µmol, 2.5 equiv.) diluted in solvent (~ 0.9 M) was slowly added over 16 min by a syringe pump. After the addition, the mixture was left to stir for another 45 min. The workup was performed according to SI, p. S19-S20. General small-scale Mn oxidation reactions: Substrate (18.5 µmol, 1.0 equiv.) and Mn catalyst (185 nmol, 1 mol%) were dissolved in 200 µL solvent in a 1 mL screw vial. After the addition of AcOH (23.3 µL, 407 µmol, 22.0 equiv.), the mixture was cooled to 0 °C. Next, a solution of commercially available aq. H_2O_2 (50% w/w, Sigma Aldrich, 51.4 µL,

Chemistry - A European Journal

10.1002/chem.202203480

WILEY-VCH

RESEARCH ARTICLE

46.2 µmol, 2.5 equiv.) diluted in solvent (~ 0.9 M) was slowly added over 16 min by a syringe pump. After the addition, the mixture was left to stir for another 45 min. The workup was performed according to SI, p. S19-S20.

Acknowledgments

We thank Dr. Michael Pfeffer for the HR-MS analysis.

Conflict of interest

The authors declare no conflict of interest.

Data Availability Statement

The data that support the findings of this study are available in the supplementary material of this article.

Keywords: C-H oxidation • supramolecular chemistry • catalysis • molecular tweezer • ammonium binding

[1] a) I. G. Denisov, T. M. Makris, S. G. Sligar, I. Schlichting, *Chem. Rev.* **2005**, *105*, 2253-2278; b) P. R. Ortiz de Montellano, *Chem. Rev.* **2010**, *110*, 932-948; c) R. Fasan, *ACS Catal.* **2012**, *2*, 647-666; d) T. L. Poulos, *Chem. Rev.* **2014**, *114*, 3919-3962.

[2] a) T. Newhouse, P. S. Baran, *Angew. Chem. Int. Ed.* **2011**, *50*, 3362-3374; b) J. Genovino, D. Sames, L. G. Hamann, B. B. Toure, *Angew. Chem. Int. Ed.* **2016**, *55*, 14218-14238; c) X.-S. Xue, P. Ji, B. Zhou, J.-P. Cheng, *Chem. Rev.* **2017**, *117*, 8622-8648; d) M. C. White, J. Zhao, *J. Am. Chem. Soc.* **2018**, *140*, 13988-14009; e) M. Milan, M. Salamone, M. Costas, M. Bietti, *Acc. Chem. Res.* **2018**, *51*, 1984-1995; f) L. D'Accolti, C. Annese, C. Fusco, *Chem. Eur. J.* **2019**, *25*, 12003-12017.

[3] a) M. S. Chen, M. C. White, *Science* **2007**, *318*, 783-787; b) M. S. Chen, M. C. White, *Science* **2010**, *327*, 566-571.

[4] P. E. Gormisky, M. C. White, *J. Am. Chem. Soc.* **2013**, *135*, 14052-14055.

[5] D. Font, M. Canta, M. Milan, O. Cussó, X. Ribas, R. J. Klein Gebbink, M. Costas, *Angew. Chem. Int. Ed.* **2016**, *55*, 5776-5779.

[6] a) K. Godula, D. Sames, *Science* **2006**, *312*, 67-72; b) H. M. Davies, J. R. Manning, *Nature* **2008**, *451*, 417-424; c) R. Jazzar, J. Hitce, A. Renaudat, J. Sofack - Kreutzer, O. Baudoin, *Chem. Eur. J.* **2010**, *16*, 2654-2672; d) T. W. Lyons, M. S. Sanford, *Chem. Rev.* **2010**, *110*, 1147-1169; e) M. P. Doyle, R. Duffy, M. Ratnikov, L. Zhou, *Chem. Rev.* **2010**, *110*, 704-724; f) H. M. Davies, D. Morton, *Chem. Soc. Rev.* **2011**, *40*, 1857-1869; g) K. M. Engle, T.-S. Mei, M. Wasa, J.-Q. Yu, *Acc. Chem. Res.* **2012**, *45*, 788-802; h) T. Brückl, R. D. Baxter, Y. Ishihara, P. S. Baran, *Acc. Chem. Res.* **2012**, *45*, 826-839; i) J. Yamaguchi, A. D. Yamaguchi, K. Itami, *Angew. Chem. Int. Ed.* **2012**, *51*, 8960-9009; j) G. Rouquet, N. Chatani, *Angew. Chem. Int. Ed.* **2013**, *52*, 11726-11743; k) Z. Chen, B. Wang, J. Zhang, W. Yu, Z. Liu, Y. Zhang, *Org. Chem. Front.* **2015**, *2*, 1107-1295; l) K. Shin, H. Kim, S. Chang, *Acc. Chem. Res.* **2015**, *48*, 1040-1052; m) T. Cernak, K. D. Dykstra, S. Tyagarajan, P. Vachal, S. W. Krska, *Chem. Soc. Rev.* **2016**, *45*, 546-576; n) J. F. Hartwig, M. A. Larsen, *ACS Cent. Sci.* **2016**, *2*, 281-292; o) J. He, M. Wasa, K. S. Chan, Q. Shao, J.-Q. Yu, *Chem. Rev.* **2017**, *117*, 8754-8786; p) D. C. Blakemore, L. Castro, I. Churcher, D. C. Rees, A. W. Thomas, D. M. Wilson, A. Wood, *Nat. Chem.* **2018**, *10*, 383-394; q) C. Sambiagio, D. Schönbauer, R. Blieck, T. Dao-Huy, G. Pototschnig, P. Schaaf, T. Wiesinger, M. F. Zia, J. Wencel-Delord, T. Besset, *Chem. Soc. Rev.* **2018**, *47*, 6603-6743; r) L. M. Stateman, K. M. Nakafuku, D. A. Nagib, *Synthesis* **2018**, *50*, 1569-1586.

[7] a) R. Breslow, S. D. Dong, *Chem. Rev.* **1998**, *98*, 1997-2012; b) P. Thordarson, E. J. Bijsterveld, A. E. Rowan, R. J. Nolte, *Nature* **2003**, *424*, 915-918; c) S. Das, G. W. Brudvig, R. H. Crabtree, *Chem. Commun.* **2008**, 413-424; d) T. Šmejkal, B. Breit, *Angew. Chem. Int. Ed.* **2008**, *47*, 311-315; e) P. Fackler, C. Berthold, F. Voss, T. Bach, *J. Am. Chem. Soc.* **2010**, *132*, 15911-15913; f) S. Carboni, C. Gennari, L. Pignataro, U. Piarulli, *Dalton Trans.* **2011**, *40*, 4355-4373; g) P. Dydio, W. I. Dzik, M. Lutz, B. de Bruin, J. N. Reek, *Angew. Chem. Int. Ed.* **2011**, *50*, 396-400; h) P. Dydio, J. N. Reek, *Chem. Sci.* **2014**, *5*, 2135-2145; i) M. Raynal, P. Ballester, A. Vidal-Ferran, P. W. van Leeuwen, *Chem. Soc. Rev.* **2014**, *43*, 1660-1733; j) Y. Kuninobu, H. Ida, M. Nishi, M. Kanai, *Nat. Chem.* **2015**, *7*, 712; k) H. J. Davis, M. T. Mihai, R. J. Phipps, *J. Am. Chem. Soc.* **2016**, *138*, 12759-12762; l) H. J. Davis, R. J. Phipps, *Chem. Sci.* **2017**, *8*, 864-877; m) S. a. Korom, P. Ballester, *J. Am. Chem. Soc.* **2017**, *139*, 12109-12112; n) M. E. Hoque, R. Bisht, C. Haldar, B. Chattopadhyay, *J. Am. Chem. Soc.* **2017**, *139*, 7745-7748; o) D. Vidal, G. Olivo, M. Costas, *Chem. Eur. J.* **2018**, *24*, 5042-5054; p) D. Vidal, M. Costas, A. Lledo, *ACS Catal.* **2018**, *8*, 3667-3672; q) N. R. Mote, S. H. Chikkali, *Chem. Asian J.* **2018**, *13*, 3623-3646; r) S. T. Bai, V. Sinha, A. M. Kluwer, P. R. Linnebank, Z. Abiri, B. de Bruin, J. N. Reek, *ChemCatChem* **2019**, *11*, 5322-5329; s) F. Burg, T. Bach, *J. Org. Chem.* **2019**, *84*, 8815-8836; t) G. Olivo, G. Capocasa, D. Del Giudice, O. Lanzalunga, S. Di Stefano, *Chem. Soc. Rev.* **2021**, *50*, 7681-7724; u) Y. Jiao, X.-Y. Chen, J. F. Stoddart, *Chem* **2022**; v) J. N. Reek, B. de Bruin, S. Pullen, T. J. Mooibroek, A. M. Kluwer, X. Caumes, *Chem. Rev.* **2022**.

[8] a) R. Breslow, X. Zhang, Y. Huang, *J. Am. Chem. Soc.* **1997**, *119*, 4535-4536; b) R. Breslow, Y. Huang, X. Zhang, J. Yang, *Proc. Natl. Acad. Sci. U.S.A.* **1997**, *94*, 11156-11158; c) J. Yang, R. Breslow, *Angew. Chem. Int. Ed.* **2000**, *39*, 2692-2695; d) J. Yang, B. Gabriele, S. Belvedere, Y. Huang, R. Breslow, *J. Org. Chem.* **2002**, *67*, 5057-5067.

[9] a) S. Das, C. D. Incarvito, R. H. Crabtree, G. W. Brudvig, *Science* **2006**, *312*, 1941-1943; b) S. Das, G. W. Brudvig, R. H. Crabtree, *J. Am. Chem. Soc.* **2008**, *130*, 1628-1637.

[10] a) J. R. Frost, S. M. Huber, S. Breitenlechner, C. Bannwarth, T. Bach, *Angew. Chem. Int. Ed.* **2015**, *54*, 691-695; b) F. Burg, M. Gicquel, S. Breitenlechner, A. Pöthig, T. Bach, *Angew. Chem. Int. Ed.* **2018**, *57*, 2953-2957; c) F. Burg, S. Breitenlechner, C. Jandl, T. Bach, *Chem. Sci.* **2020**, *11*, 2121-2129.

[11] R. V. Ottenbacher, K. P. Bryliakov, E. P. Talsi, *Adv. Synth. Catal.* **2011**, *353*, 885-889.

[12] G. Olivo, G. Farinelli, A. Barbieri, O. Lanzalunga, S. Di Stefano, M. Costas, *Angew. Chem. Int. Ed.* **2017**, *129*, 16565-16569.

[13] G. Olivo, G. Capocasa, B. Ticconi, O. Lanzalunga, S. Di Stefano, M. Costas, *Angew. Chem. Int. Ed.* **2020**, *59*, 12703-12708.

[14] A. Call, M. Cianfanelli, P. Besalú-Sala, G. Olivo, A. Palone, L. Vicens, X. Ribas, J. M. Luis, M. Bietti, M. Costas, *J. Am. Chem. Soc.* **2022**, *144*, 19542–19558.

[15] C. A. Burnett, D. Witt, J. C. Fettinger, L. Isaacs, *J. Org. Chem.* **2003**, *68*, 6184-6191.

[16] M. Knezevic, M. Heilmann, G. M. Piccini, K. Tiefenbacher, *Angew. Chem. Int. Ed.* **2020**, *59*, 12387-12391.

[17] a) C. Chen, H. Whitlock Jr, *J. Am. Chem. Soc.* **1978**, *100*, 4921-4922; b) J. Rebek Jr, B. Askew, N. Islam, M. Killoran, D. Nemeth, R. Wolak, *J. Am. Chem. Soc.* **1985**, *107*, 6736-6738; c) J. Rebek, *Science* **1987**, *235*, 1478-1484; d) C. S. Wilcox, L. M. Greer, V. Lynch, *J. Am. Chem. Soc.* **1987**, *109*, 1865-1867; e) S. C. Zimmerman, C. M. VanZyl, *J. Am. Chem. Soc.* **1987**, *109*, 7894-7896; f)

Chemistry - A European Journal

10.1002/chem.202203480

WILEY-VCH

RESEARCH ARTICLE

S. C. Zimmerman, in *Top. Curr. Chem.*, Springer, **1993**, pp. 71-102; g) A. E. Rowan, J. A. Elemans, R. J. Nolte, *Acc. Chem. Res.* **1999**, *32*, 995-1006; h) F.-G. Klärner, B. Kahlert, *Acc. Chem. Res.* **2003**, *36*, 919-932; i) M. Hardouin–Lerouge, P. Hudhomme, M. Salle, *Chem. Soc. Rev.* **2011**, *40*, 30-43; j) F.-G. Klärner, T. Schrader, *Acc. Chem. Res.* **2013**, *46*, 967-978; k) V. Valderrey, G. Aragay, P. Ballester, *Coord. Chem. Rev.* **2014**, *258*, 137-156; l) S. C. Zimmerman, *Beilstein J. Org. Chem.* **2016**, *12*, 125-138; m) S. Ganapati, L. Isaacs, *Isr. J. Chem.* **2018**, *58*, 250-263.

[18] Z. Codolà, I. Gamba, F. Acuña-Parés, C. Casadevall, M. Clémancey, J.-M. Latour, J. M. Luis, J. Lloret-Fillol, M. Costas, *J. Am. Chem. Soc.* **2018**, *141*, 323-333.

[19] L. Chiang, D. Savard, Y. Shimazaki, F. Thomas, T. Storr, *Inorg. Chem.* **2014**, *53*, 5810-5819.

[20] M. Costas, J. Que, Lawrence, *Angew. Chem.* **2002**, *114*, 2283-2285.

[21] a) A. Murphy, G. Dubois, T. Stack, *J. Am. Chem. Soc.* **2003**, *125*, 5250-5251; b) R. V. Ottenbacher, K. P. Bryliakov, E. P. Talsi, *Inorg. Chem.* **2010**, *49*, 8620-8628.

[22] a) K. Chen, M. Costas, J. Kim, A. K. Tipton, L. Que, *J. Am. Chem. Soc.* **2002**, *124*, 3026-3035; b) M. Milan, M. Bietti, M. Costas, *ACS Cent. Sci.* **2017**, *3*, 196-204.

[23] a) K. Neimann, R. Neumann, *Org. Lett.* **2000**, *2*, 2861-2863; b) A. Berkessel, J. A. Adrio, *J. Am. Chem. Soc.* **2006**, *128*, 13412-13420.

[24] V. Dantignana, M. Milan, O. Cussó, A. Company, M. Bietti, M. Costas, *ACS Cent. Sci.* **2017**, *3*, 1350-1358.

[25] a) I. Bala, N. Singh, R. A. K. Yadav, J. De, S. P. Gupta, D. P. Singh, D. K. Dubey, J.-H. Jou, R. Douali, S. K. Pal, *J. Mater. Chem. C* **2020**, *8*, 12485-12494; b) M.-K. Wong, N.-W. Chung, L. He, D. Yang, *J. Am. Chem. Soc.* **2003**, *125*, 158-162.

[26] N. A. Vermeulen, M. S. Chen, M. C. White, *Tetrahedron* **2009**, *65*, 3078-3084.

Chemistry - A European Journal

10.1002/chem.202203480

WILEY-VCH

RESEARCH ARTICLE

Entry for the Table of Contents

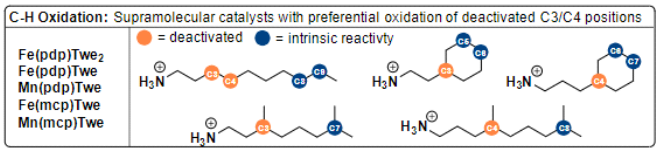

New supramolecular tweezer catalysts capable of oxidizing strongly deactivated C3/C4 positions of aliphatic ammonium salts were synthesized. The best performing catalyst **Fe(pdp)Twe** was explored in the oxidation of new substrates.

Twitter usernames: @TiefenbacherLab

10 Appendix

This chapter contains the supporting information on the two manuscripts from the tweezer project.

Angewandte Chemie
Eine Zeitschrift der Gesellschaft Deutscher Chemiker

Supporting Information

Overriding Intrinsic Reactivity in Aliphatic C–H Oxidation: Preferential C3/C4 Oxidation of Aliphatic Ammonium Substrates

*Melina Knezevic, Michael Heilmann, Giovanni Maria Piccini, and Konrad Tiefenbacher**

anie_202004242_sm_miscellaneous_information.pdf

Table of Contents

1. General Information

Experimental: All reactions with air- or moisture-sensitive substances were carried out under an atmosphere of argon (Ar 4.6). Microwave experiments were conducted using an ANTON PAAR Monowave 400 microwave synthesis reactor.

Analytical methods and instruments: For analytical thin-layer chromatography (TLC), MERCK silica gel 60 F_{254} glass-baked plates were used and analyzed under UV light (λ = 254 nm [UV]) or by immersion in a potassium permanganate solution [$KMnO_4$] (9 g $KMnO_4$, 60 g K_2CO_3, 15 mL aqueous NaOH-solution (5%) in 900 mL H_2O) and subsequent heat treatment. Column chromatography was carried out as flash chromatography using MERCK silica gel 60 (230 - 240 mesh ASTM, particle size: 40 - 63 μm) according to Still et al.[1]

^{1}H NMR spectra were recorded on a BRUKER UltraShield 500 at 500 mHz. ^{13}C NMR spectra were recorded at 126 mHz or 151 mHz, using a BRUKER UltraShield 500 or a 600 MHz BRUKER Avance III NMR spectrometer equipped with a cryogenic QCI-F probe, respectively. Chemical shifts are reported in ppm at 298 K unless stated otherwise. The ^{1}H spectra were calibrated on the signals of the residual protons of the respective solvents: $CDCl_3$ $\delta(^1H)$ = 7.26 ppm, CD_3CN $\delta(^1H)$ = 1.96 ppm, DMSO-d6 $\delta(^1H)$ = 2.50 ppm. In ^{13}C NMR spectra the signal of the deuterium coupled multiplets of the solvents are used as reference: $CDCl_3$ $\delta(^{13}C)$ = 77.16 ppm, CD_3CN $\delta(^1H)$ = 118.26 ppm, DMSO-d6 $\delta(^{13}C)$ = 39.52 ppm.[2] The coupling constants *J* are reported in hertz (Hz). Multiplicity is described as: s (singlet), br s (broad singlet), d (doublet), dd (doublet of doublets) t (triplet), m (multiplet). Apparent multiplicity of magnetically non-equivalent protons are marked as virtual (*virt.*). For characterization of compounds unknown in the literature, two-dimensional NMR experiments (HMQC, HMBC, COSY, NOESY) were conducted.

GC analyses were performed on a SHIMADZU GC-2010 Plus instrument equipped with an FID detector and a HP-5 capillary column (length = 30 m). Hydrogen was used as the carrier gas and constant-flow mode (flow rate = 40 mL/min) with a split ratio of 1:20 was used. The following temperature-program was used: 60 °C for 3 min, +15 °C/min to 250 °C, and 250 °C for 5 min.

GC-MS analyses were performed on an AGLIENT 5977B GC/MSD instrument equipped with a single quadrupole GC/MS and a HP-5MS UI capillary column (length = 30 m). Helium was used as the carrier gas and a constant-flow mode (flow rate = 1 mL/min) with a split ration of 1:100. The following temperature-program was used: 50 °C for 2.25 min, +10 °C/min to 300 °C, and 300 °C for 3 min.

Infrared spectra were measured on a BRUKER ALPHA IR spectrometer (ATR, attenuated total reflection). Abbreviations indicating intensity were used as follows: vs (very strong), s (strong), m (medium), w (weak).

High-resolution mass spectra were obtained using the electrospray ionization (ESI) technique on a BRUKER maXis 4G mass spectrometer.

Melting points were recorded on a BÜCHI Melting Point M-565 apparatus in open capillary tubes and are uncorrected.

Solvents: Anhydrous carbon tetrachloride (CCl_4), dichloroethane, toluene (PhMe), diethylamine (Et_2NH) were purchased from SIGMA-ALDRICH. Anhydrous acetonitrile (MeCN), diethyl ether (Et_2O), dichloromethane (CH_2Cl_2), DMSO, methanol (MeOH), tetrahydrofuran (THF) were purchased from ACROS ORGANICS.

Solvents for extractions, flash chromatography, filtrations and reactions under non-anhydrous conditions were purchased from VWR (HPLC grade).

Solvents for NMR spectroscopy [$CDCl_3$ (99.8%), MeCN-d3 (99.8%), DMSO-d6 (99.9%)] were purchased from CAMBRIDGE ISOTOPE LABORATORIES.

Solutions of metalorganic reagents (e.g. *n*-BuLi, LiHMDS etc.) were titrated with menthol/1,10-phenanthroline prior to use.[3]

Chemicals: Acetic anhydride, 2,2'-azobis(2-methylpropionitrile) (AIBN), biphenyl, (2*S*,2'*S*)-bipyrrolidine, *N*-bromosuccinimide (NBS), *n*-BuLi 1.6 M in hexane, (*tert*-butyldimethylsilyl)acetylene (TBS-acetylene), copper iodide, decylamine, L-(+)-diethyltartrate, ethyl formate, formaldehyde, heptylamine, iron (II) chloride, lithium aluminium hydride ($LiAlH_4$), methyl iodide, nonylamine, octylamine, phosphorus tribromide (PBr_3), potassium *tert*-butoxide (KO*t*Bu), pyridine-2-carboxaldehyde, sodium cyanoborohydride ($NaCNBH_3$), sodium peroxide water solution (50% w/w), tetrabromodurene, tetra-*n*-butylammonium bromide (TBAB), tetra-*n*-butylammonium fluoride (TBAF), tetradecylamine, tetrafluoroboric acid diethyl ether complex, triethylamine, trifluoroacetic acid (TFA), trimethylsilyl triflate, undecylamine, urea were purchased from SIGMA-ALDRICH.

Bis(triphenylphosphine)palladium(II) dichloride, dodecylamine, formic acid, potassium carbonate were purchased from ACROS ORGANICS.

2,3-Dimethylhydrochinone, 5-bromopyridine-2-carbaldehyde, 3-iodo-1,2,4,5-tetramethyl-benzene and were purchased from FLUOROCHEM.

Triphenylphosphine was purchased from ALFA AESAR.

Chemicals were used without further purifications, unless stated otherwise.

NBS used for benzylic bromination reactions was recrystallized from commercially available material according to a literature procedure and stored under an argon atmosphere at −20 °C.[4]

Employing commercially available material instead of recrystallized NBS led to aromatic bromination.

Iron (II) bis (trifluoromethanesulfonate) bis (acetonitrile) was prepared according to a literature procedure.[5]

2. Synthetic Procedures and Analytical Data

2.1.Synthesis of the Catalysts

(*syn*)-Diethyl-2,5-dioxotetrahydroimidazo[4,5-*d*]imidazole-3a,6a(1*H*,4*H*)-dicarboxylate (S1)

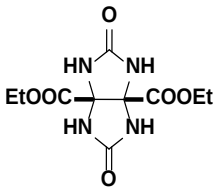

$C_{10}H_{14}N_4O_6$
MW: 286.24 g/mol

Diethyl tartrate (41.2 g, 200 mmol, 1.0 equiv.) and NBS (107 g, 600 mmol, 3.0 equiv.) were dissolved in anhydrous 1,2-dichlorethane (150 mL) and stirred at reflux for 4 h. Afterwards, the reaction was quenched by addition of Na_2SO_3 (30 g) and EtOH (40 mL) followed by removal of the solvent under reduced pressure. The oily residue was then diluted in Et_2O (100 mL), filtered and washed with Et_2O (4 x 50 mL). After removal of the solvent by rotatory evaporation, urea (30.0 g, 500 mmol. 2.5 equiv.) was added followed by PhMe (200 mL) and TFA (61.6 mL, 91.2 g, 800 mmol, 4.0 equiv.). The flask was equipped with a DEAN-STARK trap to remove emerging reaction water and was then stirred at reflux for 24 h. After cooling to room temperature, the supernatant was removed, and the residue dried in *vacuo*. Water (200 mL) was added and the mixture was heated to 80 °C for 1 h. The mixture was stored at 4 °C for 16 h and then filtered and washed with water (30 mL). The residue was dried under reduced pressure resulting in **S1** (27.0 g, 94.3 mmol, 47%) as a slightly beige solid.

^{1}H NMR (DMSO-d6, 300 K, 500 MHz) δ [ppm] = 8.00 (s, 4H), 4.09 (q, *J* = 7.1 Hz, 4H), 1.18 (t, *J* = 7.1 Hz, 6H).

^{13}C NMR (DMSO-d6, 300 K, 126 MHz) δ [ppm] = 167.3 (s), 159.5 (s), 77.8 (s), 62.0 (s), 13.8 (s).

The analytical data match literature values.[6]

1,4-Dimethoxy-2,3-dimethylbenzene (S2)

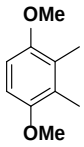

$C_{10}H_{14}O_2$
MW: 166.22 g/mol

2,3-Dimethylhydroquinone (2.76 g, 20.0 mmol, 1.0 equiv.) and KOH (5.61 g, 100 mmol, 5.0 equiv.) were dissolved in anhydrous DMSO (40 mL). Methyl iodide (2.74 mL, 6.25 g, 44.0 mmol, 2.2 equiv.) was added dropwise at room temperature with the flask being put into a water bath. The mixture was then stirred at this temperature for 2 h. After that, triethylamine (8.43 mL, 6.07 g, 60.0 mmol, 3.0 equiv.) was added and the solution was stirred for an additional 30 min. Next, water (100 mL) and concentrated HCl (10 mL) were added and the mixture was extracted with EtOAc (3 x 100 mL). The combined organic layers were washed with water (150 mL) and brine (150 mL), dried (Na_2SO_4), filtered and concentrated in *vacuo*. Purification *via* flash column chromatography (~70 g silica, Pen/Et_2O = 19/1) gave product **S2** (3.13 g, 18.8 mmol, 94%) as a white solid.

TLC R_f = 0.62 (Pen/Et_2O = 19/1) [UV, $KMnO_4$].

Mp.: 81 °C.

^{1}H NMR ($CDCl_3$, 300 K, 500 MHz) δ [ppm] = 6.66 (s, 6H), 3.78 (s, 6H), 2.16 (s, 2H).

^{13}C NMR ($CDCl_3$, 300 K, 126 MHz) δ [ppm] = 152.1 (s), 126.9 (s), 108.0 (s), 56.2 (s), 12.2 (s).

All analytical data match literature values.[7]

2,3-Bis(bromomethyl)-1,4-dimethoxybenzene (S3)

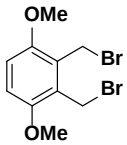

$C_{10}H_{12}Br_2O_2$
MW: 324.01 g/mol

1,4-Dimethoxy-2,3-dimethylbenzene (**S2** 5.00 g, 30.1 mmol, 1.0 equiv.), previously recrystallized NBS (11.3 g, 63.2 mmol, 2.1 equiv.) and AIBN (247 mg, 1.51 mmol, 0.05 equiv.) were dissolved in anhydrous CCl_4 (60 mL) and stirred at reflux for 3 h. Subsequently, the mixture was cooled down to room temperature and the solvent was removed by rotatory evaporation. The residue was dissolved in CH_2Cl_2 (250 mL) and 1 M NaOH (250 mL) and the mixture was extracted with CH_2Cl_2 (2 x 250 mL). The combined organic layers were washed with brine (200 mL), dried (Na_2SO_4), filtered and concentrated under

reduced pressure. The crude product was purified *via* column chromatography (~300 g silica, Pen/CH_2Cl_2 = 1/1) to give product **S3** as a white solid (9.36 g, 28.9 mmol, 96%).

TLC R_f = 0.88 (Pen/CH_2Cl_2 = 1/1) [UV, $KMnO_4$].

Mp.: 156–157 °C.

^{1}H NMR ($CDCl_3$, 300 K, 500 MHz) δ [ppm] = 6.84 (s, 2H), 4.74 (s, 4H), 3.86 (s, 6H).

^{13}C NMR ($CDCl_3$, 300 K, 151 MHz) δ [ppm] = 152.0 (s), 126.6 (s), 112.4 (s), 56.4 (s), 24.0 (s).

All analytical data match literature values.[8]

(*syn*)-Diethyl-6,9-dimethoxy-1,4-dioxo-1,2,3,4,5,10-hexahydro-2,3,4a,10a-tetraaza-benzo[g]cyclopenta[cd]azulene-2a,2a^1-dicarboxylate (7)

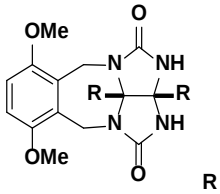

$C_{20}H_{24}N_4O_8$
MW: 448.43 g/mol

R = COOEt

Compound **S1** (3.44 g, 12.0 mmol, 2.0 equiv.) was dissolved in anhydrous DMSO (120 mL). After addition of KO*t*-Bu (2.96 g, 26.4 mmol, 4.4 equiv.), the mixture was stirred for 15 min at room temperature. Then, 2,3-bis(bromomethyl)-1,4-dimethoxybenzene (1.94 g, 6.00 mmol, 1.0 equiv.) was added and the mixture was stirred for additional 4 h at room temperature. Afterwards, the reaction was poured into a mixture of 1 M HCl (200 mL), water (100 mL) and brine (100 mL) and was extracted with EtOAc (5 x 200 mL). The combined organic layers were washed with brine (2 x 300 mL), dried (Na_2SO_4), filtered and concentrated under reduced pressure to give the crude product. Purification *via* column chromatography (~60 g silica, CH_2Cl_2/MeCN = 3/2 → 1/3) gave product **7** (1.11 g, 2.48 mmol, 41%) as a white solid.

TLC R_f = 0.43 (CH_2Cl_2/MeCN = 3/2) [$KMnO_4$].

Mp.: 235–236 °C.

^{1}H NMR ($CDCl_3$, 300 K, 500 MHz) δ [ppm] = 6.83 (s, 2H), 5.59 (d, J = 16.1 Hz, 2H), 5.44 (s, 2H), 4.26 (*virt.* dq, J = 12.8, 7.1 Hz, 4H), 4.04 (d, J = 16.1 Hz, 2H), 3.84 (s, 6H), 1.31 (t, J = 7.2 Hz, 3H), 1.30 (t, J = 7.2 Hz, 3H).

^{13}C NMR ($CDCl_3$, 300 K, 126 MHz) δ [ppm] = 166.4 (s), 166.0 (s), 157.2 (s), 151.5 (s), 127.1 (s), 113.1 (s), 83.6 (s), 73.6 (s), 63.7 (s), 63.2 (s), 57.5 (s), 36.6 (s), 14.1 (s), 14.0 (s).

All analytical data match literature values.[9]

tert-Butyldimethyl((2,3,5,6-tetramethylphenyl)ethynyl)silane (S4)

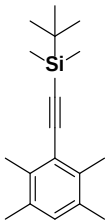

$C_{18}H_{28}Si$
MW: 272.51 g/mol

3-Iodo-1,2,4,5-tetramethyl-benzene (**5**, 2.60g, 10.0 mmol, 1.0 equiv.), $PdCl_2(PPh_3)_2$ (140 mg, 200 µmol, 0.02 equiv.) and CuI (76.2 mg, 400 µmol, 0.04 equiv.) were added to a flame-dried round-bottom flask and the flask was evacuated and refilled with argon three times. The material was then dissolved in Et_2NH (28 mL) and the solution was degassed *via* sparging with Ar for 15 min. Then, TBS acetylene (2.05 mL, 1.54 g, 11.0 mmol, 1.1 equiv.) was added dropwise and the mixture was stirred at 50 °C for 16 h. After that, water (20 mL) and CH_2Cl_2 (30 mL) were added and the separated aqueous layer was extracted with CH_2Cl_2 (2 × 20 mL). The combined organic layers were washed with brine (15 mL), dried ($MgSO_4$), filtered and concentrated *in vacuo*. Purification *via* flash column chromatography (~50 g silica, Pen) gave the desired product **S4** (2.64 g, 9.69 mmol, 97%) as a white solid.

TLC R_f = 0.66 (Pen) [UV, $KMnO_4$].

Mp.: 62–63 °C.

IR (ATR): $\tilde{\nu}$ (cm^{-1}) = 2950 (m), 2925 (m), 2853 (m), 2134 (s), 1710 (w), 1509 (w), 1461 (m), 1360 (m), 1245 (s), 1176 (w), 1074 (m), 1006 (m), 938 (w), 910 (m), 822 (s) 808 (s), 770 (vs), 698 (s), 676 (s), 647 (s), 457 (m), 423 (s).

^{1}H NMR ($CDCl_3$, 300 K, 500 MHz) δ [ppm] = 6.89 (s, 1H), 2.37 (s, 6H), 2.20 (s, 6H), 1.01 (s, 9H), 0.20 (s, 6H).

^{13}C NMR ($CDCl_3$, 300 K, 151 MHz) δ [ppm] = 136.5 (s), 133.4 (s), 131.5 (s), 123.4 (s), 104.7 (s), 100.2 (s), 26.3 (s), 20.0 (s), 17.8 (s), 16.8 (s), −4.2 (s).

tert-Butyldimethyl((2,3,5,6-tetrakis(bromomethyl)phenyl)ethynyl)silane (6)

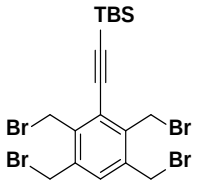

$C_{18}H_{24}Br_4Si$
MW: 588.09 g/mol

Compound **S4** (2.18 g, 8.00 mmol, 1.0 equiv.), previously recrystallized NBS[3] (8.83 g, 49.6 mmol, 6.2 equiv.) and AIBN (65.7 mg, 400 µmol, 0.05 equiv.) were dissolved in anhydrous CCl_4 (32 mL) and stirred at reflux for 72 h. Subsequently, the solvent was removed by rotatory evaporation. The residue was dissolved in CH_2Cl_2 (50 mL) and 1 M NaOH (50 mL), and the mixture was extracted with CH_2Cl_2 (3 x 50 mL). The combined organic layers were washed with brine (80 mL), dried (Na_2SO_4), filtered and concentrated under reduced pressure. The crude product was purified *via* column chromatography (~200 g silica, Pen/PhMe = 49/1) to give product **6** (2.40 g, 4.08 mmol, 51%) as a white solid.

Note: It was possible to isolate a mixture of twofold (R_f = 0.32) and threefold (R_f = 0.29) brominated byproducts (2.11 g), attempts to further convert those with another three equivalents of NBS under the same reaction conditions and work up as before resulted in more product **6** (32.7 mg, 55.6 µmol, 0.7%).

TLC R_f = 0.26 (Pen/PhMe = 49/1) [UV, $KMnO_4$].

Mp.: 120–121 °C.

IR (ATR): $\tilde{\nu}$ (cm^{-1}) = 2950 (w), 2925 (m), 2854 (m), 2151 (w), 1712 (w), 1461 (m), 1411 (m), 1361 (w), 1302 (m), 1245 (s), 1207 (s), 1141 (m), 993 (s), 930 (m), 892 (w), 820 (s), 809 (s), 772 (vs), 688 (s), 642 (s), 584 (s), 551 (s), 447 (m), 410 (s).

^{1}H NMR ($CDCl_3$, 300 K, 500 MHz) δ [ppm] = 7.32 (s, 1H), 4.86 (s, 4H), 4.57 (s, 4H), 1.06 (s, 9H), 0.28 (s, 6H).

^{13}C NMR ($CDCl_3$, 300 K, 126 MHz) δ [ppm] = 139.7 (s), 137.8 (s), 133.0 (s), 126.6 (s), 107.1 (s), 99.1 (s), 29.0 (s), 27.3 (s), 26.3 (s), 17.0 (s), −4.6 (s).

Tweezer 8a

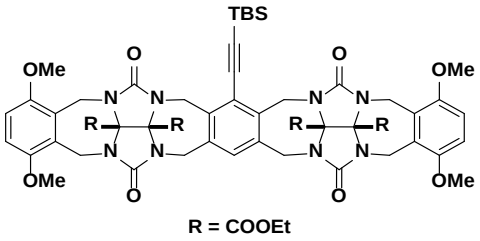

$C_{58}H_{68}N_8O_{16}Si$
MW: 1161.31 g/mol

Following a modified literature procedure,[10] compound **7** (1.52 g, 3.40 mmol, 2.0 equiv.) was dissolved in anhydrous DMSO (34 mL). After addition KO*t*Bu (839 mg, 7.48 mmol, 4.4 equiv.), the mixture was stirred for 15 min at room temperature. Then, compound **6** (1.00 g, 1.70 mmol, 1.0 equiv.) was added and the mixture was stirred for additional 16 h. The reaction mixture was poured into a mixture of 1 M HCl (10 mL) and water (10 mL) and was then extracted with CH_2Cl_2 (3 x 10 mL). The combined organic layers were washed with brine (10 mL), dried (Na_2SO_4), filtered and concentrated under reduced pressure. Purification *via* column chromatography (~50 g silica, CH_2Cl_2/MeCN = 3/1) gave product **8a** (863 mg, 743 µmol, 44%) as a off-white solid.

TLC R_f = 0.30 (CH_2Cl_2/MeCN = 3/1) [UV, $KMnO_4$].

IR (ATR): $\tilde{\nu}$ (cm^{-1}) = 2932 (w), 2854 (w), 1721 (s), 1445 (m), 1421 (m), 1365 (w), 1304 (w), 1248 (s), 1154 (m), 1076 (s), 1017 (m), 942 (m), 918 (m), 809 (m), 717 (m), 582 (w), 442 (w), 406 (w).

^{1}H NMR ($CDCl_3$, 300 K, 500 MHz) δ [ppm] = 7.17 (s, 1H), 6.76 (s, 4H), 5.27 (*virt.* dd, *J* = 15.8, 4.0 Hz, 4H), 5.20 (d, *J* = 15.6 Hz, 2H), 4.62 (d, *J* = 15.6 Hz, 2H), 4.54 (d, *J* = 15.0 Hz, 2H), 4.34 (d, *J* = 15.0 Hz, 2H), 4.21 (d, *J* = 15.9 Hz, 2H), 4.16 (d, *J* = 15.7 Hz, 2H), 4.10 (q, *J* = 7.2 Hz, 4H), 3.96 – 4.05 (m, 4H), 3.80 (s, 6H), 3.79 (s, 6H), 1.22 (t, *J* = 7.2 Hz, 6H), 1.18 (t, *J* = 7.2 Hz, 6H), 1.03 (s, 9H), 0.26 (s, 6H).

^{13}C NMR ($CDCl_3$, 300 K, 151 MHz) δ [ppm] = 166.3 (s), 166.1 (s), 156.7 (s), 156.2 (s), 151.5 (s), 151.3 (s), 138.1 (s), 135.6 (s), 131.8 (s), 126.8 (s), 126.6 (s), 124.5 (s), 112.7 (s), 112.5 (s), 105.4, 100.2 (s), 80.8 (s), 79.8 (s), 63.2 (s), 63.2 (s), 57.2 (s), 57.1 (s), 46.0 (s), 43.6 (s), 37.6 (s), 37.4 (s), 26.4 (s), 16.8 (s), 14.0 (s), 14.0 (s), −4.4 (s).

HRMS (ESI): $C_{58}H_{68}N_8O_{16}Si$ calculated: $[(M + Na)^+]$: 1183.4415

found: $[(M + Na)^+]$: 1183.4401.

Tweezer 8b

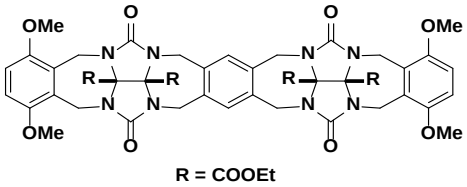

$C_{50}H_{54}N_8O_{16}$
MW: 1023.02 g/mol

Following a modified literature procedure,[10] compound **7** (897 mg, 2.00 mmol, 2.0 equiv.) was dissolved in anhydrous MeCN (20 mL). After addition KO*t*Bu (494 mg, 4.40 mmol, 4.4 equiv.), the mixture was stirred for 15 min at room temperature. Then, 1,2,4,5-tetrakis(bromomethyl)benzene (450 mg, 1.00 mmol, 1.0 equiv.) was added and the mixture was stirred for additional 6 h. The reaction was poured into a mixture of 1 M HCl (10 mL) and water (10 mL) and was then extracted with CH_2Cl_2 (3 x 10 mL). The combined organic layers were washed with brine (10 mL), dried (Na_2SO_4), filtered and concentrated under reduced pressure. Purification *via* column chromatography (60 g silica, CH_2Cl_2/MeCN = 3/1 → 2/1) gave product **8b** (288 mg, 282 µmol, 28%) as an off-white solid.

TLC R_f = 0.24 (CH_2Cl_2/MeCN = 3/1) [UV, $KMnO_4$].

^{1}H NMR ($CDCl_3$, 300 K, 500 MHz) δ [ppm] = 7.17 (s, 2H), 6.73 (s, 4H), 5.32 (d, *J* = 15.8 Hz, 4 H), 4.63 (d, *J* = 15.3 Hz, 4H), 4.34 (d, *J* = 15.3 Hz, 4H), 4.18 – 4.09 (m, 8H), 4.03 (q, *J* = 7.1 Hz, 4H), 3.78 (s, 12H), 1.23 (t, *J* = 7.1 Hz, 3H), 1.17 (t, *J* = 7.1 Hz, 3H).

^{13}C NMR ($CDCl_3$, 300 K, 151 MHz) δ [ppm] = 166.2 (s), 166.0 (s), 156.4 (s), 151.4 (s), 135.8 (s), 131.5 (s), 126.8 (s), 112.7 (s), 80.8 (s), 80.0 (s), 63.3 (s), 63.2 (s), 57.3 (s), 45.6 (s), 37.4 (s), 14.1 (s), 14.0 (s).

All analytical data match literature values.[10]

Tweezer 9

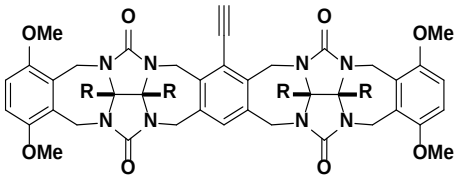

$C_{52}H_{54}N_8O_{16}$
MW: 1047.04 g/mol

Tweezer **8a** (200 mg, 172 µmol, 1.0 equiv.) was dissolved in anhydrous THF (17 mL). The reaction flask was cooled down to 0 °C and a 1 M solution of TBAF in THF (206 µL, 53.9 mg, 206 µmol, 1.2 equiv.) was added dropwise. The reaction was warmed up to room temperature and stirred for 2 h. The solvent was removed under reduced pressure and the resulting purple residue was purified *via* flash column chromatography (~7 g silica, CH_2Cl_2/acetone = 9/1) to give the desired product **9** (144 mg, 138 µmol, 80%) as a white solid.

TLC R_f = 0.12 (CH_2Cl_2/acetone = 9/1) [UV, $KMnO_4$].

IR (ATR): $\tilde{\nu}$ (cm^{-1}) = 3264 (w), 2922 (w), 2852 (w), 1721 (vs), 1595 (w), 1457 (s), 1442 (s), 1424 (s), 1365 (m), 1305 (m), 1252 (vs), 1198 (m), 1154 (m), 1079 (vs), 1015 (s), 941 (m), 918 (s), 805 (m), 717 (m) 646 (m), 582 (w), 482 (w).

^{1}H NMR ($CDCl_3$, 300 K, 500 MHz) δ [ppm] = 7.20 (s, 1H), 6.75 (s, 4H), 5.33 (*virt.* dd, *J* = 15.9, 4.6 Hz, 4H), 5.13 (d, *J* = 15.5 Hz, 2H), 4.65 (d, *J* = 15.5 Hz, 2H), 4.58 (d, *J* = 15.1 Hz, 2H), 4.36 (d, *J* = 15.0 Hz, 2H), 4.23 – 4.08 (m, 8H), 4.05 – 3.95 (m, 4H), 3.79 (s, 12H), 3.67 (s, 1H), 1.23 (t, *J* = 7.1 Hz, 6H), 1.17 (t, *J* = 7.2 Hz, 6H).

^{13}C NMR ($CDCl_3$, 300 K, 151 MHz) δ [ppm] = 166.2 (s), 166.0 (s), 156.6 (s), 156.3 (s), 151.4 (s), 151.3 (s), 138.3 (s), 135.8 (s), 132.1 (s), 126.8 (s), 126.7 (s), 123.7 (s), 112.5 (s), 112.5 (s), 88.5 (s), 80.9 (s), 79.7 (s), 78.5 (s), 63.3 (s), 63.2 (s), 57.2 (s), 46.0 (s), 43.5 (s), 37.5 (s), 37.4 (s), 14.0 (s), 14.0 (s).

HRMS (ESI): $C_{52}H_{54}N_8O_{16}$ calculated: $[(M + Na)^+]$: 1069.3550

found: $[(M + Na)^+]$: 1069.3547.

Tweezer 11

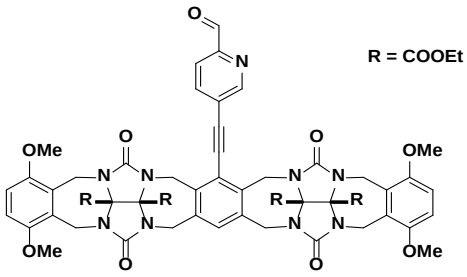

$C_{58}H_{57}N_9O_{17}$
MW: 1152.14 g/mol

In a flame-dried and argon flushed microwave tube, tweezer **9** (400 mg, 382 µmol, 1.0 equiv.), 5-bromopyridine-2-carbaldehyde (**10**) (85.3 mg, 458 µmol, 1.2 equiv.), $PdCl_2(PPh_3)_2$ (26.8 mg, 38.2 µmol, 0.1 equiv.), PPh_3 (20.0 mg, 76.4 µmol, 0.2 equiv.) and CuI (14.6 mg, 76.4 µmol, 0.2 equiv.) were dissolved in anhydrous and degassed THF (7.6 mL). The degassing of the solvent was achieved *via* sparging with Ar for 15 min. Then, NEt_3 (532 µL, 387 mg, 3.82 mol, 10 equiv.) was added and the reaction mixture was heated to 120 °C in the microwave for 90 min. Afterwards, the solvent was removed under reduced pressure and the residue was dissolved in CH_2Cl_2 (20 mL). 1 M HCl (10 mL) was added and the mixture was extracted with CH_2Cl_2 (3 × 10 mL). The combined organic layers were washed with brine (10 mL), dried (Na_2SO_4), filtered and concentrated under reduced pressure. Purification *via* column chromatography (~45 g silica, CH_2Cl_2/acetone = 14/1 → 9/1) gave product **11** (334 mg, 290 µmol, 76%) as a slightly green solid.

TLC R_f = 0.15 (CH_2Cl_2/acetone = 9/1) [UV, $KMnO_4$].

IR (ATR) $\tilde{\nu}$ (cm^{-1}) = 2981 (w), 2837 (w), 1719 (s), 1580 (w), 1447 (s), 1422 (s), 1365 (m), 1304 (w), 1252 (s), 1210 (w), 1153 (m), 1076 (m), 1016 (m), 981 (w), 942 (m), 916 (s), 848 (m), 801 (m), 772 (w), 745 (m), 718 (m), 663 (w), 582 (w), 520 (w), 475 (w), 414 (w).

^{1}H NMR ($CDCl_3$, 300 K, 500 MHz) δ [ppm] = 10.11 (d, *J* = 0.8 Hz, 1H), 9.04 (dd, *J* = 2.0, 0.9 Hz, 1H), 8.16 (ddd, *J* = 8.0, 2.0, 0.8 Hz, 1H), 7.97 (dd, *J* = 8.0, 0.9 Hz, 1H), 7.25 (s, 1H), 6.75 (s, 4H), 5.29 – 5.24 (m, 6H), 4.65 (*virt.* dd, *J* = 15.5, 4.2 Hz, 4H), 4.37 (d, *J* = 15.3 Hz, 2H), 4.22 (*virt.* dd, *J* = 15.8, 2.9 Hz, 4H), 4.11 (q, *J* = 7.1 Hz, 4H), 4.05 (p, *J* = 7.0 Hz, 4H), 3.79 (*virt.* d, *J* = 5.7 Hz, 12 H), 1.23 (t, *J* = 7.2 Hz, 6H), 1.19 (t, *J* = 7.1 Hz, 6H).

^{13}C NMR ($CDCl_3$, 300 K, 151 MHz) δ [ppm] = 193.0 (s), 166.2 (s), 166.0 (s), 156.5 (s), 156.4 (s), 152.8 (s), 151.5 (s), 151.4 (s), 140.0 (s), 138.2 (s), 136.4 (s), 132.4 (s), 126.6 (s), 126.6 (s), 124.3 (s), 123.5 (s), 121.1 (s), 112.7 (s), 112.6 (s), 95.7 (s), 91.2 (s), 80.8 (s), 79.8 (s), 63.4 (s), 63.4 (s), 57.2 (s), 57.2 (s), 45.9 (s), 43.6 (s), 37.6 (s), 37.5 (s), 14.0

HRMS (ESI): $C_{58}H_{57}N_9O_{17}$ calculated: $[(M + NH_4)^+]$: 1169.4311

found: $[(M + NH_4)^+]$: 1169.4232.

Tweezer S5

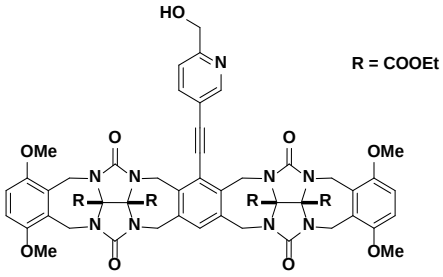

$C_{58}H_{59}N_9O_{17}$
MW: 1154.16 g/mol

Compound **11** (1.00 g, 870 µmol, 1.0 equiv.) was dissolved in a mixture of anhydrous MeOH and CH_2Cl_2 (1:1, 44 mL). Then, $NaCNBH_3$ (219 mg, 3.48 mmol, 4.0 equiv.) and trifluoroacetic acid (599 µL, 893 mg, 7.83 mmol, 9.0 equiv.) were added and the mixture was stirred for 4 h at room temperature. The reaction mixture was neutralized by addition of 4 M NaOH (8.7 mL) and was then extracted with CH_2Cl_2 (3 × 15 mL). The combined organic layers were washed with brine (15 mL), dried (Na_2SO_4), filtered and concentrated under reduced pressure to give the desired product **S5** (964 mg, 835 µmol, 96%) as an off-white solid. The material was subjected to the subsequent reaction without further purification.

TLC R_f = 0.22 (CH_2Cl_2/MeCN = 1/2) [UV, $KMnO_4$].

IR (ATR): $\tilde{\nu}$ (cm^{-1}) = 2941 (w), 2841 (w), 1721 (s), 1593 (w), 1451 (s), 1423 (s), 1367 (m), 1308 (m), 1252 (s), 1155 (m), 1075 (s), 1014 (s), 982 (m), 943 (m), 916 (s), 802 (m), 774 (w), 748 (w), 718 (m), 696 (w), 666 (m), 621 (w), 579 (w), 540 (m), 512 (w), 476 (w), 457 (w), 436 (w), 418 (w).

^{1}H NMR ($CDCl_3$, 300 K, 500 MHz) δ [ppm] = 8.84 (d, *J* = 2.0 Hz, 1H), 7.97 (dd, *J* = 8.0, 2.1 Hz, 1H), 7.26 (d, *J* = 8.2 Hz, 1H), 7.21 (s, 1H), 6.68 (s, 4H), 5.27 (*virt.* dd, *J* = 15.8, 8.2 Hz, 4H), 5.21 (d, *J* = 15.5 Hz, 2H), 4.79 (s, 2H), 4.66 (d, *J* = 15.5 Hz, 2H), 4.60 (d, *J* = 15.2 Hz, 2H), 4.37 (d, *J* = 15.1 Hz, 2H), 4.18 (*virt.* dd, *J* = 15.8, 8.3 Hz, 4H), 4.11 (q, *J* = 7.1 Hz, 4H), 4.07 – 3.99 (m, 4H), 3.78 (s, 6H), 3.76 (s, 6H), 1.22 (t, *J* = 7.1 Hz, 6H), 1.18 (t, *J* = 7.1 Hz, 6H).

^{13}C NMR ($CDCl_3$, 300 K, 151 MHz) δ [ppm] = 166.2 (s), 166.0 (s), 156.6 (s), 156.5 (s), 151.5 (s), 151.4 (s), 151.3 (s), 139.7 (s), 137.8 (s), 136.1 (s), 131.9 (s), 126.6 (s), 126.5 (s), 123.8 (s), 120.0 (s), 118.5 (s), 112.6 (s), 103.0 (s), 87.5 (s), 80.8 (s), 79.8 (s), 64.2 (s), 63.4 (s), 57.2 (s), 57.1 (s), 46.0 (s), 43.6 (s), 37.6 (s), 37.4 (s), 14.1 (s), 14.0 (s).

HRMS (ESI): $C_{58}H_{59}N_9O_{17}$ calculated: $[(M + H)^+]$: 1154.4102

found: $[(M + H)^+]$: .1154.4098.

Tweezer S6

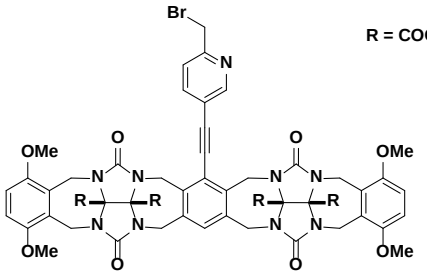

$C_{58}H_{58}BrN_9O_{16}$
MW 1217.05 g/mol

Compound **S5** (50.0 mg, 43.3 µmol, 1.0 equiv.) was dissolved in anhydrous CH_2Cl_2 (0.5 mL) and cooled to 0 °C. After dropwise addition of PBr_3 (4.48 µL, 12.9 mg, 47.6 µmol, 1.1 equiv.) and stirring for 1 h at 0 °C, the mixture was allowed to reach room temperature and stirred overnight. Next, CH_2Cl_2 (5 mL) and saturated aqueous $NaHCO_3$ solution (5 mL) were added, the two layers were separated, and the aqueous layer extracted with CH_2Cl_2 (3 x 5 mL). The combined organic layers were washed with brine (5 mL), dried (Na_2SO_4), filtered and the solvent removed under reduced pressure. The crude material was then purified *via* column chromatography (~5 g silica, CH_2Cl_2/acetone = 9/1) to give product **S6** (39.7 mg, 32.6 µmol, 75%) as a pink-colored solid.

TLC R_f = 0.13 (CH_2Cl_2/acetone = 9/1) [UV, $KMnO_4$].

IR (ATR) = $\tilde{\nu}$ (cm^{-1}) = 2930 (w), 2909 (w), 2841 (w), 1720 (s), 1593 (w), 1449 (s), 1423 (s), 1366 (m), 1307 (w), 1252 (s), 1153 (m), 1075 (m), 1015 (m), 980 (m), 942 (m), 916 (m), 848 (w), 802 (m), 773 (w), 748 (w), 718 (m), 664 (m), 612 (w), 581 (w).

^{1}H NMR ($CDCl_3$, 300 K, 500 MHz) δ [ppm] = 8.84 (d, *J* = 1.5 Hz, 1H), 7.99 (dd, *J* = 8.0, 2.1 Hz, 1H), 7.45 (d, *J* = 8.0 Hz, 1H), 7.22 (s, 1H), 6.75 (s, 4H), 5.27 (*virt.* dd, *J* = 15.8, 8.4 Hz, 4H), 5.23 (d, *J* = 15.3 Hz, 2H), 4.64 (*virt.* dd, *J* = 15.4, 8.6 Hz, 4H), 4.58 (s, 2H), 4.37 (d, *J* = 15.2 Hz, 2H), 4.21 (*virt.* dd, *J* = 15.8, 7.2 Hz, 4H), 4.11 (q, *J* = 7.1 Hz, 4H), 4.08 – 4.00 (m, 4H), 3.80 (s, 6H), 3.79 (s, 6H), 1.23 (t, *J* = 7.1 Hz, 6H), 1.19 (t, *J* = 7.1 Hz, 6H).

^{13}C NMR ($CDCl_3$, 300 K, 151 MHz) δ [ppm] = 166.2 (s), 165.9 (s), 156.5 (s), 156.3 (s), 151.9 (s), 151.2 (s), 151.1 (s), 140.2 (s), 137.8 (s), 136.1 (s), 132.0 (s), 126.4 (s), 126.3 (s), 123.8 (s), 119.2 (s), 112.3 (s), 112.3 (s), 96.0 (s), 88.5 (s), 80.8 (s), 79.7 (s), 63.3 (s), 57.0 (s), 56.9 (s), 45.8 (s), 43.5 (s), 37.5 (s), 37.3 (s), 33.3 (s), 14.0 (s), 14.0 (s).

HRMS (ESI): $C_{58}H_{58}BrN_9O_{16}$ calculated: $[(M + Na)^+]$: 1238.3077

found: $[(M + Na)^+]$: 1238.3062.

(2*S*,2'*S*)-1-(pyridin-2-ylmethyl)-2,2'-bipyrrolidine (12)

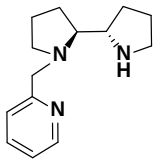

$C_{14}H_{21}N_3$
MW: 231.34 g/mol

(2*S*,2'*S*)-Bipyrrolidine (140 mg, 1.00 mmol, 1.05 equiv.) was dissolved in anhydrous MeOH (3 mL). Then, a solution of pyridine-2-carboxaldehyde (102 mg, 950 µmol, 1.0 equiv.) in MeOH (2 mL) was added dropwise and the mixture was stirred at room temperature for 16 h. After that, $NaCNBH_3$ (239 mg, 3.80 mmol, 4.0 equiv.) and trifluoroacetic acid (633 µL, 975 mg, 8.55 mmol, 9.0 equiv.) were added and the mixture was stirred for additional 3 h. The reaction mixture was neutralized by addition of 4 M NaOH (10 mL) and was then extracted with CH_2Cl_2 (3 × 15 mL). The combined organic layers were washed with brine (15 mL), dried (Na_2SO_4), filtered and concentrated under reduced pressure. The crude material was purified *via* column chromatography (10 g silica, CH_2Cl_2/MeOH/NH_4OH = 94/5/1) to give the desired product **12** (204 mg, 882 µmol, 93%) as a yellowish oil.

^{1}H NMR ($CDCl_3$, 300 K, 500 MHz) δ [ppm] = 8.54 – 8.50 (m, 1H), 7.63 (tdd, *J* = 7.7, 3.6, 1.8 Hz, 1H), 7.40 (d, *J* = 7.9 Hz, 1H), 7.16 – 7.11 (m, 1H), 4.30 (d, *J* = 14.3 Hz, 1H), 3.64 (dd, *J* = 14.3, 4.3 Hz, 1H), 3.08 (qd, *J* = 7.5, 5.1 Hz, 1H), 3.02 – 2.95 (m, 2H), 2.91 – 2.83 (m, 1H), 2.80 – 2.71 (m, 1H), 2.43 – 2.34 (m, 1H), 1.93 (dddd, *J* = 16.5, 12.1, 8.4, 3.5 Hz, 1H), 1.85 – 1.77 (m, 1H), 1.78 – 1.68 (m, 4H), 1.60 – 1.52 (m, 1H), 1.41 (dqd, *J* = 11.9, 8.1, 3.9 Hz, 1H).

^{13}C NMR ($CDCl_3$, 300 K, 126 MHz) δ [ppm] = 160.6 (s), 149.2 (s), 136.6 (s), 122.9 (s), 121.9 (s), 68.1 (s), 64.0 (s), 62.7 (s), 55.2 (s), 46.5 (s), 28.5 (s), 28.4 (s), 25.0 (s), 24.1 (s).

The spectroscopic data matched those reported in the literature.[11]

Tweezer 13

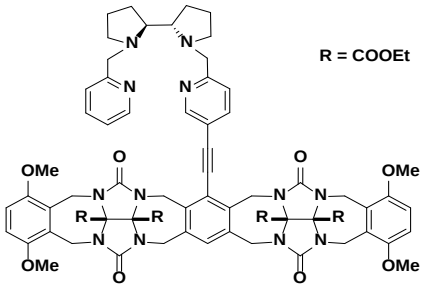

$C_{72}H_{78}N_{12}O_{16}$
MW 1367.48 g/mol

Tweezer **S6** (184 mg, 151 µmol, 1.0 equiv.) and **12** (34.9 mg, 151 µmol, 1.0 equiv.) were dissolved in anhydrous MeCN (7.5 mL). Then, K_2CO_3 (83.5 mg, 604 mmol, 4.0 equiv.) and TBAB (2.43 mg, 7.55 µmol, 0.05 equiv.) were added and the reaction mixture was stirred at reflux for 16 h. After that, the mixture was cooled down to room temperature, filtered and the residue was washed with CH_2Cl_2 (5 mL). The filtrate was concentrated under reduced pressure, 1 M NaOH (4 mL) was added and the mixture was extracted with CH_2Cl_2 (3 ×5 mL). The combined organic layers were washed with brine (5 mL), dried (Na_2SO_4), filtered and concentrated by rotatory evaporation to give compound **13** (200 mg, 146 µmol, 97%) as a slightly yellow product.

TLC R_f = 0.28 (CH_2Cl_2/MeOH/NH_4OH = 94/5/1) [UV, $KMnO_4$].

IR (ATR): $\tilde{\nu}$ (cm^{-1}) = 2939 (w), 2834 (w), 1722 (s), 1590 (w), 1483 (m), 1455 (m), 1365 (m), 1303 (w), 1253 (s), 1152 (m), 1077 (m), 1017 (m), 981 (w), 941 (w), 917 (m), 854 (w), 801 (m), 751 (m), 718 (m), 657 (w), 514 (w), 469 (w), 455 (w), 446 (w), 430 (w).

^{1}H NMR ($CDCl_3$, 300 K, 500 MHz) δ [ppm] = 8.73 (d, *J* = 2.2 Hz, 1H), 8.52 (d, *J* = 6.0 Hz, 1H), 7.87 (dd, *J* = 8.0, 2.2 Hz, 1H), 7.62 (td, *J* = 7.6, 1.9 Hz, 1H), 7.41 (*virt.* dd, *J* = 10.1, 7.8 Hz, 2H), 7.19 (s, 1H), 7.13 (dd, *J* = 7.5, 5.0 Hz, 1H), 6.65 (s, 4H), 5.28 (*virt.* dd, *J* = 15.8, 8.9 Hz, 4H), 5.17 (d, *J* = 15.5 Hz, 2H), 4.65 (d, *J* = 15.4 Hz, 2H), 4.57 (d, *J* = 15.1 Hz, 2H), 4.36 (d, *J* = 15.1 Hz, 2H), 4.27 – 4.08 (m, 10H), 4.01 (p, *J* = 7.2 Hz, 4H), 3.77 (s, 6H), 3.75 (s, 6H), 3.55 (dd, *J* = 14.5, 8.1 Hz, 2H), 3.06 – 2.97 (m, 2H), 2.88 – 2.78 (m, 2H), 2.27 (*virt.* dp, *J* = 25.2, 8.3, 7.8 Hz, 2H), 1.90 – 1.67 (m, 8H), 1.22 (t, *J* = 7.1 Hz, 6H), 1.17 (t, *J* = 7.1 Hz, 6H).

^{13}C NMR ($CDCl_3$, 300 K, 151 MHz) δ [ppm] = 166.2 (s), 166.0 (s), 160.8 (s), 160.5 (s), 156.6 (s), 156.3 (s), 151.4 (s), 151.3 (s), 151.2 (s), 149.0 (s), 139.4 (s), 137.6 (s), 137.6 (s), 136.5 (s), 135.9 (s), 135.9 (s), 131.8 (s), 126.5 (s), 126.4 (s), 124.3 (s), 122.8 (s), 122.1 (s), 121.8 (s), 117.5 (s), 112.3 (s), 97.1 (s), 87.0 (s), 80.8 (s), 79.7 (s), 65.6 (s), 65.6 (s), 63.3 (s), 63.3 (s), 61.4 (s), 61.1 (s), 57.0 (s), 57.0 (s), 55.5 (s), 55.4 (s), 46.0 (s), 43.6 (s), 37.5 (s), 37.3 (s), 26.2 (s), 26.2 (s), 23.8 (s), 23.8 (s), 14.0 (s), 14.0 (s).

HRMS (ESI): $C_{72}H_{78}N_{12}O_{16}$ calculated: $[(M + H)^+]$: 1367.5732

found: [(M + H)$^+$]: 1367.5745.

(2*S*,2'S)-1-((5-Bromopyridin-2-yl)methyl)-2,2'-bipyrrolidine (S7)

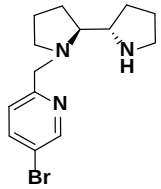

$C_{14}H_{20}BrN_3$
MW: 310.24 g/mol

(2*S*,2'*S*)-Bipyrrolidine (139 mg, 990 µmol, 1.1 equiv.) was dissolved in anhydrous MeOH (3 mL). Then, a solution of compound **10** (167 mg, 900 µmol, 1.0 equiv.) in MeOH (2 mL) was added dropwise and the solution was stirred at room temperature for 16 h. After that, $NaCNBH_3$ (249 mg, 3.96 mmol, 4.4 equiv.) and trifluoroacetic acid (689 µL, 1.03 g, 9.00 mmol, 10.0 equiv.) were added and the mixture was stirred for additional 3 h. Then, the reaction mixture was neutralized by addition of 4 M NaOH (10 mL) and extracted with CH_2Cl_2 (3 × 15 mL). The combined organic layers were washed with brine (15 mL), dried (Na_2SO_4), filtered and concentrated under reduced pressure to give the desired product **S7** (271 mg, 874 µmol, 97%) as a yellowish oil, which was subjected to the subsequent reaction without further purification.

IR (ATR): $\tilde{\nu}$ (cm^{-1}) = 3307 (br w), 2956 (m), 2868 (m), 2806 (m), 1573 (m), 1556 (m), 1464 (s), 1364 (s), 1276 (w), 1206 (w), 1088 (s), 1005 (s), 921 (w), 824 (m), 719 (w), 626 (m), 477 (m), 409 (m).

^{1}H NMR ($CDCl_3$, 500 MHz, 300 K) δ [ppm] = 8.58 (dd, *J* = 2.4, 0.7 Hz, 1H), 7.76 (dd, *J* = 8.3, 2.4 Hz, 1H), 7.34 (d, *J* = 8.3 Hz, 1H), 4.29 (d, *J* = 14.6 Hz, 1H), 3.60 (d, *J* = 14.6 Hz, 1H), 3.07 (q, *J* = 7.8 Hz, 1H), 2.94 – 3.02 (m, 2H), 2.81 – 2.92 (m, 1H), 2.73 (td, *J* = 7.8, 5.3 Hz, 1H), 2.35 (dt, *J* = 9.7, 7.9 Hz, 1H), 1.89 – 2.00 (m, 1H), 1.78 – 1.85 (m, 1H), 1.69 – 1.79 (m, 4H), 1.54 – 1.63 (m, 1H), 1.36 – 1.47 (m, 1H).

^{13}C NMR ($CDCl_3$, 300 K, 126 MHz) δ [ppm] = 159.4 (s), 150.2 (s), 139.1 (s), 124.2 (s), 118.7 (s), 68.3 (s), 64.2 (s), 62.0 (s), 55.2 (s), 46.7 (s), 28.5 (s), 24.1 (s).

HRMS (ESI): $C_{14}H_{20}BrN_3$ calculated: [(M + H)$^+$]: 310.0913

found: [(M + H)$^+$]: 310.0914.

(2*S*,2'*S*)-1-((5-Bromopyridin-2-yl)methyl)-1'-(pyridin-2-ylmethyl)-2,2'-bipyrrolidine (14)

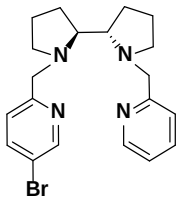

$C_{20}H_{25}BrN_4$
MW: 401.35 g/mol

Compound **S7** (754 mg, 2.43 mmol, 1.0 equiv.) and 2-(bromomethyl)pyridine hydrobromide (675 mg, 2.67 mmol, 1.1 equiv.) were dissolved in anhydrous MeCN (120 mL). Then, K_2CO_3 (1.34 g, 9.72 mmol, 4.0 equiv.) and TBAB (39.2 mg, 122 µmol, 0.05 equiv.) were added and the reaction was stirred at reflux for 16 h. After that, the mixture was cooled to room temperature, filtered, and the residue was washed with CH_2Cl_2. The filtrate was concentrated by rotatory evaporation, then, 1 M NaOH (20 mL) was added and the mixture was extracted with CH_2Cl_2 (2 ×50 mL). The combined organic layers were washed with brine (50 mL), dried (Na_2SO_4), filtered and concentrated under reduced pressure. To the resulting brownish residue *n*-hexane (30 mL) was added and the mixture was stirred for 16 h. Filtration and concentration of the filtrate resulted in a brown oil, which was purified *via* column chromatography (~100 g silica, CH_2Cl_2/MeOH/NH_4OH = 94/5/1) to give compound **14** (695 mg, 1.73 mmol, 71%) as a yellow oil.

TLC R_f = 0.38 (CH_2Cl_2/MeOH/NH_4OH = 95/5/1) [UV, $KMnO_4$].

IR (ATR): $\tilde{\nu}$ (cm^{-1}) = 3047 (w), 2960 (m), 2872 (m), 2797 (m), 1686, 1588 (s), 1570 (s), 1465 (s), 1432 (s), 1366 (m), 1206 (m), 1116 (s), 1087 (s), 1046 (m), 1005 (vs), 926 (m), 826 (m) 755 (s), 622 (m) 477 (m), 404 (s).

^{1}H NMR ($CDCl_3$, 500 MHz, 300 K) δ [ppm] = 8.53 (d, *J* = 2.4 Hz, 1H), 8.49 (dt, *J* = 4.8, 1.3 Hz, 1H), 7.69 (dd, *J* = 8.3, 2.4 Hz, 1H), 7.58 (td, *J* = 7.7, 1.8 Hz, 1H), 7.37 (d, *J* = 7.8 Hz, 1H), 7.30 (d, *J* = 8.3 Hz, 1H), 7.10 (ddd, *J* = 6.4, 4.9, 1.2 Hz, 1H), 4.17 (*virt.* dd, *J* = 16.1, 14.6 Hz, 2H), 3.49 (*virt.* dd, *J* = 31.9, 14.6 Hz, 2H), 2.98 (*virt.* dddd, *J* = 18.6, 9.2, 5.4, 3.8 Hz, 2H), 2.82 – 2.73 (m, 2H), 2.29 – 2.16 (m, 2H), 1.87 – 1.65 (m, 8H).

^{13}C NMR ($CDCl_3$, 126 MHz, 300 K) δ [ppm] = 160.5 (s), 159.4 (s), 149.9 (s), 149.0 (s), 139.0 (s), 136.4 (s), 124.1 (s), 122.8 (s), 121.8 (s), 118.6 (s), 65.8 (s), 65.8 (s), 61.4 (s), 60.7 (s), 55.5 (s), 55.4 (s), 26.4 (s), 26.3 (s), 23.8 (s).

HRMS (ESI): $C_{20}H_{25}BrN_4$ calculated: $[(M + H)^+]$: 401.1335

found: $[(M + H)^+]$: 401.1343.

Catalyst 2

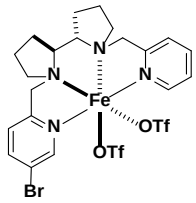

$C_{22}H_{25}BrF_6FeN_4O_6S_2$
MW: 755.32 g/mol

Following a modified literature procedure,[12] ligand **14** (20.1 mg, 50.0 µmol, 1.0 equiv.) and $Fe(OTf)_2(MeCN)_2$ (21.8 mg, 50.0 µmol, 1.0 equiv.) were dissolved in anhydrous MeCN (0.2 mL) in a glove box and stirred at room temperature for 2.5 h. Subsequently, anhydrous diethyl ether (4 mL) was added which resulted in precipitation of a yellow solid. The supernatant was removed and the solid was washed two times with diethyl ether (2x2 mL). The residue was dried under reduced pressure for 1 h to give the desired ligand **2** (22.0 mg, 29.1 µmol, 58%) as a yellow solid.

IR (ATR): $\tilde{\nu}$ (cm^{-1}) = 2970 (w), 1723 (w), 1608 (w), 1548 (w) 1445 (w), 1355 (m), 1303 (m), 1214 (m), 1098 (w), 1026 (s), 944 (w), 915 (w), 897 (w), 858 (w)825 (w), 770 (m), 762 (m), 633 (s), 571 (w), 511 (m), 453 (w), 417 (m).

^{1}H NMR (CD_3CN, 233 K, 500 MHz) δ [ppm] = 9.41 (s, 1H), 9.33 (s, 1H), 8.02 (d, *J* = 8.4 Hz, 1H), 7.84 (t, *J* = 7.6 Hz, 1H), 7.80 – 7.71 (m, 2H), 7.67 (s, 1H), 5.20 (br s, 2H), 4.08 (d, *J* = 15.5 Hz, 1H), 3.99 (d, *J* = 15.9 Hz, 1H), 3.10 – 2.91 (m, 1H), 2.86 – 2.76 (m, 1H), 2.72 – 2.56 (m, 3H), 2.37 (br s, 3H), 2.15 – 1.85 (m, 4H), 1.46 (br s, 2H).

^{13}C NMR (CD_3CN, 233 K, 126 MHz) δ [ppm] = 162.5 (s), 161.6 (s), 157.4 (s), 157.3 (s), 140.9 (s), 138.5 (s), 126.9 (s), 125.5 (s), 124.1 (s), 71.4 (s), 71.4 (s), 62.4 (s), 61.7 (s), 54.7 (s), 54.6 (s), 26.1 (s), 26.0 (s), 25.0 (s), 24.8 (s).

HRMS (ESI): $C_{22}H_{25}BrF_6FeN_4O_6S_2$ calculated: $[(M - 2OTf + 2CH_3O)^+]$: 518.0974

found: $[(M - 2OTf + 2CH_3O)^+]$: 518.0983

Catalyst 4

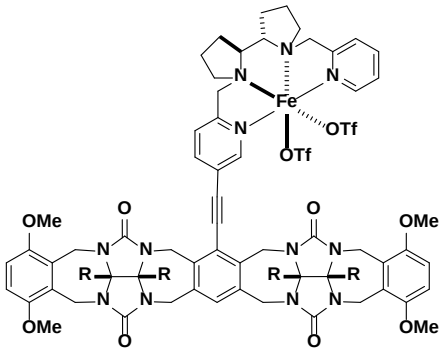

R = COOEt

$C_{74}H_{78}F_6FeN_{12}O_{22}S_2$
MW: 1721.46 g/mol

Following a modified literature procedure,[12] ligand **13** (50.0 mg, 36.6 µmol, 1.0 equiv.) and $Fe(OTf)_2(MeCN)_2$ (16.0 mg, 36.6 µmol, 1.0 equiv.) were dissolved in anhydrous MeCN (0.2 mL) in a glove box and stirred at room temperature for 2.5 h. Subsequently, anhydrous diethyl ether (4 mL) was added which resulted in precipitation of a yellow solid out of the solution. The supernatant was removed and the solid was washed two times with diethyl ether (2x2 mL) and dried under reduced pressure for 1 h resulting in the desired complex **4** (36.1 mg, 21.0 µmol, 57%) as a yellow solid.

IR (ATR): $\tilde{\nu}$ (cm^{-1}) = 2988 (w), 1722 (m), 1608 (w), 1460 (m), 1428 (m), 1367 (w), 1256 (s), 1157 (m), 1079 (m), 1028 (s), 983 (w), 941 (m), 919 (m), 850 (w), 803 (w), 761 (w), 719 (w), 637 (s), 575 (w), 516 (m), 484 (w), 471 (w), 435 (w), 416 (w).

^{1}H NMR (CD_3CN, 233 K, 500 MHz) δ [ppm] = 9.54 (s, 1H), 9.29 (s, 1H), 8.15 (d, *J* = 8.1 Hz, 1H), 7.90 (t, *J* = 7.8 Hz, 1H), 7.69 (d, *J* = 9.5 Hz, 1H), 7.14 (s, 1H), 6.95 – 6.79 (m, 4H), 5.66 (d, *J* = 16.6 Hz, 1H), 5.60 (d, *J* = 16.6 Hz, 1H), 5.36 – 5.24 (m, 3H), 5.20 (d, *J* = 16.3 Hz, 1H), 4.85 (s, 2H), 4.59 (*virt.* dd, *J* = 16.6, 5.0 Hz, 2H), 4.38 – 4.15 (m, 12H), 4.14 – 3.90 (m, 6H), 3.74 (s, 6H), 3.70 (s, 3H), 3.68 (s, 3H), 3.13 (s, 1H), 2.93 (s, 1H), 2.68 (s, 2H), 2.61 – 2.28 (m, 6H), 2.20 – 1.99 (m, 4H),1.39 (s, 2H), 1.25 (*virt.* tt, *J* = 13.9, 7.1 Hz, 12H).

^{13}C NMR (CD_3CN, 233 K, 126 MHz) δ [ppm] = 165.0, 162.1, 161.9, 158.3, 156.5, 155.0, 154.8, 149.4, 138.9, 138.3, 137.6, 137.0, 130.1, 126.0, 125.8, 125.6, 125.4, 122.7, 121.2, 110.2, 93.1, 88.5, 79.6, 79.3, 71.0, 63.7, 63.5, 62.0, 55.5, 55.3, 55.1, 54.6, 54.1, 44.0, 41.9, 41.7, 35.7, 23.7, 12.7.

HRMS (ESI): $C_{74}H_{78}F_6FeN_{12}O_{22}S_2$ calculated: $[(M - 2OTf + CH_3O)^{2+}]$: 726.7591

found: $[(M - 2OTf + CH_3O)^{2+}]$: 726.7591.

2.2.Substrate Synthesis

N,*N*-Dimethyl-decylamine (S8)

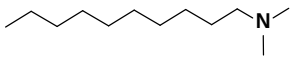

$C_{12}H_{27}N$
MW: 185.36 g/mol

Decylamine (157 mg, 1.00 mmol, 1.0 equiv.) was dissolved in a mixture of water (3 mL) and MeOH (1 mL). Aq. HCHO (36%, 1.15 mL, 15.0 mmol, 15 equiv.) and HCOOH (528 µL, 644 mg, 14.0 mmol, 14 equiv.) were added and the reaction was stirred at reflux overnight. After cooling to room temperature, 6 M KOH was added until pH ~ 12 was reached. The mixture was extracted with CH_2Cl_2 (3 x 10 mL), and the combined organic layers were washed with brine, dried (Na_2SO_4) and concentrated under reduced pressure. The crude material was purified *via* column chromatography (10 g silica, CH_2Cl_2/MeOH/NH_4OH = 96.5/2.5/1.0) to give compound **S8** (139 mg, 750 µmol, 75%) as a white solid.

TLC R_f = 0.25 (CH_2Cl_2/MeOH/NH_4OH = 96.5/2.5/1.0) [$KMnO_4$].

^{1}H NMR ($CDCl_3$, 233 K, 500 MHz) δ [ppm] = 2.25 – 2.21 (m, 2H), 2.21 (s, 6H), 1.44 (p, *J* = 7.1 Hz, 2H), 1.34 – 1.20 (m, 14H), 0.88 (t, *J* = 6.9 Hz, 3H).

^{13}C NMR($CDCl_3$, 300 K, 126 MHz) δ [ppm] = 60.1 (s), 45.7 (s), 32.1 (s), 29.8 (s), 29.5 (s), 28.0 (s), 27.7 (s), 22.8 (s), 14.2 (s).

The spectroscopic data matched those reported in the literature.[13]

N-Decyl-formamide (S9)

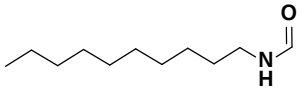

$C_{11}H_{23}NO$
MW: 185.31 g/mol

Decylamine (787 mg, 5.00 mmol, 1.0 equiv.) was dissolved in ethyl formate (15 mL) and stirred at 50 °C overnight. After cooling to room temperature, CH_2Cl_2 (20 mL) was added and the mixture was washed with 2 M H_2SO_4 (3 x 15 mL), water (15 mL) and brine (10 mL). The organic layer was dried ($MgSO_4$), filtered and concentrated under reduced pressure. The crude material was purified *via* column chromatography (20 g SiO_2, CyHex/EtOAc = 1/1) to give compound **S9** (810 mg, 4.37 mmol, 87%) as a white solid.

TLC R_f = 0.21 (CyHex/EtOAc = 1/1) [$KMnO_4$].

^{1}H NMR ($CDCl_3$, 233 K, 500 MHz) δ [ppm] = 8.16 (s, 1H), 5.52 (s, 1H), 3.40 – 3.22 (m, 2H), 1.55 – 1.49 (m, 2H), 1.34 – 1.21 (m, 14H), 0.94 – 0.82 (m, 3H).

^{13}C NMR ($CDCl_3$, 300 K, 126 MHz) δ [ppm] = 161.1 (s), 38.2 (s), 31.9 (s), 29.5 (s), 29.5 (s), 29.3 (s), 29.2 (s), 26.8 (s), 22.7 (s), 14.1 (s).

The spectroscopic data matched those reported in the literature.[14]

N-Methyldecylamine (S10)

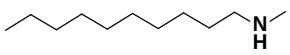

$C_{11}H_{25}N$
MW: 171.33 g/mol

$LiAlH_4$ (94.1 mg, 2.48 mmol, 1.55 equiv.) was put in a flame dried and argon flushed two-neck round-bottom flask and suspended in dry THF (7 mL). After cooling to 0 °C, *N*-decyl formamide (**S9**, 296 mg, 1.60 mmol, 1.0 equiv.) in dry THF (3.5 mL) was added dropwise over 10 min. The mixture was warmed up to room temperature and slowly heated to 80 °C for 2 h. The reaction was stirred at reflux for additional 16 h, and was then cooled to 0 °C, diluted with THF (7 mL) and neutralized by addition of 6 M KOH until a transparent solution formed with a white-grey precipitate. Subsequently, water (1 mL) and celite (1.5 g) were added. The mixture was filtered and the filtrate dried ($MgSO_4$). After filtration and removal of the solvent under reduced pressure, the yellowish oil was purified by column chromatography (~5 g SiO_2, CH_2Cl_2/MeOH/NH_4OH = 96.5/2.5/1.0) to give compound **S10** (141 mg, 823 µmol, 51%) as a yellowish oil.

TLC R_f = 0.11 (CH_2Cl_2/MeOH/NH_4OH = 96.5/2.5/1.0) [$KMnO_4$].

^{1}H NMR ($CDCl_3$, 233 K, 500 MHz) δ [ppm] = 2.57 (t, *J* = 7.2 Hz, 2H), 2.43 (s, 3H), 1.48 (t, *J* = 7.1 Hz, 2H), 1.35 – 1.20 (m, 15H), 0.88 (t, *J* = 6.9 Hz, 3 H).

^{13}C NMR ($CDCl_3$, 300 K, 126 MHz) δ [ppm] = 52.3 (s), 36.6 (s), 32.0 (s), 29.9 (s), 29.8 (s), 29.7 (s), 29.5 (s), 27.5 (s), 22.8 (s), 14.2 (s).

The spectroscopic data matched those reported in the literature.[15]

General procedure for protonation of amines:

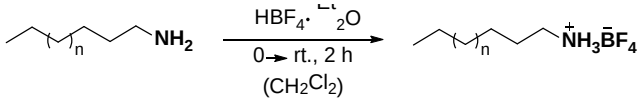

According to a literature-known procedure,[12] the free amine (1.0 equiv.) was dissolved in dry CH_2Cl_2 (~ 0.5 M) and stirred at 0 °C. Tetrafluoroboric acid diethyl ether complex (1.1 equiv.) was added dropwise leading to participation of a white solid. After stirring the mixture for 2 h at room temperature, the solvent was removed by rotatory evaporation. The residual solid was suspended in diethyl ether and stirred vigorously for a few minutes. Then the supernatant solution was removed, and the washing step was repeated two times. The final white solid was dried in *vacuo*.

Heptylammonium tetrafluoroborate (S11)

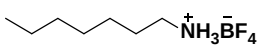

$C_7H_{18}BF_4N$
MW: 203.03 g/mol

According to the general procedure for protonation of amines, **S11** (811 mg, 3.99 mmol, 80%) was obtained from heptylamine (743 µL, 576 mg, 5.00 mmol, 1.0 equiv.) as a white solid.

^{1}H NMR (CD_3CN, 300 K, 500 MHz) δ [ppm] = 0.90 (*virt.* td, *J* = 7.0, 1.7 Hz, 3H), 1.14 – 1.38 (m, 6H), 1.61 (*virt.* t, *J* = 7.5 Hz, 2H), 2.89 – 3.14 (m, 2H), 5.93 – 6.51 (m, 3H).

^{13}C NMR (CD_3CN, 300 K, 126 MHz) δ [ppm] = 14.1 (s), 23.0 (s), 26.4 (s), 27.4 (s), 31.7 (s), 41.3 (s).

The spectroscopic data matched those reported in the literature.[12]

Octylammonium tetrafluoroborate (S12)

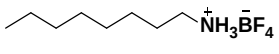

$C_8H_{20}BF_4N$
MW: 217.06 g/mol

According to the general procedure for protonation of amines, **S12** (927 mg, 4.27 mmol, 85%) was obtained from octylamine (826 µL, 646 mg, 5.00 mmol, 1.0 equiv.) as a white solid.

^{1}H NMR (CD_3CN, 300 K, 500 MHz) δ [ppm] = 0.89 (t, *J* = 6.6 Hz, 3H), 1.25 – 1.41 (m, 10H), 1.61 (t, *J* = 7.4 Hz, 2H), 2.94 (*virt.* dd, *J* = 8.7, 6.7 Hz, 2H), 6.13 (s, 3H).

^{13}C NMR (CD_3CN, 300 K, 126 MHz) δ [ppm] = 14.3 (s), 14.3 (s), 23.2 (s), 26.7 (s), 27.5, 29.5 (s), 29.5 (s), 29.6 (s), 32.3 (s), 41.3 (s).

The spectroscopic data matched those reported in the literature.[12]

Nonylammonium tetrafluoroborate (S13)

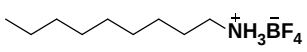

$C_9H_{22}BF_4N$
MW: 231.09 g/mol

According to the general procedure for protonation of amines, **S13** (1.04 g, 4.50 mmol, 90%) was obtained from nonylamine (908 µL, 716 mg, 5.00 mmol, 1.0 equiv.) as a white solid.

^{1}H NMR (CD_3CN, 300 K, 500 MHz) δ [ppm] = 0.89 (t, *J* = 6.7 Hz, 3H), 1.44 – 1.19 (m, 12H), 1.61 (t, *J* = 7.4 Hz, 2H), 2.87 – 3.00 (m, 2H), 5.87 – 6.34 (m, 3H).

^{13}C NMR (CD_3CN, 300 K, 126 MHz) δ [ppm] = 14.3 (s), 23.3 (s), 26.7 (s), 27.5 (s), 29.5 (s), 29.8 (s), 29.9 (s), 32.5 (s), 41.3 (s).

The spectroscopic data matched those reported in the literature.[12]

Decylammonium tetrafluoroborate (S14)

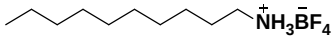

$C_{10}H_{24}BF_4N$
MW: 245.11 g/mol

According to the general procedure for protonation of amines, **S14** (86.4 mg, 352 µmol, 70%) was obtained from decylamine (99.9 µL, 78.7 mg, 500 µmol, 1.0 equiv.) as a white solid.

^{1}H NMR (CD_3CN, 300 K, 500 MHz) δ [ppm] = 0.76 – 1.00 (m, 3H), 1.15 – 1.42 (m, 14H), 1.60 (p, *J* = 7.3 Hz, 2H), 2.87 – 3.01 (m, 2H), 5.84 – 6.40 (m, 3H).

^{13}C NMR (CD_3CN, 300 K, 126 MHz) δ [ppm] = 14.3 (s), 23.3 (s), 26.7 (s), 27.5 (s), 29.5 (s), 29.9 (s), 30.0 (s), 30.1 (s), 32.5 (s), 41.3 (s).

The spectroscopic data matched those reported in the literature.[12]

Undecylammonium tetrafluoroborate (S15)

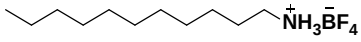

$C_{11}H_{26}BF_4N$
MW: 259.14 g/mol

According to the general procedure for protonation of amines, **S15** (1.14 g, 4.40 mmol, 88%) was obtained from undecylamine (1.08 mL, 857 mg, 5.00 mmol, 1.0 equiv.) as a white solid.

^{1}H NMR (CD_3CN, 300 K, 500 MHz) δ [ppm] = 0.88 (t, *J* = 6.7 Hz, 3H), 1.21 – 1.54 (m, 16H), 1.60 (q, *J* = 7.4 Hz, 2H), 2.94 (q, *J* = 6.8 Hz, 2H), 5.89 – 6.40 (m, 3H).

^{13}C NMR (CD_3CN, 300 K, 126 MHz) δ [ppm] = 14.3 (s), 23.3 (s), 26.7 (s), 27.5 (s), 29.5 (s), 30.0 (s), 30.0 (s), 30.2 (s), 30.2 (s), 32.6 (s), 41.3 (s).

The spectroscopic data matched those reported in the literature.[12]

Dodecylammonium tetrafluoroborate (S16)

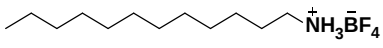

$C_{12}H_{28}BF_4N$
MW: 273.17 g/mol

According to the general procedure for protonation of amines, **S16** (93.8 mg, 343 µmol, 69%) was obtained from dodecylamine (92.7 mg, 500 µmol, 1.0 equiv.) as a white solid.

^{1}H NMR (CD_3CN, 300 K, 500 MHz) δ [ppm] = 0.81 – 0.93 (m, 3H), 1.28 (m, 18H), 1.59 (p, *J* = 7.4 Hz, 2H), 2.83 – 3.20 (m, 2H), 5.76 – 6.55 (m, 3H).

^{13}C NMR (CD_3CN, 300 K, 126 MHz) δ [ppm] = 14.3 (s), 23.3 (s), 26.7 (s), 27.5 (s), 29.6 (s), 30.0 (s), 30.0 (s), 30.2 (s), 30.3 (s), 32.6 (s), 41.3 (s).

The spectroscopic data matched those reported in the literature.[12]

Tetradeylammonium tetrafluoroborate (S17)

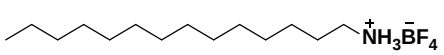

$C_{14}H_{32}BF_4N$
MW: 301.22 g/mol

According to the general procedure for protonation of amines, **S17** (646 mg, 2.14 mmol, 86%) was obtained from tetradodecylamine (623 µL,534 mg, 2.50 mmol, 1.0 equiv.) as a white solid.

^{1}H NMR (CD_3CN, 300 K, 500 MHz) δ [ppm] = 0.88 (t, *J* = 6.8 Hz, 3H), 1.28 (m, 22H), 1.60 (p, *J* = 7.4 Hz, 2H), 2.94 (*virt.* ddt, *J* = 11.6, 7.7, 3.8 Hz, 2H), 5.92 – 6.44 (m, 3H).

^{13}C NMR (CD_3CN, 300 K, 126 MHz) δ [ppm] = 14.3 (s), 23.3 (s), 26.7 (s), 27.5 (s), 29.6 (s), 30.0 (s), 30.0 (s), 30.2 (s), 30.3 (s), 30.3 (s), 30.3 (s), 30.3 (s), 32.6 (s), 41.3 (s).

The spectroscopic data matched those reported in the literature.[12]

N-Methyl-decylammonium tetrafluoroborate (S18)

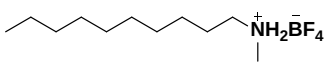

$C_{11}H_{26}BF_4N$
MW: 259.14 g/mol

According to the general procedure for protonation of amines, **S18** (36.2 mg, 140 µmol, 80%) was obtained from *N*,*N*-dimethyl-decylamine (30 mg, 175 µmol, 1.0 equiv.) as a white solid.

^{1}H NMR (CD_3CN, 300 K, 500 MHz) δ [ppm] = 0.89 (t, *J* = 6.8 Hz, 3H), 1.25 – 1.42 (m, 14H), 1.54 – 1.70 (m, 2H), 2.63 (t, *J* = 5.7 Hz, 3H), 2.95 (tdd, *J* = 8.0, 6.3, 4.4 Hz, 2H), 6.34 (t, *J* = 48.1 Hz, 2H).

^{13}C NMR (CD_3CN, 300 K, 126 MHz) δ [ppm] = 14.3 (s), 23.3 (s), 26.2 (s), 26.8 (s), 29.5 (s), 30.0 (s), 30.0 (s), 30.1 (s), 32.6 (s), 34.0 (s), 50.5 (s).

The spectroscopic data matched those reported in the literature.[12]

N,*N*-Dimethyl-decylammonium tetrafluoroborate (S19)

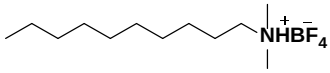

$C_{12}H_{28}BF_4N$
MW: 273.17 g/mol

According to the general procedure for protonation of amines, **S19** (43.4 mg, 159 µmol, 71%) was obtained from *N*,*N*-dimethyl-decylamine (41.3 mg, 223 µmol, 1.0 equiv.) as a white solid.

^{1}H NMR (CD_3CN, 300 K, 500 MHz) δ [ppm] = 0.80 – 1.13 (m, 3H), 1.30 (d, *J* = 12.5 Hz, 14H), 1.59 – 1.72 (m, 2H), 2.80 (dd, *J* = 5.2, 1.6 Hz, 6H), 3.04 (dtd, *J* = 9.5, 5.7, 1.4 Hz, 2H), 6.40 – 7.06 (m, 1H).

^{13}C NMR (CD_3CN, 300 K, 126 MHz) δ [ppm] = 14.3 (s), 23.3 (s), 24.9 (s), 26.7 (s), 29.6 (s), 29.9 (s), 30.0 (s), 30.1 (s), 32.6 (s), 43.9 (s), 59.1 (s).

The spectroscopic data matched those reported in the literature.[12]

3. Complex Characterization

Complex Fe-Twe **4** is paramagnetic at room temperature but becomes diamagnetic at lower temperatures. Therefore, Variable Temperature ^{1}H NMR measurements (VT-NMR) were conducted at temperatures between 25 °C and −40 °C in CD_3CN at 500 MHz using an UltraShield 500 spectrometer. ^{1}H NMR spectra of Fe-Twe **4** in 20 mM in CD_3CN at various temperatures showing a spin transition from paramagnetic to a diamagnetic form at −40 °C.

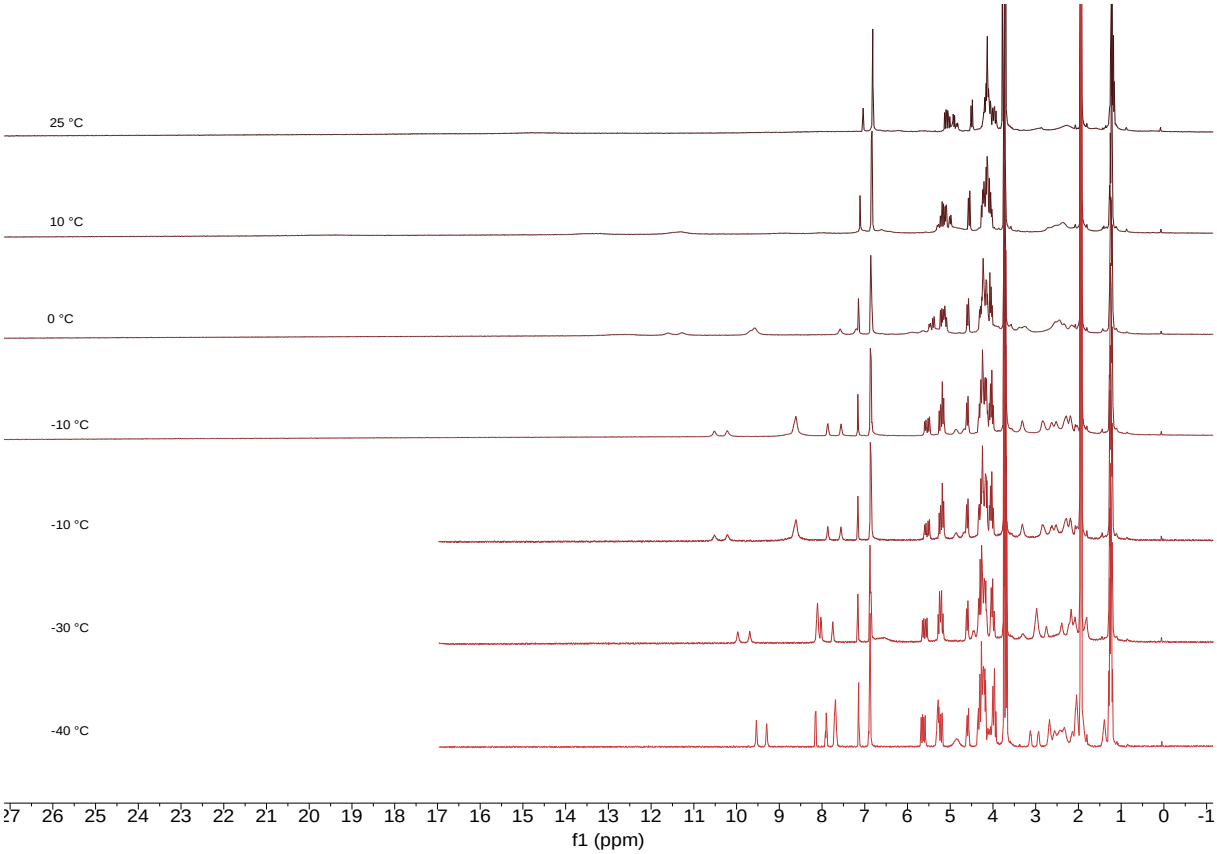

^{1}H NMR spectra of Fe-Twe **4** in 20 mM in CD_3CN at various temperatures showing a spin transition from a paramagnetic to a diamagnetic form at −40 °C.

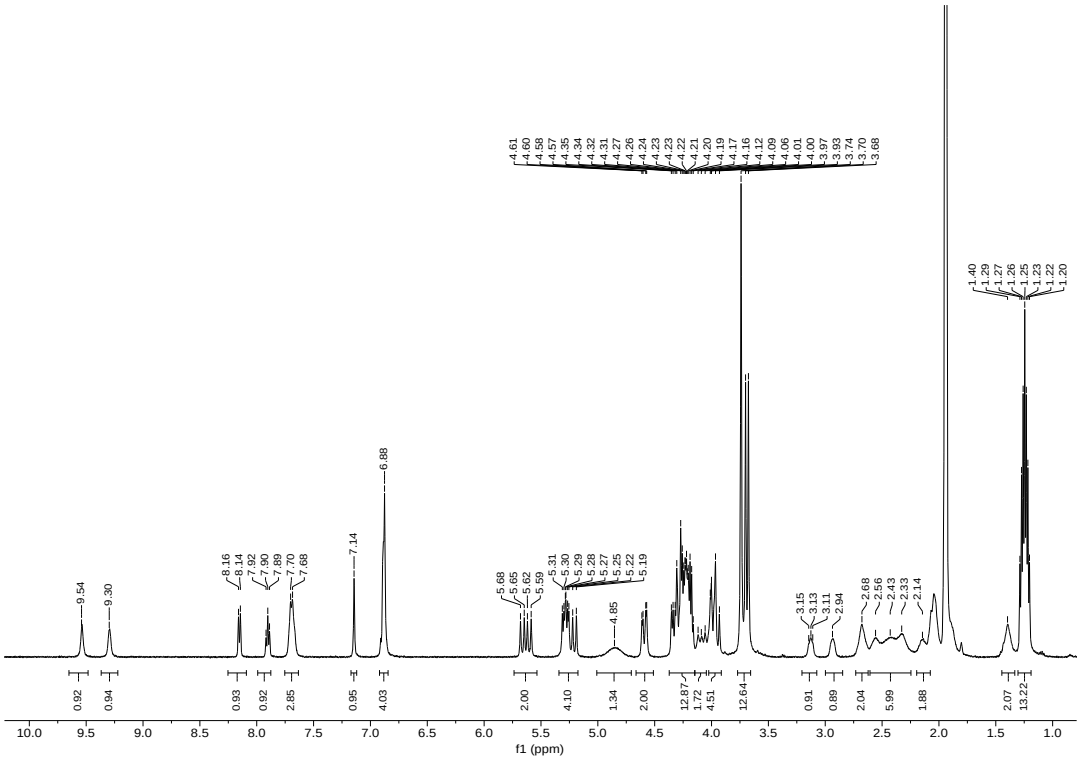

^{1}H NMR spectra of Fe-Twe **4** in CD_3CN recorded at −40 °C. The signals corresponding to the tweezer possess fine couplings, whereas the signal from the catalytic moiety are mostly broad due to closer proximity to the iron. Only in some aromatic cases couplings were observed.

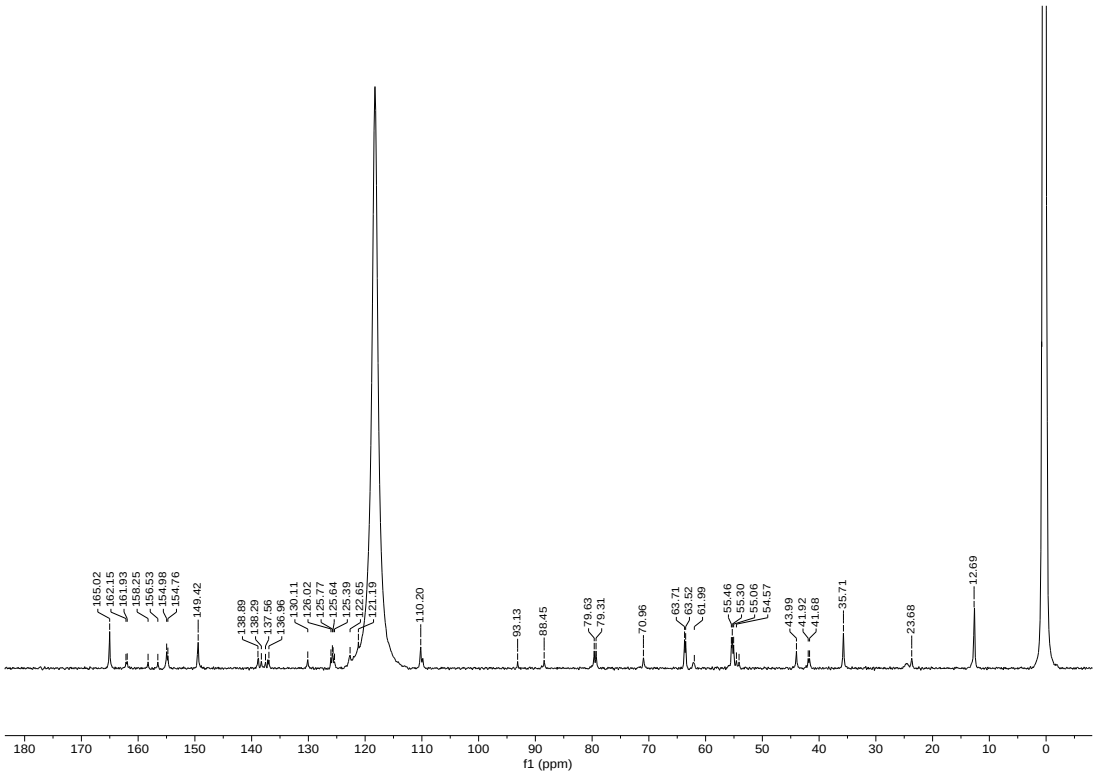

^{13}C NMR spectra of Fe-Twe **4** in CD_3CN recorded at −40 °C.

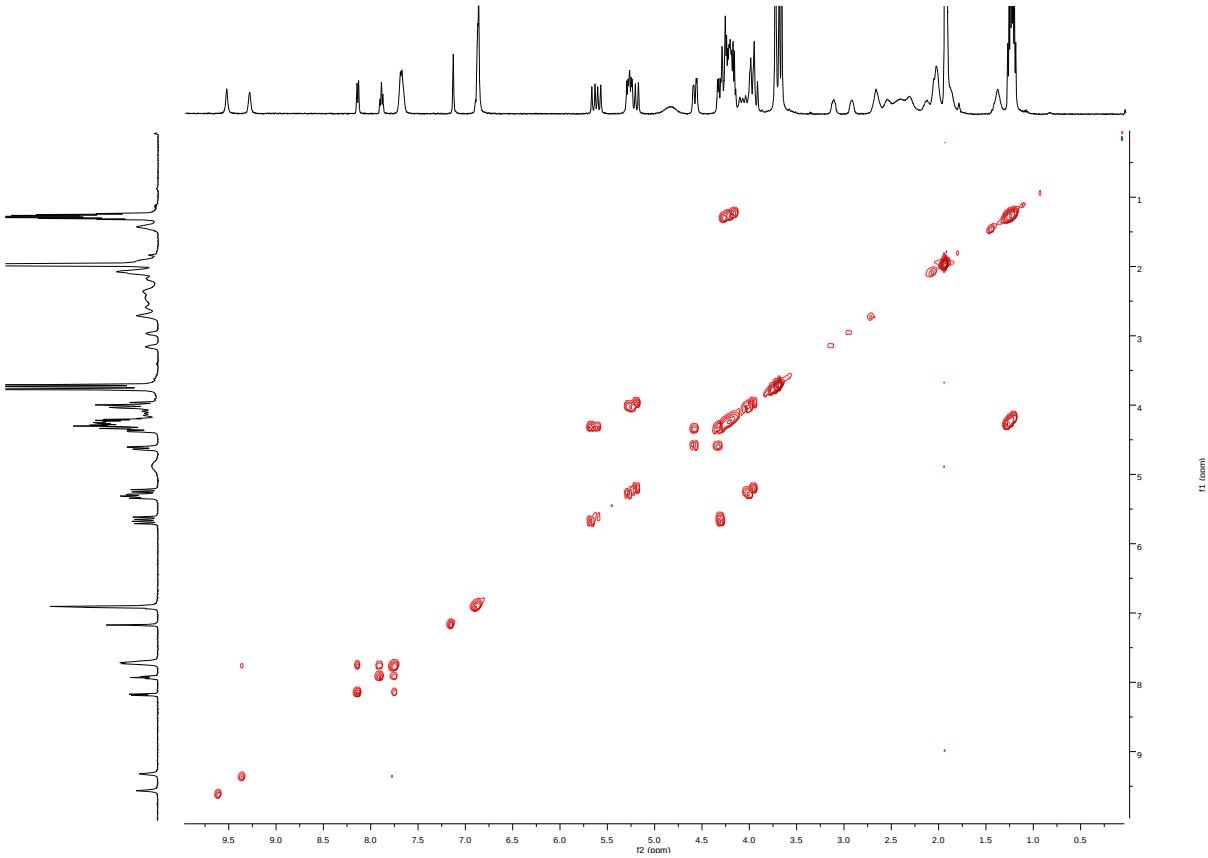

COSY of Fe-Twe **4** in CD_3CN recorded at −40 °C.

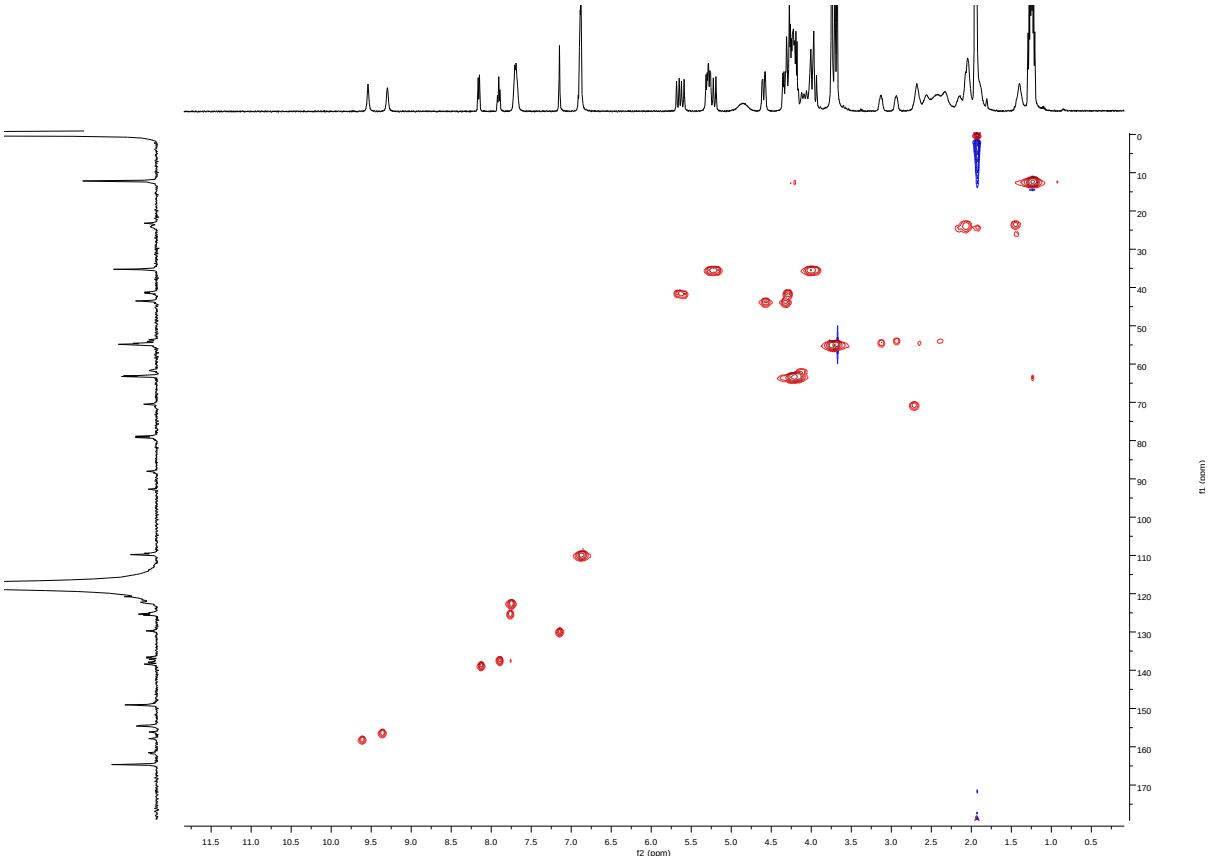

HMQC of Fe-Twe **4** in CD_3CN recorded at −40 °C.

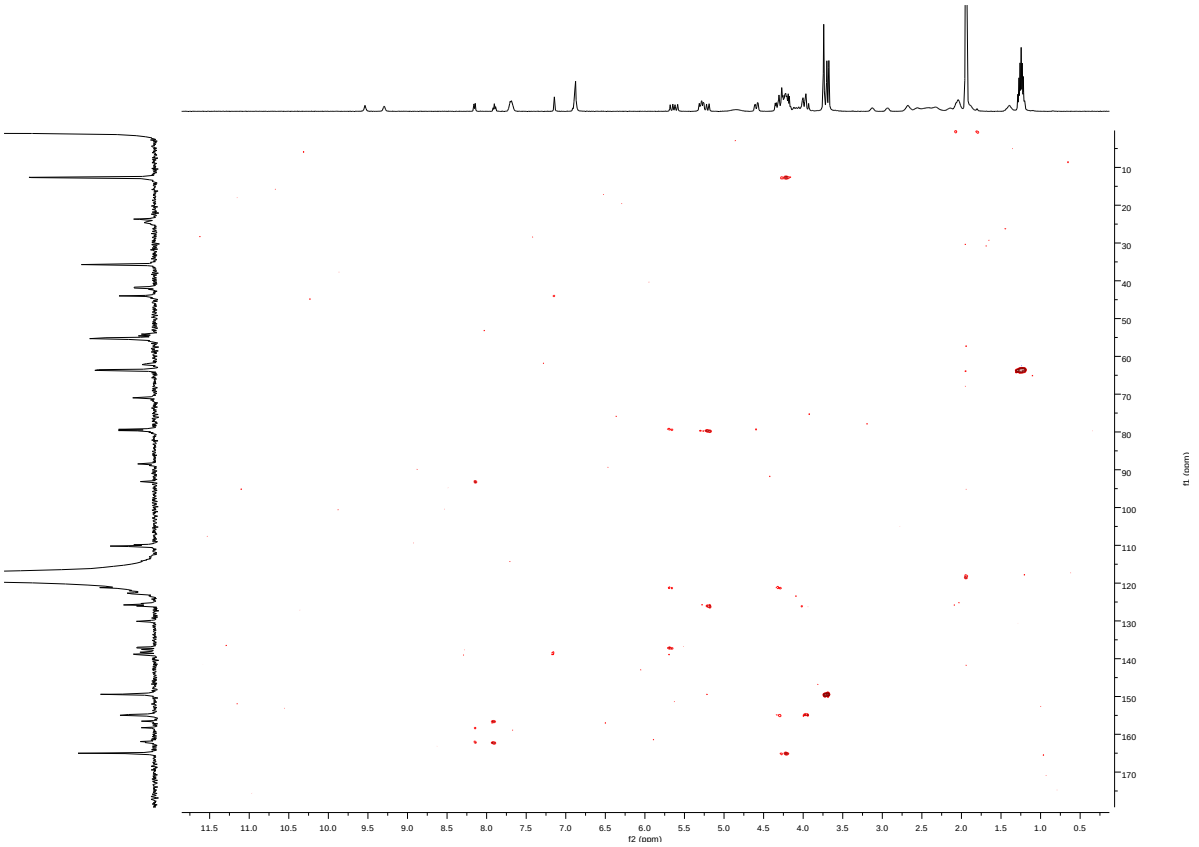

HMBC of Fe-Twe **4** in CD_3CN recorded at −40 °C.

4. Oxidation Reactions

4.1. Synthetic Procedure for the Oxidation Reactions with Fe

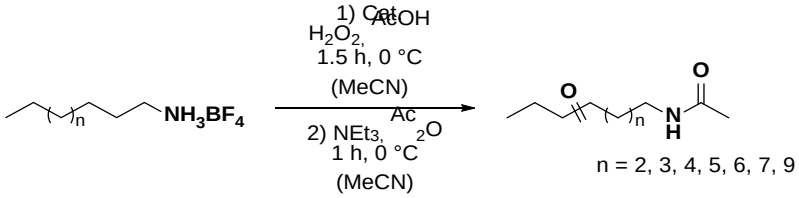

General procedure for oxidation reactions with Fe

According to a modified procedure of Costas and coworkers,[12] Fe catalyst (**2** or **4**, 699 µg or 1.59 mg respectively, 925 nmol, 5 mol%) and substrate (18.5 µmol, 1.0 equiv.) were dissolved in 200 µL MeCN in a 4 mL screw vial. After addition of a solution of AcOH in MeCN solution (~ 3 M, 49.3 µL, 148 µmol, 8.0 equiv.), the mixture was cooled to 0 °C. Next, a solution of commercially available aq. H_2O_2 (50% w/w, Sigma Aldrich) diluted in MeCN (~ 0.9 M, 308 µL, 278 µmol, 15.0 equiv.) was slowly added over 90 min by a syringe pump. After the addition, the mixture was left stirring for another 15 min.

General procedure for workup and GC analysis of primary and secondary ammonium ions

After the time indicated, biphenyl (internal standard, 9.25 µmol, 0.5 equiv.), triethylamine (100 µL) and acetic anhydride (150 µL) were added and the mixture was stirred at 0 °C for 50 min. Next, water (1 mL) was added and the mixture was left stirring for another 10 min. The solution was then extracted with CH_2Cl_2 (2 x 2 mL) and the combined organic layers were washed with a 2 M H_2SO_4 solution (2 mL), saturated aqueous $NaHCO_3$ solution (2 mL) and water (2 mL), dried (Na_2SO_4) and analyzed *via* GC and GC-MS.

General procedure for workup and GC analysis of tertiary ammonium ions

After the time indicated, biphenyl (internal standard, 9.25 µmol, 0.5 equiv.) was added. Next, 2 M NaOH (2 mL) was added and the mixture was extracted with CH_2Cl_2 (3 x 2 mL). The combined organic layers were dried (Na_2SO_4) and analyzed *via* GC and GC-MS.

Large scale procedure for the oxidation of decyl ammonium

Fe catalyst (**2**, 8.38 mg 11.1 µmol, 5 mol%) and *N*-decylammonium trifluoroborate (54.4 mg, 222 µmol, 1.0 equiv.) were dissolved in 2.4 mL MeCN. After addition of a solution of AcOH in MeCN solution (~ 3 M, 592 µL, 1.78 mmol, 8.0 equiv.), the mixture was cooled to 0 °C. Next, a solution of commercially available aq. H_2O_2 (50% w/w, Sigma Aldrich) diluted in MeCN (~ 0.9 M, 3.70 mL, 3.33 mmol, 15.0 equiv.) was slowly added over 90 min by a syringe pump. After the addition, the mixture was left stirring for another 15 min. Then, K_2CO_3 (75 mg), triethylamine (100 µL), and acetic anhydride (500 µL) were added and the mixture was stirred for additional 50 min at 0 °C. The mixture was treated with water (2.5 mL) and after additional 10 min the solution was extracted with CH_2Cl_2 (2 × 4 mL). The combined organic

layers were washed with 2 M H_2SO_4 solution (5 mL), saturated aqueous $NaHCO_3$ solution (5 mL) and water (5 mL), dried (Na_2SO_4) and concentrated under reduced pressure. Purification *via* column chromatography (5 g SiO_2, Pen/EtOAc = 1/1 → 0/1) gave unoxidized starting material as *N*-decyl acetamide (16.7 mg, 83.9 µmol, 38%) and the desired products as mixtures of different ratios (15.5 mg, 72.7 µmol, 33%) as white solids.

General procedure for the direct acetylation of amine substrates

According to a procedure of Costas and coworkers,[12] alkylamine (1.00 mmol, 1.0 equiv.) was dissolved in anhydrous MeCN (3 mL). Then, triethylamine (2.00 mmol, 2.0 equiv.) and acetic anhydride (4.00 mmol, 4.0 equiv.) were added and the mixture was stirred at 0 °C for 50 min. Afterwards, water (2 mL) was added and the mixture was stirred for additional 10 min. The mixture was further diluted with water (10 mL) and was extracted with CH_2Cl_2 (2 × 15 mL). The combined organic layers were washed with 2 M H_2SO_4 solution (2 × 15 mL), saturated aqueous $NaHCO_3$ solution (15 mL) and water (15 mL), dried (Na_2SO_4), filtered and concentrated under reduced pressure to give the pure alkylamides.

4.2. Optimization of Reaction Conditions for the Fe Catalyzed Oxidation

The oxidation reactions were optimized by testing different conditions for the oxidation of decyl ammonium tetrafluoroborate with Fe-Br **2** resp. Fe-Twe **4**.

Initially, oxidation conditions for Fe-Br **2** were optimized. Increasing the amount of catalyst (Fe-Br **2**) from 3 mol% to 10 mol% resulted in higher conversions and total yields (entry 1-3). However, 15 mol% catalyst loading did not improve the results any further (entry 4). By changing the amount of H_2O_2 (and therefore also the addition/reaction time) from 2.5 equiv. up to 15 equiv. slightly better results were obtained with higher amounts of H_2O_2 (entry 1, 5-7). Since, the selectivities increased when changing the reaction temperature to 0 °C for catalyst Fe-Twe **4** (see below), the same conditions were also applied for Fe-Br **2** giving results as at room temperature (entry 8 vs 2).

Subsequently, the optimal conditions for Fe-Twe **4** were explored. Due to the high compound value only 3 mol% were used for most of the following optimization reactions, and 5 mol% for the oxidation of different substrates (see Table S3). As the reaction temperature might play a crucial role for site-selectivity, different temperatures were explored (entry 9-14). Generally, the yields dropped with lower temperatures whereas the selectivities seemed to stay rather constant resp. slightly increased. The temperature of 0 °C was chosen for the general oxidation conditions. Addition of 10% water to the reaction decreased the yields considerably (entry 15). Oxidation with $Fe(OTf)_2(MeCN)_2$ (not shown in the table) also gave strongly decreased conversion (9.4%) and total yield (3.1%). To investigate the effect of the concentration of the reaction, the oxidation was performed 20% more diluted (entry 18) and 20% more concentrated (entry 19). However, in both cases the yields and selectivities dropped slightly. As standard reaction entry 17 was chosen. A control experiment, where the two parts of Fe-Twe **4** were added as separate entities (tweezer **8b** (5 mol%), and Fe-Br **2** (5 mol%)) was performed (entry 20). The selectivity was dramatically reduced and was close to the results of Fe-Br **2** only (entry 8), demonstrating that the tweezer has to be covalently linked to the oxidation catalyst to achieve high selectivities. Additionally, TFE and HFIP were explored as solvents. It was reported that these solvents increase yields by activating H_2O_2.[16] While this also was observed in this study, unfortunately, the selectivity for the C3-C5 CH_2-positions with Fe-Twe **4** was lost, likely due to competitive binding of the solvent (entries 21-24).

For the oxidation of the following substrates, the conditions from entry 8 resp. 17 were used.

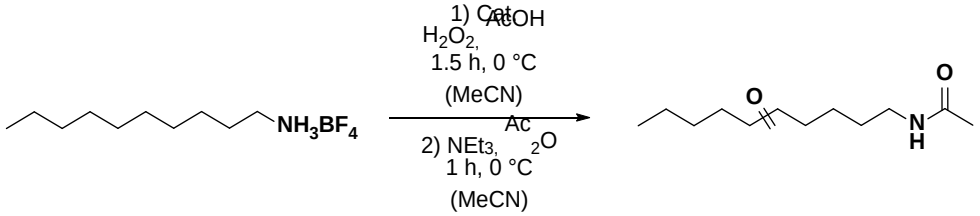

Table S1: Optimization of the reaction conditions of the oxidation of decyl ammonium tetrafluoroborate.

Enrty	Cat.	[Cat.]	AcOH [equiv.]	H_2O_2 [equiv.]	Solvent	Temp	Time of H_2O_2 Addition	Conv. [%]	Total[f] Yield [%]	Selectivity[g] K3+4 [%]	K3+5 [%]
1	Fe-Br **2**	3%	8.0	2.5	MeCN	rt	30 min	40	28	3.5	11
2	"	5%	8.0	2.5	"	rt	3 h	54	32	3.6	12
3	"	10%	8.0	2.5	"	rt	30 min	63	40	3.8	13
4	"	15%	8.0	2.5	"	rt	30 min	60	39	3.9	13
5	"	3%	8.0	5.0	"	rt	45 min	51	30	5.6	16
6	"	3%	8.0	10	"	rt	60 min	57	31	4.3	17
7	"	3%	8.0	15	"	rt	90 min	57	32	4.4	16
8	"	5%	8.0	15	"	0 °C	90 min	70	34	5.3	17
9	Fe-Twe **4**	3%	8.0	15	"	rt	90 min	43	23	18	34
10[a]	"	3%	8.0	15	"	0 °C	90 min	26	17	20	32
11	"	3%	8.0	15	"	- 10 °C	90 min	30	16	22	37
12	"	3%	8.0	15	"	- 20 °C	90 min	24	9.8	23	44
13	"	3%	8.0	15	"	- 30 °C	90 min	33	13	32	46
14	"	3%	8.0	15	"	- 40 °C	90 min	20	4.2	19	29
15[b]	"	3%	8.0	15	"	0 °C	90 min	25	9.6	20	31
16	"	5%	8.0	15	"	0 °C	90 min	39	16	29	41
17	"	5%	8.0	15	"	0 °C	90 min	47	25	28	44
18[c]	"	5%	8.0	15	"	0 °C	90 min	40	19	27	42
19[d]	"	5%	8.0	15	"	0 °C	90 min	47	22	26	41
20[e]	Fe-Br **2**	5%	8.0	15	"	0 °C	90 min	52	19	7.8	15
21	"	5%	8.0	15	TFE	0 °C	90 min	78	48	-	1.5
22	"	5%	8.0	15	HFIP	0 °C	90 min	98	59	-	-
23	Fe-Twe **4**	5%	8.0	15	TFE	0 °C	90 min	72	22	9.0	11
24	"	5%	8.0	15	HFIP	0 °C	90 min	86	52	0.8	3.8

Reaction conditions are described in the general oxidation procedure. Yields were calculated by GC and reffered to biphenyl (internal standard). (a) The screw vial was flame dried. (b) 10% H_2O was added. (c) 20% more diluted. (d) 20% more concentrated. (e) Tweezer **8b** (5 mol%) was added additionally. (f) Total yield refers tomixture of all isomers. (g) Selectivity refers to yield of selected ketones/total yield.

4.3. Competition and Control Experiments

All competition experiments were conducted according to the general protocol for oxidation reactions. The yields and conversions were obtained by GC analysis and calculated according to equation 5.2 and 5.3. In a first competition experiment, cyclohexane (18.5 µmol, 1.0 equiv.) was added as second substrate to the reaction mixture. Both substrates were oxidized by Fe-Br **2** resp. Fe-Twe **4**. However, for the oxidation with Fe-Twe **4** slightly increased selectivities for decylammonium were obtained. However, the formation of hexanol/hexanone indicates the presence of a background reaction.

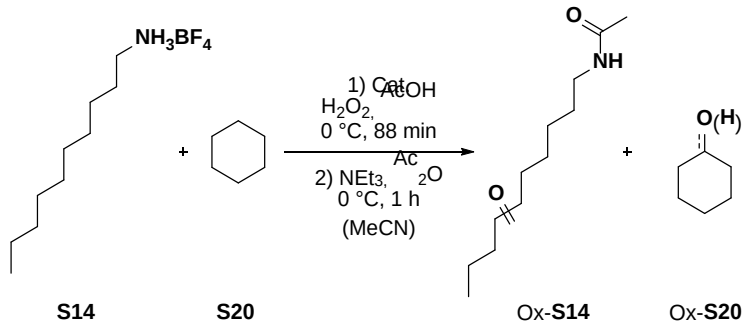

Table S2: Competition experiment of the oxidation of decylammonium tetrafluoroborate (**S14**) and cyclohexane (**S20**).

Entry	**S14** / **S20**	Cat.	Yield Ox-**S14**	Yield Ox-**S20**	Ratio Ox-**S14**/Ox-**S20**
1	1 : 1	Fe-**2**	21%	60%	1 : 2.8
2	1 : 1	Fe-**4**	14%	31%	1 : 2.2

Reaction conditions are described in the general oxidation procedure. Yields were calculated by GC and reffered to biphenyl (internal standard).

In an additional series of control experiment, different inhibitors (NH_4PF_6, NaOTf, methyl viologen dichloride dihydrate) were added to the oxidation reactions aiming at inhibting substrate binding inside Fe-Twe **4** (Table S3). All inhibitors decreased the yields of the reactions, as well as the selectivity for C3/C4 oxidation. However, these results are difficult to interpret since the inhibitor (NH_4PF_6), also inhibits oxidation of the refular catalsyst Fe-Br **2** devoid of a tweezer moiety.

Table S3: Control experiment with different inhibitors as additives.

Entry	Cat.	Additive	Conv. [%]	Yield [%]	Selectivity[a] K3-K4 [%]	K3-K5 [%]
1	Fe-Br **2**	-	75	34	5.3	17
2	Fe-Twe **4**	-	47	25	28	43
3	Fe-Twe **4**	NaOTf (2 eq.)	20	9.1	18	30
4	Fe-Twe **4**	methyl viologen dichloride dihydrate (10 mol%)	traces	traces	traces	traces
5	Fe-Twe **4**	NH_4PF_6 (10 mol%)	10	10	20	32
6	Fe-Twe **4**	NH_4PF_6 (20 mol%)	7.9	6.9	21	35
7	Fe-Twe **4**	NH_4PF_6 (40 mol%)	4.5	1.2	20	33
8	Fe-Br **2**	NH_4PF_6 (20 mol%)	traces	traces	traces	traces

Reaction conditions are described in the general oxidation procedure. Yields were calculated by GC and reffered to biphenyl (internal standard). (a) Selectivity refers to selected ketones/total yield.

4.4. Course of the Reaction Selectivity over Time

To investigate the selectivity of the oxidation reaction with Fe-Twe **4** over the reaction time, GC samples were taken after various time points (Figure S1). The selectivity did not change significantly over the reaction time.

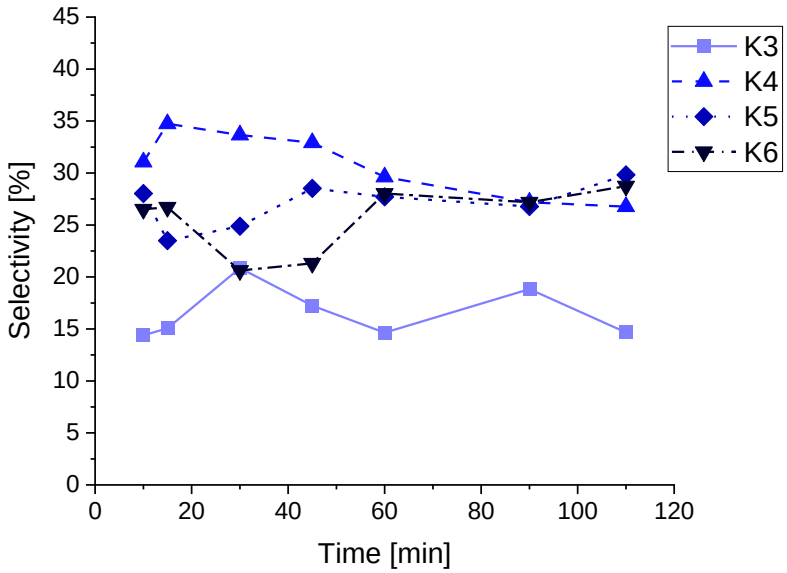

Figure S1: Reaction selectivity of the oxidation of C10-NH_3^+ with Fe-Twe **4** over the reaction course.

4.5. MS Analysis of the Catalyst Stability over the Reaction Time

MS analysis experiments were conducted to study whether the lower yields observed with catalyst Fe-Twe **4** are due to decomposition of the catalyst. Therefore, ESI MS samples of the standard oxidation reactions of Fe-Twe **4** and Fe-Br **2** were taken and analyzed after 15 min, 45 min and 90 min H_2O_2 addition. Whereas catalyst Fe-Br **2** was detectable over the whole reaction time, catalyst Fe-Twe **4** was only observed after 15 min but not anymore after 45 min, resp. 90 min. To check if this is due to the tweezer moiety itself or rather the alkyne linkage, a third experiment was conducted, in which 5 mol% tweezer **8b** was added to an oxidation experiment with Fe-Br **2**. Interestingly, already 15 min after H_2O_2 addition tweezer **8b** was not detectable in the ESI-MS anymore. These results indicate, that the tweezer moiety is not stable under the oxidation conditions and the likely cause forthe lower yields observed.

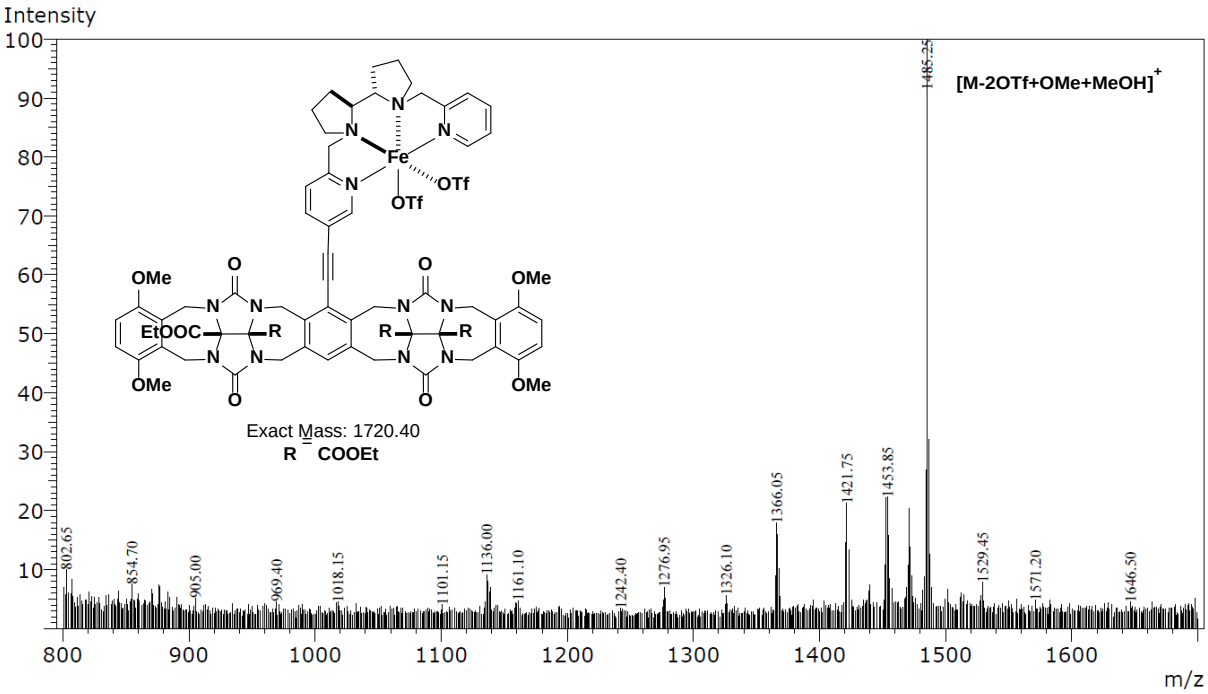

Figure S2: ESI-MS spectrum of the oxidation of C10-NH_4^+ with Fe-Twe **4** 15 min after H_2O_2 addition.

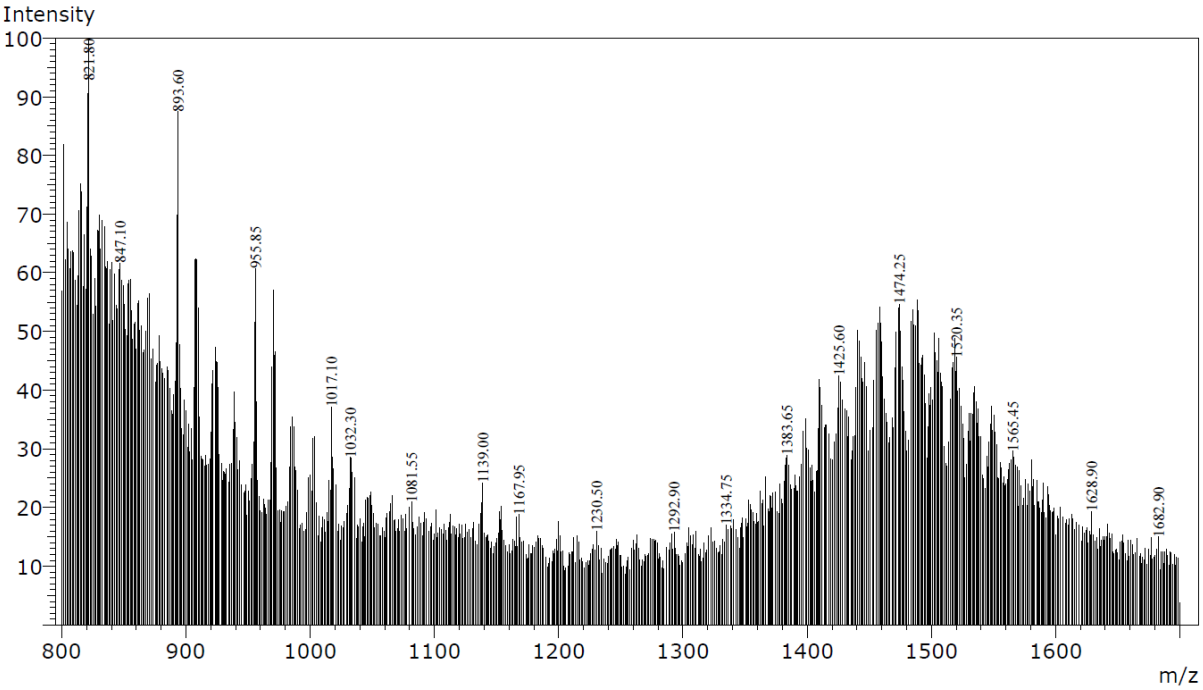

Figure S3: ESI-MS spectrum of the oxidation of C10-NH_4^+ with Fe-Twe **4** 90 min after H_2O_2 addition.

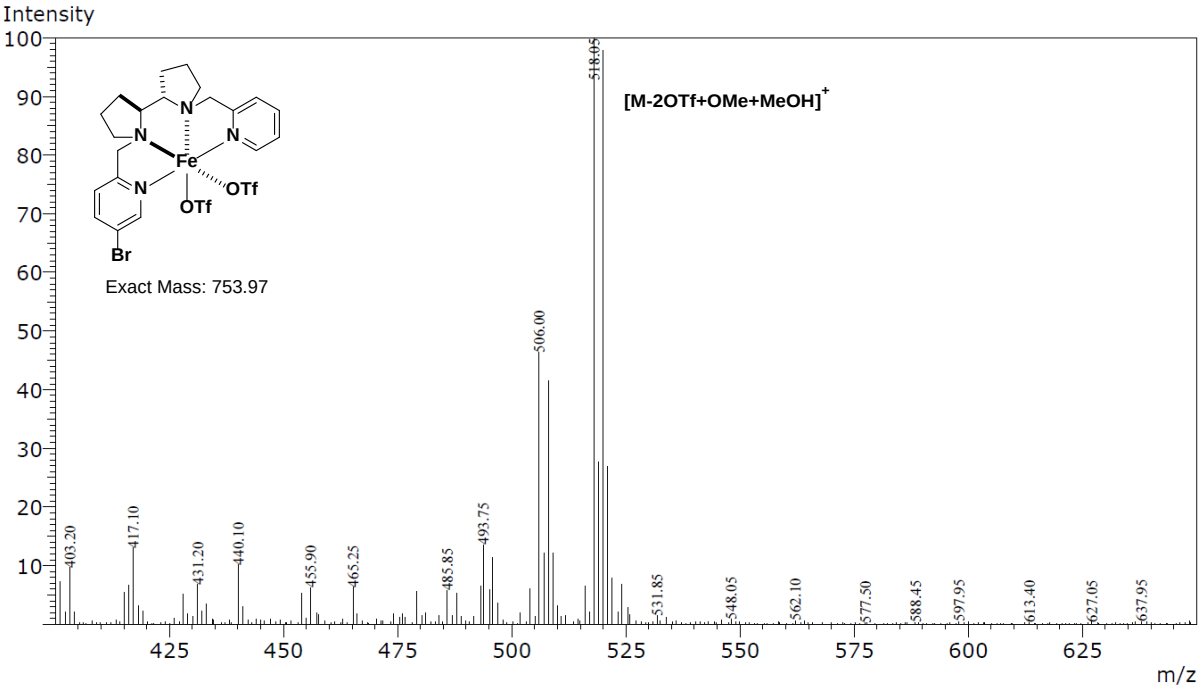

Figure 4: ESI-MS spectrum of the oxidation of C10-NH_4^+ with Fe-Br **2** 15 min after H_2O_2 addition

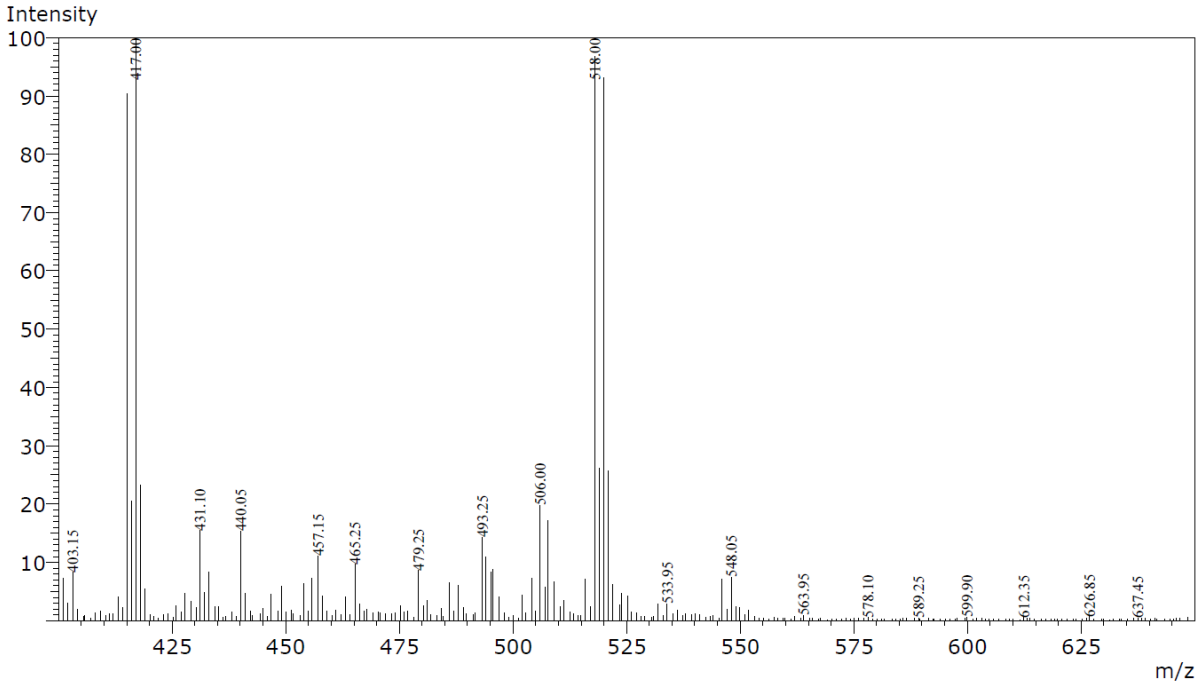

Figure 5: ESI-MS spectrum of the oxidation of C10-NH_4^+ with Fe-Br **2** 90 min after H_2O_2 addition.

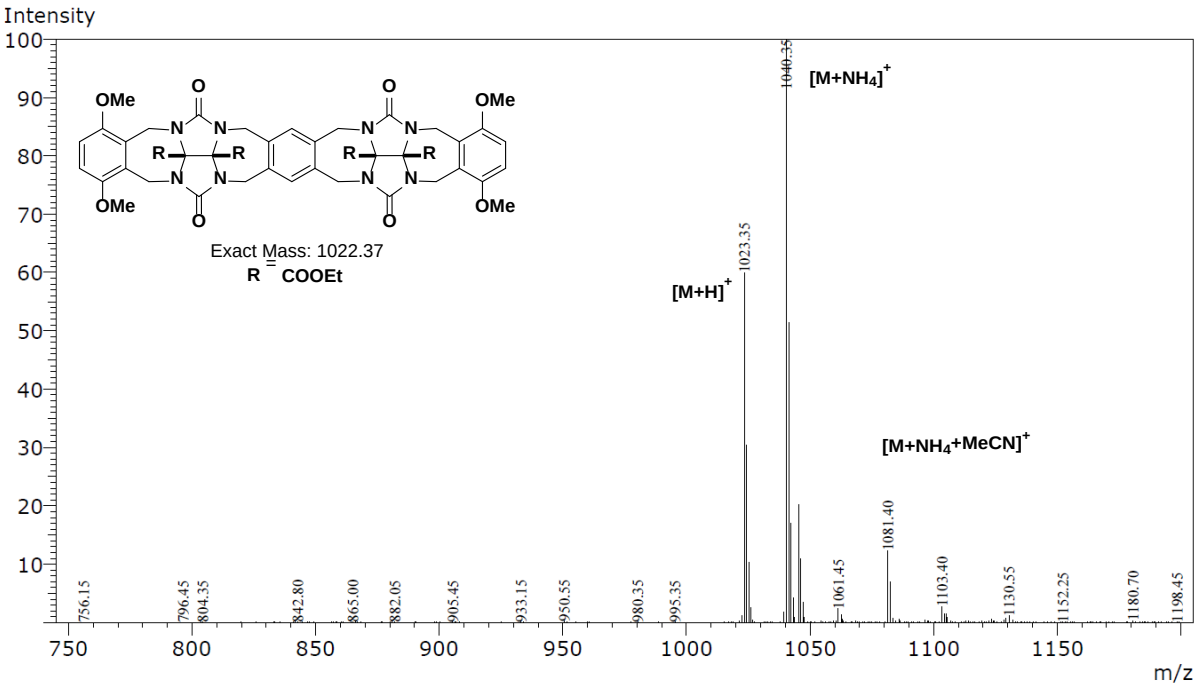

Figure S6: ESI-MS spectrum of tweezer **8b**.

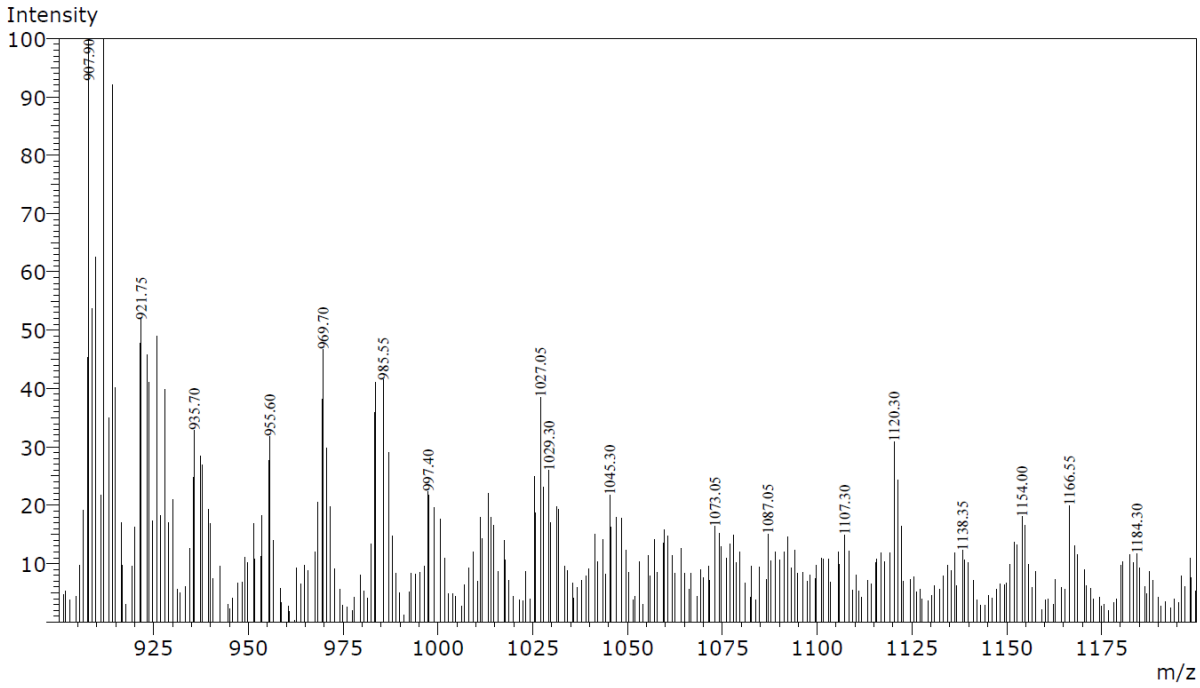

Figure S7: ESI-MS spectrum of the oxidation of C10-NH_4^+ with Fe-Br **2** in the presence of tweezer **8b** (5 mol%) 15 min after H_2O_2 addition.

4.6. Oxidation of Linear Alkyl ammonium Salts of Different Chain Length

The results of the oxidation of linear alkyl ammonium salts of the different chain length are shown in Table S3. In all cases, the general oxidation procedure with 18.5 µmol of substrate and the optimized amounts of AcOH (8.0 equiv.) and H_2O_2 (15 equiv.) were used. The yields were measured via GC analysis and calculated according to section 5.

Table S4: Oxidation of aliphatic alkylammonium salts of different chain length.

SM	Cat.	SM [%]	K13 [%]	K12 [%]	K11 [%]	K10 [%]	K9 [%]	K8 [%]	K7 [%]	K6 [%]	K5 [%]	K4 [%]	K3 [%]	Conv. [%]	Total[a] Yield [%]	Selectivity[b] K3-4 [%]	K3-5 [%]
C7-NH_3^+	Fe-**2**	66								1.1	0.9	1.0	0.8	34	3.9	46	70
C7-NH_3^+	Fe-**4**	66								0.5	0.8	2.3	2.8	34	6.4	80	92
C8-NH_3^+	Fe-**2**	63							5.9	5.0	2.9	2.3	0.9	37	17	19	36
C8-NH_3^+	Fe-**4**	78							1.3	1.6	1.1	2.5	1.6	22	8.2	51	64
C9-NH_3^+	Fe-**2**	51						8.4	7.6	6.9	4.4	2.1	0.8	49	30	10	24
C9-NH_3^+	Fe-**4**	61						2.4	2.8	2.5	2.1	4.2	2.4	39	16	40	53
C10-NH_3^+	Fe-**2**	25					7.1	7.4	7.3	6.6	4.0	1.5	0.4	75	34	5.3	17
C10-NH_3^+	Fe-**4**	53					3.8	4.4	2.7	3.4	3.7	4.8	2.2	47	25	28	43
C11-NH_3^+	Fe-**2**	43				7.9	7.7	7.5	7.7	6.3	3.4	1.3	0.4	57	42	3.9	12
C11-NH_3^+	Fe-**4**	64				3.7	4.3	1.9	2.8	2.2	3.1	3.9	1.8	36	24	24	37
C12-NH_3^+	Fe-**2**	37			3.9	4.1	5.0	5.4	3.5	3.1	1.7	0.8	0.3	63	28	3.8	9.9
C12-NH_3^+	Fe-**4**	61			1.3	1.9	0.9	1.0	0.7	0.8	1.4	1.6	0.8	39	10	23	37
C14-NH_3^+	Fe-**2**	23	3.9	4.1	4.4	3.9	3.6	3.6	4.0	2.7	2.2	0.4	0.3	77	33	2.1	8.8
C14-NH_3^+	Fe-**4**	32	1.9	1.9	1.4	1.2	1.2	1.3	1.3	1.6	2.3	2.5	1.3	68	18	21	34
C10-$NMeH_2^+$	Fe-**2**	43					5.5	4.9	5.8	5.3	3.6	1.5	0.4	57	27	7.1	20
C10-$NMeH_2^+$	Fe-**4**	57					3.5	3.6	2.6	2.3	2.7	1.9	1.0	43	18	16	32
C10-$NMe_2H^+_2$	Fe-**2**	40					7.6	7.6	5.7	5.7	3.6	1.7		60	32	5.2	17
C10-$NMe_2H^+_2$	Fe-**4**	59					4.1	4.5	1.6	1.6	1.5	0.9		41	14	6.2	17

Reaction conditions are described in the general oxidation procedure. Yields were calculated by GC and reffered to biphenyl (internal standard). (a) Total yield refers to a mixture of all isomers. (b) Selectivity refers to yield of selected ketones/total yield.

Heptylammonium Oxidation

According to the general oxidation protocol, heptylammonium tetrafluoroborate (**S11**, 3.76 mg, 18.5 µmol, 1.0 equiv.) was oxidized by Fe-Br **2** and Fe-Twe **4**. After the aqueous workup for primary ammonium ions, the mixture was analyzed by GC and GC-MS.

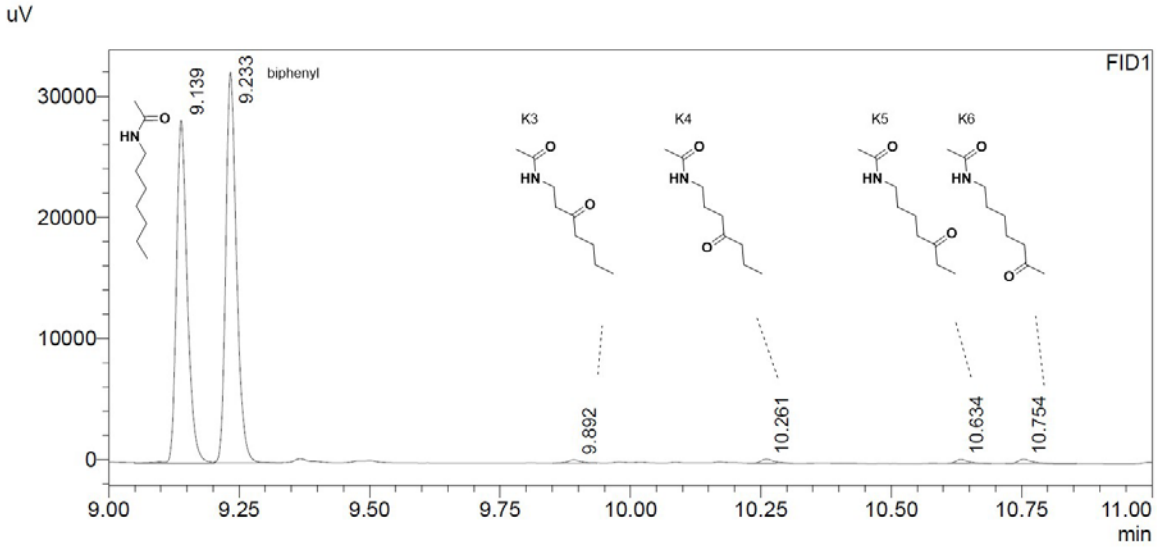

GC chromatogram of the Fe-Br **2** catalyzed oxidation of heptylammonium tetrafluoroborate.

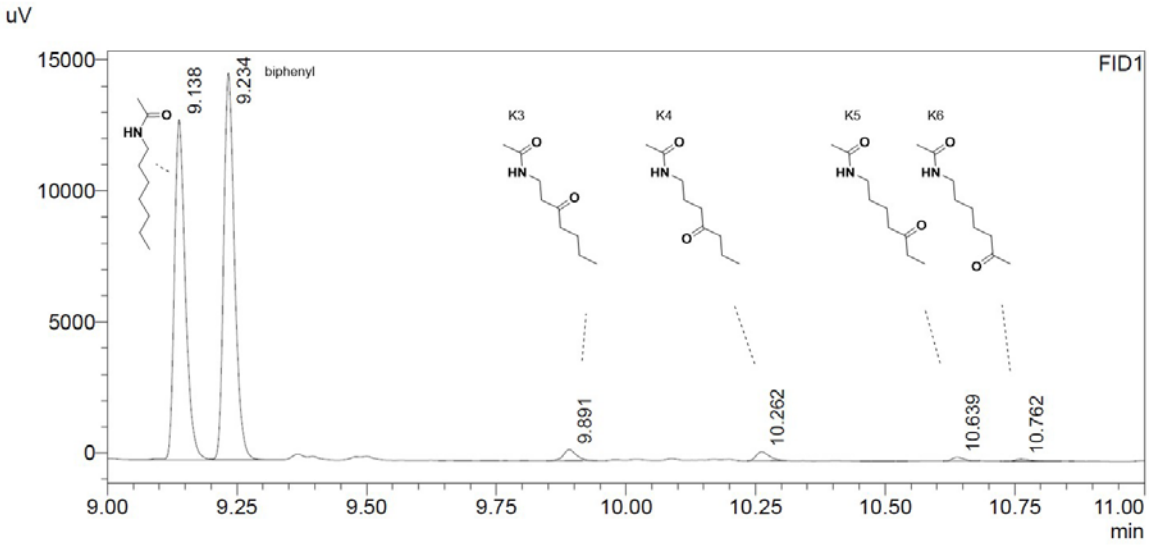

GC chromatogram of the Fe-Twe **4** catalyzed oxidation of heptylammonium tetrafluoroborate.

GC-MS chromatogram and spectra of the Fe-Twe **4** catalyzed oxidation of heptylamine tetrafluoroborate (**S11**). The different oxidation products were assigned according to their fragmentation pattern.

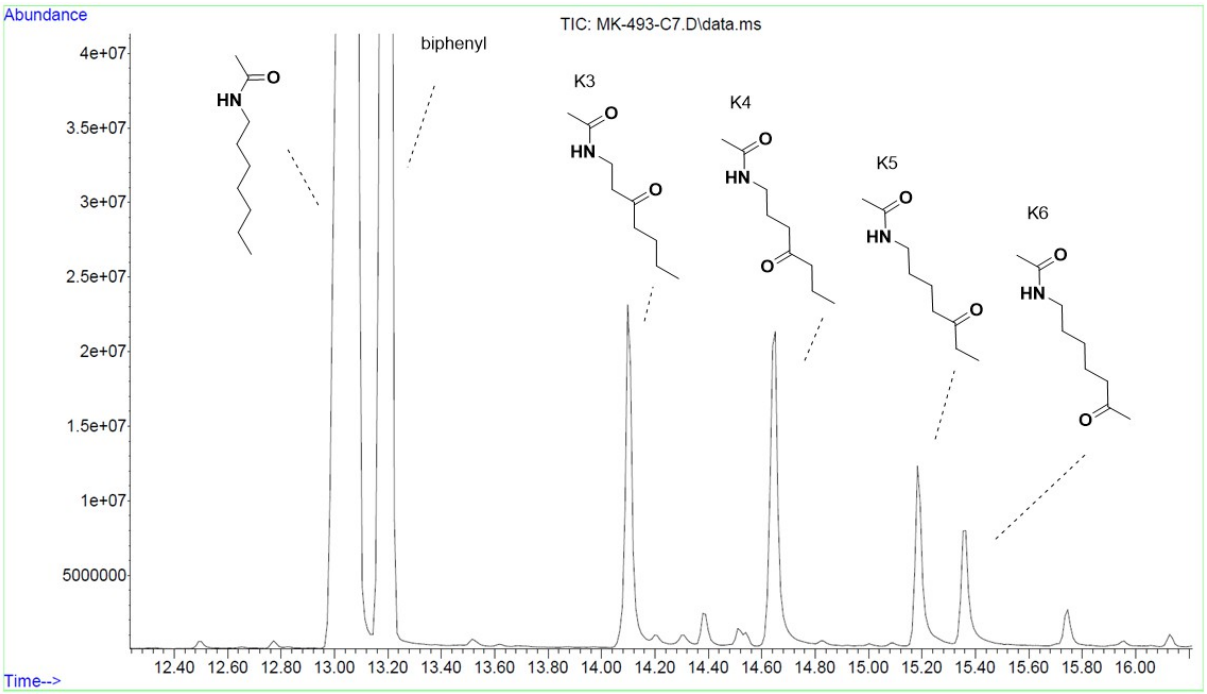

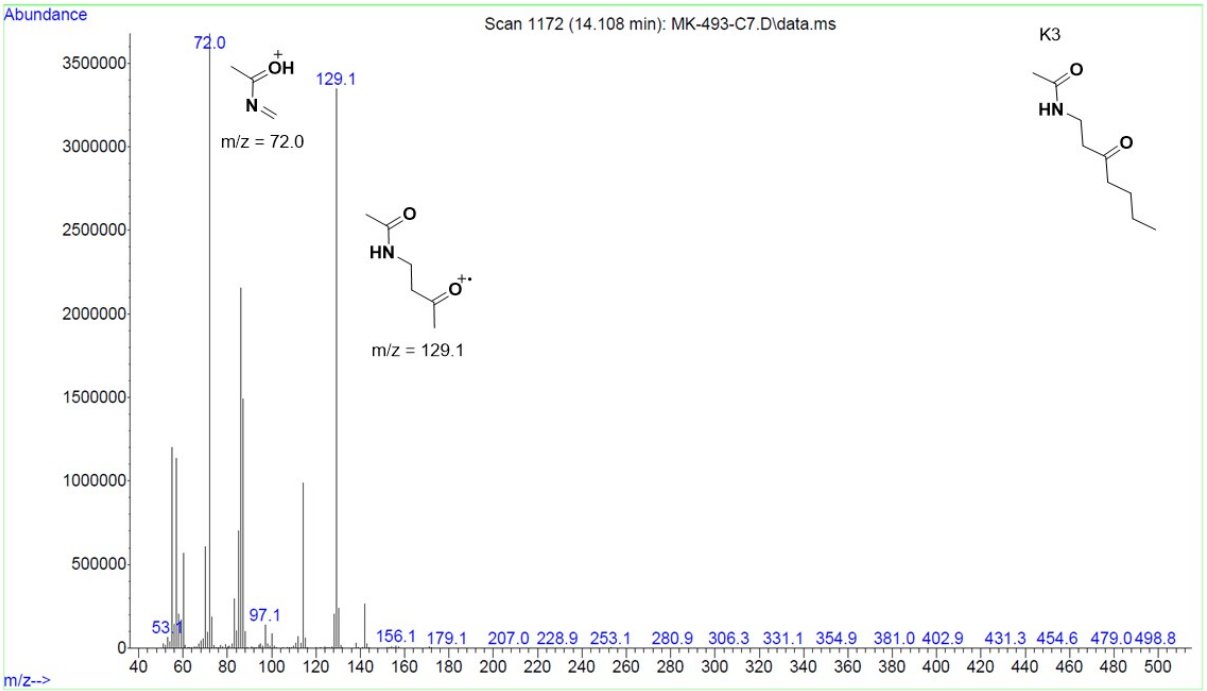

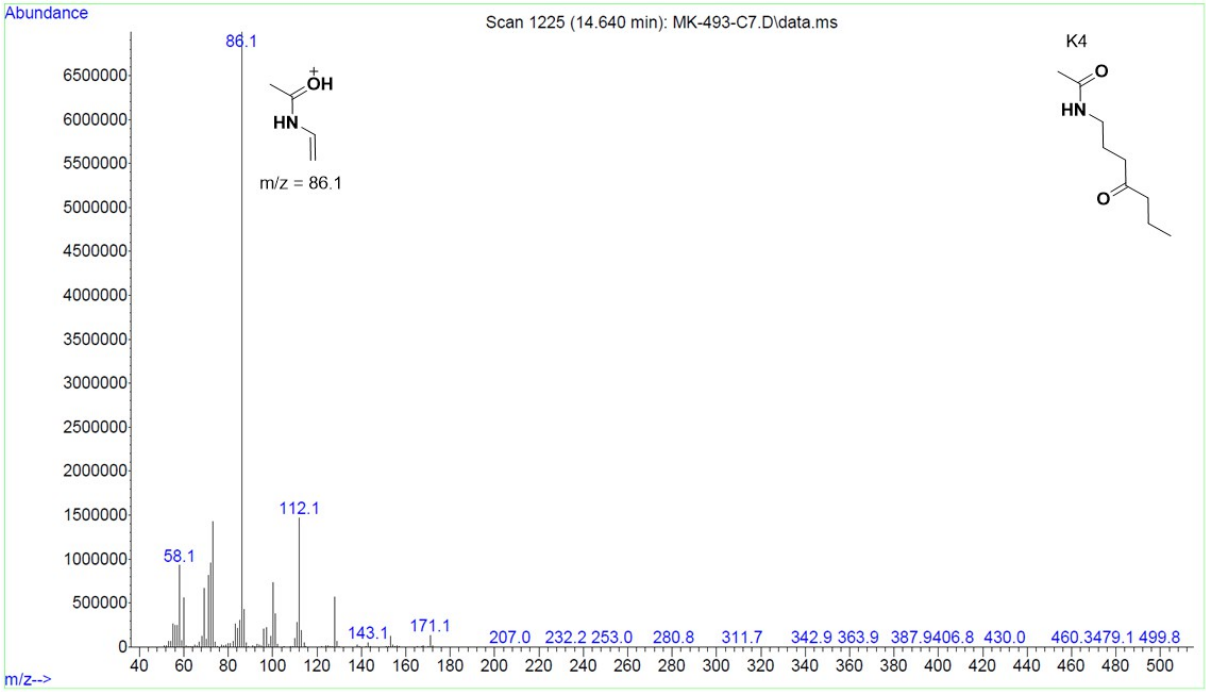
Abundance
Scan 1225 (14.640 min): MK-493-C7.D\data.ms
86.1
m/z = 86.1
K4
112.1
58.1
143.1
171.1
m/z-->

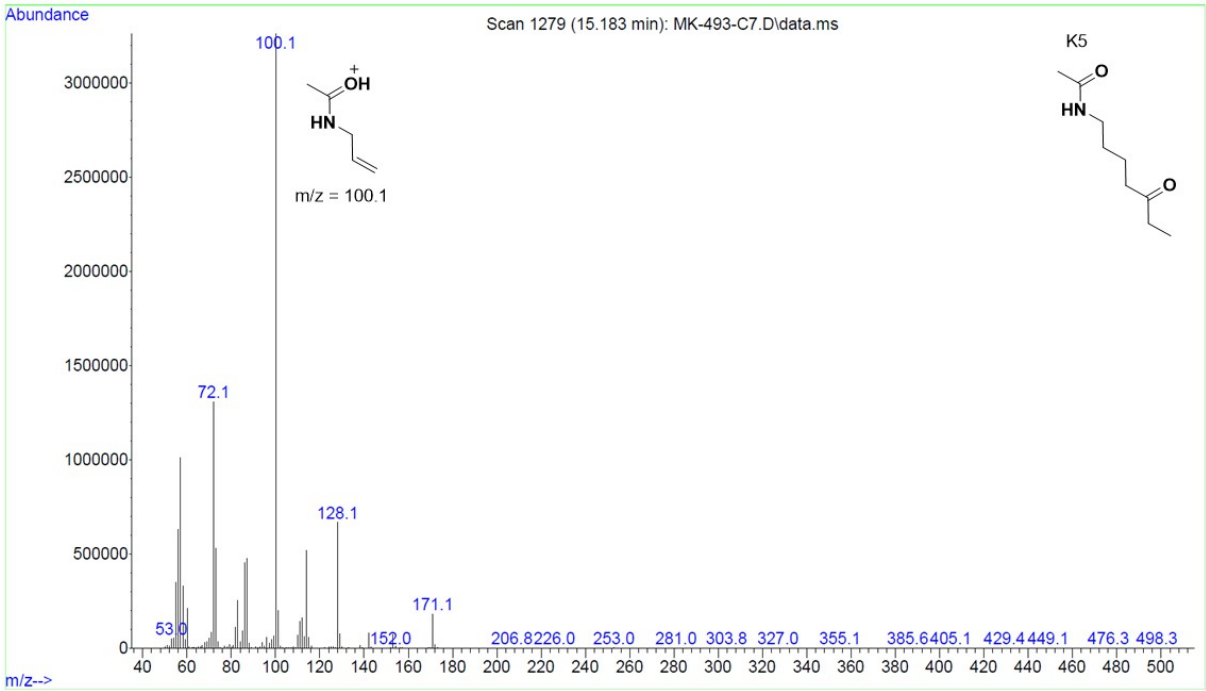
Abundance
Scan 1279 (15.183 min): MK-493-C7.D\data.ms
100.1
m/z = 100.1
K5
72.1
128.1
171.1
53.0
152.0
m/z-->

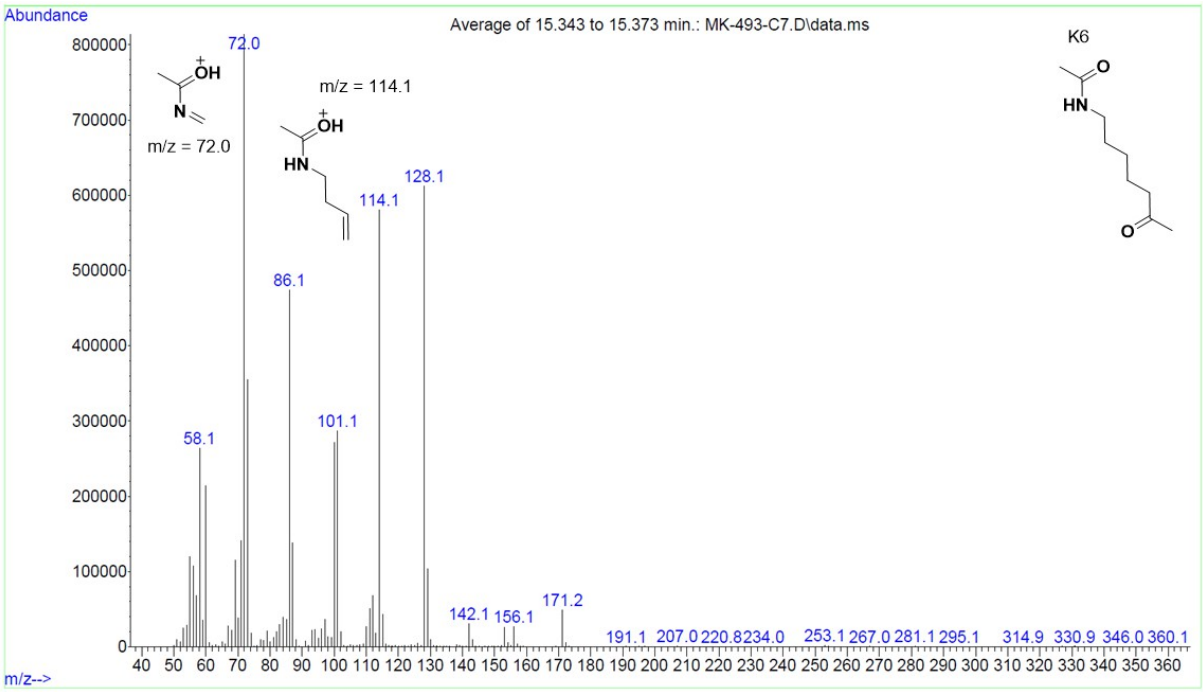
Abundance
Average of 15.343 to 15.373 min.: MK-493-C7.D\data.ms
K6
m/z = 72.0
m/z = 114.1
72.0
114.1
128.1
86.1
58.1
101.1
142.1
156.1
171.2
191.1
207.0
220.8
234.0
253.1
267.0
281.1
295.1
314.9
330.9
346.0
360.1
800000
700000
600000
500000
400000
300000
200000
100000
0
40 50 60 70 80 90 100 110 120 130 140 150 160 170 180 190 200 210 220 230 240 250 260 270 280 290 300 310 320 330 340 350 360
m/z-->

Octylammoinum Oxidation

According to the general oxidation protocol, octylammonium tetrafluoroborate (**S12**, 4.02 mg, 18.5 µmol, 1.0 equiv.) was oxidized by Fe-Br **2** and Fe-Twe **4**. After the aqueous workup for primary ammonium ions, the mixture was analyzed by GC and GC-MS.

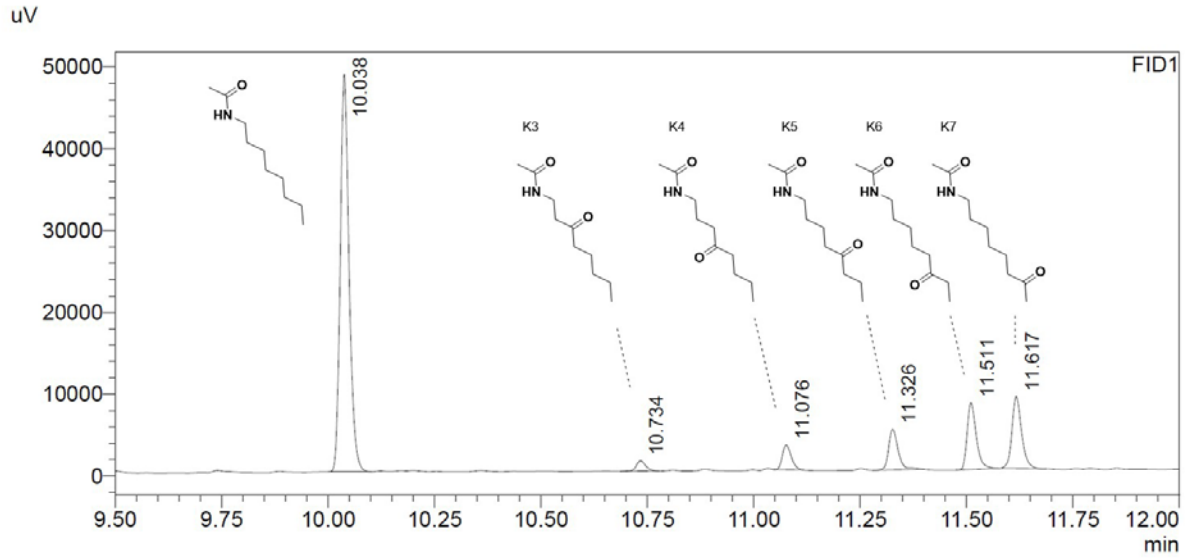

GC chromatogram of the Fe-Br **2** catalyzed oxidation of octylammonium tetrafluoroborate.

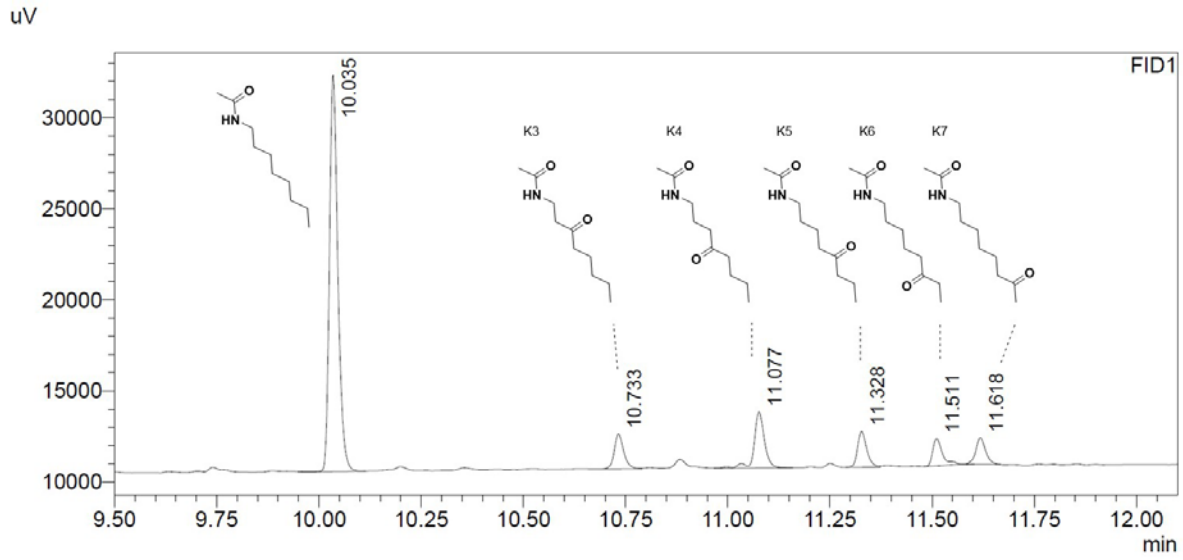

GC chromatogram of the Fe-Twe **4** catalyzed oxidation of octylammonium tetrafluoroborate.

GC-MS chromatogram and spectra of the Fe-Twe **4** catalyzed oxidation of octylammonium tetrafluoroborate (**S12**). The different oxidation products were assigned according to their fragmentation pattern.

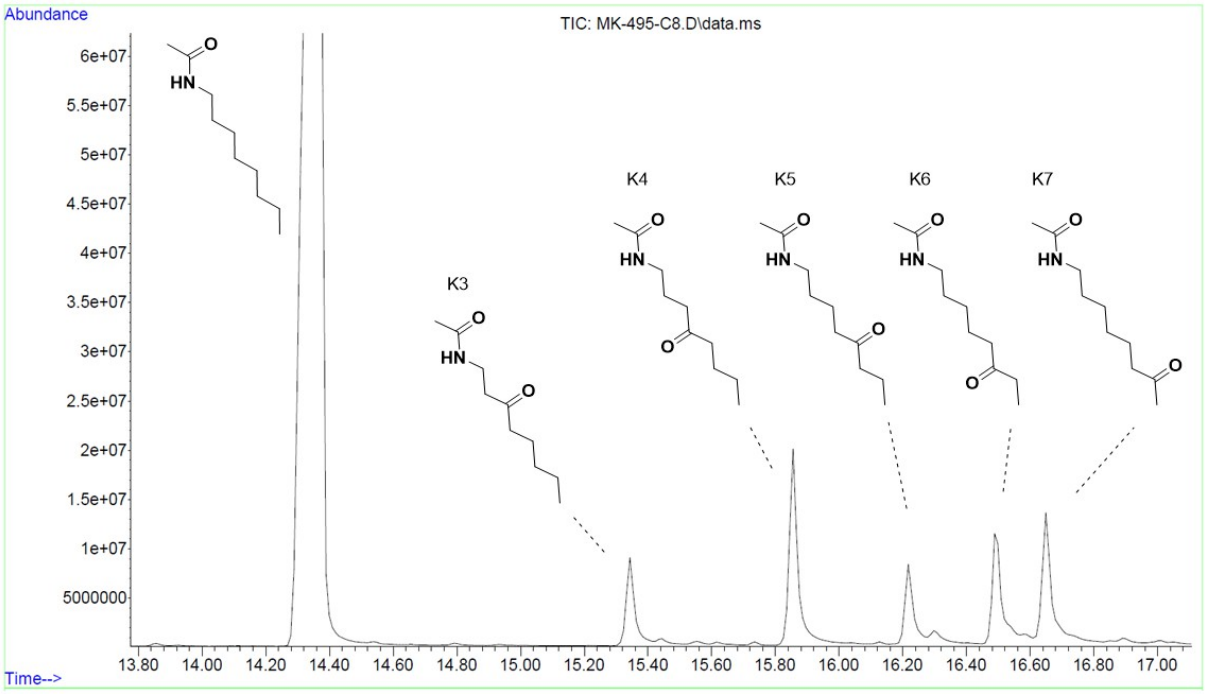

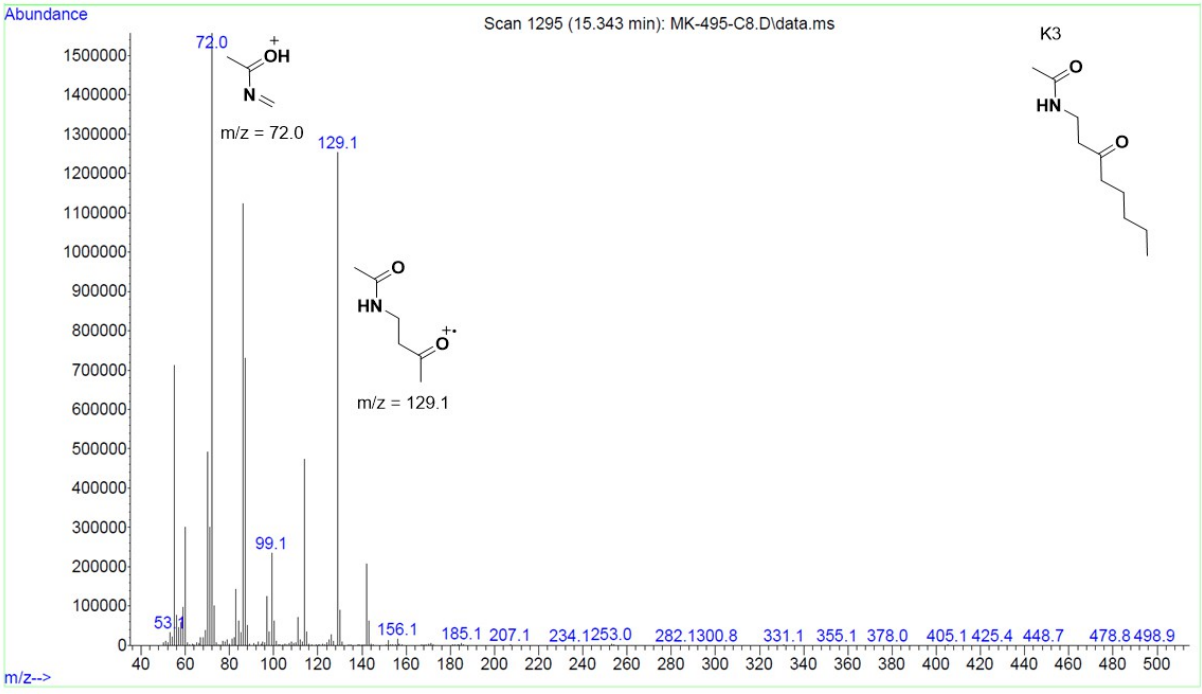

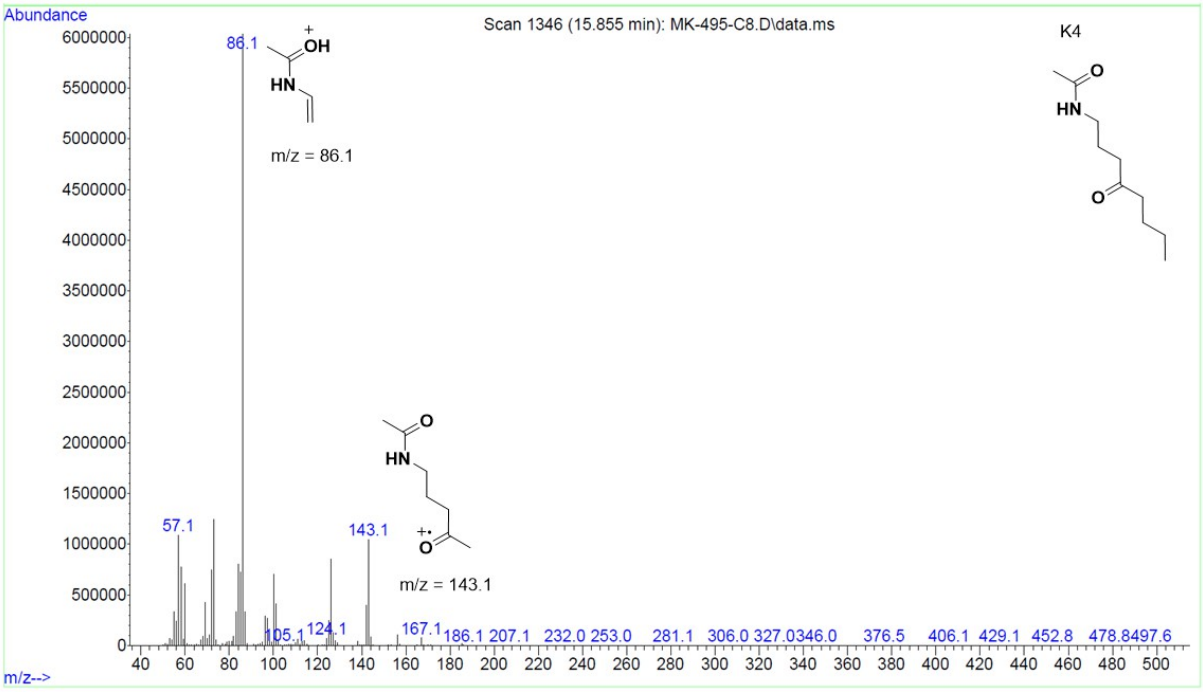
Abundance
Scan 1346 (15.855 min): MK-495-C8.D\data.ms
K4
86.1
m/z = 86.1
143.1
m/z = 143.1
57.1
105.1
124.1
167.1
m/z-->

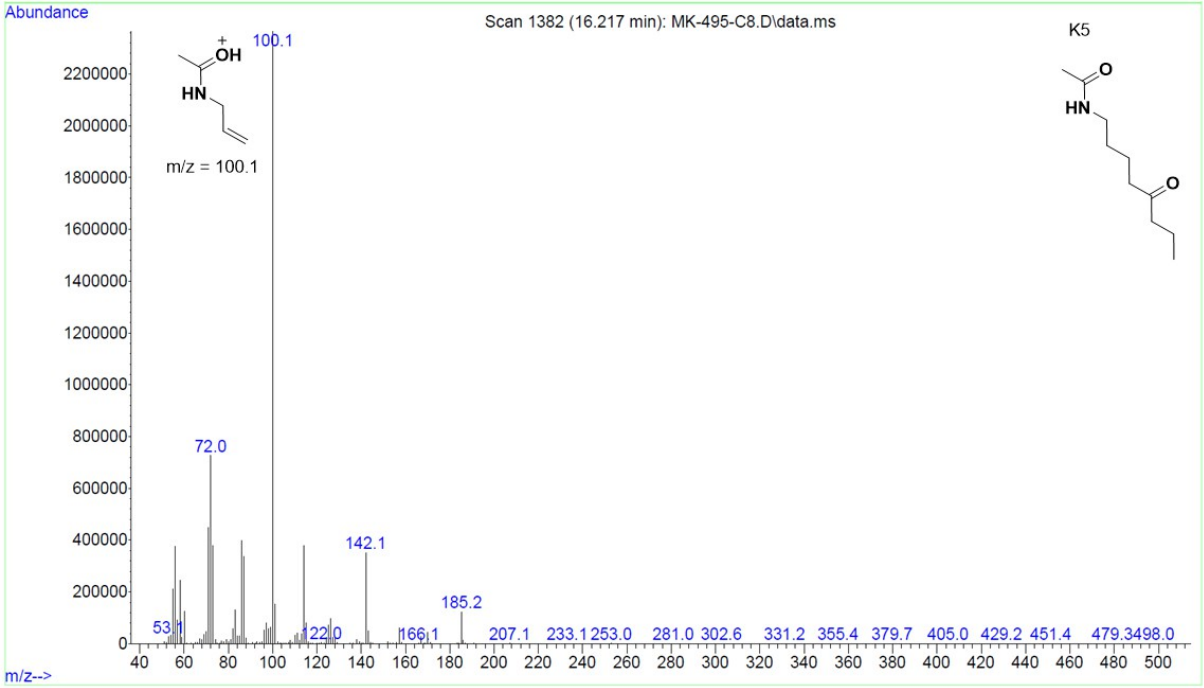
Abundance
Scan 1382 (16.217 min): MK-495-C8.D\data.ms
K5
100.1
m/z = 100.1
72.0
142.1
185.2
53.1
122.0
166.1
m/z-->

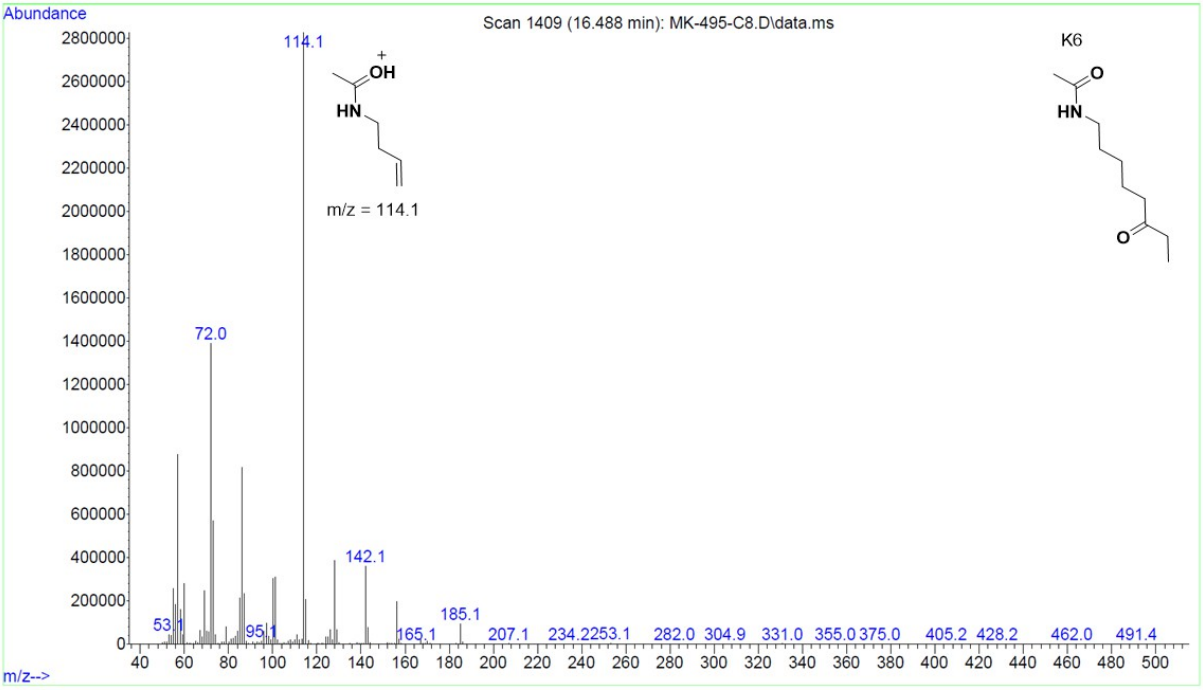
Abundance
Scan 1409 (16.488 min): MK-495-C8.D\data.ms
K6
114.1
72.0
142.1
185.1
m/z = 114.1
m/z-->

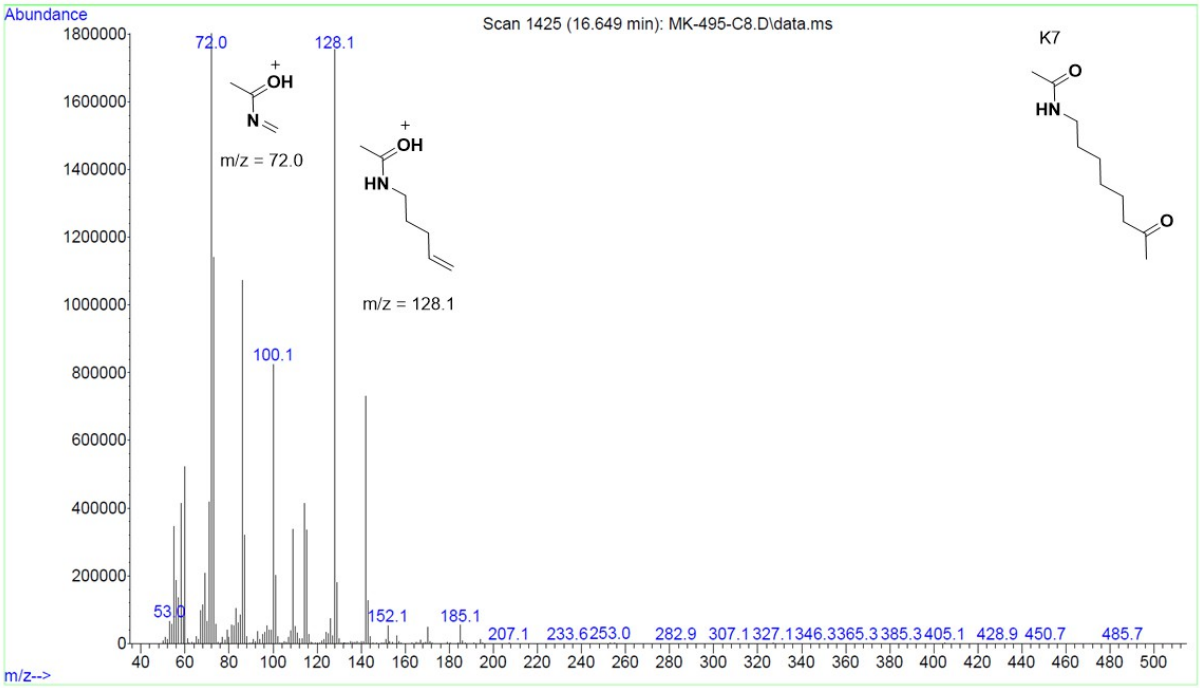
Abundance
Scan 1425 (16.649 min): MK-495-C8.D\data.ms
K7
72.0
128.1
100.1
152.1
185.1
m/z = 72.0
m/z = 128.1
m/z-->

Nonylammonium Oxidation

According to the general oxidation protocol, nonylammonium tetrafluoroborate (**S13**, 4.28 mg, 18.5 µmol, 1.0 equiv.) was oxidized by Fe-Br **2** and Fe-Twe **4**. After the aqueous workup for primary ammonium ions, the mixture was analyzed by GC and GC-MS.

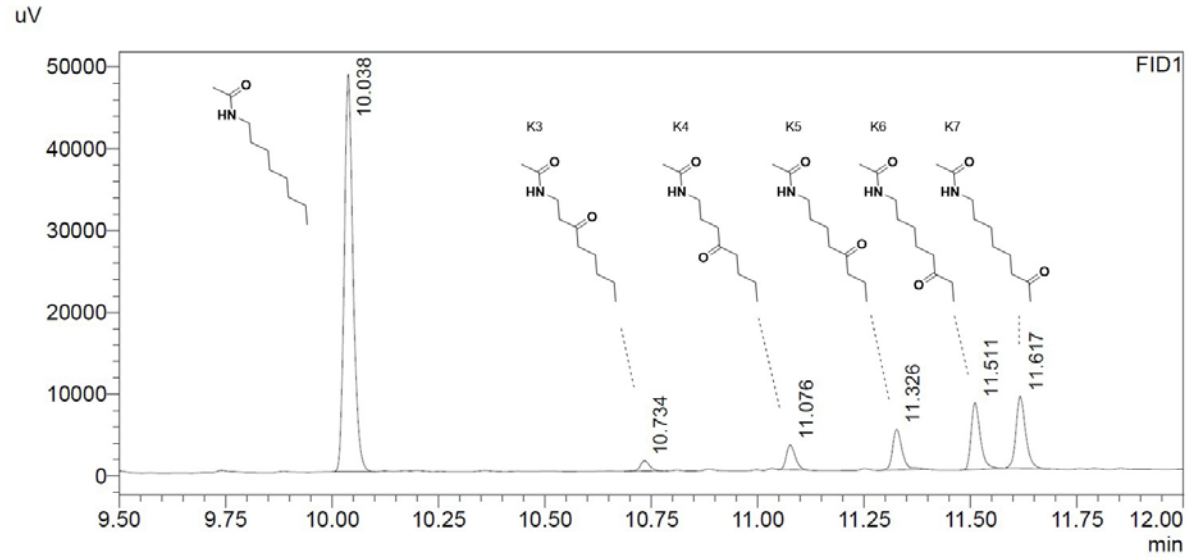

GC chromatogram of the Fe-Br **2** catalyzed oxidation of nonylammonium tetrafluoroborate.

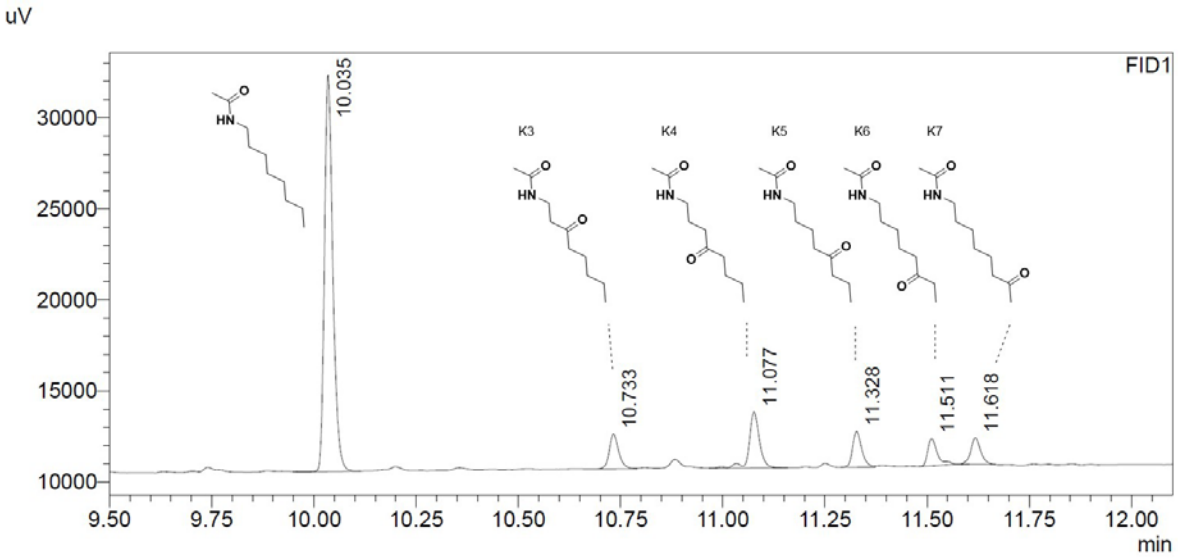

GC chromatogram of the Fe-Twe **4** catalyzed oxidation of nonylammonium tetrafluoroborate.

GC-MS chromatogram and spectra of the Fe-Twe **4** catalyzed oxidation of nonylammonium tetrafluoroborate (**S13**). The different oxidation products were assigned according to their fragmentation pattern.

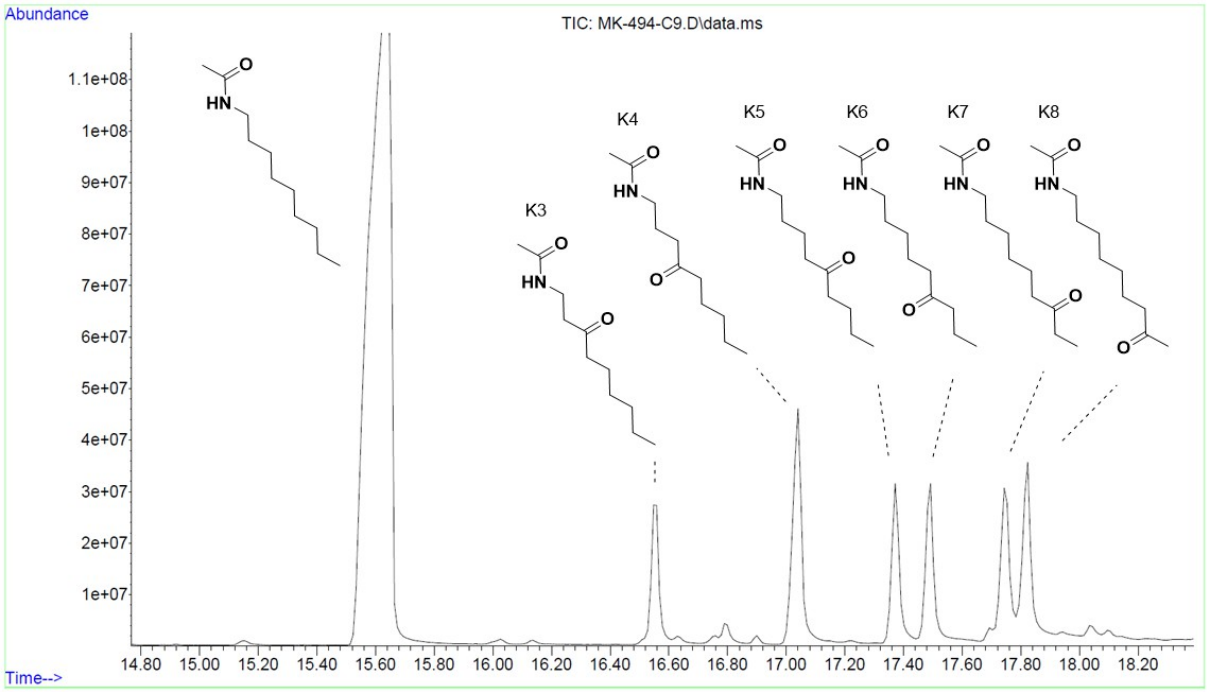

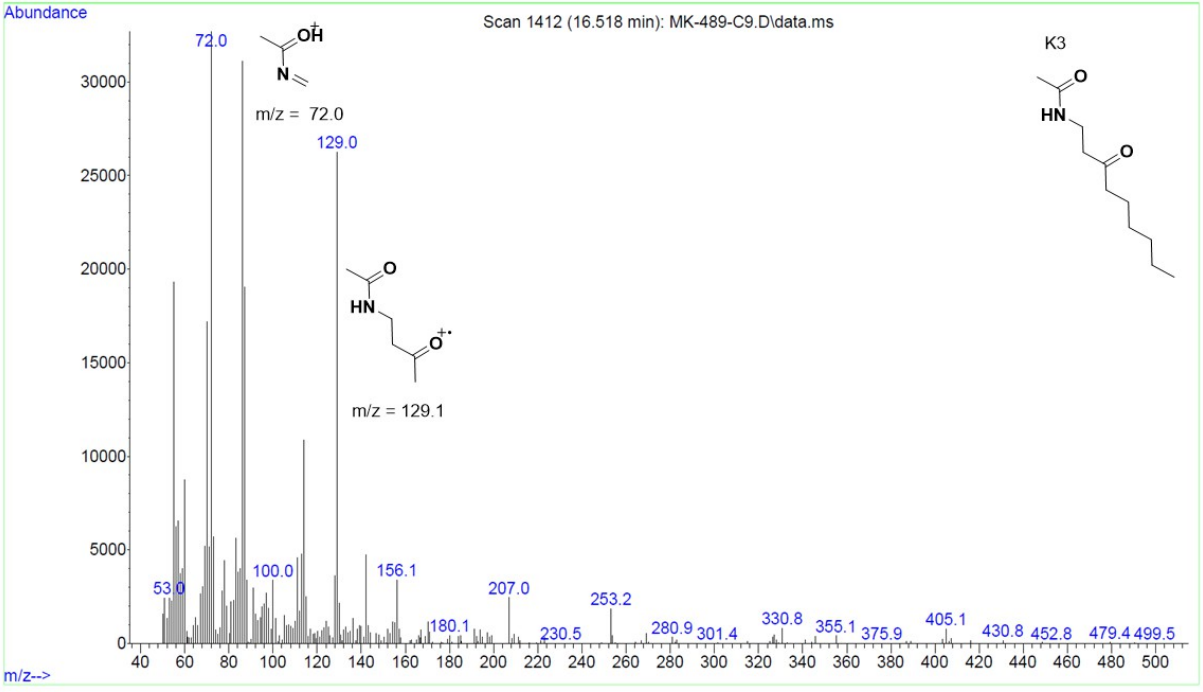

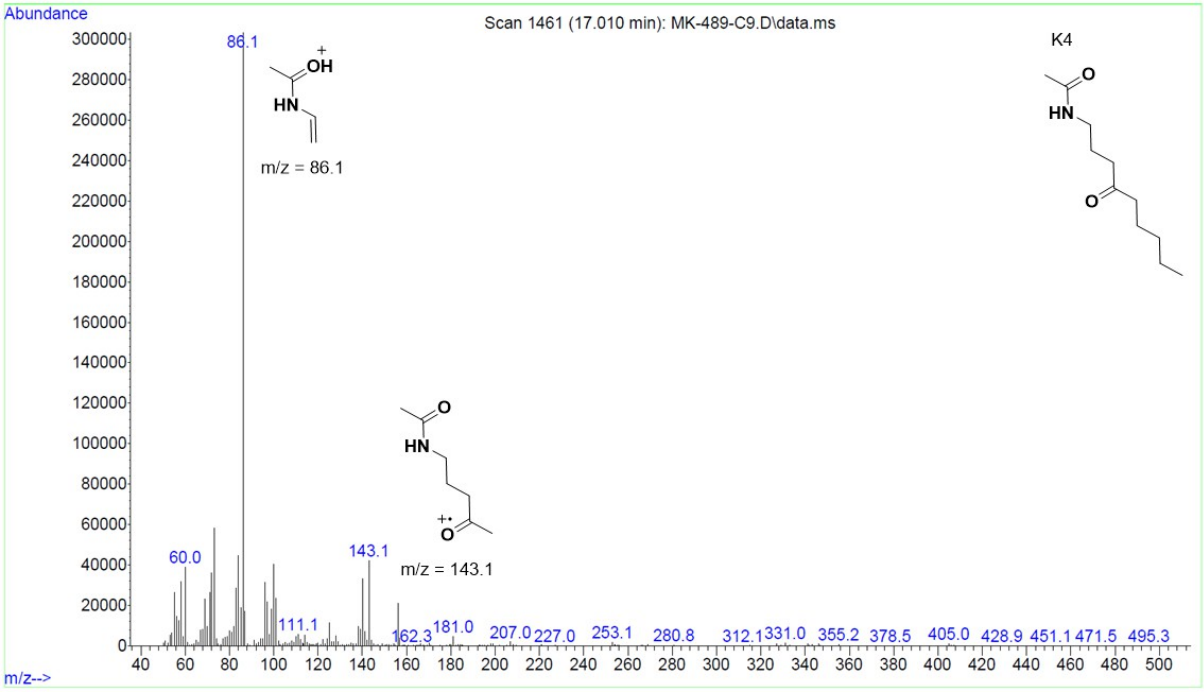
Abundance
Scan 1461 (17.010 min): MK-489-C9.D\data.ms
K4
86.1
m/z = 86.1
143.1
m/z = 143.1
60.0
111.1
162.3
181.0
207.0
227.0
253.1
280.8
312.1
331.0
355.2
378.5
405.0
428.9
451.1
471.5
495.3
m/z-->

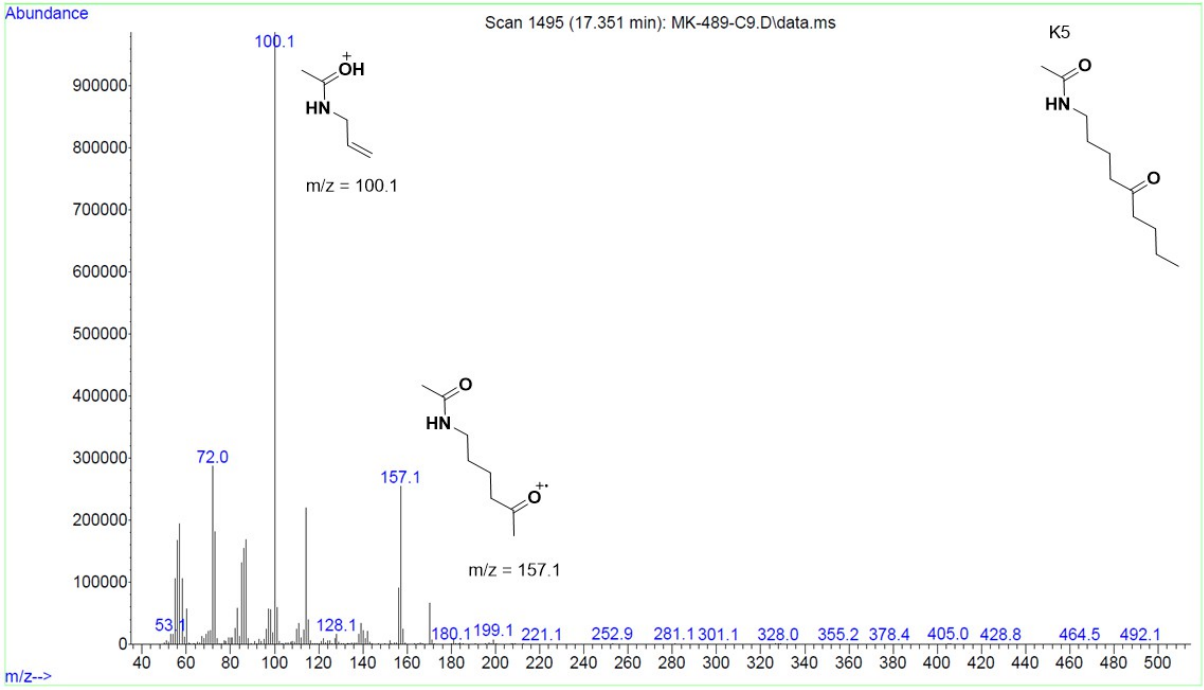
Abundance
Scan 1495 (17.351 min): MK-489-C9.D\data.ms
K5
100.1
m/z = 100.1
157.1
m/z = 157.1
72.0
53.1
128.1
180.1
199.1
221.1
252.9
281.1
301.1
328.0
355.2
378.4
405.0
428.8
464.5
492.1
m/z-->

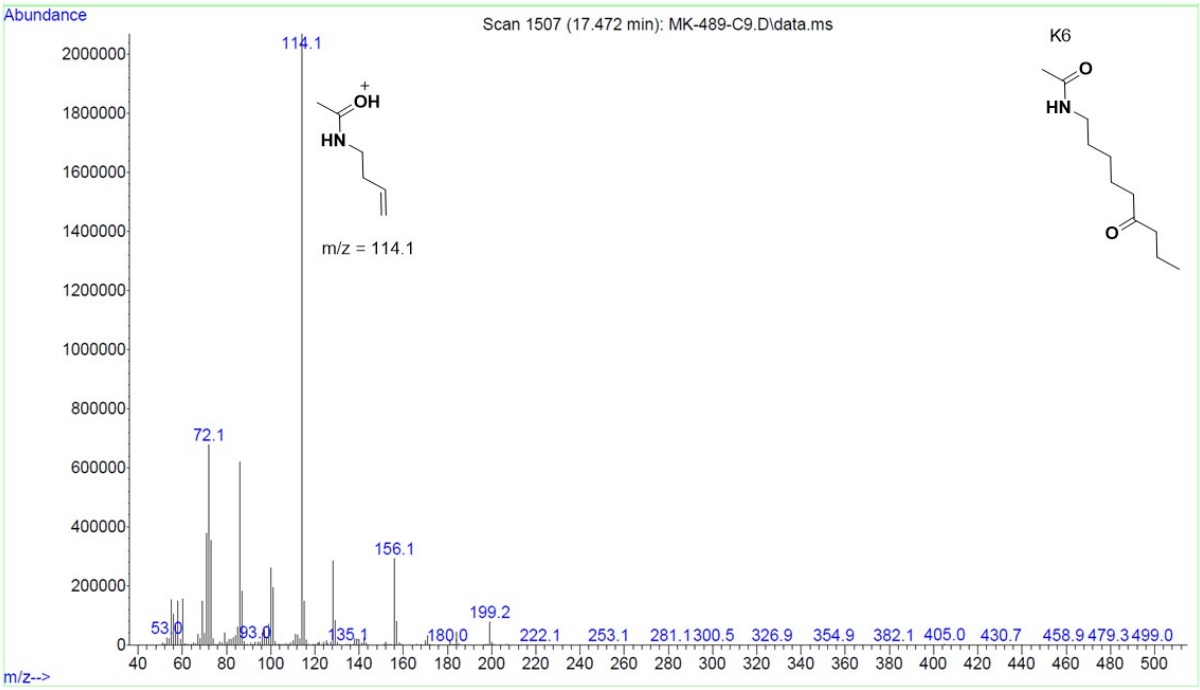
Abundance
Scan 1507 (17.472 min): MK-489-C9.D\data.ms
K6
114.1
72.1
156.1
199.2
m/z = 114.1
m/z-->

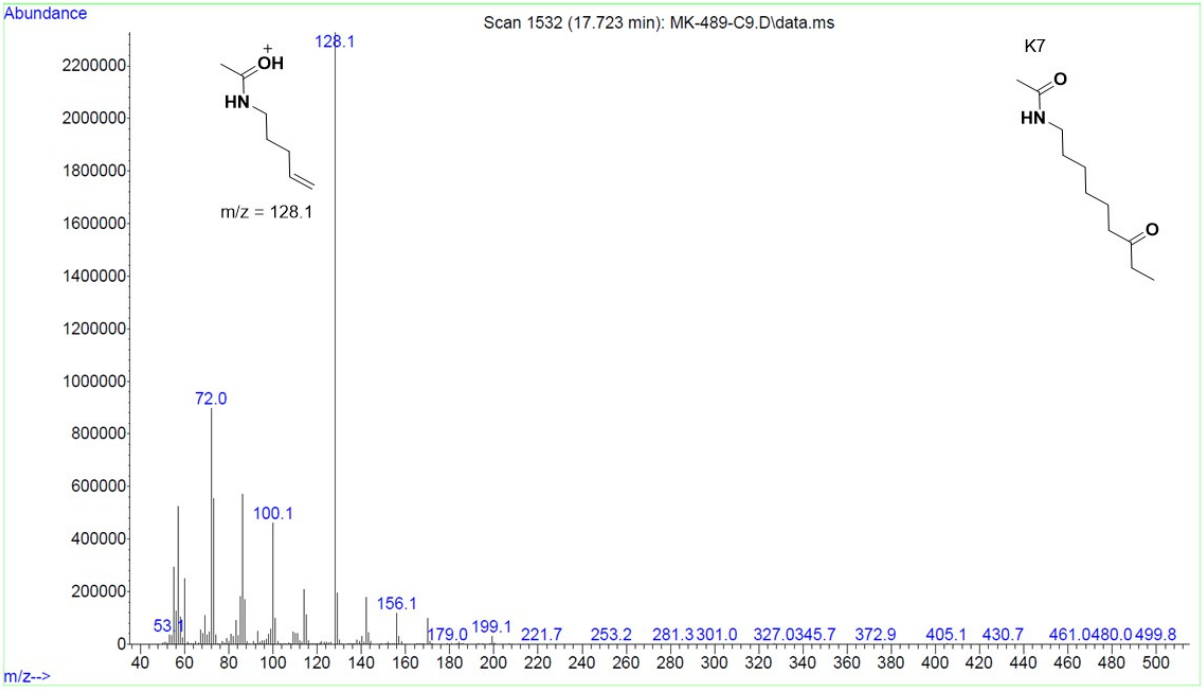
Abundance
Scan 1532 (17.723 min): MK-489-C9.D\data.ms
K7
128.1
72.0
100.1
156.1
199.1
m/z = 128.1
m/z-->

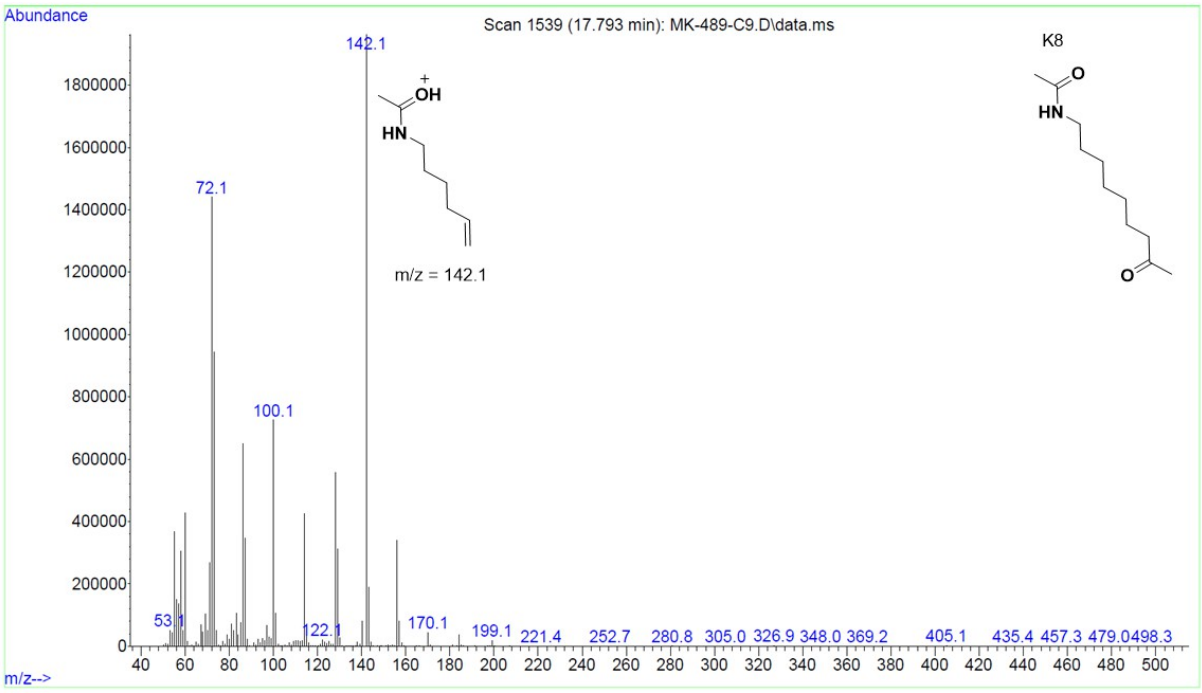
Abundance
Scan 1539 (17.793 min): MK-489-C9.D\data.ms
142.1
72.1
100.1
53.1
122.1
170.1
199.1
221.4
252.7
280.8
305.0
326.9
348.0
369.2
405.1
435.4
457.3
479.0498.3
m/z = 142.1
K8
m/z-->

Decylammonium Oxidation

According to the general oxidation protocol, decylammonium tetrafluoroborate (**S14**, 4.53 mg, 18.5 µmol, 1.0 equiv.) was oxidized by Fe-Br **2** and Fe-Twe **4**. After the aqueous workup for primary ammonium ions, the mixture was analyzed by GC and GC-MS.

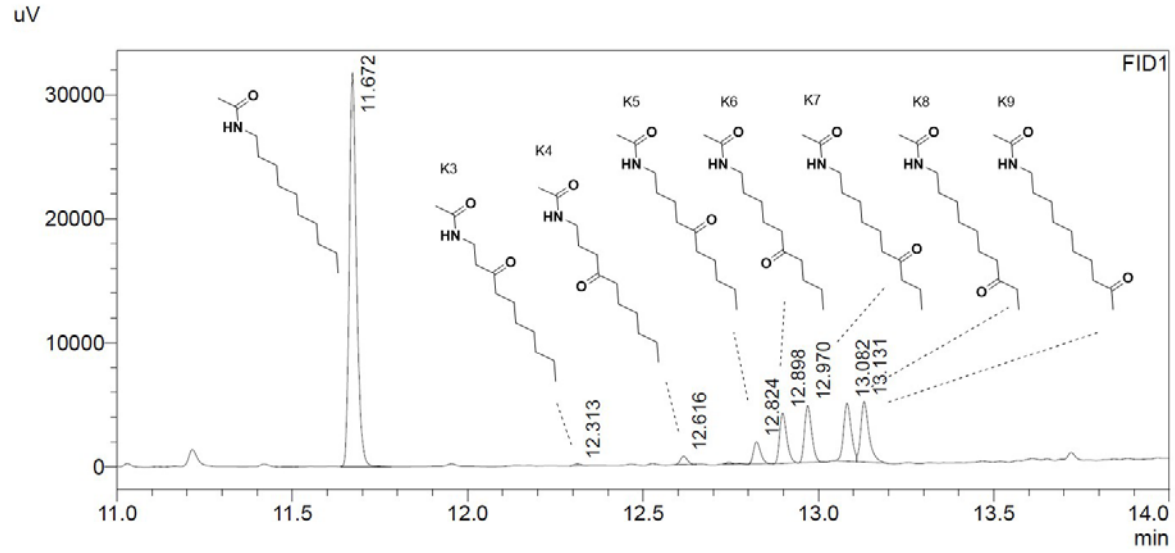

GC chromatogram of the Fe-Br **2** catalyzed oxidation of decylammonium tetrafluoroborate.

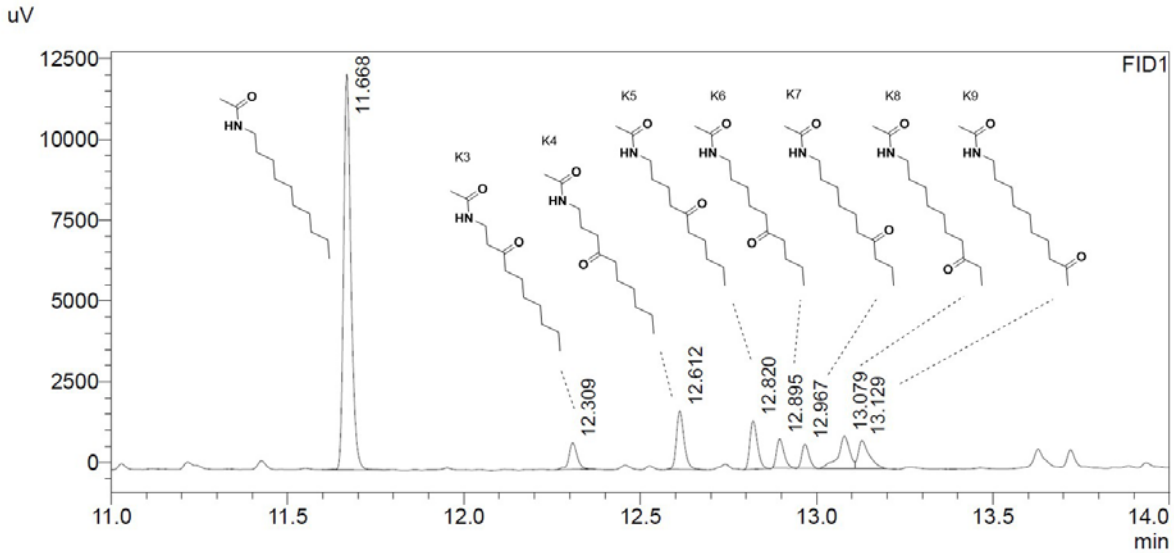

GC chromatogram of the Fe-Twe **4** catalyzed oxidation of decylammonium tetrafluoroborate.

GC-MS chromatogram and spectra of the Fe-Twe **4** catalyzed oxidation of decylammonium tetrafluoroborate (**S14**). The different oxidation products were assigned according to their fragmentation pattern.

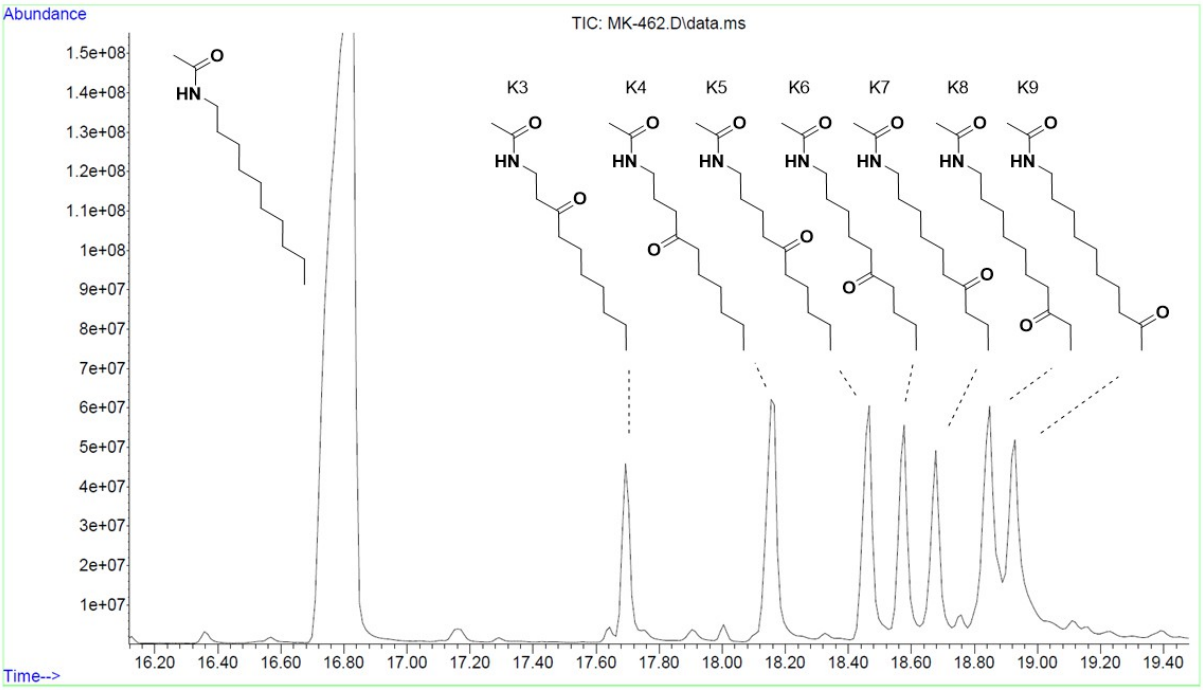

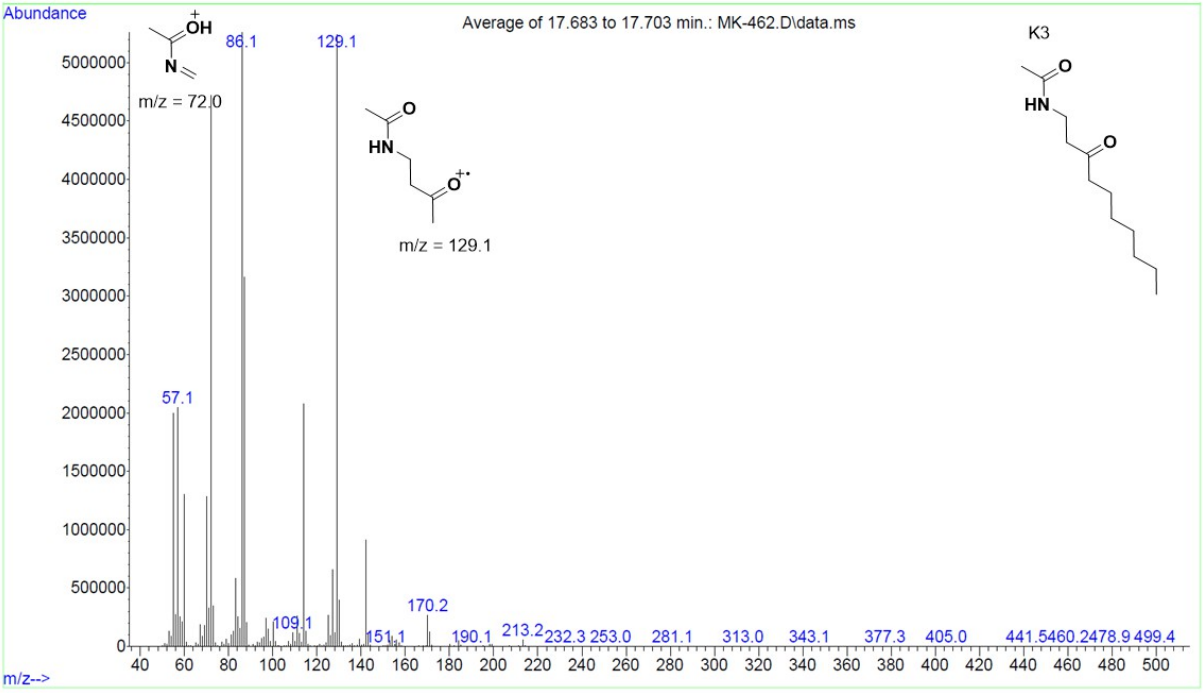

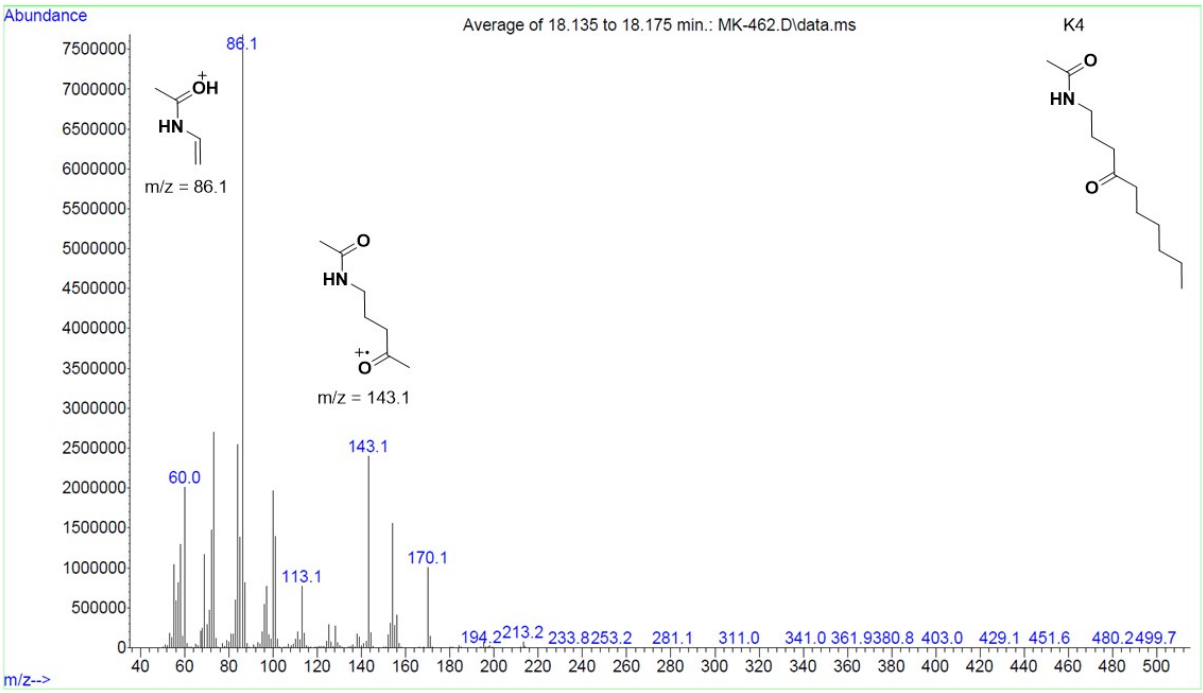
Abundance
Average of 18.135 to 18.175 min.: MK-462.D\data.ms
K4
86.1
m/z = 86.1
m/z = 143.1
143.1
60.0
113.1
170.1
m/z-->

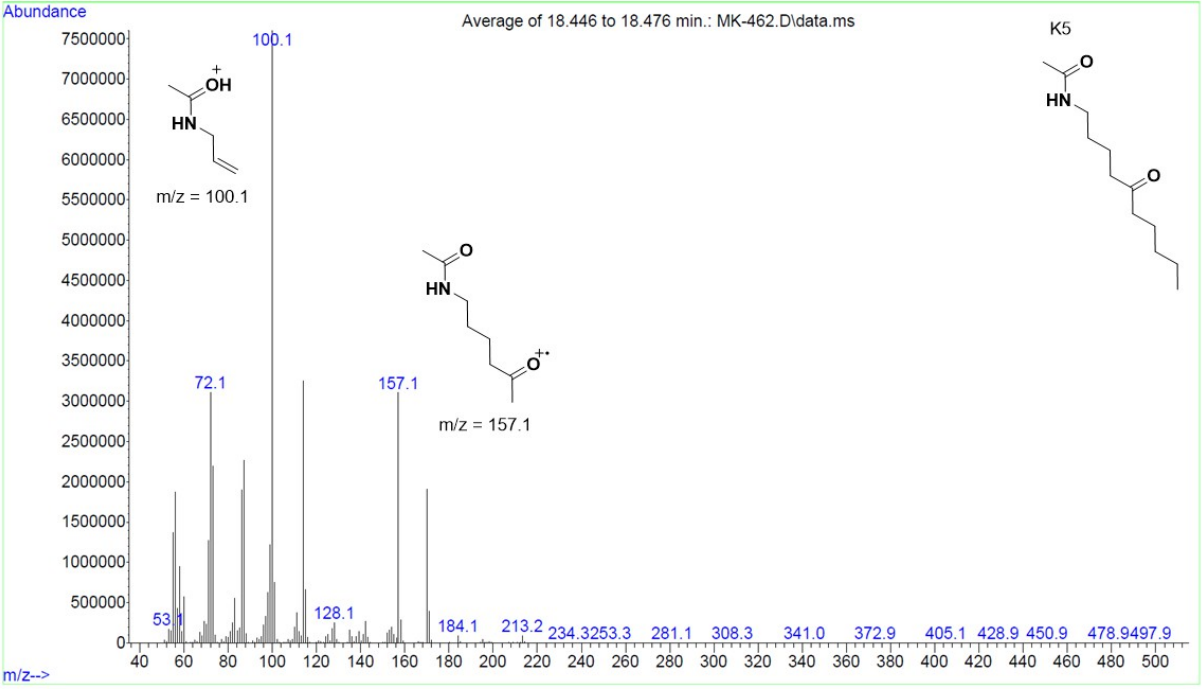
Abundance
Average of 18.446 to 18.476 min.: MK-462.D\data.ms
K5
100.1
m/z = 100.1
m/z = 157.1
72.1
157.1
128.1
m/z-->

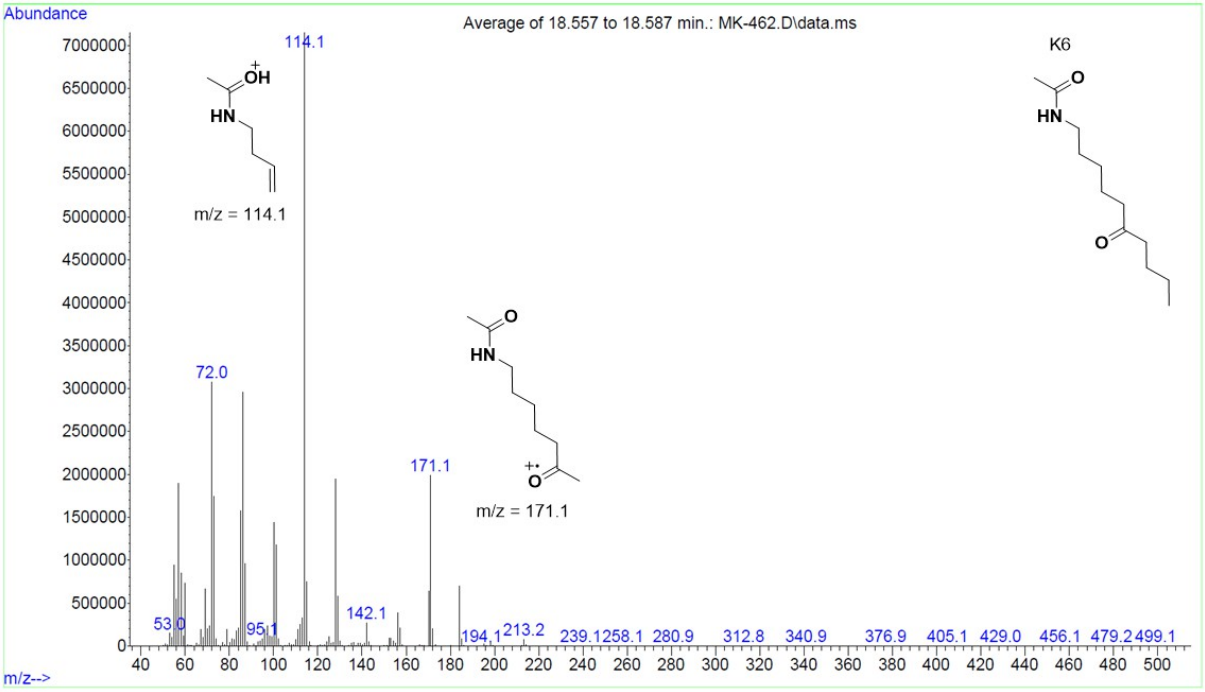
Abundance
Average of 18.557 to 18.587 min.: MK-462.D\data.ms
K6
m/z = 114.1
m/z = 171.1
114.1
72.0
171.1
142.1
53.0
95.1
194.1
213.2
m/z-->

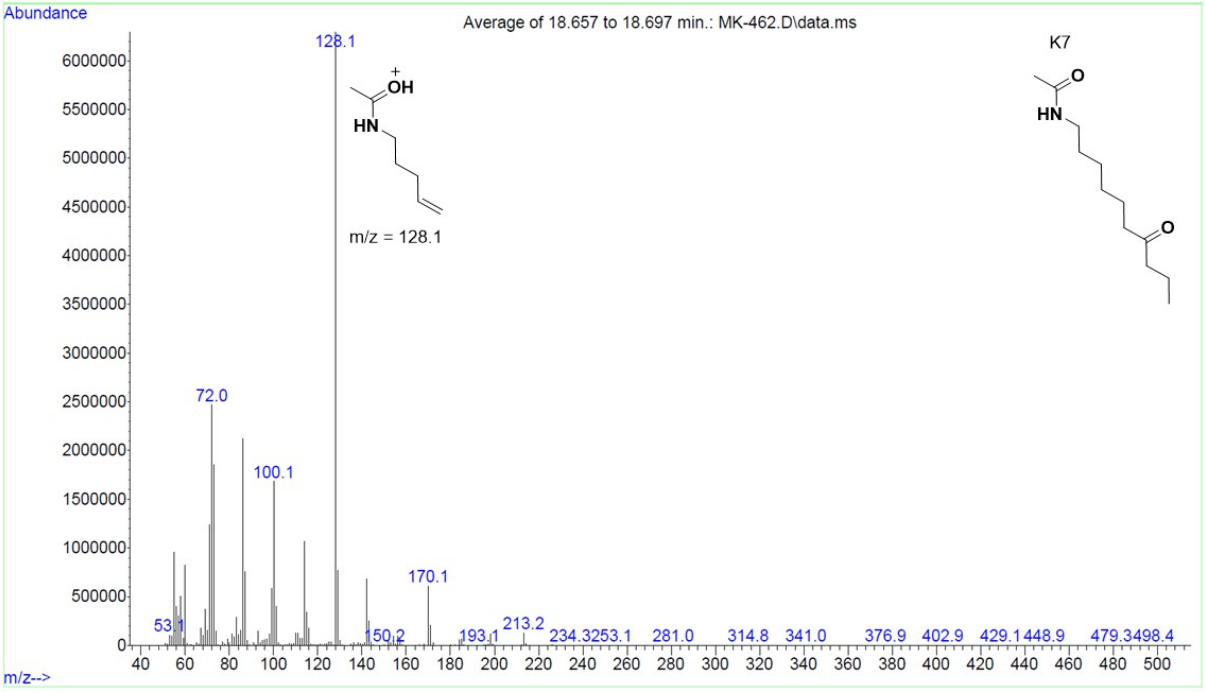
Abundance
Average of 18.657 to 18.697 min.: MK-462.D\data.ms
K7
m/z = 128.1
128.1
72.0
100.1
170.1
53.1
150.2
193.1
213.2
m/z-->

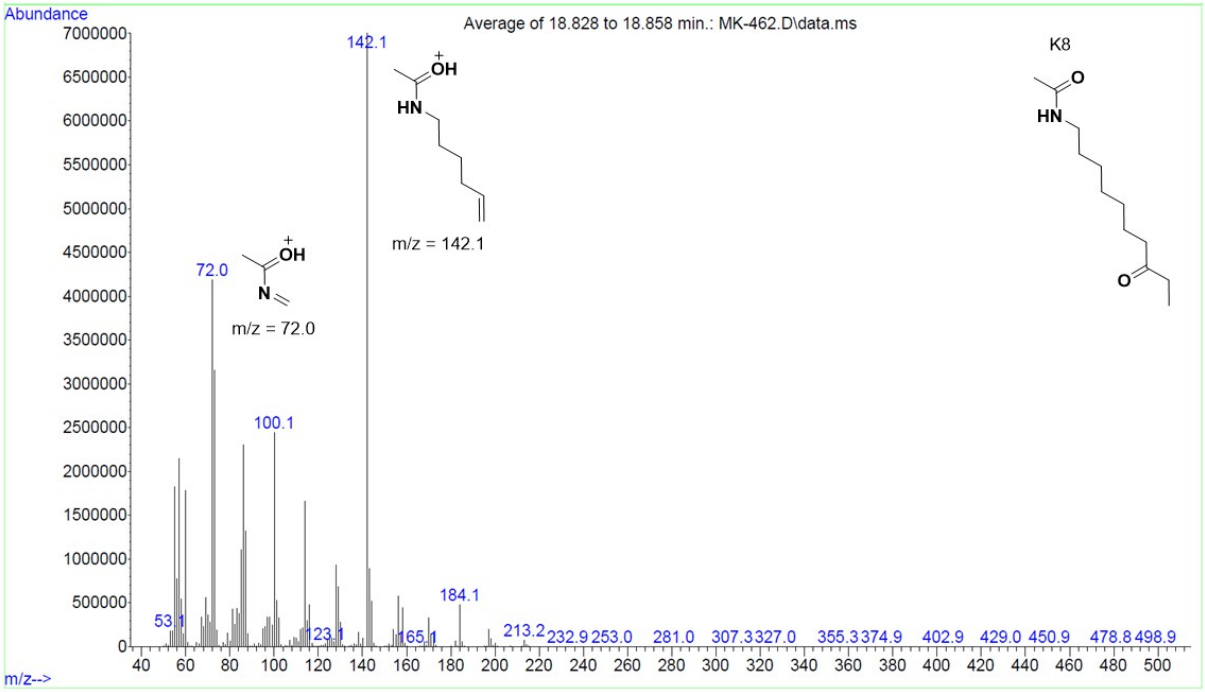
Abundance
Average of 18.828 to 18.858 min.: MK-462.D\data.ms
142.1
72.0
100.1
184.1
53.1
123.1
165.1
213.2
m/z = 142.1
m/z = 72.0
K8
m/z-->

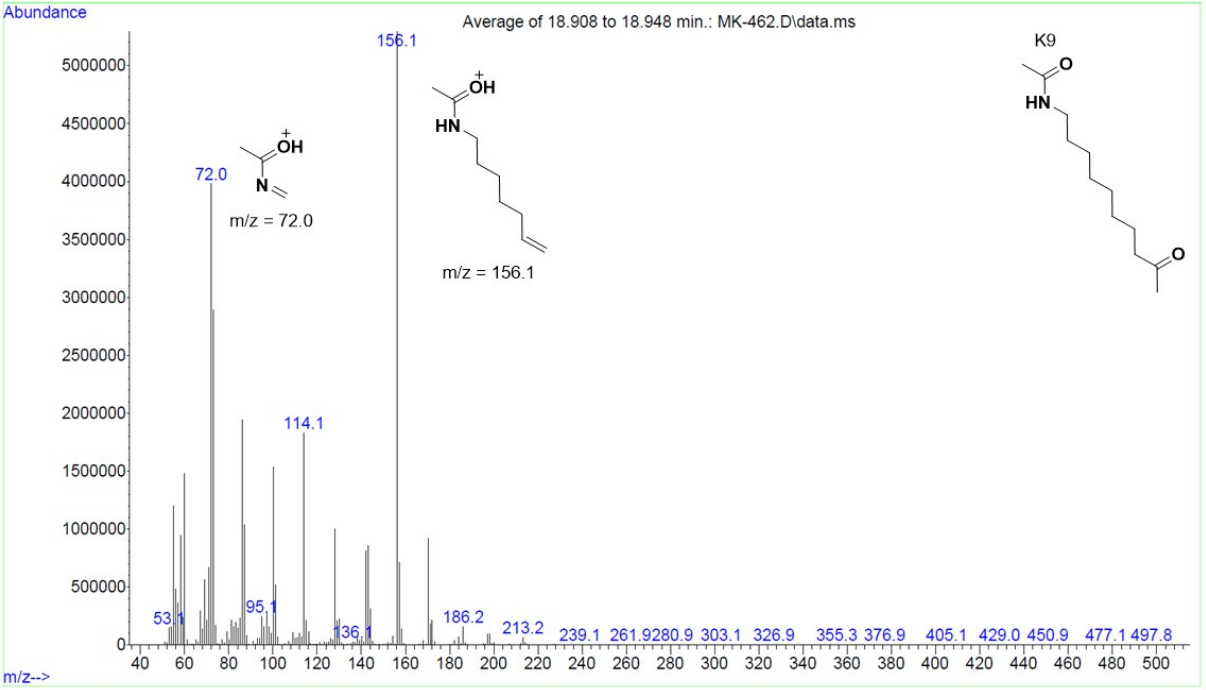
Abundance
Average of 18.908 to 18.948 min.: MK-462.D\data.ms
156.1
72.0
114.1
53.1
95.1
136.1
186.2
213.2
m/z = 156.1
m/z = 72.0
K9
m/z-->

Undecylammonium Oxidation

According to the general oxidation protocol, undecylammonium tetrafluoroborate (**S15**, 4.79 mg, 18.5 µmol, 1.0 equiv.) was oxidized by Fe-Br **2** and Fe-Twe **4**. After the aqueous workup for primary ammonium ions, the mixture was analyzed by GC and GC-MS.

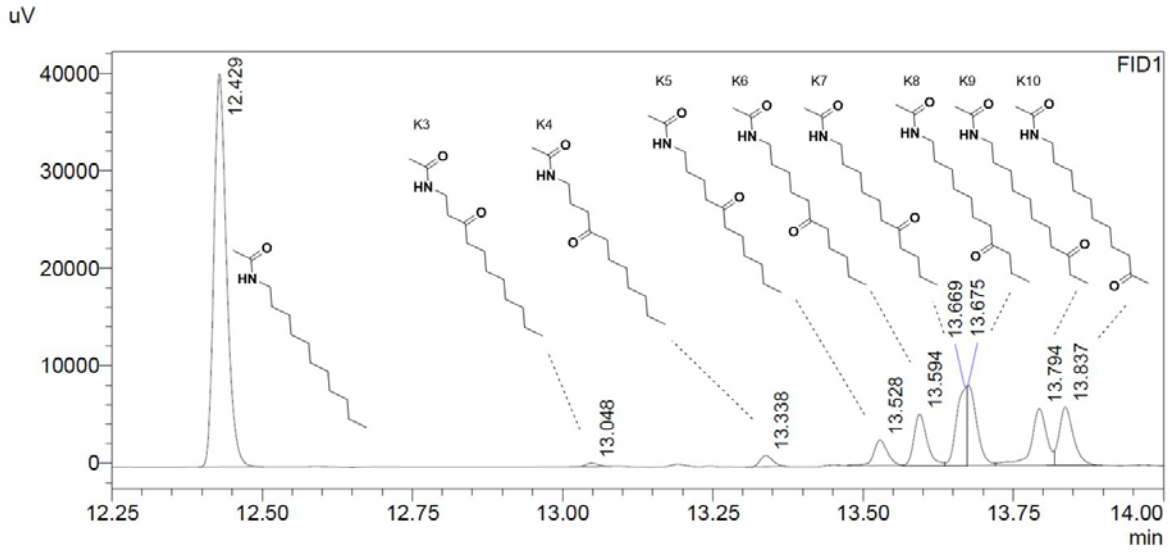

GC chromatogram of the Fe-Br **2** catalyzed oxidation of undecylammonium tetrafluoroborate.

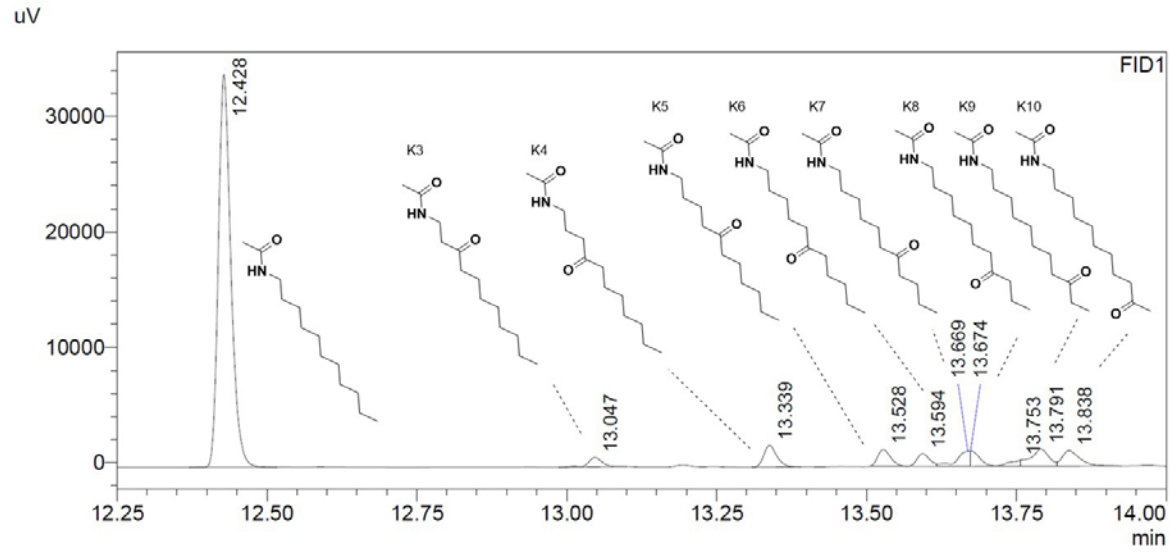

GC chromatogram of the Fe-Twe **4** catalyzed oxidation of undecylammonium tetrafluoroborate.

GC-MS chromatogram and spectra of the Fe-Twe **4** catalyzed oxidation of undecylammonium tetrafluoroborate (**S15**). The different oxidation products were assigned according to their fragmentation pattern.

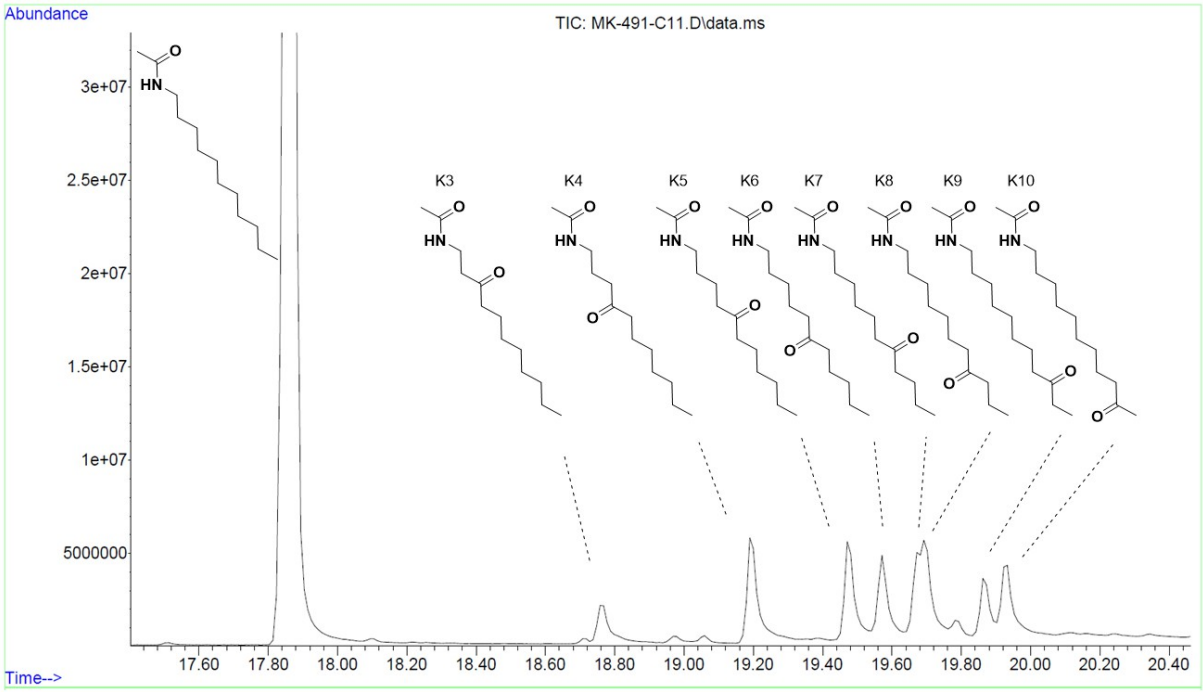

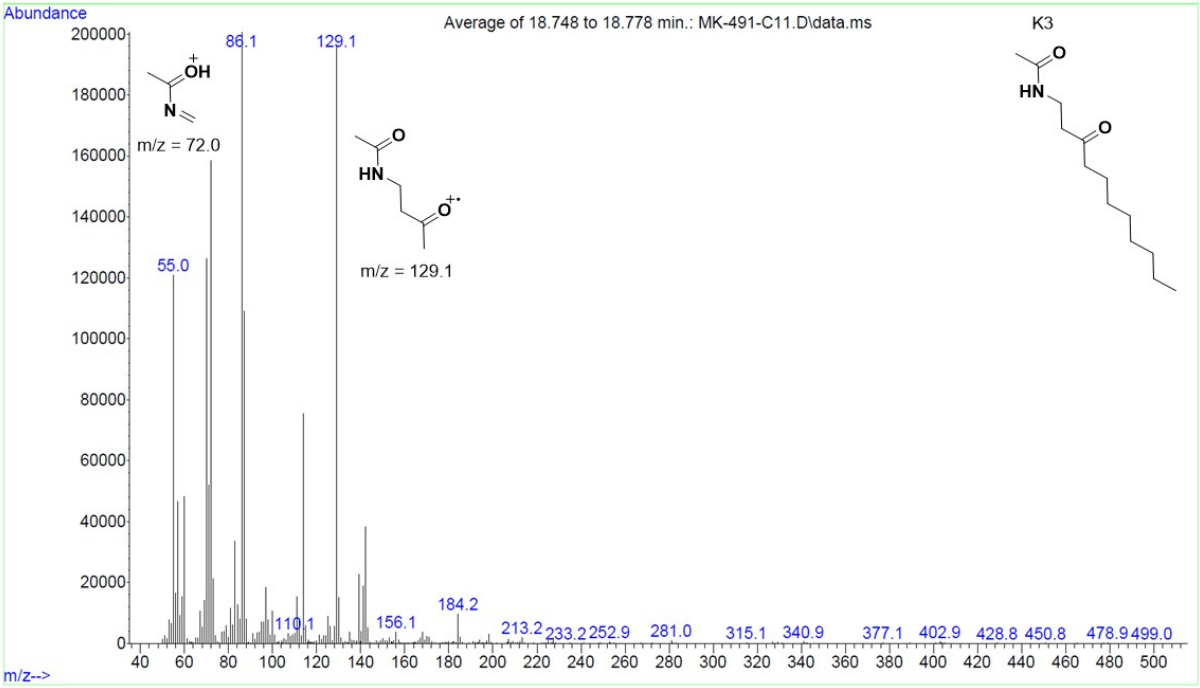

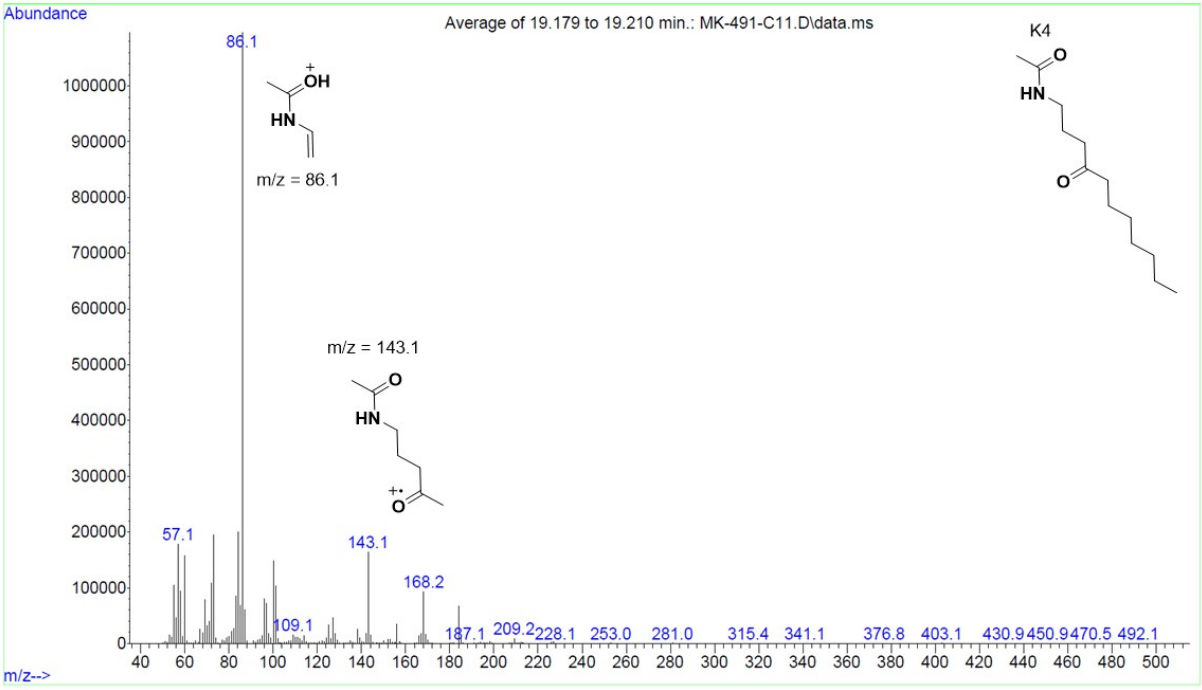
Abundance
Average of 19.179 to 19.210 min.: MK-491-C11.D\data.ms
K4
86.1
m/z = 86.1
m/z = 143.1
57.1
143.1
168.2
109.1
187.1
209.2
228.1
253.0
281.0
315.4
341.1
376.8
403.1
430.9
450.9
470.5
492.1
m/z-->

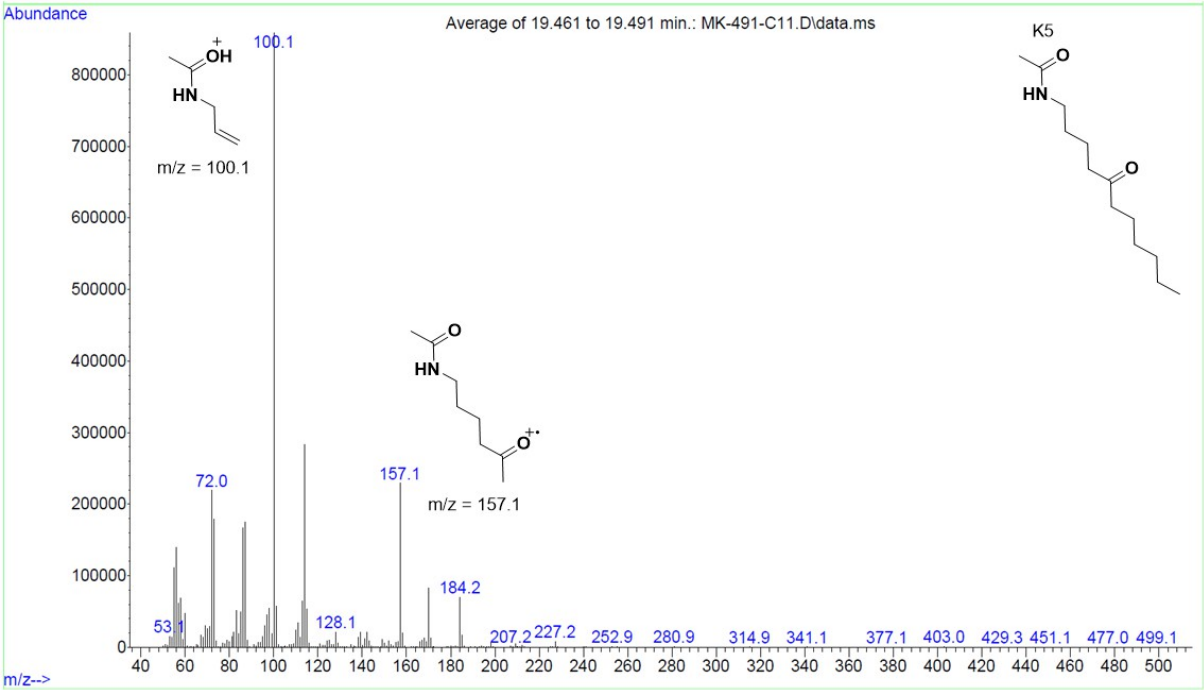
Abundance
Average of 19.461 to 19.491 min.: MK-491-C11.D\data.ms
K5
100.1
m/z = 100.1
m/z = 157.1
72.0
157.1
184.2
53.1
128.1
207.2
227.2
252.9
280.9
314.9
341.1
377.1
403.0
429.3
451.1
477.0
499.1
m/z-->

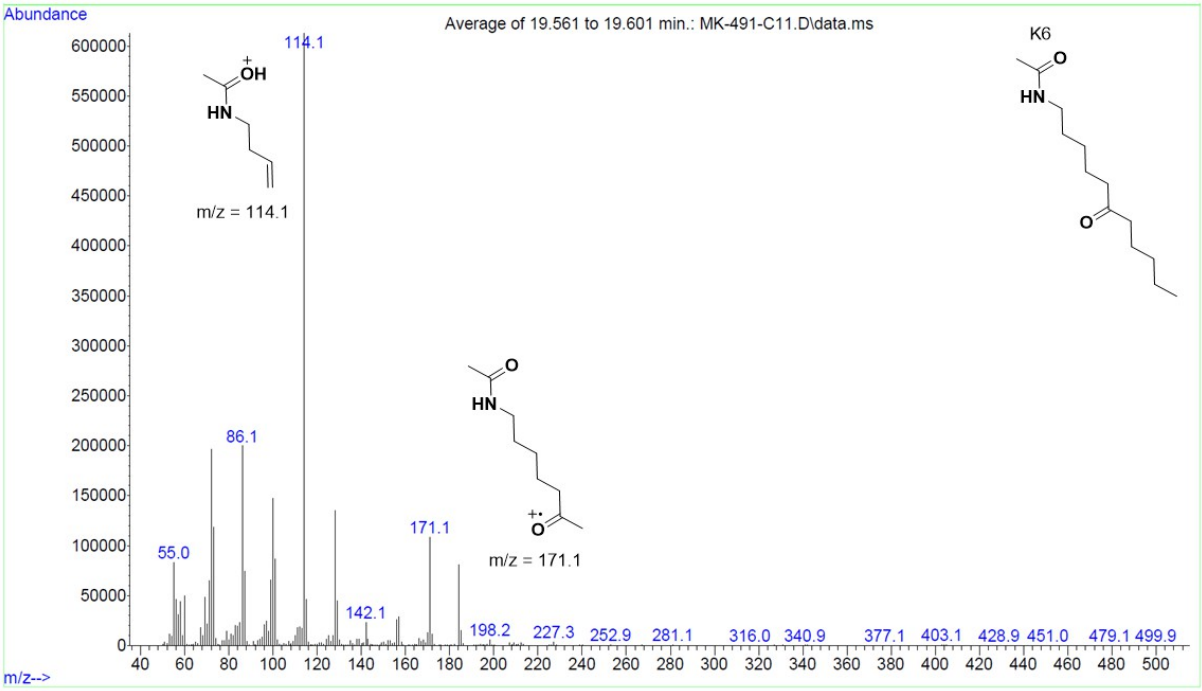
Abundance
Average of 19.561 to 19.601 min.: MK-491-C11.D\data.ms
K6
114.1
m/z = 114.1
86.1
55.0
171.1
m/z = 171.1
142.1
198.2
227.3
252.9
281.1
316.0
340.9
377.1
403.1
428.9
451.0
479.1
499.9
m/z-->

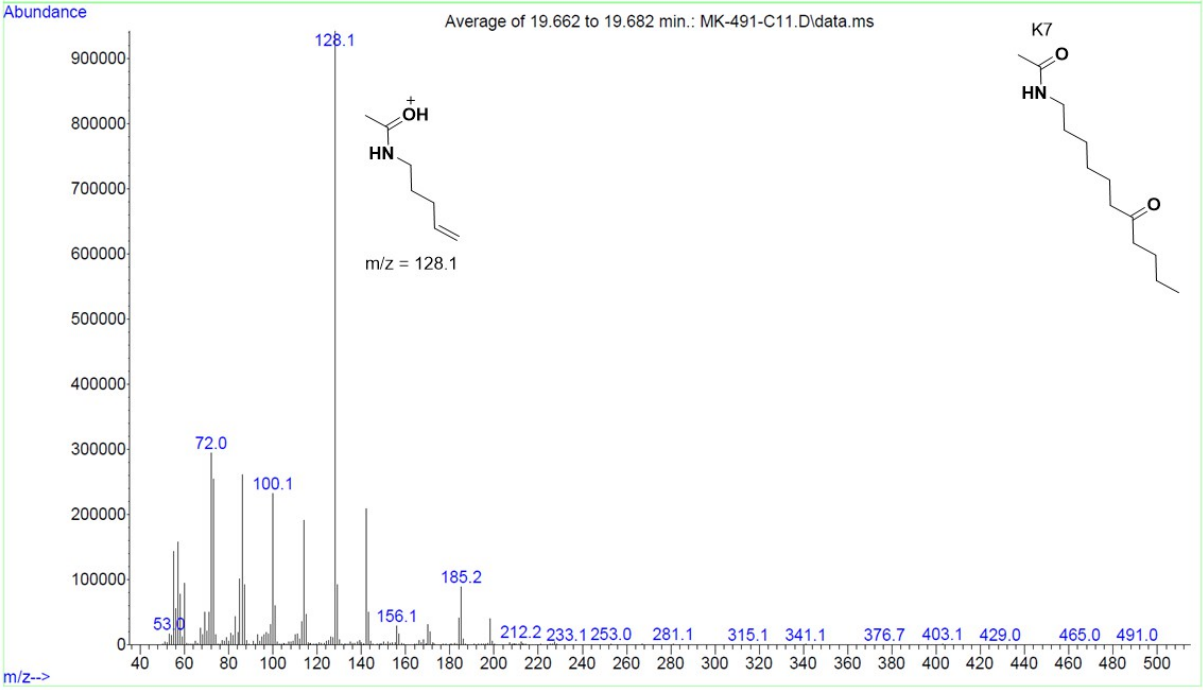
Abundance
Average of 19.662 to 19.682 min.: MK-491-C11.D\data.ms
K7
128.1
m/z = 128.1
72.0
100.1
185.2
53.0
156.1
212.2
233.1
253.0
281.1
315.1
341.1
376.7
403.1
429.0
465.0
491.0
m/z-->

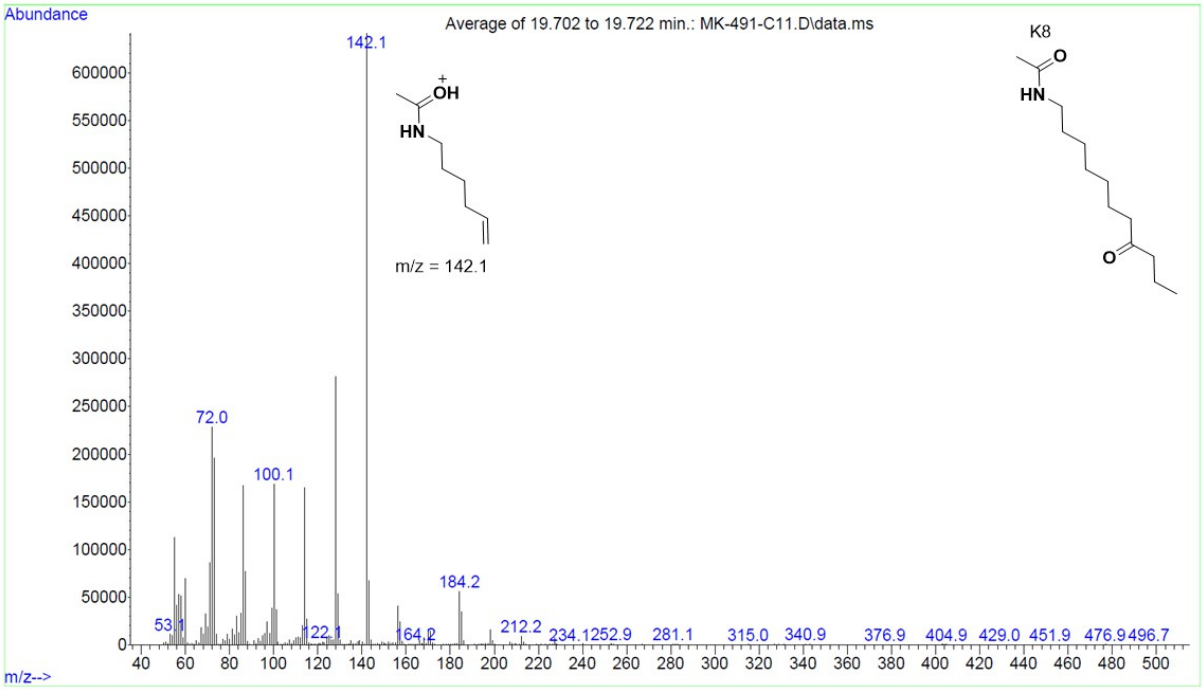
Abundance
Average of 19.702 to 19.722 min.: MK-491-C11.D\data.ms
K8
142.1
m/z = 142.1
72.0
100.1
184.2
m/z-->

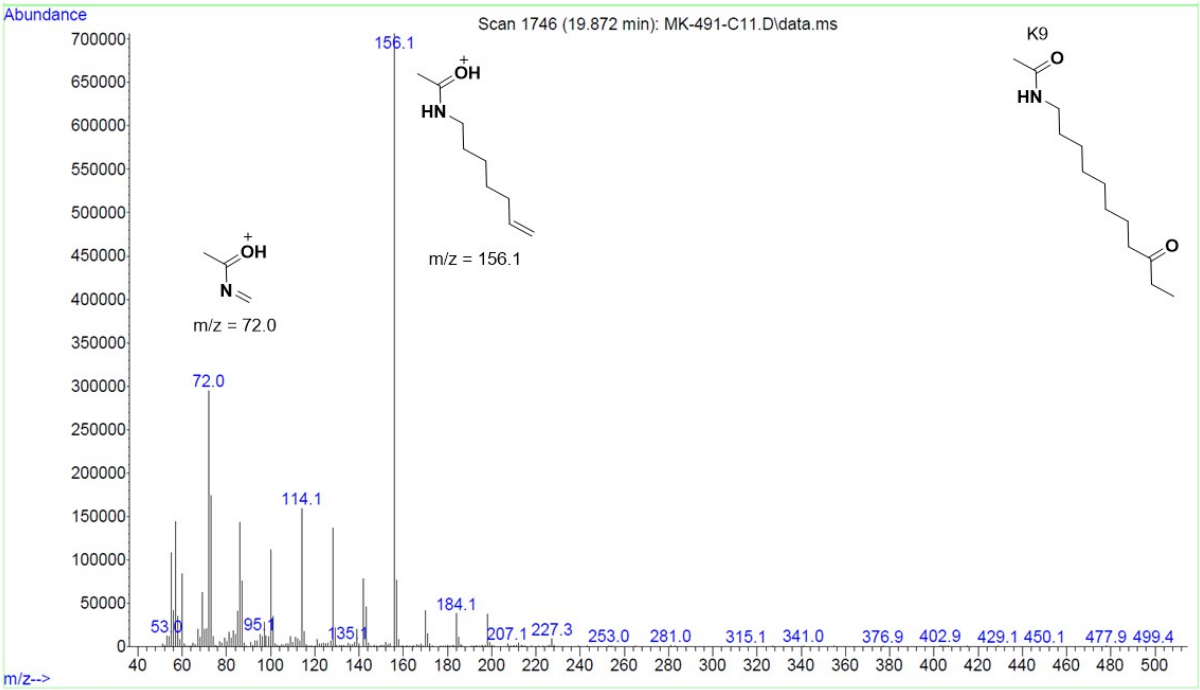
Abundance
Scan 1746 (19.872 min): MK-491-C11.D\data.ms
K9
156.1
m/z = 156.1
m/z = 72.0
72.0
114.1
184.1
m/z-->

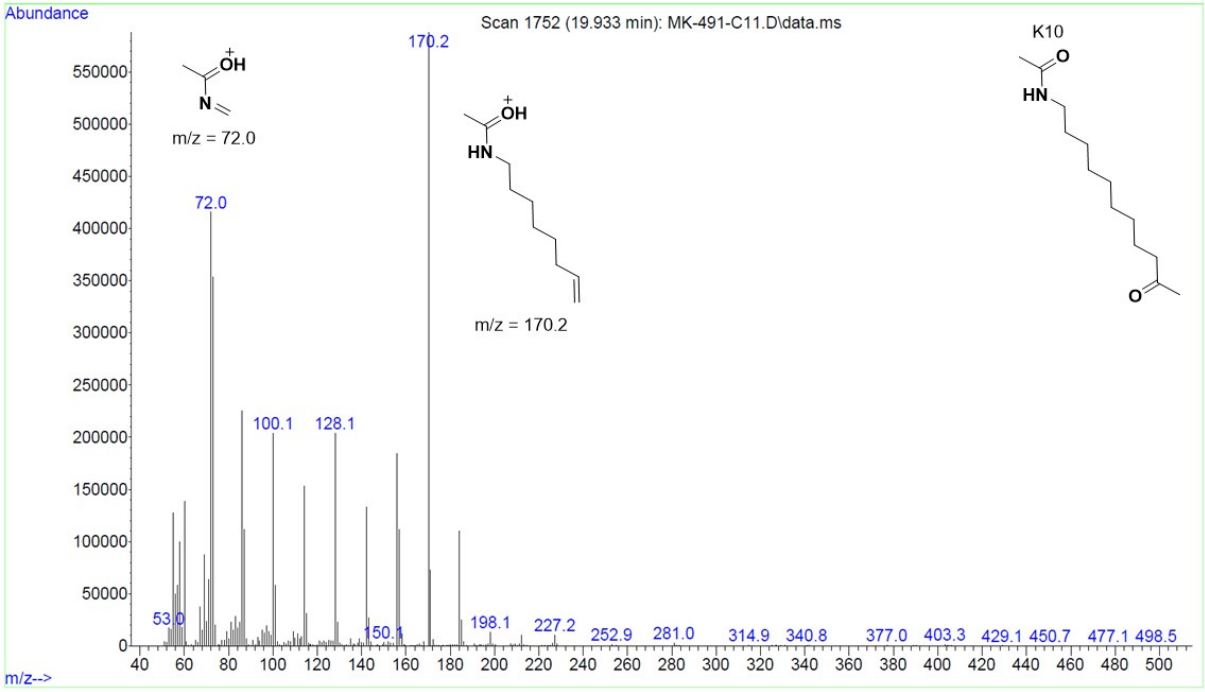
Abundance
Scan 1752 (19.933 min): MK-491-C11.D\data.ms
K10
m/z = 72.0
m/z = 170.2
72.0
100.1
128.1
170.2
198.1
227.2
m/z-->

Dodecylammonium Oxidation

According to the general oxidation protocol, dodecylammonium tetrafluoroborate (**S16**, 5.05 mg, 18.5 µmol, 1.0 equiv.) was oxidized by Fe-Br **2** and Fe-Twe **4**. After the aqueous workup for primary ammonium ions, the mixture was analyzed by GC and GC-MS.

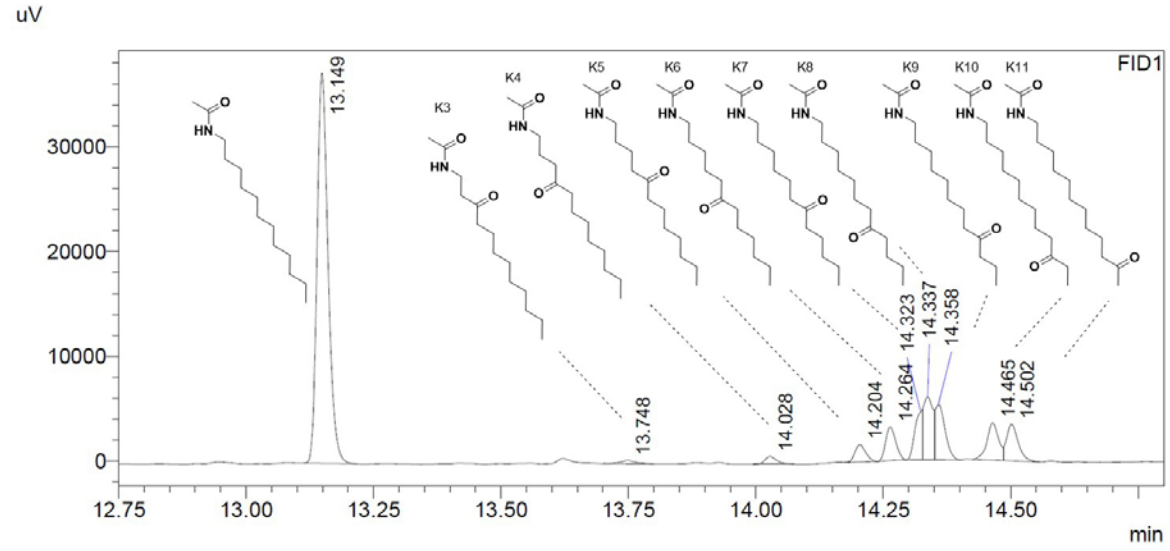

GC chromatogram of the Fe-Br **2** catalyzed oxidation of dodecylammonium tetrafluoroborate.

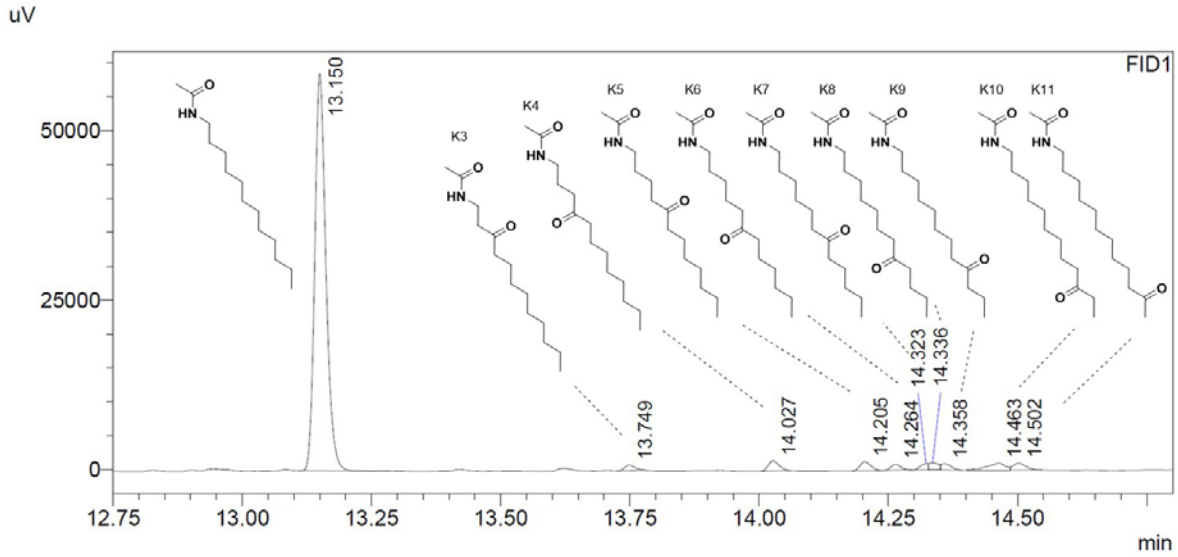

GC chromatogram of the Fe-Twe **4**catalyzed oxidation of dodecylammonium tetrafluoroborate.

GC-MS chromatogram and spectra of the Fe-Twe **4** catalyzed oxidation of docylammonium tetrafluoroborate (**S16**). The different oxidation products were assigned according to their fragmentation pattern.

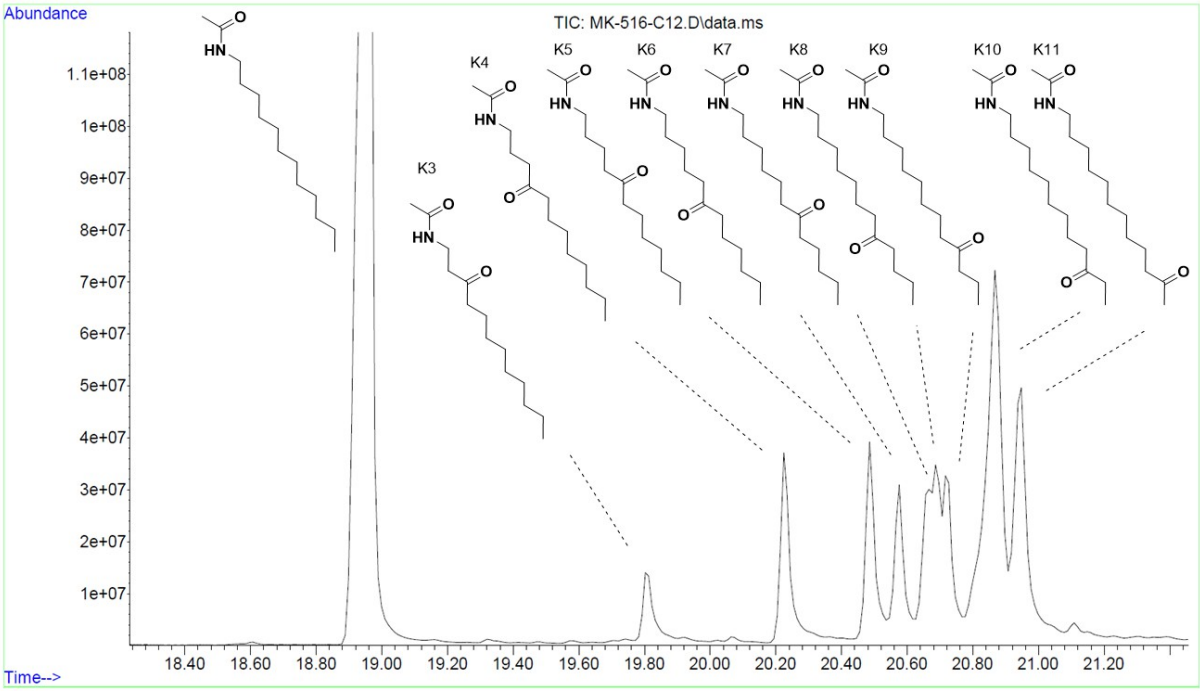

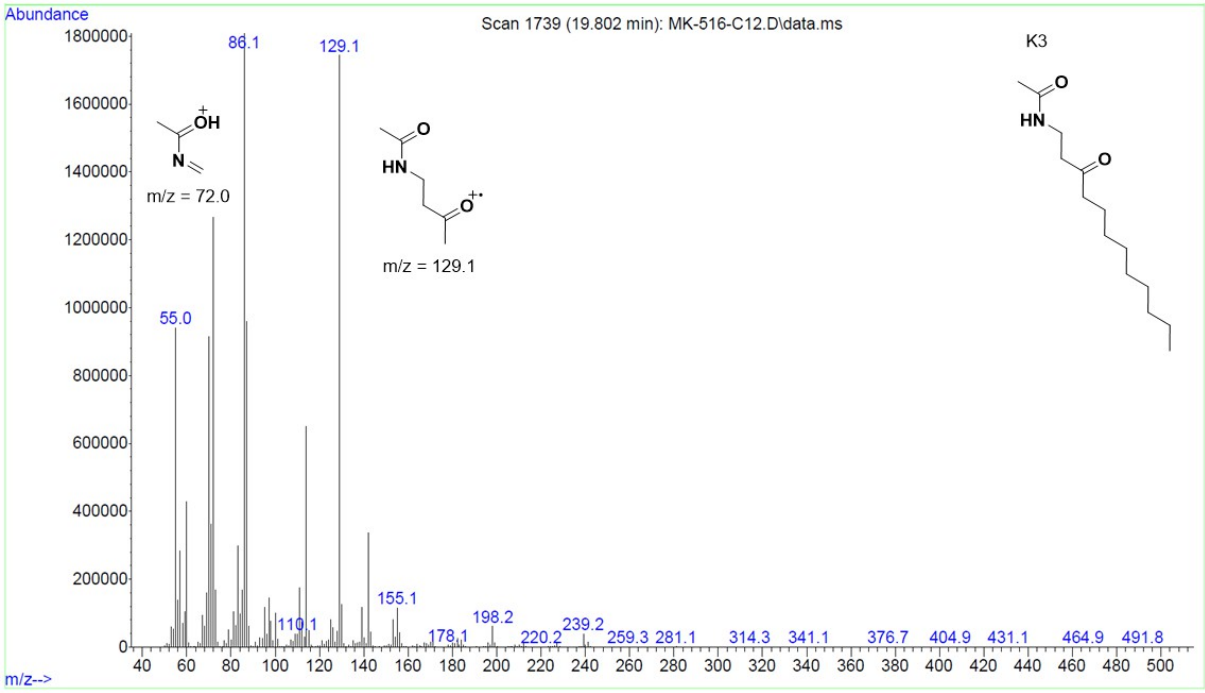

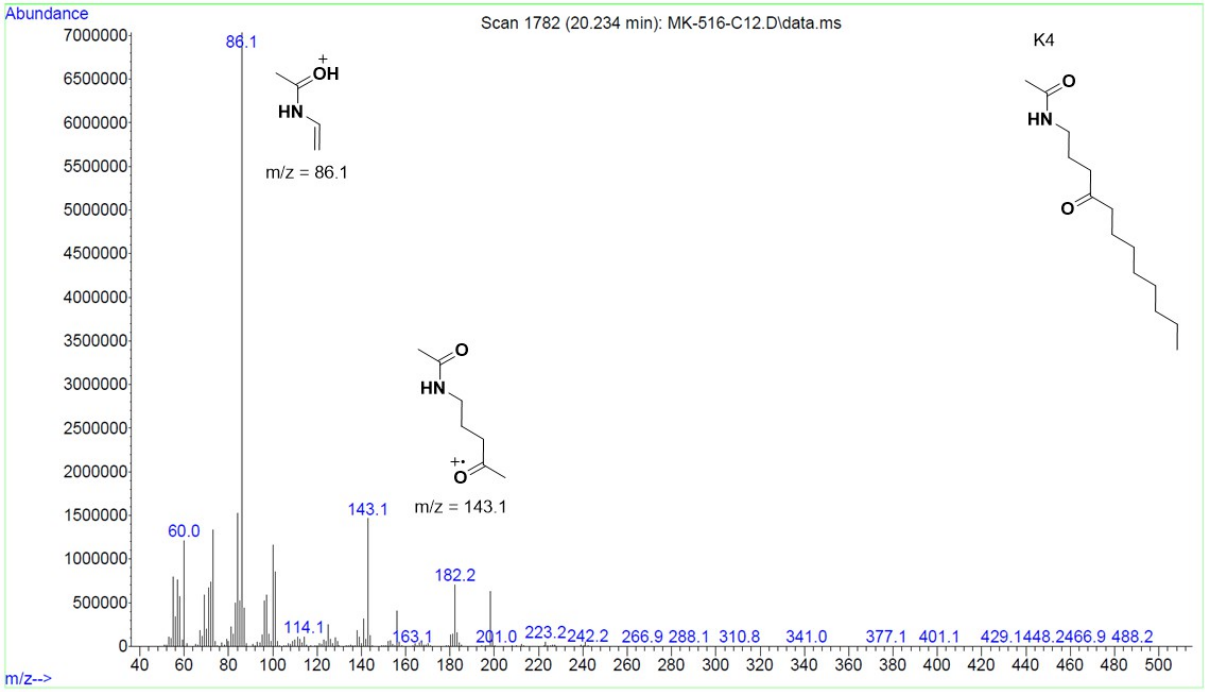
Abundance
Scan 1782 (20.234 min): MK-516-C12.D\data.ms
K4
86.1
m/z = 86.1
m/z = 143.1
143.1
60.0
182.2
114.1
m/z-->

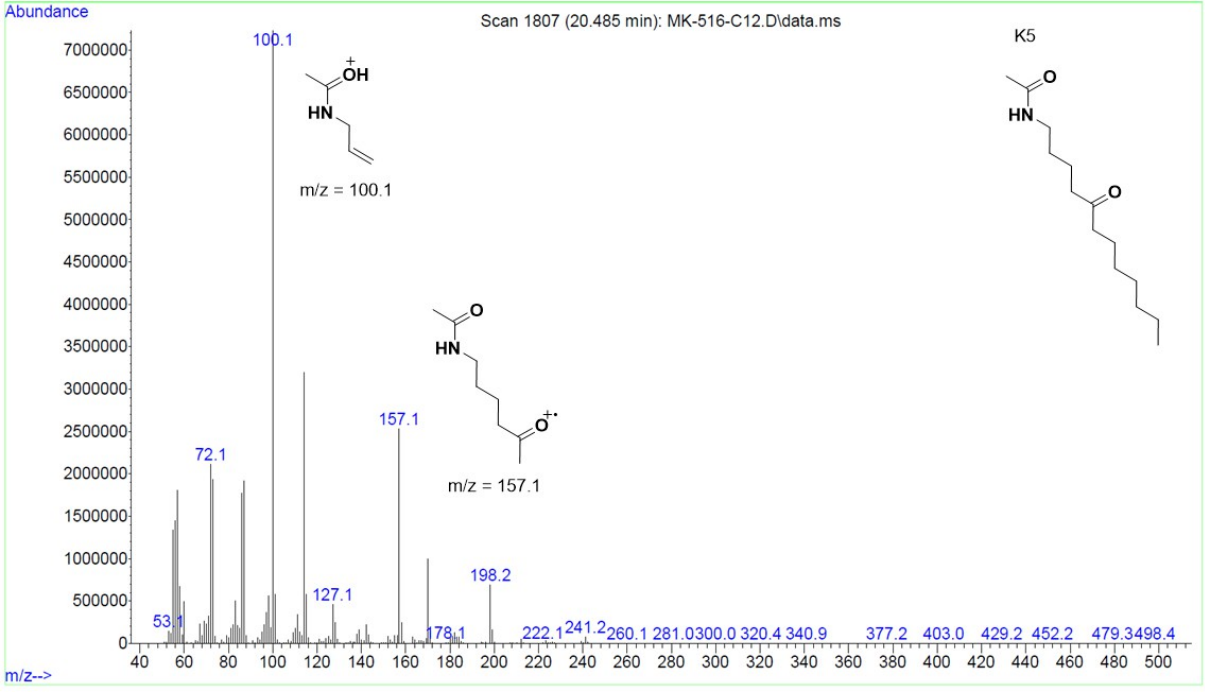
Abundance
Scan 1807 (20.485 min): MK-516-C12.D\data.ms
K5
100.1
m/z = 100.1
m/z = 157.1
157.1
72.1
198.2
127.1
53.1
m/z-->

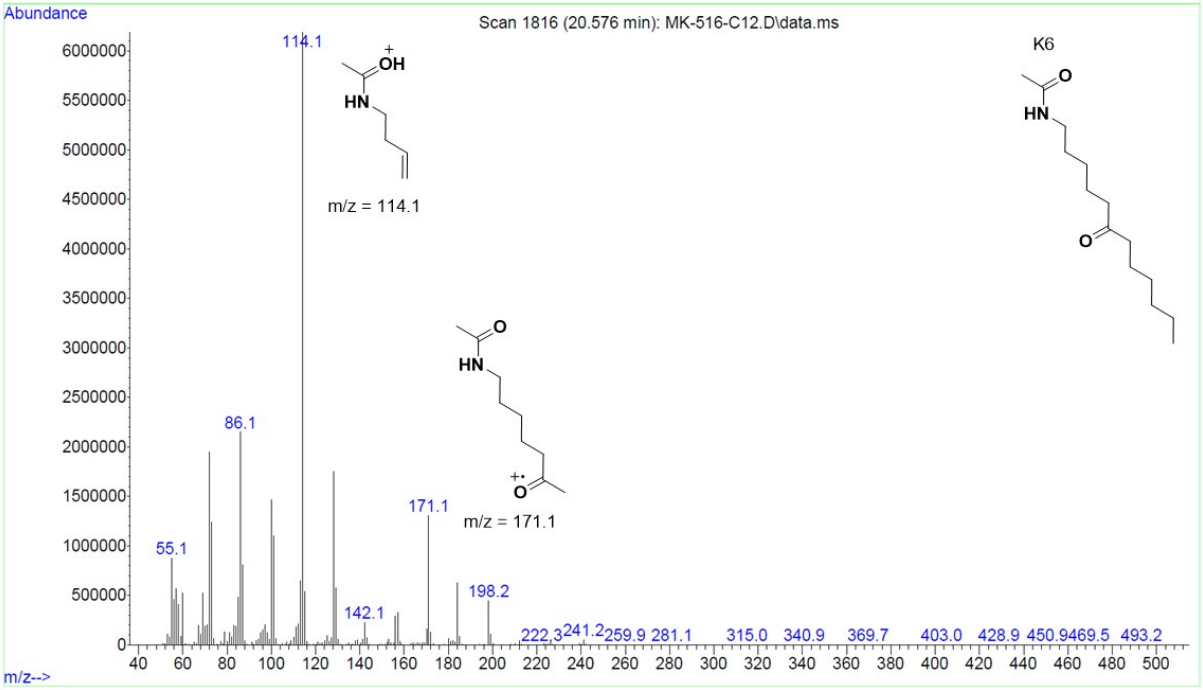
Abundance
Scan 1816 (20.576 min): MK-516-C12.D\data.ms
K6
m/z = 114.1
m/z = 171.1
114.1
86.1
55.1
171.1
142.1
198.2
m/z-->

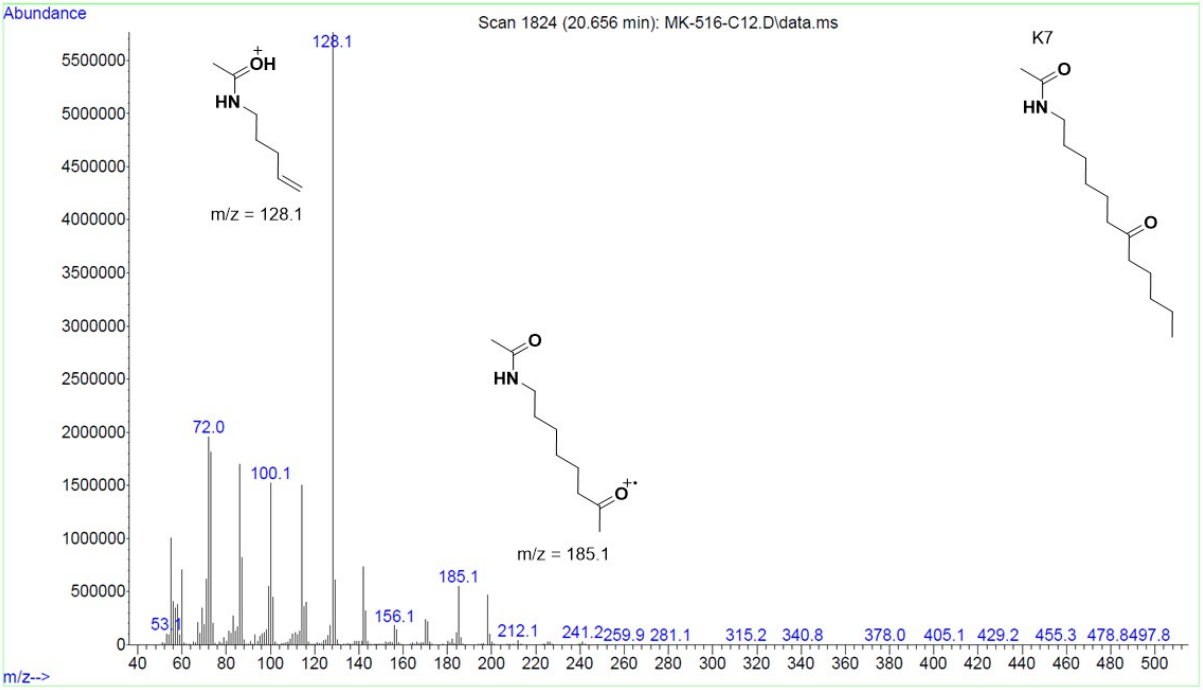
Abundance
Scan 1824 (20.656 min): MK-516-C12.D\data.ms
K7
m/z = 128.1
m/z = 185.1
128.1
72.0
100.1
185.1
53.1
156.1
212.1
m/z-->

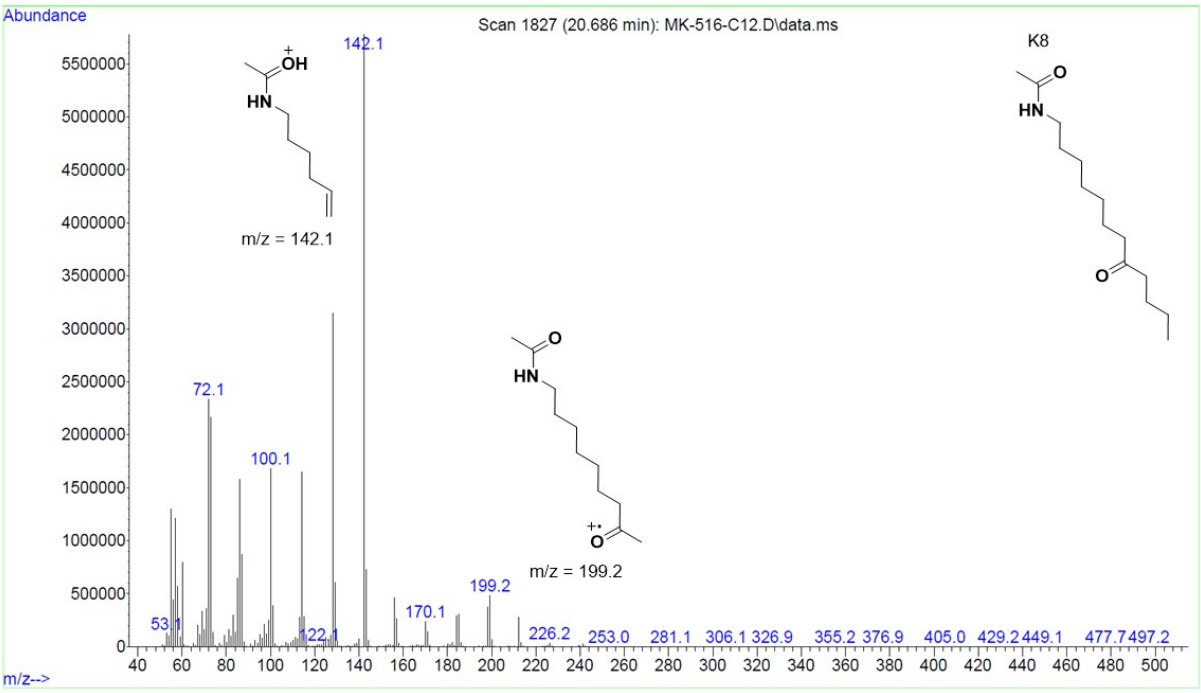
Abundance
Scan 1827 (20.686 min): MK-516-C12.D\data.ms
K8
142.1
72.1
100.1
199.2
170.1
m/z = 142.1
m/z = 199.2
m/z-->

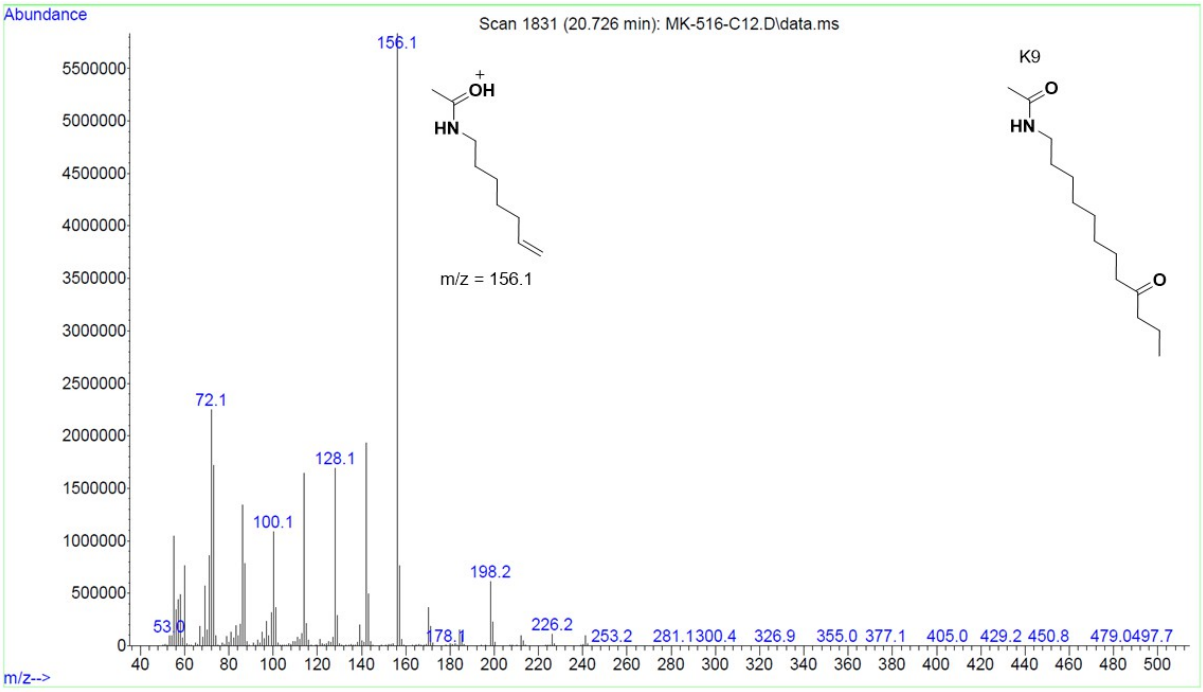
Abundance
Scan 1831 (20.726 min): MK-516-C12.D\data.ms
K9
156.1
72.1
128.1
100.1
198.2
m/z = 156.1
m/z-->

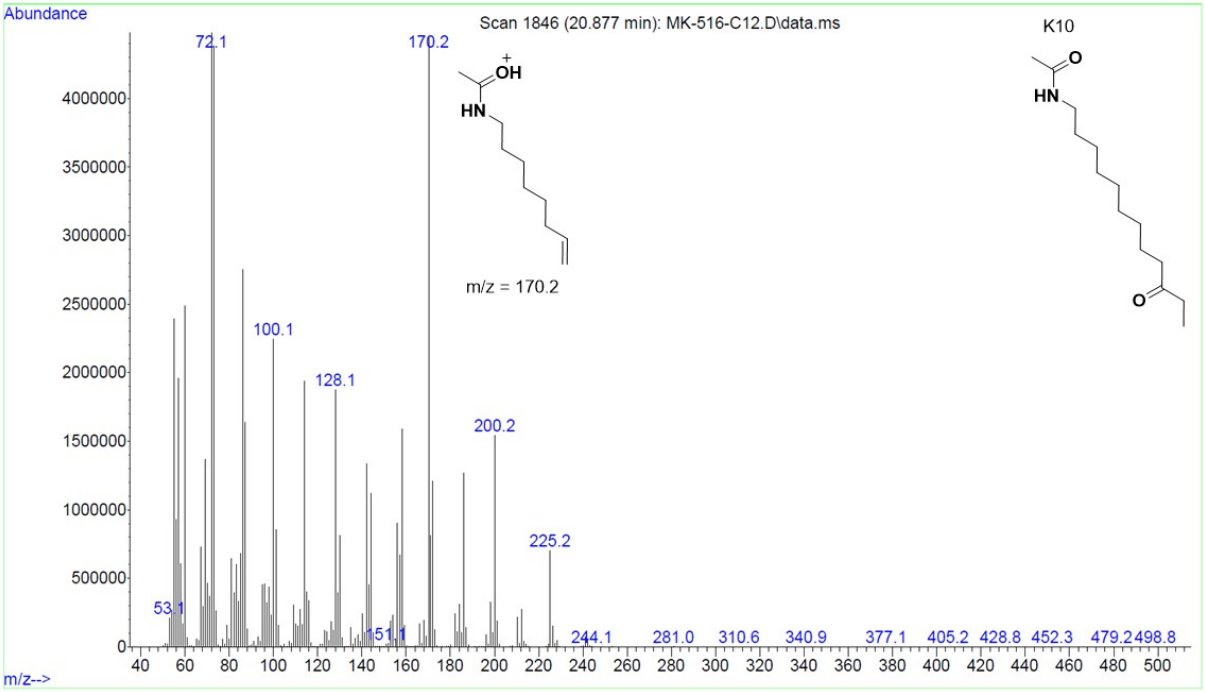
Abundance
Scan 1846 (20.877 min): MK-516-C12.D\data.ms
K10
72.1
170.2
100.1
128.1
200.2
225.2
53.1
151.1
244.1
281.0
310.6
340.9
377.1
405.2
428.8
452.3
479.2
498.8
m/z = 170.2
m/z-->

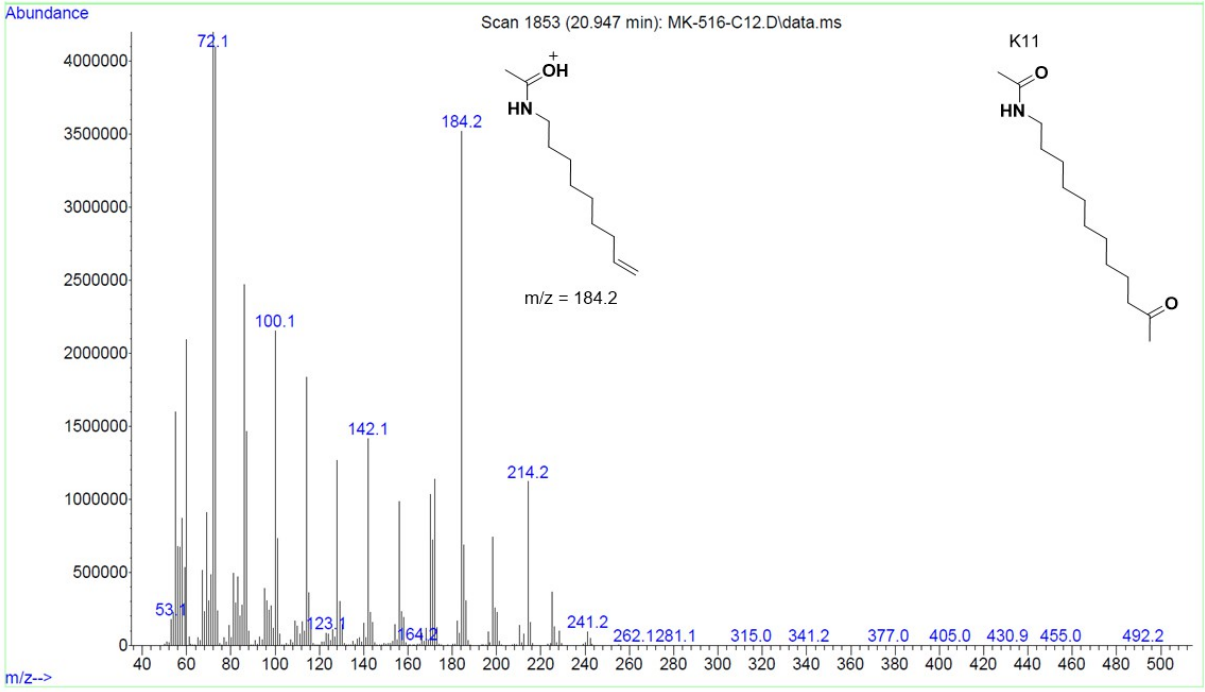
Abundance
Scan 1853 (20.947 min): MK-516-C12.D\data.ms
K11
72.1
184.2
100.1
142.1
214.2
53.1
123.1
164.2
241.2
262.1
281.1
315.0
341.2
377.0
405.0
430.9
455.0
492.2
m/z = 184.2
m/z-->

Tetradecylammonium Oxidation

According to the general oxidation protocol, tetradecylammonium tetrafluoroborate (**S17**, 5.57 mg, 18.5 µmol, 1.0 equiv.) was oxidized by Fe-Br **2** and Fe-Twe **4**. After the aqueous workup for primary ammonium ions, the mixture was analyzed by GC and GC-MS.

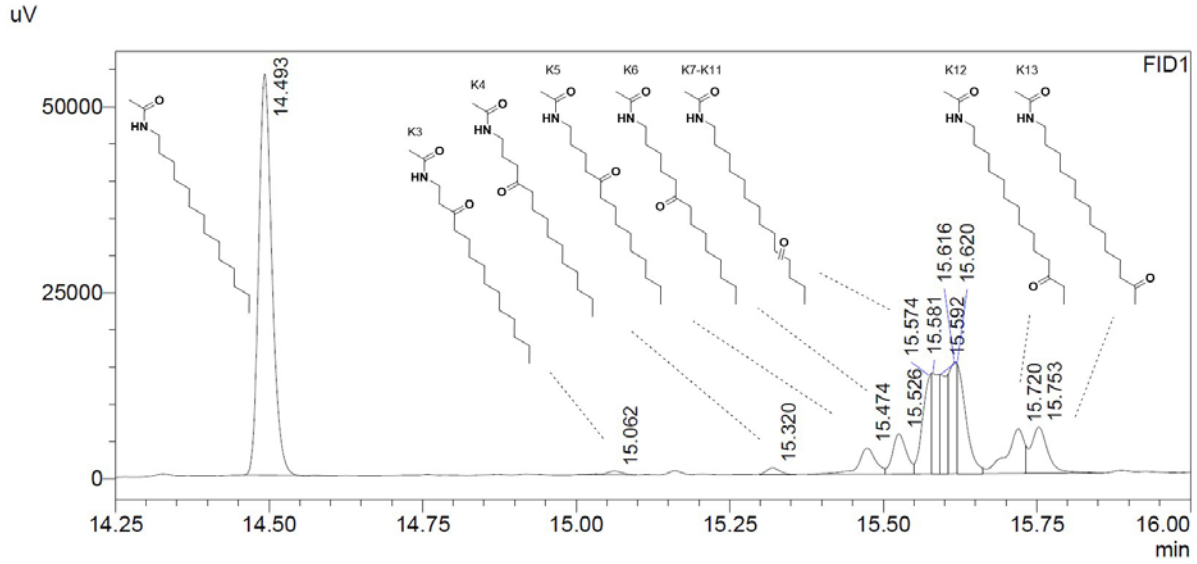

GC chromatogram of the Fe-Br **2** catalyzed oxidation of tetradecylammonium tetrafluoroborate.

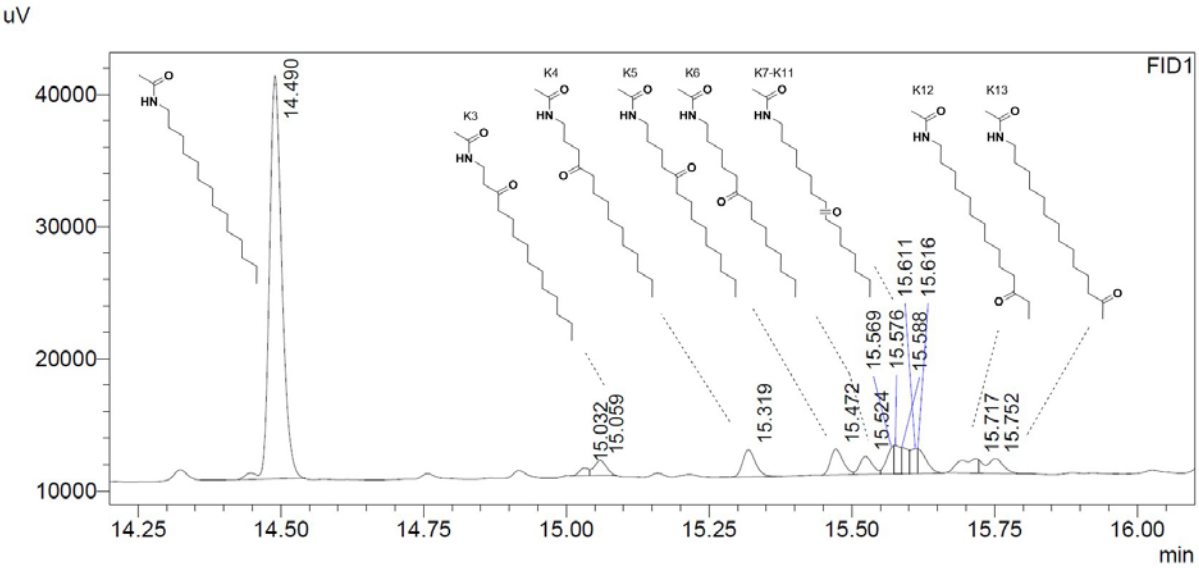

GC chromatogram of the Fe-Twe **4** catalyzed oxidation of tetradecylammonium tetrafluoroborate.

GC-MS chromatogram and spectra of the Fe-Twe **4** catalyzed oxidation of tetradecylammonium tetrafluoroborate (**S17**). The different oxidation products were assigned according to their fragmentation pattern.

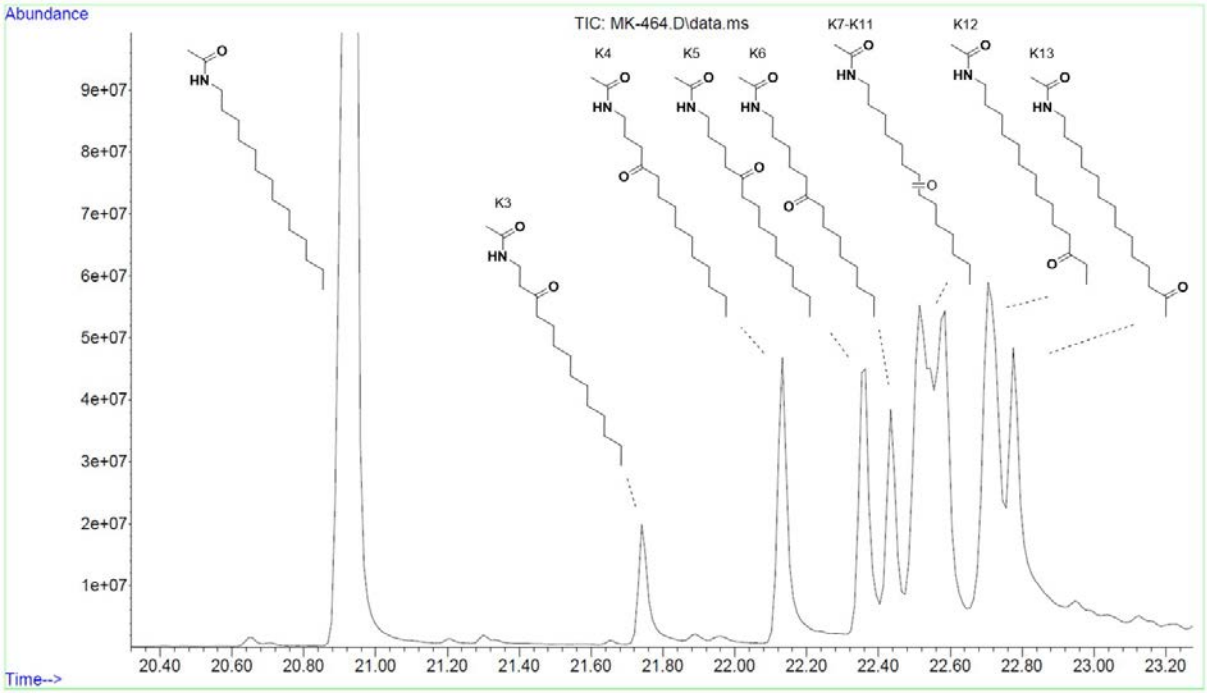

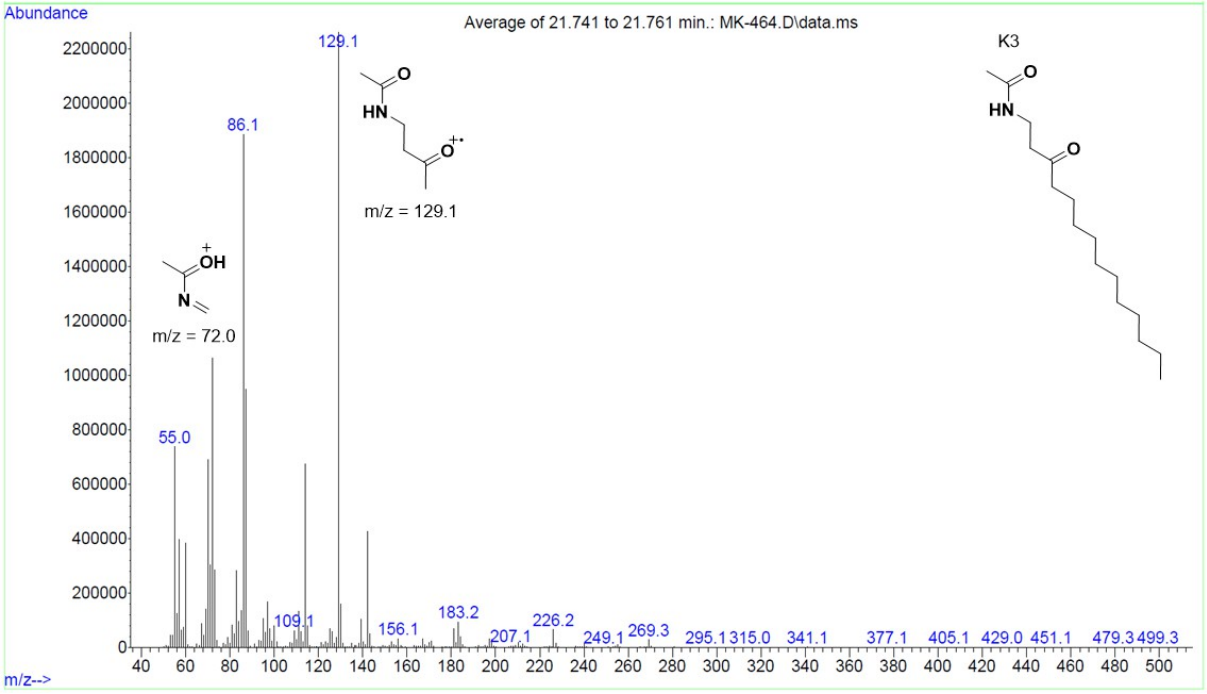

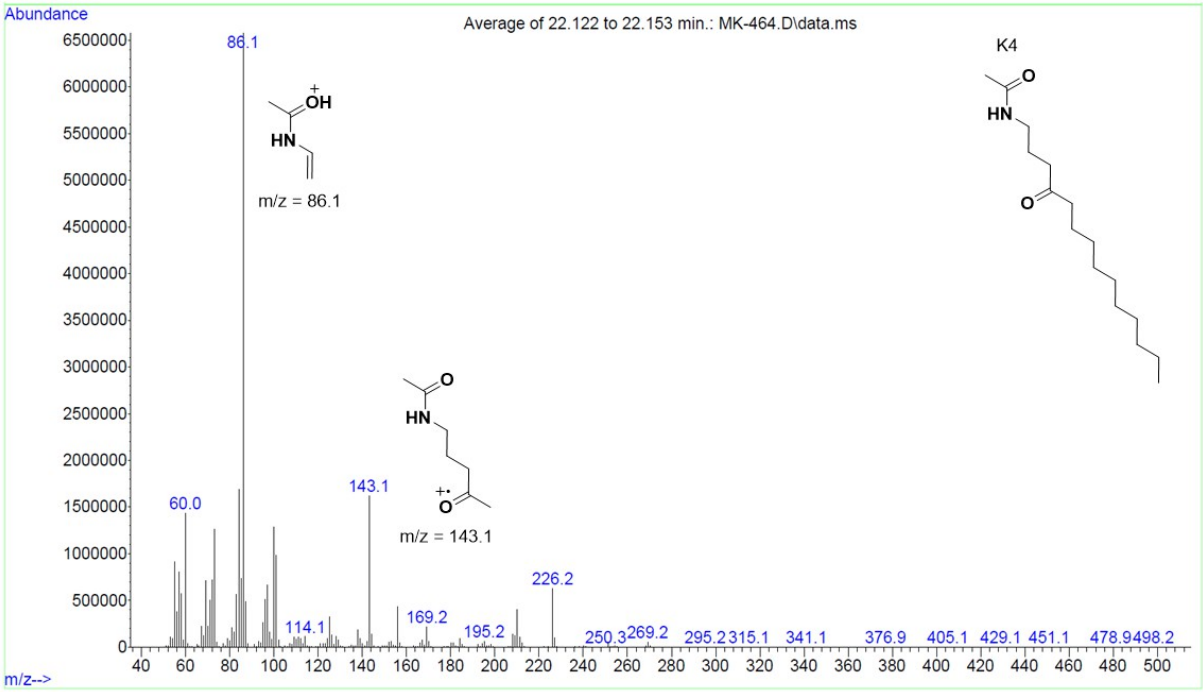
Abundance
Average of 22.122 to 22.153 min.: MK-464.D\data.ms
K4
m/z = 86.1
m/z = 143.1
m/z-->

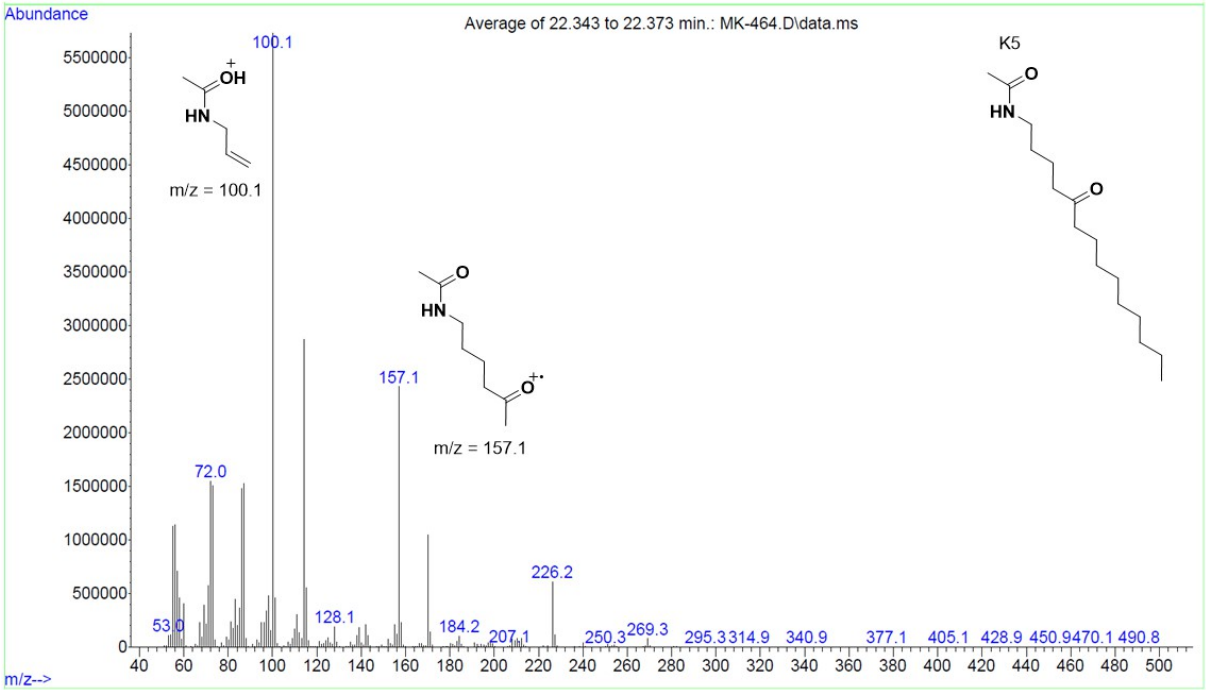
Abundance
Average of 22.343 to 22.373 min.: MK-464.D\data.ms
K5
m/z = 100.1
m/z = 157.1
m/z-->

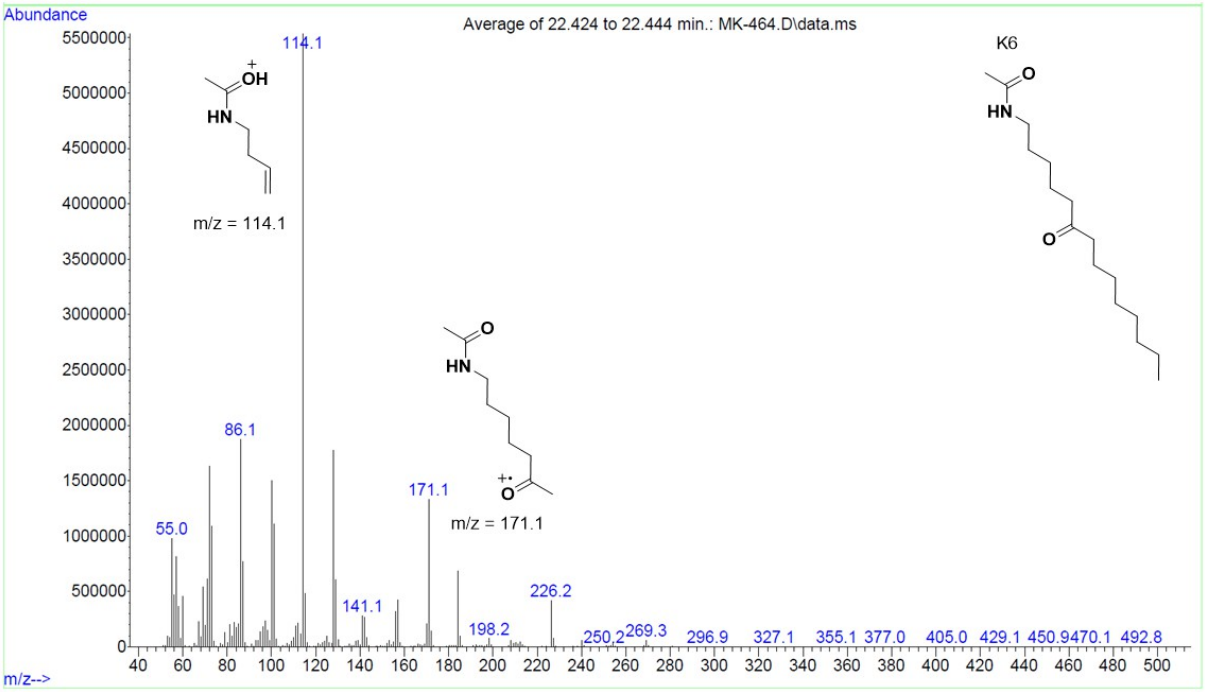
Abundance
Average of 22.424 to 22.444 min.: MK-464.D\data.ms
K6
m/z = 114.1
m/z = 171.1
114.1
86.1
171.1
55.0
141.1
198.2
226.2
m/z-->

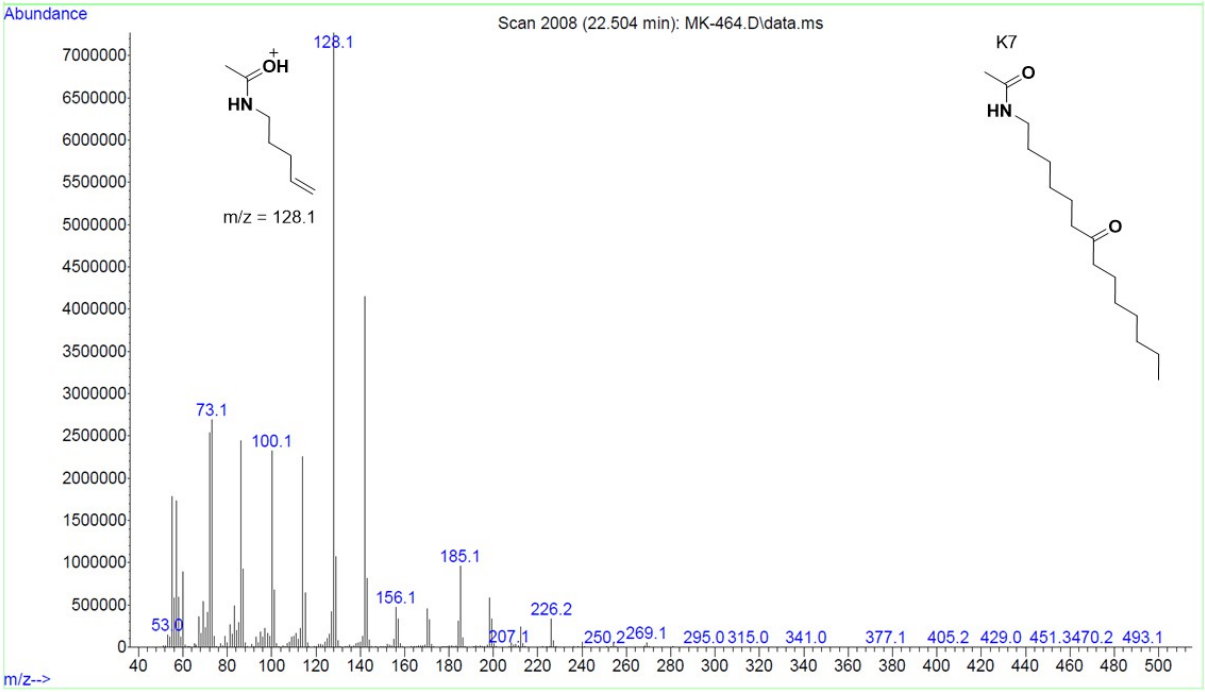
Abundance
Scan 2008 (22.504 min): MK-464.D\data.ms
K7
m/z = 128.1
128.1
73.1
100.1
185.1
156.1
226.2
53.0
m/z-->

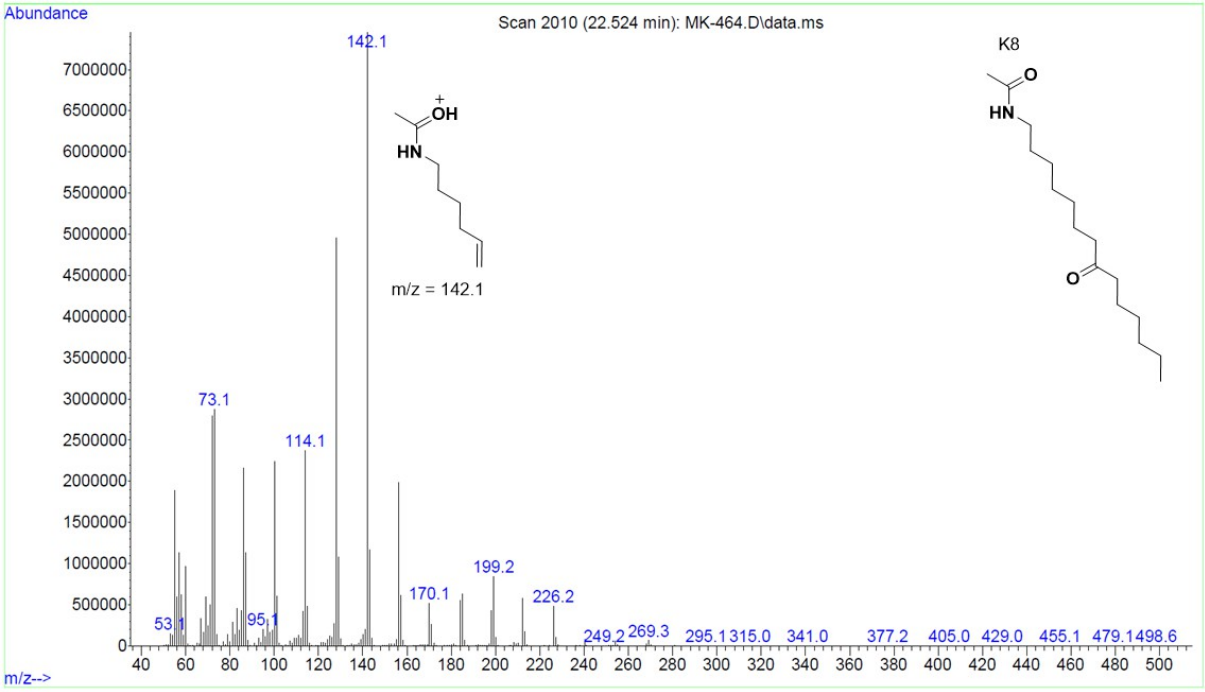
Abundance
Scan 2010 (22.524 min): MK-464.D\data.ms
142.1
73.1
114.1
199.2
170.1
226.2
53.1
95.1
249.2
269.3
295.1
315.0
341.0
377.2
405.0
429.0
455.1
479.1
498.6
m/z = 142.1
K8
m/z-->

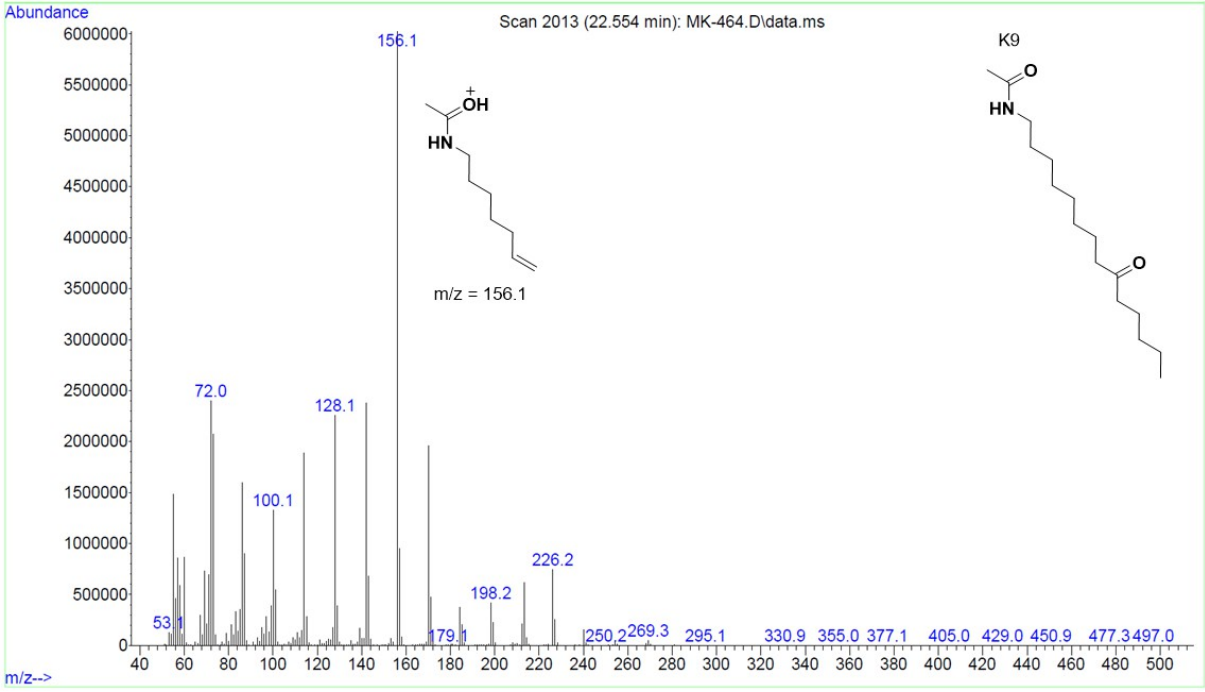
Abundance
Scan 2013 (22.554 min): MK-464.D\data.ms
156.1
72.0
128.1
100.1
226.2
198.2
53.1
179.1
250.2
269.3
295.1
330.9
355.0
377.1
405.0
429.0
450.9
477.3
497.0
m/z = 156.1
K9
m/z-->

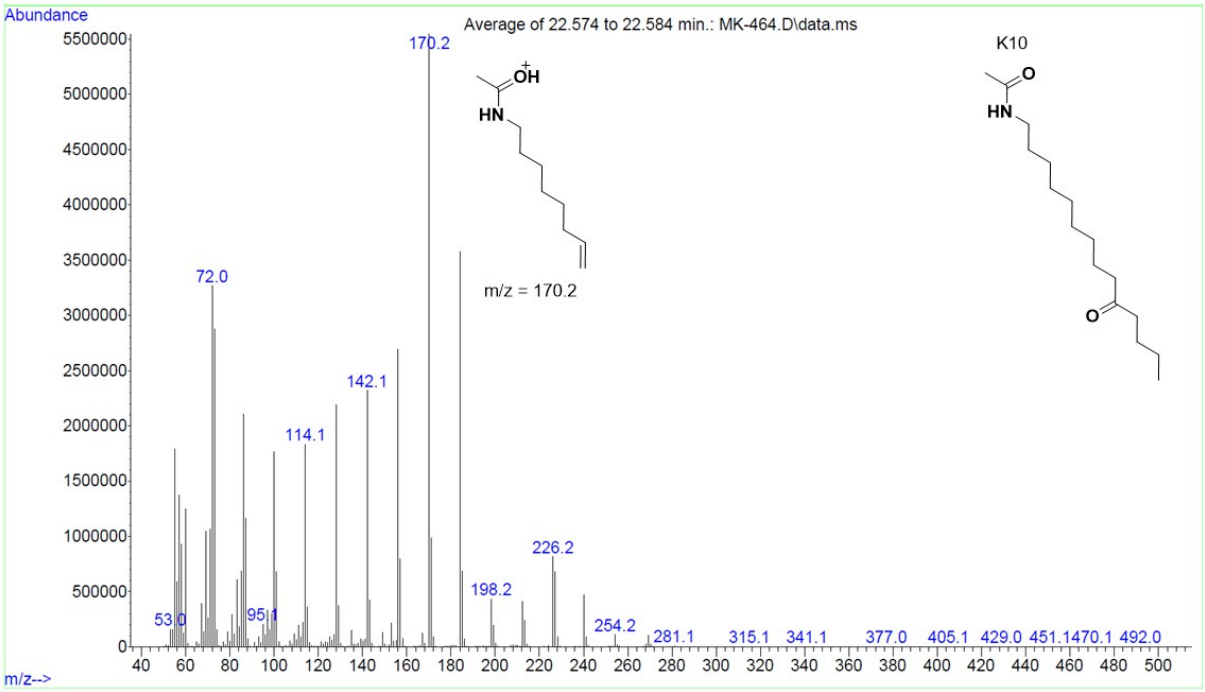
Abundance
Average of 22.574 to 22.584 min.: MK-464.D\data.ms
K10
m/z = 170.2
m/z-->

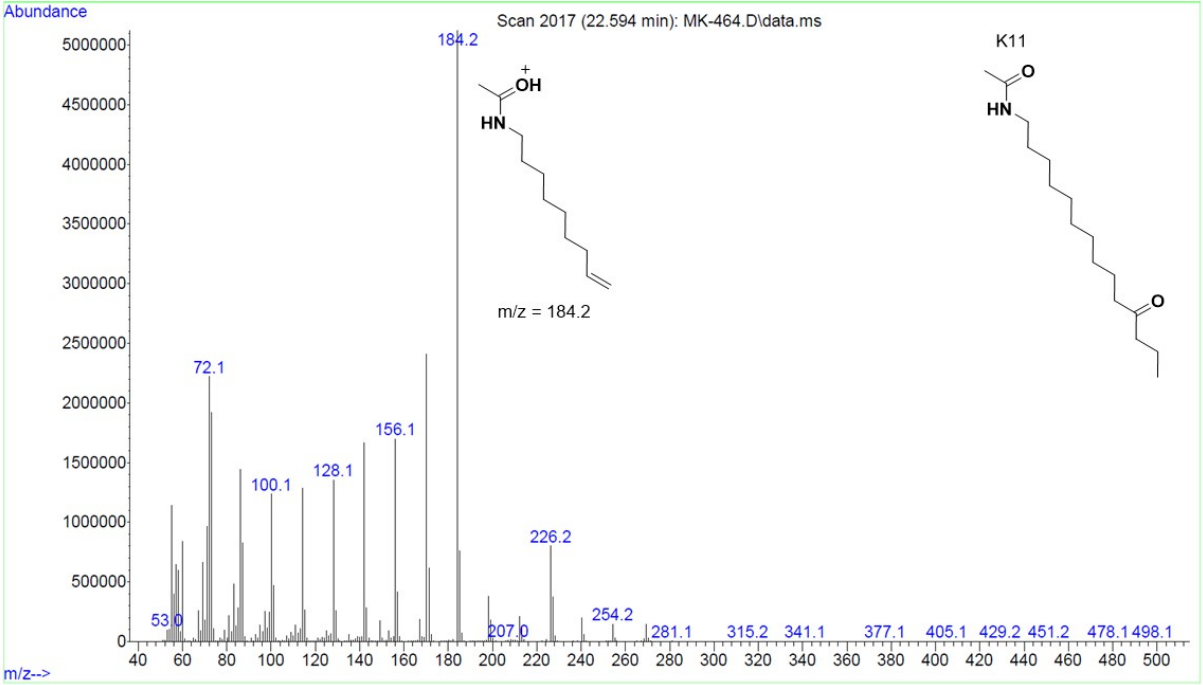
Abundance
Scan 2017 (22.594 min): MK-464.D\data.ms
K11
m/z = 184.2
m/z-->

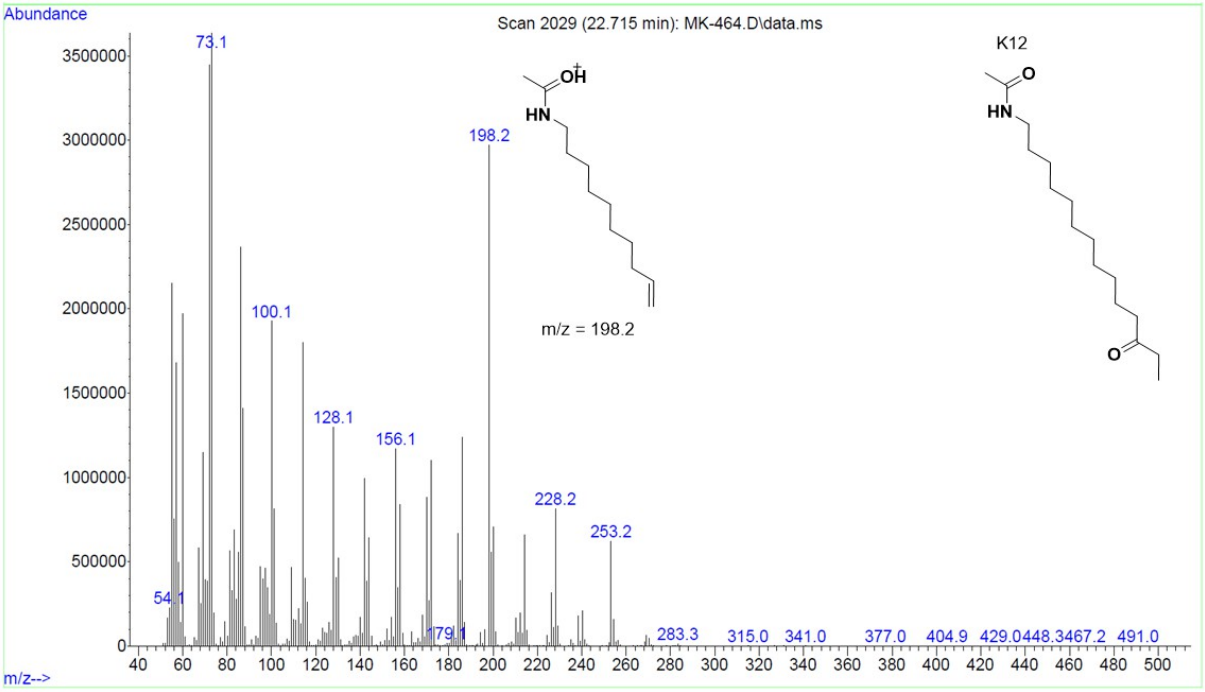
Abundance
Scan 2029 (22.715 min): MK-464.D\data.ms
K12
73.1
198.2
100.1
128.1
156.1
228.2
253.2
54.1
179.1
283.3
315.0
341.0
377.0
404.9
429.0
448.3
467.2
491.0
m/z = 198.2
m/z-->

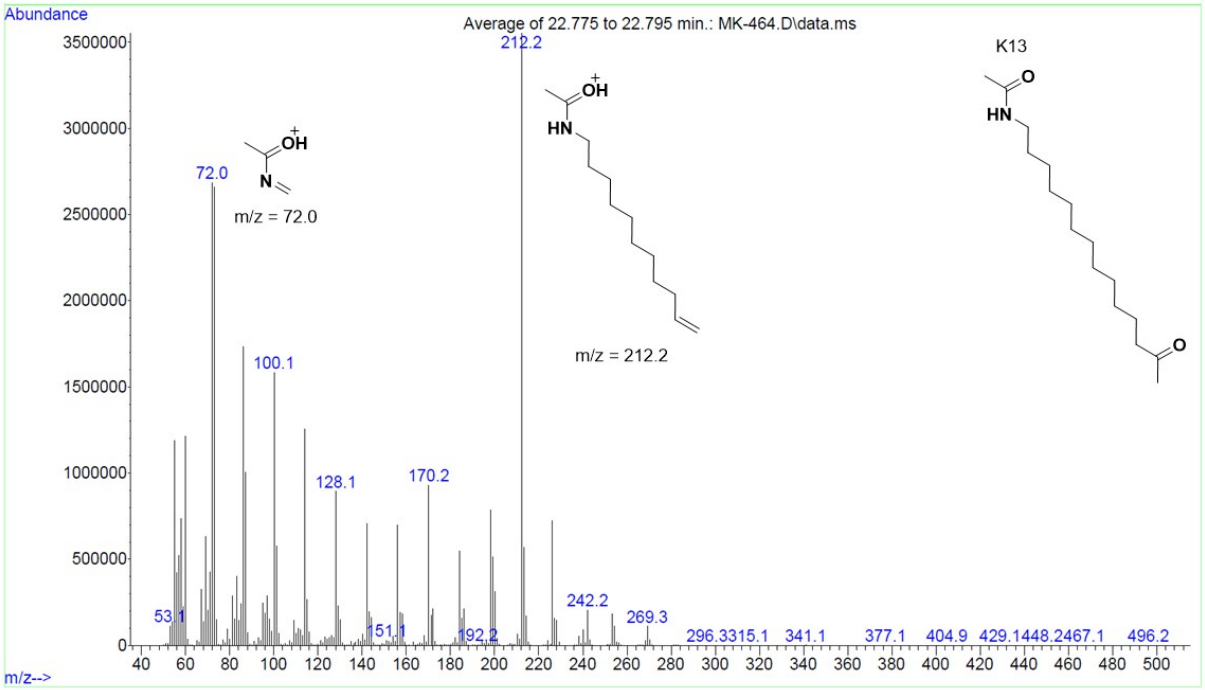
Abundance
Average of 22.775 to 22.795 min.: MK-464.D\data.ms
K13
212.2
72.0
m/z = 72.0
100.1
128.1
170.2
242.2
269.3
53.1
151.1
192.2
296.3
315.1
341.1
377.1
404.9
429.1
448.2
467.1
496.2
m/z = 212.2
m/z-->

N-Methyl-decylammonium Oxidaiton

According to the general oxidation protocol, *N*-methyl-decylammonium tetrafluoroborate (**S18**, 4.79 mg, 18.5 µmol, 1.0 equiv.) was oxidized by Fe-Br **2** and Fe-Twe **4**. After the aqueous workup for secondary ammonium ions, the mixture was analyzed by GC and GC-MS.

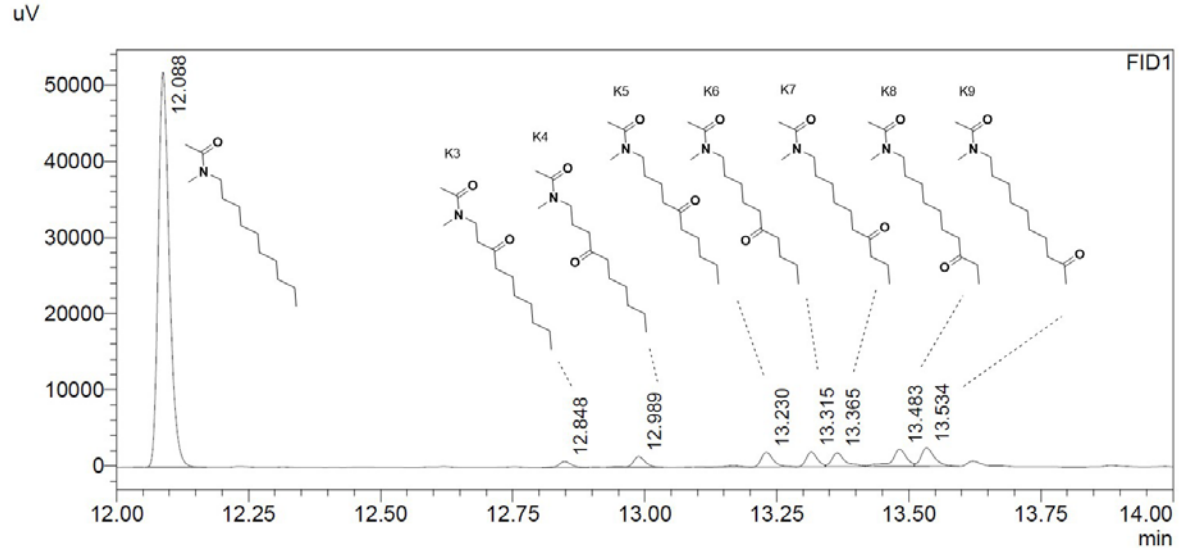

GC chromatogram of the Fe-Br **2** catalyzed oxidation of *N*-methyl-decylammonium tetrafluoroborate.

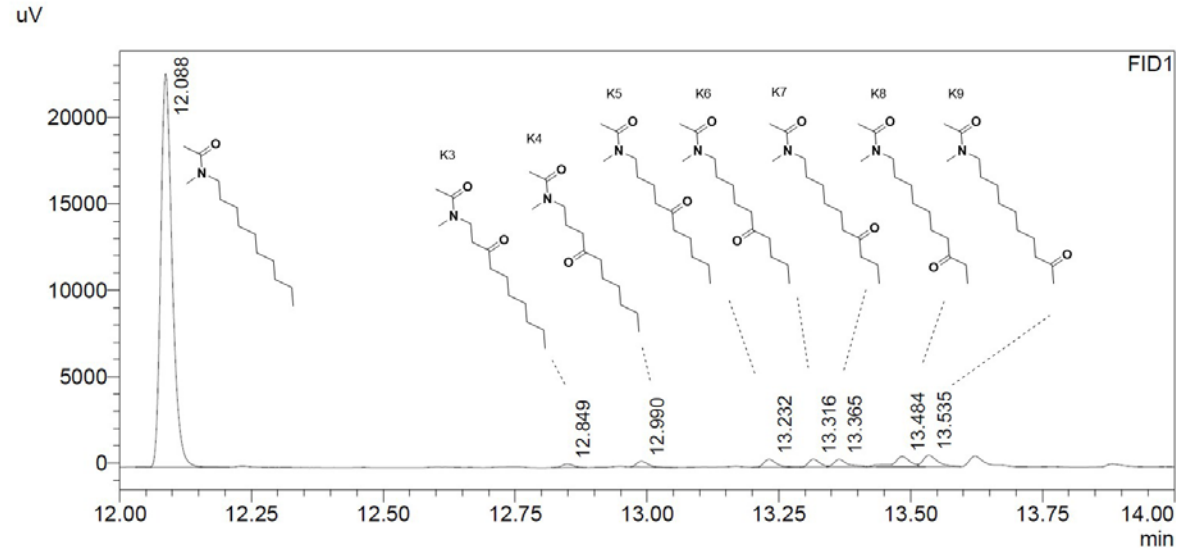

GC chromatogram of the Fe-Twe **4** catalyzed oxidation of *N*-methyl-decylammonium tetrafluoroborate.

GC-MS chromatogram and spectra of the Fe-Twe **2** catalyzed oxidation of *N*-methyl-decylammonium tetrafluoroborate. The different oxidation products were assigned according to their fragmentation pattern.

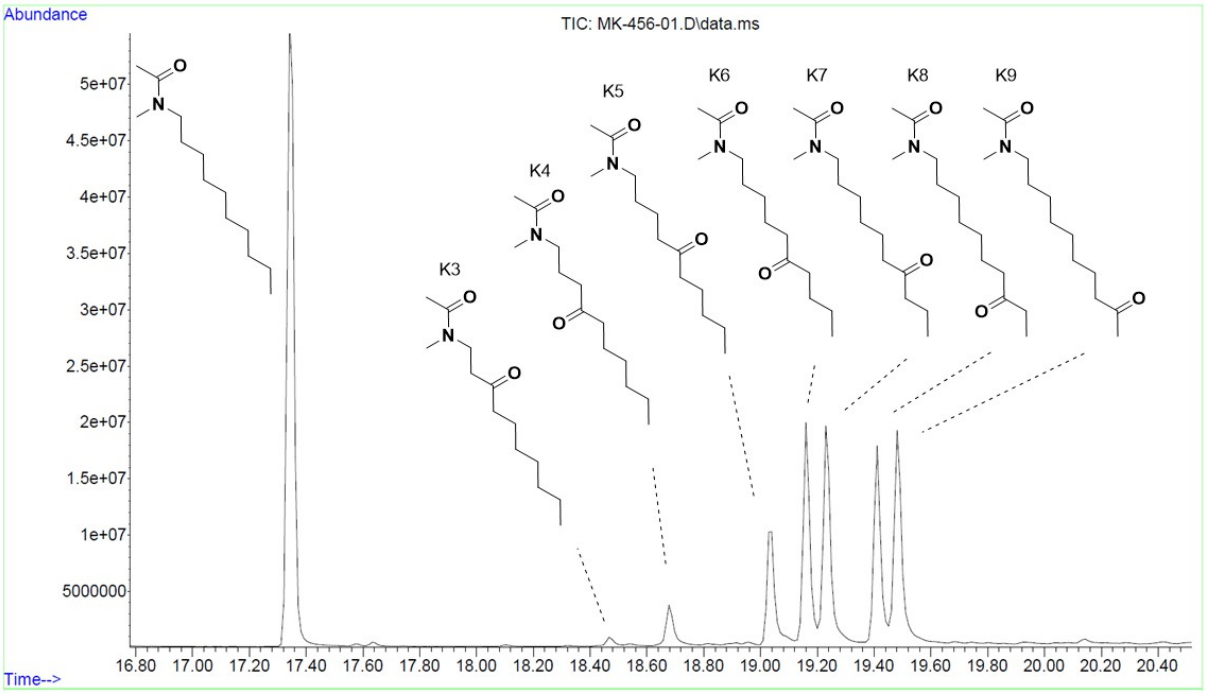

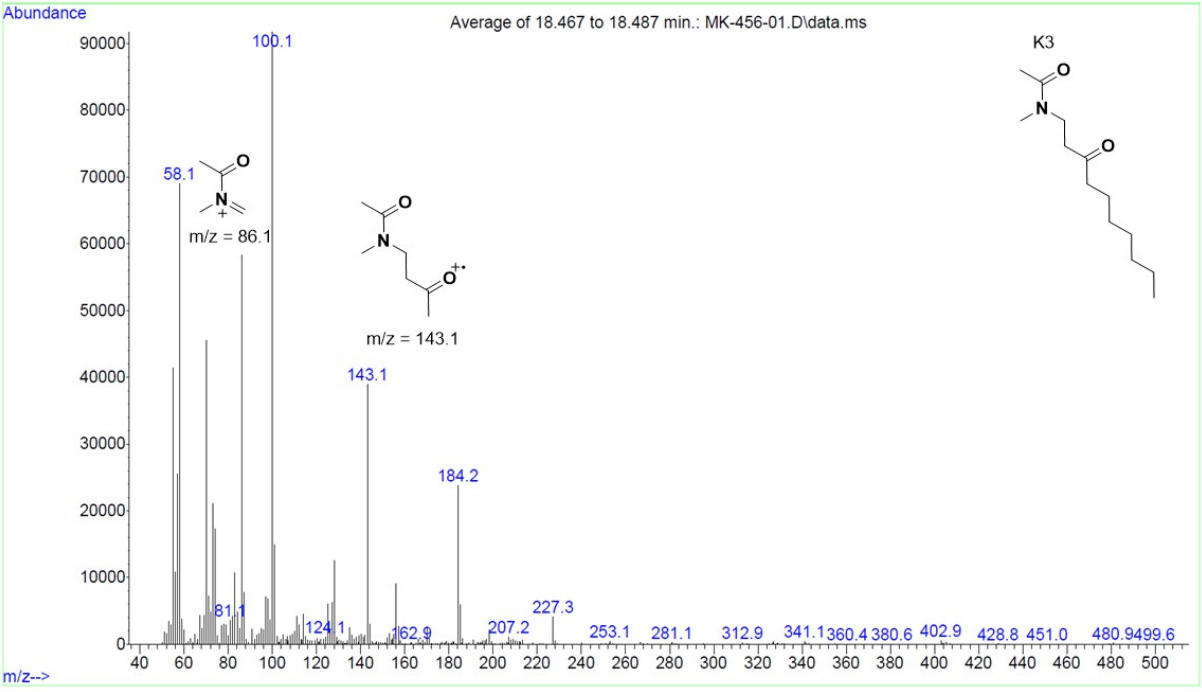

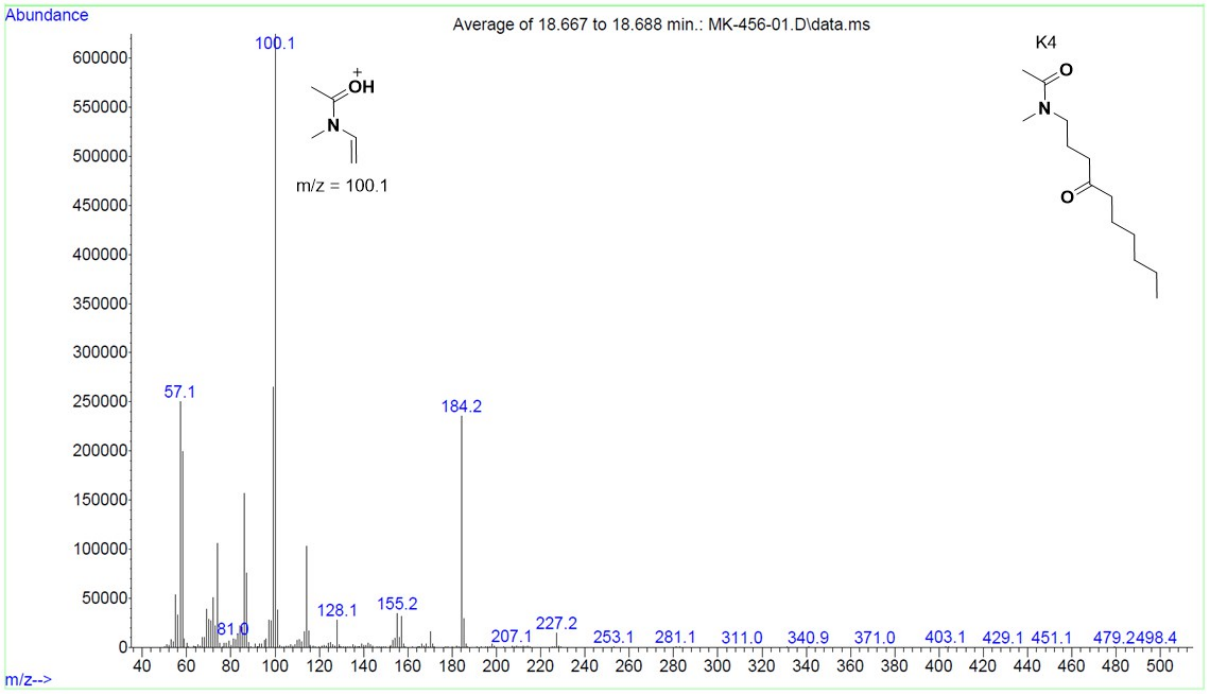
Abundance
Average of 18.667 to 18.688 min.: MK-456-01.D\data.ms
K4
100.1
m/z = 100.1
57.1
184.2
128.1
155.2
81.0
207.1
227.2
253.1
281.1
311.0
340.9
371.0
403.1
429.1
451.1
479.2498.4
m/z-->

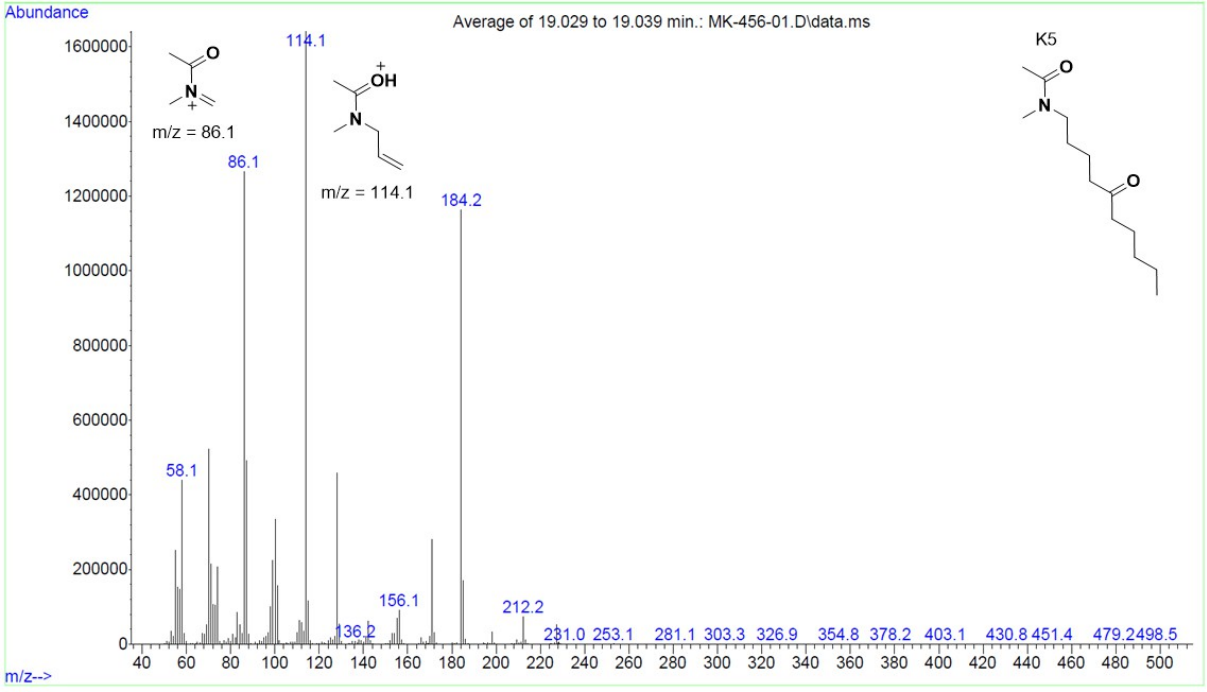
Abundance
Average of 19.029 to 19.039 min.: MK-456-01.D\data.ms
K5
114.1
m/z = 86.1
86.1
m/z = 114.1
184.2
58.1
156.1
212.2
136.2
231.0
253.1
281.1
303.3
326.9
354.8
378.2
403.1
430.8
451.4
479.2498.5
m/z-->

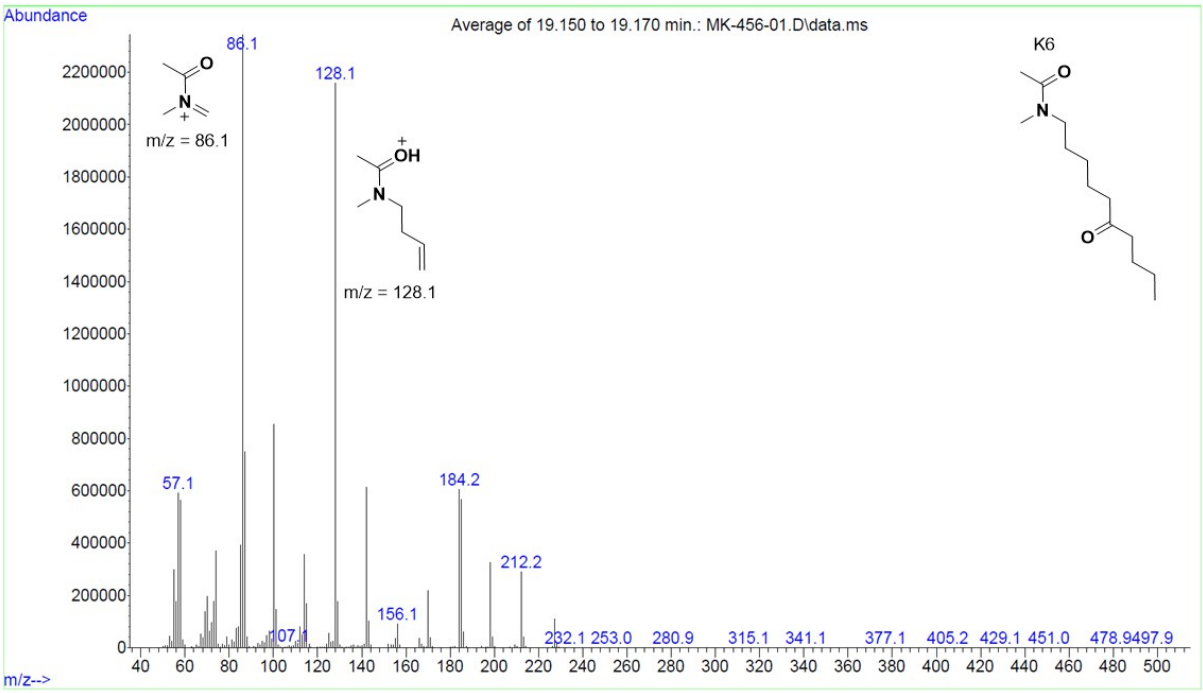
Abundance
Average of 19.150 to 19.170 min.: MK-456-01.D\data.ms
86.1
128.1
m/z = 86.1
m/z = 128.1
K6
57.1
184.2
212.2
156.1
107.1
m/z-->

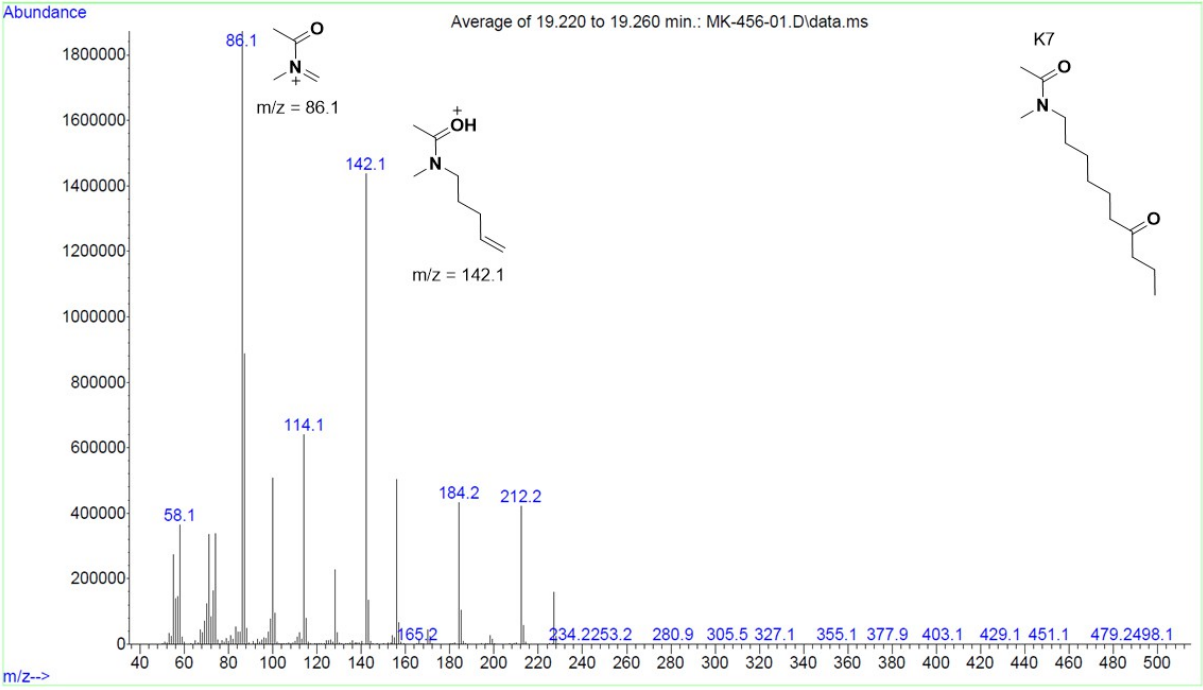
Abundance
Average of 19.220 to 19.260 min.: MK-456-01.D\data.ms
86.1
m/z = 86.1
142.1
m/z = 142.1
K7
114.1
58.1
184.2
212.2
m/z-->

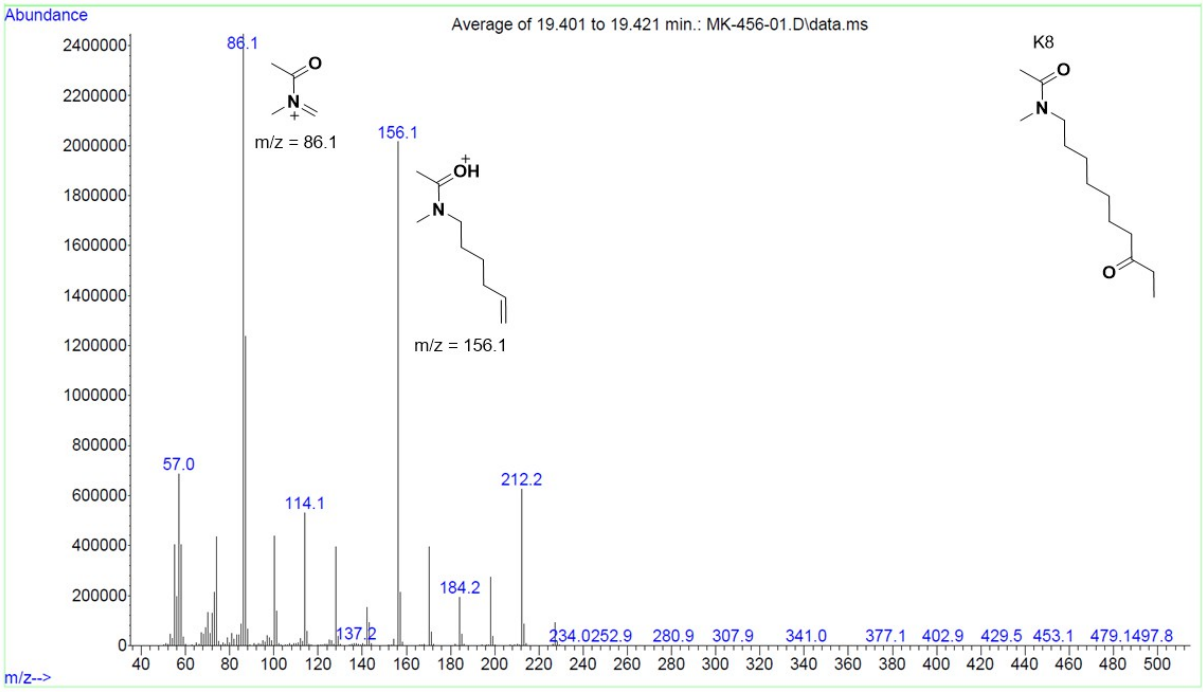
Abundance
Average of 19.401 to 19.421 min.: MK-456-01.D\data.ms
86.1
m/z = 86.1
156.1
m/z = 156.1
K8
57.0
114.1
212.2
184.2
137.2
234.0252.9
280.9
307.9
341.0
377.1
402.9
429.5
453.1
479.1497.8
m/z-->

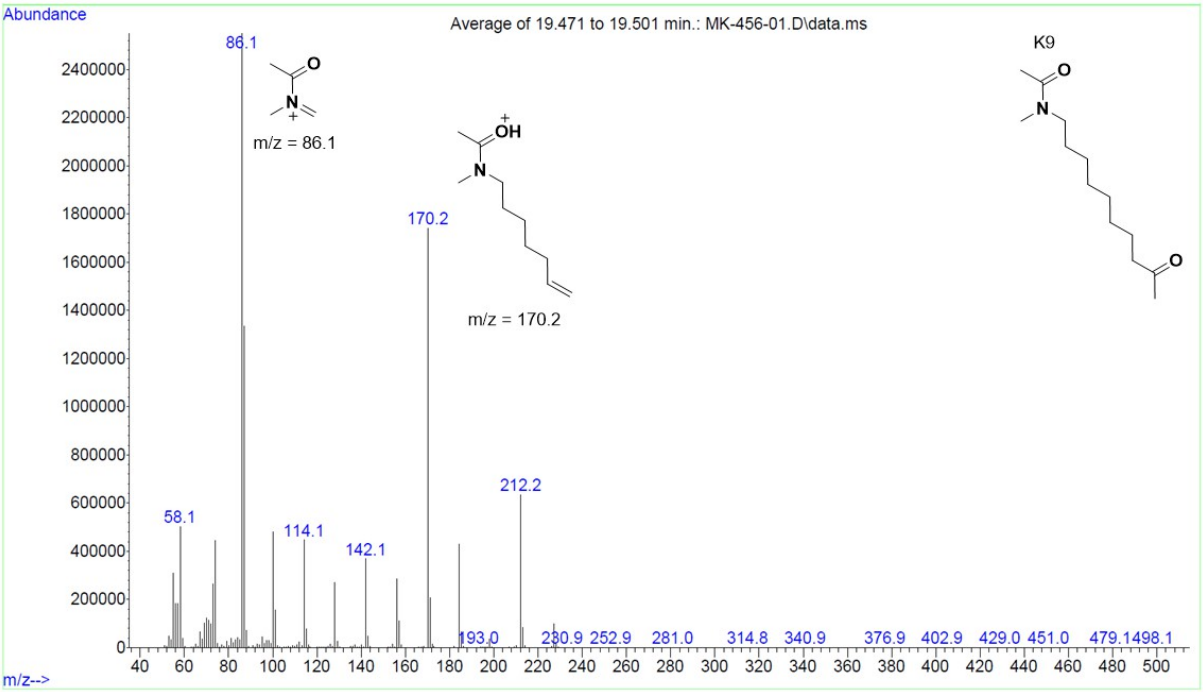
Abundance
Average of 19.471 to 19.501 min.: MK-456-01.D\data.ms
86.1
m/z = 86.1
170.2
m/z = 170.2
K9
58.1
114.1
142.1
212.2
193.0
230.9
252.9
281.0
314.8
340.9
376.9
402.9
429.0
451.0
479.1498.1
m/z-->

N,*N*-Dimethyl-decylammonium Oxidation

According to the general oxidation protocol, *N*,*N*-dimethyl-decylammonium tetrafluoroborate (**S19**, 5.05 mg, 18.5 µmol, 1.0 equiv.) was oxidized by Fe-Br **2** and Fe-Twe **4**. After the aqueous workup for tertiary ammonium ions, the mixture was analyzed by GC and GC-MS.

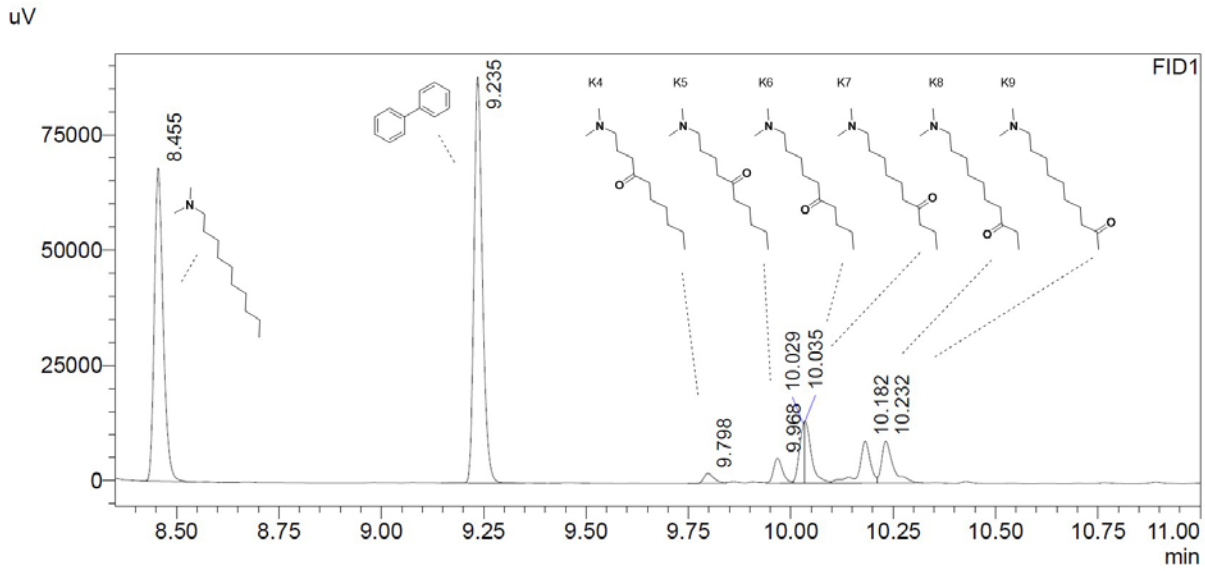

GC chromatogram of the Fe-Br **2** catalyzed oxidation of *N*,*N*-dimethyl-decylammonium tetrafluoroborate.

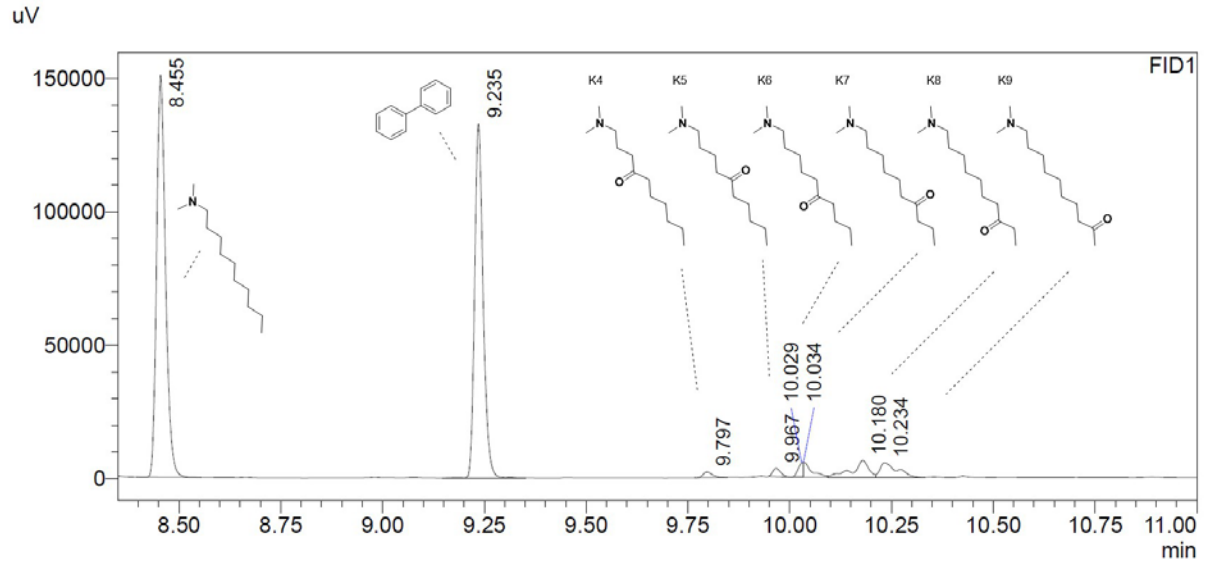

GC chromatogram of the Fe-Twe **4** catalyzed oxidation of *N*,*N*-dimethyl-decylammonium tetrafluoroborate.

GC-MS chromatogram and spectra of the Fe-Twe **2** catalyzed oxidation of *N*,*N*-dimethyl-decylammonium tetrafluoroborate. The different oxidation products were assigned according to their fragmentation pattern.

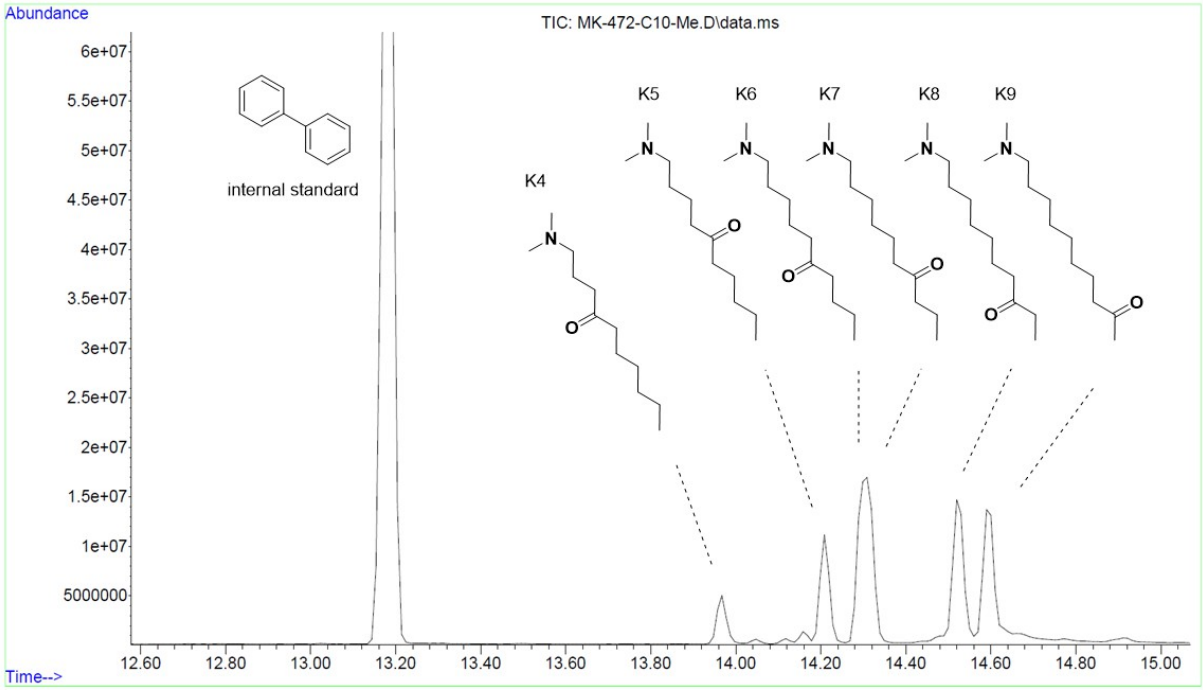

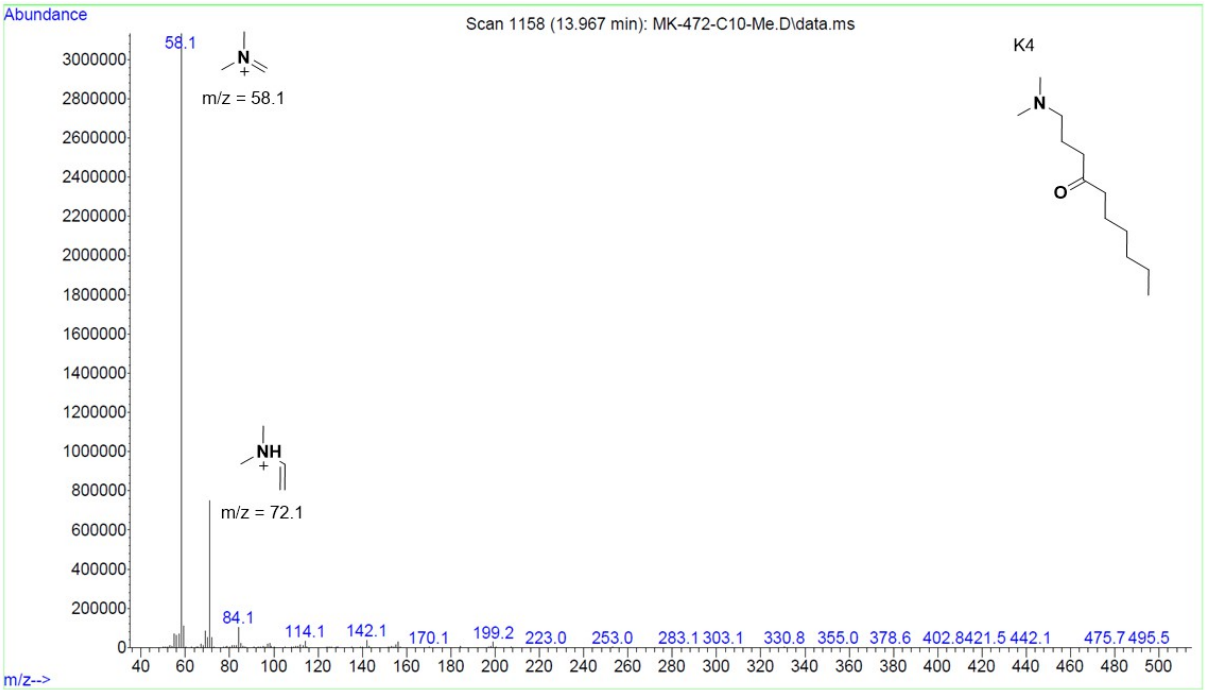

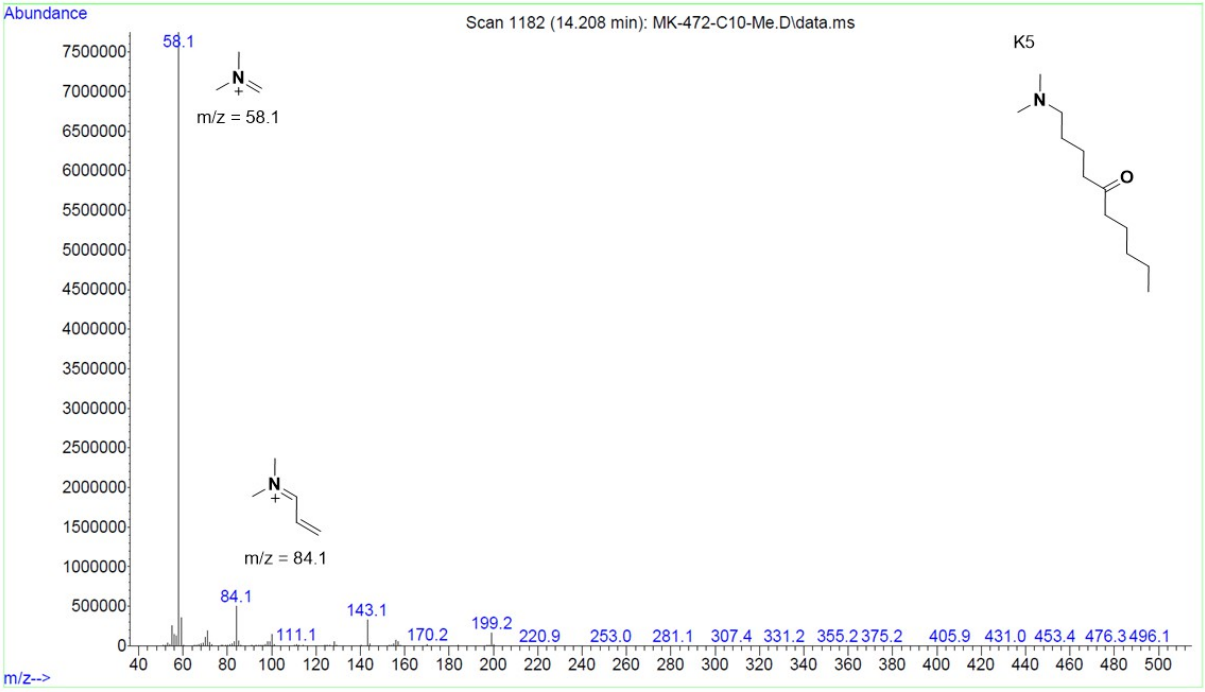
Abundance
Scan 1182 (14.208 min): MK-472-C10-Me.D\data.ms
K5
58.1
m/z = 58.1
m/z = 84.1
84.1
143.1
111.1
170.2
199.2
m/z-->

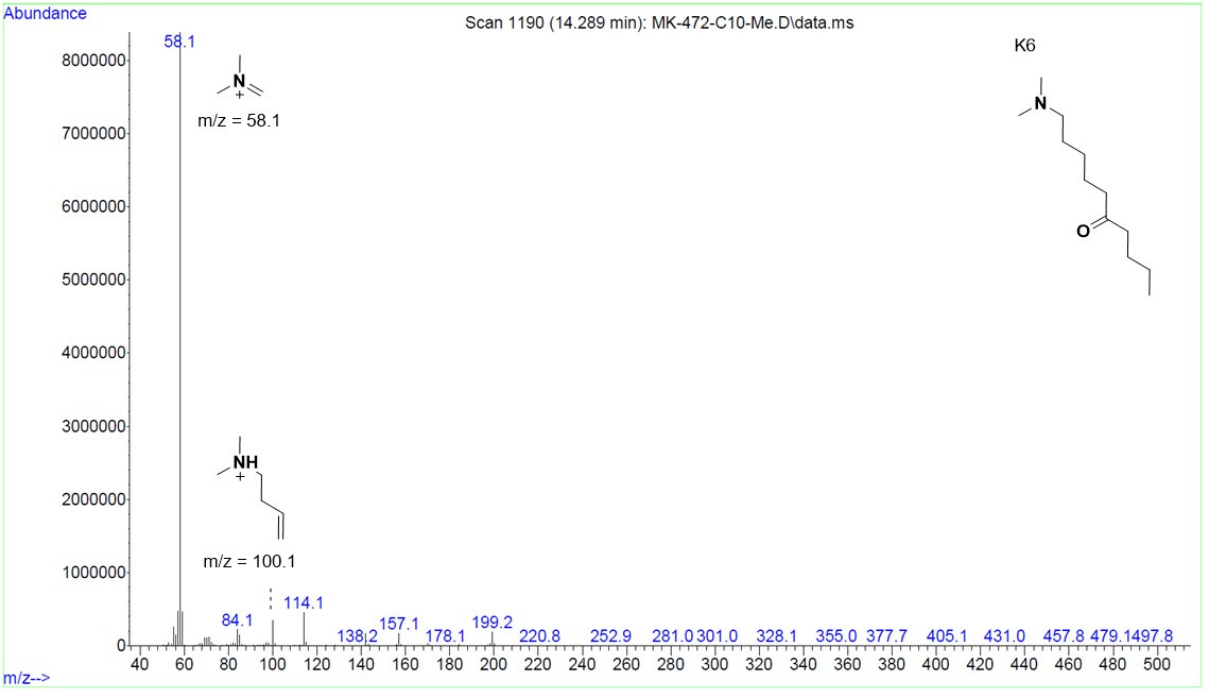
Abundance
Scan 1190 (14.289 min): MK-472-C10-Me.D\data.ms
K6
58.1
m/z = 58.1
m/z = 100.1
114.1
84.1
157.1
199.2
m/z-->

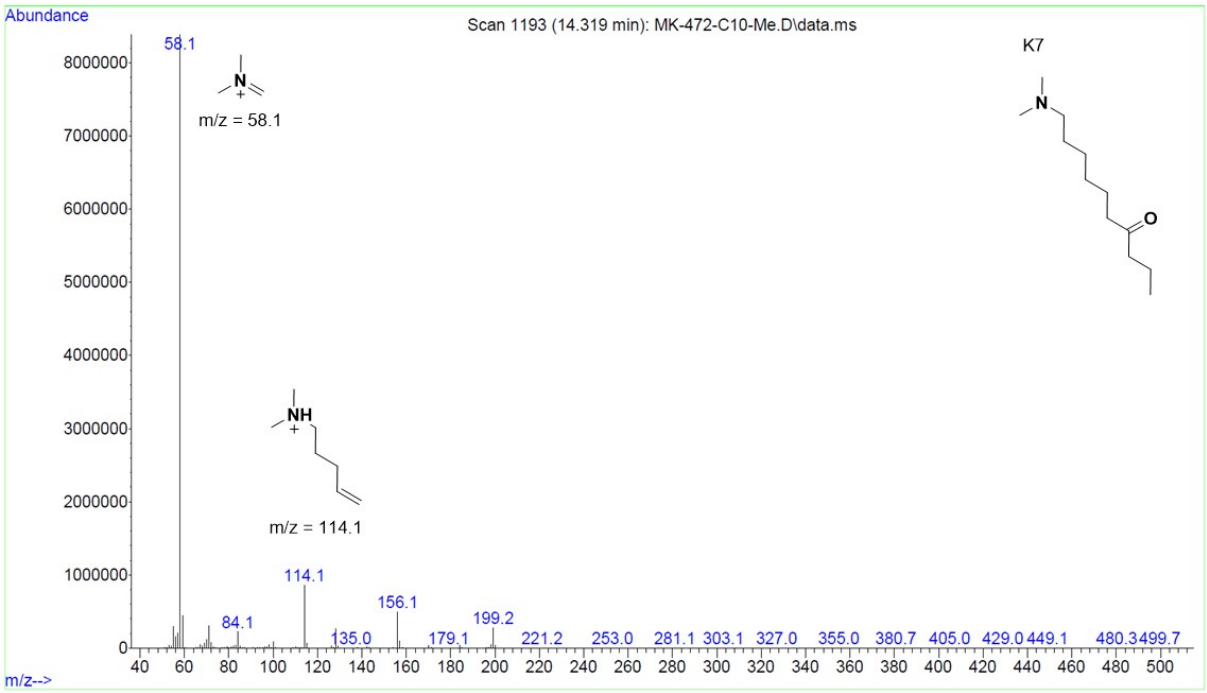
Abundance
Scan 1193 (14.319 min): MK-472-C10-Me.D\data.ms
58.1
m/z = 58.1
K7
m/z = 114.1
114.1
156.1
84.1
199.2
135.0
179.1
221.2
253.0
281.1
303.1
327.0
355.0
380.7
405.0
429.0
449.1
480.3
499.7
m/z-->

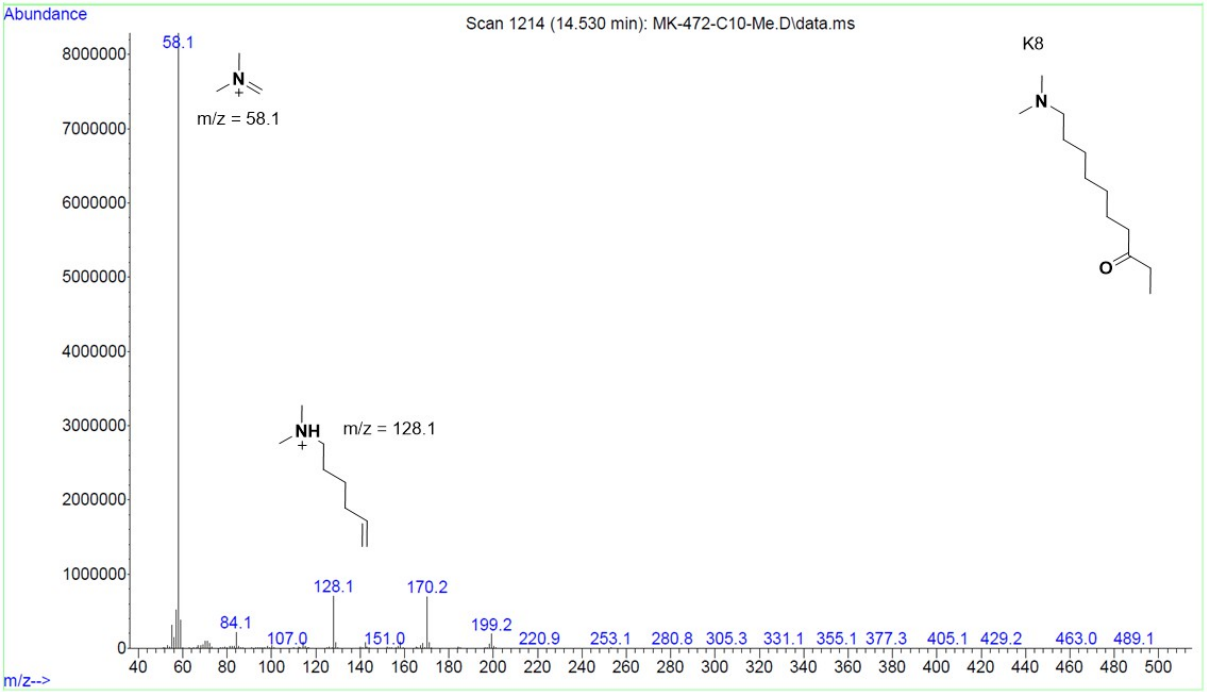
Abundance
Scan 1214 (14.530 min): MK-472-C10-Me.D\data.ms
58.1
m/z = 58.1
K8
m/z = 128.1
128.1
170.2
84.1
199.2
107.0
151.0
220.9
253.1
280.8
305.3
331.1
355.1
377.3
405.1
429.2
463.0
489.1
m/z-->

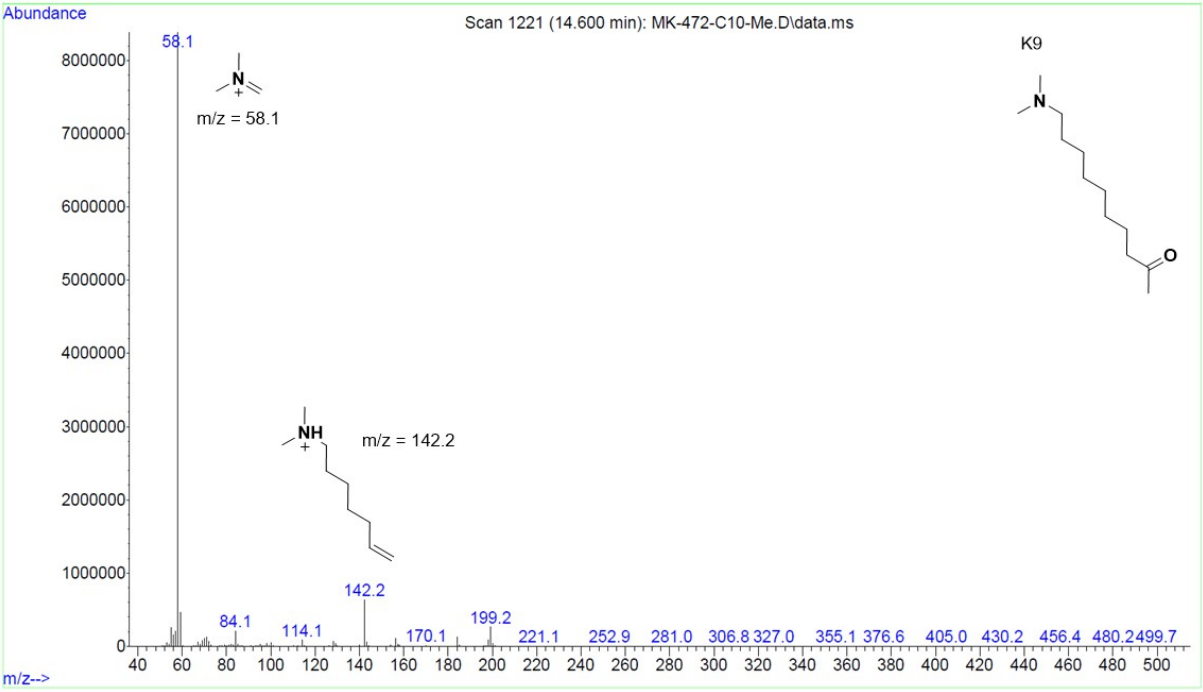
Abundance
Scan 1221 (14.600 min): MK-472-C10-Me.D\data.ms
58.1
m/z = 58.1
K9
m/z = 142.2
142.2
84.1
114.1
170.1
199.2
221.1
252.9
281.0
306.8
327.0
355.1
376.6
405.0
430.2
456.4
480.2
499.7
m/z-->

5. Determination of Response Factors

The response factors were determined according to equation 5.1. Each substrate was subjected to GC analysis three times with three different ratios of internal standard to substrate.

$$RF = \frac{(A_x \cdot C_{IS})}{(A_{IS} \cdot C_x)} \quad (5.1)$$

RF = response factor; A_x = GC area of analyte; A_{IS} = GC area of internal standard; C_x = concentration of analyte; C_{IS} = concentration of internal standard.

Table S5: Response factor determination for decylamide.

Compound	C_x/C_{IS}	A_x/A_{IS}	RF	Mean value
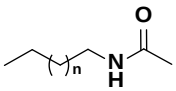 n = 7; decylamide	1.0	0.90	0.90	0.90
	2.0	1.80	0.90	
	3.0	2.67	0.89	

The response factor of heptylamide, octylamide, nonylamide, undecylamide, dodecylamide, tetradecylamide, hexanol and hexanone were determined in the same manner. The values are shown in Table S5 (Mean value). Prediction of the response factors using the Effective Carbon Number Concept by Scanlon and Willis resulted in comparable results (Theory).[17]

Table S6: Response factors of substrates heptylamide, octylamide, nonylamide, undecylamide, dodecylamide, tetradecylamide, hexanol and hexanone.

Compound	RF (Mean value)	RF (Theory)
heptylamide	0.67	0.67
octylamide	0.77	0.75
nonylamide	0.84	0.83
decylamide	0.90	0.92
undecylamide	1.00	1.00
dodecylamide	1.07	1.08
tetradecylamide	1.30	1.25
hexanol	0.41	0.44
hexanone	0.40	0.42

Since, it was not possible to separate the different oxidation products (K3, K4, K5, etc.), the RF values for the products were approximated based on two assumptions: First, all the different oxidation products of one substrate (constitutional isomers K3, K4, K5, etc.) possess the same RF value, and second, that the products with different length follow the rules described by Scanlon and Willis.[17] In our opinion, these assumptions are reasonable, especially since we observed a very good agreement with the predicted values for the substrates (Table S5). The predicted values are shown in Table S6 following the same trend as the determined for the

acetylated starting materials. Both, the predicted and measured RF values for the substrates are depicted in Figure S1.

Table S7: Approximated response factors for the oxidation products.

Compound	RF (Theory)
Ox. Prod. of C7-NH_3^+	0.58
Ox. Prod. of C8-NH_3^+	0.67
Ox. Prod. of C9-NH_3^+	0.75
Ox. Prod. of C10-NH_3^+	0.83
Ox. Prod. of C11-NH_3^+	0.92
Ox. Prod. of C12-NH_3^+	1.00
Ox. Prod. of C14-NH_3^+	1.17
Ox. Prod. of C10-$NMeH_2^+$	0.92
Ox. Prod. of C10-NMe_2H^+	0.92

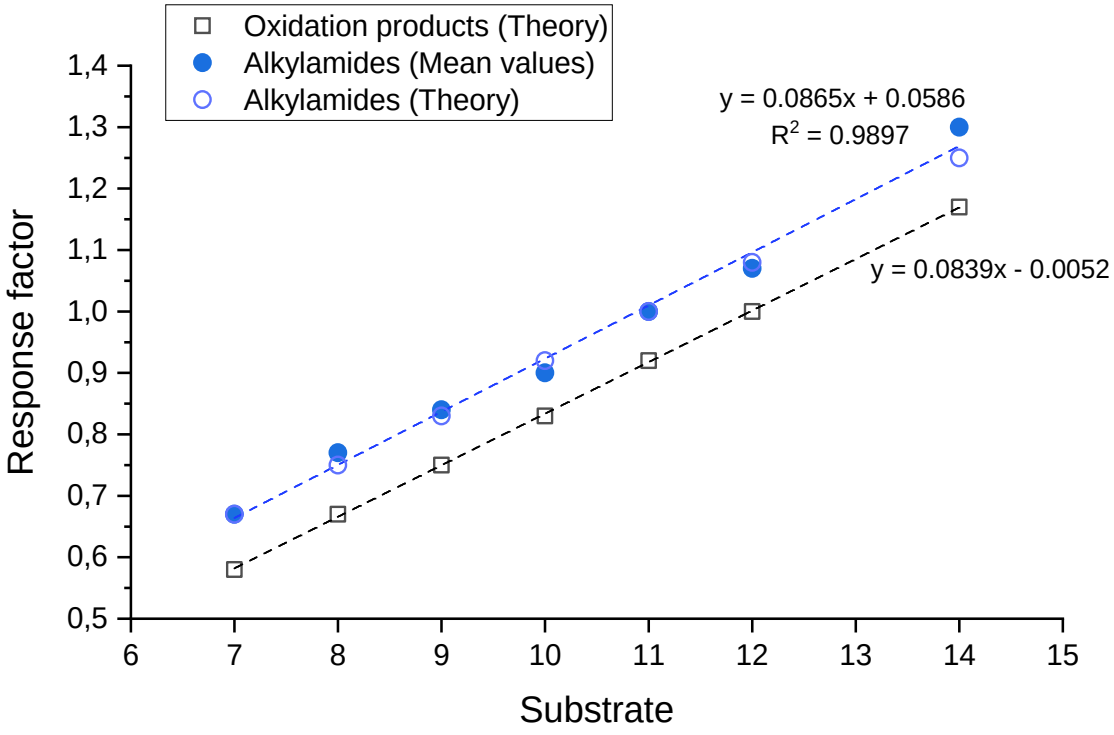

Figure S8: Depiction of the determined and predicted RF values.

Calculation for GC analysis

For GC analysis, conversions and yields were calculated utilizing the mentioned response factors. Since only 0.5 equiv. of internal standard was added to the reaction, the area of internal standard A_{IS} was multiplied by 2.

$$yield(p) = \frac{A_P}{2 \cdot A_{IS} \cdot RF_P} \tag{5.2}$$

$$conv.(SM) = 1 - \frac{A_{SM}}{2 \cdot A_{IS} \cdot RF_{SM}} \tag{5.3}$$

A_P = area of product signal; A_{SM} = area of starting material, A_{IS} = area of internal standard; RF_P = approximated response factor of product; RF_{SM} = response factor of starting material.

6. NMR Titration Experiments

NMR titrations were performed at 298 K, measuring ^{1}H NMR spectra at 500 MHz using a UltraShield 500 spectrometer.

If not stated otherwise, to a solution of tweezer **8b** resp. Fe-Twe **4** (host, H) in MeCN was added a stock solution of corresponding guest (G) with the same host concentration [H] as the host solution, so that 500 µL of a solution with constant [H] of 10 mM and with varying concentrations [G] were obtained. The NMR samples were adjusted to the original pD of buffer when necessary.[10, 18]

Fast exchange on an NMR timescale was observed for the formation the host-guest complexes; therefore changes in chemical shift were observed and plotted using nonlinear regression *via* the bindfit app (THORDARSON *et al.*, http://app.supramolecular.org/bindfit/)[19] for signals that could be observed over the entire course of the titration experiment. The resulting fits were used to calculate K_a in addition to an error margin for 95% confidence of fit and the root mean square (RMS) for the entire signal set.

6.1. Dilution Titration Tweezer 8b

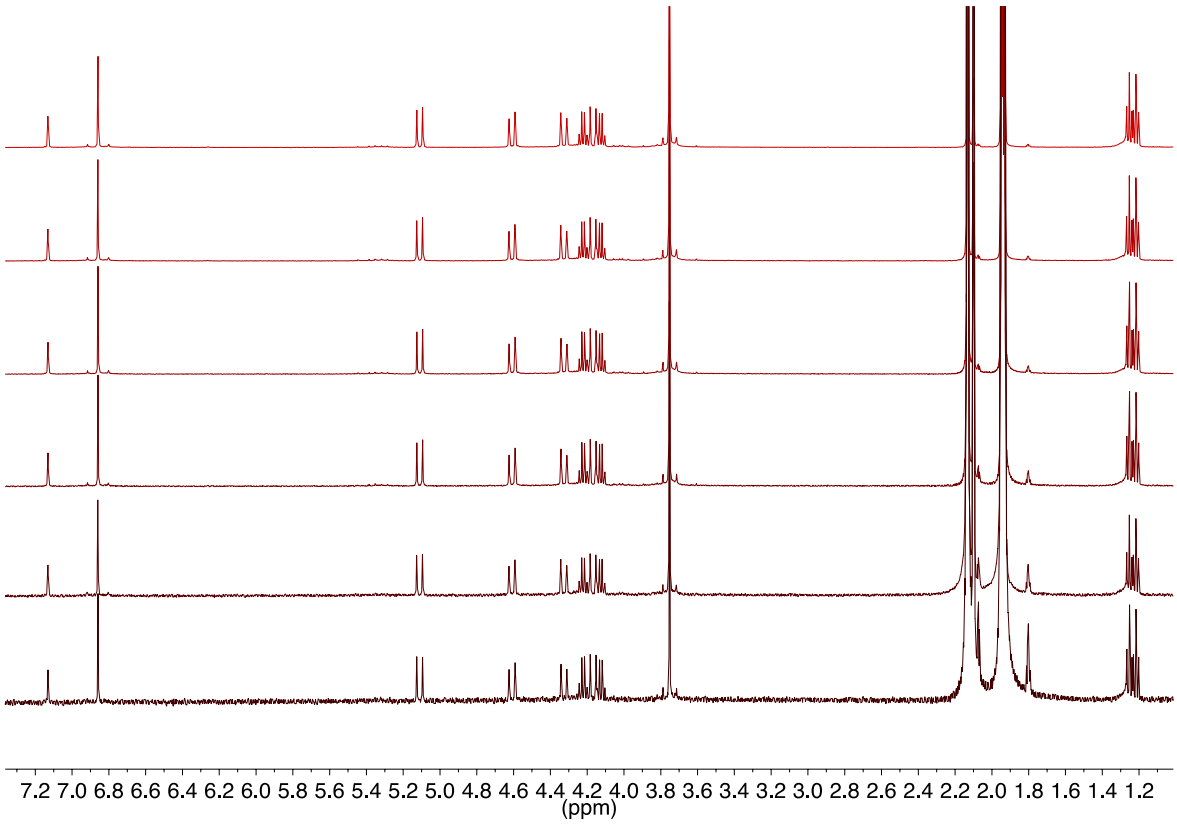

No perturbations in chemical shifts were observed over the concentration range of 100 µM ... 2.0 mM.

6.2. Titration of Decylammonium Tetrafluoroborate (S14@8b)

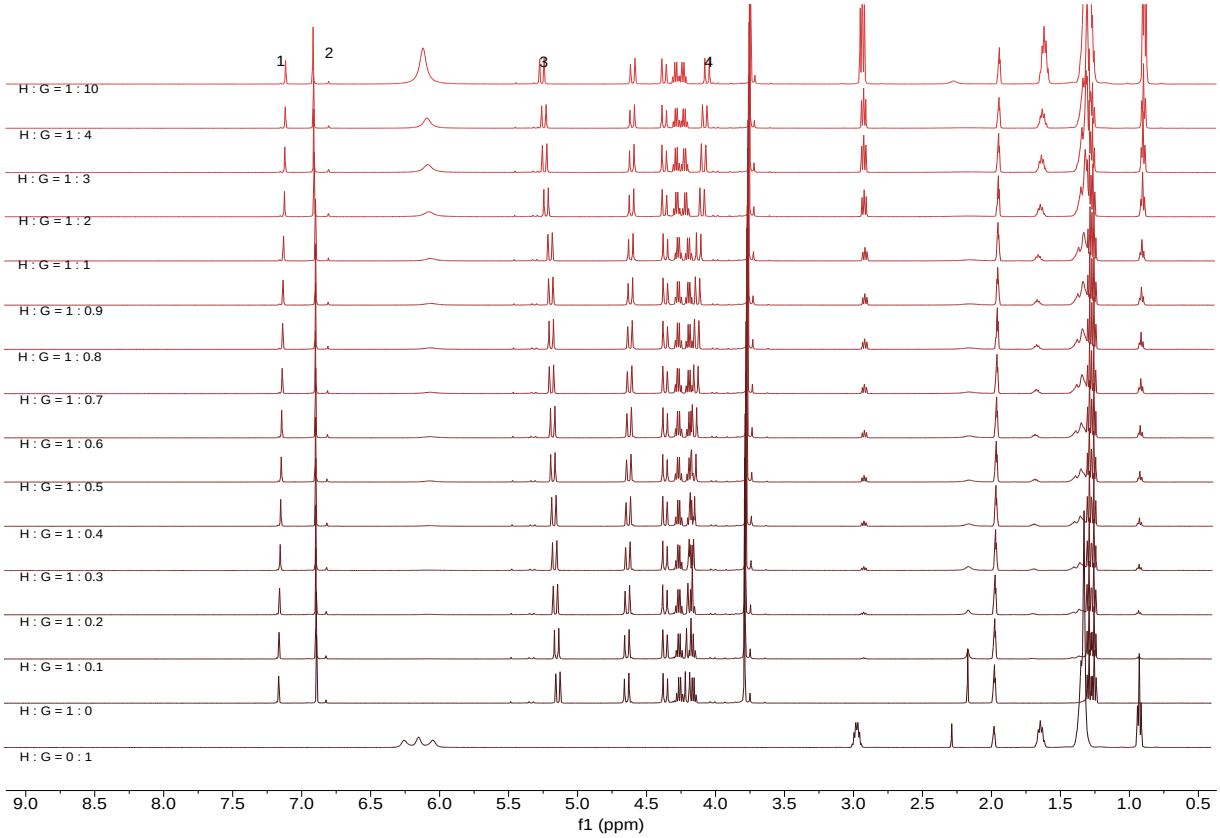

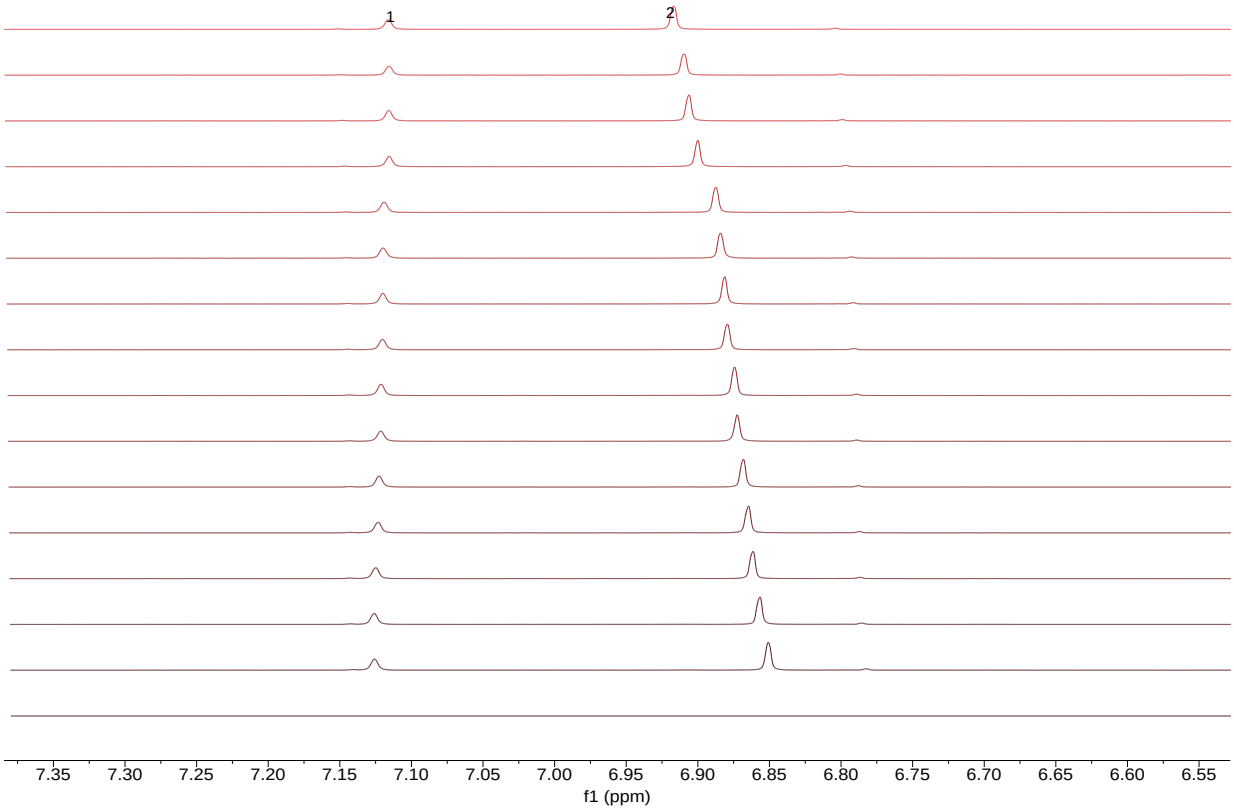

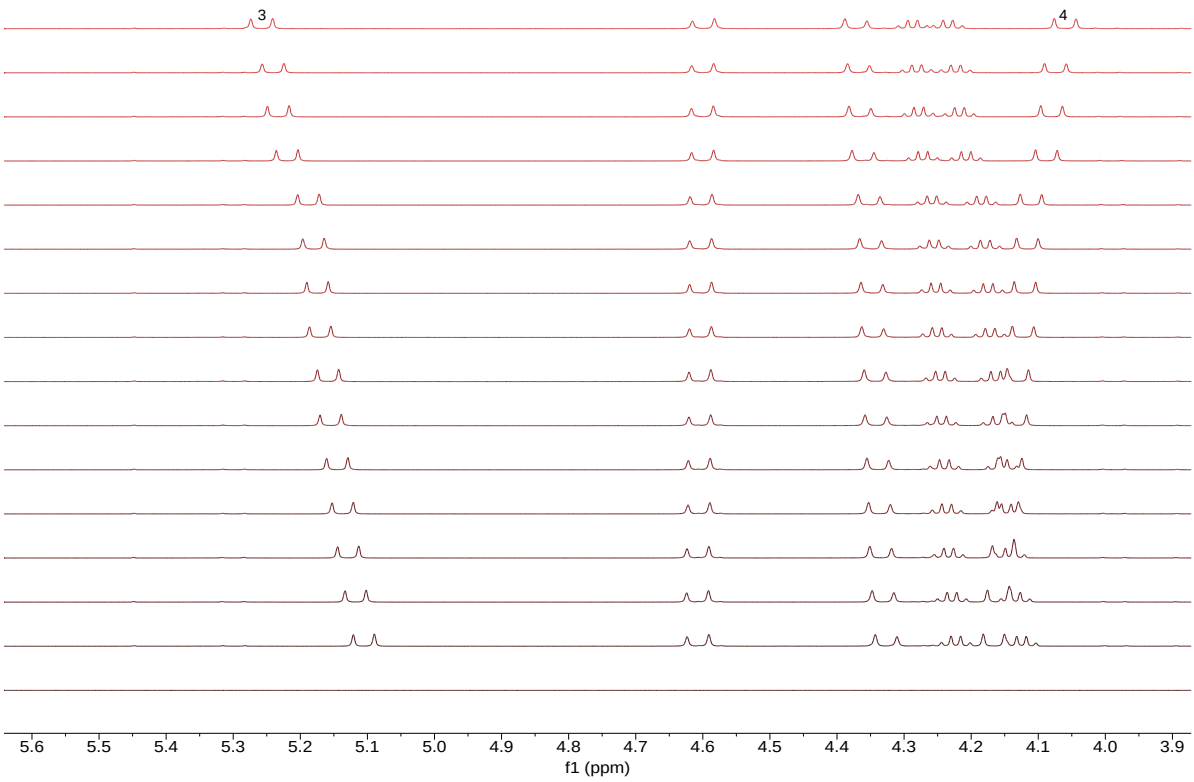

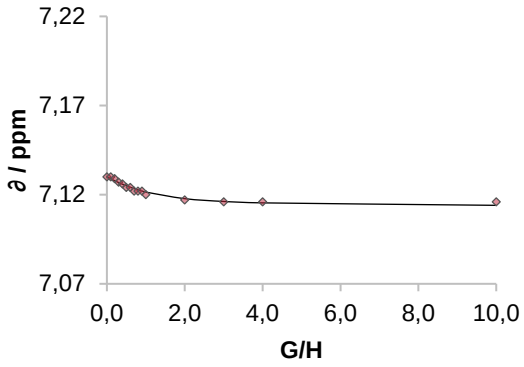

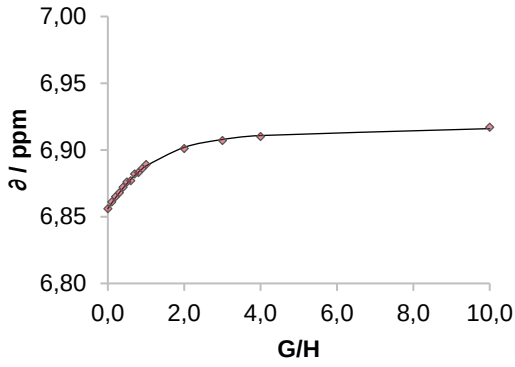

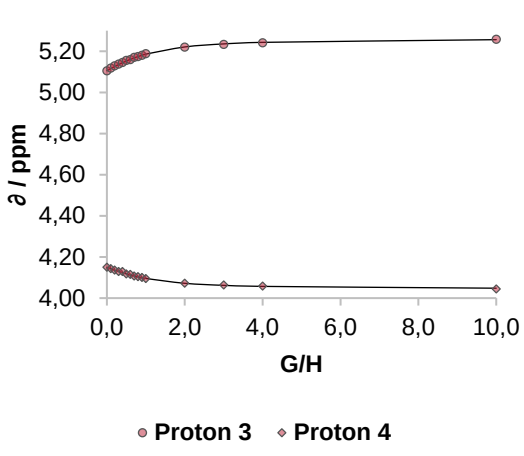

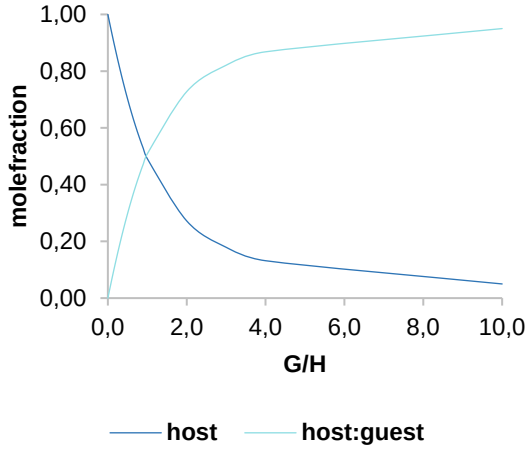

Titrated at 10 mM [H]. $K_a = 210 \pm 7.6$ M^{-1}. RMS = $1.5192 \cdot 10^{-3}$.

6.3. Dilution Titration Fe-Twe 4

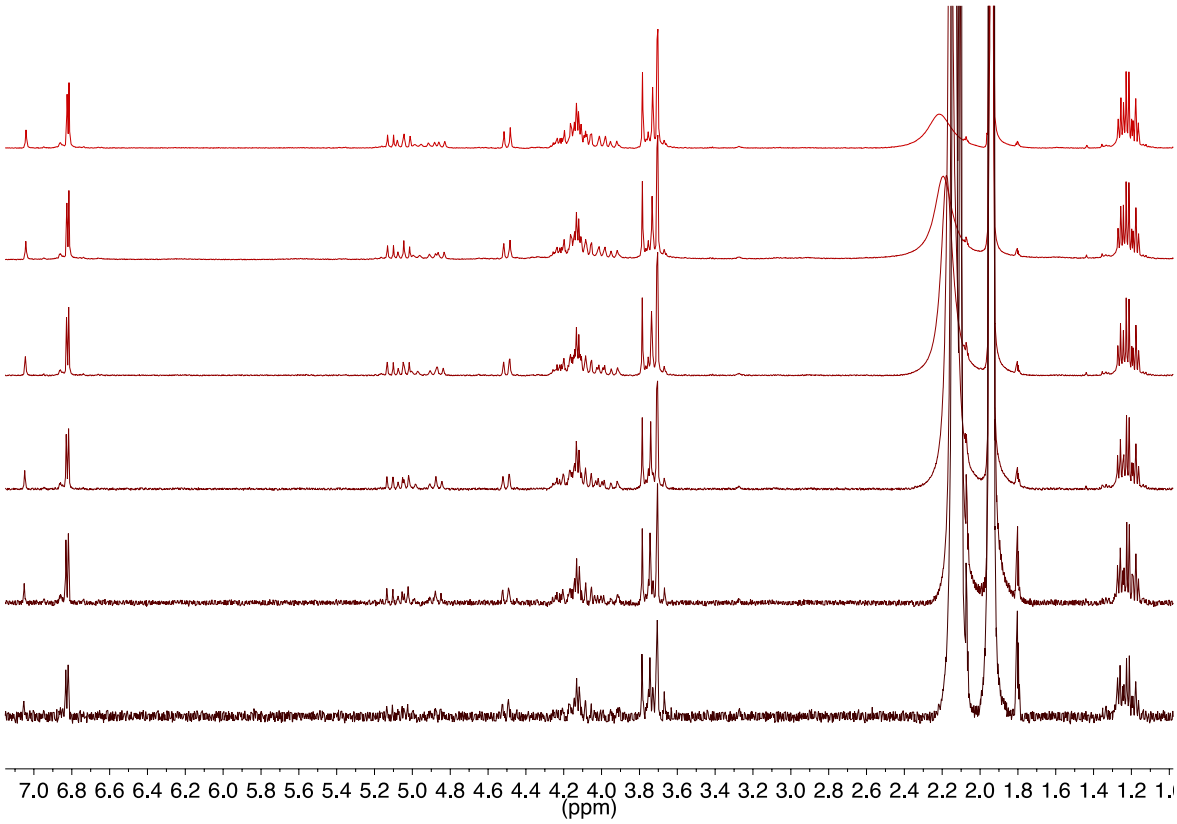

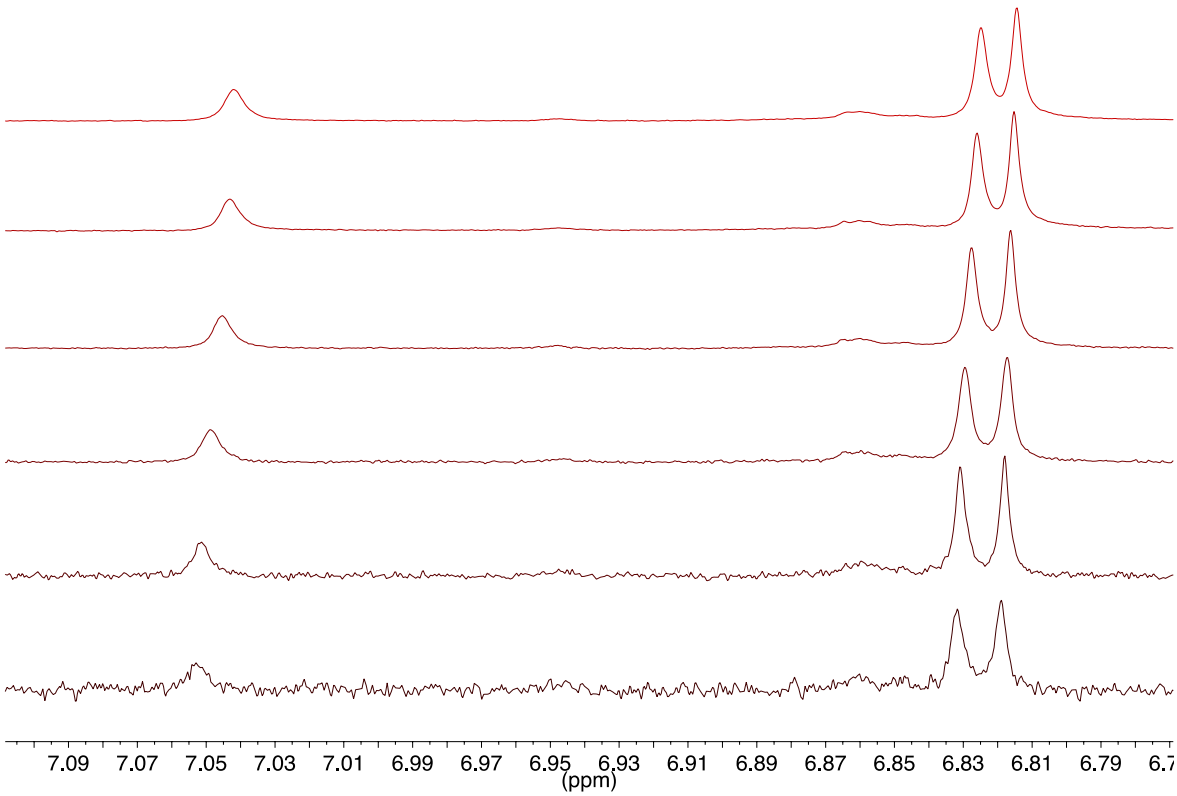

Titrated at 100 µM ... 2.0 mM [H]. K_{dim} = 160 ± 2.2 M^{-1}. RMS = $2.2720 \cdot 10^{-4}$.

6.4. Titration Fe-Twe 4 with Decylammonium Tetrafluoroborate (S14@4)

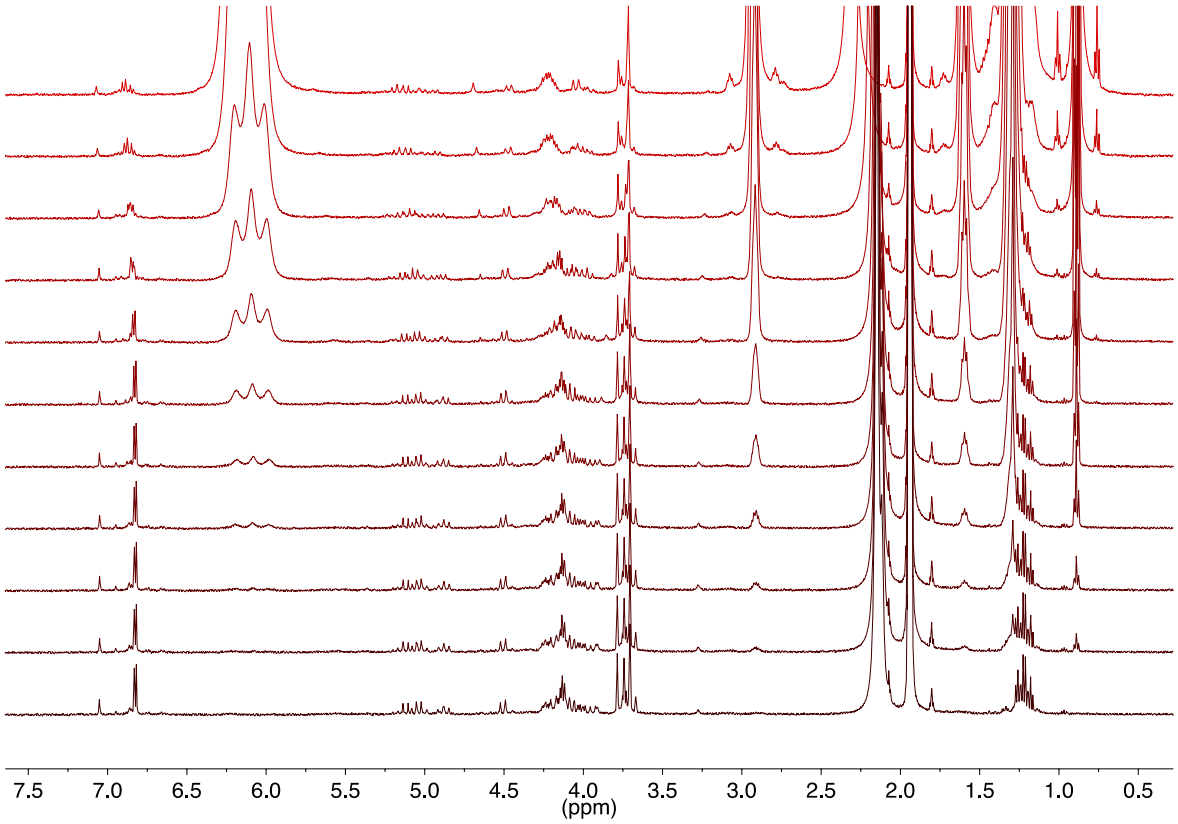

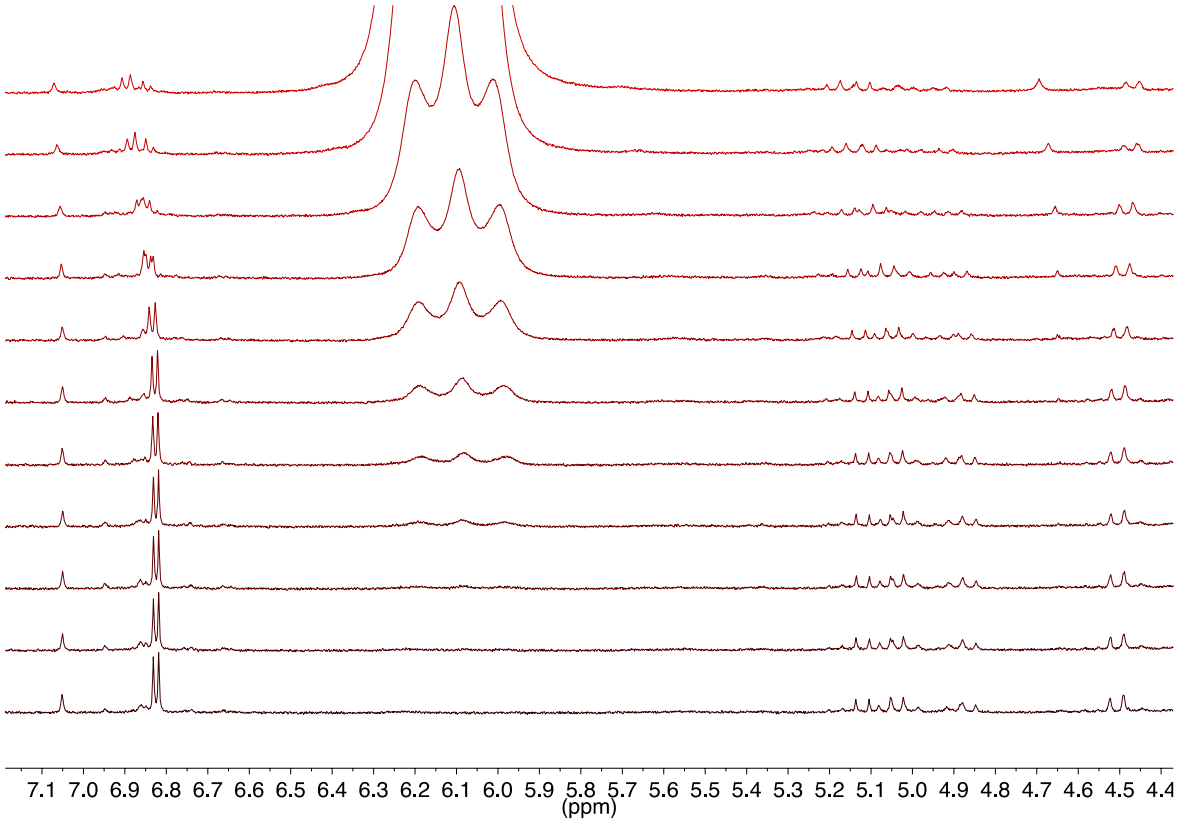

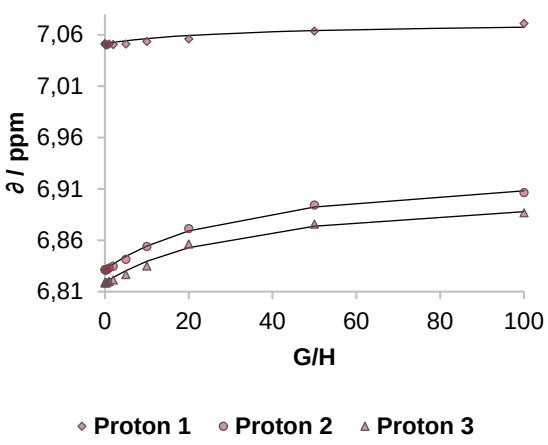

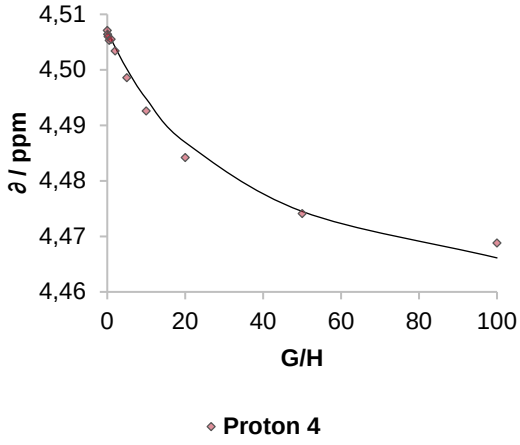

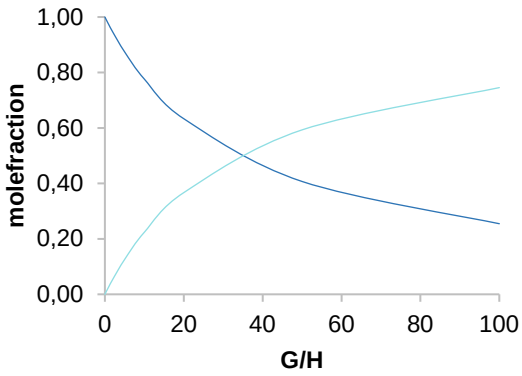

Titrated at 1.0 mM [H].

K_a = 29.5 ± 1.9 M^{-1}.

RMS = 1.9878•10^{-3}.

7. Additional Models of Tweezer and Guests

Models were compiled using the Spartan chemistry software (equilibrium geometry, PM3 semiempirical method; gas phase). Two possible binding motifs are depicted of the binding of Fe-Twe **4** and decylammonium **S14**. In the first model, the ammonium ion binds deeper into the tweezer pocket so that the more distant methylene groups (C7-C9) are close to the active oxidation site (Figure S2). In the second model, the binding of the aliphatic ammonium salt is shallower, leading to a proximity of the C3-C5 methylene groups to the active oxidation site (Figure S3).

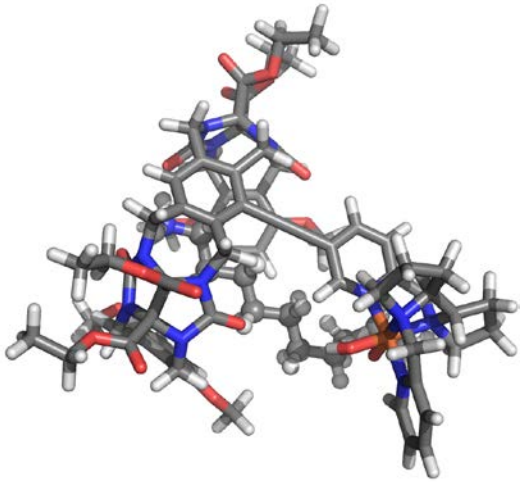

Figure S9: PM3 semi-empirical model I of Fe-Twe **4** and deeply binding decylammonium **S14** (binding mode 1).

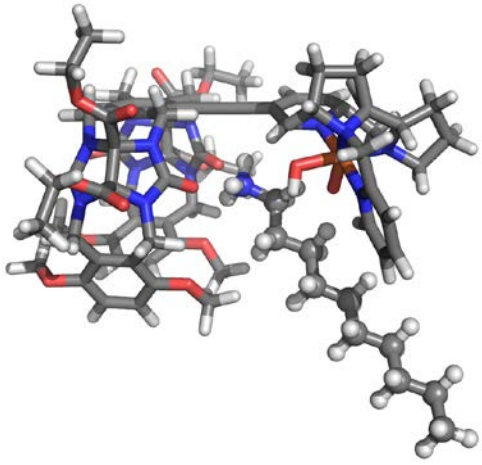

Figure S10: PM3 semi-empirical model I of Fe-Twe **4** and shallow binding decylammonium-**S14** (binding mode 2).

8. Molecular dynamics simulations and free energy calculation

To investigate the differences in the relative binding energies of binding modes 1 and 2 (see Fig. S9-10), we performed enhanced sampling metadynamics[20] simulations using the General Amber Force Field (GAFF)[21] with ab initio derived RESP charges[22]. The GAFF/RESP parametrization has proven to describe properly binding thermodynamics of host-guest chemistry, including cucurbiturils-hydrocarbons complexes[23] and glycoluril-derived molecular tweezers-hydrocarbons complexes,[24] that are structurally very similar to those investigated in this study. Metadynamics provides an acceleration to molecular dynamics sampling allowing us studying the slow interconversion mechanism between Mode 1 and Mode 2 and at the same time obtaining the free energy profile associated to this process, thus including both enthalpic and entropic contributions.

To model the host-guest complex we simplified the structure of the tweezer excluding the Fe(pdp) catalytic chain and retaining only the binding glycoluril tweezer forming a complex with a pentylammonium ion. This choice is motivated by the fact that the catalytic oxidation occurs on much shorter time scales that those of conformational rearrangements. Thus, we may assume that the oxidation selectivity is directly driven by a specific binding state whose lifetime is longer by orders of magnitude than the one of the catalytic step. Furthermore, the host-guest binding is mostly driven by the interaction of the ammonium cation with the glycoluril and ether oxygen atoms of the tweezer and, therefore, the influence of the catalytic tail on the conformational dynamics can be reasonable neglected.

To mimic realistic experimental conditions the complex has been placed in a 30 Å simulation box with periodic boundary conditions surrounded by 203 acetonitrile solvent molecules and a BF_4^- counterion neutralizing the overall charge of the system reproducing the experimental concentration of 0.1 M for the alkylammonium salt. The simulation has been performed at 300 K sampling a 2.4 μs trajectory with a 2 fs timestep using GROMACS[25] patched with the PLUMED2 code[26] for the additional metadynamics bias. To drive the interconversion between binding modes the metadynamic bias has been progressively added along two specific Collective Variables (CVs) relevant to the description of the binding process. The first CV (C_{Mode12}) accounts for the binding of the ammonium group to site 1 or 2 of the molecular tweezer. The second CV (d_{BF4-}) describes the distance between the ammonium group and its counterion BF_4^-. Detailed information on the design and selection of the CVs as well as further computational details can be found below.

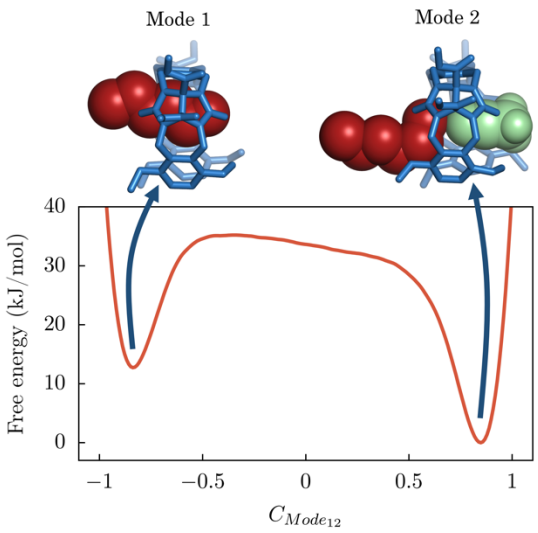

Figure S11: Free energy profile along C_{Mode12} displaying the large thermodynamic stability of binding Mode 2. Structure snapshots of the sampled trajectory are reported above the two minima where in blue sticks is depicted the tweezer host structure, in red balls the pentylammonium guest, and in pale green balls the acetonitrile molecule always present in binding Mode 2.

To illustrate the results of our calculations we projected the free energy surface along C_{Mode12} only as reported in Figure S11. As expected, Mode 2 is thermodynamically more stable than Mode 1. By integrating the free energy basins between -1.5 and 0 for Mode 1 and between 0 and +1.5 for Mode 2 we estimate a free energy difference for the process of ΔG_{21} = -5.0 kJ/mol. This free energy difference at 300 K corresponds to a relative Boltzmann population of 9:1 for Mode2:Mode1. This result confirms the experimental observations for which the relative abundance of C3-C4 oxidation is ascribed to the larger stability of Mode 2 compared to Mode 1. The reason of this stability can be found in the interaction of the complex with the acetonitrile solvent molecules. Figure S12 reports the free energy surface calculated by reweighting procedure[27] along C_{Mode12} and a CV that accounts for the coordination of acetonitrile molecules to the binding site associated with Mode 1 ($C_{ACN\text{-}Mode1}$, vide infra). It is clear from this picture that whenever the guest is bound in Mode 2 (C_{Mode12} = 1), the vacant coordination site of Mode 1 is most likely occupied by an acetonitrile unit ($C_{ACN\text{-}Mode1}$ = 1). Acetonitrile is a strongly polar molecule where the cyano carbon atom as well as the methyl group are positively polarized whereas the ending nitrogen atom is negative (see, e.g.[28]). This feature has a double effect. First, the positive part of the acetonitrile molecule interacts with the partial negative polarization provided by the glycoluril and ether oxygen atoms of the guest stabilizing the system. Second, the lone pair of the cyano group is a hydrogen bond acceptor that can easily bind of the ammonium hydrogen atoms stabilizing further binding Mode 2 (see Figure S15).

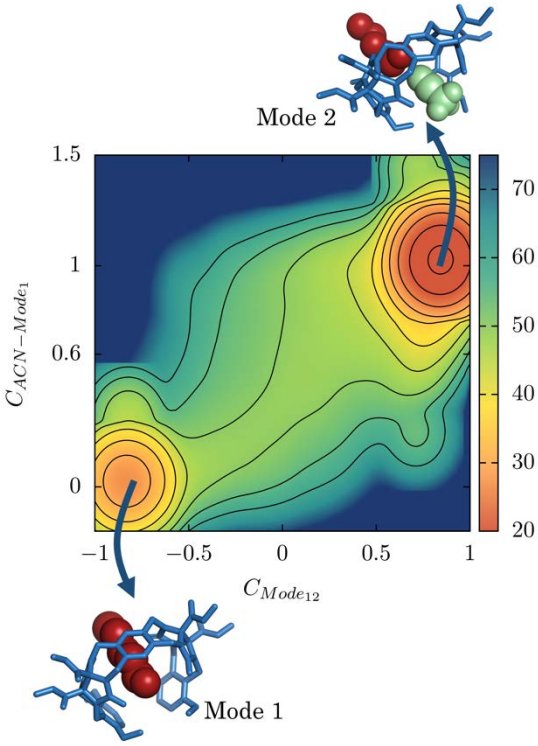

Figure S12: Free energy surface reweighted along C_{Mode12} and $C_{ACN\text{-}Mode1}$ showing that the larger stability of Mode 2 is also ascribed by the constant presence of an acetonitrile molecules occupying binding site 1 and, thus, stabilizing the host-guest complex. Structure snapshots of the sampled trajectory are reported above the two minima where in blue sticks is depicted the tweezer host structure, in red balls the pentylammonium guest, and in pale green balls the acetonitrile molecule always present in binding Mode 2. The color bar on the righthand side represent the energy reported in kJ/mol.

As final remark, we discuss the effect of the counterion on the transition between the two binding modes. Whereas C_{Mode12} is the most relevant descriptor of the process of interest, the distance with the counterion plays a fundamental role in lowering the barrier for the transition between Mode 1 and 2 as it can be seen in Figure S16. We observed that the vicinity of the counterion to the complex does not affect significantly the relative stability of the two binding states. However, it is responsible of a significant lowering of the barrier separating the two free energy minima when the BF_4^- ion is close to the host-guest complex at about 4 Å from the ammonium group. This fact is motivated by the electrostatic stabilization exerted by the anion during the transition between the two binding modes. In fact, when shifting from Mode 1 to Mode 2 the ammonium cation is not stabilized anymore by the tweezer's negatively charged oxygens of site 1 or 2. The effect of the BF_4^- ion is to partially neutralize the charge lying close to the ammonium cation separated only by the host structure. This results in a much lower energic cost in transitioning between binding modes.

8.1. Collective Variables Design

C_{Mode12} - Binding mode

To describe the binding of the pentylammonium ion to the two sites of the glycoluril molecular tweezers, we considered the proximity of the ammonium group to the glycoluril and ether groups present on the external sides of the tweezer. Chemically, the ammonium group binds these oxygen atoms via hydrogen bond and electrostatic interactions, determining the binding to Mode 1 or Mode 2. However, this is a very dynamic type of bonding whose fluctuations within a specific binding mode are large. Thus, a direct counting of the hydrogen bonds between the ammonium group and the oxygen atoms of Mode 1 and 2 would result in a very noisy signal not suitable for describing the overall binding mode interconversion.

To simplify this description, we define the centers of mass of the four oxygen atoms on each side of the host molecule as dummy atoms representing the binding site. We then consider the coordination number of these two dummy atoms with the nitrogen atom of the ammonium group. The coordination number is a smoothly decaying switching function counting the presence of the ammonium nitrogen atom within a sphere of 4 Å placed around the dummy atoms of Mode 1 and 2. These coordination numbers, here defined as C_{Mode1} and C_{Mode2}, are approach 1 and 0 when the guest is bound in Mode 1 respectively, and vice versa for Mode 2.

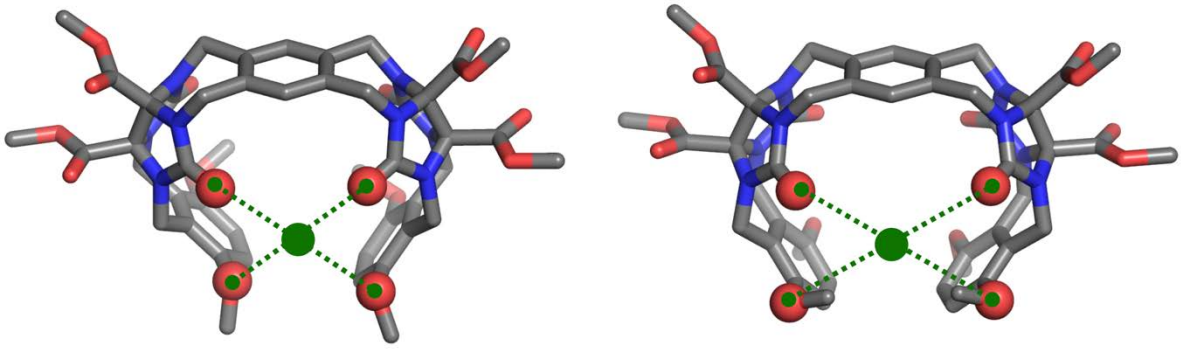

Figure S13: Oxygen atoms used to calculate the center of mass defining the dummy atom for Mode 1 and Mode 2.

To simplify further the collective variable, we combined the two coordination numbers in a one-dimensional anti-symmetric linear combination of the form $C_{Mode12} = C_{Mode2} - C_{Mode1}$.[29] In this way we can describe the binding to Mode 1 or 2 with one single collective variable that corresponds to −1 when the guest is bound to Mode 1 and to +1 when it is bound to Mode 2.

d_{BF4-} - Counterion distance

As it became clear from the first test simulations, the presence of the BF_4^- counterion is not negligible and it appeared to play a fundamental role in interconversion process. Therefore, we decided to include the effect of its vicinity to the host-guest complex by using the distance (d_{BF4-}) between the boron atom of BF_4^- and the nitrogen atom of the ammonium group interreacting electrostatically although screened by the host and solvent molecules.

$C_{ACN\text{-}Mode1}$ - Binding of acetonitrile to site 1

Similarly to C_{Mode1}, this CV measures the coordination of the methyl carbon atom of any of the 203 acetonitrile molecules to the center of mass of the oxygen atoms at binding site 1 within a 2 Å sphere.

8.2. Simulation Details

System preparation

The host and guest molecules have been parametrized using an all-atoms GAFF/RESP procedure as implemented in the antechamber program.[30] RESP charges were calculated using Gaussian code at the HF/6-31G* level. Acetonitrile parameters have been obtained from the AMBER database of the Bryce group (http://research.bmh.manchester.ac.uk/bryce/amber/).[31] BF_4^- parameters have been obtained from the AMBER tutorial (https://ambermd.org/tutorials/advanced/tutorial15/Tutorial2.xhtml).[32]

1 host molecule, 1 guest molecule, 1 BF_4^- molecule, and 203 acetonitrile molecules were placed in a 30 Å simulation box. The system has been first minimized for 3281 optimization steps, heated in NVT ensemble up to 300 K for 2500000 steps, the pressure has been subsequently adjusted using two NPT simulations using first the Berendsen barostat for 100000 steps followed by a further equilibration using the Parrinello-Rahman barostat for 500000 steps. The step used was 2 fs.

Metadynamics

One single walker well-tempered metadynamics simulation has been performed using a 2 fs integration step for 2.4 μs. Two dimensional Gaussian kernels have been deposited along C_{Mode12} and d_{BF4-} every picosecond of simulation (each 500 steps) with an initial height of 0.5 kJ/mol and a sigma corresponding to 0.05 and 0.1 for the two variables. To ensure dimensional homogeneity of the two CVs d_{BF4-} has been scaled by a factor of 20.

Convergence of the free energy difference after removal of a 0.6 μs transient is reported in Figure S14.

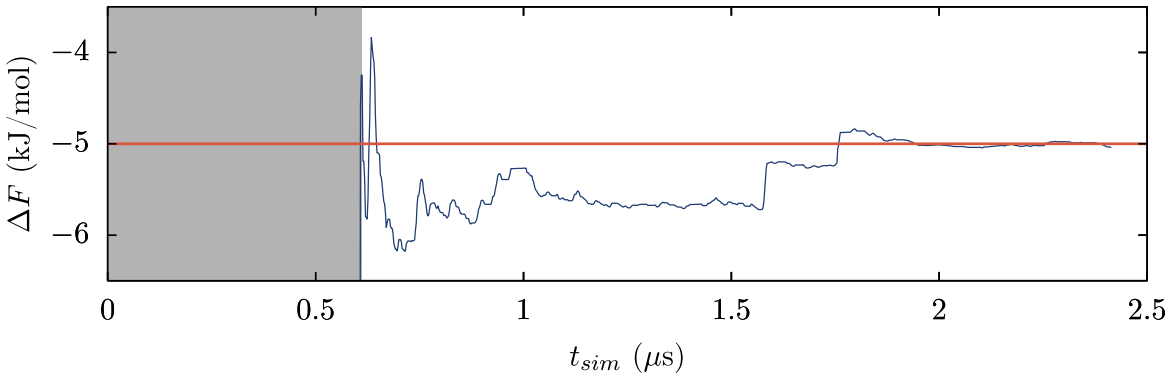

Figure S14: Free energy convergence to the -5 kJ/mol value (orange line) obtained by progressive reweighting of the metadynamics trajectory. The blue line indicates the oscillation of the free energy difference between basin of Mode 2 and Mode 1. The grey region indicates the metadynamics transient of 0.6 μs removed to ensure equilibrium dynamics.

Hydrogen Bonding with Cyano Group in Mode 2

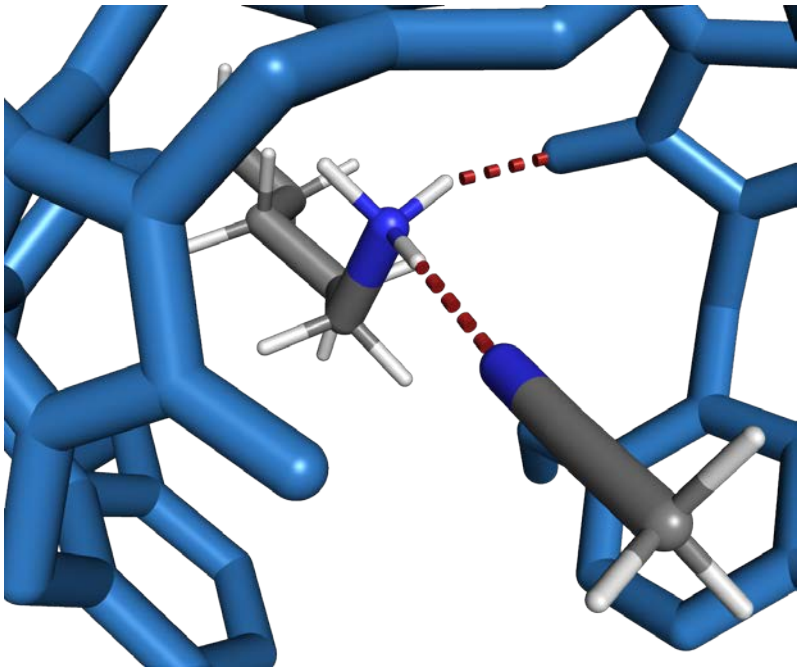

Figure S15: Complexation of one acetonitrile molecule in binding site 1 forming one hydrogen bond with the ammonium group. The surrounding solvent molecules and the BF_4^- unit are omitted for clarity.

Free Energy Surface along $C_{Moder12}$ and d_{BF4-}

Figure S16 reports the Free Energy Surface along C_{Mode12} and d_{BF4-} obtained by sampling the process using metadynamics. It can be observed how the distance of the counterion plays a fundamental role in lowering the barrier of the transition between Mode 1 and Mode 2 but does

not affect significantly the relative stability of the two binding modes. Three main "reaction channels" are observed at 4, 8, and 13 Å corresponding to different solvation shells of the host-guest complex in acetonitrile. It is evident that the lowest barrier is observed at 4 Å, corresponding to the BF_4^- ion in close proximity to the complex. This result is reasonable as acetonitrile, although polar, at relatively high concentrations as 0.1 M cannot screen sufficiently the electrostatic interaction between BF_4^- and the complexed ammonium cation. Therefore, the most likely path to interconversion between Mode 1 and 2 is the one at 4 Å where the two charges are much closer. It may be possible that at lower ionic concentrations the lowest transition barrier could be observed at large distances at which the two ions are be separated by several solvation shells, thus enabling a more effective electrostatic screening.

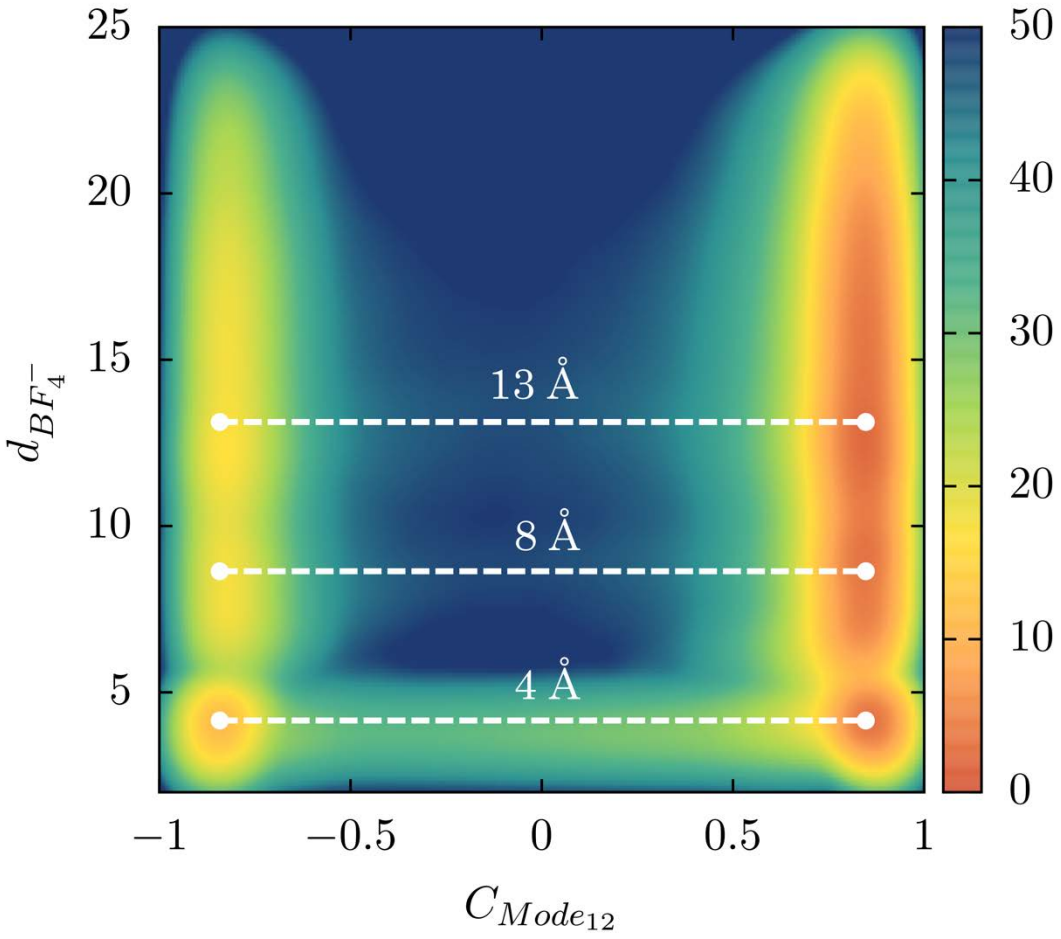

Figure S16: Free energy surface obtained by reweighting metadynamics data along C_{Mode12} and d_{BF4-}. C_{Mode12} is a dimensionless quantity whereas d_{BF4-} is a distance in Å. The color bar on the righthand side represent the energy reported in kJ/mol.

9. 1H- and 13C-NMR Spectra of New and Key Compounds

S4 – ^{1}H

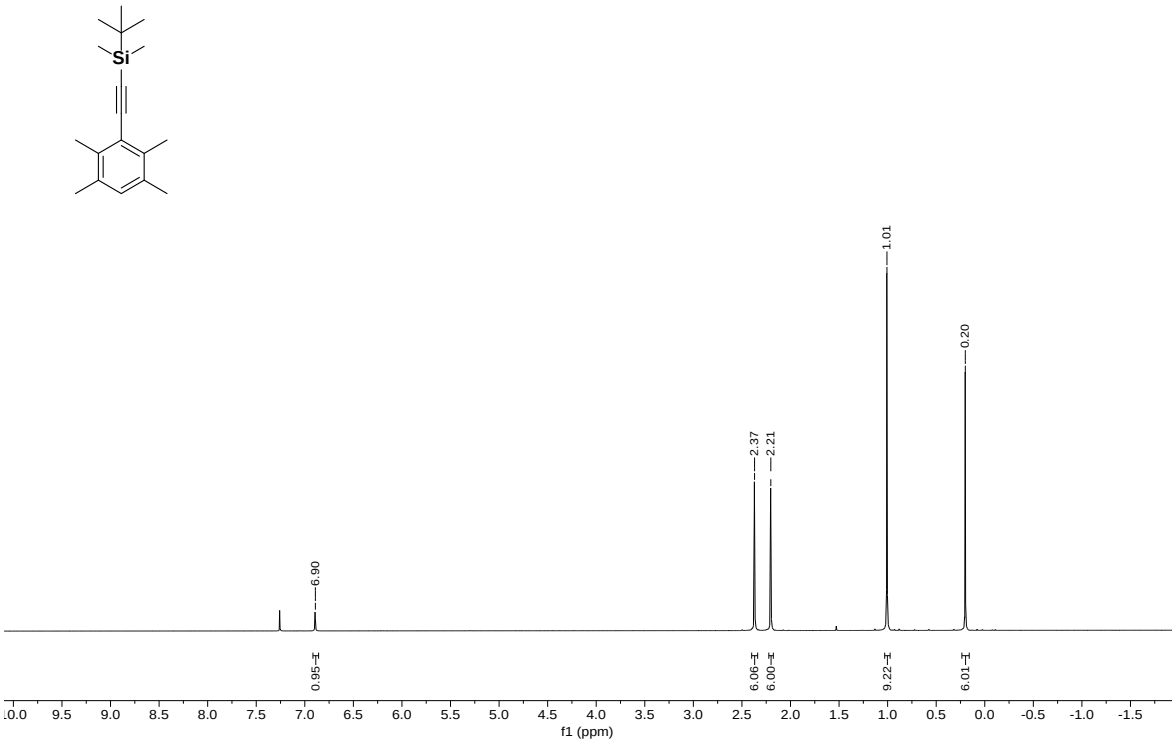

S4 – ^{13}C

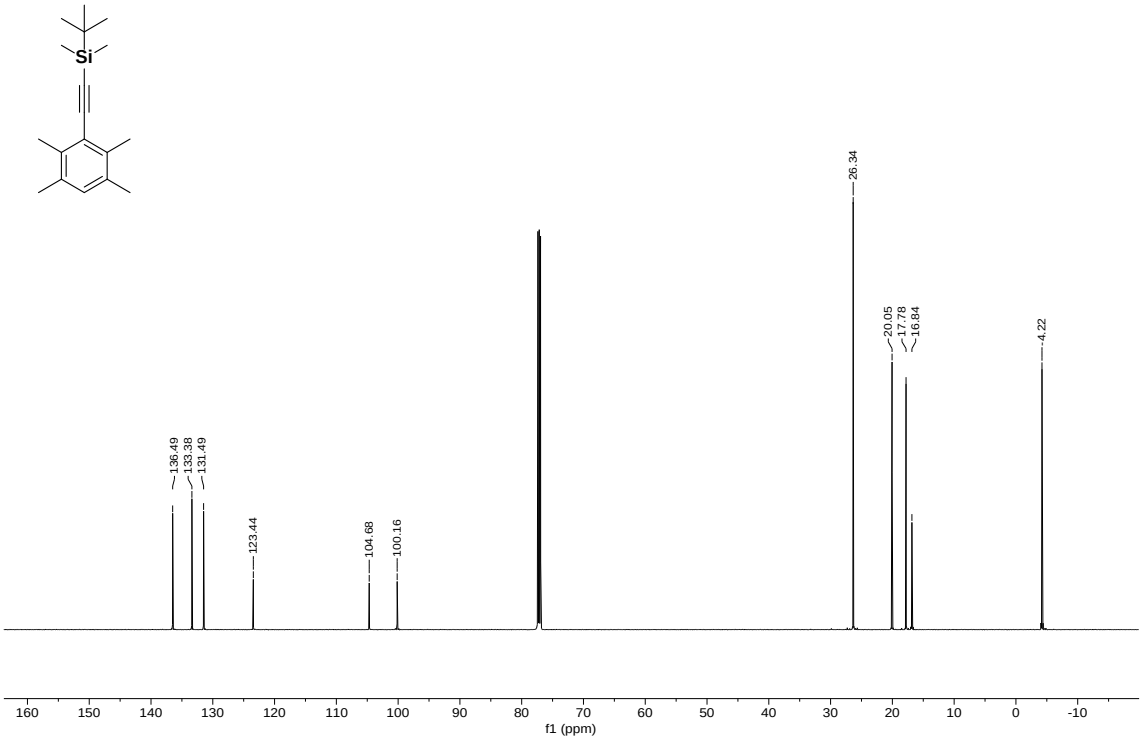

6 – ^{1}H

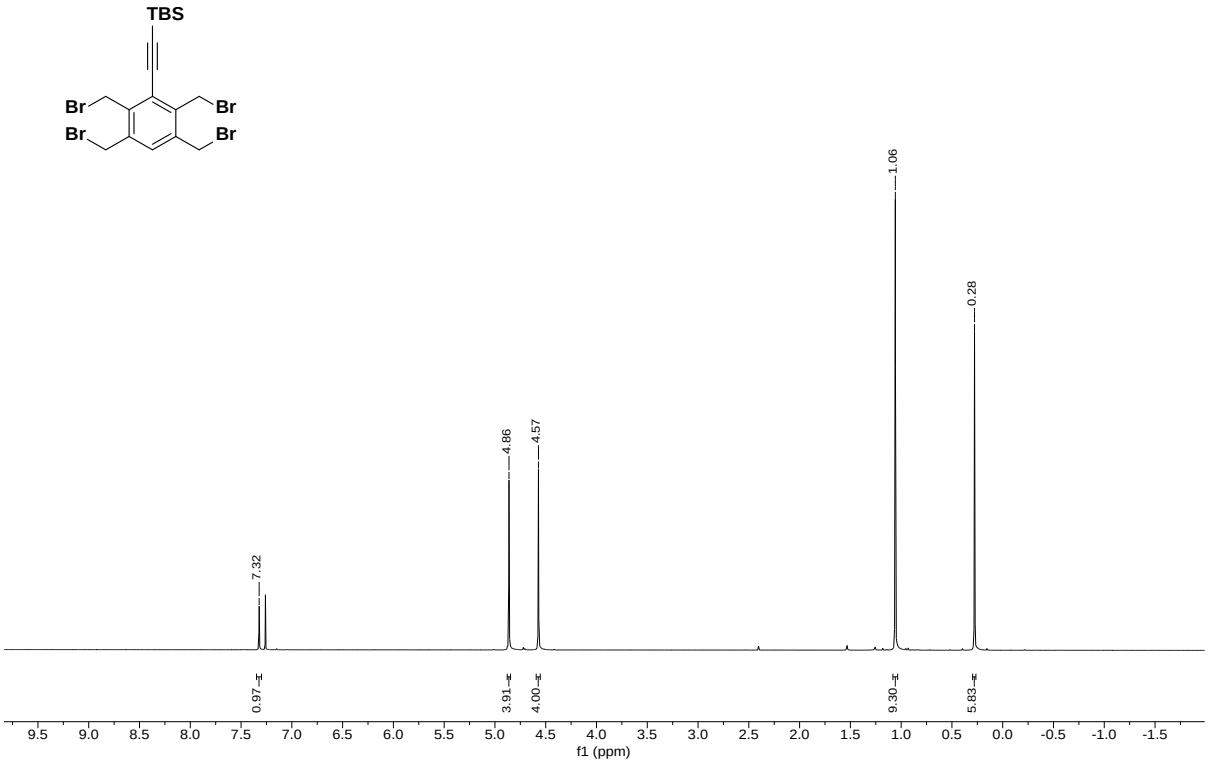
TBS
Br
Br
Br
Br
7.32
4.86
4.57
1.06
0.28
0.97
3.91
4.00
9.30
5.83
f1 (ppm)

6 – ^{13}C

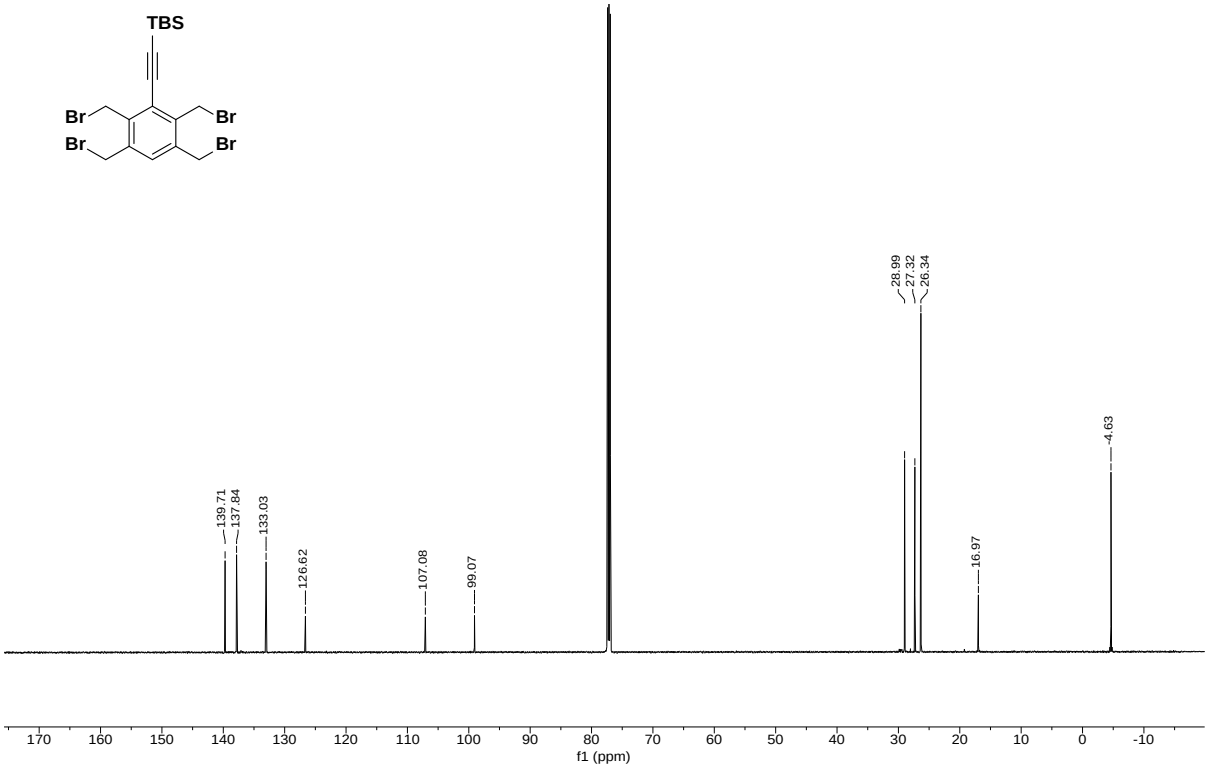
TBS
Br
Br
Br
Br
139.71
137.84
133.03
126.62
107.08
99.07
28.99
27.32
26.34
16.97
-4.63
f1 (ppm)

S7 – ^{1}H

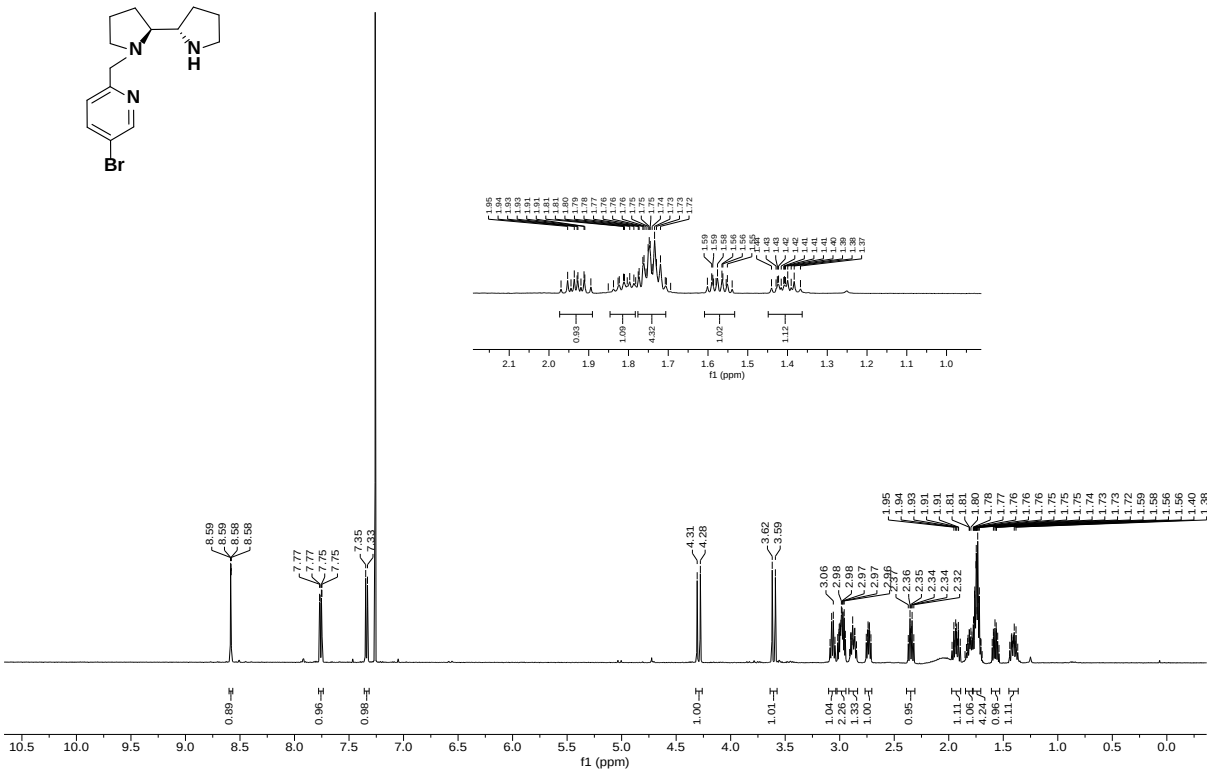
N
N
H
N
Br
f1 (ppm)

S7 – ^{13}C

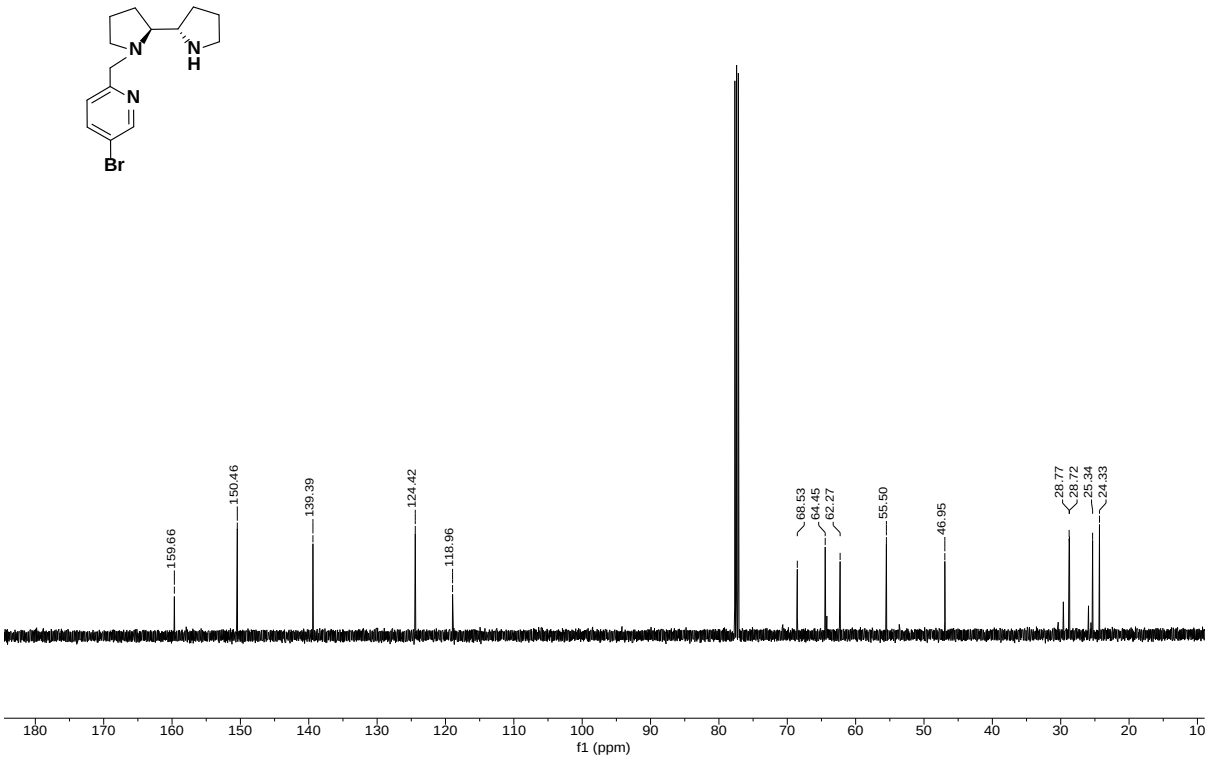
N
N
H
N
Br
159.66
150.46
139.39
124.42
118.96
68.53
64.45
62.27
55.50
46.95
28.77
28.72
25.34
24.33
f1 (ppm)

14 – ^{1}H

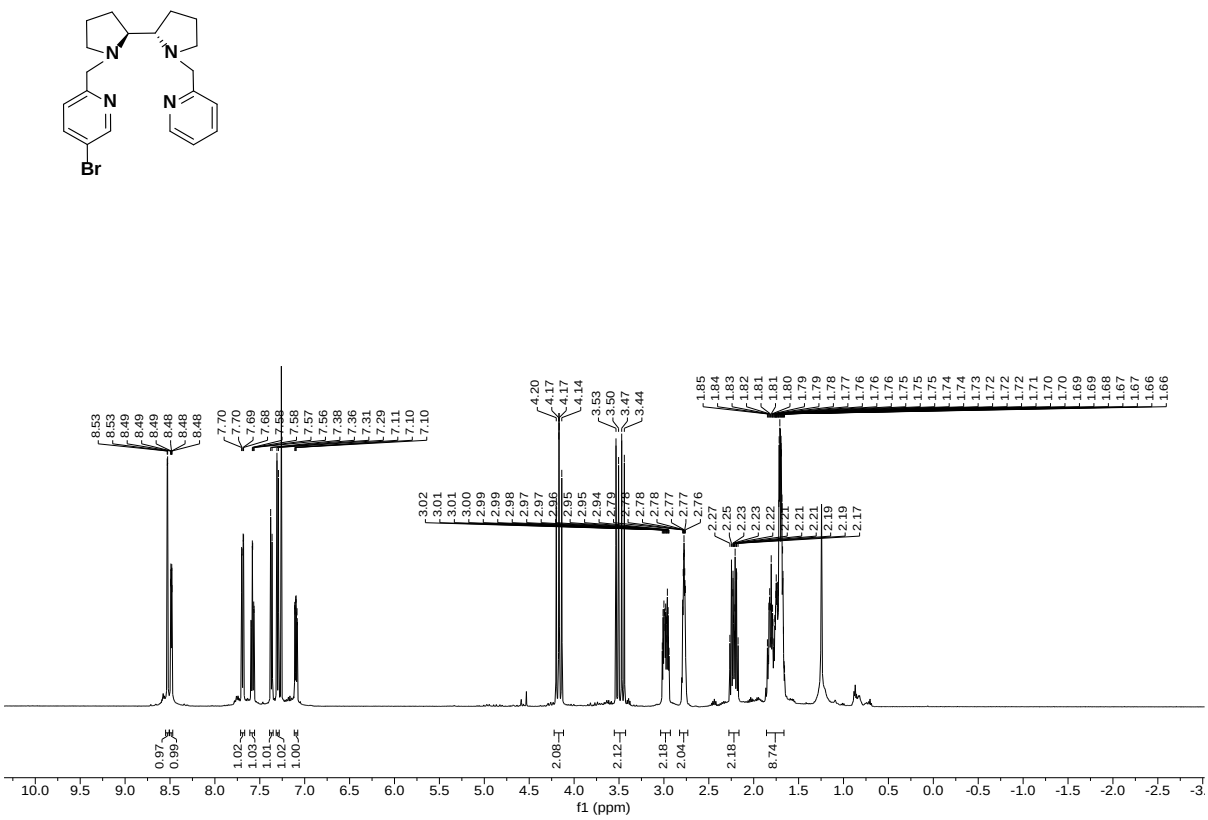
Br
8.53 8.53 8.49 8.49 8.49 8.48 8.48 8.48
7.70 7.70 7.69 7.68 7.68 7.58 7.57 7.56 7.38 7.36 7.31 7.29 7.11 7.10 7.10
4.20 4.17 4.17 4.14
3.53 3.50 3.47 3.44
3.02 3.01 3.01 3.00 2.99 2.99 2.98 2.97 2.97 2.96 2.95 2.95 2.94 2.79 2.78 2.78 2.78 2.77 2.77 2.76
2.27 2.25 2.23 2.23 2.22 2.21 2.21 2.21 2.19 2.19 2.17
1.85 1.84 1.83 1.82 1.81 1.81 1.80 1.79 1.79 1.78 1.77 1.76 1.76 1.76 1.75 1.75 1.75 1.74 1.74 1.73 1.72 1.72 1.72 1.71 1.70 1.70 1.69 1.69 1.68 1.67 1.67 1.66 1.66
0.97 0.99 1.02 1.03 1.01 1.02 1.00 2.08 2.12 2.18 2.04 2.18 8.74
f1 (ppm)

14 – ^{13}C

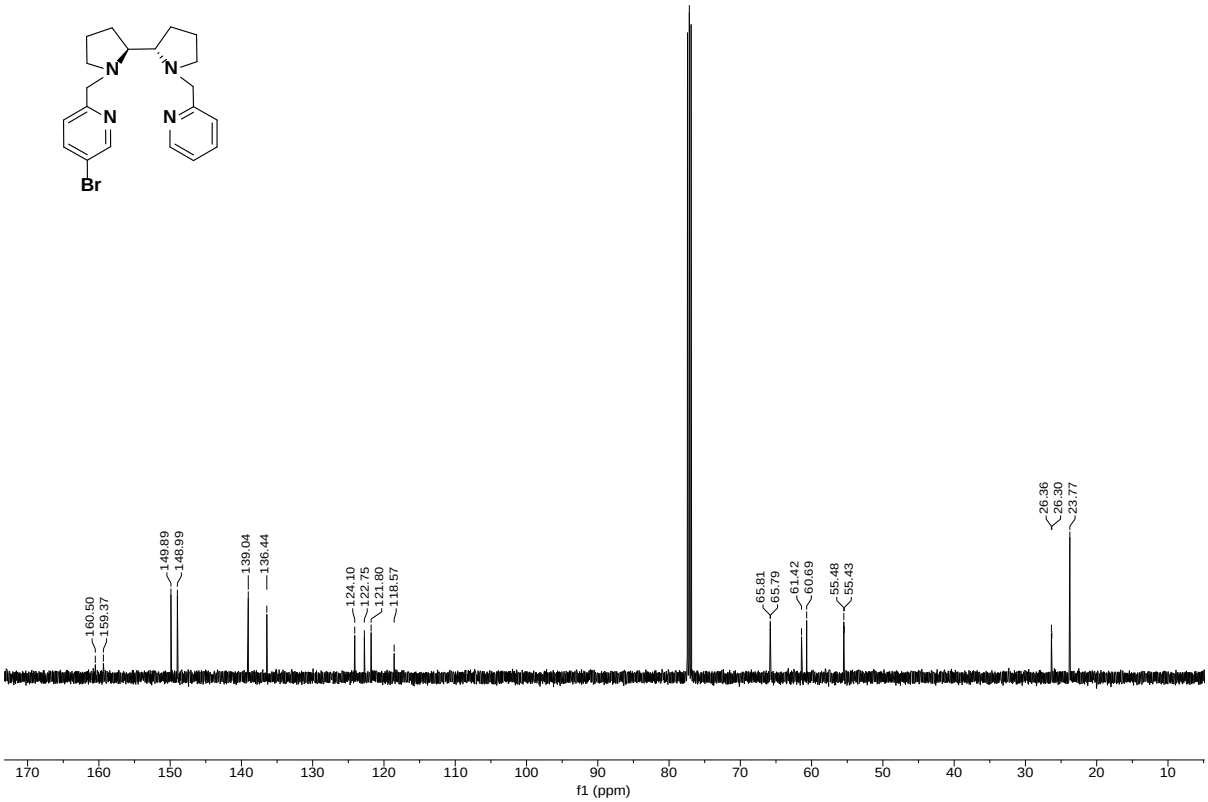
Br
160.50 159.37
149.89 148.99
139.04 136.44
124.10 122.75 121.80 118.57
65.81 65.79 61.42 60.69 55.48 55.43
26.36 26.30 23.77
f1 (ppm)

2 – ^{1}H

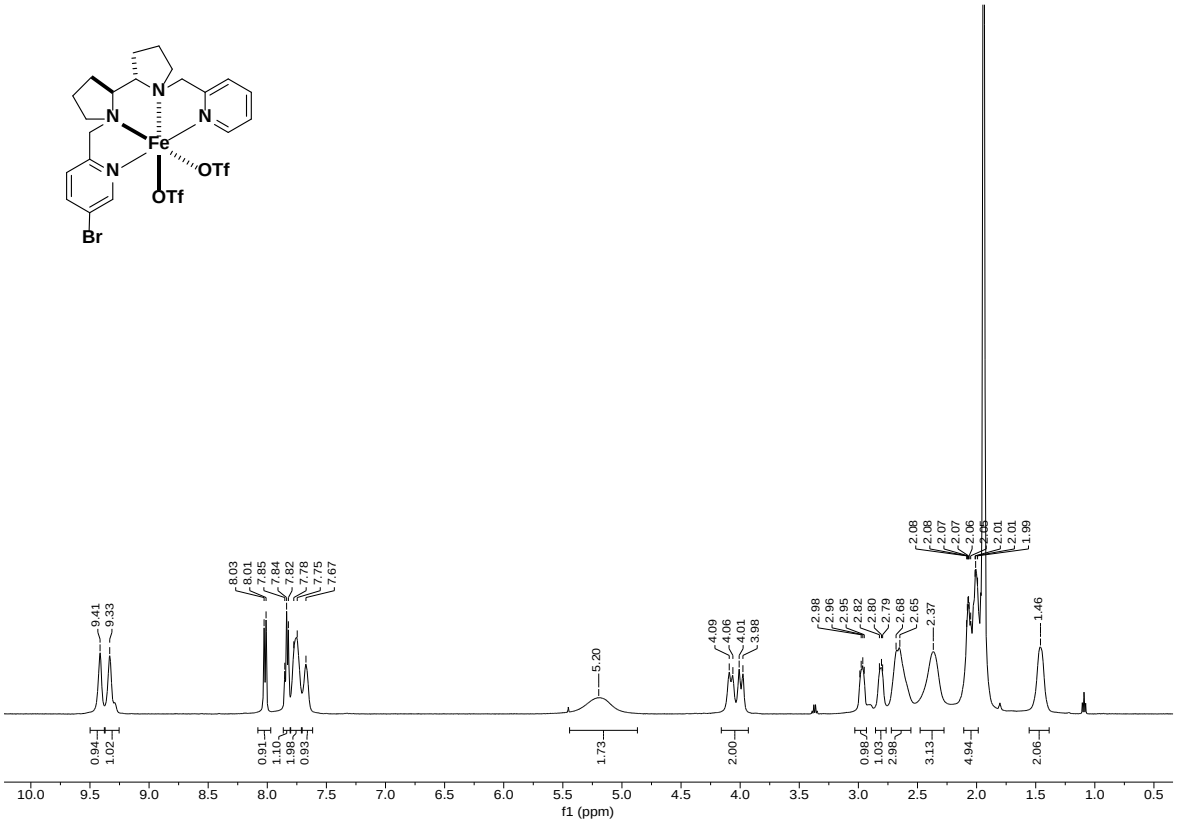
N
N
N
Fe
N
OTf
OTf
Br
9.41
9.33
8.03
8.01
7.85
7.84
7.82
7.78
7.75
7.67
5.20
4.09
4.06
4.01
3.98
2.98
2.96
2.95
2.82
2.80
2.79
2.68
2.65
2.37
2.08
2.08
2.07
2.07
2.06
2.01
2.01
1.99
1.46
0.94
1.02
0.91
1.10
1.98
0.93
1.73
2.00
0.98
1.03
2.98
3.13
4.94
2.06
f1 (ppm)

2 – ^{13}C

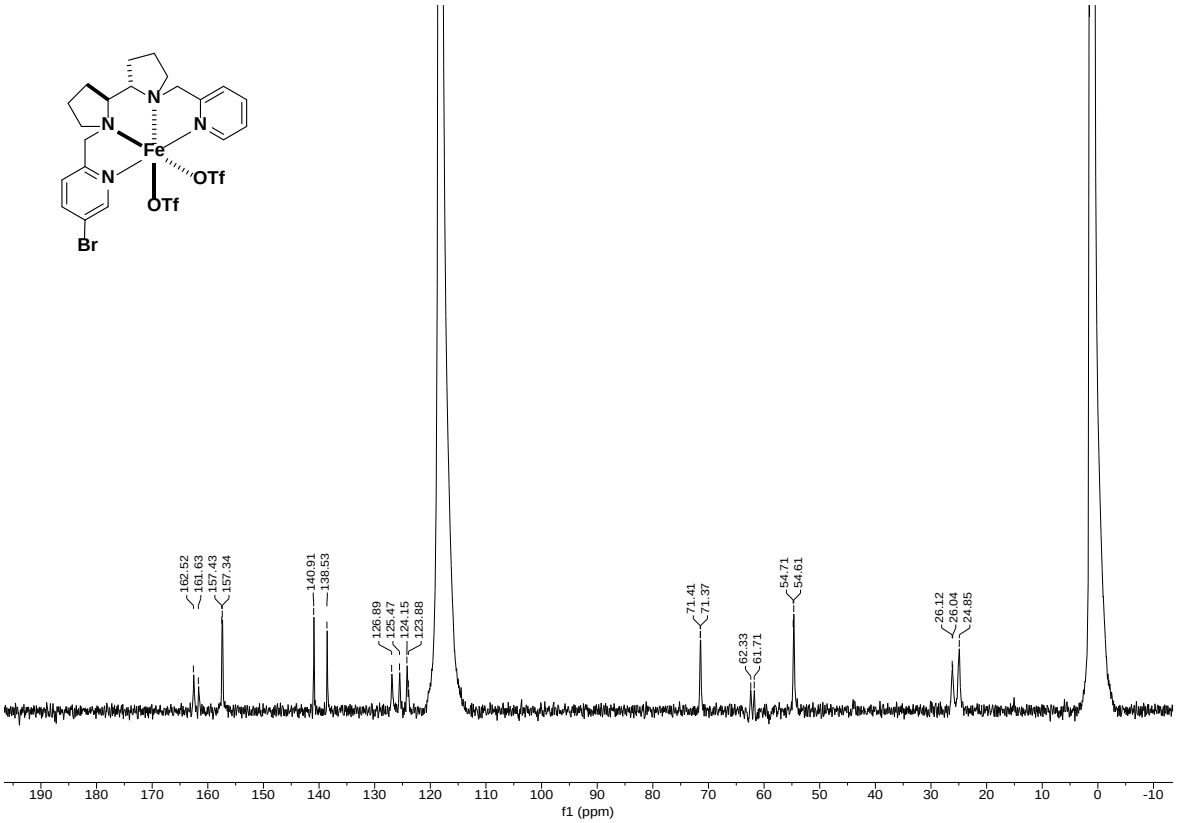
N
N
N
Fe
N
OTf
OTf
Br
162.52
161.63
157.43
157.34
140.91
138.53
126.89
125.47
124.15
123.88
71.41
71.37
62.33
61.71
54.71
54.61
26.12
26.04
24.85
f1 (ppm)

8a – ^{1}H

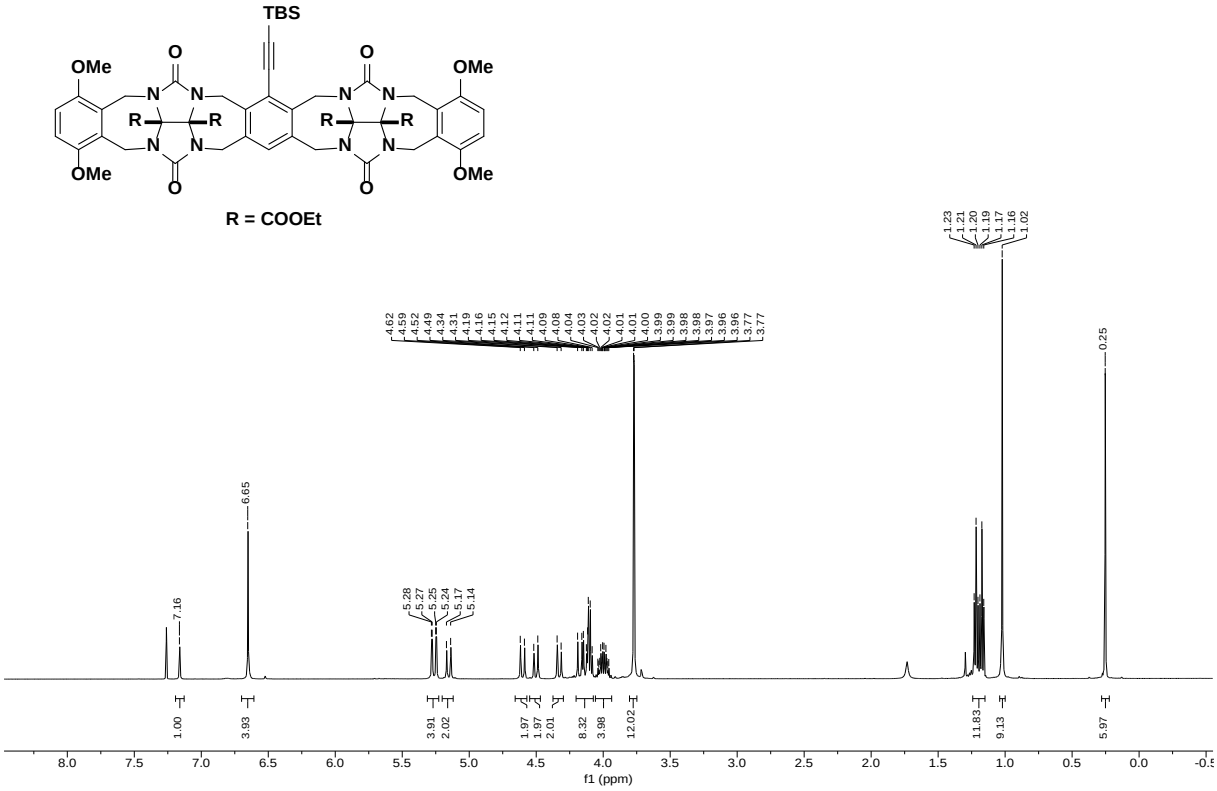
TBS
OMe
OMe
OMe
OMe
R = COOEt
1.23
1.21
1.20
1.19
1.17
1.16
1.02
4.62
4.59
4.52
4.49
4.34
4.31
4.19
4.16
4.15
4.12
4.11
4.11
4.09
4.08
4.04
4.03
4.02
4.02
4.01
4.01
4.00
3.99
3.99
3.98
3.98
3.97
3.96
3.96
3.77
3.77
0.25
6.65
7.16
5.28
5.27
5.25
5.24
5.17
5.14
1.00
3.93
3.91
2.02
1.97
1.97
2.01
8.32
3.98
12.02
11.83
9.13
5.97
f1 (ppm)

8a – ^{13}C

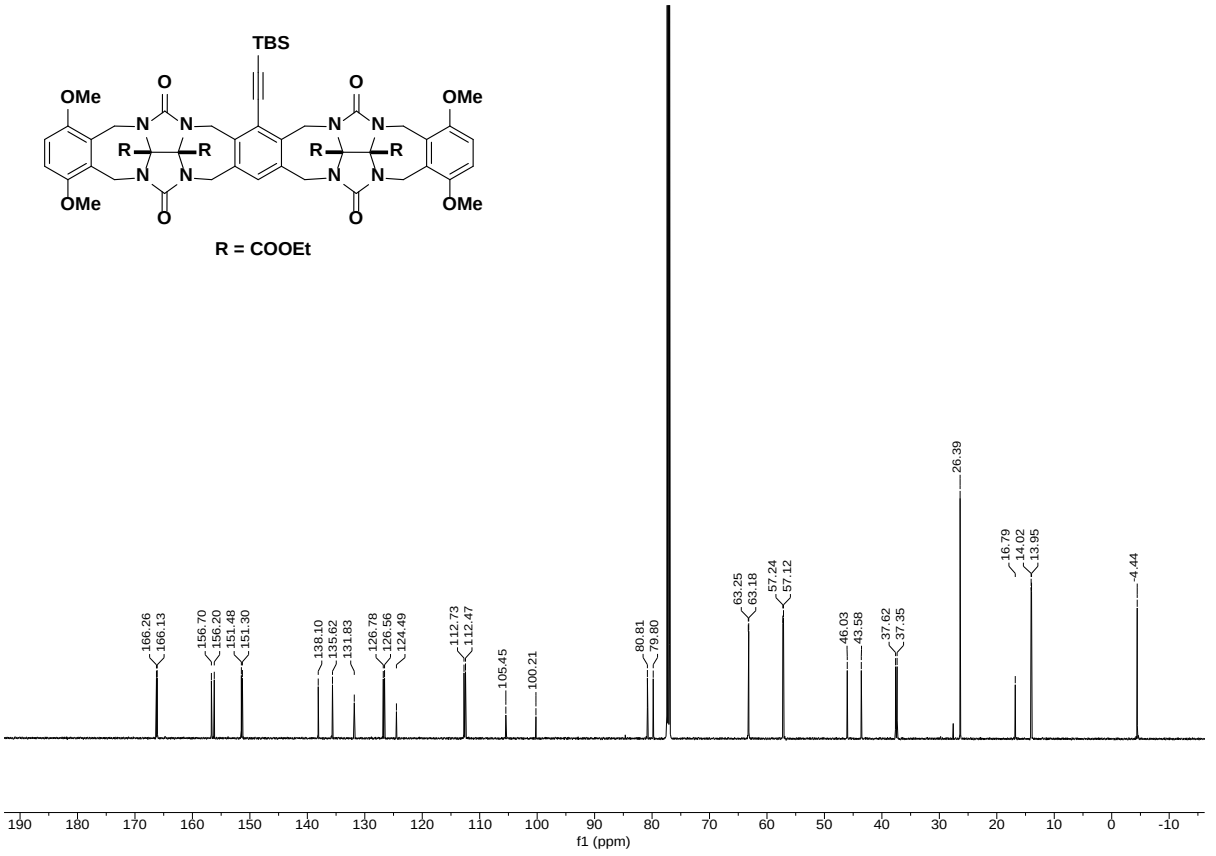
TBS
OMe
OMe
OMe
OMe
R = COOEt
166.26
166.13
156.70
156.20
151.48
151.30
138.10
135.62
131.83
126.78
126.56
124.49
112.73
112.47
105.45
100.21
80.81
79.80
63.25
63.18
57.24
57.12
46.03
43.58
37.62
37.35
26.39
16.79
14.02
13.95
-4.44
f1 (ppm)

9 – ^{1}H

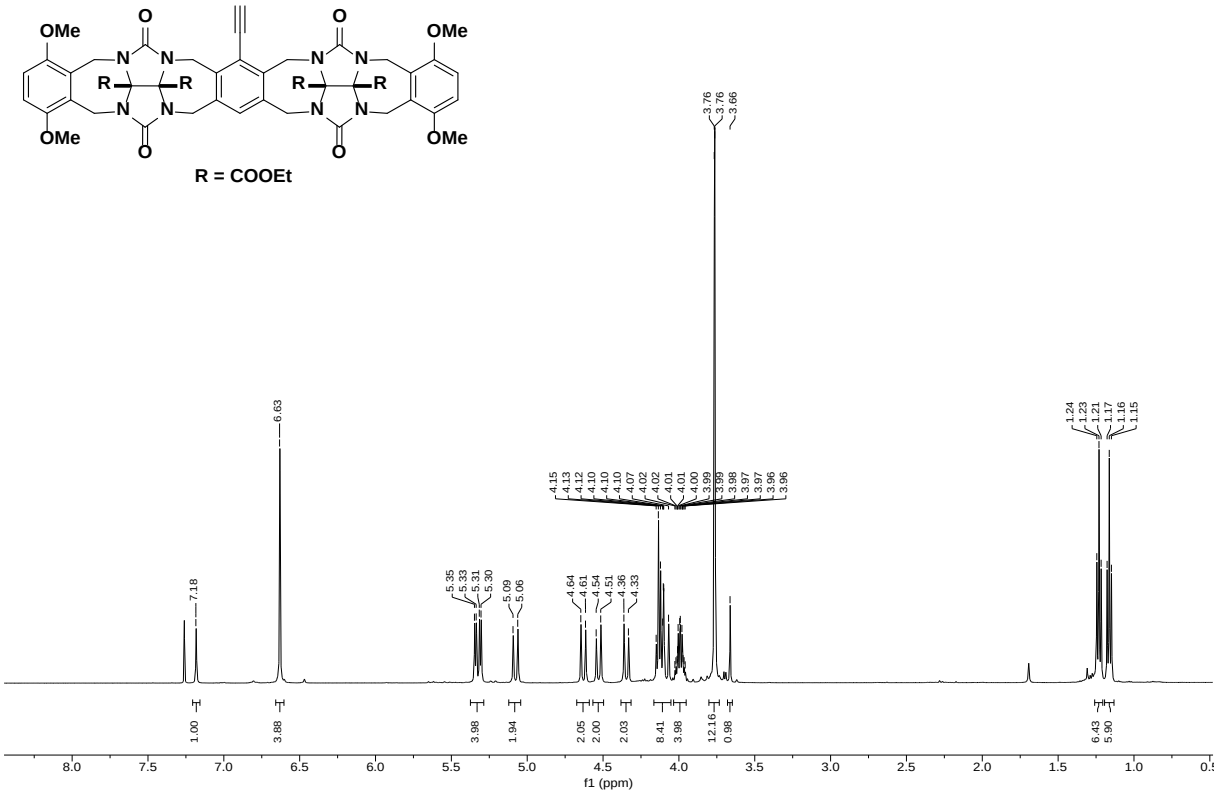
OMe
O
N
R
R = COOEt
3.76
3.76
3.66
6.63
7.18
5.35
5.33
5.31
5.30
5.09
5.06
4.64
4.61
4.54
4.51
4.36
4.33
4.15
4.13
4.12
4.10
4.10
4.07
4.02
4.02
4.01
4.01
4.00
3.99
3.99
3.98
3.97
3.97
3.96
3.96
1.24
1.23
1.21
1.17
1.16
1.15
1.00
3.88
3.98
1.94
2.05
2.00
2.03
8.41
3.98
12.16
0.98
6.43
5.90
f1 (ppm)

9 – ^{13}C

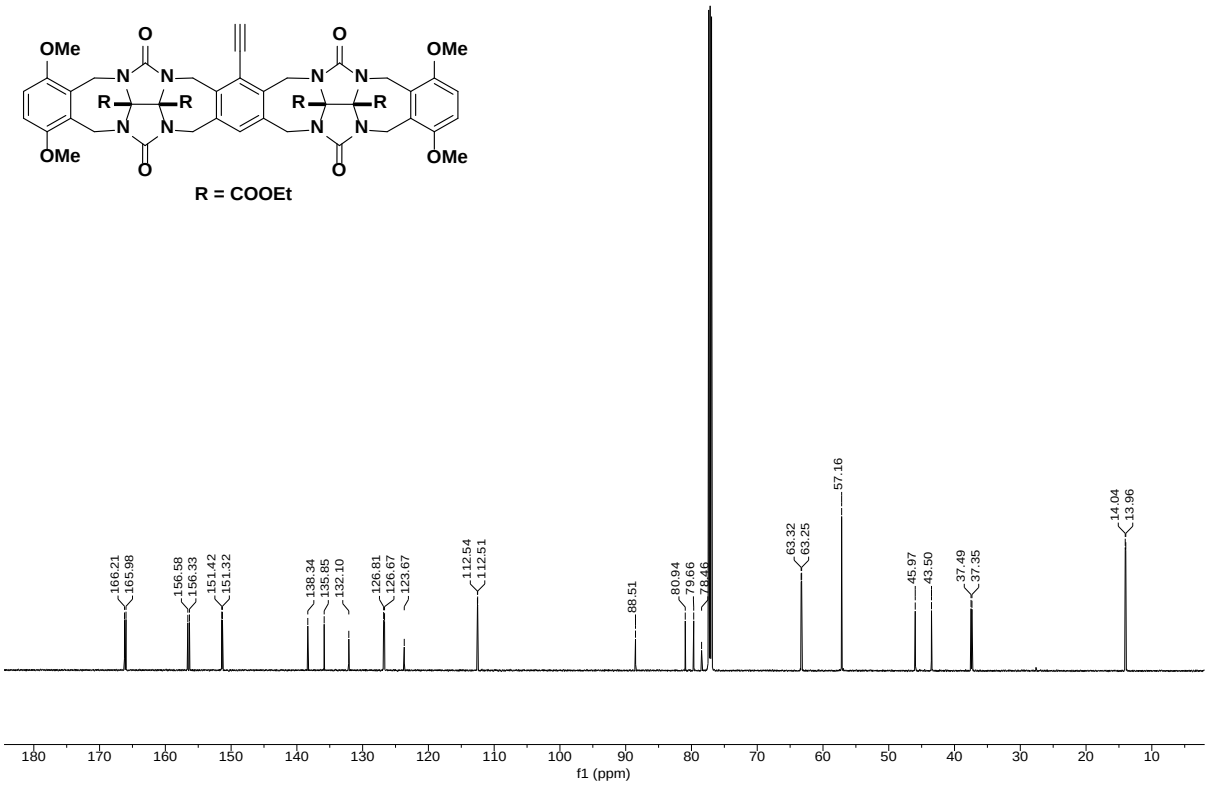
OMe
O
N
R
R = COOEt
166.21
165.98
156.58
156.33
151.42
151.32
138.34
135.85
132.10
126.81
126.67
123.67
112.54
112.51
88.51
80.94
79.66
78.46
63.32
63.25
57.16
45.97
43.50
37.49
37.35
14.04
13.96
f1 (ppm)

11 – ^{1}H

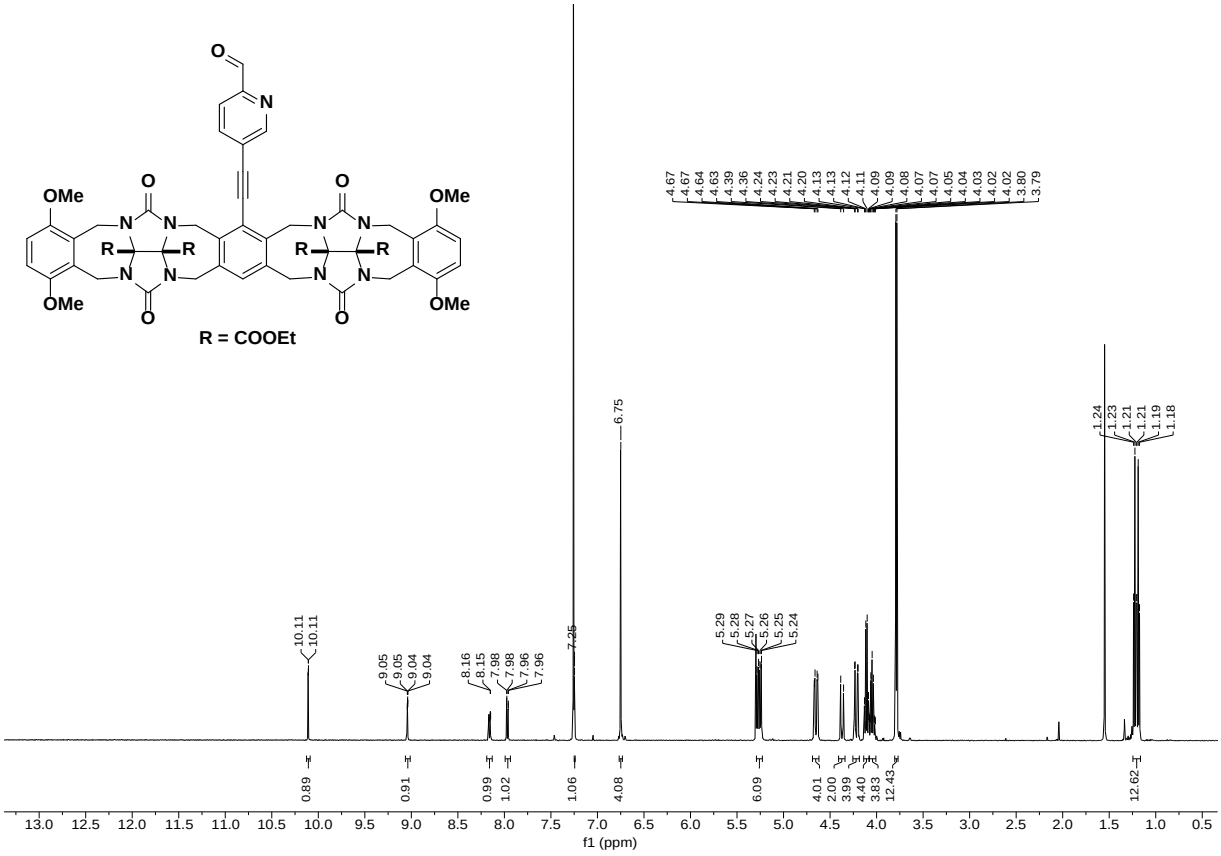

11 – ^{13}C

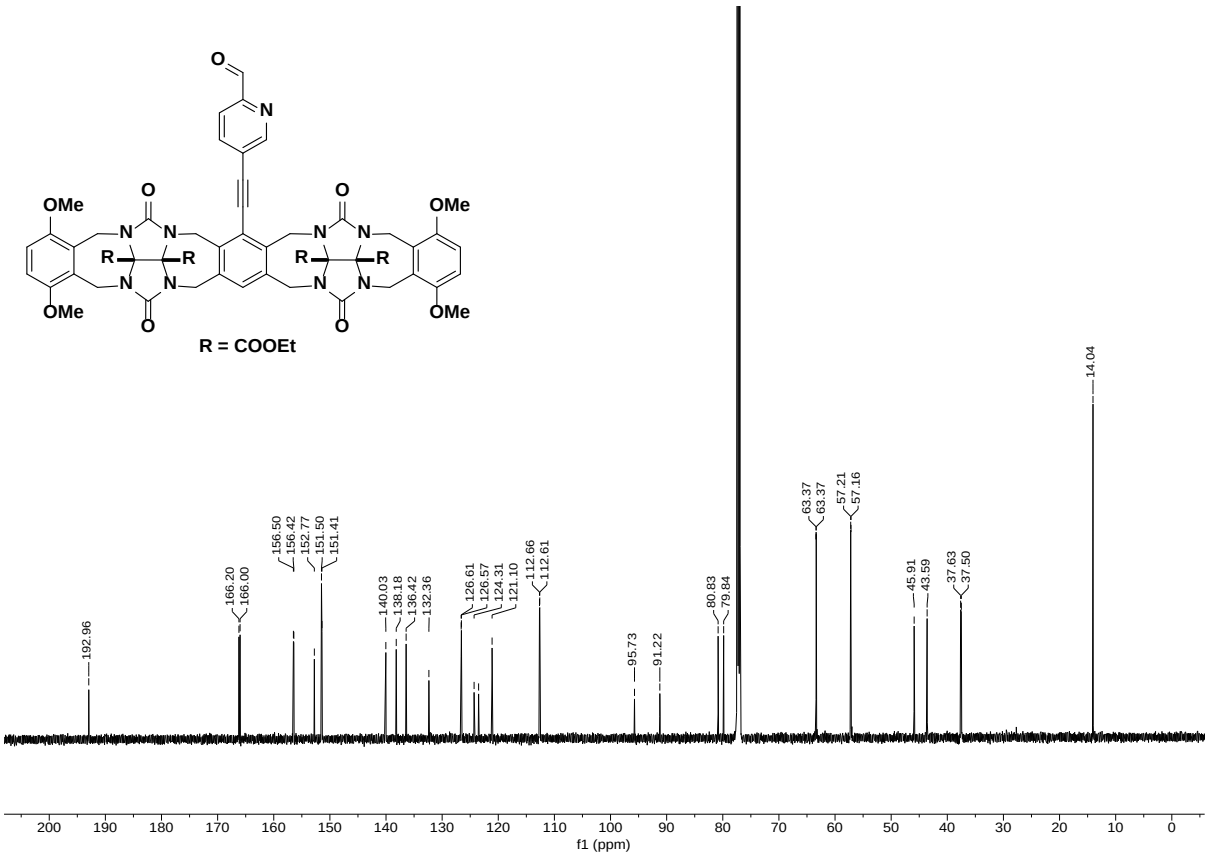

S5 – ^{1}H

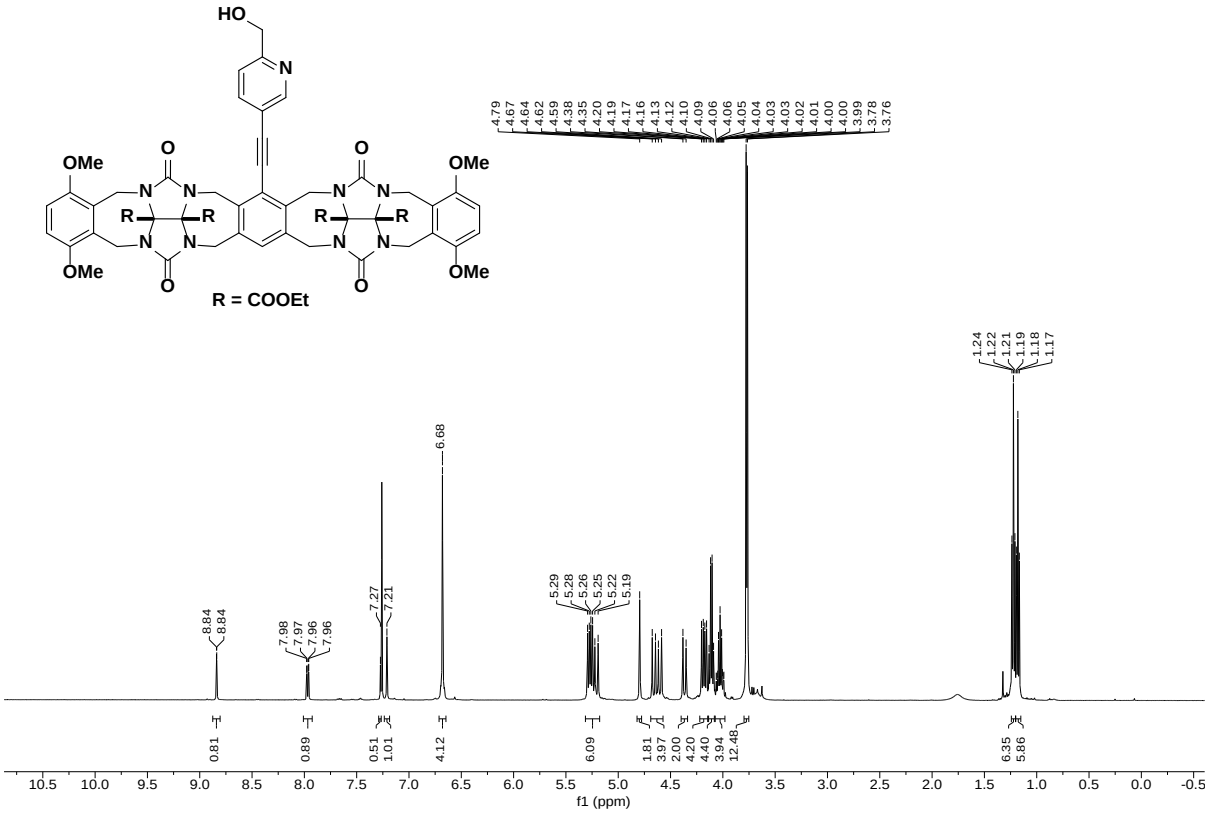
HO
N
OMe
O
N
R
R = COOEt
4.79
4.67
4.64
4.62
4.59
4.38
4.35
4.20
4.19
4.17
4.16
4.13
4.12
4.10
4.09
4.06
4.06
4.05
4.04
4.03
4.03
4.02
4.01
4.00
4.00
3.99
3.78
3.76
1.24
1.22
1.21
1.19
1.18
1.17
6.68
8.84
8.84
7.98
7.97
7.96
7.96
7.27
7.21
5.29
5.28
5.26
5.25
5.22
5.19
0.81
0.89
0.51
1.01
4.12
6.09
1.81
3.97
2.00
4.20
4.40
3.94
12.48
6.35
5.86
f1 (ppm)

S5 – ^{13}C

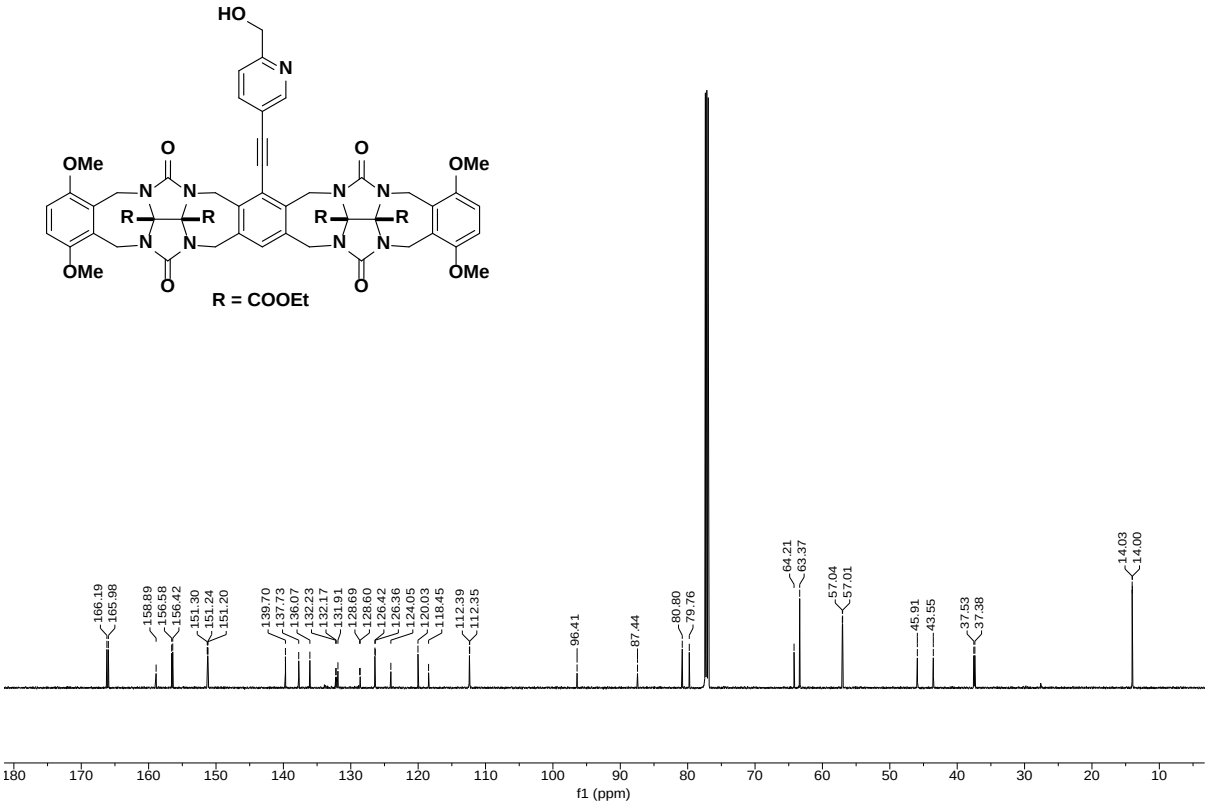
HO
N
OMe
O
N
R
R = COOEt
166.19
165.98
158.89
156.58
156.42
151.30
151.24
151.20
139.70
137.73
136.07
132.23
132.17
131.91
128.69
128.60
126.42
126.36
124.05
120.03
118.45
112.39
112.35
96.41
87.44
80.80
79.76
64.21
63.37
57.04
57.01
45.91
43.55
37.53
37.38
14.03
14.00
f1 (ppm)

S6 – ^{1}H

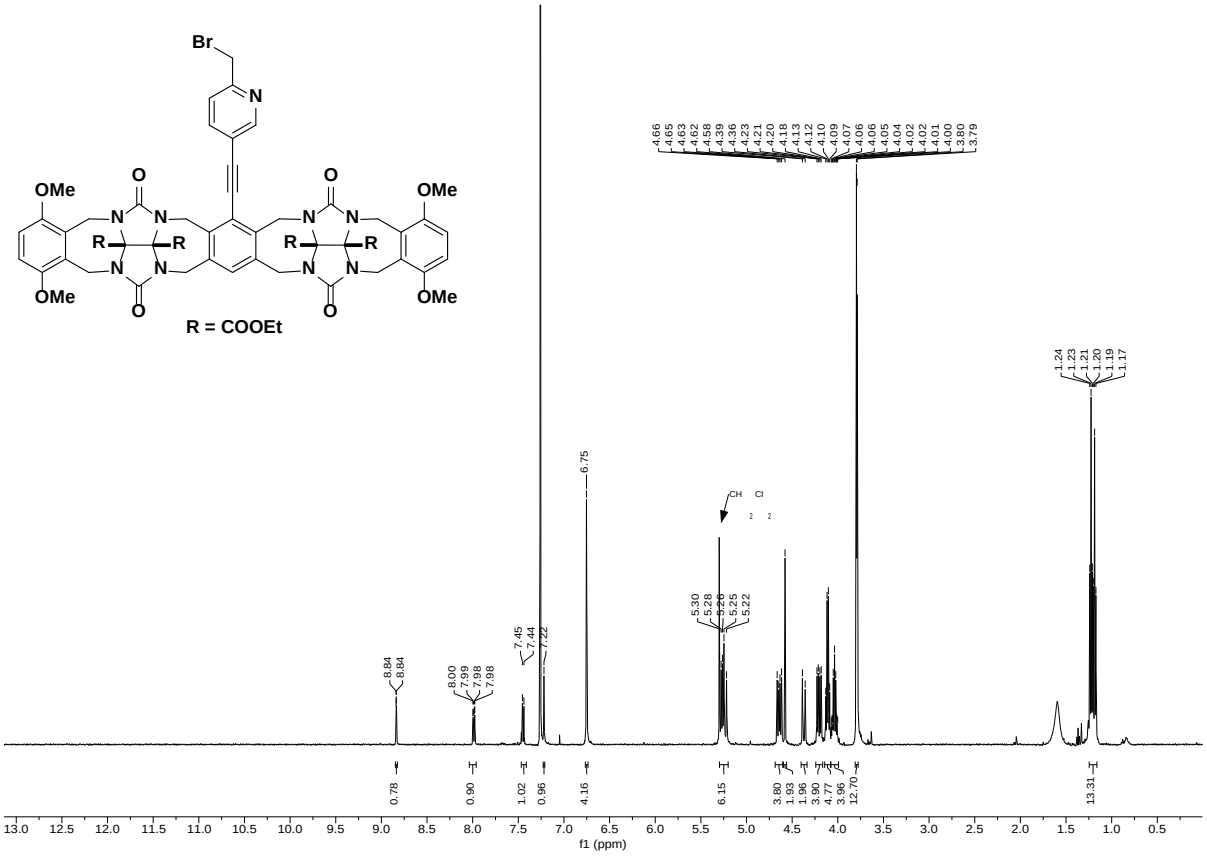
Br
N
OMe
O
N
R
R
R = COOEt
4.66
4.65
4.63
4.62
4.58
4.39
4.36
4.23
4.21
4.20
4.18
4.13
4.12
4.10
4.09
4.07
4.06
4.06
4.05
4.04
4.02
4.02
4.01
4.00
3.80
3.79
1.24
1.23
1.21
1.20
1.19
1.17
6.75
CH2Cl2
5.30
5.28
5.26
5.25
5.22
8.84
8.84
8.00
7.99
7.98
7.98
7.45
7.44
7.22
0.78
0.90
1.02
0.96
4.16
6.15
3.80
1.93
1.96
3.90
4.77
3.96
12.70
13.31
f1 (ppm)

S6 – ^{13}C

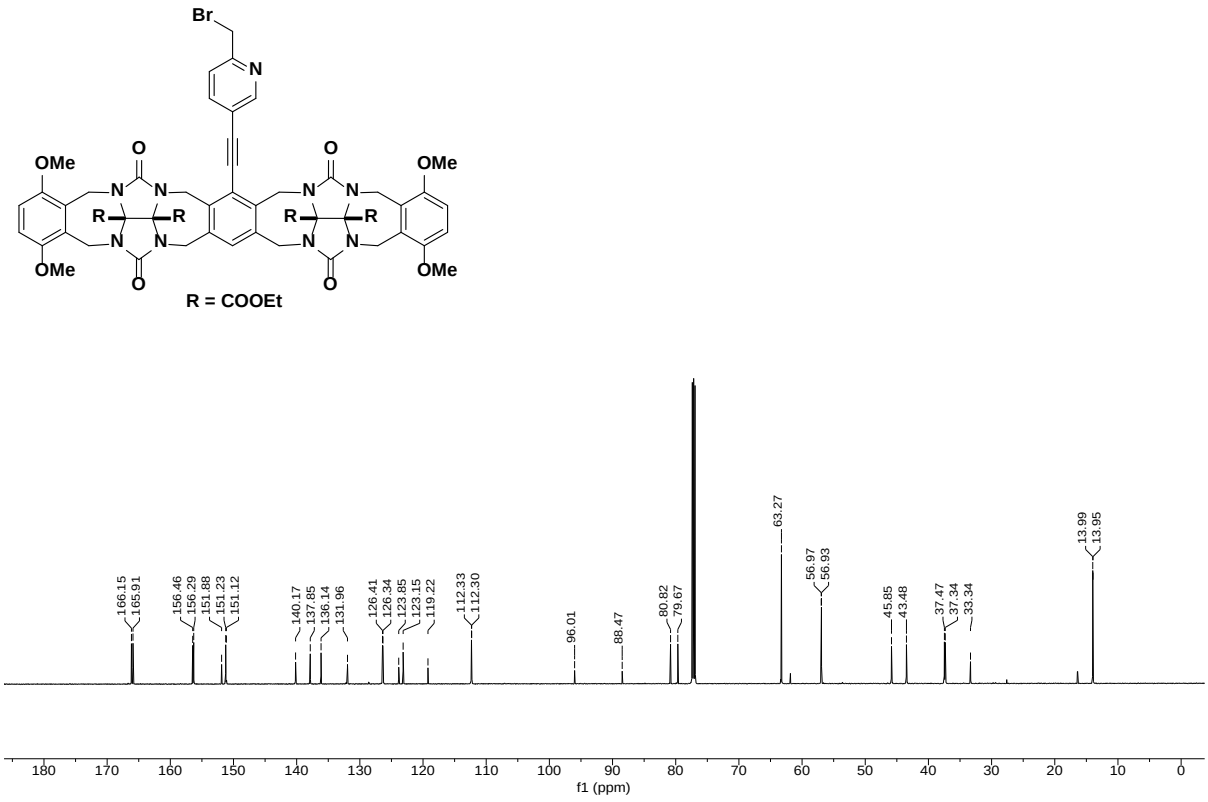
Br
N
OMe
O
N
R
R
R = COOEt
166.15
165.91
156.46
156.29
151.88
151.23
151.12
140.17
137.85
136.14
131.96
126.41
126.34
123.85
123.15
119.22
112.33
112.30
96.01
88.47
80.82
79.67
63.27
56.97
56.93
45.85
43.48
37.47
37.34
33.34
13.99
13.95
f1 (ppm)

13 – ^{1}H

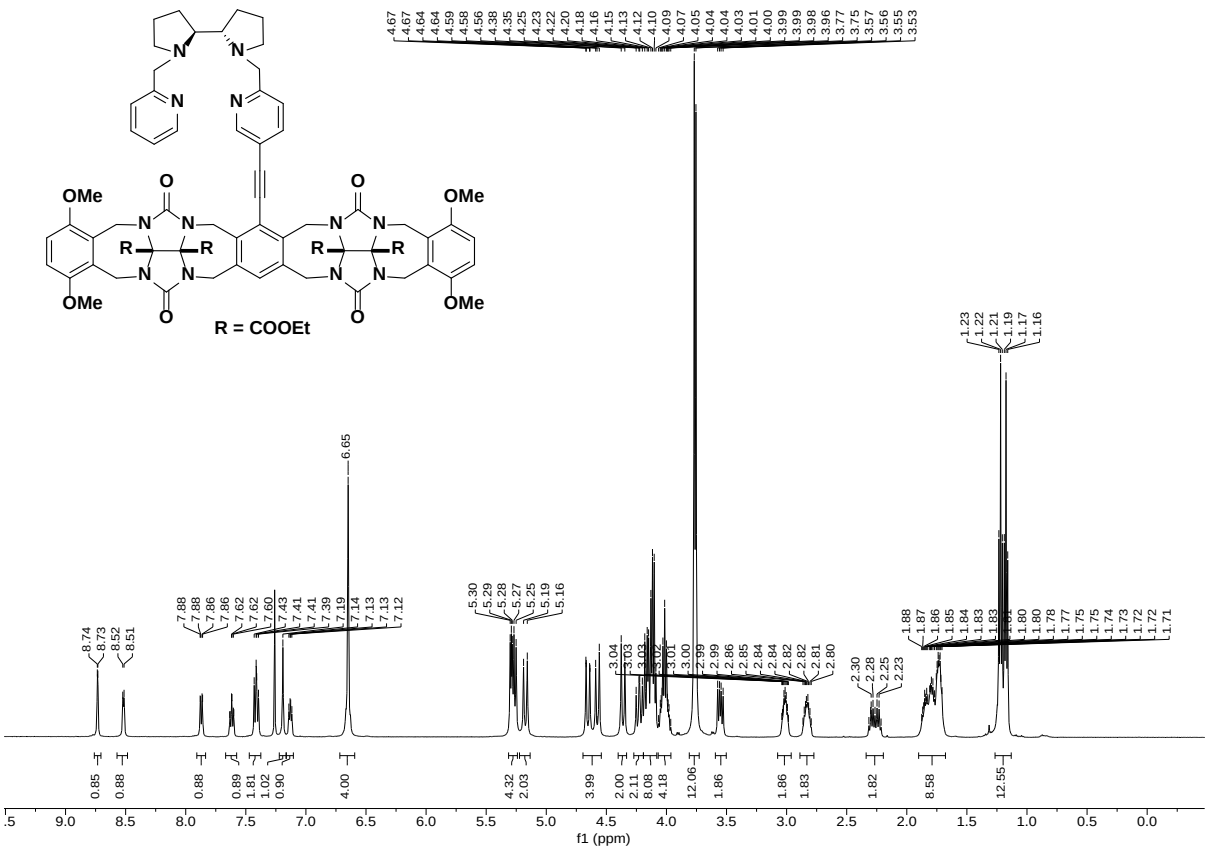

13 – ^{13}C

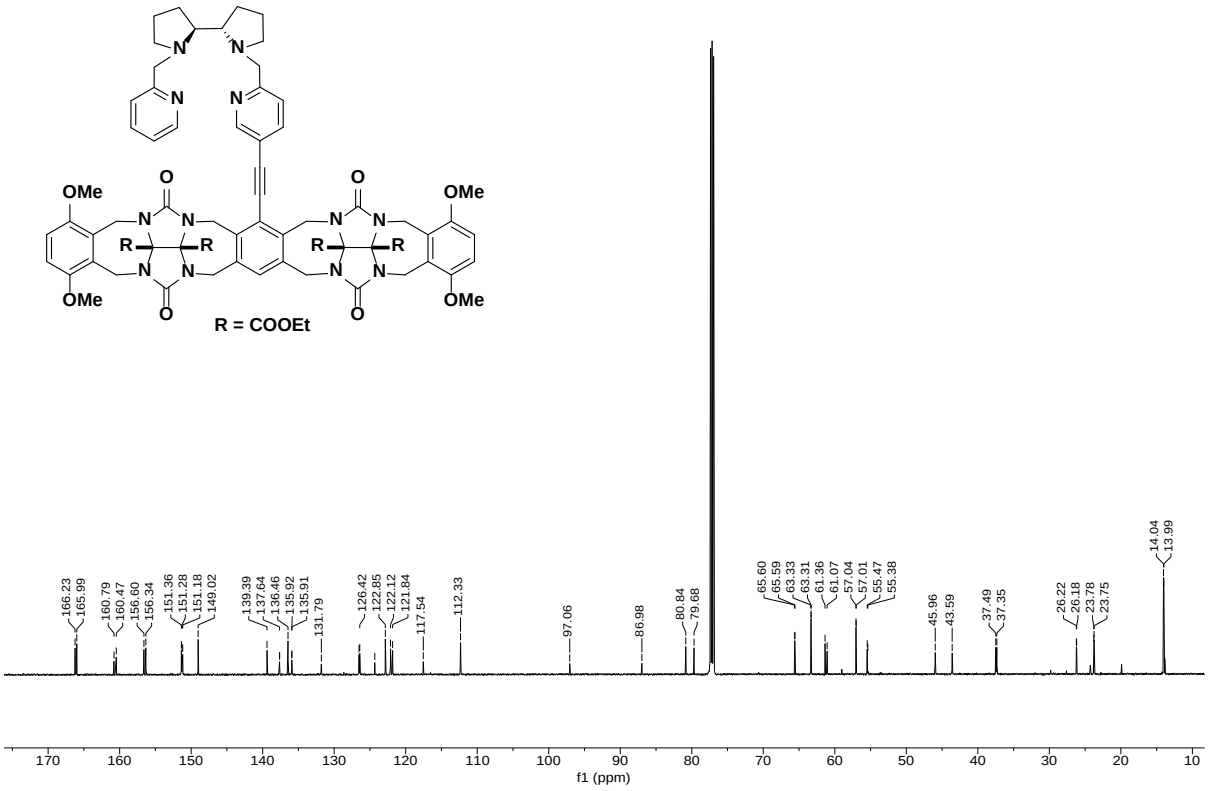

4 – ^{1}H

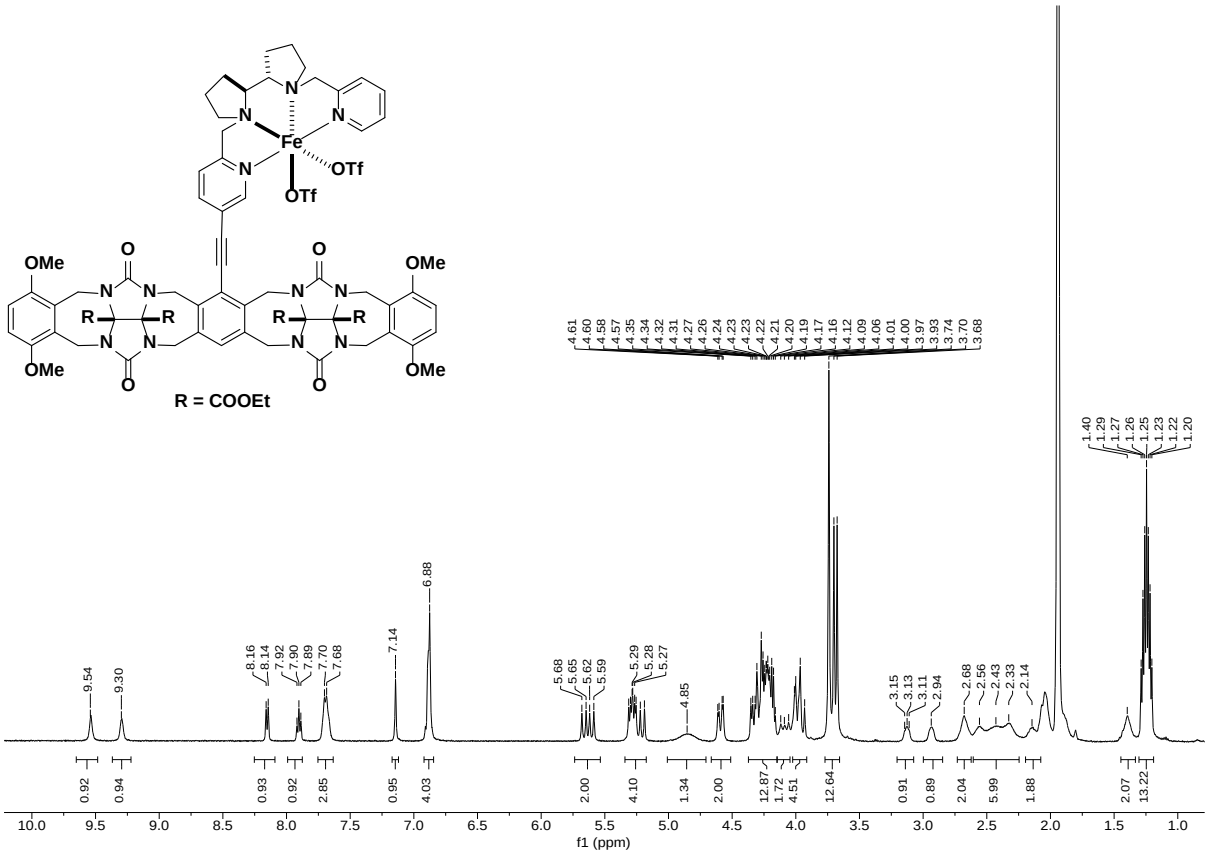

4 – ^{13}C

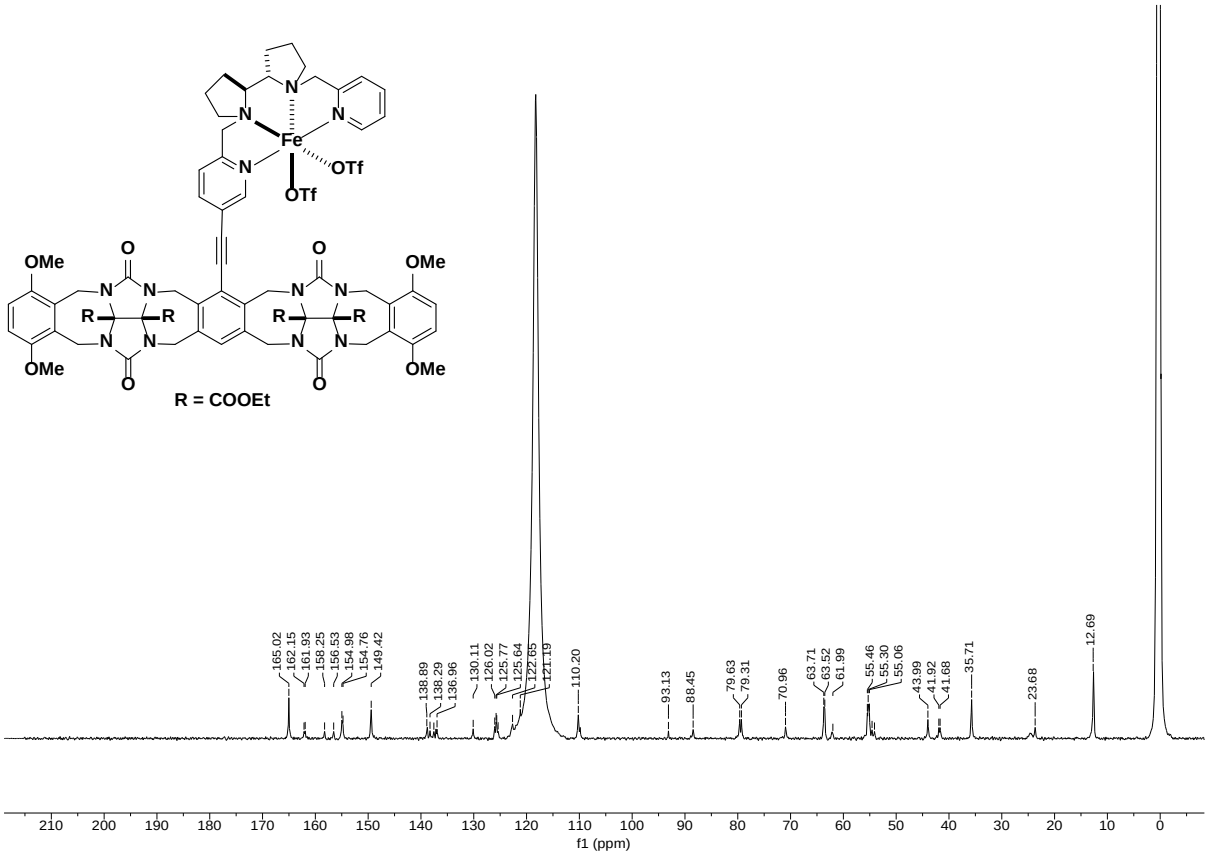

10. References

[1] W. C. Still, M. Kahn, A. Mitra, *J. Org. Chem.* **1978**, *43*, 2923-2925.
[2] H. E. Gottlieb, V. Kotlyar, A. Nudelman, *J. Org. Chem.* **1997**, *62*, 7512-7515.
[3] H.-S. Lin, L. A. Paquette, *Synth. Commun.* **1994**, *24*, 2503-2506.
[4] H. J. Dauben Jr, L. L. McCoy, *J. Am. Chem. Soc.* **1959**, *81*, 4863-4873.
[5] A. Diebold, A. Elbouadili, K. S. Hagen, *Inorg. Chem.* **2000**, *39*, 3915-3923.
[6] M. Shin, et al., *Tetrahedron* **2014**, *70*, 1617-1620.
[7] B. M. Trost, H. C. Shen, L. Dong, J.-P. Surivet, C. Sylvain, *J. Am. Chem. Soc.* **2004**, *126*, 11966-11983.
[8] F. Mazzini, F. Galli, P. Salvadori, *Eur. J. Org. Chem.* **2006**, *2006*, 5588-5593.
[9] L. Isaacs, D. Witt, J. Lagona, *Org. Lett.* **2001**, *3*, 3221-3224.
[10] C. A. Burnett, D. Witt, J. C. Fettinger, L. Isaacs, *J. Org. Chem.* **2003**, *68*, 6184-6191.
[11] M. Soler, et al., *Inorg. Chem.* **2015**, *54*, 10542-10558.
[12] G. Olivo, et al., *Angew. Chem.* **2017**, *129*, 16565-16569.
[13] H. Sasakuma, Y. Motoyama, H. Nagashima, *Chem Commun (Camb)* **2007**, 4916-4918.
[14] Z. Ke, Y. Zhang, X. Cui, F. Shi, *Green Chem.* **2016**, *18*, 808-816.
[15] D. Enjalbert, C. Bassilana, V. Krier, S. Szönyi, A. Cambon, *J. Fluorine Chem.* **1999**, *93*, 145-152.
[16] a) K. Neimann, R. Neumann, *Org. Lett.* **2000**, *2*, 2861-2863; b) A. Berkessel, J. A. Adrio, *J. Am. Chem. Soc.* **2006**, *128*, 13412-13420.
[17] J. T. Scanlon, D. E. Willis, *J. Chromatogr. Sci.* **1985**, *23*, 333-340.
[18] M. Heilmann, K. Tiefenbacher, *Chem. Eur. J.* **2019**, *25*, 12900-12904.
[19] P. Thordarson, *Chem. Soc. Rev.* **2011**, *40*, 1305-1323.
[20] a) A. Laio, M. Parrinello, *Proc. Natl. Acad. Sci. U. S. A.* **2002**, *99*, 12562-12566; b) A. Barducci, G. Bussi, M. Parrinello, *Phys. Rev. Lett.* **2008**, *100*, 020603.
[21] J. Wang, R. M. Wolf, J. W. Caldwell, P. A. Kollman, D. A. Case, *J. Comput. Chem.* **2004**, *25*, 1157-1174.
[22] R. Woods, R. Chappelle, *J. Mol. Struc. (Theochem)* **2000**, *527*, 149-156.
[23] a) A. T. Fenley, N. M. Henriksen, H. S. Muddana, M. K. Gilson, *J. Chem. Theory Comput.* **2014**, *10*, 4069-4078; b) K. I. Assaf, et al., *J. Phys. Chem. B* **2017**, *121*, 11144-11162.
[24] a) J. Yin, et al., *J. Comput.-Aided Mol. Des.* **2017**, *31*, 1-19; b) A. Rizzi, et al., *J. Comput.-Aided Mol. Des.* **2018**, *32*, 937-963.
[25] H. J. Berendsen, D. van der Spoel, R. van Drunen, *Comput. Phys. Commun.* **1995**, *91*, 43-56.
[26] a) G. A. Tribello, M. Bonomi, D. Branduardi, C. Camilloni, G. Bussi, *Comput. Phys. Commun.* **2014**, *185*, 604-613; b) M. Bonomi, et al., *Nat. Methods* **2019**, *16*, 670-673.
[27] M. Invernizzi, M. Parrinello, *J. Phys. Chem. Lett* **2020**, *11*, 2731-2736.
[28] K. Remya, C. H. Suresh, *Phys. Chem. Chem. Phys.* **2015**, *17*, 18380-18392.
[29] a) G. Piccini, J. J. McCarty, O. Valsson, M. Parrinello, *J. Phys. Chem. Lett* **2017**, *8*, 580-583; b) D. Mendels, G. Piccini, M. Parrinello, *J. Phys. Chem. Lett* **2018**, *9*, 2776-2781.
[30] J. Wang, W. Wang, P. A. Kollman, D. A. Case, *J. Mol. Graphics Modell.* **2006**, *25*, 247-260.
[31] X. Grabuleda, C. Jaime, P. A. Kollman, *J. Comput. Chem.* **2000**, *21*, 901-908.

[32] X. Wu, Z. Liu, S. Huang, W. Wang, *Phys. Chem. Chem. Phys.* **2005**, *7*, 2771-2779.

Chemistry–A European Journal

Supporting Information

Tweezer-Based C–H Oxidation Catalysts Overriding the Intrinsic Reactivity of Aliphatic Ammonium Substrates

Melina Knezevic and Konrad Tiefenbacher*

Table of Content

1. General Information

Experimental: Reactions were carried out under an atmosphere of argon in dried glassware unless otherwise indicated. Analytical thin-layer chromatography (TLC) was performed on Merck silica gel 60 F254 glass-backed plates, which were analyzed under UV light or after exposure to standard staining solutions (CAM: cerium ammonium molybdate or basic $KMnO_4$).[1] Medium Pressure Liquid Chromatography (MPLC) was carried out with RediSep® Silica Gel Disposable Flash Columns SiO_2 columns (particle size 40-63 μm) and Al_2O_3 basic columns (particle size 40-63 μm) on a CombiFlash NextGen 300+ version 5.0.55 by Teledyne ISCO with a fraction collector version 00.92.00, detector version 11, and a pump version: 1.47. For all the runs the column type and size, flow rate [ml/min], solvent mixture, column volumes (CV) and run time [min] is given. All NMR experiments were performed on a Bruker Avance Neo and a Bruker Avance III HD NMR spectrometer operating at 500 MHz and 600 MHz proton frequency, respectively. The instruments were equipped with a direct observe 5-mm BBFO smart probe (500 MHz) or a five-channel cryogenic 5 mm QCI probe (600 MHz). All probes were equipped with actively shielded z-gradients (10 A). The experiments were performed at 300 K. Chemical shifts of ^{1}H NMR and ^{13}C NMR are given in ppm. The following solvent residual signals of the deuterated solvents were used as reference: $CDCl_3$: 7.26 ppm (δ^1H), 77.16 ppm (δ^{13}C), MeCN-d3: 1.96 ppm (δ^1H), 118.26 ppm (δ^{13}C).[2] Coupling constants (*J*) are reported in Hertz (Hz). Standard abbreviations indicating multiplicity were used as follows: br (broad), s (singlet), d (doublet), t (triplet), dd (doublet of doublets), etc., m (multiplet). Infrared spectra were measured on a Brucker Alpha IR spectrometer (ATR, attenuated total reflection). Abbreviations indicating intensity were used as follows: s (strong), m (medium), w (weak). Melting points were recorded on a Büchi Melting Point M-565 apparatus using open capillary tubes. GC analyses were carried out on a Shimadzu GC-2010 Plus instrument equipped with a flame ionization detector (FID) and an Rtx-5 capillary column (length = 30 m). Hydrogen was used as the carrier gas and the constant-flow mode was used (flow rate = 40 mL/min) with a split ratio of 1:20. The following temperature program was used: 60 °C for 3 min, 15 °C/min to 250 °C, and 250 °C for 5 min. The response factors of the analyzed compounds were calculated as previously reported.[3] For the determination of enantiopurity via GC, a Shimadzu GC-2010 Plus instrument equipped with a FID and an Rt-bDEXsm capillary column (length = 30 m) was used. Hydrogen was used as the carrier gas and the constant-flow mode was used (flow rate = 50 mL/min) with a split ratio of 1:20. The following temperature program was used: 60 °C for 1 min, 1 °C/min to 220 °C, and 220 °C for 10 min. High-resolution mass spectra were obtained on a Thermo Scientific LTQ-FT Ultra via electrospray ionization (ESI) or a Finnigan MAT 8200 (EI) (ESI source parameters for positive polarity mode were: spray voltage, 4.0 kV; capillary temperature, 275 °C; capillary voltage, 48 V; and tube lens, –120 V).

Sources of chemicals: Anhydrous acetonitrile (MeCN), dichloromethane (CH_2Cl_2), diethyl ether (Et_2O), dimethylformamide (DMF), methanol (MeOH), and tetrahydrofuran (THF) were purchased from Acros Organics. Deuterated acetonitrile (MeCN-d_3 99.8%) and chloroform (stabilized over silver foil) ($CDCl_3$, 99.8%) were purchased from Cambridge Isotope Laboratories. Acetic acid, acetic anhydride, aluminum oxide (activated, basic, Brockmann I), biphenyl, (2*S*,2'*S*)-bipyrrolidine, decylamine, iron (II) chloride, lithium aluminum hydride ($LiAlH_4$), pyridine-2-carboxaldehyde, silver trifluoromethanesulphonate (AgOTF), sodium azide (NaN_3), sodium cyanide (NaCN), sodium

cyanoborohydride ($NaCNBH_3$), sodium peroxide water solution (50% w/w), tetra-*n*-butylammonium bromide (TBAB), tetrafluoroboric acid diethyl ether complex, triethylamine, trifluoroacetic acid (TFA), and trifluoroethanol (TFE) were purchased from Sigma-Aldrich. Potassium carbonate was purchased from Acros Organics. 2-Cyclohexylethanamine, 2-cyclohexylpropan-1-amine, 1-bromo-3,7-dimethyloctane, 1,1,1,3,3,3-hexafluoro-2-isopropanol, (1*S*,2*S*)-*N*,*N*'-dimethyl-1,2-cyclohexane-diamine were purchased from FluoroChem. Manganese bis(trifluoromethanesulphonate) was purchased from Apollo. Iron (II) bis (trifluoromethanesulfonate) bis (acetonitrile) was prepared according to a literature procedure.[4] Silica gel (0.040-0.063 mm, 230-400 mesh ASTM) and Celite 545 (0.02-0.1 mm) were purchased from Merck KGaA. All chemicals were used as received.

2. Synthesis of Catalysts and Substrates

2.1 Ligand Synthesis:

Synthesis of **pdp(Twe)** was carried out as previously described.[3a]

(1*S*,2*S*)-*N*^{1},*N*^{2}-Dimethyl-*N*1-(4yridine-2-ylmethyl)cyclohexane-1,2-diamine (5)

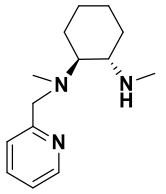

$C_{14}H_{23}N_3$
MW: 233.36 g/mol

According to a modified literature procedure,[5] (2*S*,2'*S*)-*N*^{1},*N*^{2}-dimethylcyclohexane-1,2-diamine (142 mg, 1.00 mmol, 1.0 equiv.) was dissolved in anhydrous MeOH (2 mL). Then, a solution of pyridine-2-carboxaldehyde (107 mg, 1.00 mmol, 1.0 equiv.) in MeOH (2 mL) was added dropwise and the mixture was stirred at room temperature for 16 h. Thereafter, $NaCNBH_3$ (251 mg, 4.00 mmol, 4.0 equiv.) and trifluoroacetic acid (693 µL, 1.02 g, 9.00 mmol, 9.0 equiv.) were added and the reaction was stirred for additional 3 h. The reaction mixture was neutralized by the addition of 4 M NaOH (10 mL) and was then extracted with CH_2Cl_2 (3 × 15 mL). The combined organic layers were washed with brine (15 mL), dried (Na_2SO_4), filtered, and concentrated under reduced pressure. The crude material was purified *via* MPLC (RediSep® Column: Alumina, basic 8 g, 13 mL/min; CH_2Cl_2/CH_2Cl_2:MeOH (9:1) 100:0 to 0:100, 24.0 CV, 11.4 min) to give the desired product **5** (156 mg, 668 µmol, 67%) as a yellowish oil.

TLC R_f = 0.34 (CH_2Cl_2/MeOH/NH_4OH = 90/8/2) [UV, $KMnO_4$].

^{1}H NMR ($CDCl_3$, 500 MHz, 300 K) δ [ppm] = 8.51 (ddd, *J* = 4.9, 1.9, 0.9 Hz, 1H), 7.66 (td, *J* = 7.7, 1.8 Hz, 1H), 7.42 (d, *J* = 7.8 Hz, 1H), 7.14 (ddd, *J* = 7.6, 4.9, 1.2 Hz, 1H), 3.81 (d, *J* = 14.3 Hz, 1H), 3.62 (d, *J* = 14.3 Hz, 1H), 2.40 (s, 3H), 2.40 – 2.36 (m, 1H), 2.27 (td, *J* = 10.5, 4.1 Hz, 1H), 2.21 (s, 3H), 2.17 – 2.08 (m, 1H), 1.95 – 1.88 (m, 1H), 1.81 (td, *J* = 5.0, 2.5 Hz, 1H), 1.75 – 1.66 (m, 1H), 1.35 – 1.13 (m, 3H), 1.00 (d, *J* = 12.1 Hz, 1H).

^{13}C NMR ($CDCl_3$, 126 MHz, 300 K) δ [ppm] = 160.6 (s), 149.1 (s), 136.7 (s), 122.6 (s), 122.0 (s), 67.1 (s), 60.5 (s), 59.7 (s), 37.1 (s), 34.1 (s), 31.4 (s), 25.7 (s), 24.8 (s), 22.3 (s).

The analytical data match literature values.[6]

***S,S*-(Mcp)Twe**

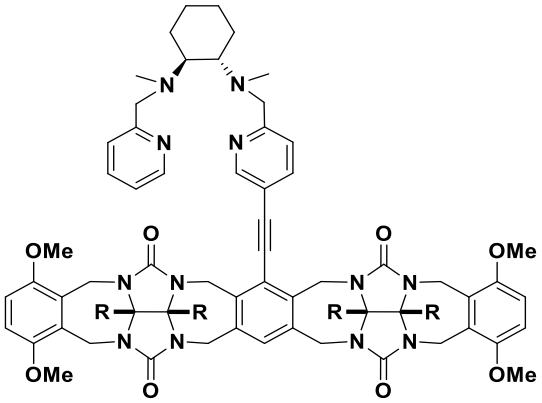

$C_{72}H_{80}N_{12}O_{16}$
MW: 1369.50 g/mol
R = COOEt

Tweezer bromide **3**[3a] (79.1 mg, 65.0 µmol, 1.0 equiv.) and **5** (15.2 mg, 65.0 µmol, 1.0 equiv.) were dissolved in anhydrous MeCN (3.5 mL). Then, K_2CO_3 (35.9 mg, 260 µmol, 4.0 equiv.) and TBAB (1.05 mg, 3.25 µmol, 0.05 equiv.) were added and the reaction mixture was stirred at reflux for 16 h. Thereafter, the mixture was cooled down to room temperature, filtered and the residue was washed with CH_2Cl_2 (10 mL). The filtrate was concentrated under reduced pressure, 1 M NaOH (10 mL) was added and the mixture was extracted with CH_2Cl_2 (3 ×10 mL). The combined organic layers were washed with brine (10 mL), dried (Na_2SO_4), filtered, and concentrated by rotatory evaporation. The crude compound was purified by flash chromatography (10 g silica, CH_2Cl_2/MeOH/NH_4OH = 93/5/2) to obtain ***S,S*-(Mcp)Twe** (83.7 mg, 61.1 µmol, 94%) as a yellow solid.

TLC R_f = 0.37 (CH_2Cl_2/MeOH/NH_4OH = 90/8/2) [UV, $KMnO_4$].

M.P.: 174 – 178 °C (decomp.)

IR (ATR): $\tilde{\nu}$ (cm^{-1}) = 2931 (w), 2834 (w), 1720 (s), 1592 (w), 1484 (w), 1447 (s), 1423 (s), 1366 (m), 1305 (m), 1252 (s) 1152 (m), 1076 (m), 1017 (m), 981 (w), 941 (m), 916 (m), 852 (m), 801 (m), 762 (m), 718 (m), 662 (m).

^{1}H NMR ($CDCl_3$, 500 MHz, 300 K) δ [ppm] = 8.75 (s, 1H), 8.52 (d, *J* = 4.9 Hz, 1H), 7.87 (dd, *J* = 8.0, 2.1 Hz, 1H), 7.68 (t, *J* = 7.8 Hz, 1 H), 7.62 (d, *J* = 8.1 Hz, 1H), 7.56 (d, *J* = 7.8 Hz, 1H), 7.21 (s, 1H), 7.21 – 7.15 (m, 1H), 6.76 (s, 4H), 5.28 (*virt.* Dd, *J* = 15.8, 6.5 Hz, 4H), 5.24 (*virt.* Dd, *J* = 15.6, 2.5 Hz, 2H), 4.68 (*virt.* Dd, *J* = 15.6, 3.9 Hz, 2H), 4.62 (d, *J* = 15.2 Hz, 2H), 4.38 (d, *J* = 15.1 Hz, 2H), 4.20 (*virt.* Dd, *J* = 15.7, 11.7 Hz, 4H), 4.11 (q, *J* = 7.1 Hz, 4H), 4.07 – 3.99 (m, 4H), 3.96 (d, *J* = 15.0 Hz, 1H), 3.92 (d, *J* = 14.5 Hz, 1H), 3.84 – 3.74 (m, 14 H), 2.70 – 2.65 (m, 2H), 2.31 (s, 3H), 2.30 (s, 3H), 2.04 – 1.97 (m, 2H), 1.79 (br s, 2H), , 1.36 – 1.20 (m, 4H), 1.23 (t, *J* = 7.1 Hz, 6H), 1.19 (*virt.* Td, *J* = 7.1, 1.3 Hz, 6H).

^{13}C NMR ($CDCl_3$, 126 MHz, 300 K) δ [ppm] = 166.2 (s), 166.0 (s), 161.9 (s), 161.3 (s), 156.6 (s), 156.4 (s), 151.3 (s), 151.3 (s), 151.2 (s), 148.8 (s), 139.4 (s), 137.7 (s), 137.6 (s), 136.7 (s), 136.0 (s), 135.9 (s), 131.8 (s), 126.5 (s), 126.5 (s), 124.4 (s), 123.1 (s), 122.4 (s), 121.9 (s), 117.5 (s), 112.4 (s), 112.4 (s), 112.3 (s), 97.2 (s), 86.9 (s), 80.8(s), 80.8 (s), 79.7 (s), 64.8 (s), 64.6 (s), 63.3 (s), 63.3 (s), 60.6 (s),

60.2 (s), 57.1 (s), 57.0 (s), 57.0 (s), 46.0 (s), 43.6 (s), 37.5 (s), 37.4 (s), 37.0 (s), 36.6 (s), 26.1 (s), 25.9 (s), 25.2 (s), 14.0 (s), 14.0 (s).

HRMS (ESI): $C_{72}H_{80}N_{12}O_{16}$ calculated: $[(M + 2H)^{2+}]$: 685.2980

found: $[(M + 2H)^{2+}]$: 685.2978.

***S,S*-(Pdp)Twe$_2$**

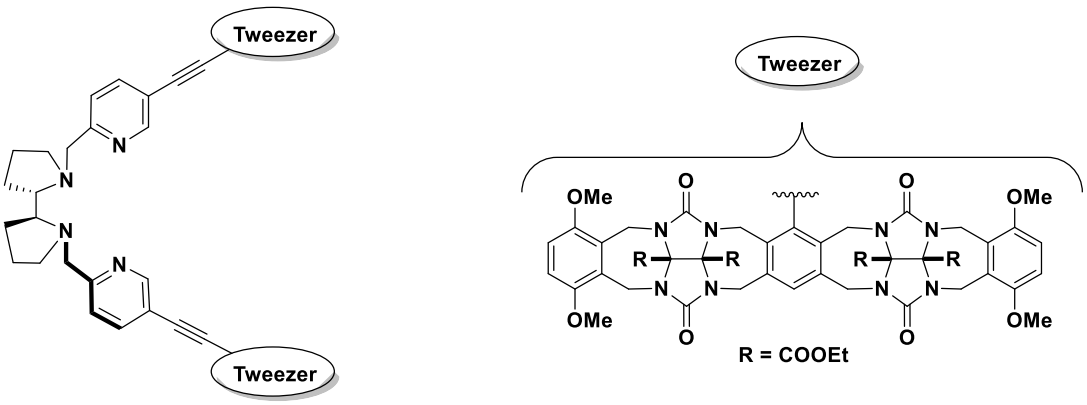

$C_{124}H_{130}N_{20}O_{32}$
MW: 2412.51 g/mol

Tweezer bromide **3**[3a] (39.9 mg, 32.8 µmol, 2.0 equiv.) and (2*S*,2'*S*)-bipyrrolidine (**4**, 2.30 mg, 16.4 µmol, 1.0 equiv.) were dissolved in anhydrous MeCN (1.0 mL). Then, K_2CO_3 (9.07 mg, 65.6 µmol, 4.0 equiv.) and TBAB (264 µg, 820 nmol, 0.05 equiv.) were added and the reaction mixture was stirred at reflux for 16 h. Thereafter, the mixture was cooled down to room temperature, filtered and the residue was washed with CH_2Cl_2 (5 mL). The filtrate was concentrated under reduced pressure, 1 M NaOH (4 mL) was added and the mixture was extracted with CH_2Cl_2 (3 ×5 mL). The combined organic layers were washed with brine (5 mL), dried (Na_2SO_4), filtered, and concentrated by rotatory evaporation. The crude compound was purified *via* MPLC (RediSep® Column: Alumina, Basic 8 g, 13 mL/min; CH_2Cl_2/CH_2Cl_2:MeOH (9:1) 100:0 to 0:100, 18.0 CV, 8.5 min) to obtain the desired **(pdp)Twe$_2$** (35.1 mg, 14.5 µmol, 88%) as a yellow solid.

TLC R_f = 0.49 (CH_2Cl_2/MeOH/NH_4OH = 90/8/2) [UV, $KMnO_4$].

M.P.: 123 – 125 °C (decomp.)

IR (ATR): $\tilde{\nu}$ (cm^{-1}) = 2920 (w), 2840 (w), 1718 (s), 1595 (w), 1458 (s), 1423 (s), 1366 (m), 1305 (m), 1253 (s), 1153 (m), 1076 (m), 1015 (m), 981 (m), 941 (m), 916 (m), 851 (w), 801 (m), 772 (w), 750 (w), 718 (w), 662 (w).

^{1}H NMR ($CDCl_3$, 500 MHz, 300 K) δ [ppm] =8.85 – 8.74 (m, 2H), 7.94 (dd, *J* = 8.0, 2.2 Hz, 2H), 7.49 (d, *J* = 8.0 Hz, 2H), 7.20 (s, 2H), 6.67 (m, 8H), 5.34 – 5.24 (m, 8H), 5.24 – 5.10 (m, 4H), 4.67 (dd, *J* = 15.5, 4.8 Hz, 4H), 4.58 (dd, *J* = 15.1, 3.5 Hz, 4H), 4.37 (d, *J* = 15.1 Hz, 4H), 4.21 – 4.08 (m, 18H), 4.02 (*virt.* qdd, *J* = 10.8, 7.0, 4.0 Hz, 8H), 3.77 (*virt.* t, *J* = 3.0 Hz, 24H), 3.56 (d, *J* = 14.6 Hz, 2H), 3.02 (ddd, *J* = 8.9, 6.1, 2.6 Hz, 2H), 2.94 – 2.84 (m, 2H), 2.28 (td, *J* = 9.2, 7.3 Hz, 2H), 1.86 (q, *J* = 7.8,

7.1 Hz, 4H), 1.82 – 1.71 (m, 4H), 1.24 (*virt.* dt, *J* = 14.4, 7.1 Hz, 12H), 1.19 (*virt.* td, *J* = 7.2, 1.3 Hz, 12H).

^{13}C NMR ($CDCl_3$, 126 MHz, 300 K) δ [ppm] = 166.2 (s), 166.0 (s), 160.8 (s), 156.6 (s), 156.6 (s), 156.4 (s), 156.3 (s), 151.4 (s), 151.3 (s), 151.3 (s), 151.3 (s), 151.3 (s), 151.2 (s), 139.5 (s), 137.7 (s), 137.7 (s), 136.0 (s), 135.9 (s), 131.8 (s), 126.6 (s), 126.4 (s), 124.3 (s), 122.3 (s), 117.7 (s), 112.4 (s), 97.1 (s), 87.1 (s), 80.9 (s), 80.8 (s), 80.8 (s), 79.7 (s), 79.7 (s), 65.1 (s), 63.3 (s), 60.8 (s), 57.1 (s), 57.1 (s), 55.4 (s), 46.0 (s), 43.6 (s), 37.5 (s), 37.4 (s), 29.8 (s), 27.6 (s), 25.7 (s), 23.8 (s), 14.1 (s), 14.0 (s).

HRMS (ESI): $C_{124}H_{130}N_{20}O_{32}$ calculated: $[(M + H + Na)^{2+}]$: 1217.4562

found: $[(M + H + Na)^{2+}]$: 1217.4587.

2.2 Complex Synthesis

All reactions were performed in a glove box and anhydrous and degassed (*via* freeze-pump-thaw) solvents were used.

Synthesis of (*S*,*S*)-**Fe(pdp)**,[7] (*S*,*S*)-**Fe(pdp)Twe**,[3a] (*S*,*S*)-**Mn(pdp)**,[8] (*S*,*S*)-**Fe(mcp)**[9] and (*S*,*S*)-**Mn(mcp)**[10] were carried out as previously described.

***S,S*-Fe(mcp)Twe**

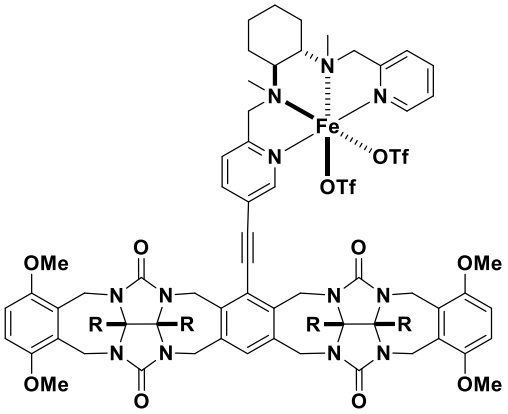

$C_{74}H_{80}F_6FeN_{12}O_{22}S_2$
MW: 1723.47 g/mol

R = COOEt

To a solution of **(mcp)Twe** (10.9 mg, 7.96 µmol, 1.0 equiv.) in MeCN (0.1 mL) was added dropwise a solution of $FeCl_2$ (1.01 mg, 7.96 µmol, 1.0 equiv.) in MeCN (0.1 mL). The reaction was stirred at room temperature for 2.5 h leading to the formation of a yellow suspension. Subsequently, AgOTf (4.09 mg, 15.9 µmol, 2.00 equiv.) was added and the reaction mixture was stirred for another 2 h. Then, the mixture was filtered over Celite. Slow diffusion of Et_2O resulted in the formation of the desired *S,S*-**Fe(mcp)Twe** complex (11.6 mg, 6.73 µmol, 85%) as a yellow film at the glass walls.

IR (ATR): $\tilde{\nu}$ (cm^{-1}) = 2940 (w), 1715 (s), 1607 (w), 1456 (s), 1428 (s), 1366 (m), 1252 (s), 1153 (m) 1077 (m), 1028 (s), 978 (w), 941 (m), 916 (m), 882 (w), 855 (w), 802 (w), 760 (w), 718 (w), 664 (w), 636 (s), 572 (w), 512 (m), 418 (w).

HRMS (ESI): $C_{74}H_{80}F_6FeN_{12}O_{22}S_2$ calculated: $[(M - 2OTf)^{2+}]$: 712.2578

found: $[(M - 2OTf)^{2+}]$: 712.2586.

***S*,*S*-Mn(mcp)Twe**

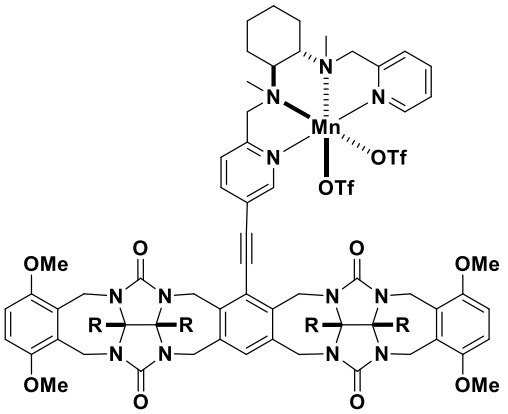

$C_{74}H_{80}F_6MnN_{12}O_{22}S_2$
MW: 1722.56 g/mol

R = COOEt

The **(mcp)Twe** (41.1 mg, 30.0 µmol, 1.0 equiv.) and $Mn(OTf)_2$ (10.6 mg, 30.0 µmol, 1.0 equiv.) were dissolved in MeCN (0.2 mL) and stirred at room temperature for 2.5 h. Subsequently, diethyl ether (4 mL) was added which resulted in the precipitation of a yellow solid out of the solution. The supernatant was removed and the solid was washed two times with diethyl ether (2x2 mL) and dried under reduced pressure for 30 min resulting in the desired complex *S*,*S*-**Mn(mcp)Twe** (30.0 mg, 17.4 µmol, 58%) as an off-white solid.

IR (ATR): $\tilde{\nu}$ (cm^{-1}) = 2940 (w), 1717 (s), 1607 (w), 1460 (s), 1366 (m), 1255 (s), 1157 (m), 1080 (m), 1029 (s), 983 (w), 941 (w), 917 (m), 856 (w), 803 (w), 760 (w), 719 (w), 637 (s), 574 (w), 516 (m), 410 (w).

HRMS (ESI): $C_{74}H_{80}F_6MnN_{12}O_{22}S_2$ calculated: $[(M - 2OTf)^{2+}]$: 711.7592

found: $[(M - 2OTf)^{2+}]$: 711.7594.

***S,S*-Mn(pdp)Twe**

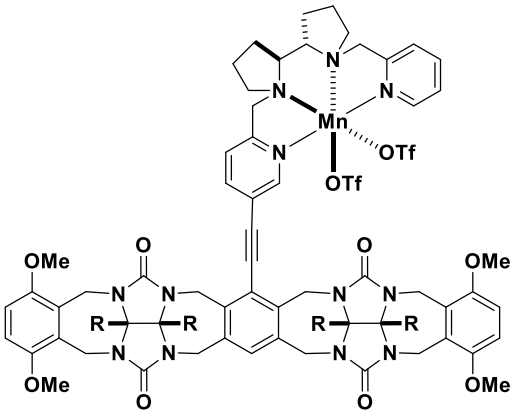

$C_{74}H_{78}F_6MnN_{12}O_{22}S_2$
MW: 1720.55 g/mol

R = COOEt

The **(pdp)Twe** (41.0 mg, 30.0 µmol, 1.0 equiv.) and $Mn(OTf)_2$ (10.6 mg, 30.0 µmol, 1.0 equiv.) were dissolved in MeCN (0.2 mL) and stirred at room temperature for 2.5 h. Subsequently, diethyl ether (4 mL) was added which resulted in the precipitation of a yellow solid out of the solution. The supernatant was removed and the solid was washed two times with diethyl ether (2x2 mL) and dried under reduced pressure resulting in the desired complex ***S,S*-Mn(pdp)Twe** (40.1 mg, 23.3 µmol, 78%) as an off-white solid.

IR (ATR): $\tilde{\nu}$ (cm^{-1}) = 2984 (w), 2913 (w), 1751 (m), 1719 (m), 1638 (w), 1460 (m), 1438 (w), 1257 (s), 1223 (m), 1157 (m), 1079 (m), 1030 (s), 985 (w), 942 (w), 917 (w), 895 (w), 845 (w), 810 (w), 761 (w), 720 (w), 638 (s), 574 (w), 518 (m), 412 (m).

HRMS (ESI): $C_{74}H_{78}F_6MnN_{12}O_{22}S_2$ calculated: $[(M - 2OTf)^{2+}]$: 710.7514

found: $[(M - 2OTf)^{2+}]$: 710.7519.

***S,S*-Fe(pdp)Twe$_2$**

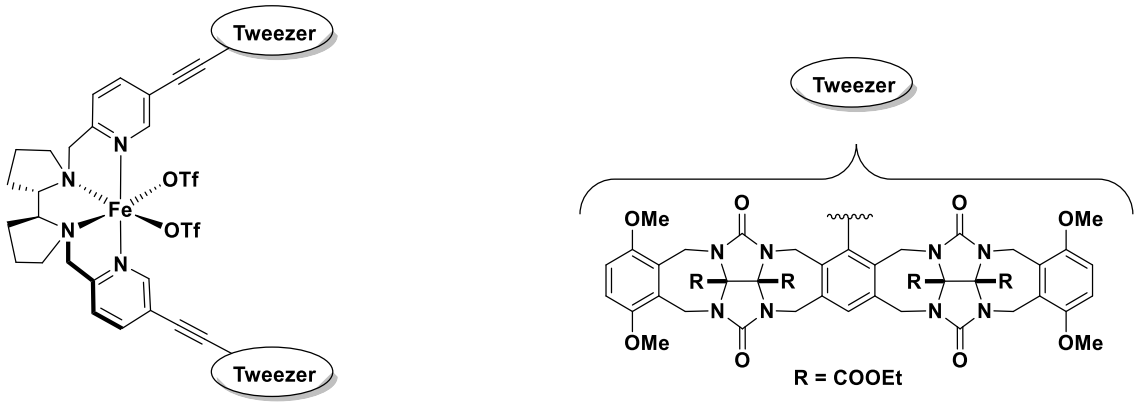

$C_{126}H_{130}F_6FeN_{20}O_{38}S_2$
MW: 2766.48 g/mol

The **(pdp)Twe$_2$** (20.0 mg, 8.29 µmol, 1.0 equiv.) and $Fe(OTf)_2(MeCN)_2$ (3.62 mg, 8.29 µmol, 1.0 equiv.) were dissolved in MeCN (0.2 mL) and stirred at room temperature for 2.5 h. Subsequently, diethyl ether (4 mL) was added which resulted in the precipitation of a yellow solid out of the solution. The supernatant was removed and the solid was washed two times with diethyl ether (2x2 mL) and dried under reduced pressure for 1 h resulting in the desired complex ***S,S*-Fe(pdp)Twe$_2$** (9.19 mg, 3.32 µmol, 40%) as a yellow solid.

IR (ATR): $\tilde{\nu}$ (cm^{-1}) = 2988 (w), 1719 (m), 1598 (w), 1460 (m), 1428 (m), 1366 (w), 1255 (s), 1155 (m), 1079 (m), 1030 (m), 983 (w), 942 (w), 917 (m), 854 (w), 804 (w), 755 (w), 719 (w), 663 (w), 638 (m), 573 (w), 517 (m).

HRMS (ESI): $C_{126}H_{130}F_6FeN_{20}O_{38}S_2$ calculated: $[(M - 2OTf)^{2+}]$: 1233.4250

found: $[(M - 2OTf)^{2+}]$: 1233.4272.

2.3 Substrate Synthesis

Decylammonium tetrafluoroborate was synthesized as previously described.[3a]

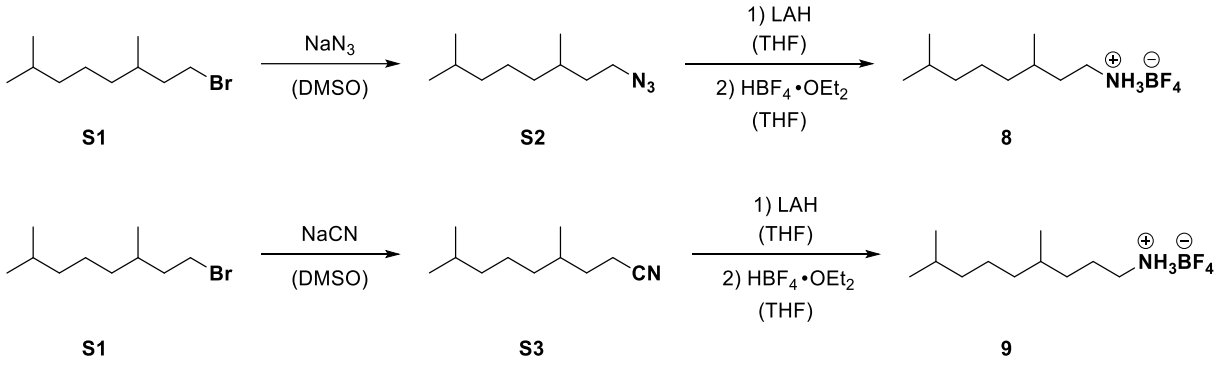

Scheme S1: Synthetic route to ammonium tetrafluoroborate **8** and **9**.

Azide **S2** was synthesized as previously described.[11]

4,8-Dimethylnonanenitrile (S3)

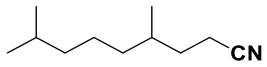

S3

$C_{11}H_{21}N$
MW: 167.30 g/mol

1-Bromo-3,7-dimethyloctane (**S1**, 1.04 mL, 1.11 g, 5.00 mmol, 1.0 equiv.) was added dropwise to a solution of NaCN (270 mg, 5.50 mmol, 1.1 equiv.) in anhydrous DMF (10 mL) at 0 °C. The reaction was left stirring at room temperature overnight. Then, water (25 mL) was added and the mixture was extracted with Et_2O (3 x 25 mL). The combined organic layers were washed with brine (25 mL), dried (Na_2SO_4), filtered, and concentrated under reduced pressure. The crude material was purified *via* MPLC (RediSep® Column: Silica, 12 g, 30 mL/min; CyHex/EtOAc 100:0 to 70:30, 16.0 CV, 9.5 min) to obtain nitrile **S3** (718 mg, 4.29 mmol, 86%) as a colorless oil.

TLC R_f = 0.67 (CyHex/EtOAc = 3/1) [$KMnO_4$].

^{1}H NMR ($CDCl_3$, 500 MHz, 300 K) δ [ppm] = 2.56 – 2.19 (m, 2H), 1.69 (dtd, *J* = 13.3, 7.6, 5.4 Hz, 1H), 1.62 – 1.42 (m, 3H), 1.37 – 1.20 (m, 3H), 1.14 (dddd, *J* = 12.0, 9.7, 8.1, 5.1 Hz, 3H), 0.91 (d, *J* = 6.6 Hz, 3H), 0.87 (*virt.* dd, *J* = 6.6, 1.0 Hz, 6H).

^{13}C NMR (MeCN-d_3, 151 MHz, 300 K) δ [ppm] = 120.2 (s), 39.2 (s), 36.6 (s), 32.4 (s), 32.2 (s), 28.1 (s), 24.6 (s), 22.8 (s), 22.7 (s), 19.0 (s), 15.1 (s).

All analytical data match literature values.[12]

General procedure A for azide/nitrile reduction and ammonium salt formation

Following a modified literature procedure,[13] a two-necked flask was charged with LAH (3.0 equiv.) under Ar atmosphere. Then, anhydrous THF (0.04 M) was added and the mixture was cooled down to

0 °C. Azide **S2** or nitrile **S3** (1.0 equiv.) was added and the mixture was allowed to reach room temperature followed by stepwise heating to reflux (Caution: N_2 and H_2 formation). After stirring the reaction for 16 h at this temperature, the mixture was cooled down to 0 °C and 10 M NaOH solution was added until a clear solution with slurry precipitation was formed, followed by the addition of water (8 mL) and Celite (8 g). The mixture was filtered, and the solvents were removed under reduced pressure. Next, 1 M NaOH (4 mL) was added and the mixture was extracted with CH_2Cl_2 (3 ×5 mL). The combined organic phases were dried over Na_2SO_4, filtered, and concentrated by rotatory evaporation. The crude amine was dissolved in anhydrous CH_2Cl_2 (0.5 M) without further purification. Then, tetrafluoroboric acid diethyl ether complex (1.1 equiv.) was added dropwise at 0 °C leading to the precipitation of a white solid. After stirring the mixture for 2 h at room temperature, the solvent was removed by rotatory evaporation. The residual solid was suspended in diethyl ether and stirred vigorously for a few minutes. Then the supernatant solution was removed, and the washing step was repeated two times. The final compound was dried in *vacuo* leading to the desired ammonium salt.

3,7-Dimethyloctan-1-ammonium tetrafluoroborate (8)

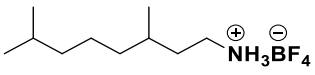

8

$C_{10}H_{24}BF_4N$
MW: 245.11 g/mol

Following general procedure A, azide **S2** (367 mg, 2.00 mmol, 1.0 equiv.) was converted into the corresponding white ammonium salt **8** (293 mg, 1.20 mmol) in 60% yield.

M.P.: 179 – 181 °C.

IR (ATR): $\tilde{\nu}$ (cm^{-1}) = 3277 (m), 2957 (m), 2927 (m), 2870 (w), 1606 (w), 1511 (m), 1469 (w), 1405 (w), 1384 (w), 1366 (w), 1291 (w), 1013 (s), 909 (m), 860 (w), 769 (m), 734 (w), 525 (m).

^{1}H NMR (MeCN-d_3, 600 MHz, 300 K) δ [ppm] = 6.08 (br s, 3H), 3.25 – 2.71 (m, 2H), 1.67 – 1.58 (m, 1H), 1.57 – 1.38 (m, 3H), 1.36 – 1.23 (m, 3H), 1.20 – 1.10 (m, 3H), 0.99 – 0.76 (m, 9H).

^{13}C NMR (MeCN-d_3, 151 MHz, 300 K) δ [ppm] = 39.7 (s), 39.6 (s), 37.3 (s), 34.4 (s), 30.9 (s), 28.6 (s), 25.1 (s), 22.8 (s), 22.8 (s), 19.3 (s).

HRMS (ESI): $C_{10}H_{24}BF_4N$ calculated: $[(M + Na)^+]$: 268.1832

found: $[(M + Na)^+]$: 268.1825.

4,8-Dimethylnonan-1-ammonium tetrafluoroborate (9)

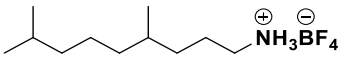

9

$C_{11}H_{26}BF_4N$
MW: 259.14 g/mol

Following general procedure A, nitrile **S3** (335 mg, 2.00 mmol, 1.0 equiv.) was converted into the corresponding white ammonium salt **9** (190 mg, 733 μmol) in 37% yield.

M.P.: 187 – 188 °C.

IR (ATR): $\tilde{\nu}$ (cm^{-1}) = 3276 (m), 2956 (m), 2924 (m), 2870 (w), 1606 (m), 1512 (m), 1467 (m), 1403 (w), 1383 (w), 1367 (w), 1293 (w), 1020 (s), 939 (m), 862 (w), 818 (w), 748 (w), 526 (m).

^{1}H NMR (MeCN-d_3, 600 MHz, 300 K) δ [ppm] = 6.07 (br s, 3H), 2.91 (ddd, J = 8.7, 6.7, 2.4 Hz, 2H), 1.71 – 1.48 (m, 3H), 1.46 – 1.38 (m, 1H), 1.38 – 1.21 (m, 4H), 1.21 – 1.06 (m, 4H), 0.96 – 0.83 (m, 9H).

^{13}C NMR (MeCN-d_3, 151 MHz, 300 K) δ [ppm] = 41.5 (s), 39.9 (s), 37.6 (s), 33.9 (s), 32.9 (s), 28.6 (s), 25.3 (s), 25.1 (s), 22.9 (s), 22.8 (s), 19.6 (s).

HRMS (ESI): $C_{11}H_{26}BF_4N$ calculated: [(M + Na)$^+$]: 282.1989

found: [(M + Na)$^+$]: 282.1984.

General procedure B for ammonium salt formation

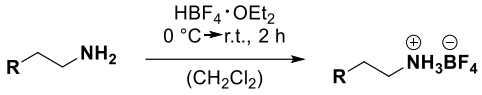

According to a literature procedure,[14] the free amine (1.0 equiv.) was dissolved in dry CH_2Cl_2 (~ 0.5 M) and stirred at 0 °C. Tetrafluoroboric acid diethyl ether complex (1.1 equiv.) was added dropwise leading to the precipitation of a white solid. After stirring the mixture for 2 h at room temperature, the solvent was removed by rotatory evaporation. The residual solid was suspended in diethyl ether and stirred vigorously for a few minutes. Then the supernatant solution was removed, and the washing step was repeated two times. The final white solid was dried in *vacuo*.

2-Cyclohexylethan-1-ammonium tetrafluoroborate (10)

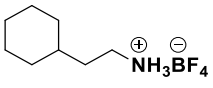

10

$C_8H_{18}BF_4N$
MW: 215.04 g/mol

Following general procedure B, 2-cyclohexylethanamine (**S4**, 254 mg, 2.00 mmol, 1.0 equiv.) was converted into the corresponding white ammonium salt **10** (388 mg, 1.80 mmol) in 91% yield.

M.P.: 241 – 242 °C.

IR (ATR): $\tilde{\nu}$ (cm^{-1}) = 3274 (m), 3179 (w), 2919 (m), 2852 (m), 1612 (w), 1594 (w), 1507 (m), 1477 (w), 1465 (m), 1449 (w), 1410 (w), 1347 (w), 1289 (w), 1020 (s), 1007 (s), 966 (w), 931 (m), 885 (w), 866 (m), 842 (w), 793 (w), 759 (w), 568 (w), 524 (m), 470 (w).

^{1}H NMR (MeCN-d_3, 500 MHz, 300 K) δ [ppm] = 6.45 – 5.74 (m, 3H), 2.97 (s, 2H), 1.84 – 1.61 (m, 5H), 1.55 – 1.41 (m, 2H), 1.37 – 1.13 (m, 4H), 1.00 – 0.87 (m, 2H).

^{13}C NMR (MeCN-d_3, 126 MHz, 300 K) δ [ppm] = 39.3 (s), 35.4 (s), 34.9 (s), 33.4 (s), 27.0 (s), 26.7 (s).

HRMS (ESI): $C_8H_{18}BF_4N$ calculated: $[(M + Na)^+]$: 238.1362

found: $[(M + Na)^+]$: 238.1356.

3-Cyclohexylpropan-1-ammonium tetrafluoroborate (11)

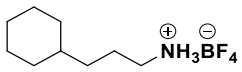

11

$C_9H_{20}BF_4N$
MW: 229.07 g/mol

Following general procedure B, 2-cyclohexylpropan-1-amine (**S5**, 150 mg, 1.06 mmol, 1.0 equiv.) was converted into the corresponding white ammonium salt **11** (171 mg, 746 μmol) in 70% yield.

M.P.: 263 – 265 °C.

IR (ATR): $\tilde{\nu}$ (cm^{-1}) = 3276 (m), 2919 (m), 2851 (m), 1607 (w), 1510 (m), 1475 (w), 1450 (w), 1404 (w), 1291 (w), 1020 (s), 960 (m), 928 (m), 884 (w), 867 (w), 843 (w), 821 (w), 779 (w), 746 (w), 564 (w), 524 (m), 479 (w), 421 (w).

^{1}H NMR (MeCN-d_3, 500 MHz, 300 K) δ [ppm] = 6.52 – 5.81 (m, 3H), 3.13 – 2.75 (m, 2H), 1.78 – 1.42 (m, 7H), 1.40 – 1.05 (m, 6H), 1.00 – 0.83 (m, 2H).

^{13}C NMR (MeCN-d_3, 126 MHz, 300 K) δ [ppm] = 41.5 (s), 37.7 (s), 34.3 (s), 33.7 (s), 27.2 (s), 26.9 (s), 24.9 (s).

HRMS (ESI): $C_9H_{20}BF_4N$ calculated: $[(M + Na)^+]$: 252.1519

found: $[(M + Na)^+]$: 252.1519.

General procedure C for acetylation of primary ammonium salts

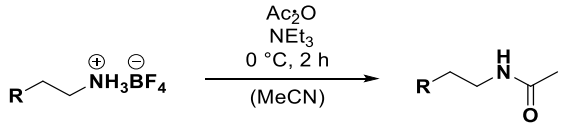

The ammonium salt (1.0 equiv.) was dissolved in dry MeCN (~ 0.5 M) and stirred at 0 °C. Triethylamine (2.0 equiv.) and acetic anhydride (3.0 equiv.) were added and the mixture was allowed to stir for 2 h at this temperature. Then, water was added and the solution was extracted with CH_2Cl_2 (2 x 2 mL). The combined organic layers were washed with saturated NH_4Cl solution (2 mL) and saturated aqueous $NaHCO_3$ solution (2 mL), dried (Na_2SO_4), and concentrated under reduced pressure. Column chromatography *via* MPLC (RediSep® Column: Silica, 4 g, 13 mL/min; CH_2Cl_2/ CH_2Cl_2:MeOH (9:1) 100:0 to 20:80, 20.0 CV, 9.5 min) resulted in the desired acetylated products.

***N*-(3,7-Dimethyloctyl)acetamide (S6)**

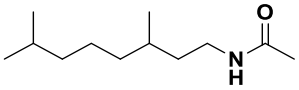

S6

$C_{12}H_{25}NO$
MW 199.34 g/mol

According to general procedure C, compound **8** (12.2 mg, 50.0 µmol) resulted in the desired acetylated product **S6** (7.77 mg, 39.0 µmol, 78%) as a colorless liquid.

TLC R_f = 0.28 (CH_2Cl_2/MeOH = 95/5) [CAM].

IR (ATR): $\tilde{\nu}$ (cm^{-1}) = 3282 (m), 3089 (w), 2954 (m), 2926 (m), 2869 (m), 1650 (s), 1555 (s), 1464 (m), 1438 (m), 1367 (m), 1295 (m), 1230 (w) 1169 (w), 1146 (w),1102 (w), 1040 (w), 995 (w), 733 (m), 602 (m), 490 (w), 468 (w), 440 (w), 413 (w).

^{1}H NMR ($CDCl_3$, 500 MHz, 300 K) δ [ppm] = 5.36 (s, 1H), 3.42 – 2.90 (m, 2H), 1.97 (s, 2H), 1.56 – 1.43 (m, 3H), 1.35 – 1.19 (m, 5H), 1.17 – 1.09 (m, 3H), 0.89 (d, *J* = 6.5 Hz, 3H), 0.86 (*virt.* dd, *J* = 6.6, 0.8 Hz, 6H).

^{13}C NMR ($CDCl_3$, 126 MHz, 300 K) δ [ppm] = 170.1 (s), 39.4 (s), 38.0 (s), 37.3 (s), 36.9 (s), 30.8 (s), 28.1 (s), 24.8 (s), 23.5 (s), 22.8 (s), 22.7 (s), 19.6 (s).

HRMS (ESI): $C_{12}H_{25}NO$ calculated: $[(M + H)^+]$: 200.2009

found: $[(M + H)^+]$: 200.2010.

***N*-(4,8-Dimethylnonyl)acetamide (S7)**

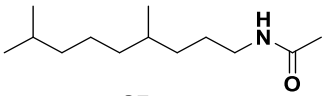

S7

$C_{13}H_{27}NO$
MW: 213.37 g/mol

According to general procedure C, compound **9** (12.9 mg, 50.0 µmol) resulted in the desired acetylated product **S7** (9.83 mg, 46.1 µmol, 92%) as a colorless liquid.

TLC R_f = 0.29 (CH_2Cl_2/MeOH = 95/5) [CAM].

IR (ATR): $\tilde{\nu}$ (cm^{-1}) = 3286 (m), 3089 (w), 2954 (m), 2926 (m), 2868 (m), 1650 (s), 1555 (s), 1461 (m), 1438 (m), 1367 (m), 1293 (m), 1213 (w), 1189 (w), 1147 (w), 1101 (w), 1039 (w), 990 (w), 920 (w), 733 (m), 603 (m), 453 (w).

^{1}H NMR ($CDCl_3$, 500 MHz, 300 K) δ [ppm] = 5.50 (s, 1H), 3.21 (dddd, *J* = 7.9, 6.7, 5.7, 4.0 Hz, 2H), 1.96 (s, 3H), 1.56 – 1.35 (m, 4H), 1.34 – 1.17 (m, 4H), 1.16 – 1.04 (m, 4H), 0.85 (*virt.* dd, *J* = 6.6, 0.7 Hz, 6H), 0.85 (d, *J* = 6.6 Hz, 3H).

^{13}C NMR ($CDCl_3$, 126 MHz, 300 K) δ [ppm] = 170.1 (s), 40.2 (s), 39.4 (s), 37.3 (s), 34.3 (s), 32.7 (s), 28.1 (s), 27.3 (s), 24.9 (s), 23.5 (s), 22.8 (s), 22.7 (s), 19.7 (s).

HRMS (ESI): $C_{13}H_{27}NO$ calculated: $[(M + H)^+]$: 214.2165

found: $[(M + H)^+]$: 214.2167.

***N*-(2-Cyclohexylethyl)acetamide (S8)**

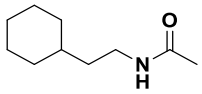

S8

$C_{10}H_{19}NO$
MW: 169.29 g/mol

According to general procedure C, compound **10** (21.4 mg, 100 μmol) resulted in the desired acetylated product **S8** (14.2 mg, 83.9 μmol, 84%) as a colorless liquid.

TLC R_f = 0.28 (CH_2Cl_2/MeOH = 95/5) [CAM].

IR (ATR): $\tilde{\nu}$ (cm^{-1}) = 3297 (m), 3092 (w), 2918 (s), 2850 (s), 1646 (s), 1552 (s), 1445 (m), 1366 (s), 1313 (w), 1291 (s), 1249 (w), 1203 (m), 1183 (w), 1154 (m), 1103 (m), 1092 (w), 1035 (m), 995 (w), 964 (w), 921 (w), 890 (w), 844 (w), 732 (m), 631 (w), 602 (s), 569 (w), 491 (m), 452 (w), 424 (m).

^{1}H NMR ($CDCl_3$, 500 MHz, 300 K) δ [ppm] = 5.50 (s, 1H), 3.70 – 2.88 (m, 2H), 1.95 (s, 3H), 1.75 – 1.59 (m, 5H), 1.41 – 1.33 (m, 2H), 1.33 – 1.07 (m, 4H), 0.97 – 0.84 (m, 2H).

^{13}C NMR ($CDCl_3$, 126 MHz, 300 K) δ [ppm] = 170.1 (s), 37.6 (s), 37.2 (s), 35.5 (s), 33.3 (s), 26.6 (s), 26.3 (s), 23.5 (s).

HRMS (ESI): $C_{10}H_{19}NO$ calculated: $[(M + H)^+]$: 170.1539

found: $[(M + H)^+]$: 170.1542.

***N*-(3-Cyclohexylpropyl)acetamide (S9)**

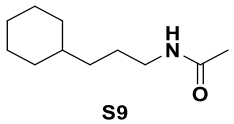

S9

$C_{11}H_{21}NO$
MW: 183.30 g/mol

According to general procedure C, compound **11** (22.8 mg, 100 μmol) resulted in the desired acetylated product **S9** (18.3 mg, 99.8 μmol, *quant.*) as a colorless liquid.

TLC R_f = 0.28 (CH_2Cl_2/MeOH = 95/5) [CAM].

IR (ATR): $\tilde{\nu}$ (cm^{-1}) = 3281 (m), 3091 (w), 2920 (s), 2850 (m), 1649 (s), 1553 (s), 1446 (m), 1368 (m), 1290 (m), 1194 (w), 1179 (w), 1153 (w), 1108 (w), 1038 (w), 992 (w), 888 (w), 843 (w), 735 (m), 602 (m), 502 (w), 452 (w).

^{1}H NMR ($CDCl_3$, 500 MHz, 300 K) δ [ppm] = 5.41 (br s, 1H), 3.21 (td, *J* = 7.3, 5.8 Hz, 2H), 1.97 (s, 3H), 1.77 – 1.57 (m, 5H), 1.58 – 1.42 (m, 2H), 1.42 – 1.07 (m, 6H), 0.97 – 0.71 (m, 2H).

^{13}C NMR ($CDCl_3$, 126 MHz, 300 K) δ [ppm] = 170.1 (s), 40.2 (s), 37.5 (s), 34.7 (s), 33.5 (s), 27.1 (s), 26.8 (s), 26.5 (s), 23.5 (s).

HRMS (ESI):	$C_{11}H_{21}NO$	calculated:	$[(M + H)^+]$: 184.1696
		found:	$[(M + H)^+]$: 184.1699.

3. Oxidation Reactions

3.1. Synthetic Procedure for the Oxidation Reactions

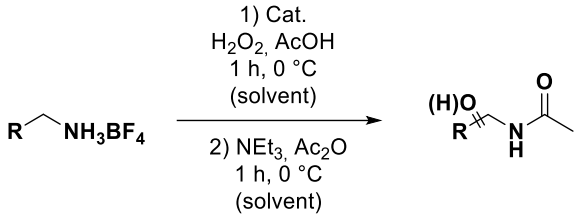

Small-scale oxidation procedure with Fe catalysts

Fe catalyst (555 nmol, 3 mol%) and substrate (18.5 µmol, 1.0 equiv.) were dissolved in 200 µL solvent in a 1 mL screw vial. After the addition of AcOH (8.5 µL, 148 µmol, 8.0 equiv.), the mixture was cooled to 0 °C. Next, a solution of commercially available aq. H_2O_2 (50% w/w, Sigma Aldrich, 51.4 µL, 46.2 µmol, 2.5 equiv.) diluted in solvent (~ 0.9 M) was slowly added over 16 min by a syringe pump. After the addition, the mixture was left to stir for another 45 min.

Small-scale oxidation procedure with Mn catalysts

Mn catalyst (185 nmol, 1 mol%) and substrate (18.5 µmol, 1.0 equiv.) were dissolved in 200 µL solvent in a 1 mL screw vial. After the addition of AcOH (23.3 µL, 407 µmol, 22.0 equiv.), the mixture was cooled to 0 °C. Next, a solution of commercially available aq. H_2O_2 (50% w/w, Sigma Aldrich, 51.4 µL, 46.2 µmol, 2.5 equiv.) diluted in solvent (~ 0.9 M) was slowly added over 16 min by a syringe pump. After the addition, the mixture was left to stir for another 45 min.

General procedure for workup and GC analysis for decyl ammonium substrate

After the time indicated, biphenyl (internal standard, 9.25 µmol, 0.5 equiv.), triethylamine (100 µL), and acetic anhydride (150 µL) were added and the mixture was stirred at 0 °C for 50 min. Next, water (1 mL) was added and the mixture was left stirring for another 10 min. The solution was then extracted with CH_2Cl_2 (2 x 2 mL) and the combined organic layers were washed with a 2 M H_2SO_4 solution (2 mL), saturated aqueous $NaHCO_3$ solution (2 mL), and water (2 mL), dried (Na_2SO_4) and analyzed *via* GC.

General procedure for workup and GC analysis for all other substrates

After the time indicated, biphenyl (internal standard, 9.25 µmol, 0.5 equiv.), triethylamine (100 µL), and acetic anhydride (150 µL) were added and the mixture was stirred at 0 °C for 50 min. Next, water (1 mL) was added and the mixture was left stirring for another 10 min. The solution was then extracted with CH_2Cl_2 (2 x 2 mL) and the combined organic layers were washed with a saturated NH_4Cl solution (2 mL), saturated aqueous $NaHCO_3$ solution (2 mL), dried (Na_2SO_4), and analyzed *via* GC.

Second step for small-scale oxidation reactions in TFE/HFIP

For the analysis via GC, the oxidation of the alcohol products obtained in TFE/HFIP as solvents turned out to be advantageous due to better separation. Therefore, after the workup, the crude material was dissolved in anhydrous EtOAc (0.5 mL) and IBX (10.4 mg, 37 µmol, 2.00 equiv.) was added. The mixture was stirred at 70 °C overnight, cooled down to r.t., filtered over Celite, and analyzed *via* GC.

Large-scale oxidation procedure with Fe catalysts

Fe catalyst (2.78 µmol, 3 mol%) and substrate (92.5 µmol, 1.0 equiv.) were dissolved in 1 mL MeCN in a screw vial. After the addition of AcOH (42.4 µL, 740 mmol, 8.0 equiv.), the mixture was cooled to 0 °C. Next, a solution of commercially available aq. H_2O_2 (50% w/w, Sigma Aldrich, 257 µL, 231 µmol, 2.5 equiv.) diluted in MeCN (~ 0.9 M) was slowly added over 16 min by a syringe pump. After the addition, the mixture was left to stir for another 45 min. Then, triethylamine (500 µL), and acetic anhydride (750 µL) were added and the mixture was stirred for an additional 50 min at 0 °C. The solvent was removed under reduced pressure and the mixture was treated with water (3 mL) and extracted with CH_2Cl_2 (3 × 4 mL). The combined organic layers were washed with saturated NH_4Cl solution (5 mL), saturated aqueous $NaHCO_3$ solution (5 mL), dried (Na_2SO_4), and concentrated under reduced pressure. The crude material was purified *via* MPLC.

Large-scale oxidation procedure with Mn catalysts

Mn catalyst (3.70 µmol, 1 mol%) and substrate (370 µmol, 1.0 equiv.) were dissolved in 4 mL MeCN in a 25 mL round-bottomed flask. After the addition of AcOH (233 µL, 4.07 mmol, 11.0 equiv.), the mixture was cooled to 0 °C. Next, a solution of commercially available aq. H_2O_2 (50% w/w, Sigma Aldrich, 1.03 mL, 925 µmol, 2.5 equiv.) diluted in MeCN (~ 0.9 M) was slowly added over 16 min by a syringe pump. After the addition, the mixture was left to stir for another 45 min. Then, triethylamine (1 mL), and acetic anhydride (1.5 mL) were added and the mixture was stirred for an additional 50 min at 0 °C. The solvent was removed under reduced pressure and the mixture was treated with water (3 mL) and extracted with CH_2Cl_2 (3 × 4 mL). The combined organic layers were washed with saturated NH_4Cl solution (5 mL), saturated aqueous $NaHCO_3$ solution (5 mL), dried (Na_2SO_4), and concentrated under reduced pressure. The crude material was purified *via* MPLC.

Privous small-scale procedure for oxidation reactions with Fe[3a]

Fe catalyst (925 nmol, 5 mol%) and substrate (18.5 µmol, 1.0 equiv.) were dissolved in 200 µL MeCN in a 4 mL screw vial. After addition of a solution of AcOH in MeCN solution (~ 3 M, 49.3 µL, 148 µmol, 8.0 equiv.), the mixture was cooled to 0 °C. Next, a solution of commercially available aq. H_2O_2 (50% w/w, Sigma Aldrich) diluted in MeCN (~ 0.9 M, 308 µL, 278 µmol, 15.0 equiv.) was slowly added over 90 min by a syringe pump. After the addition, the mixture was left stirring for another 15 min.

3.2 Oxidation Results

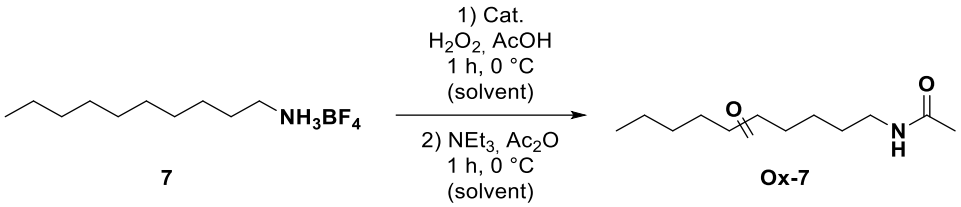

All reactions were performed as described in the *small-scale oxidation procedure with Fe or Mn catalysts*, followed by the *general procedure for workup and GC analysis for decyl ammonium* substrate. In the case of entries 9 to 12, the second step for *small-scale oxidation reactions in TFE/HFIP was done after the work-up.*

Table S1: Results of the oxidation of decylammonium tetrafluoroborate using different catalysts and solvents.

Entry	Cat.	Cat. [mol%]	Solvent	SM [%]	K9 [%]	K8 [%]	K7 [%]	K6 [%]	K5 [%]	K4 [%]	K3 [%]	Conv. [%]	Total Yield[a] [%]	Selectivity[b] K3-4 [%]	K3-5 [%]
1	**Mn(mcp)**	1	MeCN	31	16	11	9.9	9.5	5.2	2.3	0.9	69	55	5.8	15
2	**Mn(mcp)Twe**	1	"	42	9.3	7.7	5.2	6.3	5.9	4.3	1.2	58	40	14	29
3	**Mn(pdp)**	1	"	42	9.0	6.9	5.4	5.4	2.8	1.7	0.6	58	32	7.2	16
4	**Mn(pdp)Twe**	1	"	55	6.1	5.4	3.0	3.8	3.8	2.7	0.7	45	26	13	28
5[c]	**Fe(mcp)**	3	"	82	5.6	4.7	1.8	2.0	0.7	0.5	0.1	18	15	3.6	7.9
6	**Fe(mcp)Twe**	3	"	93	0.5	0.7	0.2	0.2	0.1	0.2		6.8	2.0	9.0	15
7	**Fe(pdp)**	3	"	65	7.9	7.5	5.6	5.7	2.1	1.7	0.3	35	31	6.4	13
8	**Fe(pdp)Twe**	3	"	83	3.1	2.9	1.3	1.8	1.3	2.8	0.9	17	14	27	36
9[d]	**Fe(pdp)**	3	TFE	37	11	7.5	7.0	5.5	2.7	0.5		63	34	1.6	9.5
10[d]	**Fe(pdp)Twe**	3	"	62	5.9	4.0	3.2	3.0	2.8	1.1		38	20	5.6	20
11[d]	**Fe(pdp)**	3	HFIP	6.0	35	17	12	6.2	1.9	0.5		94	73	0.7	3.3
12[d]	**Fe(pdp)Twe**	3	"	55	8.4	5.1	3.2	3.5	5.7	3.7	0.7	45	30	15	34
13[e]	**Fe(pdp)Twe**	5	MeCN	53	3.8	4.4	2.7	3.4	3.7	4.8	2.2	47	25	28	43
14[e]	**Fe(pdp)Twe$_2$**	5	"	66	4.8	6.0	1.7	3.1	3.5	3.1	1.3	34	23	19	34

Reaction conditions are described in the general oxidation procedure (small scale). Yields were calculated via GC analysis utilizing biphenyl as an internal standard. (a) Total yield refers to a mixture of all isomers. (b) Selectivity refers to yield of selected ketones/total yield. (c) 37.0 umol scale. (d) Different reaction conditions (small scale reactions in TFE/HIFP). (e) 15. equiv. of H_2O_2 were added over 90 min.

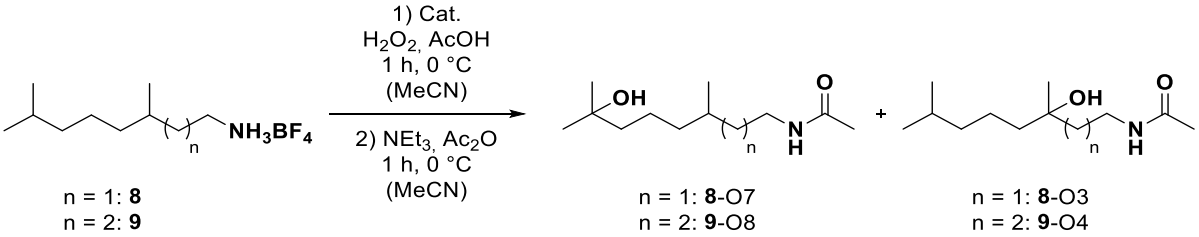

All reactions were performed as described in the *large-scale oxidation procedure with Fe catalysts*.

Table S2: Results of the oxidation of **8** and **9** using **Fe(pdp)** and **Fe(pdp)Twe**, respectively.

Entry	Substrate	Cat.	Cat. [mol%]	SM [%]	O7/O8 [%]	O3/O4 [%]	Conv. [%]	Total [a] Yield [%]	Selectivity[b] O3/O4 [%]
1	**8**	**Fe(pdp)**	3	51	30	3.6	49	34	11
2	**8**	**Fe(pdp)Twe**	3	76	9.4	6.6	24	16	41
3	**9**	**Fe(pdp)**	3	45	18	6.0	55	24	25
4	**9**	**Fe(pdp)Twe**	3	62	6.4	8.6	38	15	57

Reaction conditions are described in the general oxidation procedure (large scale). Yields were calculated via GC analysis utilizing biphenyl as an internal standard. (a) Total yield refers to a mixture of all isomers. (b) Selectivity refers to yield of selected ketones/total yield and was determined via NMR.

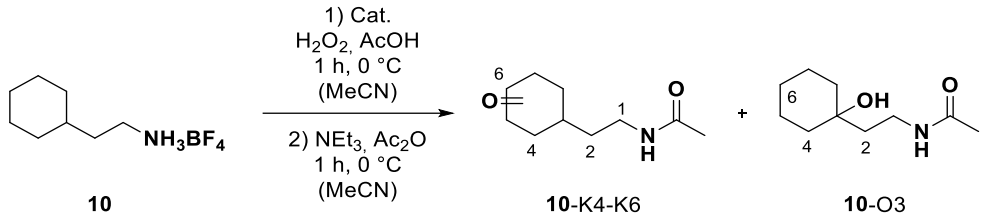

All reactions were performed as described in the *small-scale oxidation procedure with Fe catalysts* followed by the general *procedure for workup and GC analysis for all other substrates*.

Table S3: Results of the oxidation of **10** using **Fe(pdp)** and **Fe(pdp)Twe**, respectively.

Entry	Substrate	Cat.	Cat. [mol%]	SM [%]	K6 [%]	K5 [%]	K4 [%]	O3 [%]	Conv. [%]	Total [a] Yield [%]	Selectivity[b] K4 [%]	Selectivity[b] O3 [%]
1	**10**	**Fe(pdp)**	3	50	7.0	16	3.4	1.4	50	28	13	4.9
2	**10**	**Fe(pdp)Twe**	3	74	1.2	5.6	2.7	1.8	26	11	24	16

Reaction conditions are described in the general oxidation procedure (small scale). Yields were calculated via GC analysis utilizing biphenyl as an internal standard. (a) Total yield refers to a mixture of all isomers. (b) Selectivity refers to yield of selected product/total yield.

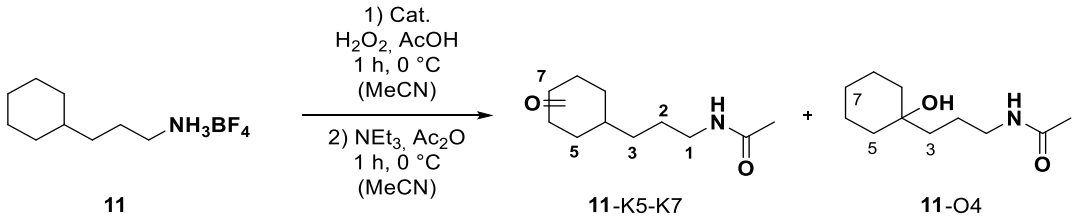

All reactions were performed as described in the *small-scale oxidation procedure with Fe catalysts* followed by the general *procedure for workup and GC analysis for all other substrates*.

Table S4: Results of the oxidation of **11** using **Fe(pdp)** and **Fe(pdp)Twe**, respectively.

Entry	Substrate	Cat.	Cat. [mol%]	SM [%]	K7 [%]	K6 [%]	K5 [%]	O4 [%]	Conv. [%]	Total [a] Yield [%]	Selectivity[b] K5 [%]	Selectivity[b] O4 [%]
1	**11**	**Fe(pdp)**	3	39	8.6	22	2.2	3.2	61	36	6.2	9.0
2	**11**	**Fe(pdp)Twe**	3	64	1.8	6.5	2.0	3.8	36	14	14	27

Reaction conditions are described in the general oxidation procedure (small scale). Yields were calculated via GC analysis utilizing biphenyl as an internal standard. (a) Total yield refers to a mixture of all isomers. (b) Selectivity refers to yield of selected product/total yield.

3.3 Isolation and Characterization of Oxidation Products

The oxidation products of decylammonium tetrafluoroborate were characterized according to previous work.[3a]

3.3.1 Oxidation Products of 3,7-Dimethyloctan-1-ammonium tetrafluoroborate (8)

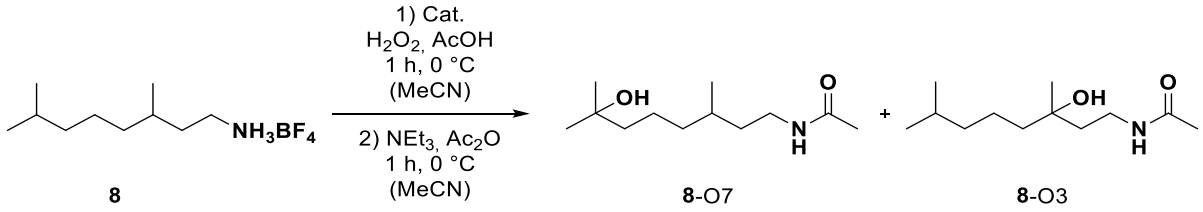

8 **8**-O7 **8**-O3

According to the large-scale oxidation procedure with Fe catalysts, 3,7-dimethyloctan-1-ammonium tetrafluoroborate (**8**, 22.6 mg, 92.5 µmol, 1.00 equiv.) was oxidized by **Fe(pdp)** or **Fe(pdp)Twe**, respectively. After the aqueous workup, the crude mixture was analyzed via GC. Purification via MPLC (RediSep® Column: Silica, 4 g, 13 mL/min; CH_2Cl_2 : CH_2Cl_2/MeOH (9/1) 75:25 to 0:100, 25.2 CV, 11.9 min) gave the tertiary alcohol products as an inseparable mixture.

8-O3/O7: **TLC** R_f = 0.09 (CH_2Cl_2/MeOH = 95/5 [CAM].

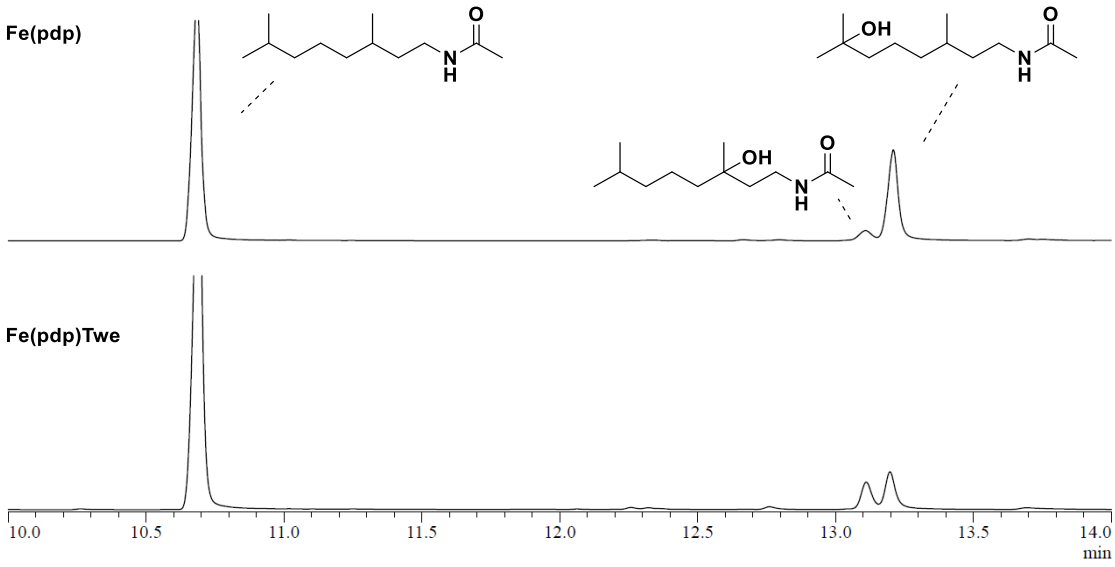

Figure S1: GC spectra of the crude mixtures of the oxidation of **8**.

GC spectra of the crude materials. The tertiary alcohol products **8**-O3 / **8**-O7 could not be separated and were analyzed as a mixture via MS and NMR. The products were assigned via analysis of the corresponding NMR spectra (see SI, Figure S3-S8).

MS Analysis of Mixture of Alcohol products

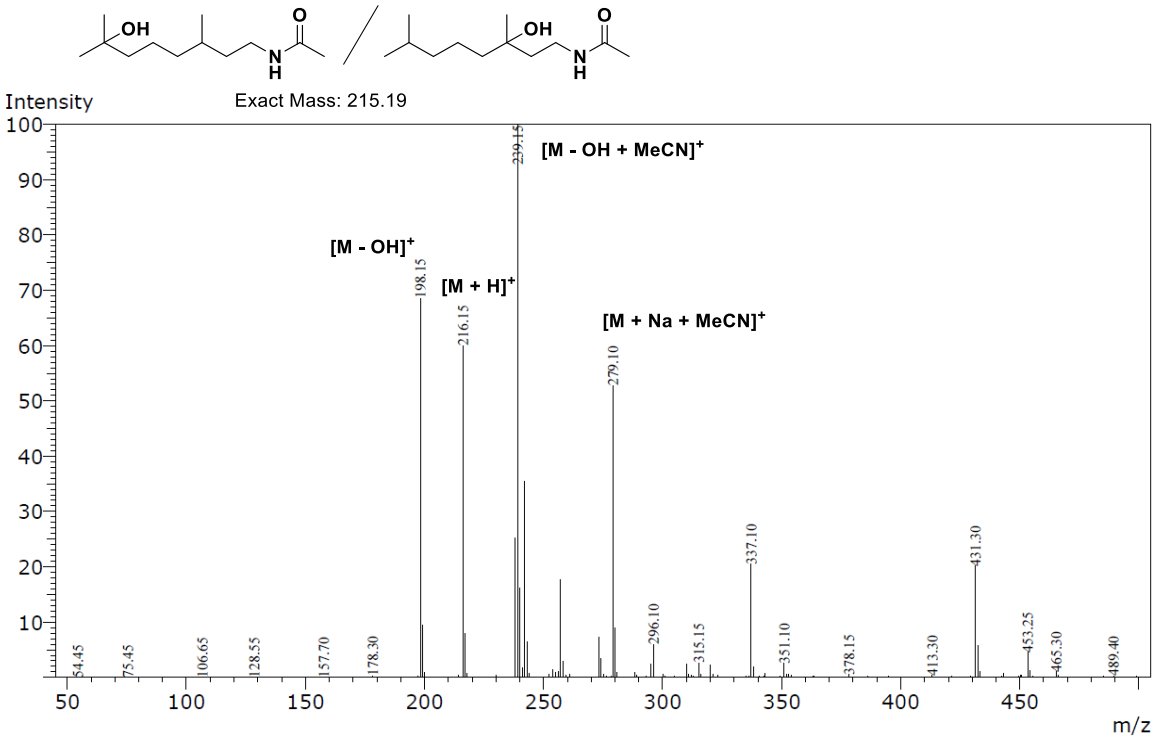

Figure S2: MS spectra of the alcohol products **8**-07 and **8**-03.

Note: MS/MS analysis was conducted but did not result in any conclusive fragments.

Oxidation with **Fe(pdp)**

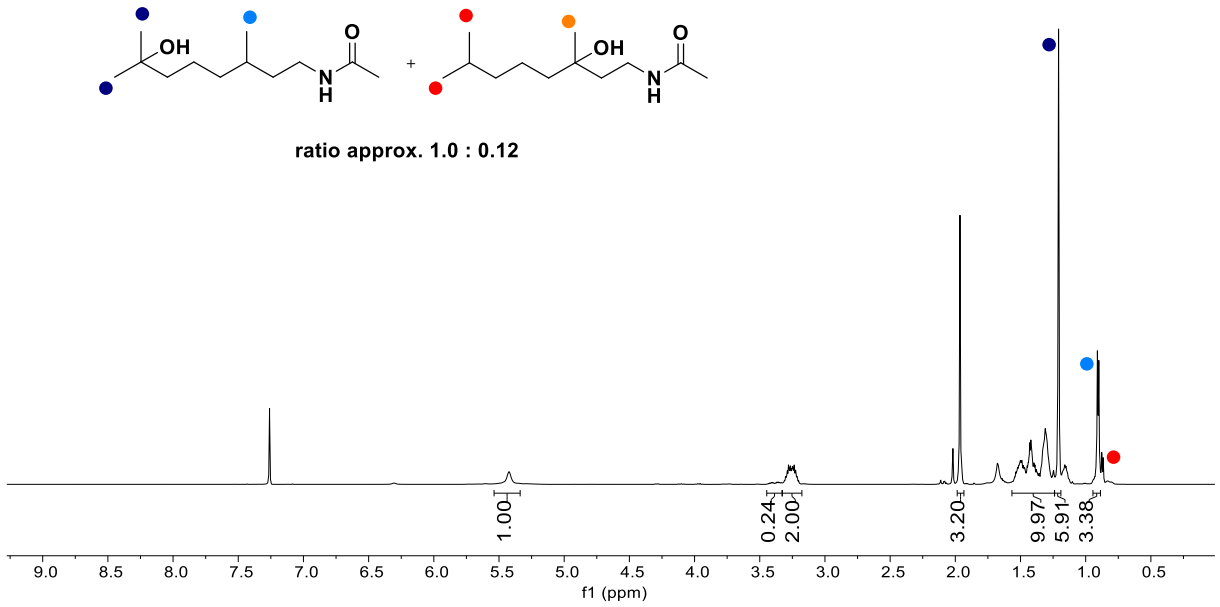

Figure S3: ^{1}H NMR spectra of **8**-O3 / **8**-O7 mixture.

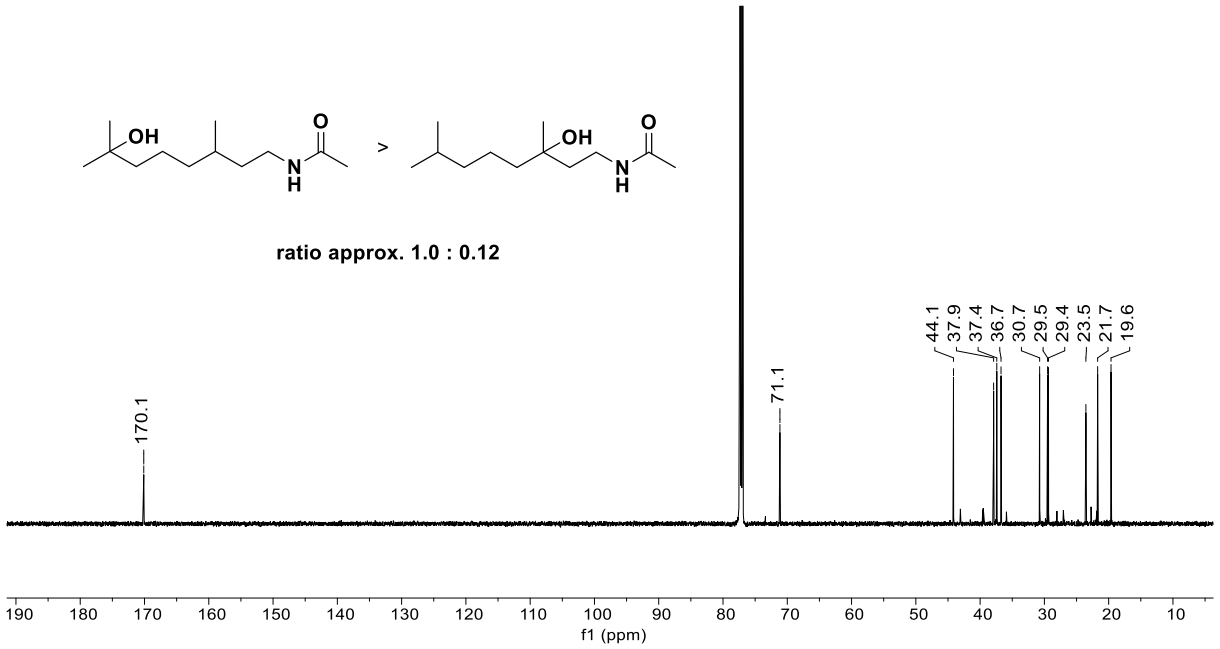

Figure S4: ^{13}C NMR spectra of **8**-O3 / **8**-O7 mixture.

Oxidation with **Fe(pdp)Twe**

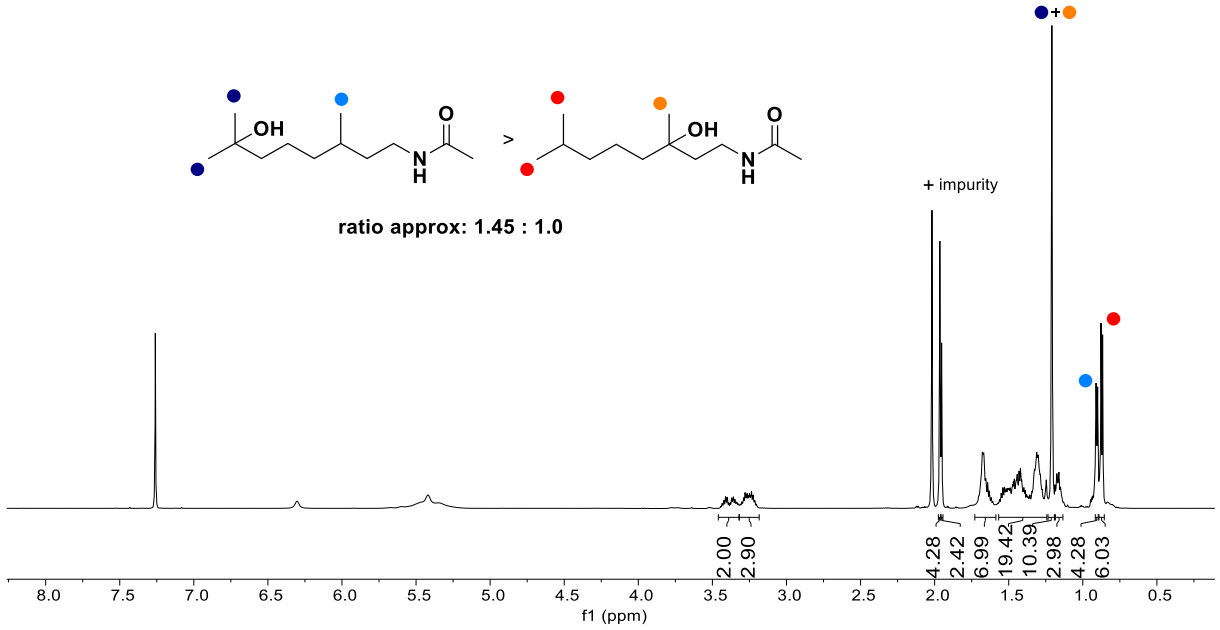

Figure S5: ^{1}H NMR spectra of **8**-O3 / **8**-O7 mixture

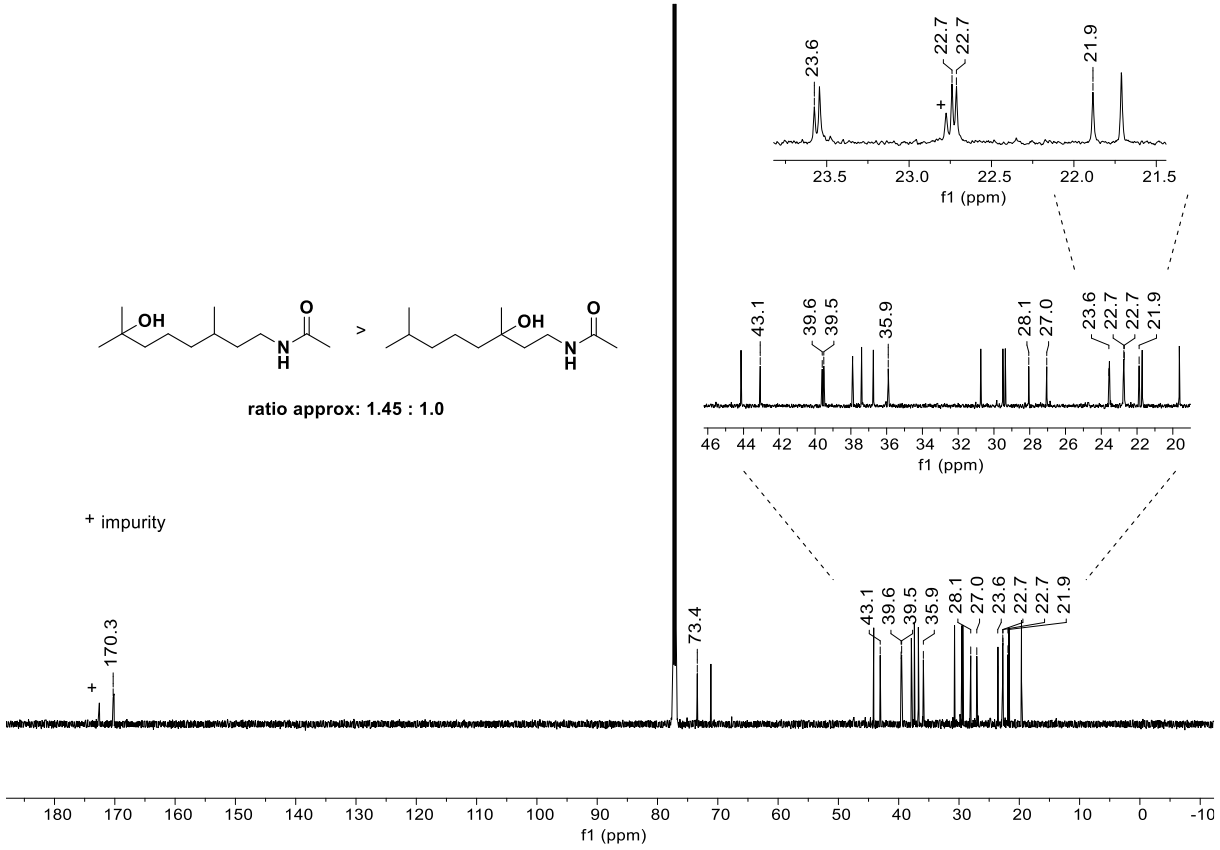

Figure S6: ^{13}C NMR spectra of **8**-O3 / **8**-O7 mixture.

Comparison of Oxidation of **8** with **Fe(pdp)** and **Fe(pdp)Twe**

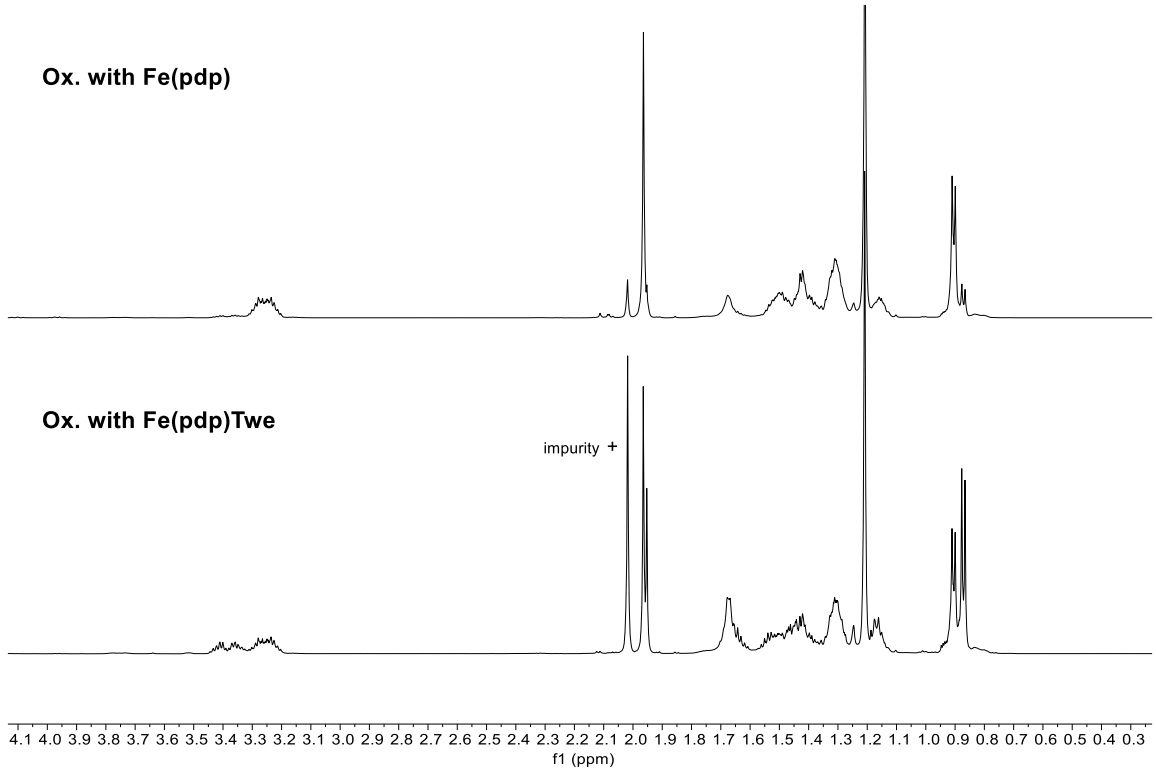

Figure S7: Stacked ^{1}H NMR spectra of the product mixtures of the oxidation of **8** with **Fe(pdp)**/**Fe(pdp)Twe**.

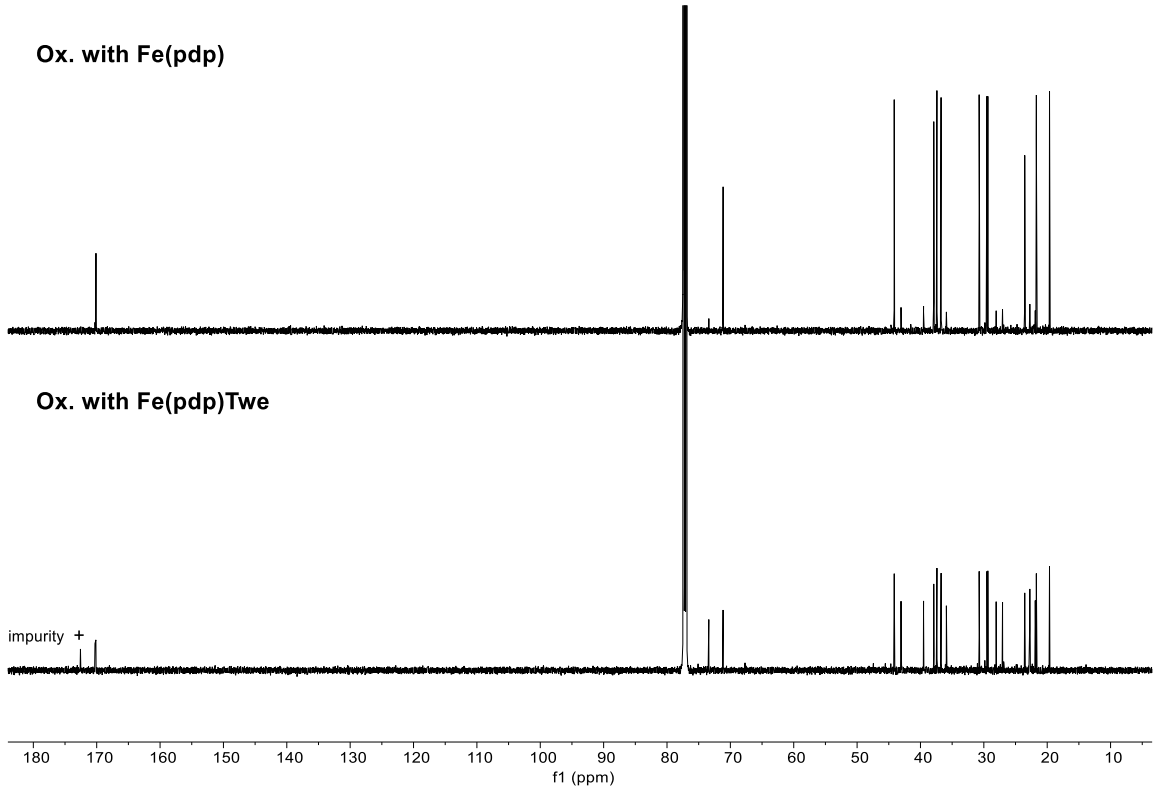

Figure S8: Stacked ^{13}C NMR spectra of product mixtures of the oxidation of **8** with **Fe(pdp)** and **Fe(pdp)Twe**.

3.3.2 Oxidation Products of 4,8-Dimethylnonan-1-ammonium tetrafluoroborate (9)

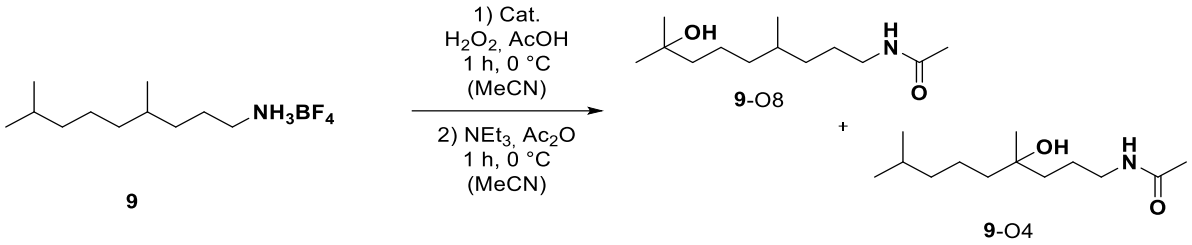

According to the large-scale oxidation procedure with Fe catalysts, 4,8-dimethylnonan-1-ammonium tetrafluoroborate (**9**, 23.9 mg, 92.5 µmol, 1.0 equiv.) was oxidized by **Fe(pdp)** or **Fe(pdp)Twe**, respectively. After the aqueous workup, the crude mixture was analyzed via GC. Purification *via* MPLC (RediSep® Column: Silica, 4 g, 13 mL/min; CH_2Cl_2 : CH_2Cl_2/MeOH (9/1) 70:30 to 0:100, 25.2 CV, 11.9 min) gave the tertiary alcohol products as an inseparable mixture. *Note*: Purification *via* HPLC led to no improvement in separation.

9-O4/O8: **TLC** R_f = 0.17 (CH_2Cl_2/MeOH = 95/5 [CAM].

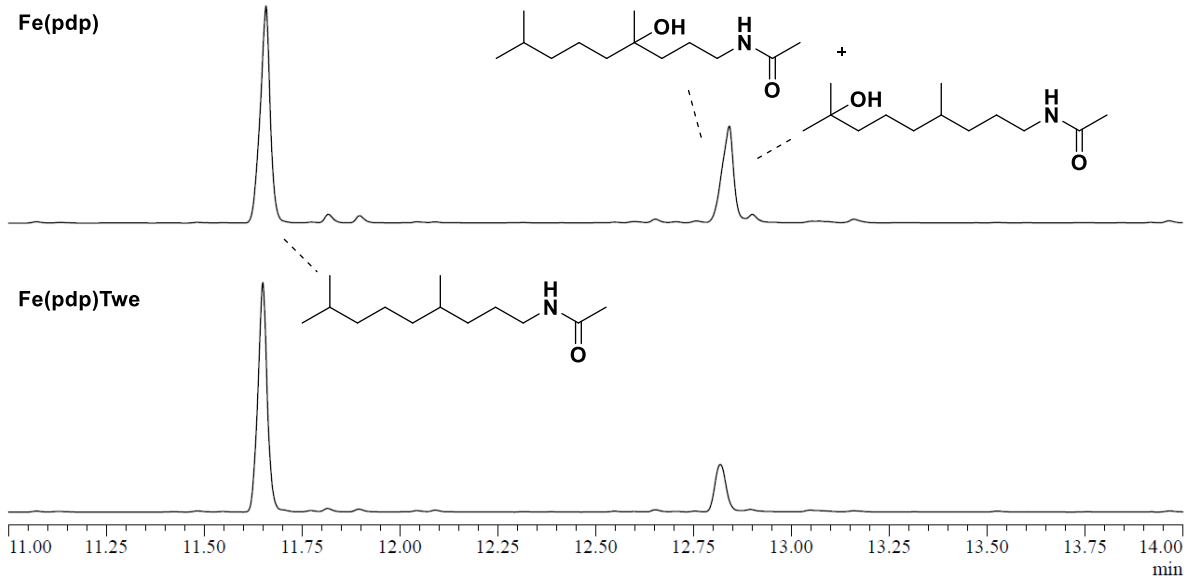

Figure S9: GC spectra of the crude mixtures of the oxidation of **9**.

GC spectra of the crude materials. The tertiary alcohol products **9**-O8 and **9**-O4 could not be separated *via* column chromatography and were analyzed as mixtures. The products were assigned via analysis of the corresponding NMR spectra (see SI, Figure S11-S16). Also, the ratio of the alcohol products was determined via NMR since there was no separation on the GC observed even after optimization of the conditions.

MS Analysis of Mixture of Alcohol products

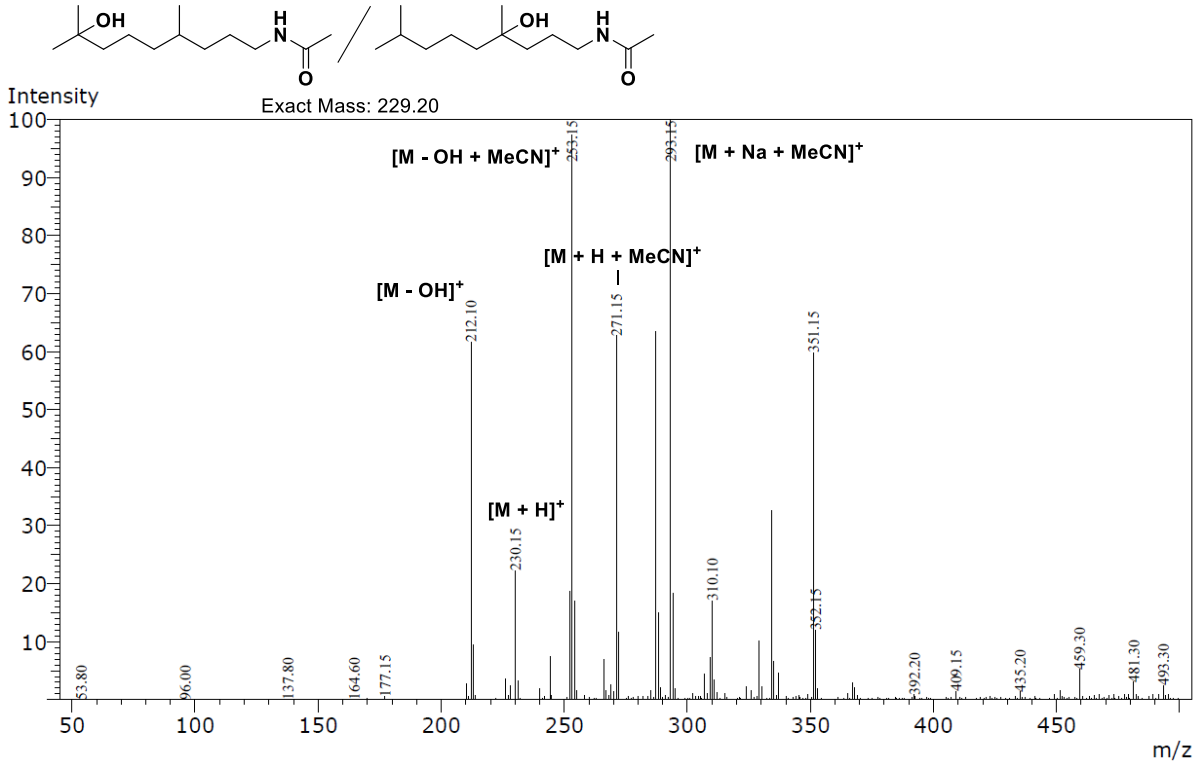

Figure S10: MS spectra of the alcohol products **9**-O8 and **9**-O4.

Note: MS/MS analysis was conducted but did not result in any conclusive fragments.

Oxidation with **Fe(pdp)**

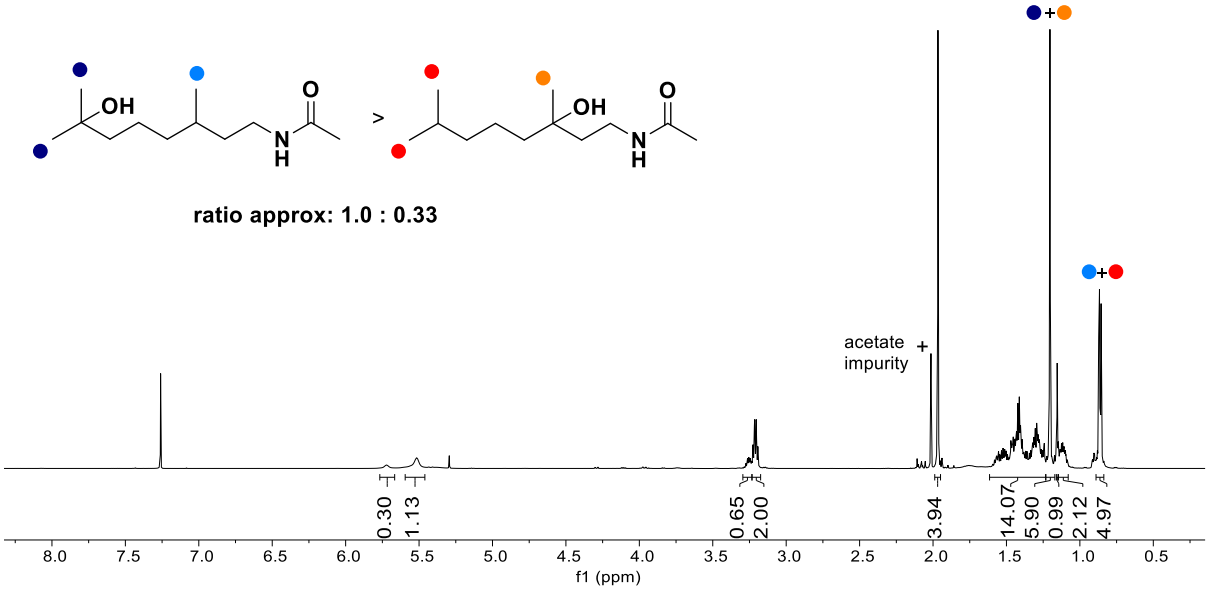

Figure S11: ^{1}H NMR spectra of the **9**-O8 / **9**-O4 mixture.

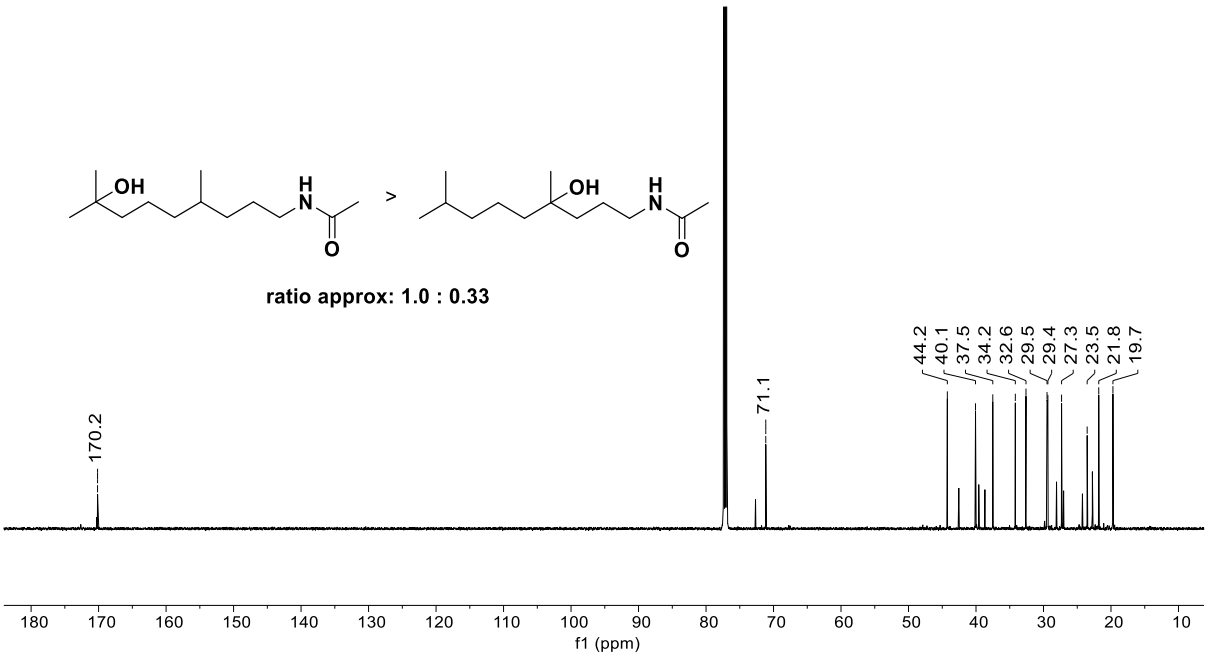

Figure S12: ^{13}C NMR spectra of the **9**-O8 / **9**-O4 mixture.

Oxidation with **Fe(pdp)Twe**

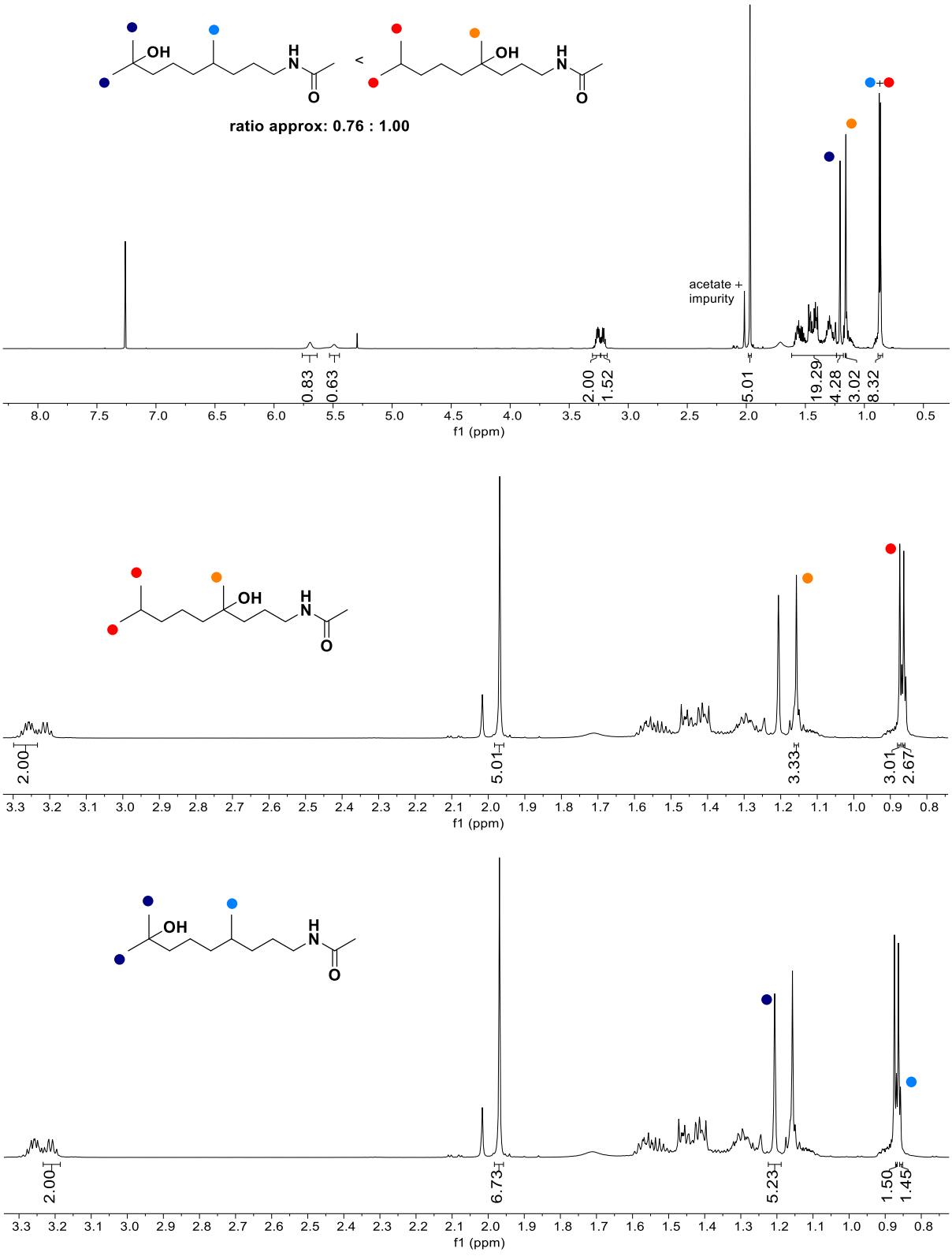

Figure S13: Top: ^{1}H NMR spectra of the alcohol product mixture **9**-O8 and **9**-O4; Middle: Zoom in with the selection of important product signals of the **9**-O4 product; Bottom: Zoom in with the selection of important product signals of **9**-O8 product. Assigned via the integrals and shifts of the corresponding methyl groups at C-4 and C-8, respectively.

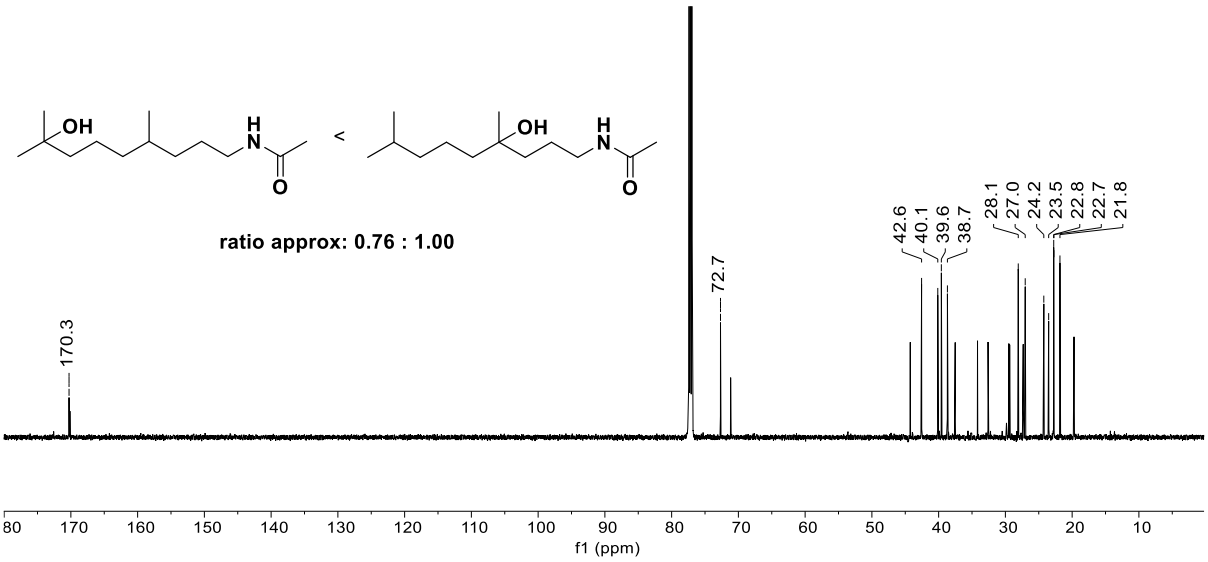

Figure S14: ^{13}C NMR spectra of the alcohol product mixture **9**-O8 and **9**-O4.

Comparison of the Oxidation of **9** with **Fe(pdp)** and **Fe(pdp)Twe**

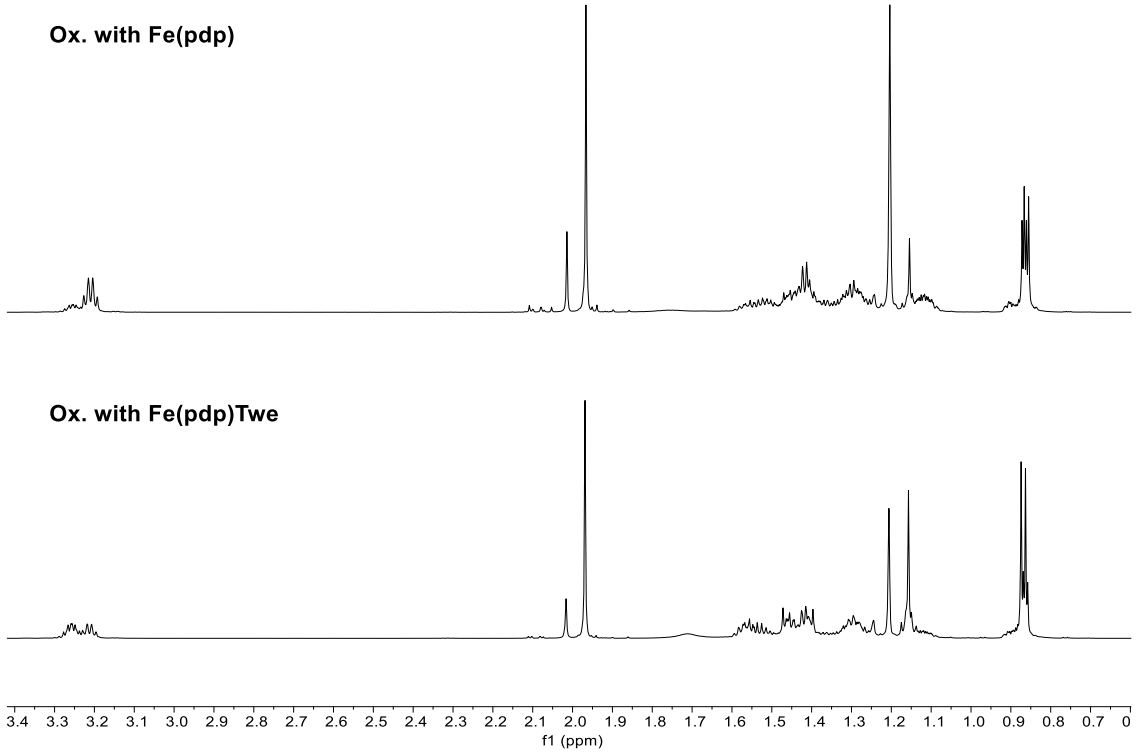

Figure S15: Stacked ^{1}H NMR spectra of **9**-O8 / **9**-O4 mixtures obtained from the oxidation with **Fe(pdp)** and **Fe(pdp)Twe**, respectively.

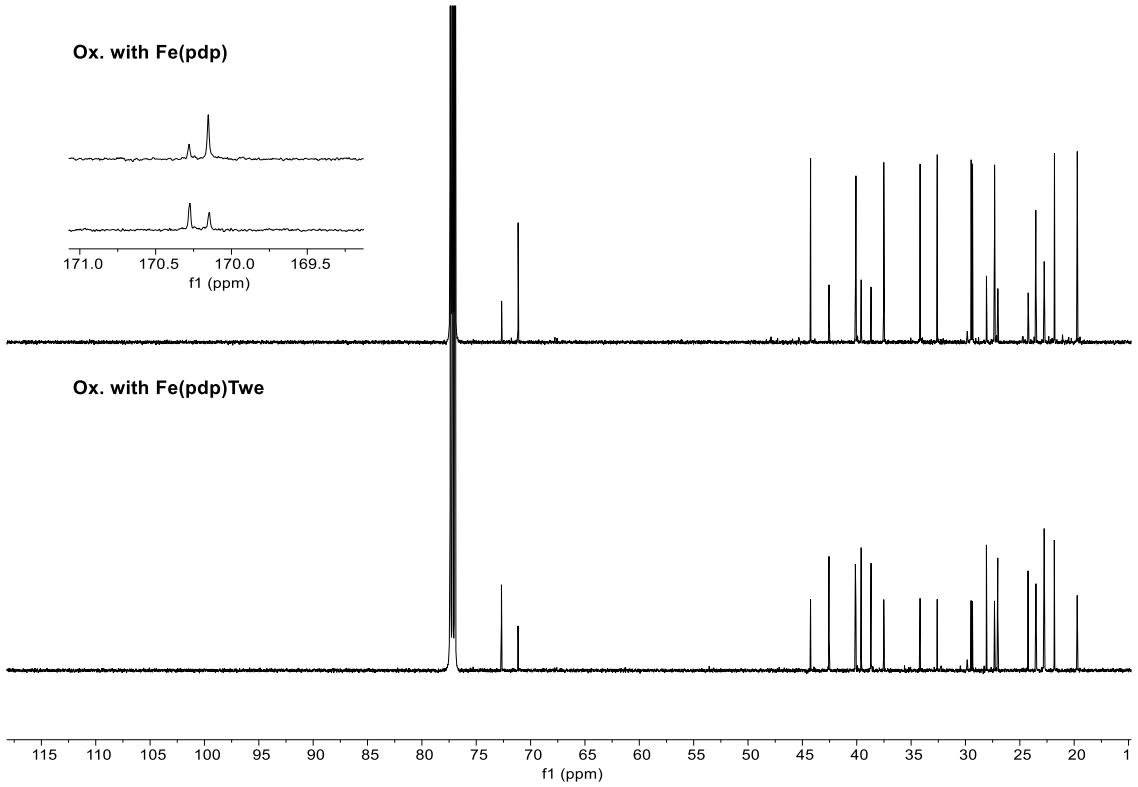

Figure S16: Stacked ^{13}C NMR spectra of **9**-O8 / **9**-O4 mixtures obtained from the oxidation with **Fe(pdp)** and **Fe(pdp)Twe**, respectively.

3.3.3 Oxidation Products of 2-Cyclohexylethan-1-ammonium tetrafluoroborate (10)

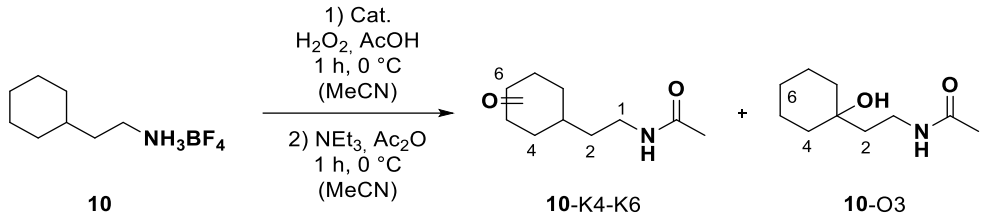

According to the large-scale oxidation procedure with Mn catalysts, 2-cyclohexylethan-1-ammonium tetrafluoroborate (**10**, 19.8 mg, 92.5 µmol, 1.0 equiv.) was oxidized by **Mn(mcp)**. After the aqueous workup, the crude mixture was purified *via* MPLC (RediSep® Column: Silica, 4 g, 13 mL/min; CH_2Cl_2: CH_2Cl_2/MeOH (9/1) 100:0 to 0:100, 30.0 CV, 14.2 min), however, **10**-K4 could only be obtained as a mixture with acetylated starting material, and **10**-K5 and **10**-K6 as a mixture.

10-K4: **TLC** R_f = 0.24 (CH_2Cl_2/MeOH = 95/5 [CAM].

10-K5/6: **TLC** R_f = 0.22 (CH_2Cl_2/MeOH = 95/5 [CAM].

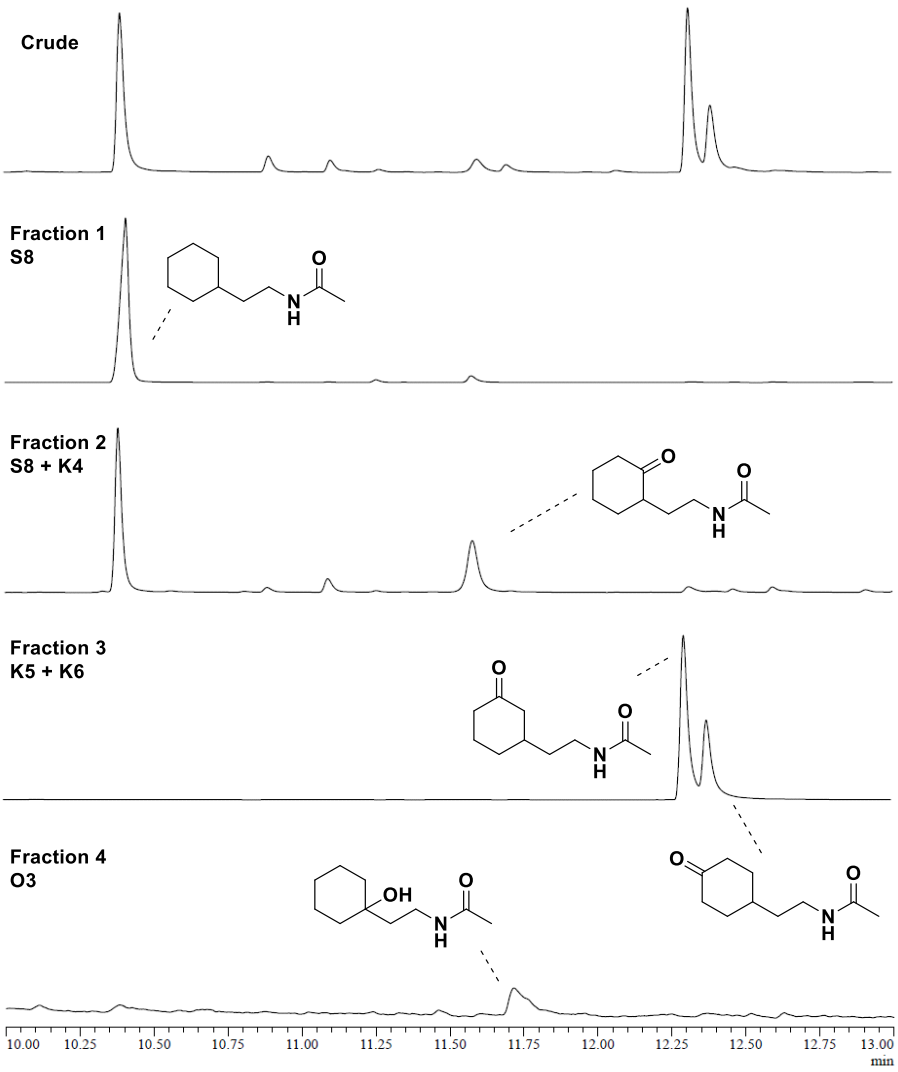

Figure S17: Stacked GC spectra of crude and isolated fractions of the oxidation of **10**.

Stacked GC spectra of crude and isolated fractions of the oxidation of **10**. The products were assigned via analysis of the corresponding NMR spectra (see SI, Figure S18-S38).

Characterization of products via NMR

Acetylated Starting Material (S8) (for comparison with **10-K4**)

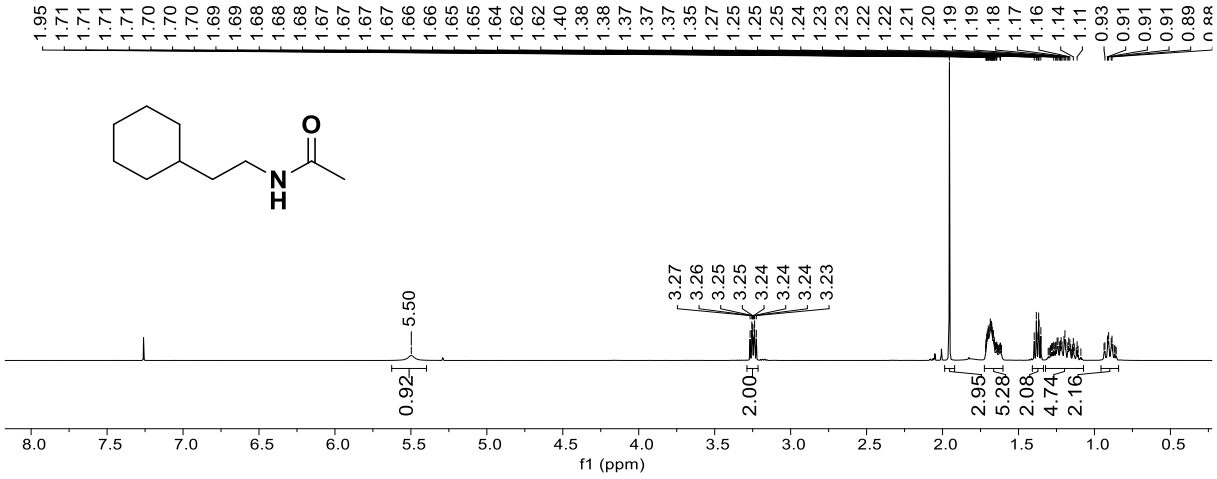

Figure S18: ^{1}H NMR spectra of **S8**.

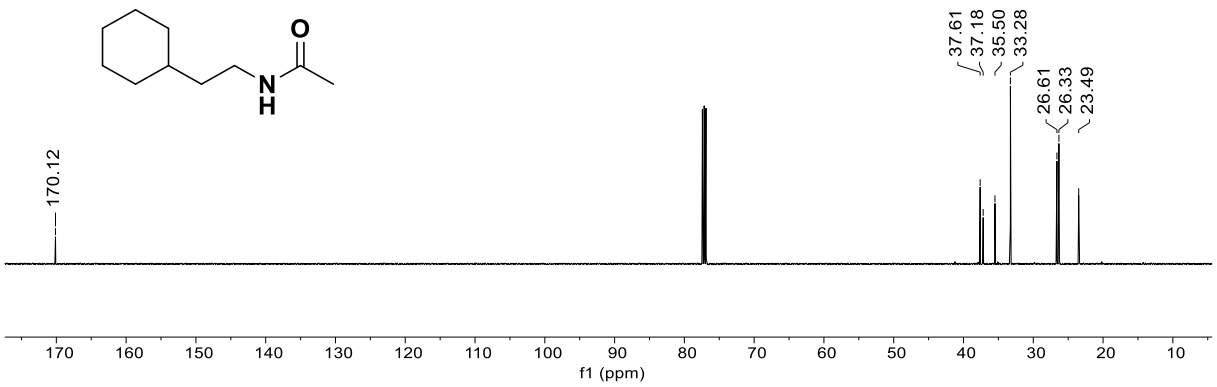

Figure S19: ^{13}C NMR spectra of **S8**.

S8 / 10-K4 mixture

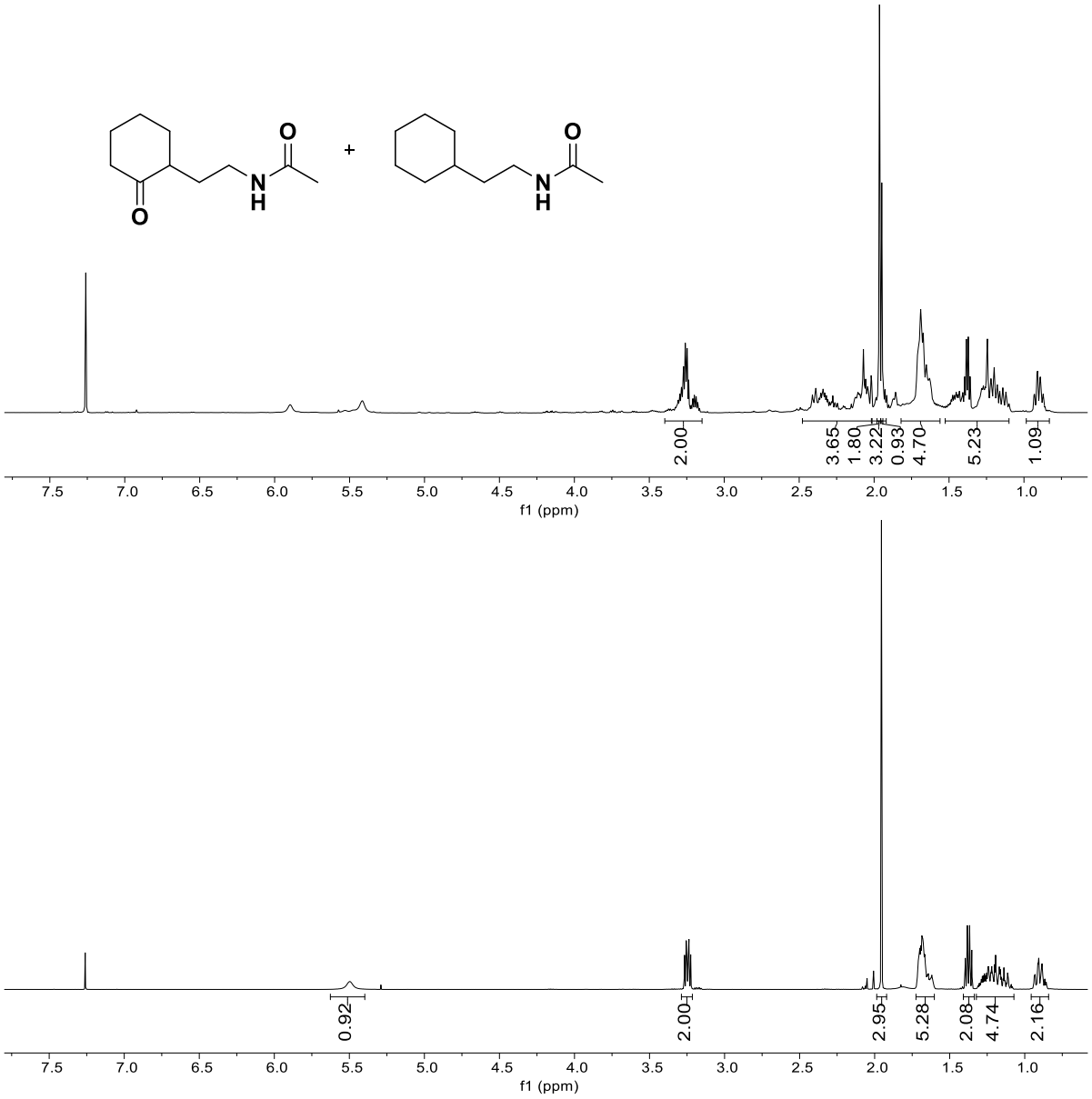

Figure S20: Top: ^{1}H NMR spectra of **S8 / 10**-K4 mixture; Bottom: ^{1}H NMR spectra of **S8**.

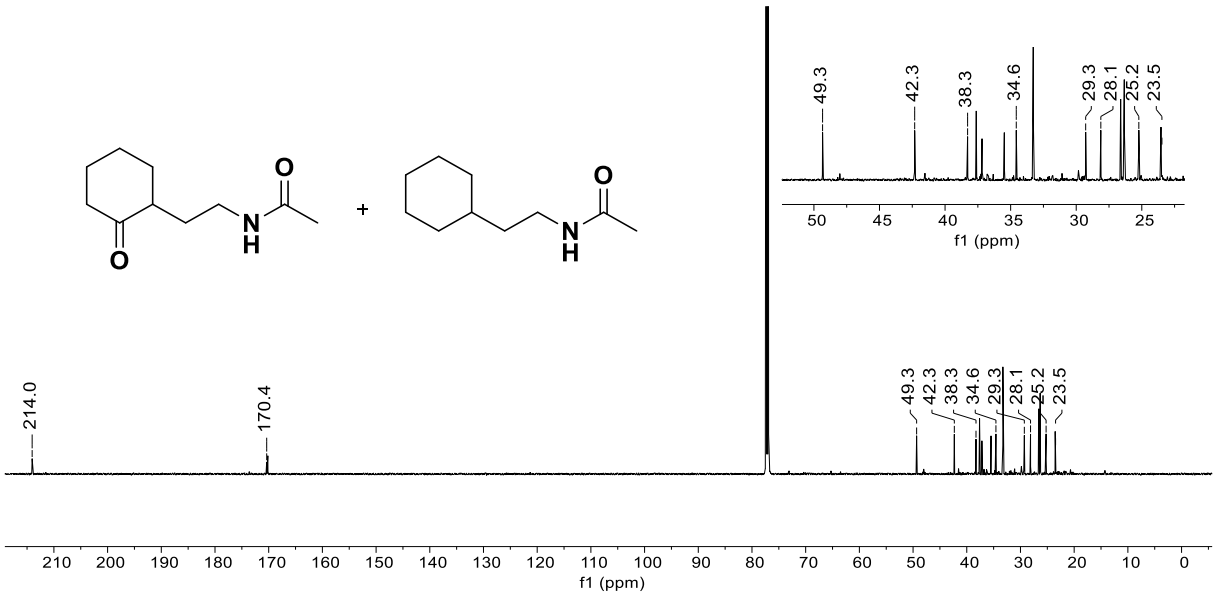

Figure S21: ^{13}C NMR spectra of **S8 / 10**-K4 mixture.

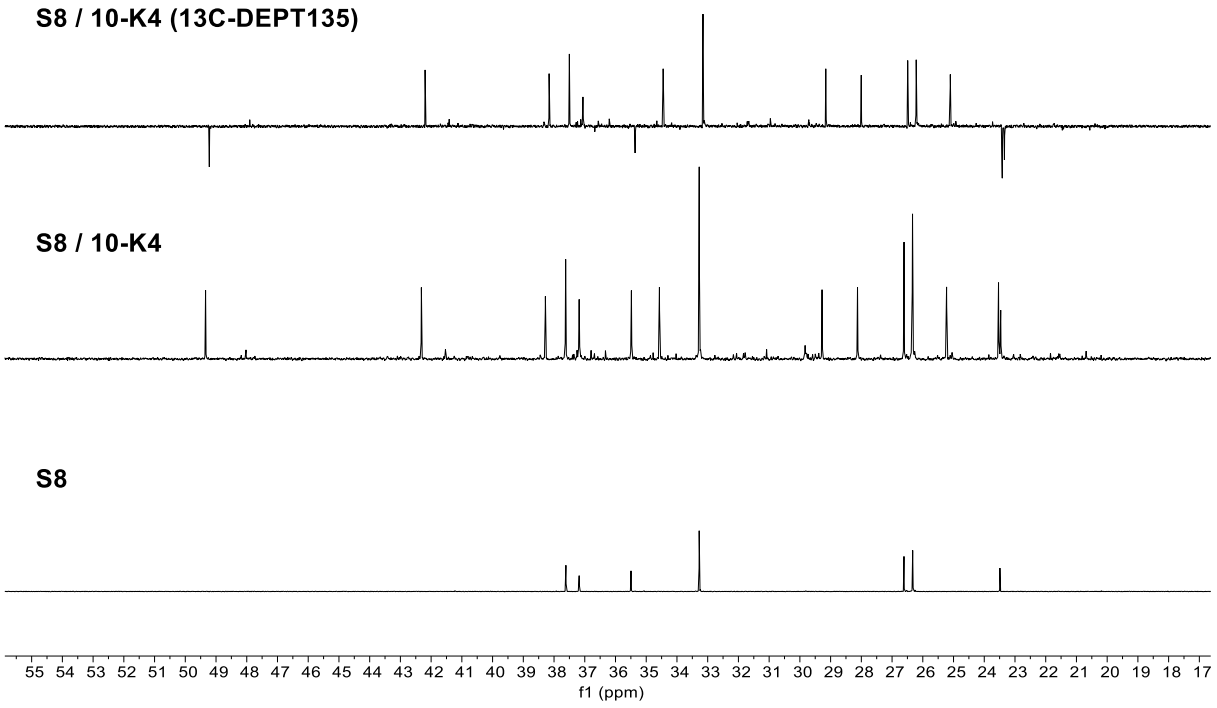

Figure S22: Stacked ^{13}C NMR spectra of **S8 / 10**-K4 mixture and pure **S8**.

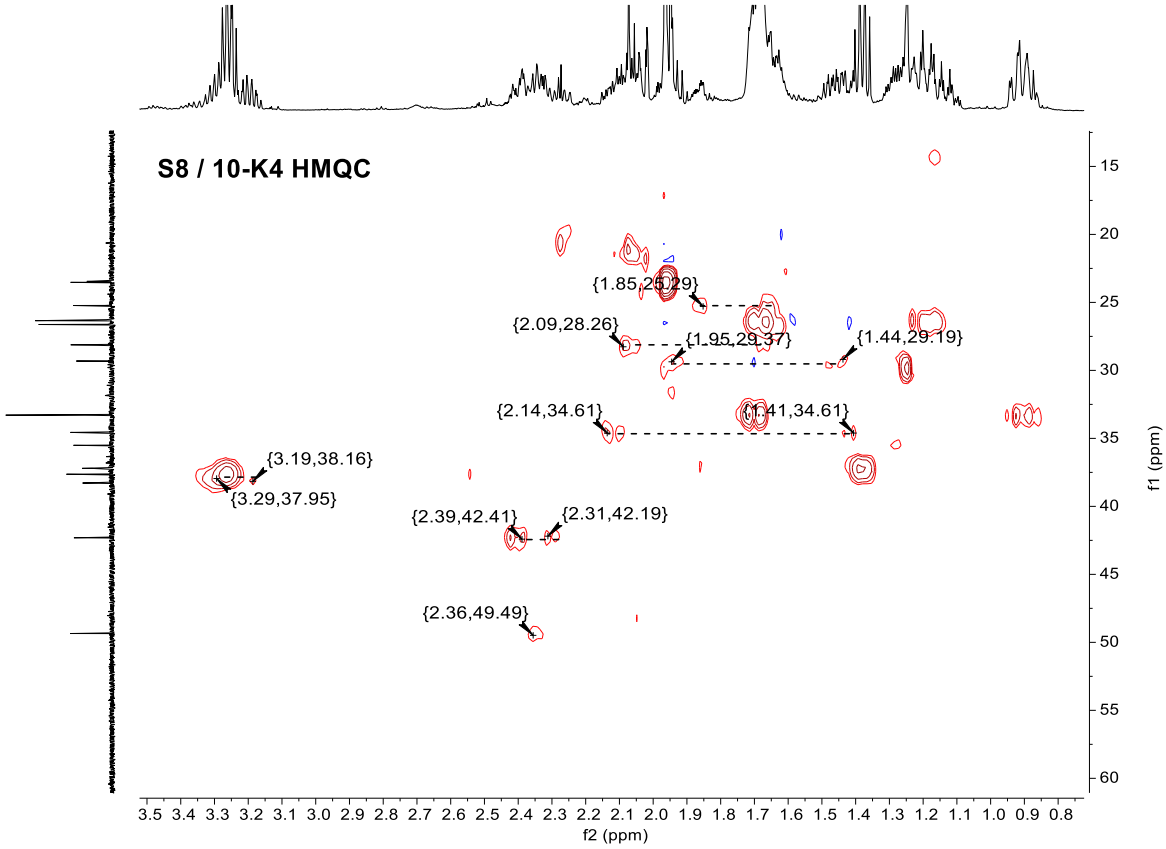

Figure S23: ^{1}H,^{13}C-HMQC spectra of **S8 / 10**-K4.

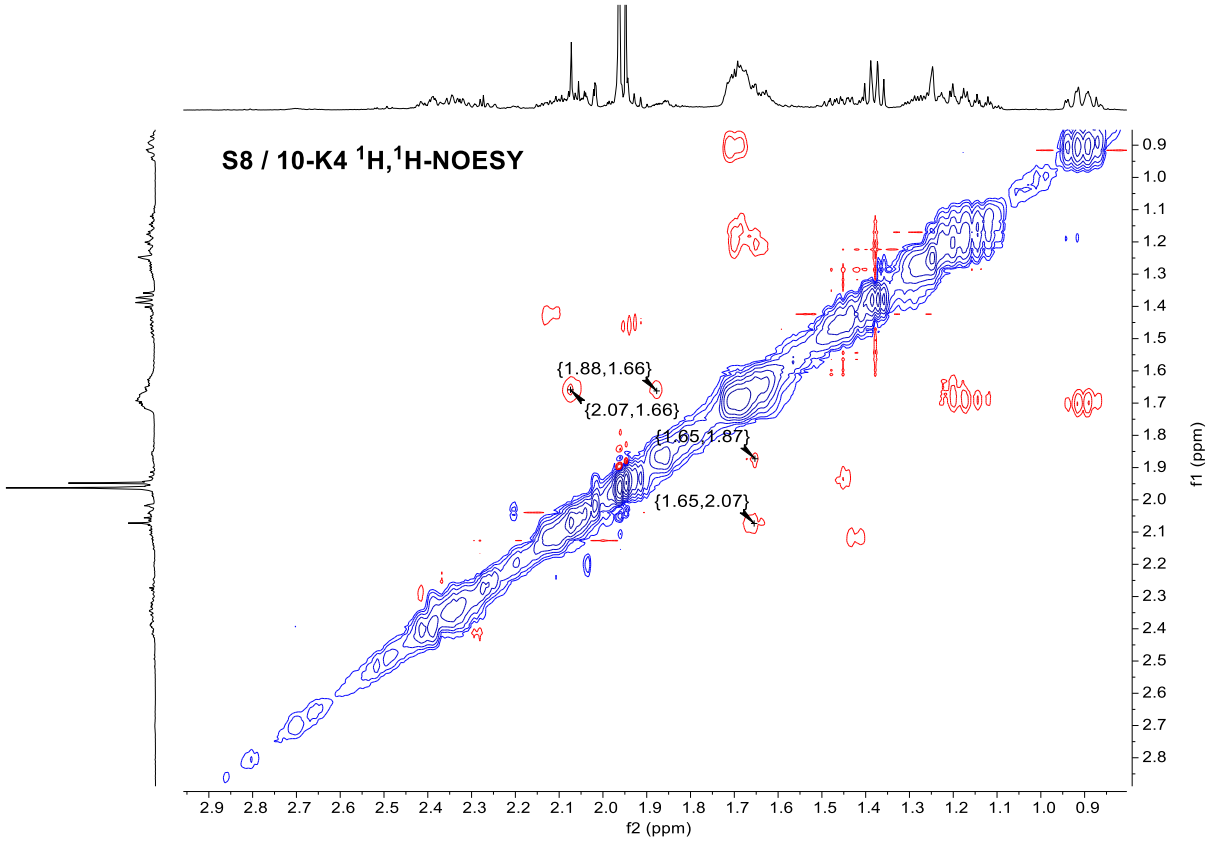

Figure S24: ^{1}H,^{1}H-NOESY spectra of **S8 / 10**-K4 mixture.

10-K5/10-K6 (2:1) mixture

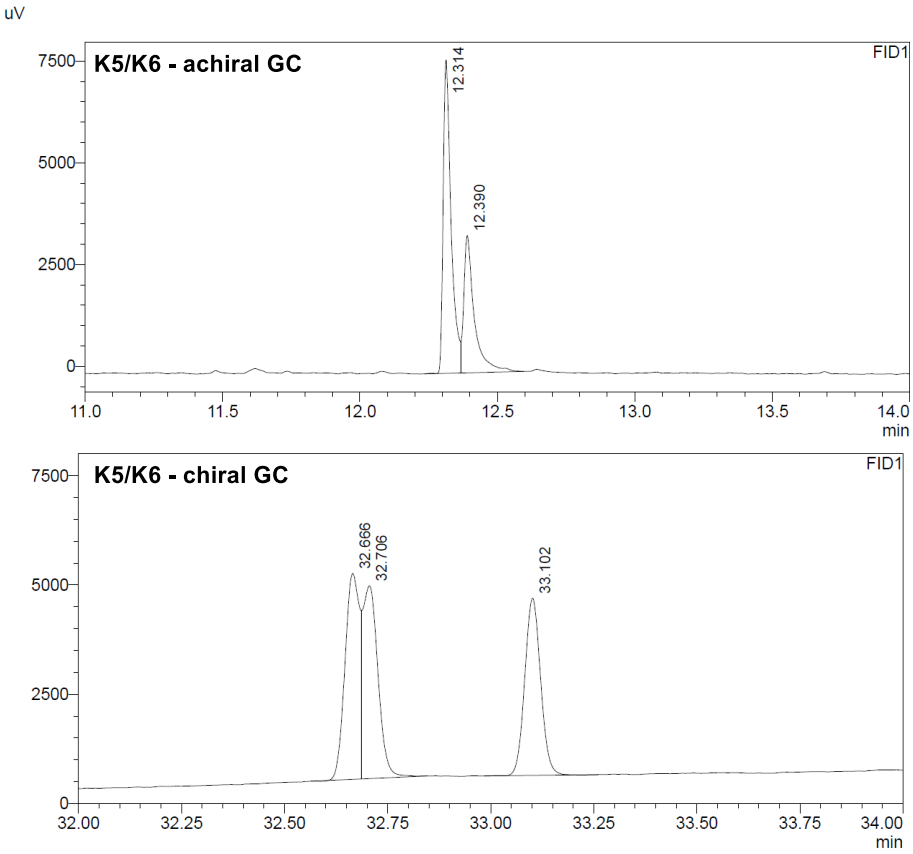

Figure S25: Stacked achiral (top) and chiral (bottom) GC spectra of **10**-K5 / **10**-K6 mixture.

On the chiral GC, the main peak splits into two, providing the first hint that this peak corresponds to the racemic mixture of **10**-K5, whereas the smaller peak represents the achiral **10**-K6 product.

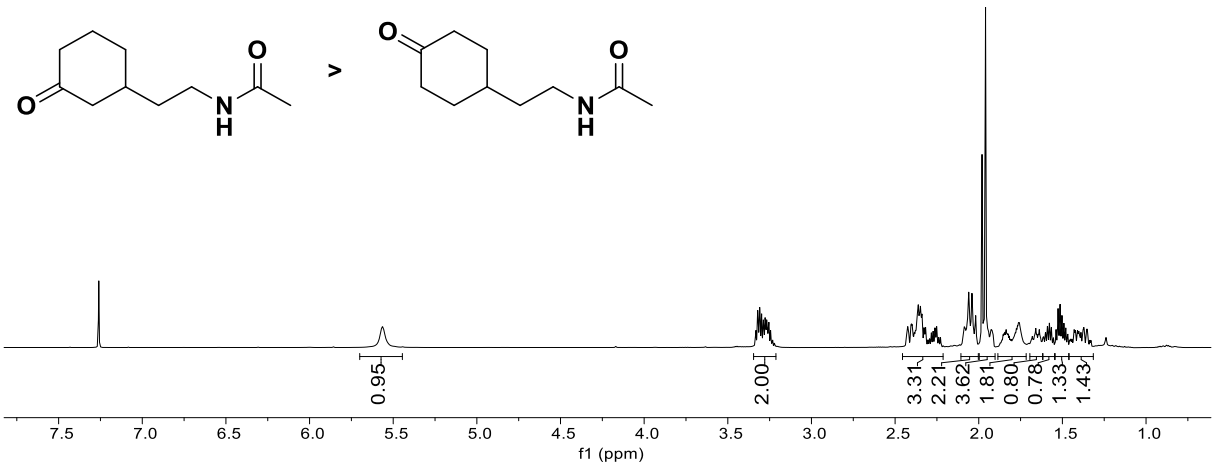

Figure S26: ^{1}H NMR spectra of **10**-K5 / **10**-K6 mixture.

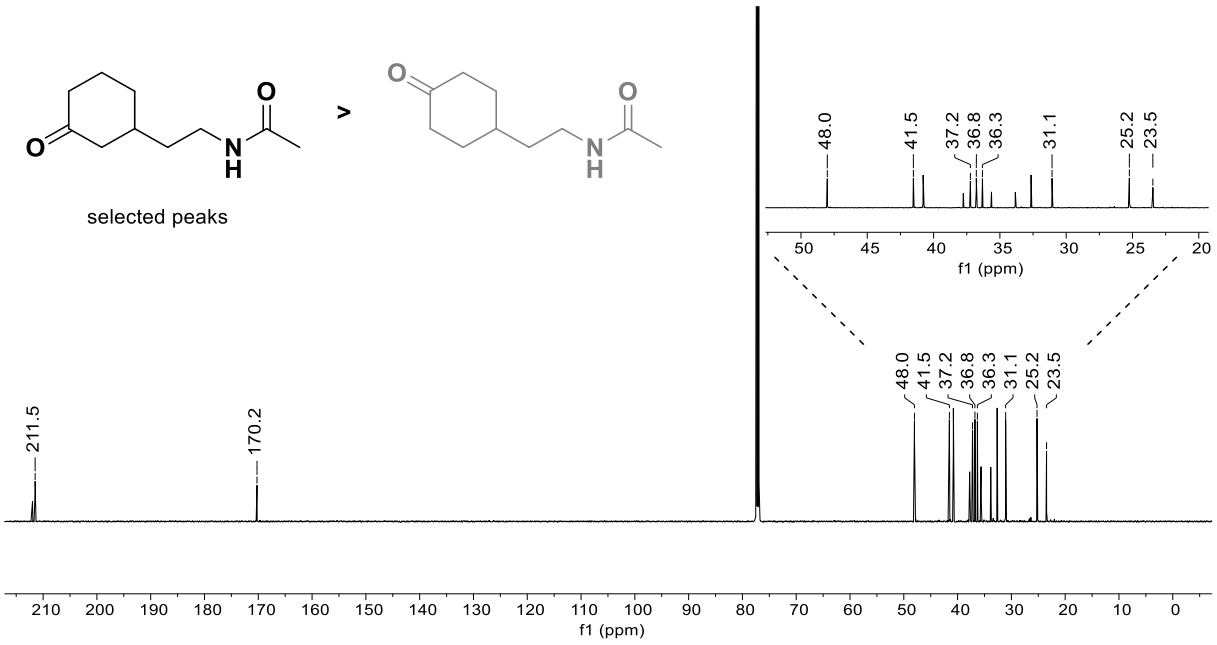

Figure S27: ^{13}C NMR spectra of **10**-K5 / **10**-K6 mixture with the selection of key **10**-K5 signals. Assigned according to signal intensity, DEPT, and 2D NMR spectra.

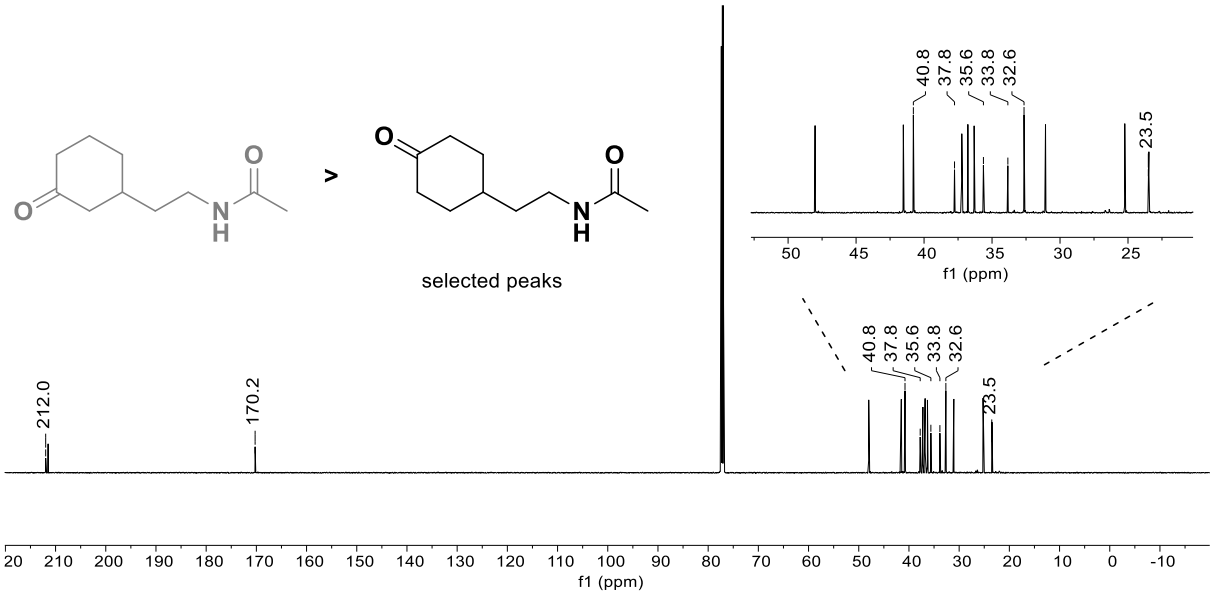

Figure S28: ^{13}C NMR spectra of **10**-K5 / **10**-K6 mixture with the selection of the **10**-K6 signals. Assigned according to signal intensity, DEPT, and 2D NMR spectra.

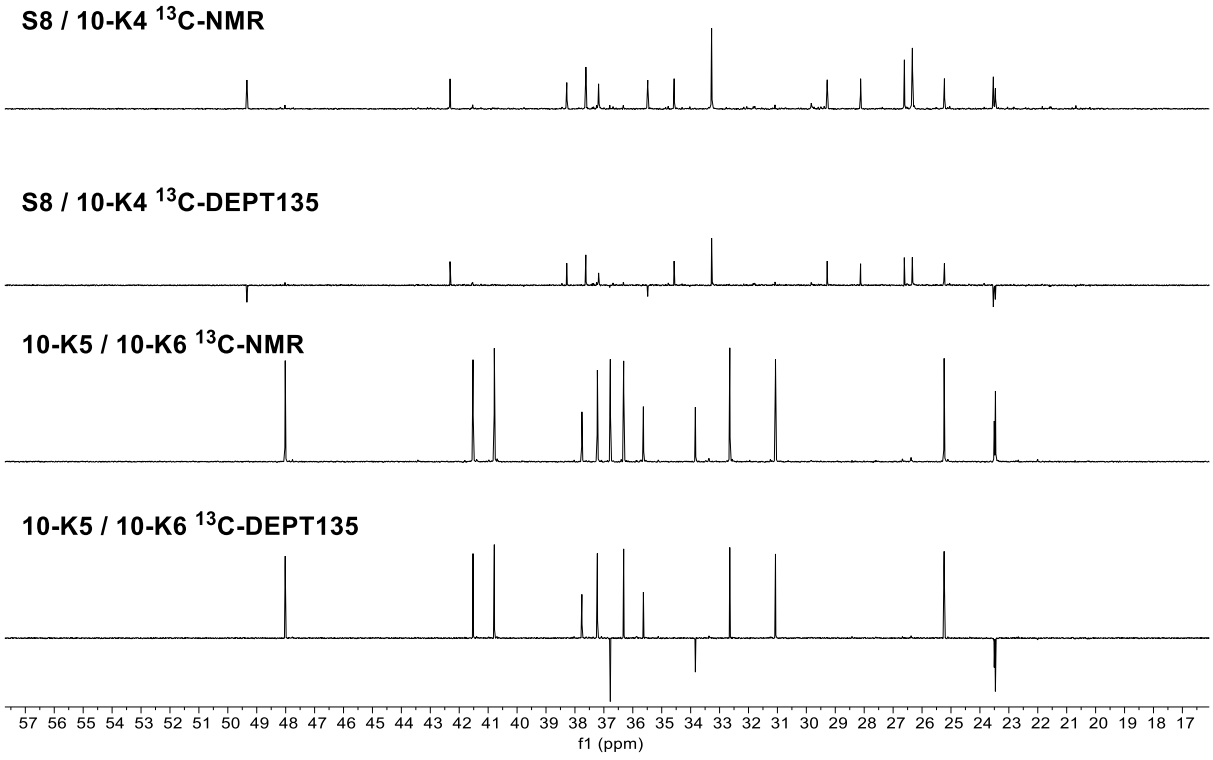

Figure S29: Stacked ^{13}C NMR spectra of **S8 / 10**-K4 mixture and **10**-K5 / **10**-K6 mixture. *Note:* Minor amounts of **10**-K5 product in the **S8 / 10**-K4 mixture are visible.

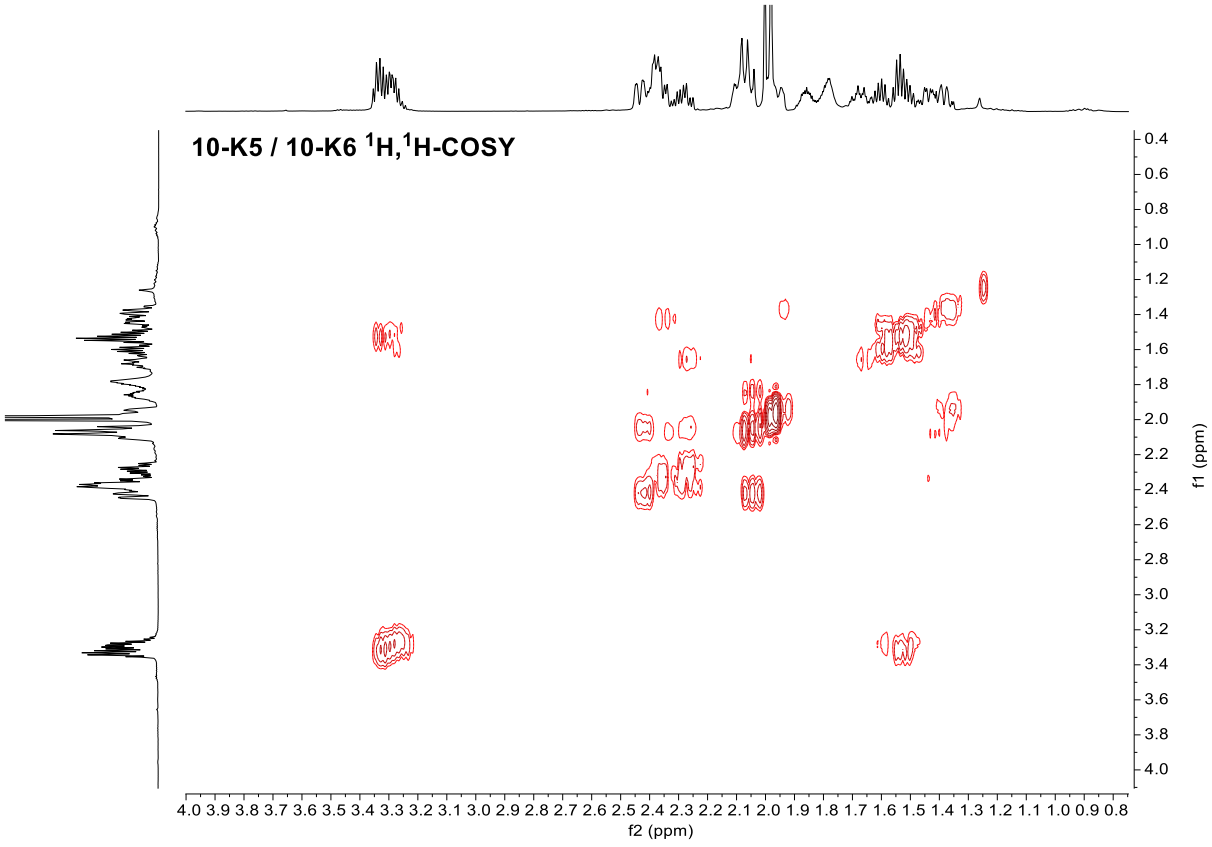

Figure S30: ^{1}H,^{1}H-COSY spectra of **10**-K5 / **10**-K6 mixture.

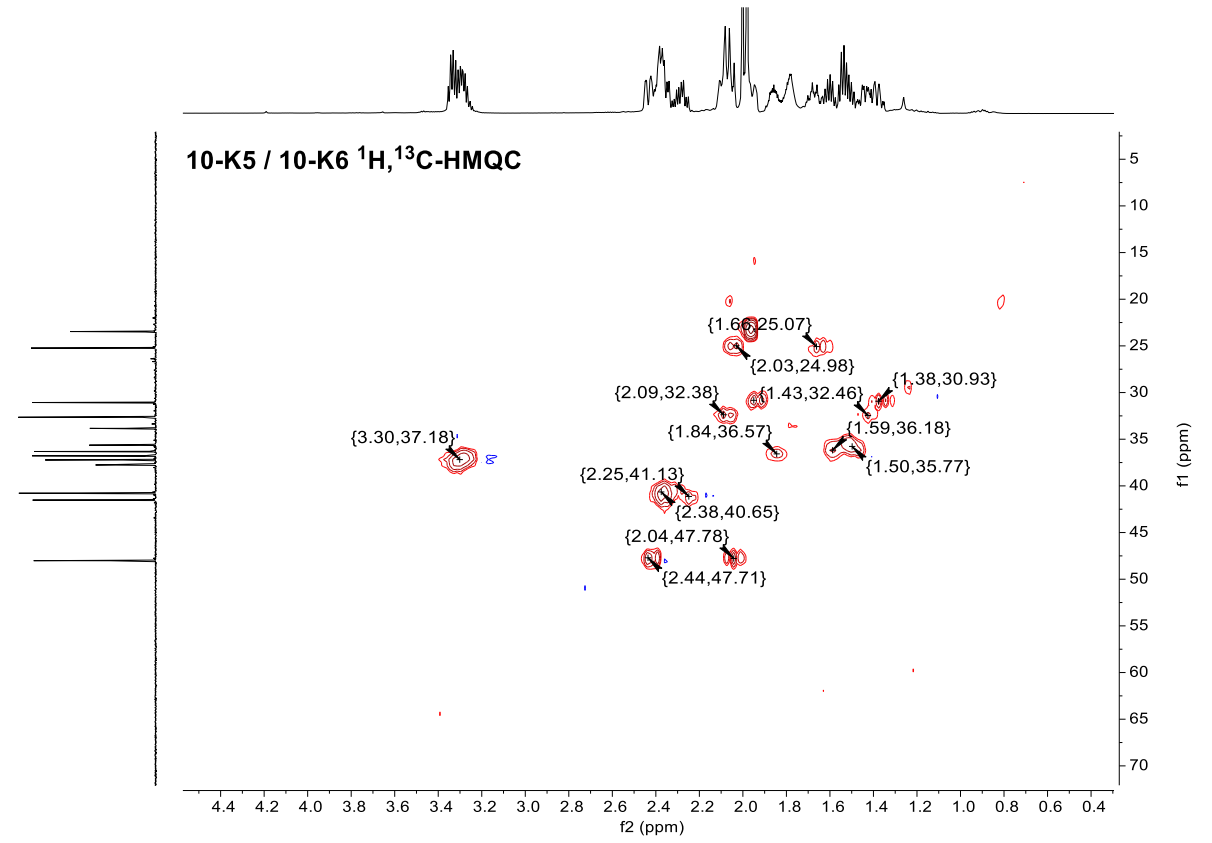

Figure S31: ^{1}H,^{13}C-HMQC spectra of **10**-K5 / **10**-K6 mixture.

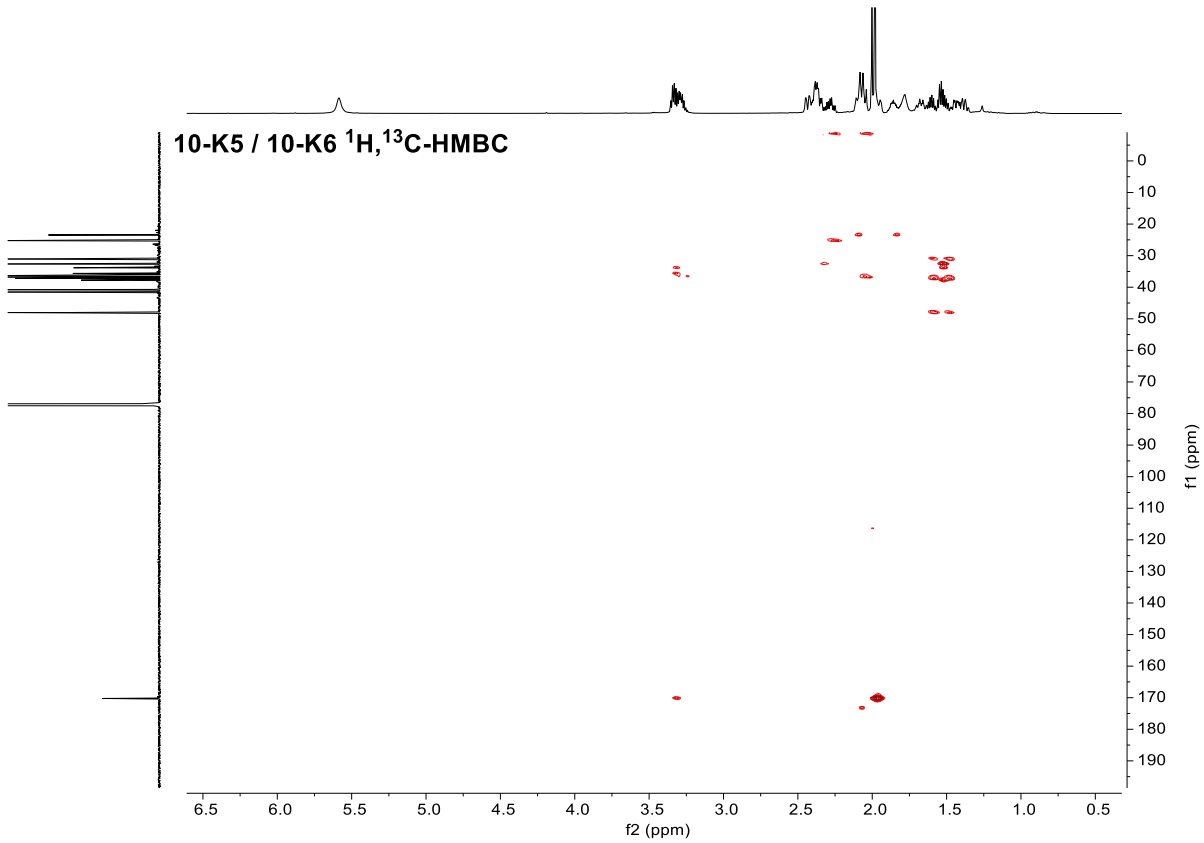

Figure S32: ^{1}H,^{13}C-HMBC spectra of **10**-K5 / **10**-K6 mixture.

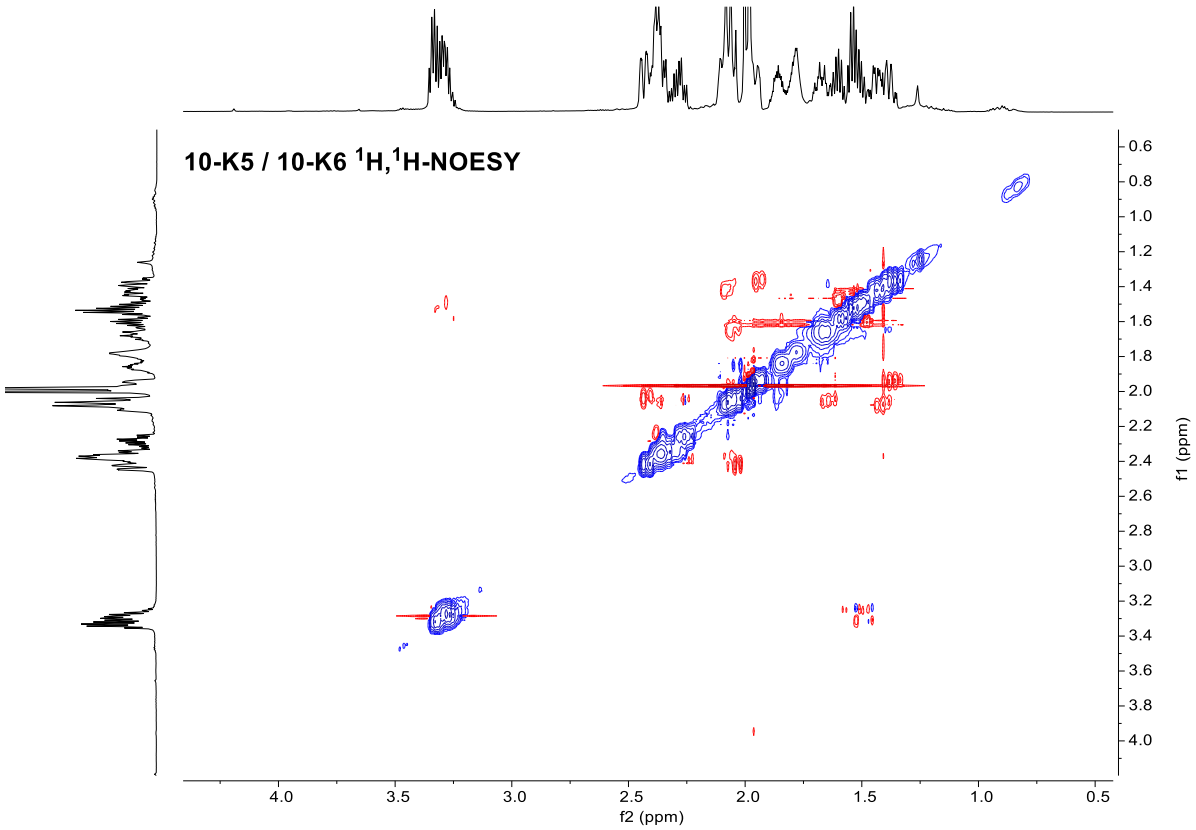

Figure S33: ^{1}H,^{1}H-NOESY spectra of **10**-K5 / **10**-K6 mixture.

10-O3 Product

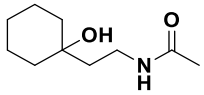

$C_{10}H_{19}NO_2$
MW: 185.27 g/mol

TLC R_f = 0.08 (CH_2Cl_2/MeOH = 95/5) [CAM].

IR (ATR): $\tilde{\nu}$ (cm^{-1}) = 3297 (m), 3092 (w), 2926 (m), 2854 (m), 1712 (w), 1630 (s), 1552 (m), 1446 (m), 1369 (m), 1291 (m), 1262 (m), 1164 (w), 1140 (w), 1115 (w), 1039 (w), 971 (m), 903 (w), 851 (w), 837 (w), 730 (w), 600 (m), 454 (w).

^{1}H NMR ($CDCl_3$, 500 MHz, 300 K) δ [ppm] = 6.30 (br s, 1H), 3.89 – 2.91 (m, 2H), 1.95 (s, 3H), 1.72 – 1.62 (m, 2H), 1.62 – 1.43 (m, 10H).

^{13}C NMR ($CDCl_3$, 151 MHz, 300 K) δ [ppm] = 170.3 (s), 72.2 (s), 37.8 (s), 35.3 (s), 29.9 (s), 25.8 (s), 23.6 (s), 22.3 (s).

HRMS (ESI): $C_{10}H_{19}NO_2$ calculated: $[(M + H)^+]$: 186.1489

found: $[(M + H)^+]$: 186.1486.

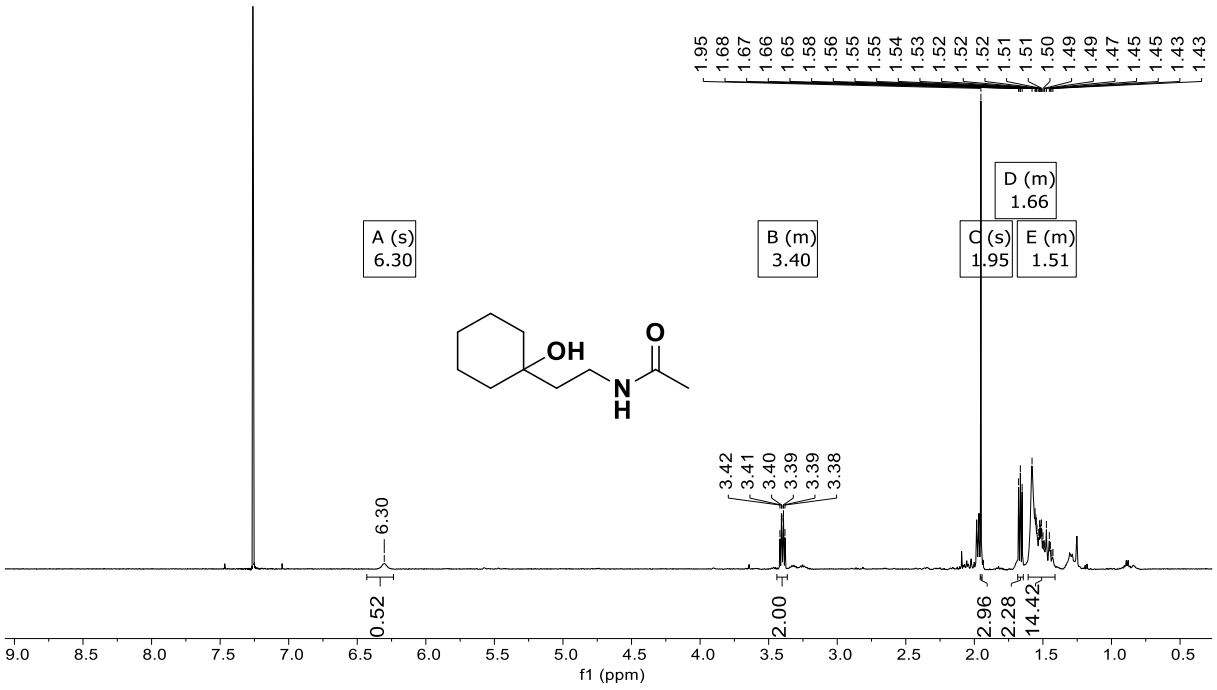

Figure S34: ^{1}H NMR spectra of **10**-O3.

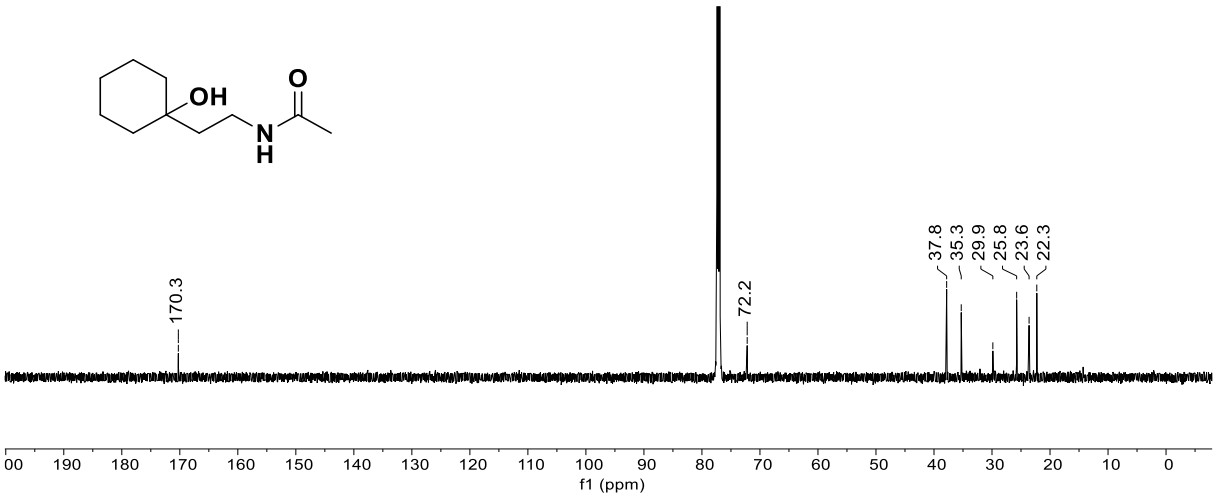

Figure S35: ^{13}C NMR spectra of **10**-O3.

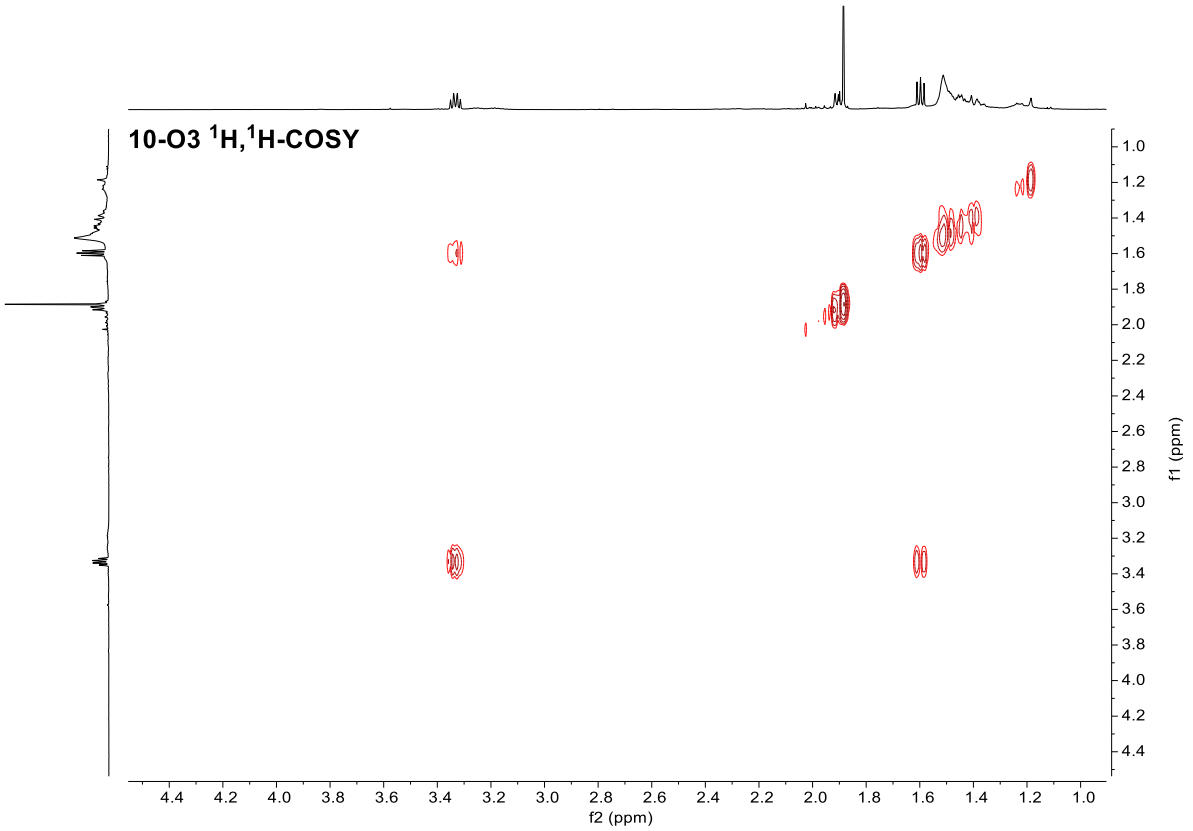

Figure S36: ^{1}H,^{1}H-COSY spectra of **10**-O3.

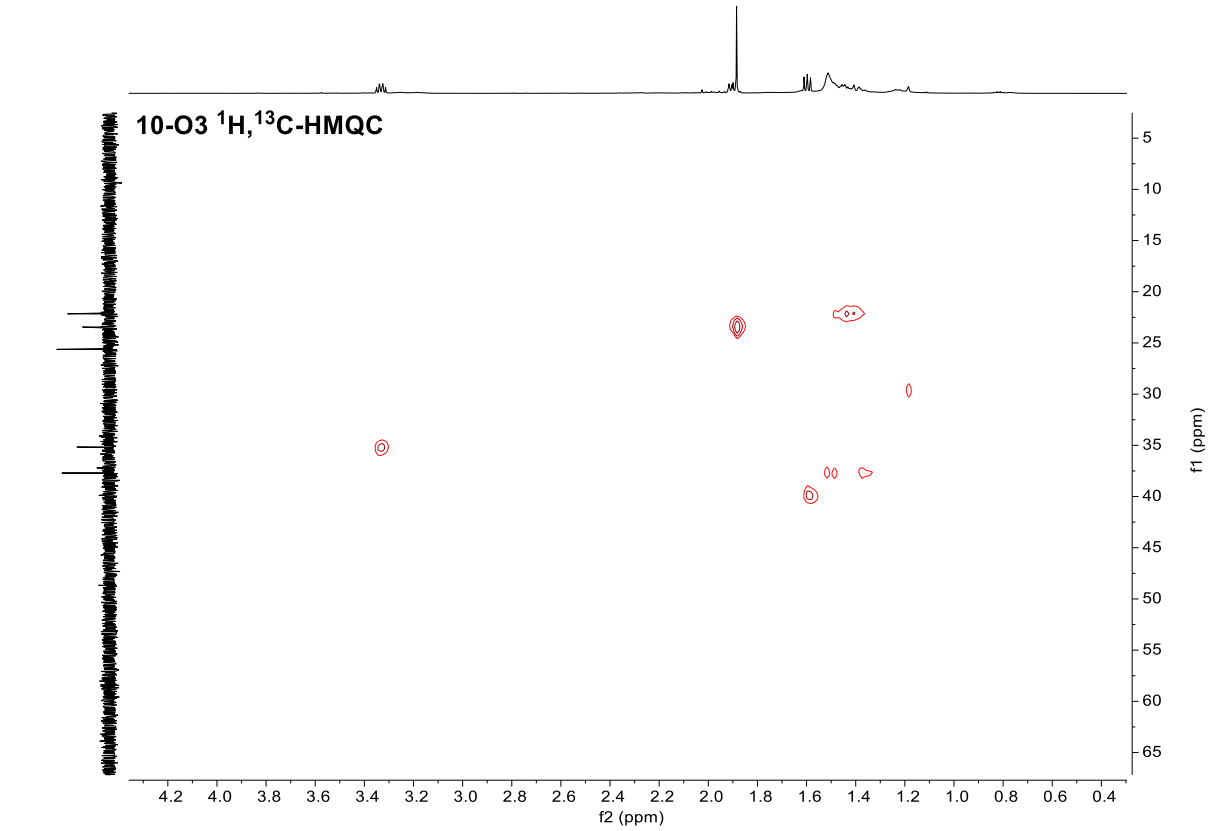

Figure S37: ^{1}H,^{13}C-HMQC spectra of **10**-O3.

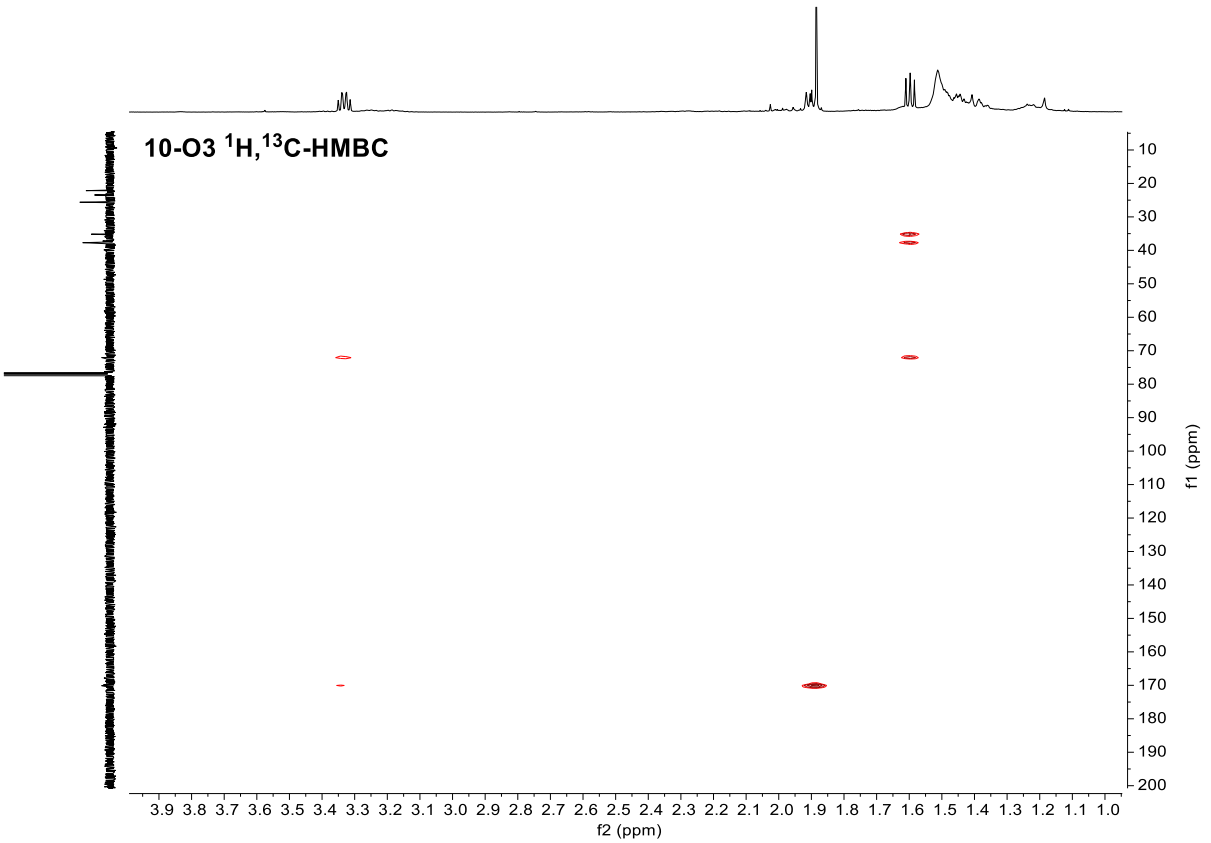

Figure S38: ^{1}H,^{13}C-HMBC spectra of **10**-O3.

3.3.4 Oxidation Products of 2-Cyclohexylpropan -1-ammonium tetrafluoroborate (11)

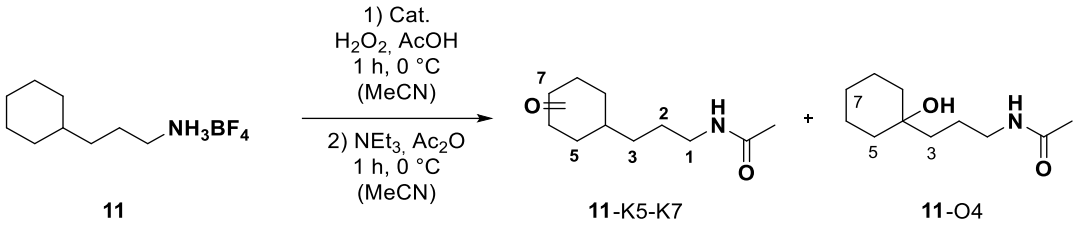

According to the large-scale oxidation procedure with Mn catalysts, 2-cyclohexylpropan-1-ammonium tetrafluoroborate (**11**, 84.4 mg, 370 µmol, 1.0 equiv.) was oxidized with **Mn(mcp)**. After the aqueous workup, the crude mixture was purified *via* MPLC (RediSep® Column: Silica, 12 g, 30 mL/min; CH_2Cl_2: CH_2Cl_2/MeOH (9/1) 100:0 to 0:100, 23.0 CV, 13.6 min), however, **11**-K5 could only be obtained as a mixture with acetylated starting material, and **11**-K6 and **11**-K7 as a mixture.

11-K5: **TLC** R_f = 0.25 (CH_2Cl_2/MeOH = 95/5 [CAM].

11-K6/7: **TLC** R_f = 0.23 (CH_2Cl_2/MeOH = 95/5 [CAM].

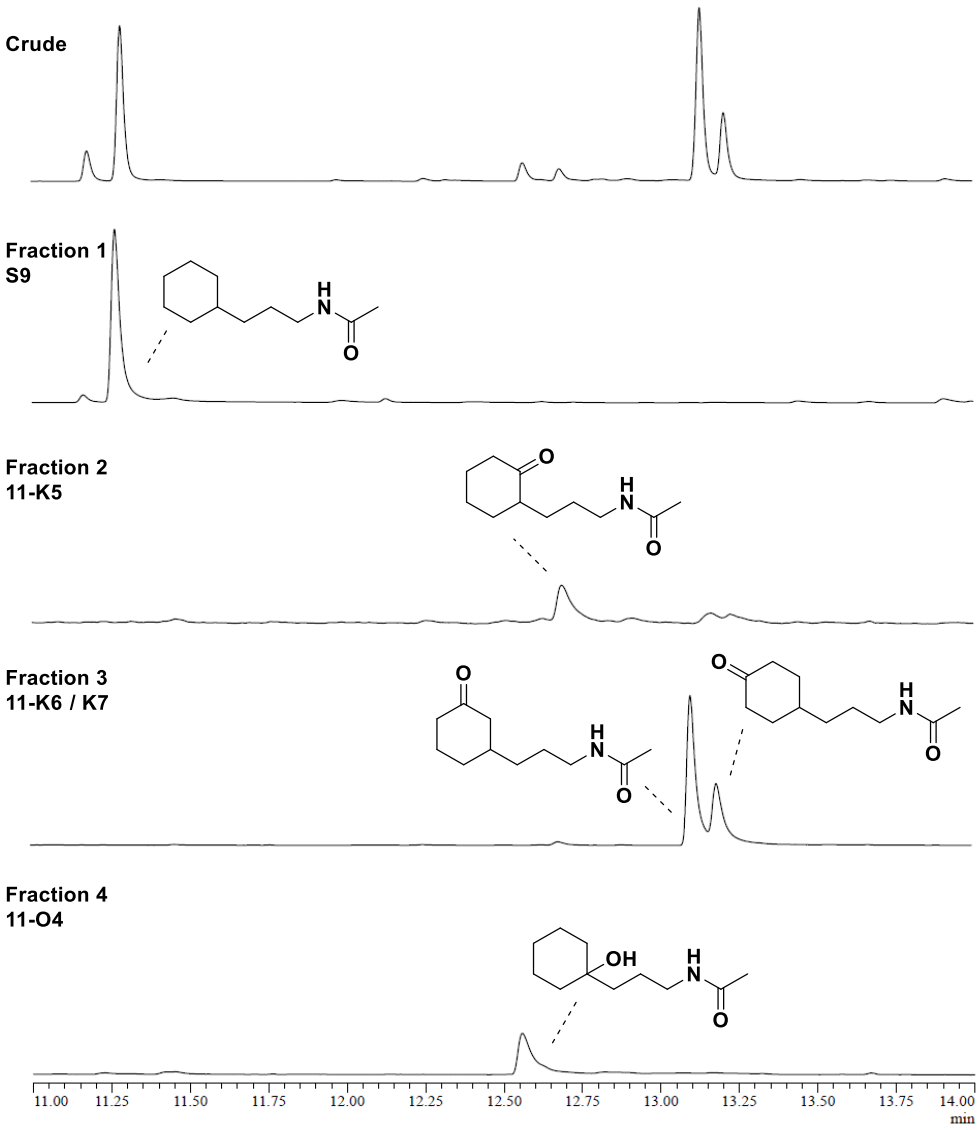

Figure S39: Stacked GC spectra of crude and isolated fractions of the oxidation of **11**.

Stacked GC spectra of crude and isolated fractions of the oxidation of **11**. The products were assigned via analysis of the corresponding NMR spectra (see SI, Figure S40-S58).

11-K5 mixture (minor amounts of 11-K6/K7)

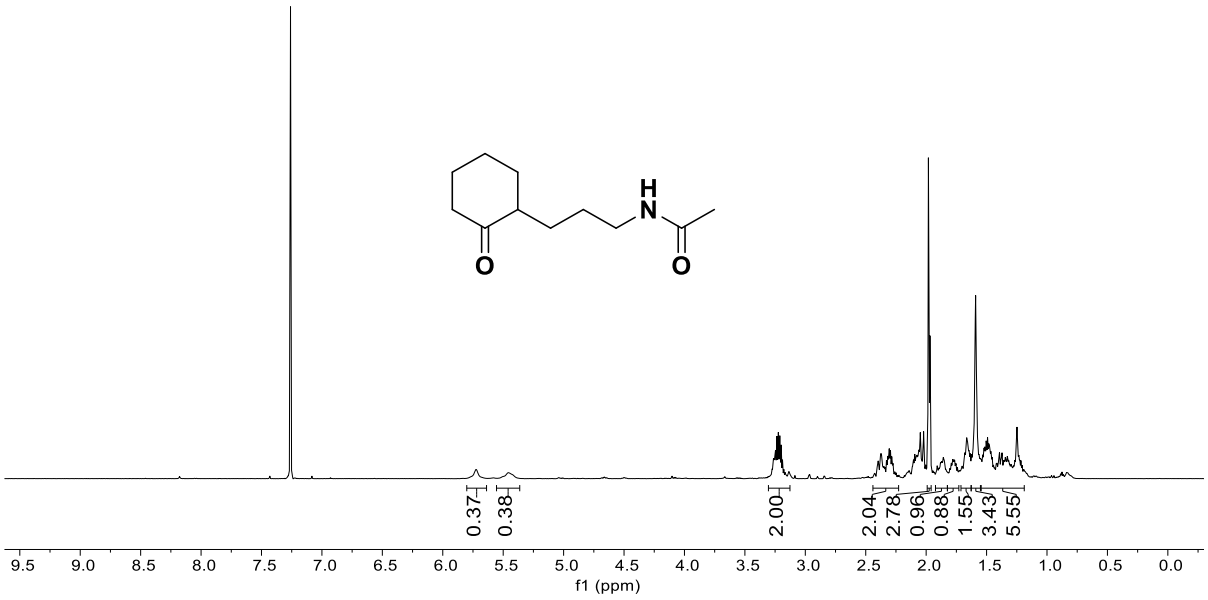

Figure S40: ^{1}H NMR spectra of **11**-K5 (+**11**-K6/K7) mixture.

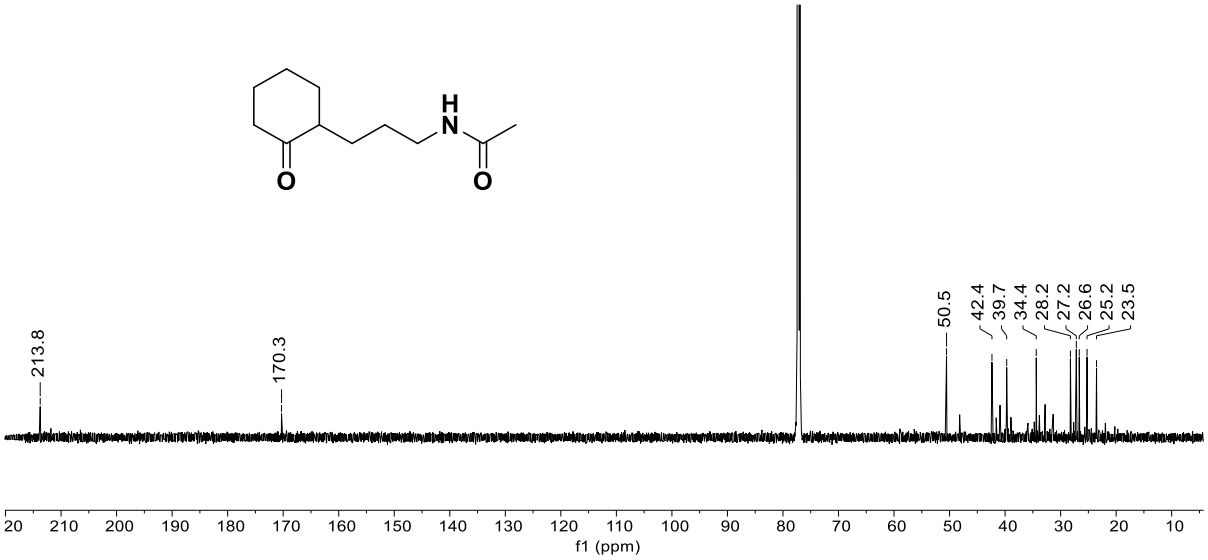

Figure S41: ^{13}C NMR spectra of **11**-K5 (+**11**-K6/K7) mixture.

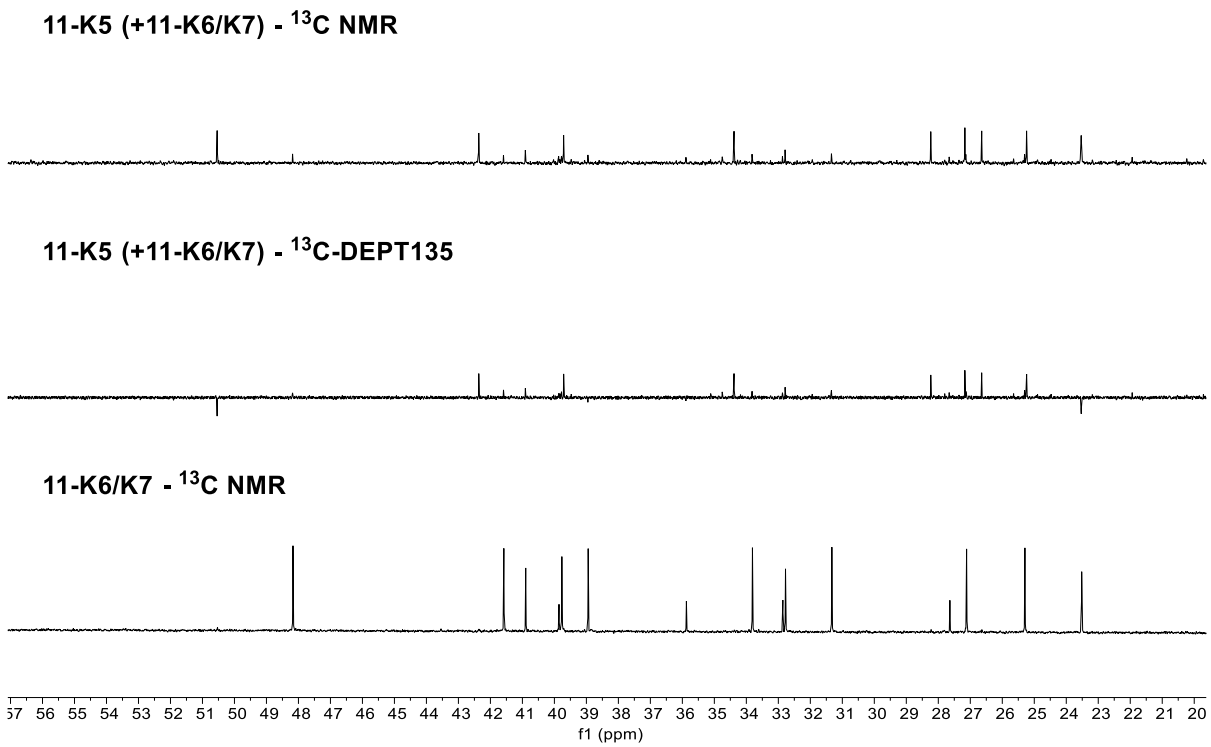

Figure S42: Stacked ^{13}C spectra of **11**-K5 and **11**-K6 / **11**-K7 mixture.

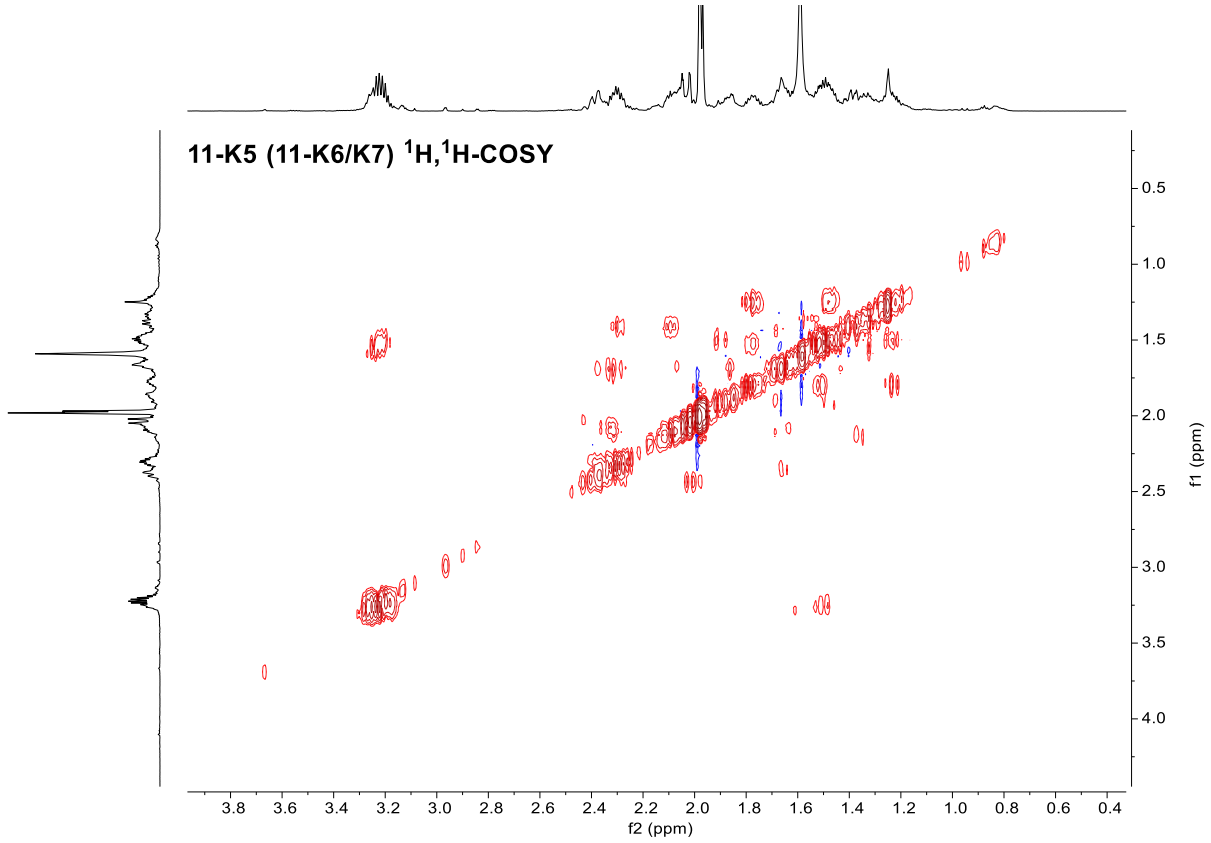

Figure S43: ^{1}H,^{1}H-COSY spectra of **11**-K5 (+**11**-K6/K7) mixture.

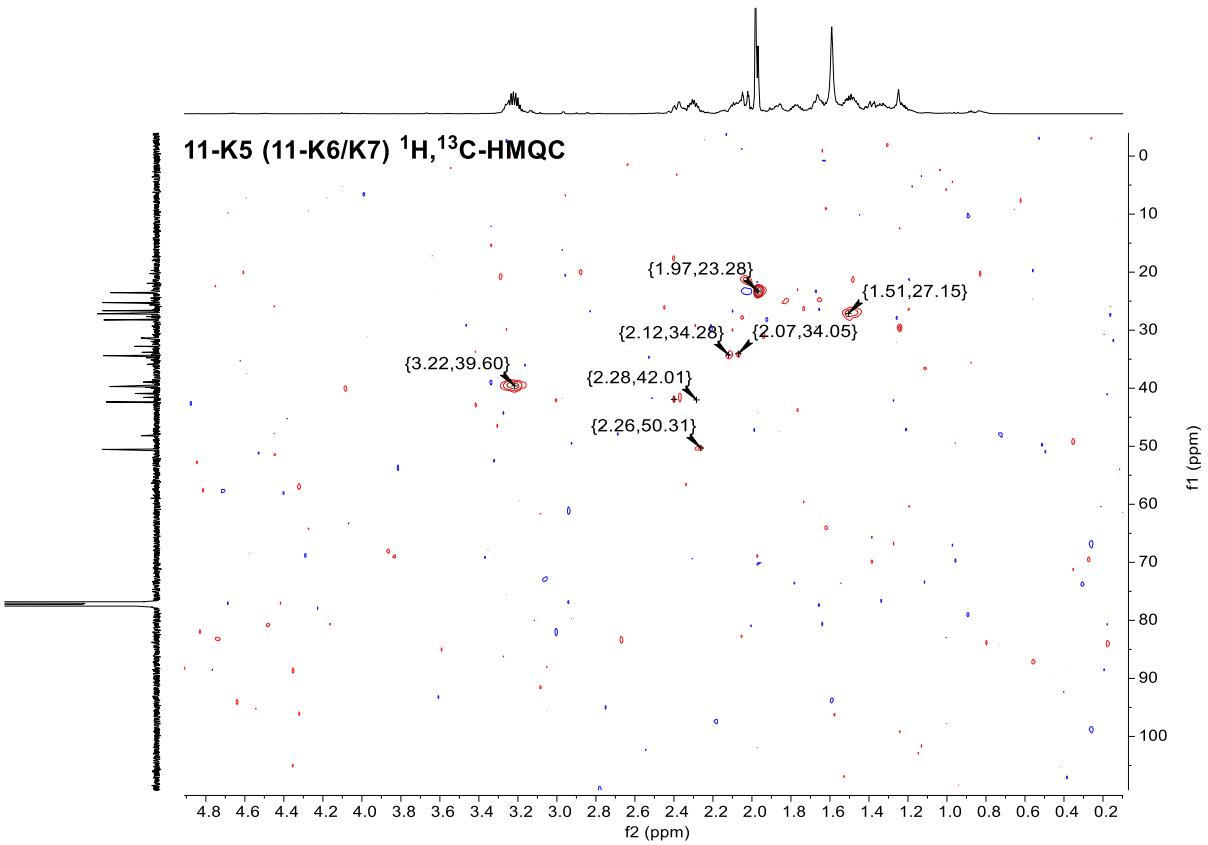

Figure S44: ^{1}H,^{13}C-HMQC spectra of **11**-K5 (+**11**-K6/K7) mixture.

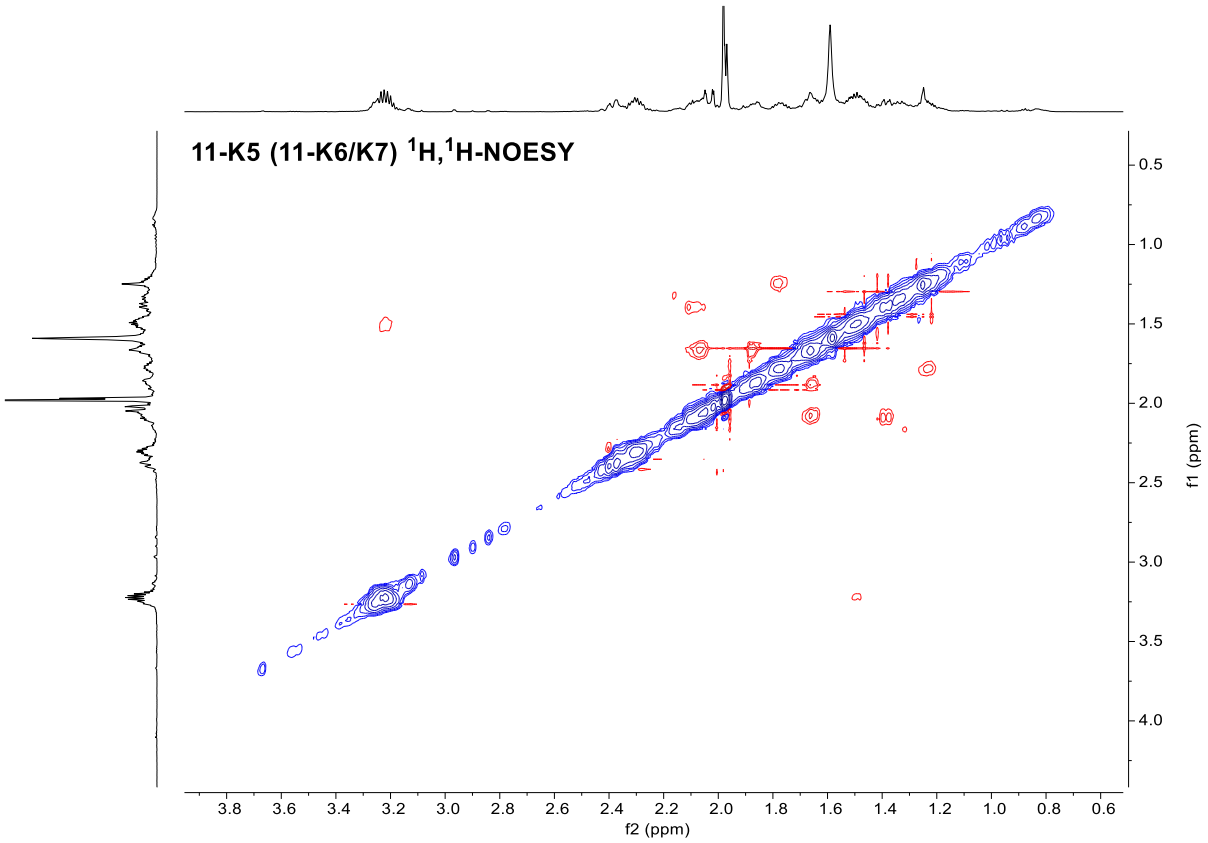

Figure S45: ^{1}H,^{1}H-NOESY spectra of **11**-K5 (+**11**-K6/K7) mixture.

11-K6/K7 (3:1) mixture

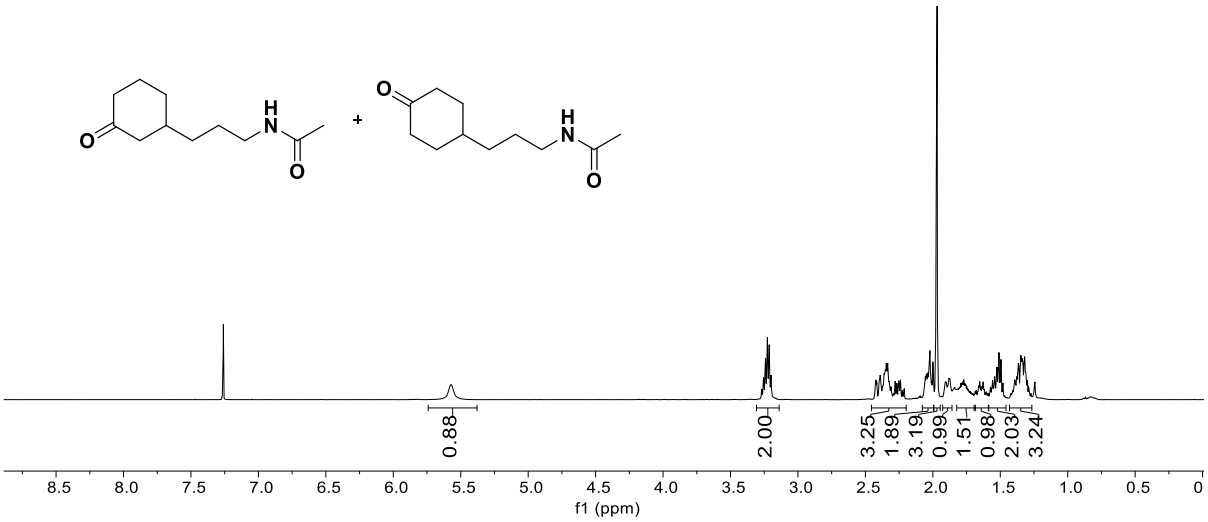

Figure S46: [1]H NMR spectra of **11**-K6 / **11**-K7 mixture.

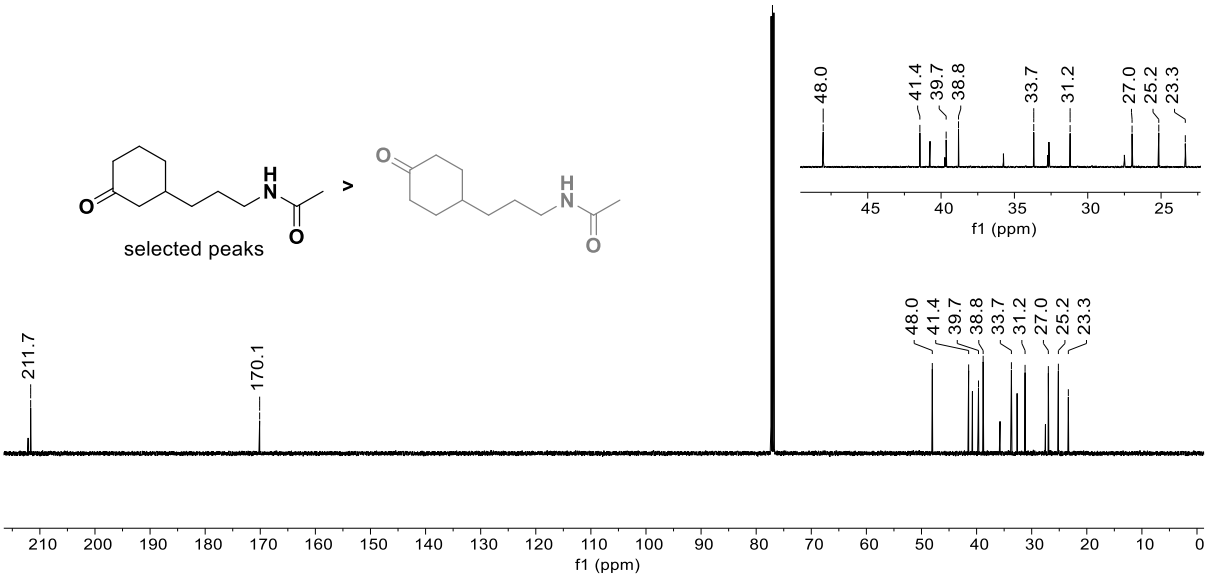

Figure S47: [13]C NMR spectra of **11**-K6 / **11**-K7 mixture with the selection of the **11**-K6 signals. Assigned according to signal intensity, DEPT, and 2D NMR spectra.

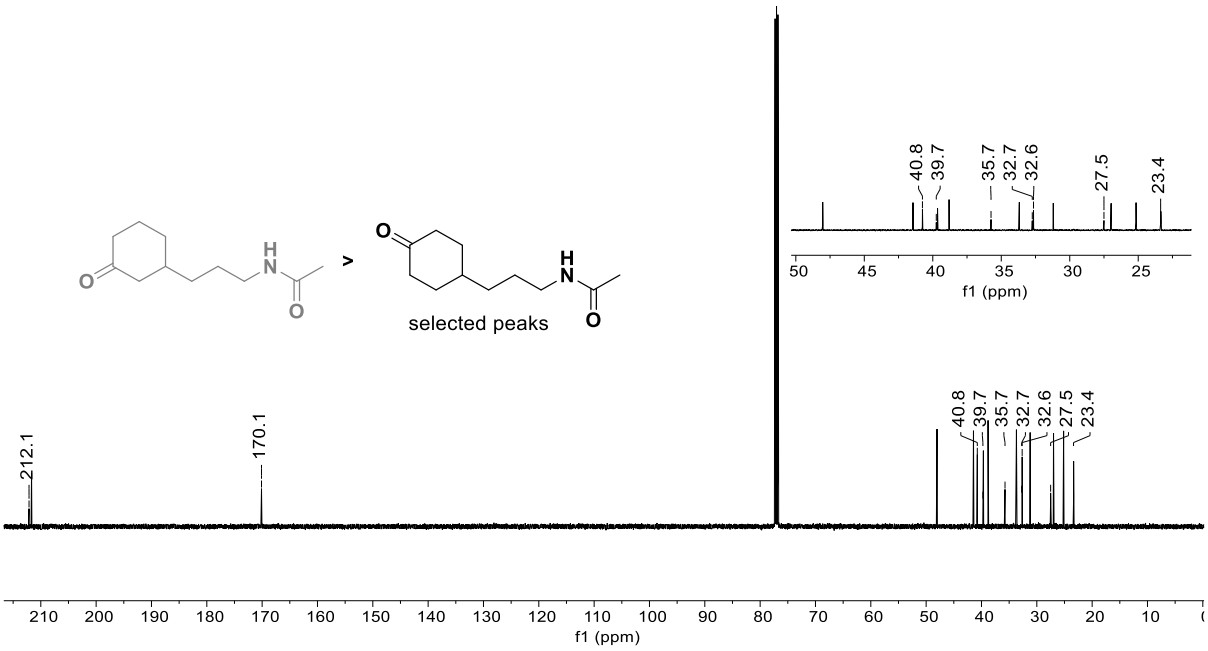

Figure S48: ^{13}C NMR spectra of **11**-K6 / **11**-K7 mixture with the selection of the **11**-K7 signals. Assigned according to signal intensity, DEPT, and 2D NMR spectra.

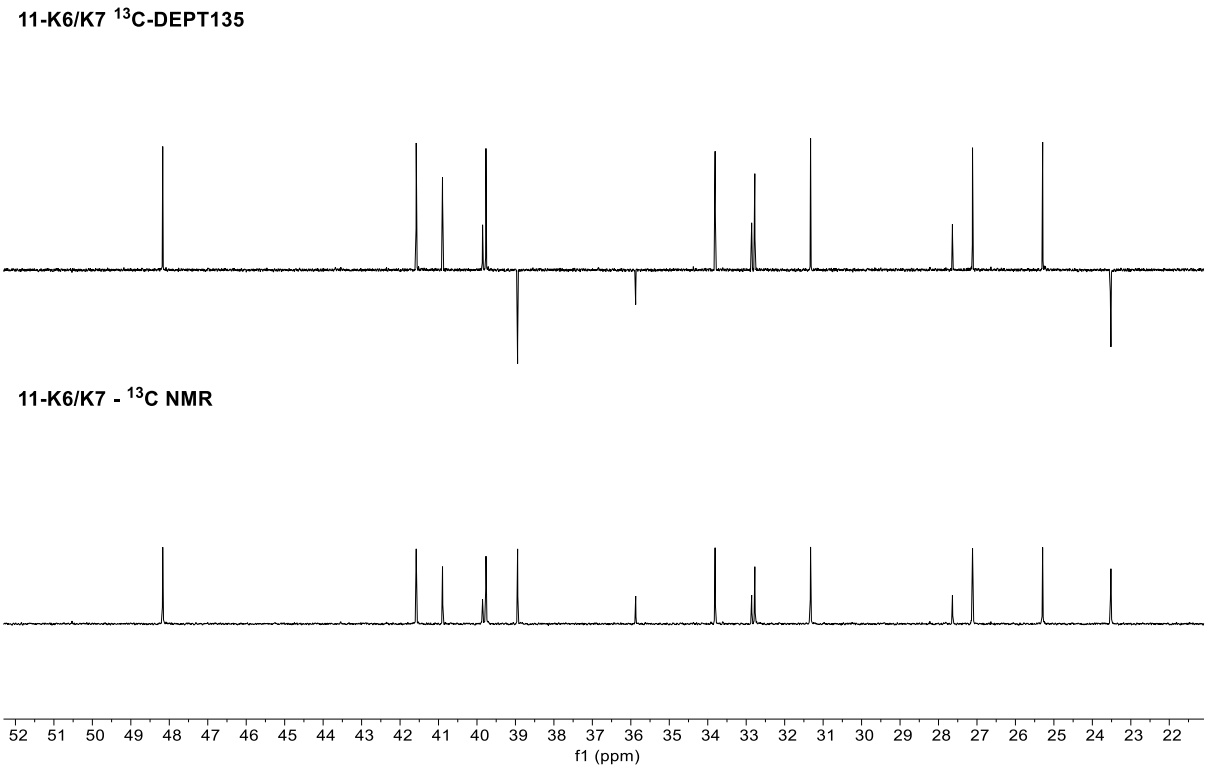

Figure S49: Stacked ^{13}C NMR and ^{13}C-DEPT135 spectra of **11**-K6 / **11**-K7 mixture.

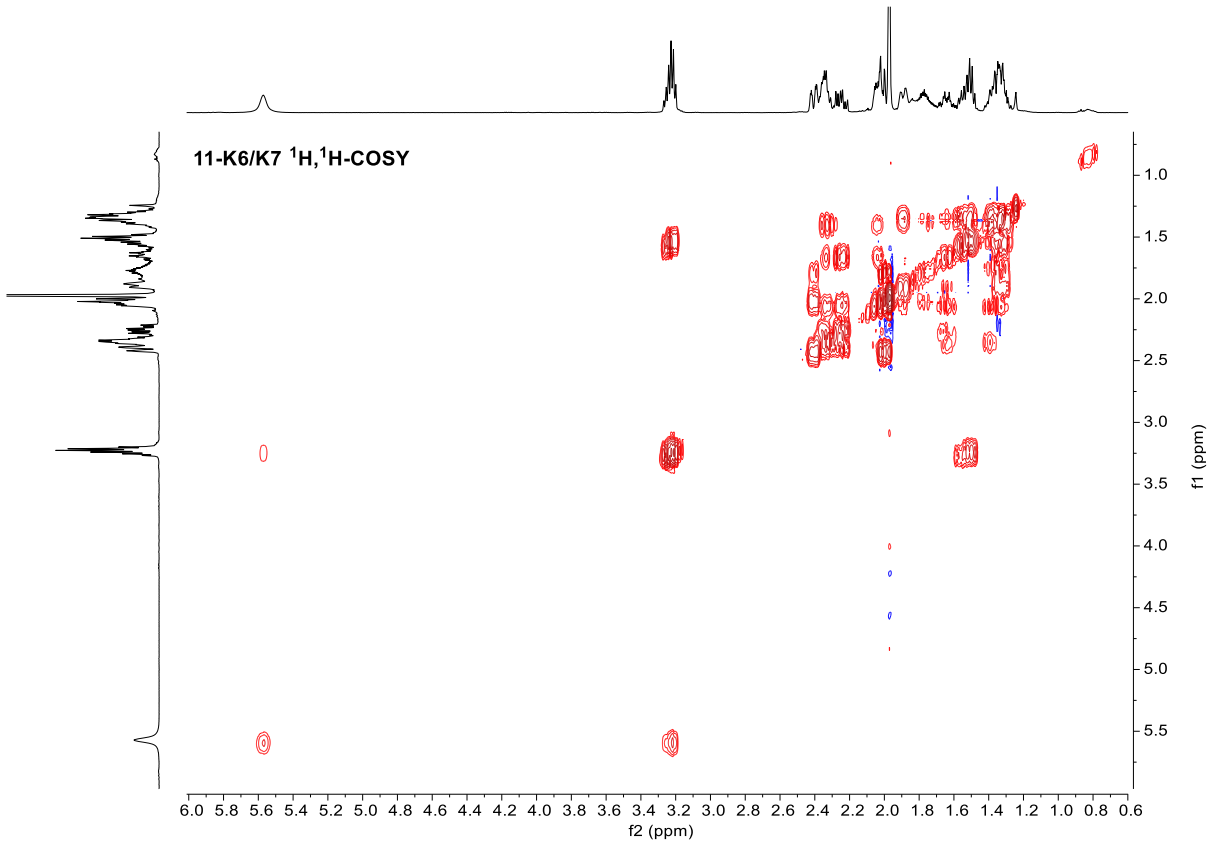

Figure S50: ^{1}H,^{1}H-COSY spectra of **11**-K6 / **11**-K7.

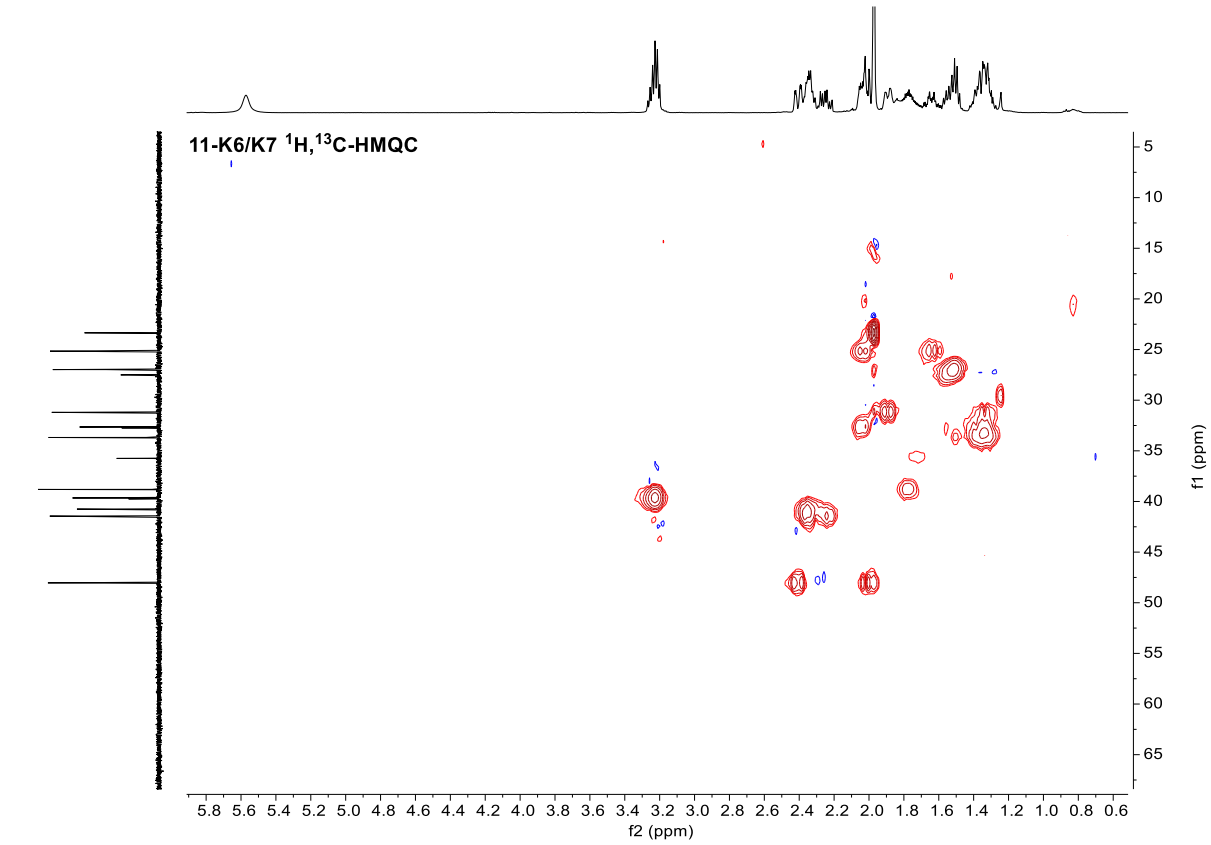

Figure S51: ^{1}H,^{13}C-HMQC spectra of **11**-K6 / **11**-K7.

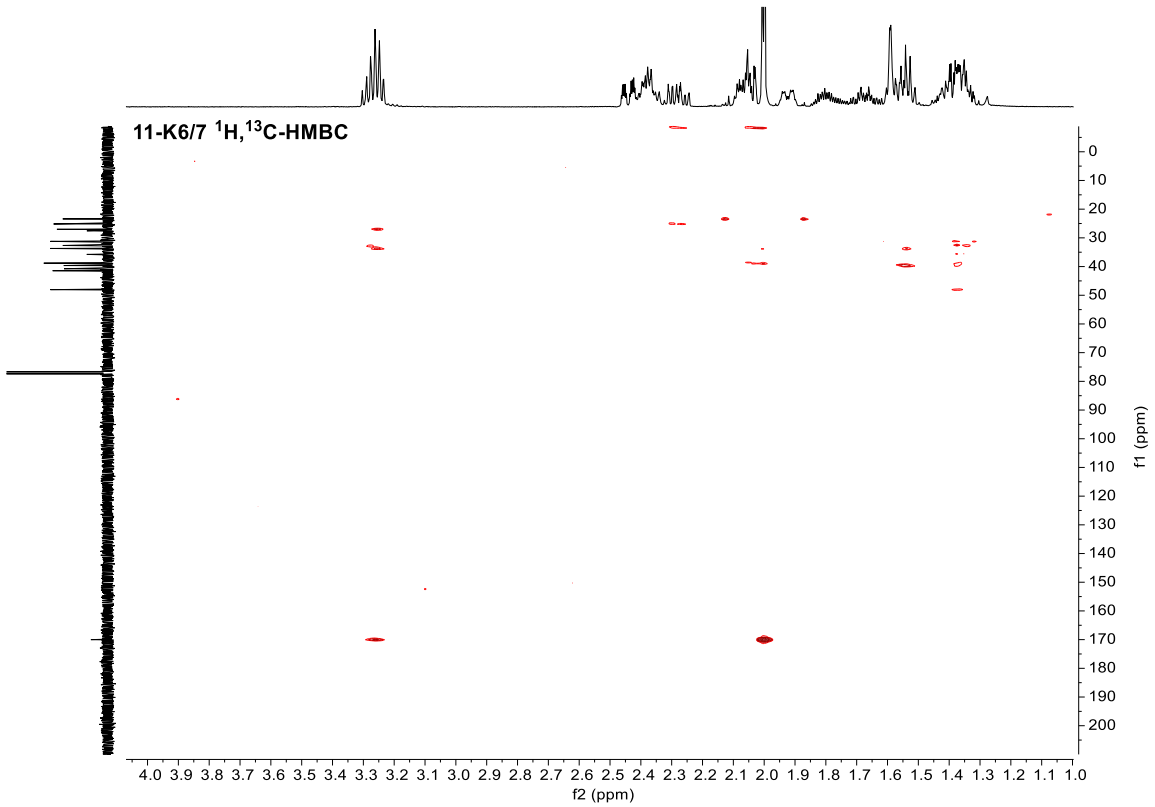

Figure S52: ^{1}H,^{13}C-HMBC spectra of **11**-K6 / **11**-K7.

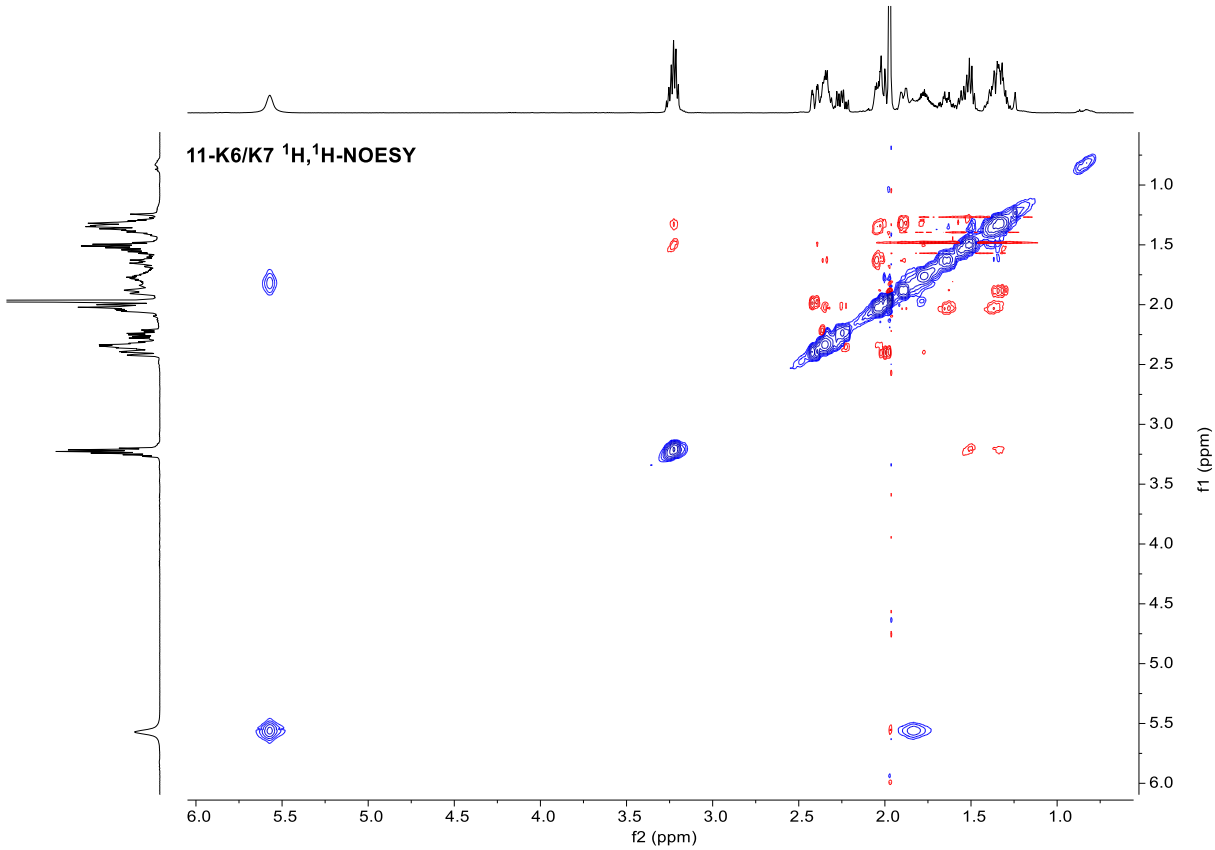

Figure S53: ^{1}H,^{1}H-NOESY spectra of **11**-K6 / **11**-K7.

11-O4 Product

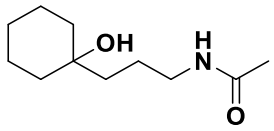

$C_{11}H_{21}NO_2$
MW: 199.29 g/mol

TLC R_f = 0.11 (CH_2Cl_2/MeOH = 95/5) [CAM].

IR (ATR): $\tilde{\nu}$ (cm^{-1}) = 3294 (m), 3087 (w), 2929 (m), 2858 (m), 1707 (m), 1649 (s), 1550 (m), 1447 (m), 1369 (m), 1289 (m), 1239 (m), 1187 (w), 1125 (w), 1033 (w), 811 (w), 717 (w), 602 (w), 523 (w), 430 (w), 412 (w).

^{1}H NMR ($CDCl_3$, 500 MHz, 300 K) δ [ppm] = 5.65 (br s, 1H), 3.26 (td, *J* = 7.0, 5.8 Hz, 2H), 19.7 (s, 3H), 1.69 – 1.34 (s, 14H),

^{13}C NMR ($CDCl_3$, 151 MHz, 300 K) δ [ppm] = 170.3 (s), 71.4 (s), 40.2 (s), 39.2 (s), 37.7 (s), 25.9 (s), 23.5 (s), 23.4 (s), 22.4 (s).

HRMS (ESI): $C_{11}H_{21}NO_2$ calculated: [(M + H)$^+$]: 200.1645

found: [(M + H)$^+$]: 200.1643.

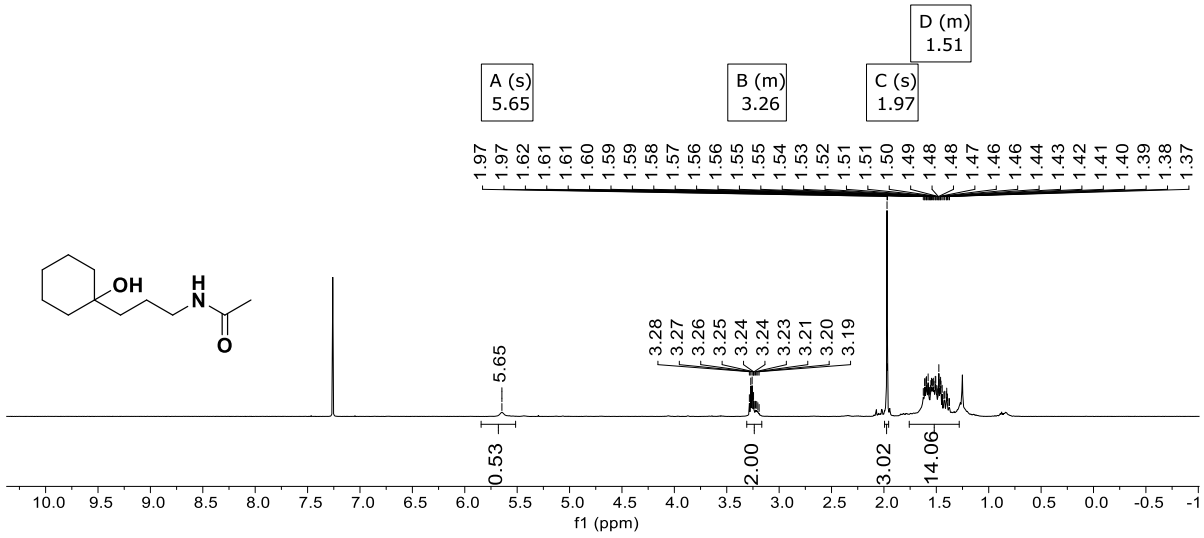

Figure S54: ^{1}H NMR spectra of **11**-O4.

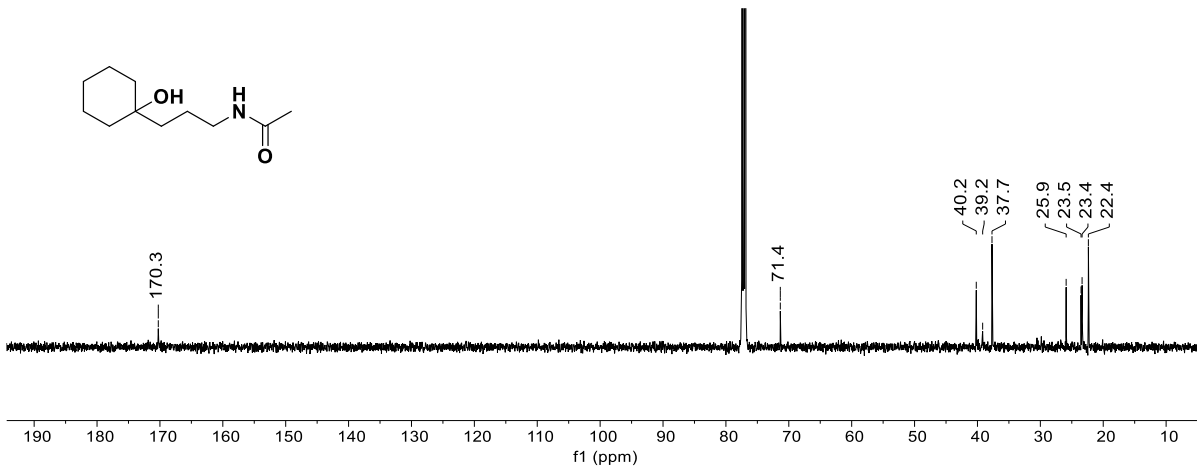

Figure S55: ^{13}C NMR spectra of **11**-O4.

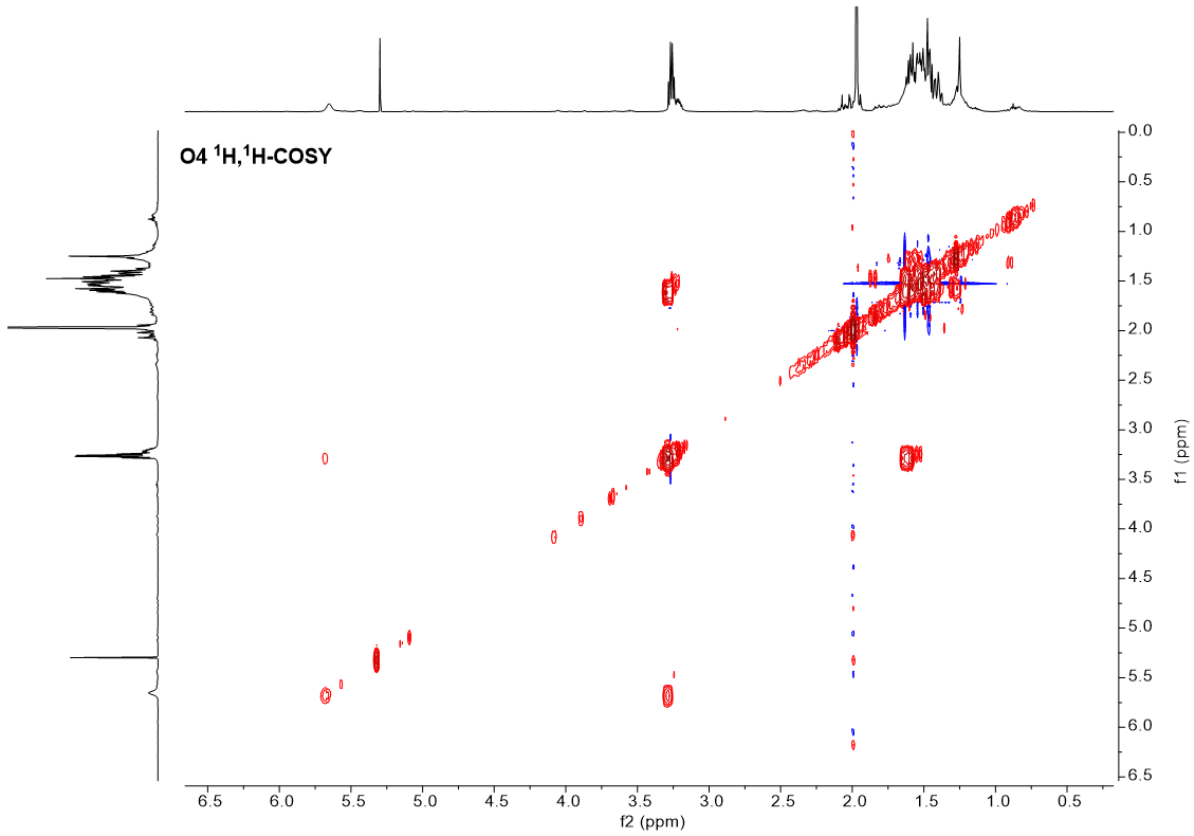

Figure S56: ^{1}H,^{1}H-COSY spectra of **11**-O4.

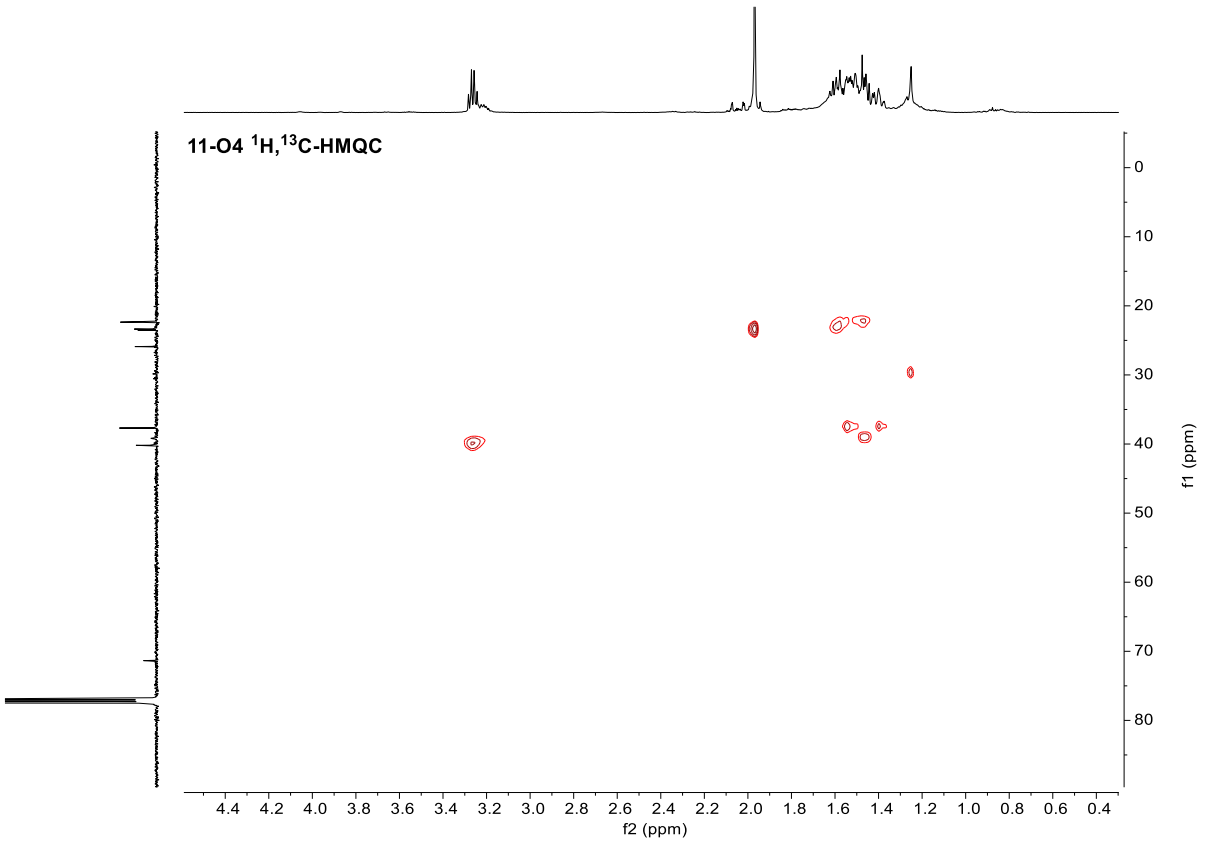

Figure S57: ^{1}H,^{13}C-HMQC spectra of **11**-O4.

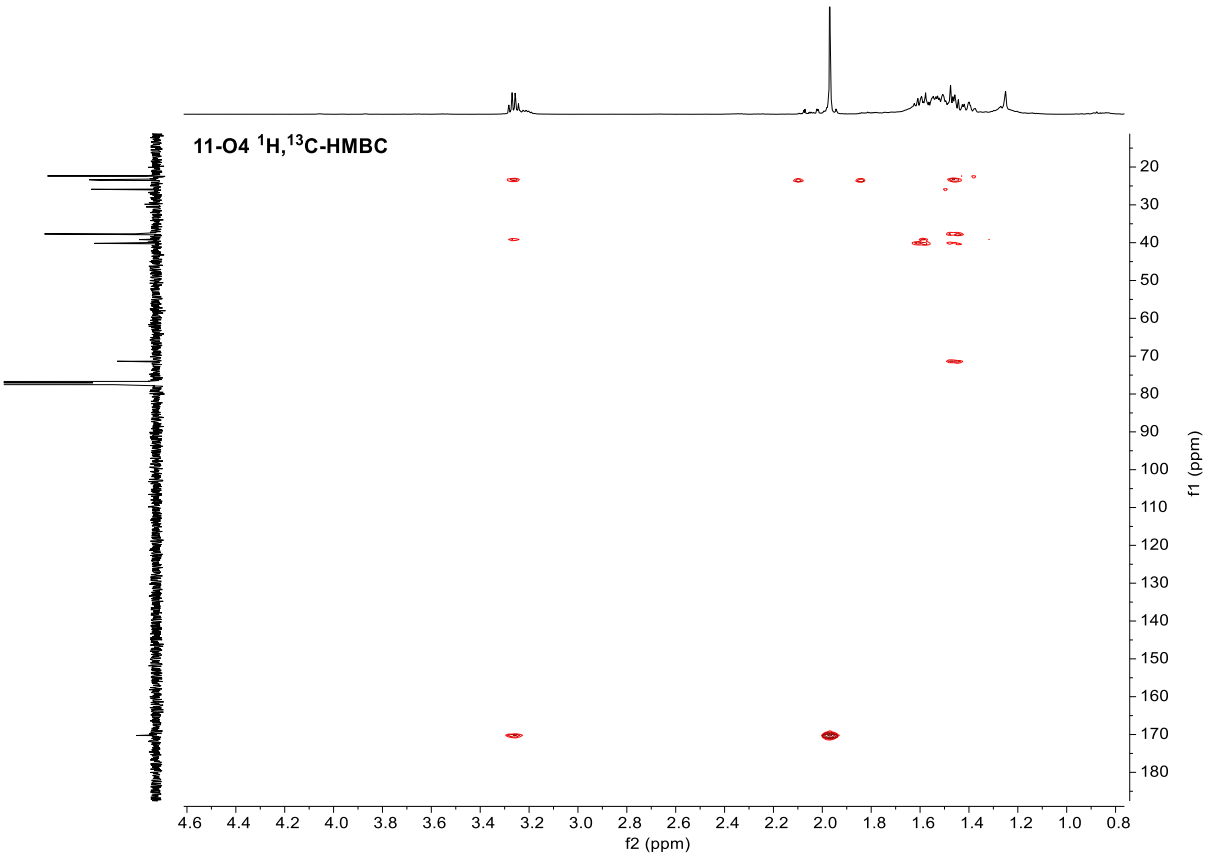

Figure S58: ^{1}H,^{13}C-HMBC spectra of **11**-O4.

3.4 Exploring Potential Oxidation Selectivity Changes with Conversion

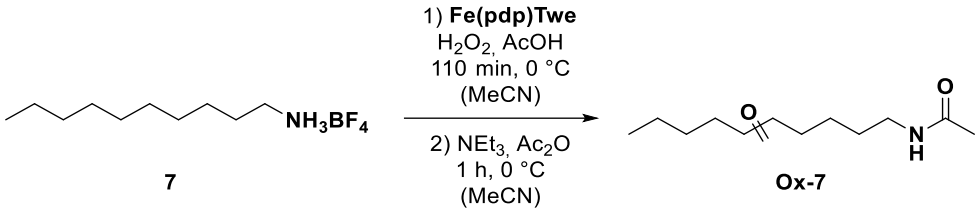

Decylammonium **7** was oxidized according to the previous small-scale procedure (see p. S20) for oxidation reactions with Fe (applying only 3 mol% catalyst). The reaction course was followed by taking samples after 3 min, 15 min, 30 min, 45 min, 60 min, and 110 min. The samples were then subjected to the general procedure for workup and GC analysis for decyl ammonium substrate. Note that no internal standard was added, and the obtained results were analyzed only qualitatively. The results do not indicate any distinct changes in the oxidation pattern over the reaction course. For details regarding assignments of the products, see our previous publication.[3a]

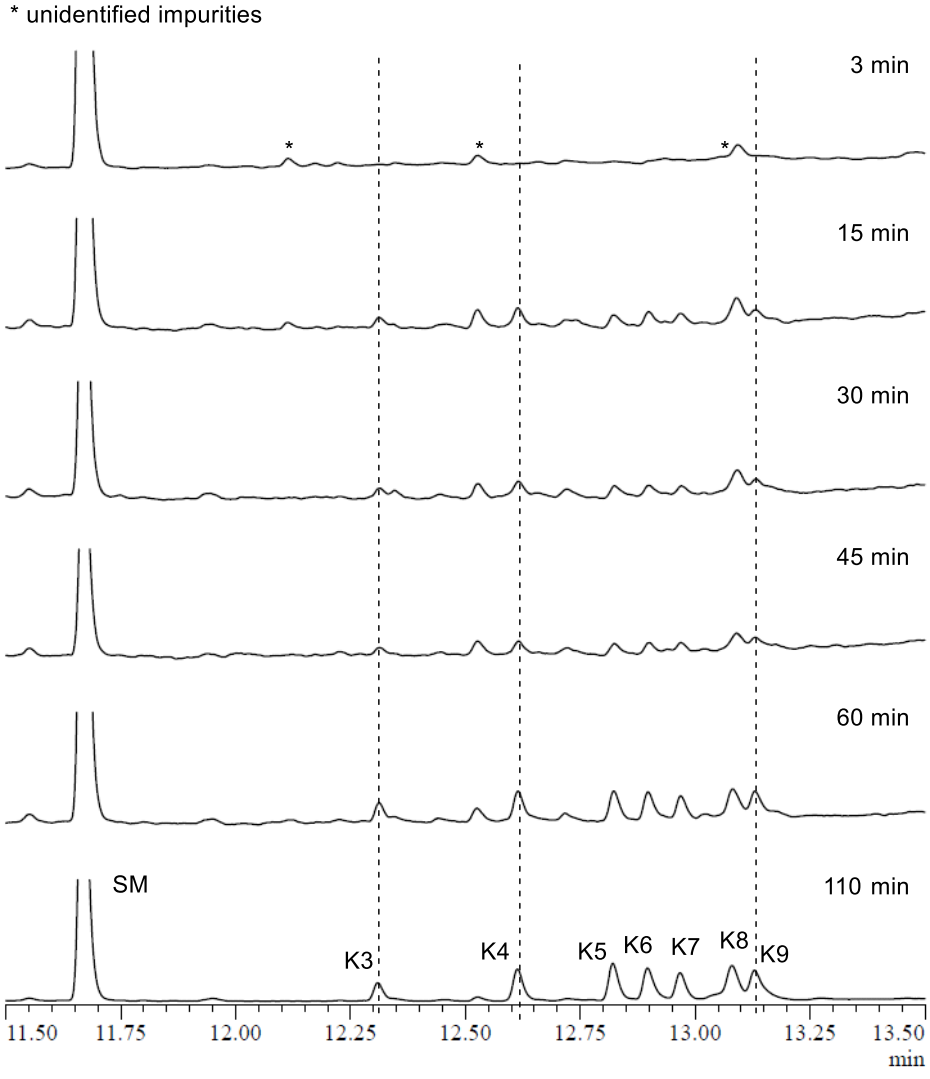

Figure S59: Oxidation pattern of decylammonium with **Fe(pdp)Twe** at different reaction times.

4. NMR Titration Experiments

NMR titrations were performed at 298 K, measuring ^{1}H NMR spectra at 500 MHz using a UltraShield 500 spectrometer. To a solution of **Fe(pdp)Twe$_2$** (host, H) in MeCN was added a stock solution of corresponding guest (G) with the same host concentration [H] as the host solution, so that 500 µL of a solution with constant [H] of 100 µM and with varying concentrations [G] were obtained.

Fast exchange on an NMR timescale was observed for the formation of the host-guest complex; therefore changes in chemical shift were observed and plotted using nonlinear regression *via* the bindfit app (THORDARSON *et al.*, http://app.supramolecular.org/bindfit/)[15] for signals that could be observed over the entire course of the titration experiment. The resulting fit was used to calculate K_a in addition to an error margin for 90% confidence of fit and the root mean square (RMS) for the entire signal set.

Titration of Decylammonium Tetrafluoroborate (7@Fe(pdp)Twe$_2$)

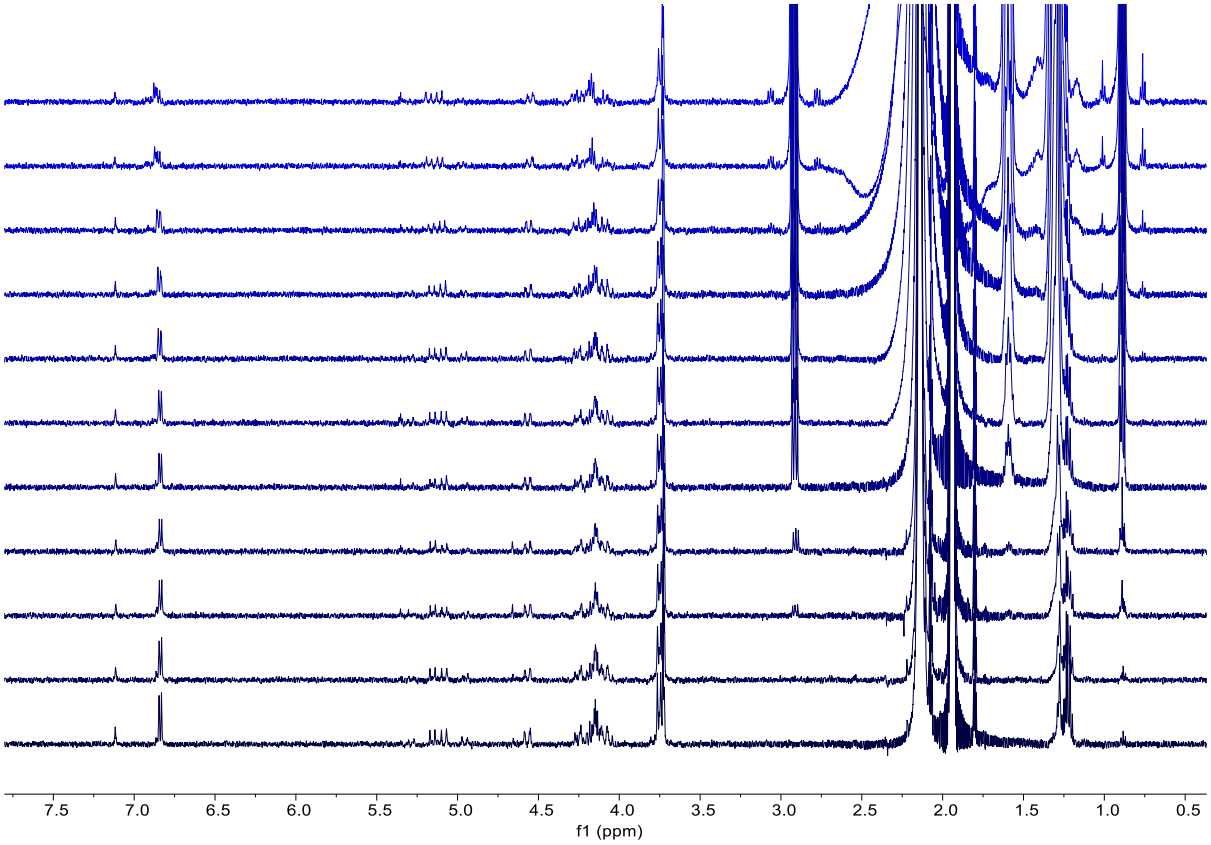

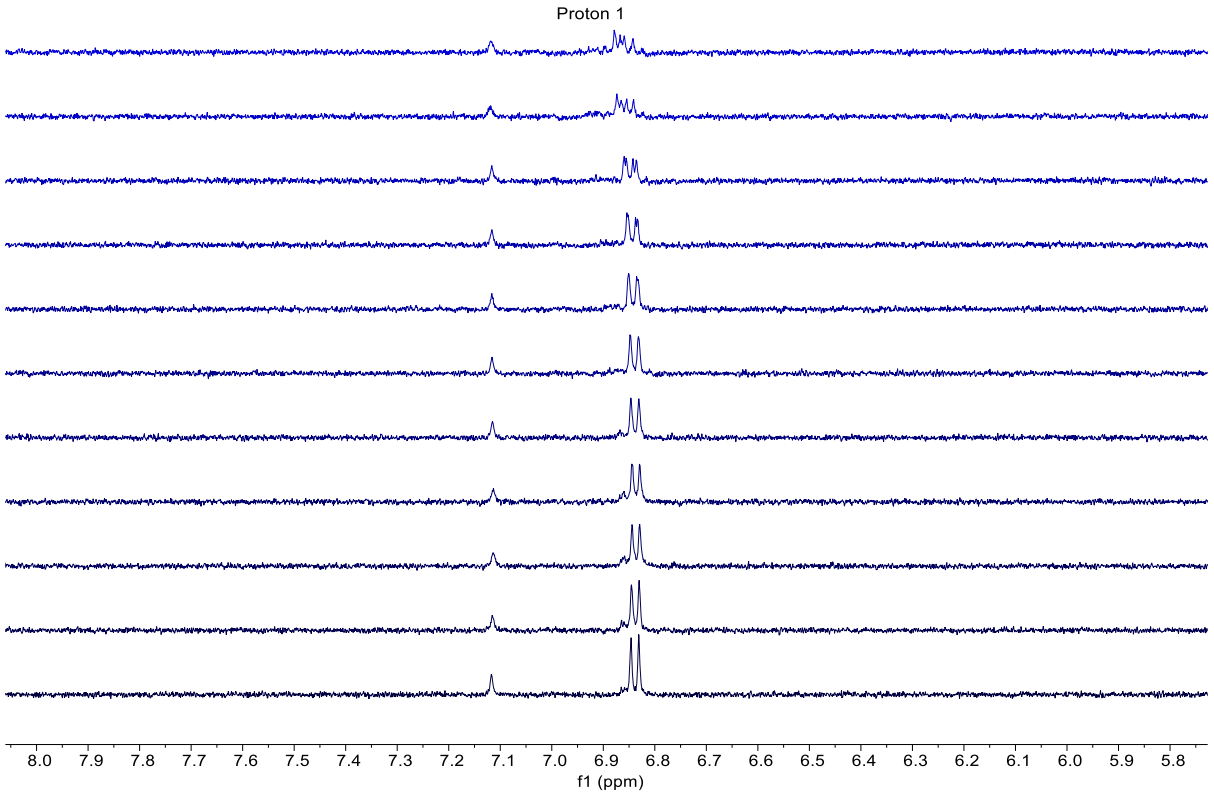
Proton 1
8.0 7.9 7.8 7.7 7.6 7.5 7.4 7.3 7.2 7.1 7.0 6.9 6.8 6.7 6.6 6.5 6.4 6.3 6.2 6.1 6.0 5.9 5.8
f1 (ppm)

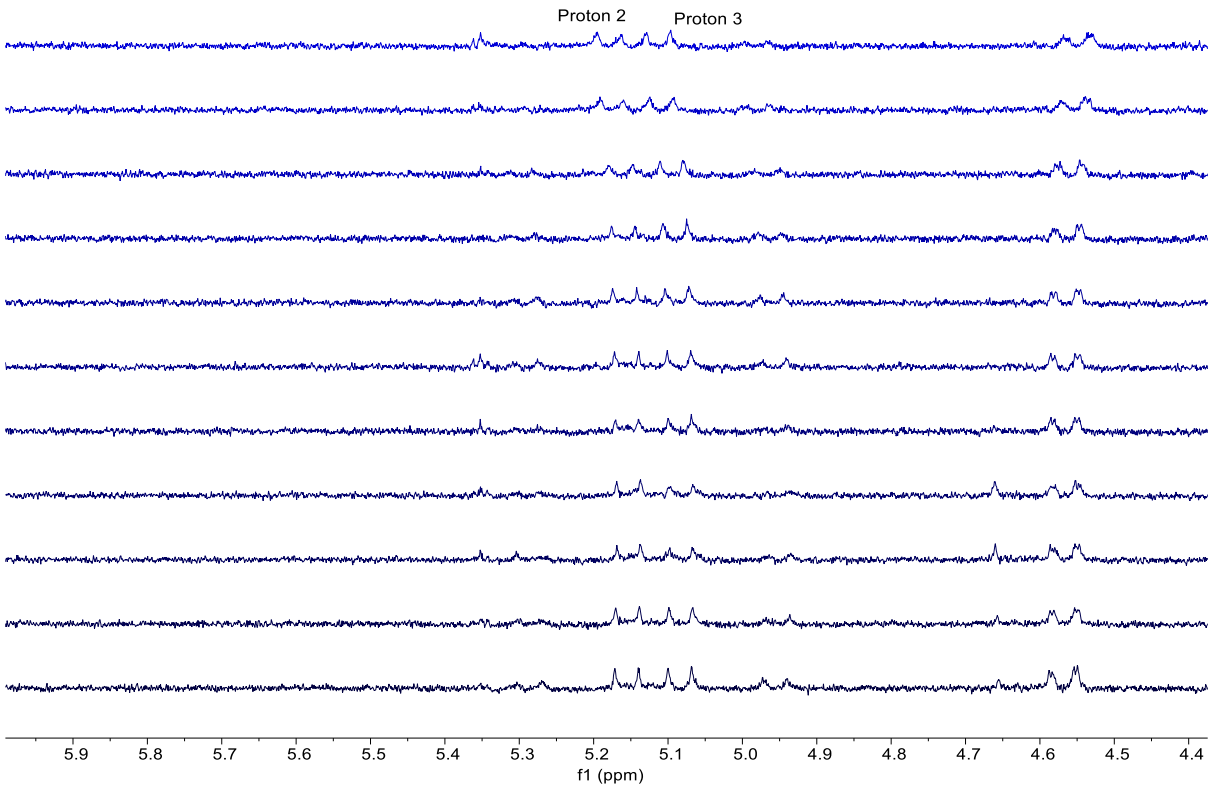
Proton 2
Proton 3
5.9 5.8 5.7 5.6 5.5 5.4 5.3 5.2 5.1 5.0 4.9 4.8 4.7 4.6 4.5 4.4
f1 (ppm)

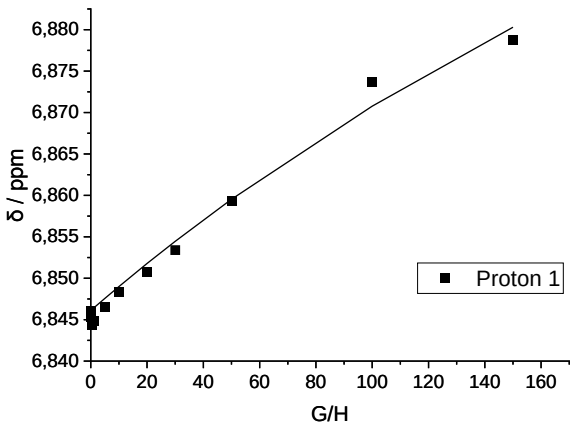

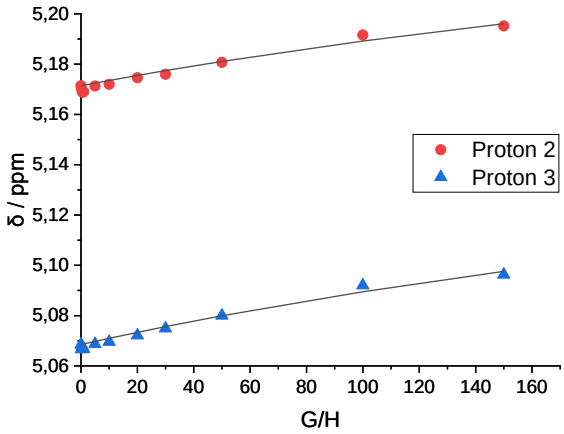

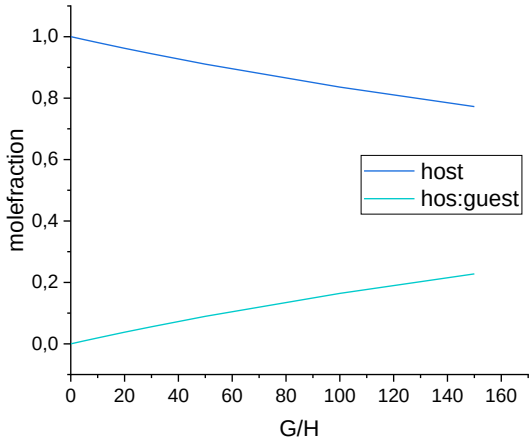

<u>Titrated at 100 μM [H].</u>

K_a = 19.7 ± 1.15 M^{-1}.

RMS = $1.4700 \cdot 10^{-3}$

5. Additional Models of Tweezer Catalysts

Models for **Fe(pdp)** and **Fe(pdp)Twe$_2$** were compiled using the Spartan chemistry software (equilibrium conformer, MMFF, gas phase).

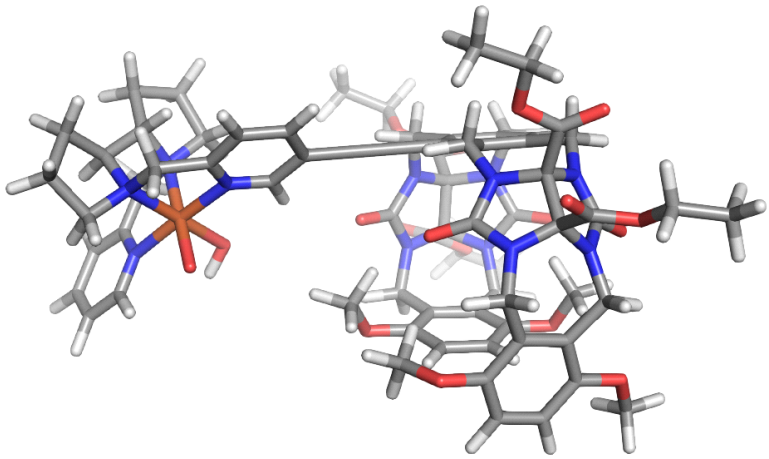

Figure S60: MMFF model of **Fe(pdp)Twe**.

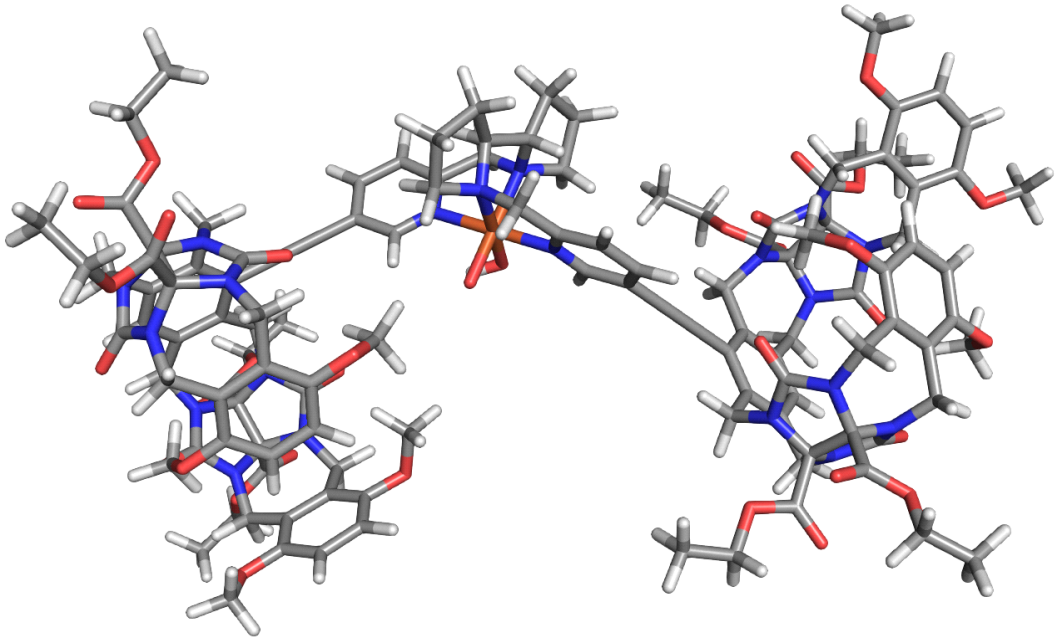

Figure 61: MMFF model of **Fe(pdp)Twe$_2$**.

6. References

[1] W. C. Still, M. Kahn, A. Mitra, *J. Org. Chem.* **1978**, *43*, 2923-2925.

[2] H. E. Gottlieb, V. Kotlyar, A. Nudelman, *J. Org. Chem.* **1997**, *62*, 7512-7515.

[3] a) M. Knezevic, M. Heilmann, G. M. Piccini, K. Tiefenbacher, *Angew. Chem. Int. Ed.* **2020**, *59*, 12387-12391; b) J. T. Scanlon, D. E. Willis, *J. Chromatogr. Sci.* **1985**, *23*, 333-340.

[4] A. Diebold, A. Elbouadili, K. S. Hagen, *Inorg. Chem.* **2000**, *39*, 3915-3923.

[5] Z. Codolà, I. Gamba, F. Acuña-Parés, C. Casadevall, M. Clémancey, J.-M. Latour, J. M. Luis, J. Lloret-Fillol, M. Costas, *J. Am. Chem. Soc.* **2018**, *141*, 323-333.

[6] Z. Codolà, I. Gamba, F. Acuña-Parés, C. Casadevall, M. Clémancey, J.-M. Latour, J. M. Luis, J. Lloret-Fillol, M. Costas, *J. Am. Chem. Soc.* **2018**, *141*, 323-333.

[7] a) M. S. Chen, M. C. White, *Science* **2007**, *318*, 783-787; b) L. Gomez, M. Canta, D. Font, I. Prat, X. Ribas, M. Costas, *J. Org. Chem.* **2013**, *78*, 1421-1433.

[8] R. V. Ottenbacher, K. P. Bryliakov, E. P. Talsi, *Adv. Synth. Catal.* **2011**, *353*, 885-889.

[9] M. Costas, J. Que, Lawrence, *Angew. Chem. Int. Ed.* **2002**, *114*, 2283-2285.

[10] a) A. Murphy, G. Dubois, T. Stack, *J. Am. Chem. Soc.* **2003**, *125*, 5250-5251; b) R. V. Ottenbacher, K. P. Bryliakov, E. P. Talsi, *Inorg. Chem.* **2010**, *49*, 8620-8628.

[11] I. Bala, N. Singh, R. A. K. Yadav, J. De, S. P. Gupta, D. P. Singh, D. K. Dubey, J.-H. Jou, R. Douali, S. K. Pal, *J. Mater. Chem. C* **2020**, *8*, 12485-12494.

[12] M.-K. Wong, N.-W. Chung, L. He, D. Yang, *J. Am. Chem. Soc.* **2003**, *125*, 158-162.

[13] G. Olivo, G. Capocasa, B. Ticconi, O. Lanzalunga, S. Di Stefano, M. Costas, *Angew. Chem. Int. Ed.* **2020**, *59*, 12703-12708.

[14] G. Olivo, G. Farinelli, A. Barbieri, O. Lanzalunga, S. Di Stefano, M. Costas, *Angew. Chem. Int. Ed.* **2017**, *129*, 16565-16569.

[15] P. Thordarson, *Chem. Soc. Rev.* **2011**, *40*, 1305-1323.

Appendix: ^{1}H and ^{13}C NMR Spectra

^{1}H NMR (500 MHz, 300 K, $CDCl_3$)

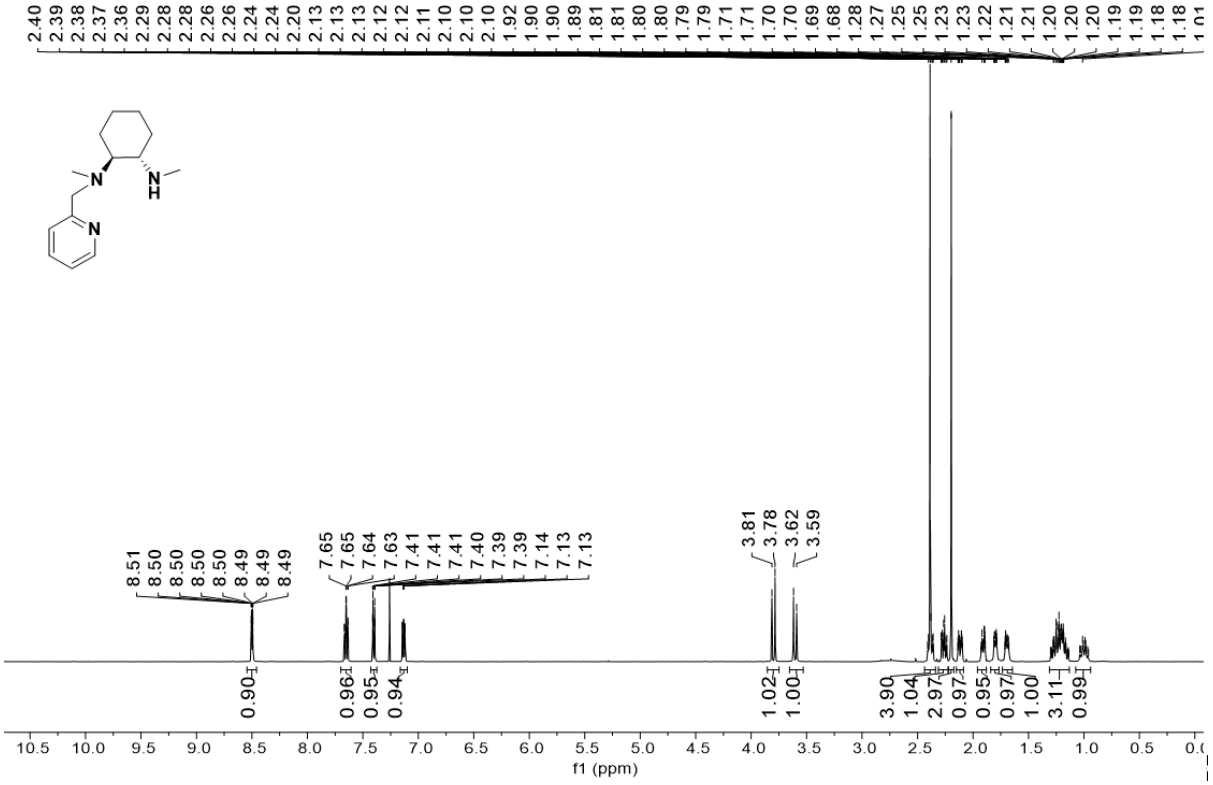

^{13}C NMR (126 MHz, 300 K, $CDCl_3$)

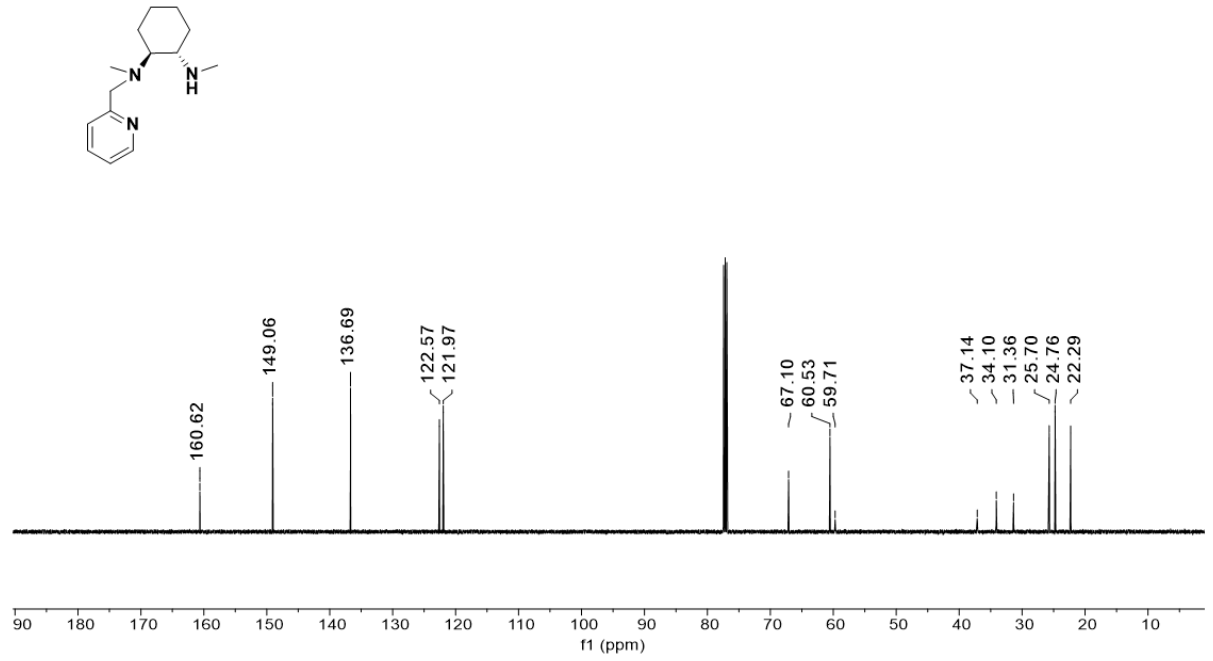

^{1}H NMR (500 MHz, 300 K, $CDCl_3$)

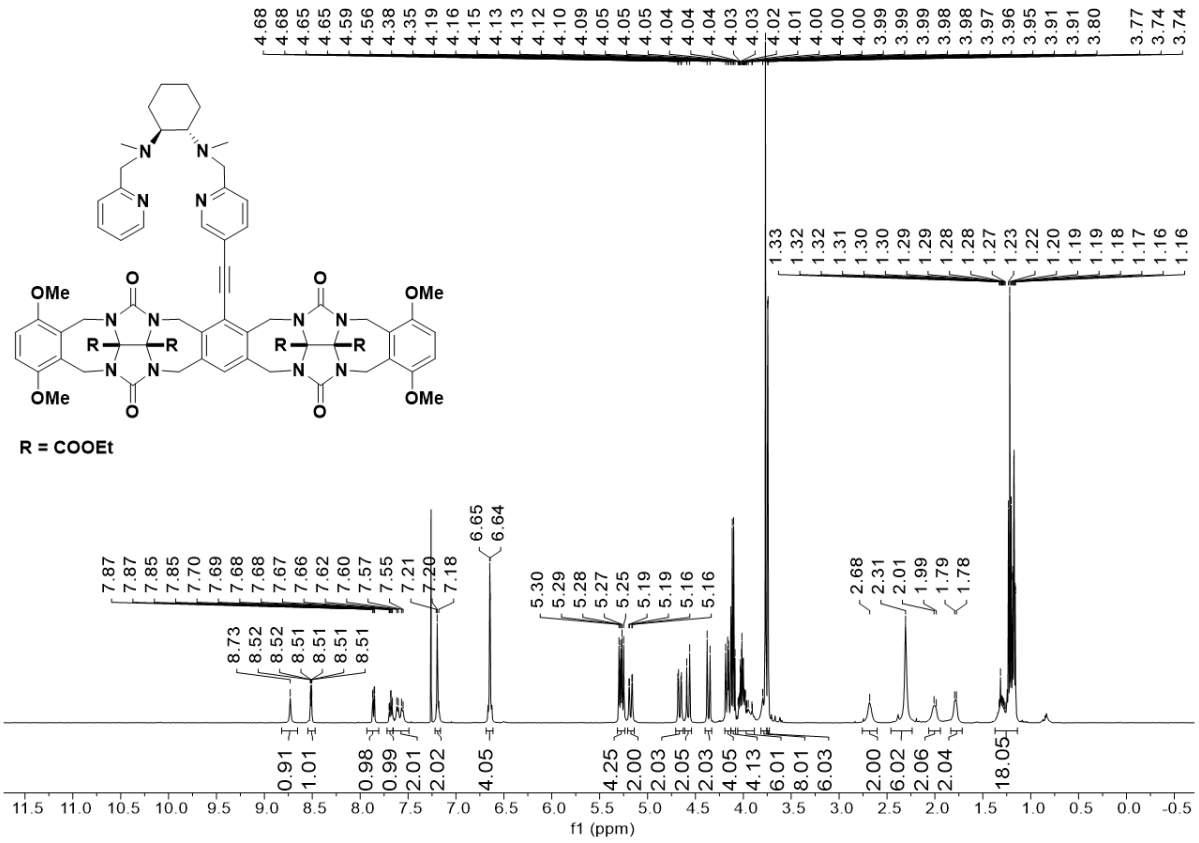

^{13}C NMR (151 MHz, 300 K, $CDCl_3$)

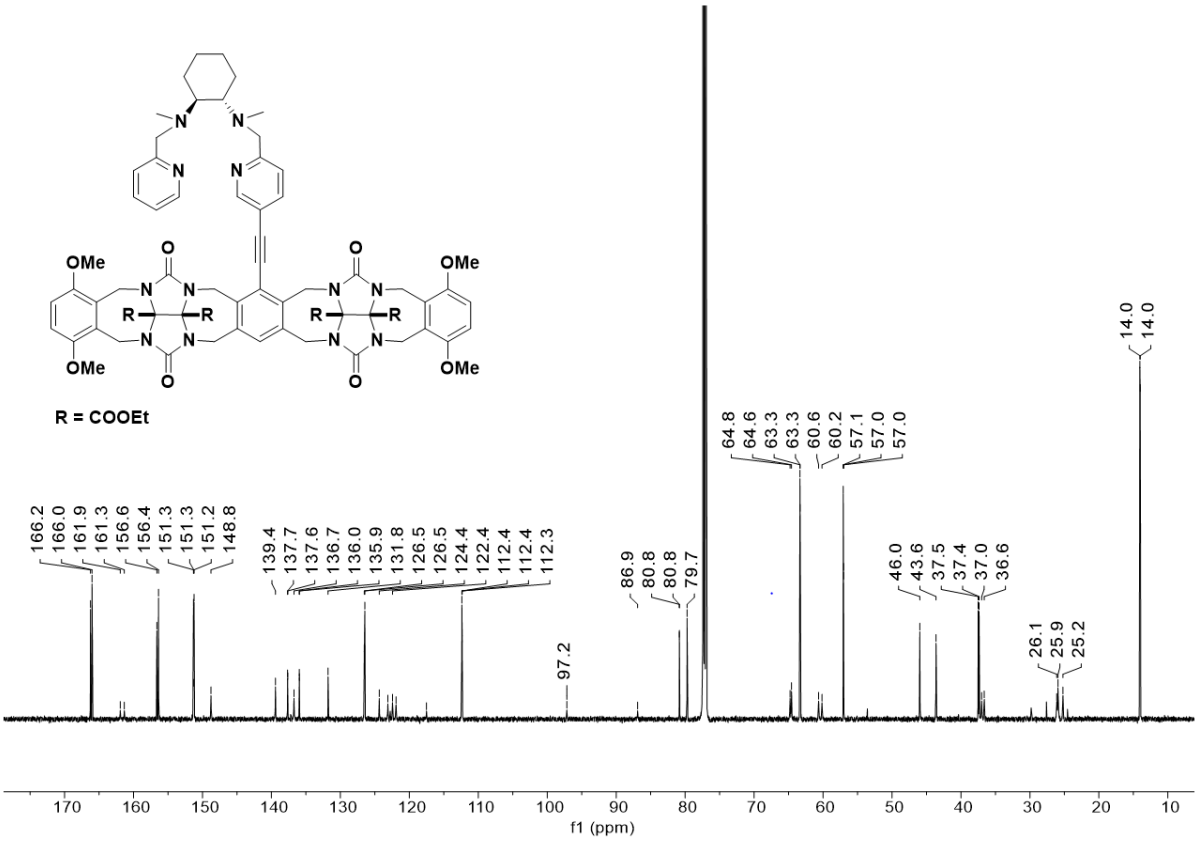

^{1}H NMR (500 MHz, 300 K, $CDCl_3$)

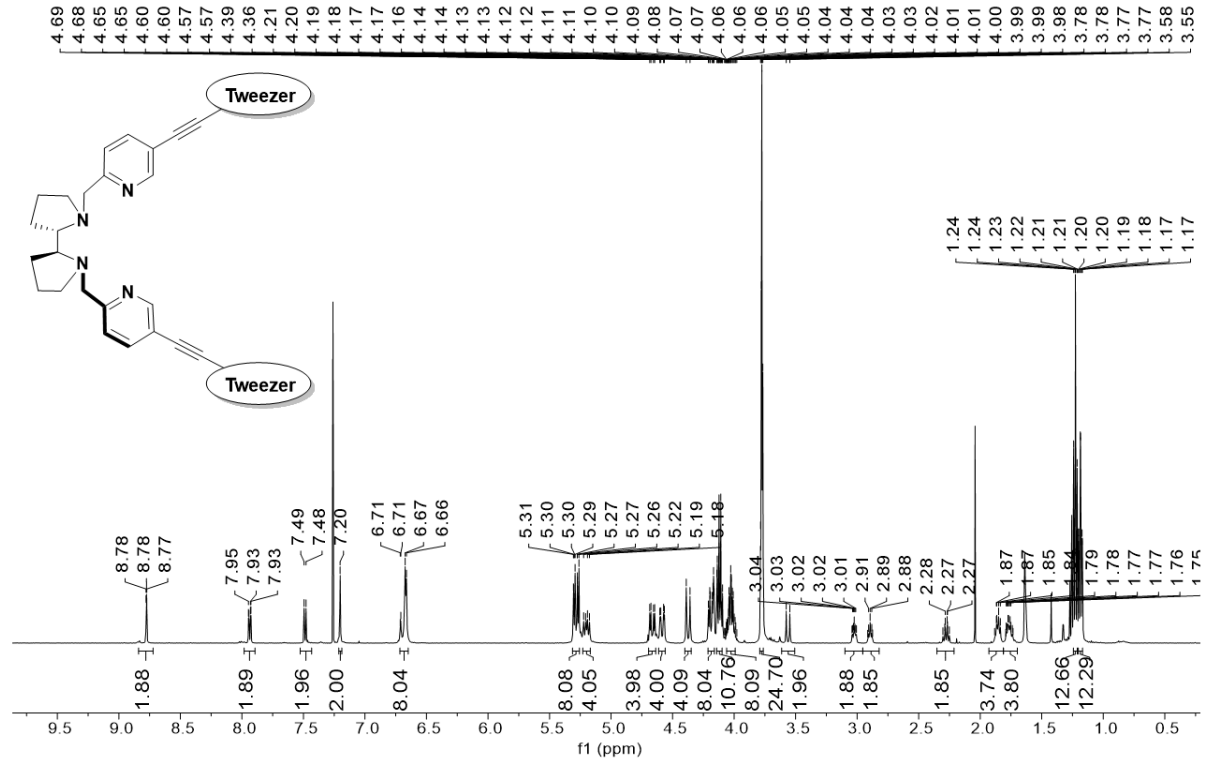

^{13}C NMR (151 MHz, 300 K, $CDCl_3$)

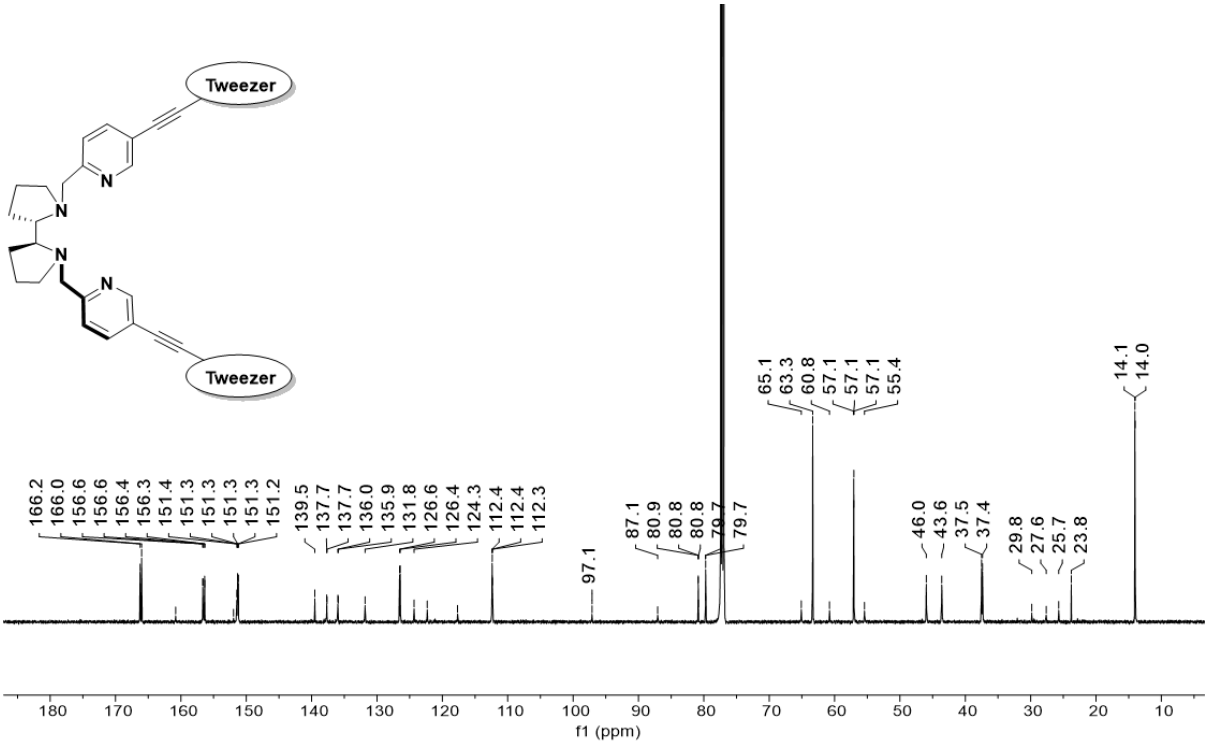

^{1}H NMR (500 MHz, 300 K, $CDCl_3$)

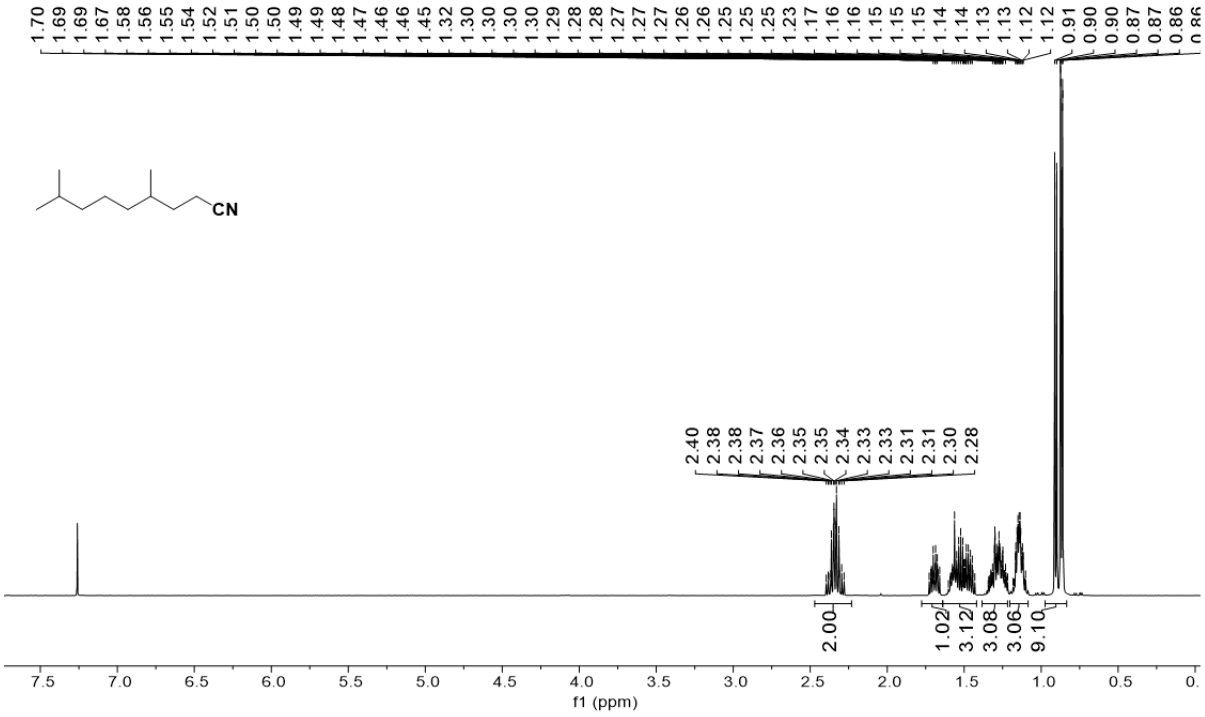

^{13}C NMR (126 MHz, 300 K, $CDCl_3$)

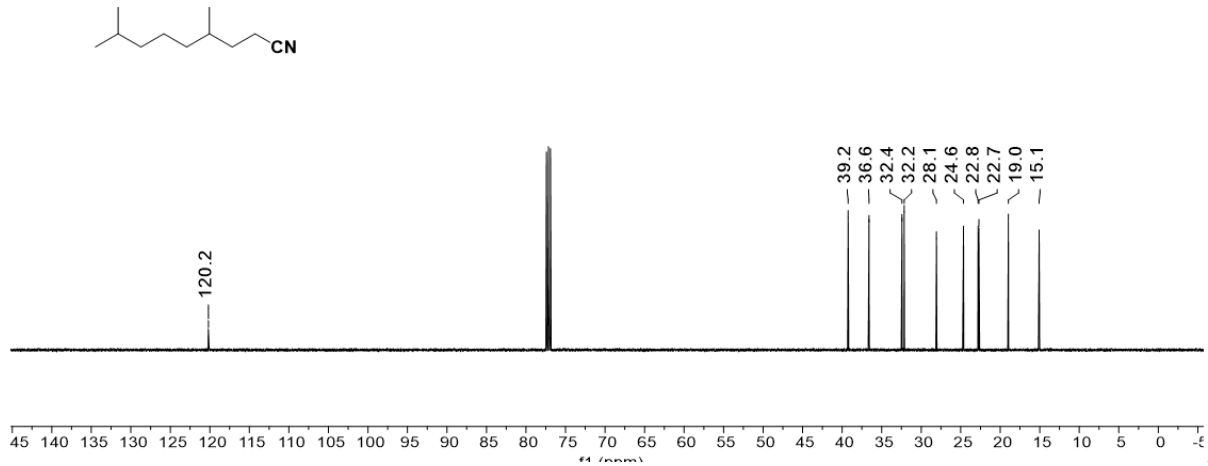

^{1}H NMR (600 MHz, 300 K, MeCN-d_3)

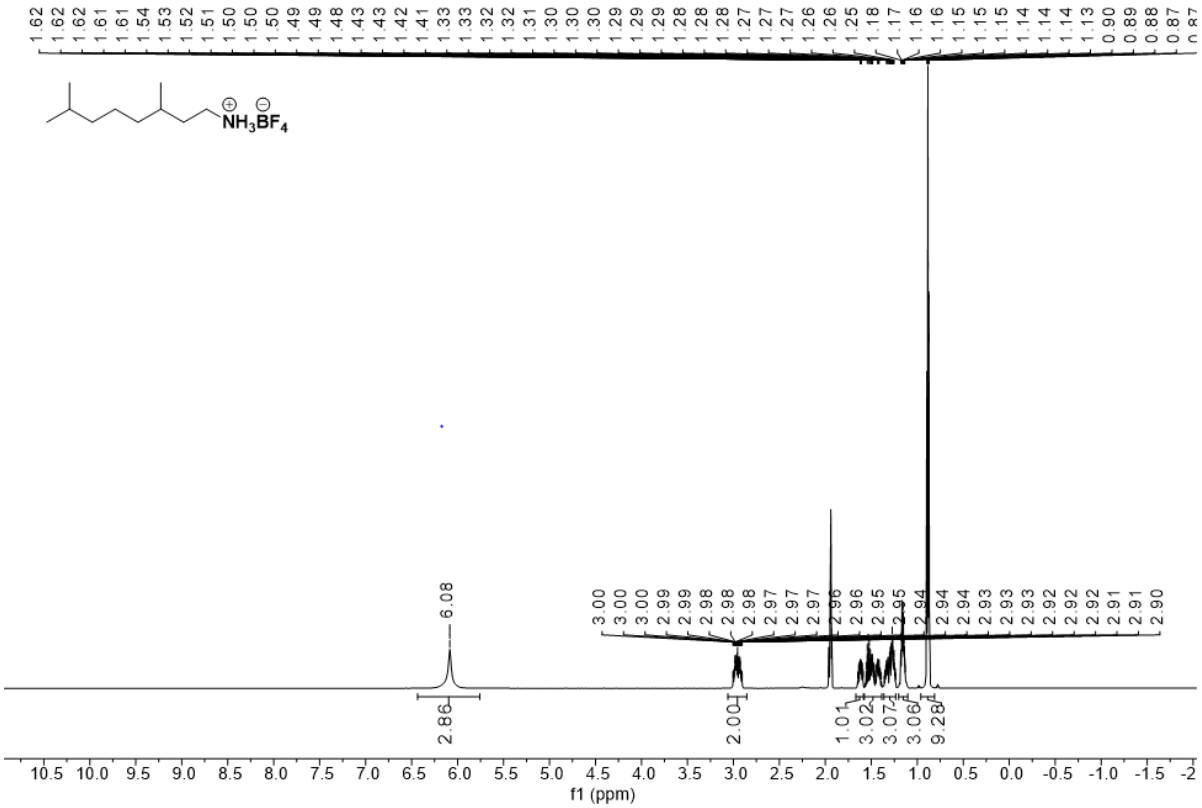

^{13}C NMR (151 MHz, 300 K, MeCN-d_3)

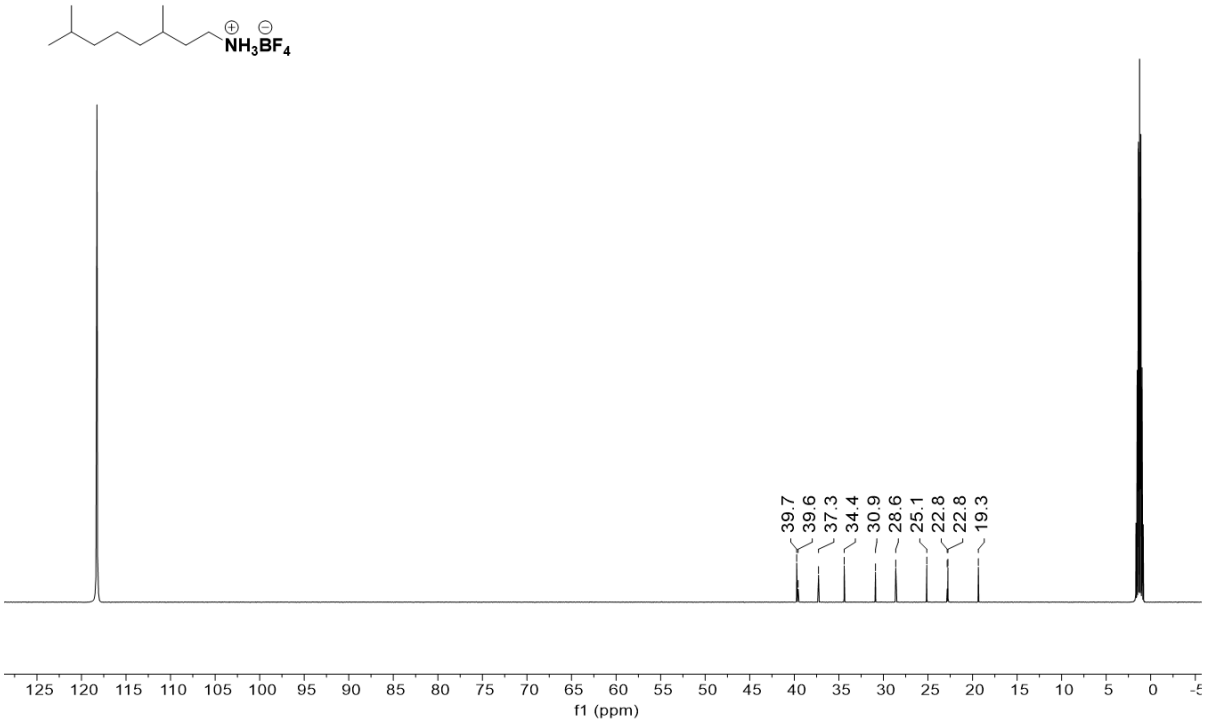

^{1}H NMR (600 MHz, 300 K, MeCN-d_3)

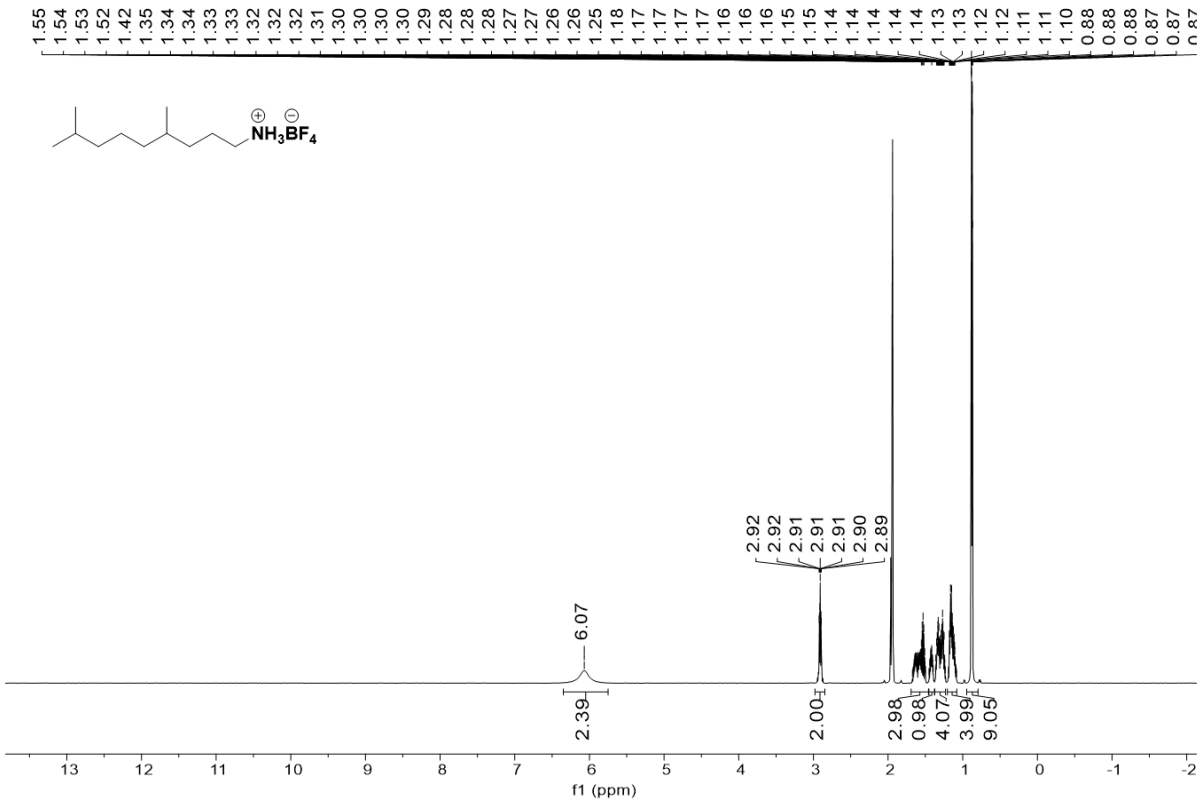

^{13}C NMR (151 MHz, 300 K, MeCN-d_3)

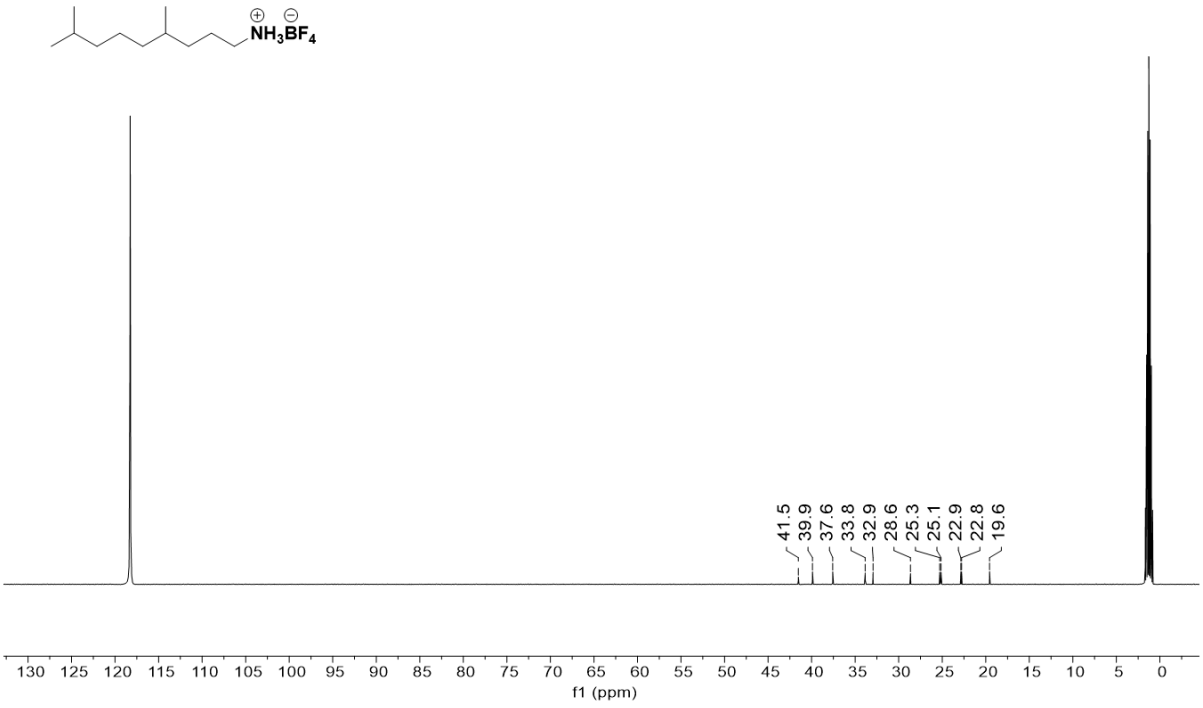

^{1}H NMR (500 MHz, 300 K, MeCN-d_3)

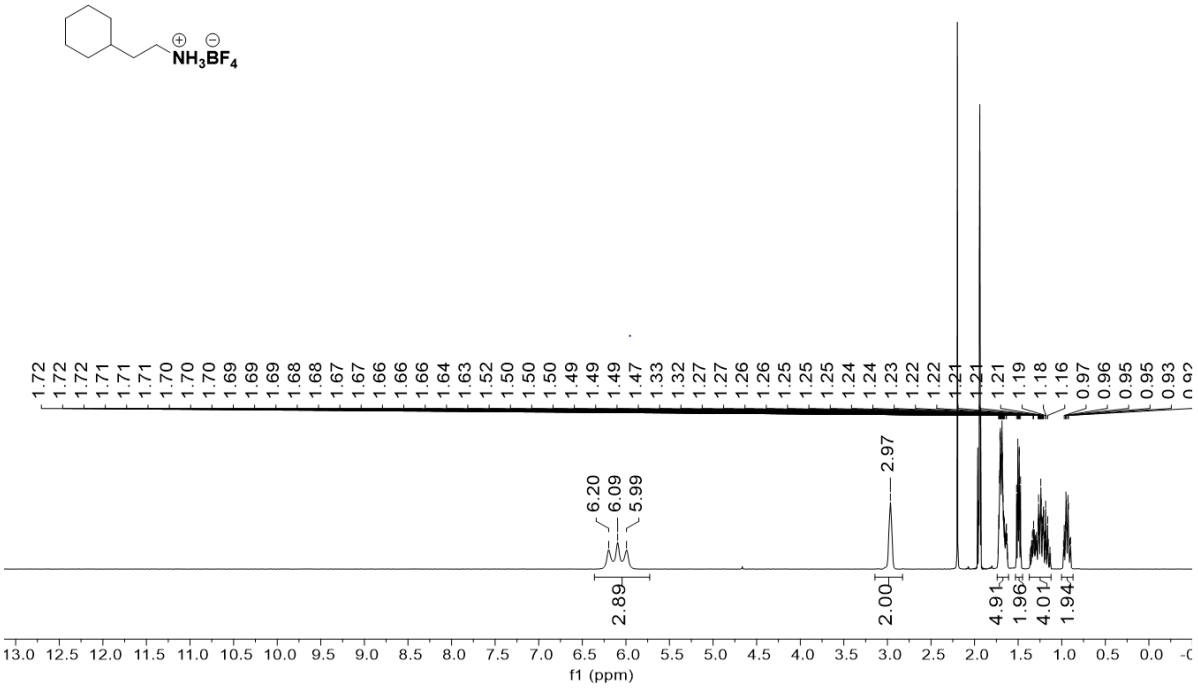

^{13}C NMR (126 MHz, 300 K, MeCN-d_3)

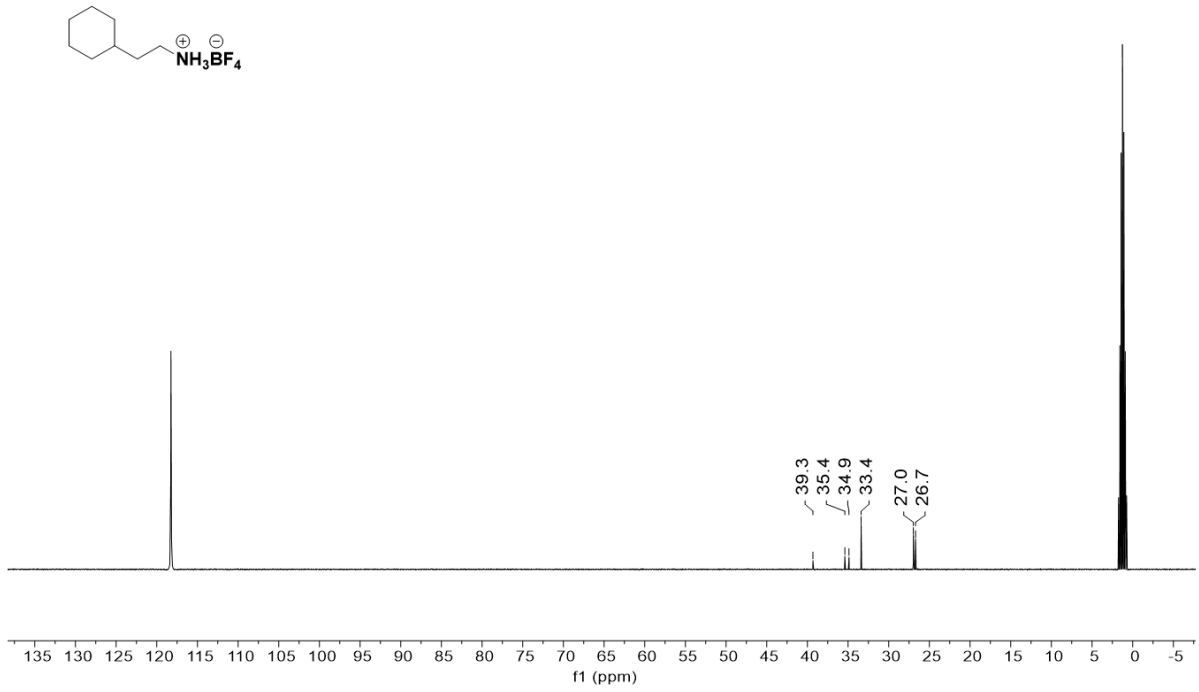

^{1}H NMR (500 MHz, 300 K, MeCN-d_3)

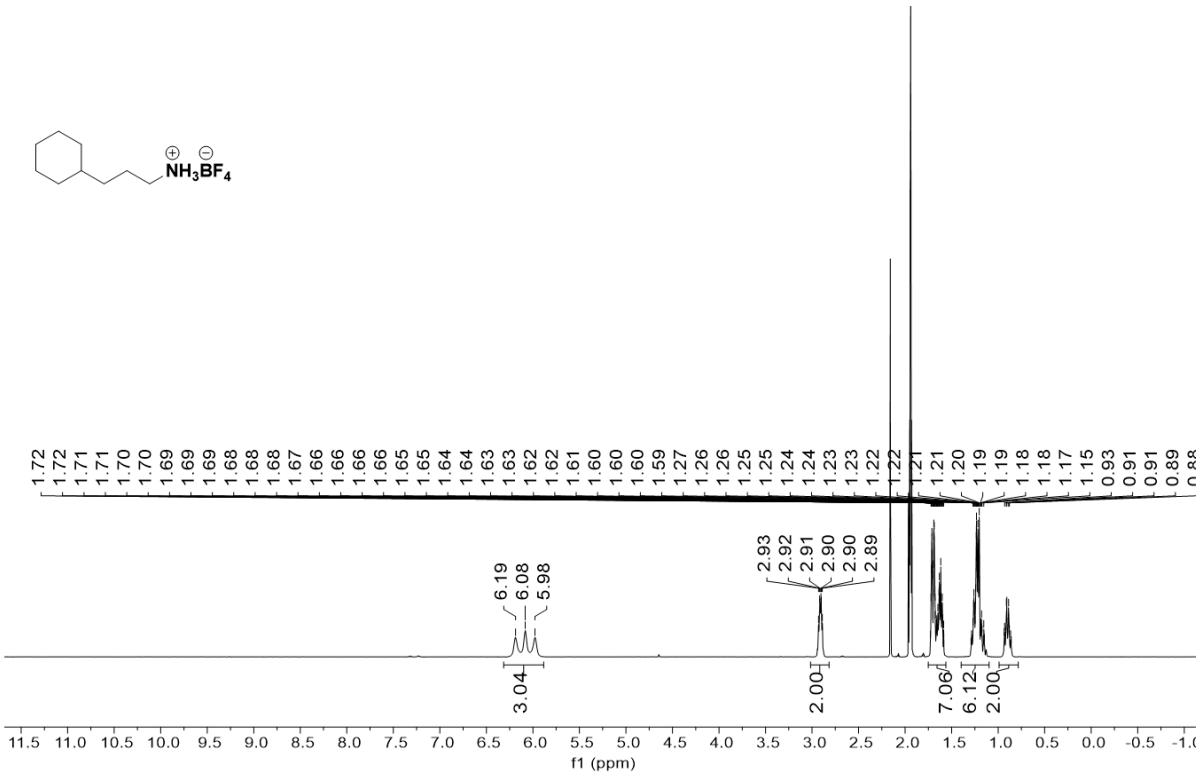

^{13}C NMR (126 MHz, 300 K, MeCN-d_3)

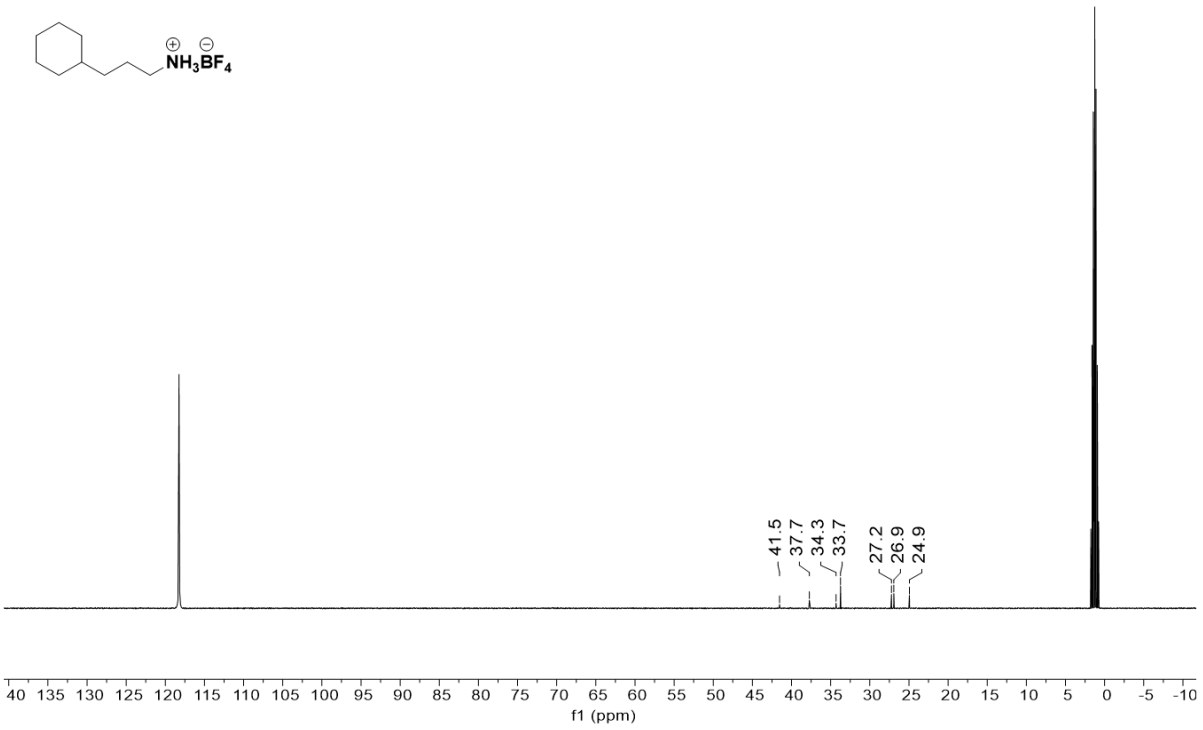

^{1}H NMR (500 MHz, 300 K, $CDCl_3$)

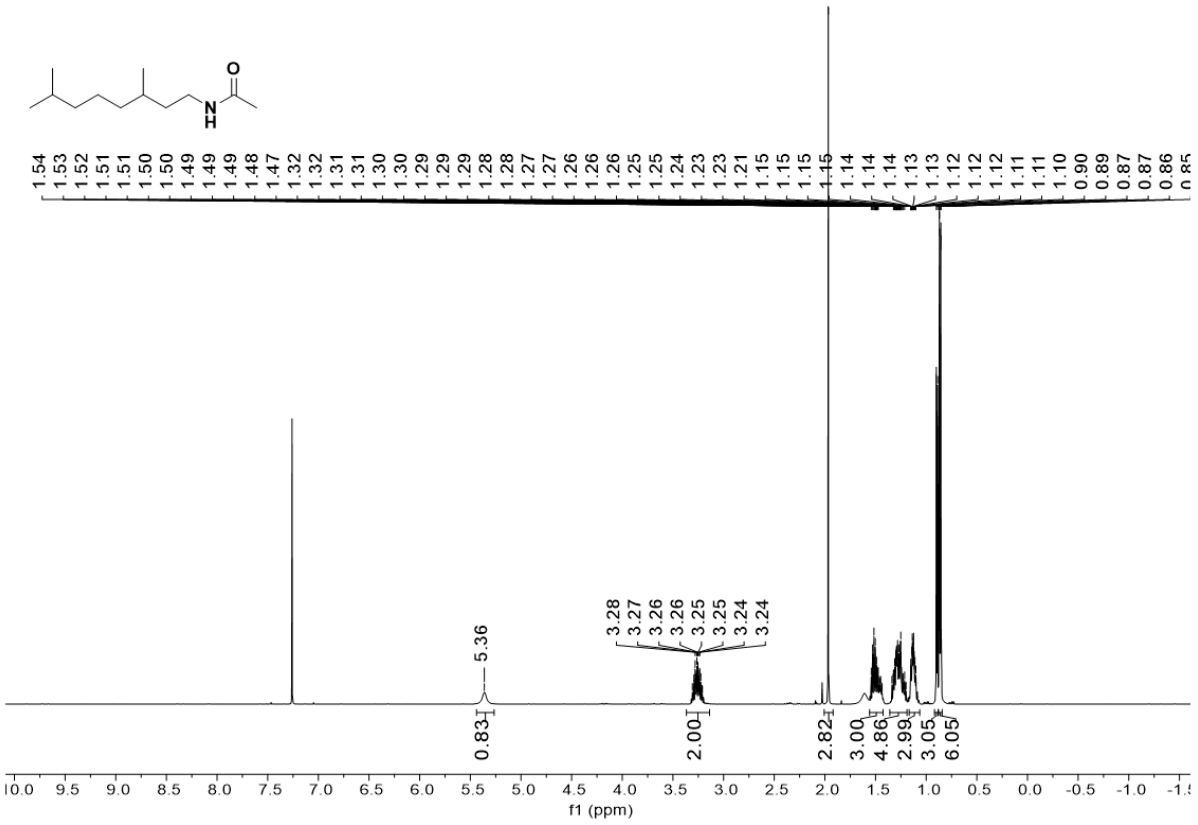

^{13}C NMR (126 MHz, 300 K, $CDCl_3$)

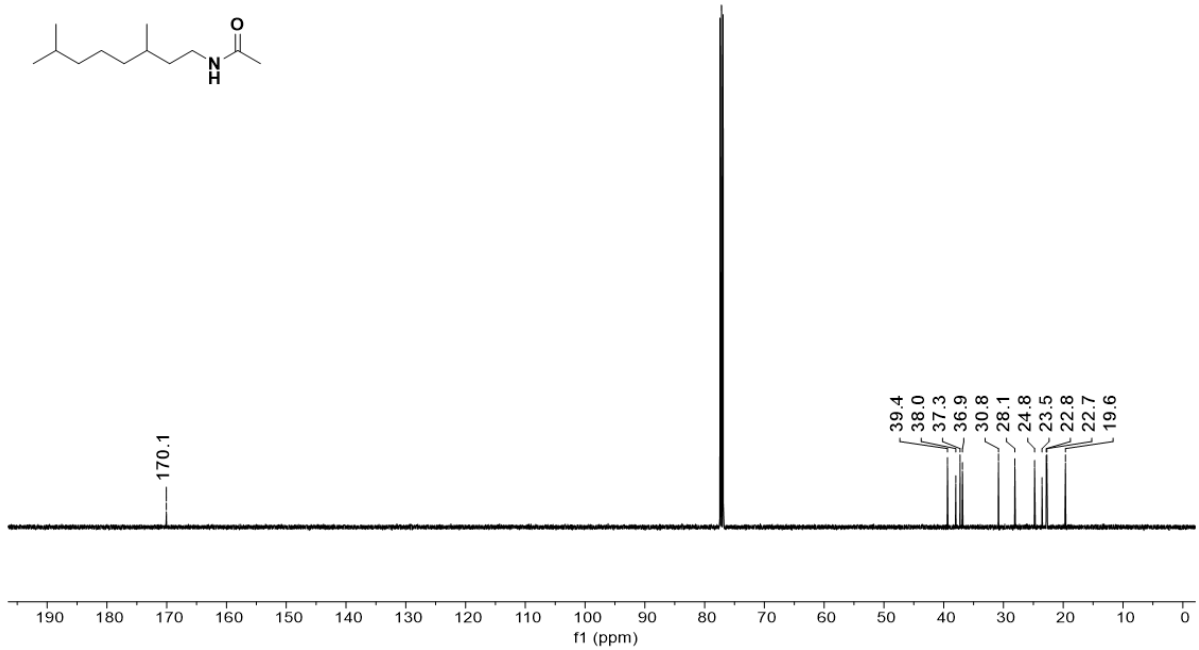

^{1}H NMR (500 MHz, 300 K, $CDCl_3$)

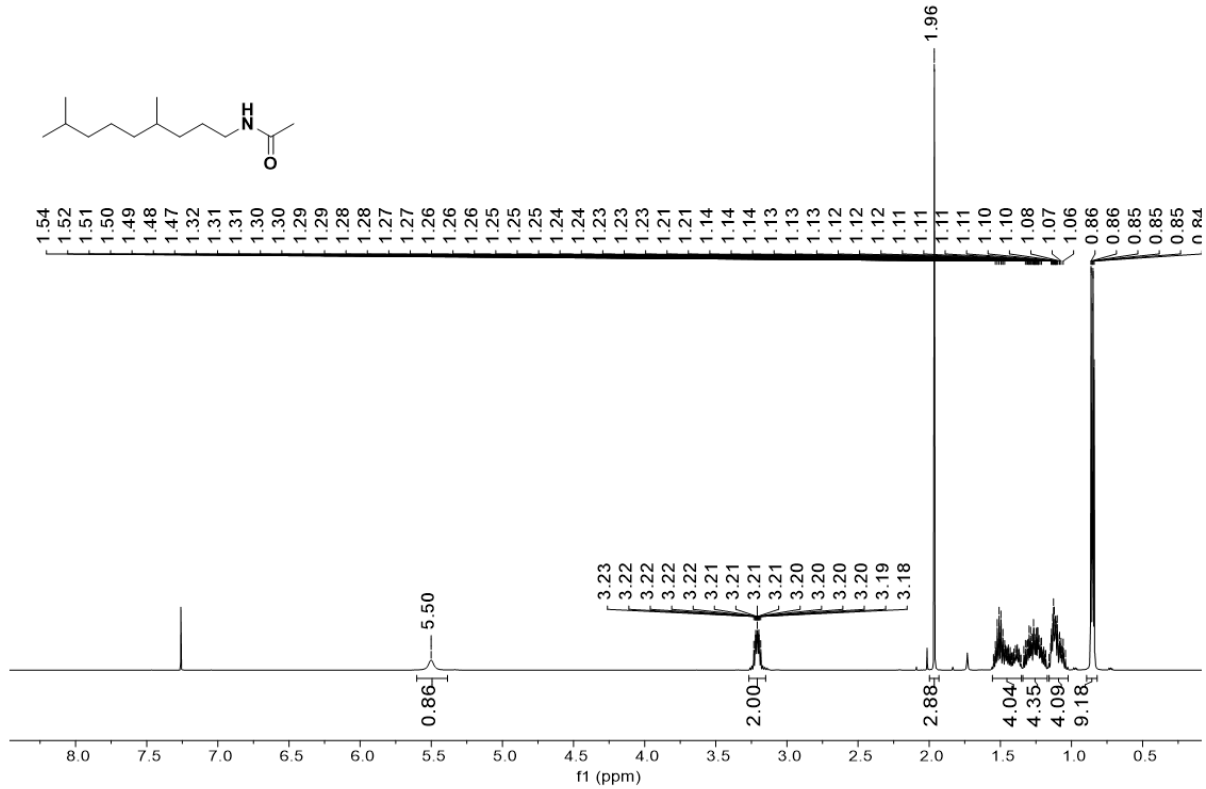

^{13}C NMR (126 MHz, 300 K, $CDCl_3$)

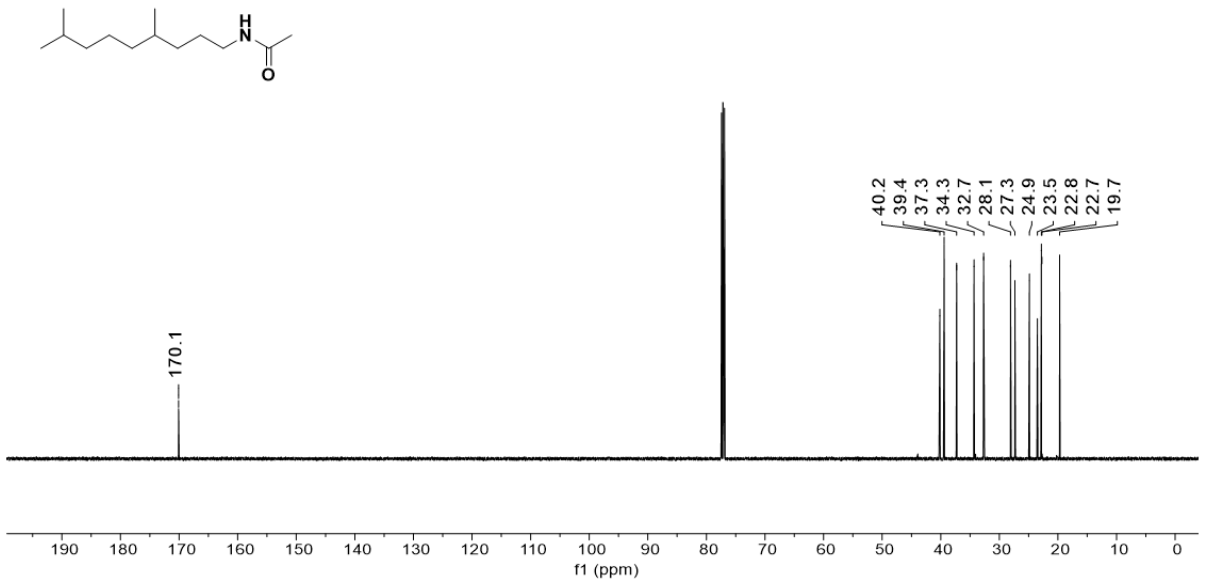

^{1}H NMR (500 MHz, 300 K, $CDCl_3$)

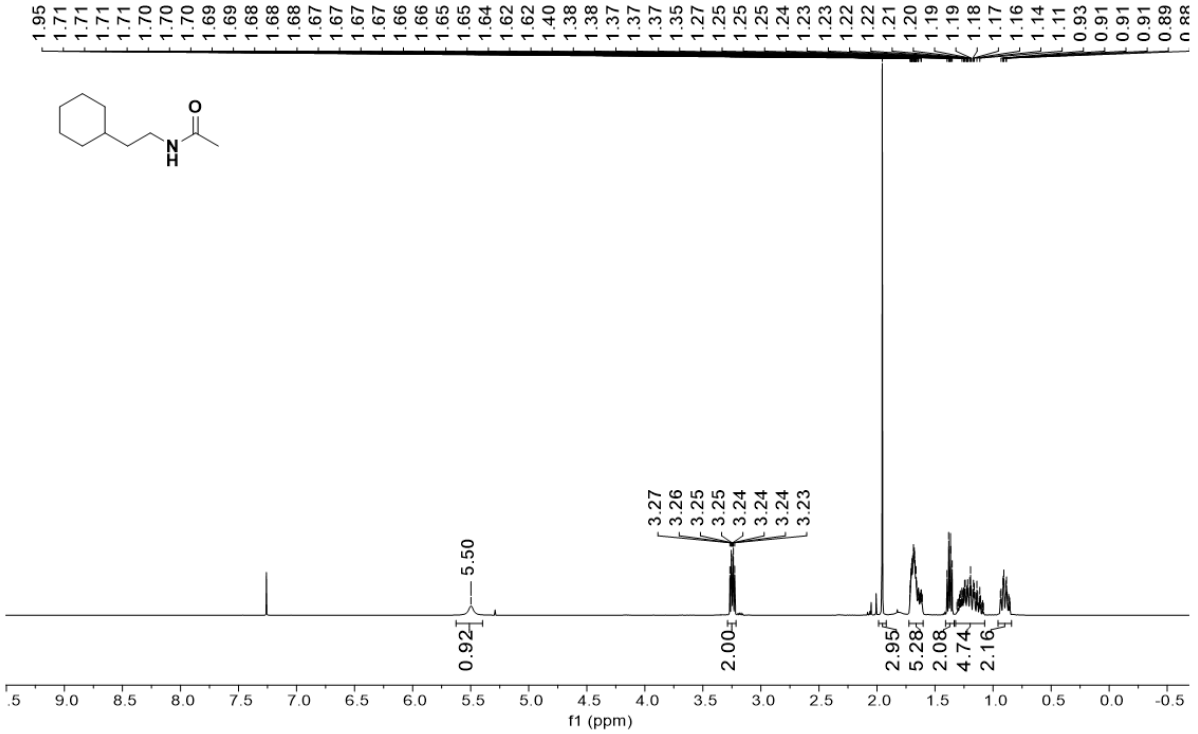

^{13}C NMR (126 MHz, 300 K, $CDCl_3$)

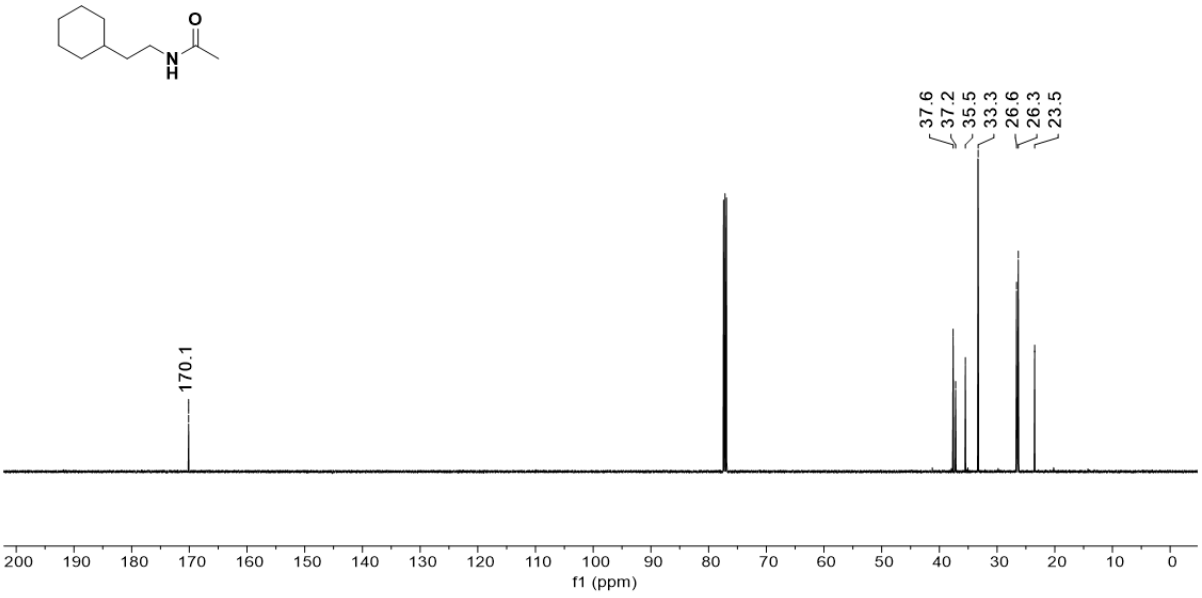

^{1}H NMR (500 MHz, 300 K, $CDCl_3$)

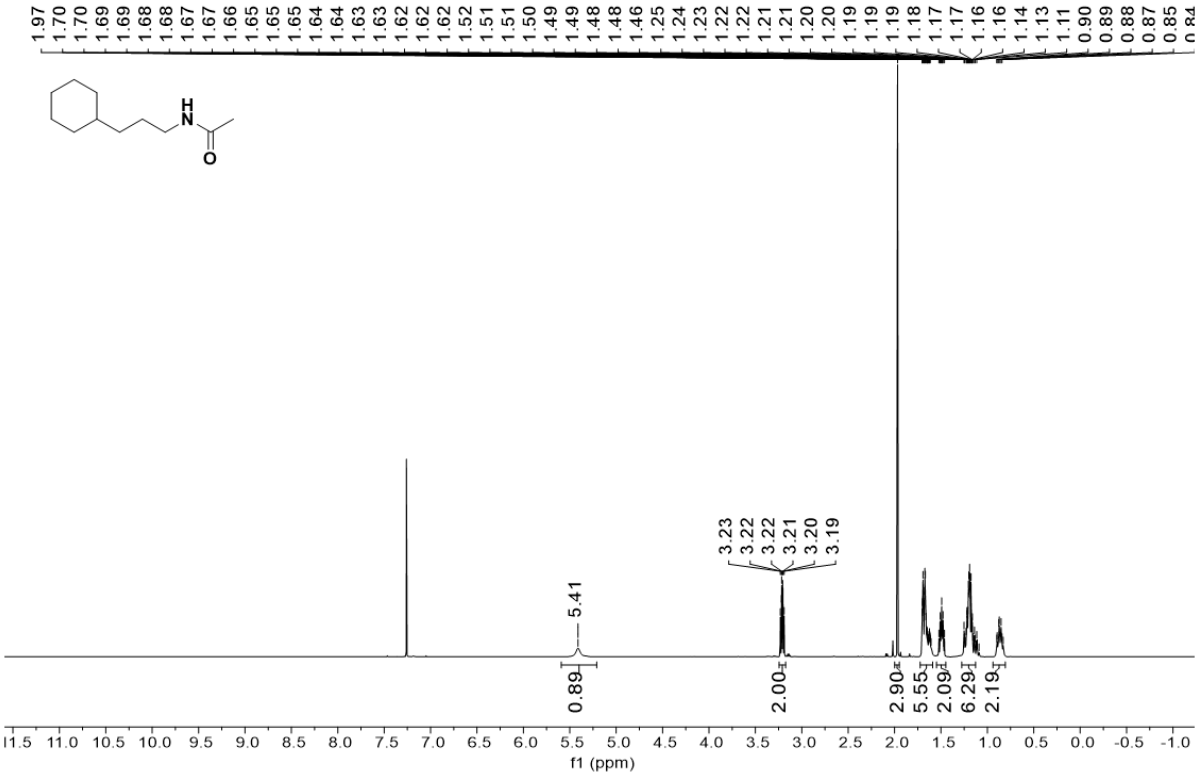

^{13}C NMR (126 MHz, 300 K, $CDCl_3$)